PROCEEDINGS

OF THE

ROYAL SOCIETY OF LONDON

SERIES A. MATHEMATICAL AND PHYSICAL SCIENCES

VOL CLXVII

CONTENTS

SERIES A   VOL CLXVII

No. A 928. 7 July 1938

Contents

Contents

PAGE

The Zeeman and Paschen-Back effects in strong magnetic fields

By P. Kapitza, F.R.S., P. G. Strelkov and E. Laurman

Institute for Physical Problems of the Academy of Science of the U.S.S.R., Moscow

[Plates 1, 2]

1. Introduction

The Zeeman effect in strong magnetic fields was first studied by Kapitza and Skinner (1925), the fields being obtained by a method developed by one of us (Kapitza 1924), in which an accumulator battery of small capacity was discharged through a coil. In this way it was possible to obtain magnetic fields up to 140,000 gauss during a time of $\frac{1}{100}$ sec. It turned out that in such fields the majority of the spectral lines which were studied, split up (within the limits of experimental error) proportionally to the applied field, in accordance with the theory which had previously been verified only in weaker magnetic fields. An exception, however, was the zinc line at 4680 A, which gave a splitting about 10 % greater than that predicted by the theory, this discrepancy being outside the limits of experimental error.

Since then the method of producing strong magnetic fields has been considerably developed (Kapitza 1927); instead of the discharge of an accumulator the powerful current impulse from a short-circuited generator has been used, which has made possible the production of fields more than twice as great as those formerly obtained, and, moreover, in considerably larger volumes. At the same time the technique of measuring the magnetic field has also been improved. Using these improvements we have made a new investigation of the Zeeman effect in fields up to 320,000 gauss, in which we have been able to increase considerably the accuracy of the measurements, and to explain the cause of the discrepancies previously found. We have also been able to investigate the Paschen-Back effect and to verify the theory of this effect.

2. The experimental arrangement

The experiments were made only in longitudinal fields, since this was the most convenient under our experimental conditions.

In its essentials the experimental arrangement is similar to that used in the former research; it is shown schematically in fig. 1.
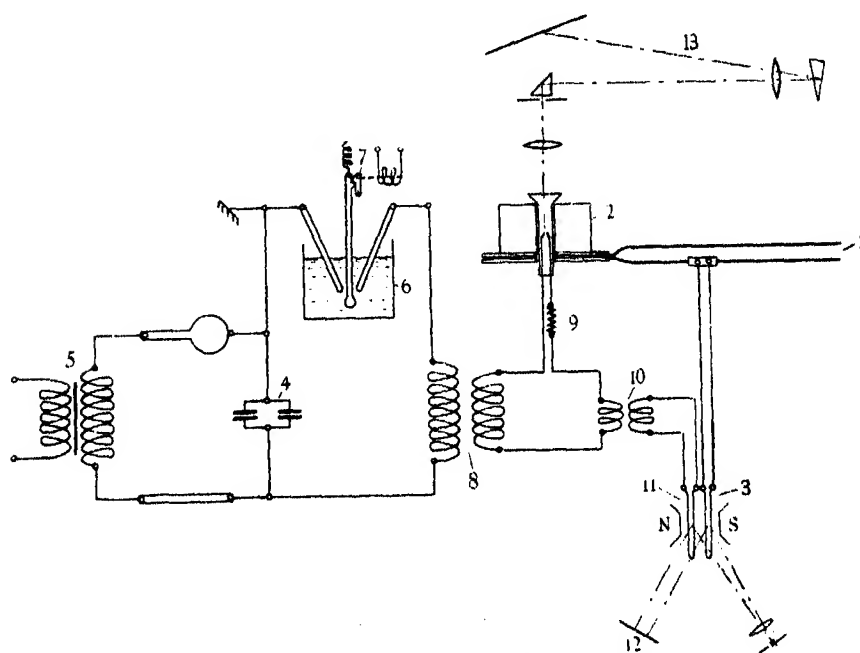
FIG. 1. General experimental arrangement.

The current from the short-circuited generator passes along the leads (1) and through the coil (2) in which the magnetic field is produced, the strength of the current being measured by means of the shunted oscillograph (3). A spark is produced by the discharge of two condensers (4), each of capacity $0 \cdot 1 \mu$F, charged to a potential of 30,000 V through a kenotron and a water resistance from the transformer (5); the condensers are discharged at the required moment by means of an oil switch (6), which is provided with an electromagnetic release mechanism (7). The discharge takes place through an iron-free transformer (8) whose secondary is connected in series with the spark gap, which is situated at the centre of the coil (2). In this circuit is included also a resistance (9) and a transformer (10), whose secondary is connected directly to the other coil of the oscillograph (11), which marks the time of passage of the current of the spark on the same photographic plate (12) on which is recorded the current passing through the coil (2). The spectrum is produced by means of a Hilger E 1 quartz spectrograph (13) (some of the spectra, for instance fig. 4 a (Plate 1), were, however, produced

with a spectrograph with glass optical parts, made by the State Optical Institute).

The transformer (8) consists of a primary of 320 turns, wound on a glass cylinder of diameter 270 mm., and a secondary of 50 turns also wound on a glass cylinder, with oil insulation. The use of this transformer is to regulate the voltage of the spark, which was chosen to be lower than that of the condenser; with this arrangement no high tension has to be introduced into the centre of the coil. By means of the resistance (9) the current strength in the spark can be adjusted, which is very important since the current has a strong influence on the breadth of the spectral lines produced.

The whole arrangement works in the following way. The condensers are first charged, and then when the generator is short circuited through the coil by pressing a button (for the detailed description of this mechanism see Kapitza 1927), current is passed from sliding contacts connected with the special switch of the big generator, through the release mechanism (7), thus bringing the oil switch into action. The contacts are so arranged as to synchronize the action of the release mechanism with that of the big generator, so that the spark is produced at the moment at which the current through the coil has its maximum value. This synchronization is checked by the oscillogram produced on the photographic plate (12); a typical oscillogram is shown in fig. 2 (Plate 1).
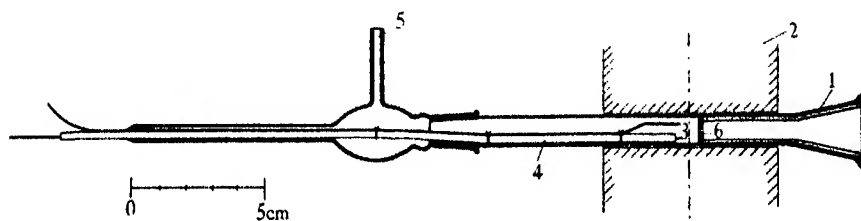
Fig. 3. The discharge tube.

The arrangement of the spark gap is shown in fig. 3. It consists of a glass tube (1) which is inserted into the hollow of the coil (2) (shown schematically here). In some of the experiments the diameter of this tube was 10 mm. and in the others 12 mm., according to the size of the hollow of the coil used in the particular experiment. The spark takes place between the electrodes (3) and (4), one of which (4) is insulated from the other by a quartz tube which surrounds it. This whole system can be evacuated, and usually the spark is produced at a pressure of 1 mm. Hg. A small window (6) of fused quartz is placed in front of the spark gap to limit the spreading of the spark along the axis of the coil.

3. MEASUREMENT OF THE MAGNETIC FIELD

The magnetic field was measured by the same method as used in the previous research (Kapitza 1927). The coil (2) was calibrated by placing inside it an accurately measured search coil, which was connected by means of a specially synchronized switch to a ballistic galvanometer at the moment of maximum current in the coil (2). By comparing the throw of the galvanometer with that produced by a standard mutual inductance, the strength of the magnetic field was determined; the current in the coil was deduced from an oscillogram, and so the constant of the coil (2) could be determined. Since the coil (2) is surrounded by a steel bandage in order to strengthen it, the magnetic field is not strictly proportional to the current in the coil, the deviation from proportionality being of the order of a few per cent. The calibration was therefore carried out for several different current strengths, and from the results the curve showing the relation between magnetic field and current was constructed. The oscillograms were measured after a fivefold magnification, produced by means of a special pantograph, one end of which was automatically guided along the curve of the oscillogram with the help of a photoelectric cell.* We estimate the accuracy of measurement of the magnetic field in the coil as from 1 to $1\frac{1}{2}$ %.

In fig. 2 (Plate 1) we reproduce one of the oscillograms of the current in the coil (2), from which the values of the magnetic field at the moment of the beginning and end of the spark, as indicated by the other oscillograph, could be deduced. It can be seen from the oscillogram that the time occupied by the spark is 0·001 sec., and in this time the current through the coil did not generally change by more than 1–$1\frac{1}{2}$ %.

The inhomogeneity of the field in the volume in which the discharge occurs was also studied, the search coil being placed at various points along the axis of the coil. It was found that in the space between the spark gap (3) and the quartz window (6) (fig. 3) the field did not vary by more than $\frac{1}{2}$ %.

The spectra were investigated in fields from 60,000 to 320,000 gauss.

4. PRODUCTION OF THE SPARK AND MEASUREMENT OF THE SPECTRAL LINES

The precision of the results of our research depends to a large extent on the possibility of producing sharp narrow spectral lines, and as in the

* A detailed account of this pantograph, constructed by P. Kapitza and E. Laurman, is to be published shortly.

previous work (Kapitza and Skinner 1925), we found that the most suitable method was to use the required elements not in their pure form but as impurities in some other material. Thus in our experiments the main substance of the electrodes was either copper or tungsten.

The breadth of the spectral lines was found to be extremely sensitive to the experimental conditions, a minute change of the latter being sufficient to spoil the quality of the lines quite appreciably.

An improvement in the sharpness of the lines obtained, as compared with the earlier experiments, was brought about by the larger available volume in which the spark was produced; in the previous experiments the coil diameter was only 0·4 cm., while now it was nearly three times greater. The main factor, however, in determining the sharpness of the lines was the current density: by suitable choice of the resistance (9) (fig. 1), the line could be considerably sharpened. Evacuation of the tube diminished the rise of pressure during the time of the discharge, and thus also increased the sharpness of the line.

In fig. 4 (Plate 1) we show, for comparison, photographs of the zinc triplet (4680, 4722 and 4811 A), the first of which was taken at the beginning of the research before the various measures described above had been taken, and the others after the experimental technique had been improved.

The breadth also depends appreciably on the strength of the magnetic field itself, apparently because the character of the spark is changed by the presence of the magnetic field. In a magnetic field, the ions of the evaporated metal can depart from the electrodes only along screw-like trajectories of very small diameter round the lines of forces of the field, and consequently their concentration is greatly increased. In this connexion it is interesting to mention that after each discharge a well-blackened spot was noticed in the centre of the window (6) (fig. 3) just opposite the electrode; the formation of this spot was presumably due to the ions moving along the lines of forces settling on the quartz. After each experiment it was necessary to use a new quartz window. In a magnetic field the relative intensities of the various spectral lines were also strongly affected, especially the lines of impurities in the main metal of the electrode; the lines of some impurities, hardly noticeable without a magnetic field, sometimes became even more intense in a magnetic field than the lines of the main metal. This is illustrated by fig. 5 (Plate 2), where the spectra taken without a field, and in a field of 320,000 gauss, are superimposed on the same plate, and it will be seen for instance that the lines of the doublet Ca ^2S–^2P, which in the absence of a field do not appear on the plate, have a considerable intensity in the field.

The spectra of each electrode used were generally taken at various fields up to 300,000 gauss, and there was a large number of lines which had to be measured on each plate. It turned out that the best method of measuring up the plates was by means of a travelling microscope, this method giving an accuracy exceeding 0·01 mm. The measuring technique was improved by the application of Linnik's vibrating objective method (Linnik 1931), which increases the accuracy by weakening the influence of the grain of the photographic plate. Any possible lateral displacement of the objective by the vibrations was excluded by suspending it on bronze strips which were vibrated electromagnetically. We also tried using a microphotometer but, in spite of the longer time required and the more tedious nature of the measurements, no increase in accuracy was obtained. In order to translate the microscope measurements of the splittings into wave-lengths the plate was calibrated, using for the greater part the lines investigated themselves as standards. Since linear interpolation over 30–40 A would have given an error of order 1·5 %, we introduced a dispersion correction, differentiating the dispersion formula for quartz

$$n^2 = a^2 + \frac{M_1}{\lambda^2 - \lambda_1^2} - \frac{M_2}{\lambda_2^2 - \lambda^2}, \tag{1}$$

with the following values of the constants:

$$a = 3\cdot4629 \qquad\qquad \lambda_1^2 = 0\cdot010627$$

$$M_1 = 0\cdot010654 \qquad\qquad \lambda_2^2 = 100\cdot77$$

$$M_2 = 111\cdot47$$

The accuracy of our determinations of the Zeeman splitting varied from 1 to 3 % according to the breadth of the line and the strength of the magnetic field.

5. Verification of the proportionality of the Zeeman splitting to the magnetic field

First of all we investigated the zinc line $2\,^3P_0 - 2\,^3S_1$, $\lambda = 4680\cdot20$ A, which in the previous research had not shown strict proportionality between splitting and field. Using stronger magnetic fields, we discovered at once that the apparent increase of splitting in the previous experiments was caused by a neighbouring line, apparently $a\,^4F_3 - c\,^4D_3$ of copper, $\lambda = 4674\cdot76$ A. In the photographs without a field this line was absent, and became observable in the photographs with a field on account of the change in the conditions

of discharge. Even in a field this line was very weak, but its splitting, superimposed on one of the components of $\lambda = 4680$ A, displaced the corresponding position of maximum blackening on the plate, and caused an apparent increase of the splitting. The use of stronger fields definitely established the accidental character of the discrepancy; in fig. 4 (Plate 1) can be seen the superposition of the splitting of the zinc and copper lines in a field of 126,000 gauss.

By a suitable choice of the spark conditions we were subsequently able to eliminate the disturbing line. In fig. 4 *b* (Plate 1) we show the splitting of the triplet in a field of 275,000 gauss; as can be seen from Tables I, II and VI, the 4680 zinc line is split proportionally to the field up to 275,000 gauss within the limits of experimental error.

The proportionality of the splitting and the field was verified also on a number of other lines; a summary of the results is given in Tables I–VII. We tried to investigate as large as possible a variety of spectral terms, but were limited by the optical aperture of the spectrograph and the sensitivity of the plates. High terms, having a complicated splitting, could not be sufficiently accurately studied, owing to the limited resolving power of the spectrograph, so we had to confine ourselves to the first lines of the principal and sharp series. Each of the tables refers to a separate photograph, and we have chosen seven of the most characteristic. From the experimental splitting $(\varDelta\lambda)$ the magnetic field was deduced in each case by means of the theoretical formula

$$\varDelta\lambda = \varDelta(mg)\frac{\mu H}{ch}\lambda^2 = 4.69 \times 10^{-5}\lambda^2, \text{ in A,}$$

where $\varDelta(mg)$ is the difference of the mg values for the levels which give rise to the displaced component, and is known as the splitting type. It will be seen that the magnetic field deduced in this way agrees fairly well with the field deduced from the oscillogram, so that the theory, and in particular the law of proportionality to the magnetic field, is confirmed up to the strongest field we were able to use.

It will be noticed on more detailed examination of the tables that the splitting of the lines is systematically slightly less than could be expected from the accuracy of measurement of the magnetic field: thus the magnetic field deduced from the splitting is usually 2–3 % less than that deduced from the oscillograms. Probably the discrepancy is due to the fact that all the experimental errors tend to diminish the measured splitting below its true value. Firstly, each of the components has a diffuse tail, which, superimposed on the corresponding opposite component, slightly displaces the

position of maximum blackening towards the centre; this error, however, is not large. A more serious error is caused by the fact that the spark in our discharge tube is limited only in the forward direction. Part of the excited atoms falling into the back part of the tube, farthest removed from the window, may radiate already in a region of weaker magnetic fields. The radiation of these atoms, though weak in intensity, causes a spreading of the split lines towards the centre of the pattern and thus causes an apparent reduction of the splitting.

Since various atoms will be distributed with varying concentration in the discharge gap of our tube, according to their ionizations, quantities and temperatures, the apparent diminution of the splitting should be different for the various spectral lines, and this can also be seen from the tables.

It should be noticed that in the doublets and triplets investigated the Paschen-Back effect is still of negligible influence, causing departure from proportionality much less than the errors of measurement.

In this way we can conclude from our experiments that the fundamental laws of the Zeeman splitting are perfectly valid for the spectral terms investigated in magnetic fields up to 320,000 gauss.

Further, we investigated whether there was any displacement of the centre of gravity of the splitting pattern in a strong magnetic field, by superimposing on the same plate exposures in the absence of a field and in a field of 320,000 gauss. The results of such double exposures are shown in fig. 5 (Plate 2); it will be seen that the split lines lie exactly symmetrically about the line obtained in the absence of a field. Accurate measurements showed that there was no common displacement greater than 0·01 mm., so that our experiments confirm that the centre of gravity of the pattern is not displaced by a strong magnetic field, in accordance with theory.

6. THE PASCHEN-BACK EFFECT

In order to trace the development of the Paschen-Back effect and to verify the theory of this effect* we examined the beryllium doublet, Be II, principal series $\lambda = 3131\cdot32$ and $3131\cdot97$ A. In our magnetic fields the splitting of this line was as great as 5·5 A, which considerably exceeds the natural splitting of the level (0·65 A), so that the conditions were suitable for the occurrence of the Paschen-Back effect.

This doublet was easily obtained by using electrodes of ordinary beryllium copper. The exposures were made at various field strengths and are repro-

* For theory and experiments see for instance Bethe (1933).

duced in fig. 6 (Plate 2). Since the doublet occurs close to the already investigated copper doublet, we could check the magnetic field by the splitting of the copper lines which are adjacent to the beryllium lines.

We were able to trace clearly all the stages of the development of the Paschen-Back effect. The splitting of the beryllium doublet can be calculated exactly; for the energies of the longitudinal components we have:

$$
\left.
\begin{aligned}
&\pm \mu H + \frac{\varDelta}{2}, \\[2mm]
&+\frac{3\mu H \pm \sqrt{(\mu^2 H^2 + \tfrac{2}{3}\mu H \varDelta + \varDelta^2)}}{2}, \\[2mm]
&-\frac{3\mu H \pm \sqrt{(\mu^2 H^2 - \tfrac{2}{3}\mu H \varDelta + \varDelta^2)}}{2},
\end{aligned}
\right\}
\tag{2}
$$

where $\varDelta$ is energy difference between the doublet levels in the absence of a field. The intensities of these components are respectively given by

$$
\left.
\begin{aligned}
&\frac{I}{2}, \\[2mm]
&\frac{I}{4}\left[1 \pm \frac{\mu H + \dfrac{\varDelta}{3}}{\sqrt{(\mu^2 H^2 + \tfrac{2}{3}\mu H \varDelta + \varDelta^2)}}\right], \\[2mm]
&\frac{I}{4}\left[1 \pm \frac{\mu H - \dfrac{\varDelta}{3}}{\sqrt{(\mu^2 H^2 + \tfrac{2}{3}\mu H \varDelta + \varDelta^2)}}\right],
\end{aligned}
\right\}
\tag{3}
$$

where I is the intensity of the weaker component of the doublet.

The splittings in wave-lengths calculated from these formulae are plotted against the magnetic fields in fig. 7 (full curve). In reducing the plates of the Paschen-Back effect obtained experimentally, we generally determined only the difference of wave-lengths between the components, the results being plotted in fig. 7 in such a way that the points departed approximately equally from the theoretical curves. In one case (261,900 gauss), however, the wave-lengths of all the components of the splitting were directly determined by comparison with the lines of Be II doublet without field (superimposed on the same plate); the results of this measurement are indicated by full black circles.

As can be seen from fig. 7, the discrepancy between our experimental results and the theory is well within the limits of experimental error, so that we can conclude that the theoretical formulae correctly describe the phenomenon up to the highest magnetic field used in our experiments.

The asymmetry predicted by the formula can, in fact, even be seen visually; thus for the largest splitting on the photograph (fig. 5, Plate 2), it can be seen that the right-hand pair of more intense lines is slightly less split than the left-hand pair, which coresponds to the theoretical prediction, as is evident from the diagram (fig. 7).
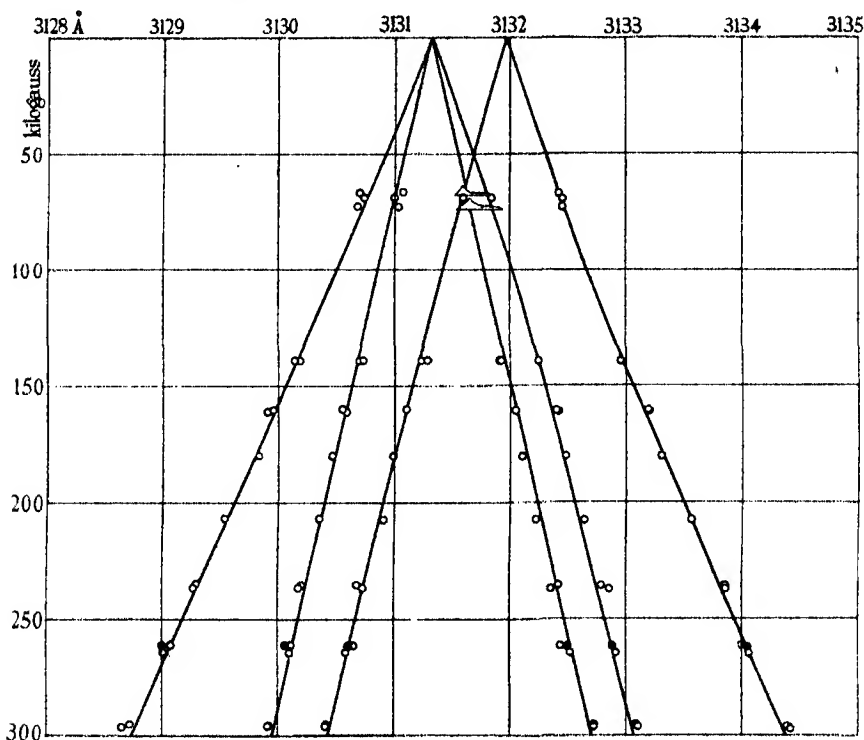
FIG. 7. Dependence of splitting of the Be II doublet on field strength: the full lines are the theoretical curves, and the circles experimental points.

We were not able to carry out a thorough investigation of the intensities of the components, but made microphotometric intensity curves which are compared in fig. 8, with the theoretically predicted intensity relations. Although only qualitative comparison is possible, it can be seen that the experimental results are in agreement with the theoretical predictions. The intensity of the extreme components rapidly diminishes with increase of magnetic field, while the inner components approach equal intensities, the ratio of intensities of the components of the original doublet being 1 : 2, as can be seen from the microphotometer curve. The theoretical value of the intensity ratio of the central components to the weaker extreme components is 20 : 1, and if the blackening of the plate is taken as a measure
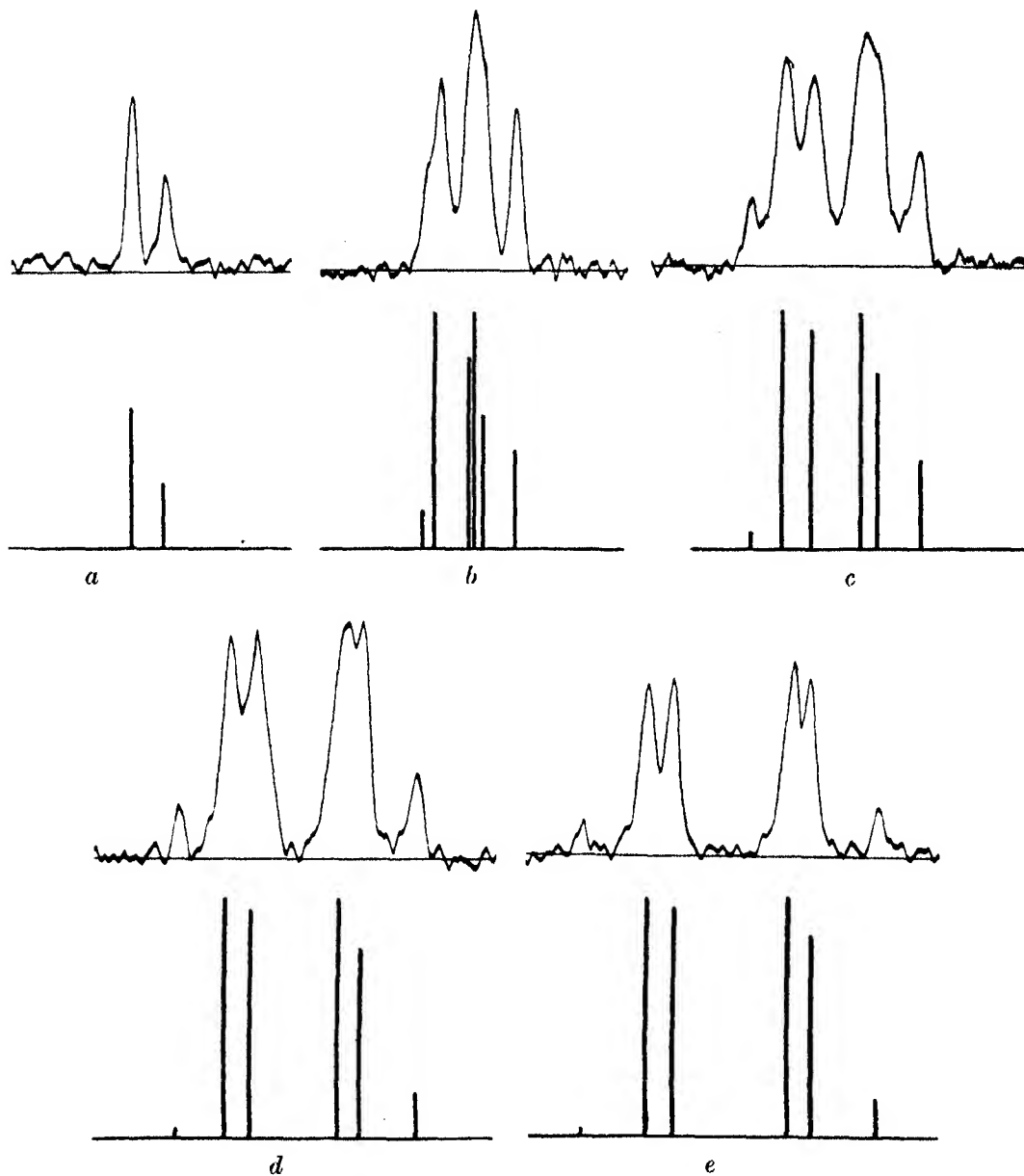
FIG. 8. Comparison of microphotometer intensity curves with the theoretically predicted intensities for the components of the split Be II doublets.

of intensity it will be seen that, allowing for the roughness of the method, the agreement of the experiment with theory is quite satisfactory.

The initial stages of the Paschen-Back effect can be traced also with the zinc triplet $^3P-^3S$; in fig. 4 b (Plate 1) it can even be observed visually that the line 4722 A of the triplet is not symmetrically split, the separation between the longer wave-length components being greater than between the shorter wave-length components. Measurement showed that these separations were 1·5 and 1·3 A respectively, which agree very well with an approximate calculation, kindly made by Dr L. D. Landau, predicting separations 1·55 and 1·31 A for the particular magnetic field used.

TABLE I

Description of spectral lines	Wave-length A	Type of splitting	Amount of splitting A	Field deduced from splitting, in kilogauss	
Si (?)	3905·52	1/1 (?)	2·69	—	187·6
Ca II $^2S-^2P$	3933·66	5/3	4·50	185·7	183·1
		3/3	2·62	180·5	
Ca II $^2S-^2P$	3968·46	4/3	3·70	—	187·8
Zn I $^3P-^3S$	4680·20	4/2	7·53	—	183·2

Field deduced from oscillogram 186·8–189·1

TABLE II

Description of spectral lines	Wave-length A	Type of splitting	Amount of splitting A	Field deduced from splitting, in kilogauss	
Si (?)	3905·52	1/1 (?)	3·98	—	277·8
Ca II $^2S-^2P$	3933·66	5/3	6·72	277·7	275·0
		3/3	3·96	272·3	
Ca II $^2S-^2P$	3968·46	4/3	5·44	—	275·8
Zn I $^3P-^3S$	4680·20	4/2	11·27	—	274·2
Zn I $^3P-^3S$	4722·16	4/2	11·53	275·3	275·5
		3/2	8·46	269·6	

Field deduced from oscillogram 278·0–279·6

TABLE III

Description of spectral lines	Wave length A	Type of splitting	Amount of splitting A	Field deduced from splitting, in kilogauss	
Si (?)	3905·52	1/1 (?)	3·89	—	272·0
Ca II $^2S-^2P$	3933·66	5/3	6·68	276·0	269·7
		3/3	3·83	263·4	
Ca II $^2S-^2P$	3968·46	4/3	5·34	—	271·0
Ca I $^1S-^1P$	4226·73	1/1	4·51	—	269·1
Cd I $^3P-^3S$	4678·19	4/2	11·25	—	270·5

Field deduced from oscillogram 266·8–275·2

TABLE IV

Description of spectral lines	Wave-length A	Type of splitting	Amount of splitting A	Field deduced from splitting, in kilogauss	
Cu I ^{2}S–^{2}P	3247·55	5/3	4·34	263·0	264·2
		3/3	2·63	265·4	
Cu I ^{2}S–^{2}P	3273·97	4/3	3·59	—	267·6
Si (?)	3905·52	1/1 (?)	3·78	—	264·0
Ca II ^{2}S–^{2}P	3933·66	5/3	6·35	262·3	262·8
		3/3	3·82	263·2	
Ca II ^{2}S–^{2}P	3968·46	4/3	5·21	—	264·2
Hg I ^{3}P–^{3}S	4046·56	4/2	8·06	—	262·2

Field deduced from oscillogram 273·4–275·9

TABLE V

Description of spectral lines	Wave-length A	Type of splitting	Amount of splitting A	Field deduced from splitting, in kilogauss	
Cu I ^{2}S–^{2}P	3247·55	5/3	4·51	273·3	276·0
		3/3	2·77	278·7	
Cu I ^{2}S–^{2}P	3273·97	4/3	3·70	—	275·6
Si (?)	3905·52	1/1 (?)	3·89	—	272·3
Ca II ^{2}S–^{2}P	3933·66	5/3	6·62	273·7	273·9
		3/3	3·98	274·1	
Ca II ^{2}S–^{2}P	3968·46	4/3	5·41	—	274·3
Hg I ^{3}P–^{3}S	4046·56	4/2	8·42	—	274·0
Hg I ^{3}P–^{1}S	4077·83	3/2	6·37	—	272·1

Field deduced from oscillogram 275·2–276·9

TABLE VI

Description of spectral lines	Wave-length A	Type of splitting	Amount of splitting A	Field deduced from splitting, in kilogauss	
Cu I ^{2}S–^{2}P	3247·55	5/3	4·38	265·2	265·2
		3/3	2·62	265·1	
Cu I ^{2}S–^{2}P	3273·97	4/3	3·59	—	267·6
Ca II ^{2}S–^{2}P	3933·66	5/3	6·42	265·0	266·0
		3/3	3·88	267·0	
Ca II ^{2}S–^{2}P	3968·46	4/3	5·27	—	267·5
Hg I ^{3}P–^{3}S	4046·56	4/2	8·21	—	267·1
Hg I ^{3}P–^{1}S	4077·83	3/2	6·23	—	266·0
Zn I ^{3}P–^{3}S	4680·20	4/2	10·97	—	266·8
Zn I ^{3}P–^{3}S	4722·16	4/2	11·17	268·8	268·7
		3/2	8·43	268·6	

Field deduced from oscillogram 274·4–276·3

TABLE VII

Description of spectral lines	Wave-length A	Type of splitting	Amount of splitting A	Field deduced from splitting, in kilogauss	
Cu I ^{2}S–^{2}P	3247·55	5/3	5·27	319·1	320·3
		3/3	3·18	321·5	
Cu I ^{2}S–^{2}P	3273·97	4/3	4·30	—	320·2
Si (?)	3905·52	1/1 (?)	4·61	—	322·3
Ca II ^{2}S–^{2}P	3933·66	5/3	7·73	325·2	322·3
		3/3	4·72	319·3	
Ca II ^{2}S–^{2}P	3968·46	4/3	6·35	—	322·2
Hg I ^{3}P–^{3}S	4046·56	4/2	9·87	—	321·1
Hg I ^{3}P–^{1}S	4077·83	3/2	7·39	—	315·9

Field deduced from oscillogram 319·6–323·8

TABLE VIII

Measured wave-length of the component A	Calculated wave-length of the component A	Difference: measured minus calculated wave-length A
3134·05	3134·04	+ 0·01
3132·90	3132·88	+ 0·02
3132·49	3132·53	− 0·04
3130·61	3130·61	0·00
3130·06	3130·12	− 0·06
3129·00	3129·07	− 0·07

SUMMARY

1. A method is described for studying the Zeeman and Paschen-Back effects in magnetic fields up to 320,000 gauss.

2. It is shown that the Zeeman splitting is within the limits of experimental error proportional to the magnetic field and obeys the theoretical predictions previously verified only in weaker fields.

3. In strong magnetic fields we were unable to discover any displacement of the centre of gravity of the splitting pattern, which again is in agreement with the theoretical prediction.

4. The Paschen-Back effect was studied in fields up to 300,000 gauss on a beryllium doublet, and it was shown that the splitting accurately followed the theoretical predictions, and that the intensities of the various components agreed qualitatively with the theory.

5. The initial stages of the Paschen-Back effect were also observed for a zinc triplet ^{3}P–^{3}S.

Cu 3273·97 — Cu 3277·55 — Si 3905·52 — Ca 3968·46 — Ca 3933·66 — Hg 4046·56 — Hg 4077·83 —

Fig. 5

a

b

c

d

e

× 10
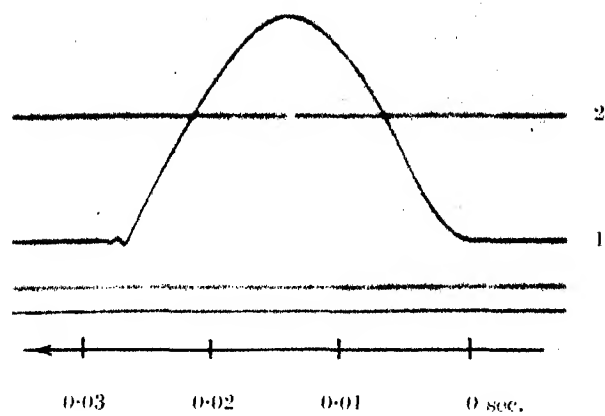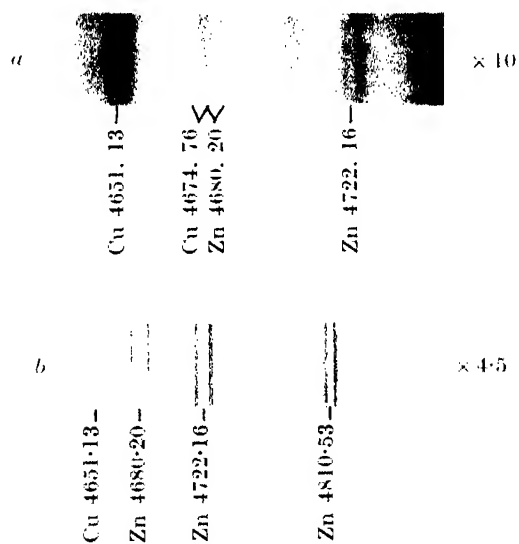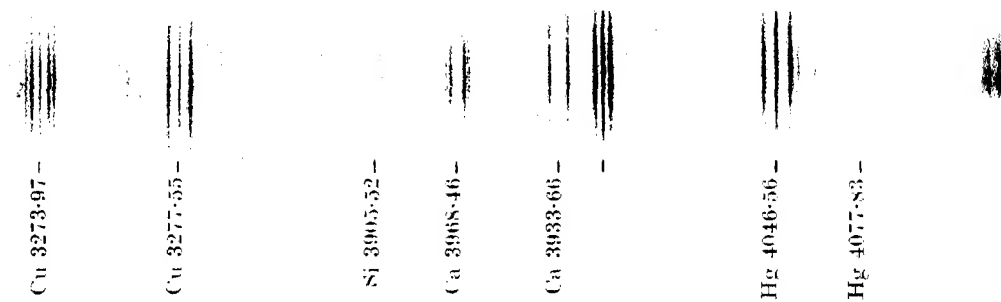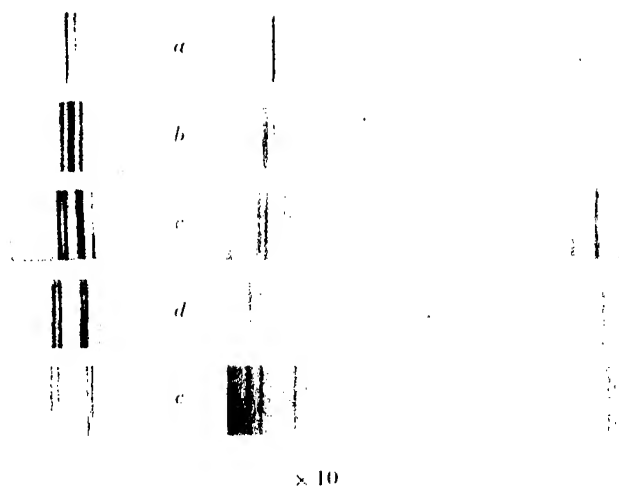
Fig. 6

REFERENCES

Bethe 1933 *Handbuch der Physik*, **24**.
Kapitza 1924 *Proc. Roy. Soc.* A, **105**, 691.
— 1927 *Proc. Roy. Soc.* A, **115**, 658.
Kapitza and Skinner 1925 *Proc. Roy. Soc.* A, **109**, 224.
Linnik 1931 *Trans. Opt. Inst. Leningrad,* **5**, No. 52.

DESCRIPTION OF PLATES

PLATE 1

FIG. 2. Oscillogram showing (1) current in the coil, and (2) current in the spark.

FIG. 4. Splitting of the zinc triplet $^3P-^3S$: (a) at 126 kilogauss with badly chosen current density, (b) at 275 kilogauss with improved spark conditions.

PLATE 2

FIG. 5. Superimposed spectra with field of 320 kilogauss and without field.

FIG. 6. Paschen-Back effect for the beryllium doublet $^2S-^2P$. On the left is shown the splitting of the doublet in increasing fields (a) 0, (b) 74·3, (c) 168·4, (d) 241·8, (e) 307·0 kilogauss; on the right the splitting of the copper doublet 3248, 3274 A for the same fields.

The primary decomposition of ethane, and the reaction between ethane and nitric oxide

By T. J. GRAY, MORRIS W. TRAVERS, F.R.S., AND F. T. WHITE

In a recent paper published in this journal, Staveley (1937) has shown that the effect of adding nitric oxide to ethane is to reduce the rate of increase in pressure when the gas is heated at constant volume in the neighbourhood of 600°. Assuming that the nitric oxide remains sensibly unchanged, he concludes that the effect of the addition of this gas is to inhibit the primary decomposition of the ethane, and explains this on the supposition that the nitric oxide removes free radicals, which initiate reaction chains. In the present paper we shall show that some important facts have been overlooked, and particularly that nitric oxide itself reacts with ethane at a rate which is comparable with that of the primary decomposition process.

EXPERIMENTAL WORK

The method which we have used is substantially the same as we have employed in this laboratory in a number of other investigations, and has been referred to as the method of *detailed analyses*. It is admittedly laborious, and for this reason we have only been able to carry out a single series of experiments, in which the initial concentration of the ethane was 0·01 g.mol.-litre, and that of the nitric oxide one-tenth of this amount. The temperature at which the experiments were carried out was 590°. Two silica reaction tubes of capacity close to 59 c.c. were used, and each of these cracked on chilling after it had been used for about twenty experiments.

An accurately measured quantity of the gas was condensed in a reaction tube, which was then sealed. Ethane, having a negligibly small vapour pressure at − 180°, could be condensed completely, but using a mixture of ethane and nitric oxide, a small quantity of gas remained in the dead space of the filling apparatus, and this was collected, analysed, and allowed for. After heating the reaction tube for varying periods up to 20 min., it was chilled, and fractions of the gas were taken off at − 180° and − 80°, a method of refractionation being used so as to secure the practically complete separation of the low- and high-boiling constituents.

In the case of the experiments with pure ethane, the − 180° fraction contained hydrogen, which was estimated by combustion over copper oxide at 290°, small quantities of methane, estimated by combustion at 600°, and nitrogen accumulated in the course of the processes of manipulation. The − 80° fraction contained ethane and ethylene. The latter was difficult to estimate accurately as the difference between two relatively large quantities. However, the results of the first four experiments with pure ethane show that the hydrogen and ethylene are formed in quantities which (g.mol.-litre/min.) are closely equivalent, thus:

TABLE I

Time interval	C_2H_4	H_2
10	0·00024	0·00023
15	0·00032	0·00032
5	0·00017	0·00013
20	0·00058	0·00053

The rate of primary decomposition of the ethane can be determined with the same accuracy from the increase in volume, taken as the sum of the volumes of the two fractions, as from the quantity of hydrogen formed, the

quantity of methane and of condensate formed being too small to measure. These quantities are plotted in fig. 1.
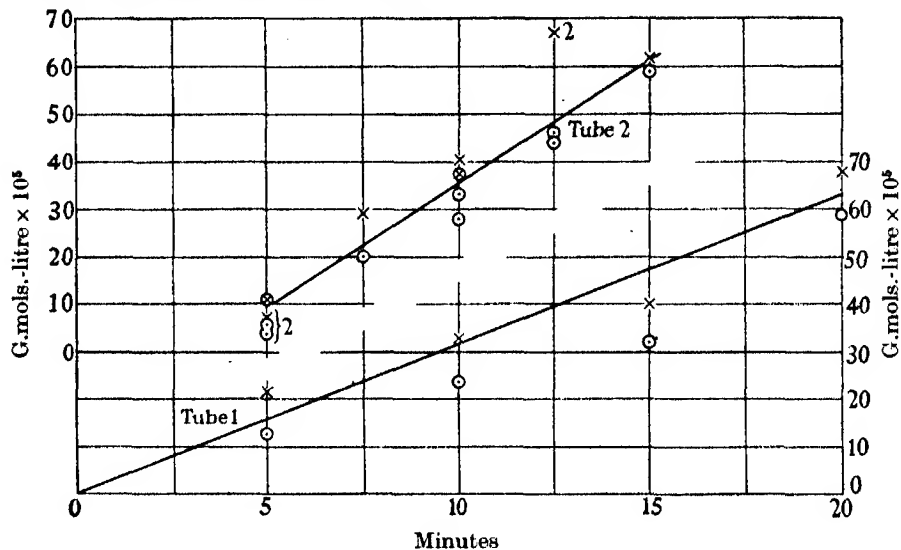
Fig. 1. Ethane experiments: Hydrogen ⊙, increase in volume ×.

The quantities of methane and nitrogen (total in two fractions) found in the −180° fraction were:

TABLE II

(G.mol.-litre × 10^5, min.)

Tube 1

Time	10	15	5	23
N_2	5	10	5	7
CH_4	24	12	12	11

Tube 2

Time	10	5	$12\frac{1}{2}$	10	$7\frac{1}{2}$	5	15	20	10	5	$12\frac{1}{2}$
N_2	4	5	3	5	3	4	4	5	5	1	5
CH_4	8	20	11	15	11	9	10	12	9	12	——

It is obvious that the methane is formed mainly in the first few moments of the reaction, and its formation is probably a surface phenomenon, and not the result of the homogeneous reaction of ethane and ethylene (Travers 1937a). The two tubes did not behave very differently so far as the formation of methane is concerned, but in the case of the second tube the formation of hydrogen, and the increase in volume, was delayed initially. This was confirmed by repeated experiments carried out at the 5 min. interval, the experiments being the second, sixth, and tenth in the series. Check

experiments showed that hydrogen could be introduced into a reaction tube under the conditions of the experiment, and recovered without loss. The nitrogen is the quantity accumulated in the two fractions in the manipulative process. Apart from one or two erratic results, the quantity is close to 0·00005 g.mol.-litre per fraction. We shall refer to this quantity later.

In the experiments with ethane and nitric oxide the $-180°$ fraction contained unreacted nitric oxide, hydrogen, and small quantities of carbon monoxide, methane, and nitrogen. The $-80°$ fraction contained a gas which was absorbed by bromine, and which was partly ethylene and partly a nitrogen-containing carbon compound, unchanged ethane, and a nitrogen-containing gas the nature of which will be discussed later. The sums of the volumes of the two fractions, for the intervals up to about 12·5 min., did not differ sensibly from the volume of the original gas, 0·00110 g.mol.-litre, and then increased slowly (fig. 2 A). This fact does not necessarily imply that if the pressure change were observed at constant volume and at the reaction temperature, no change of pressure would be observed at first, since a little water, or carbon compound non-volatile at $-80°$ might have been formed. However, it offers a partial explanation of Staveley's results (Staveley 1937), and, taken with facts to be presented later, shows that the nitric oxide and ethane react with decrease in volume.
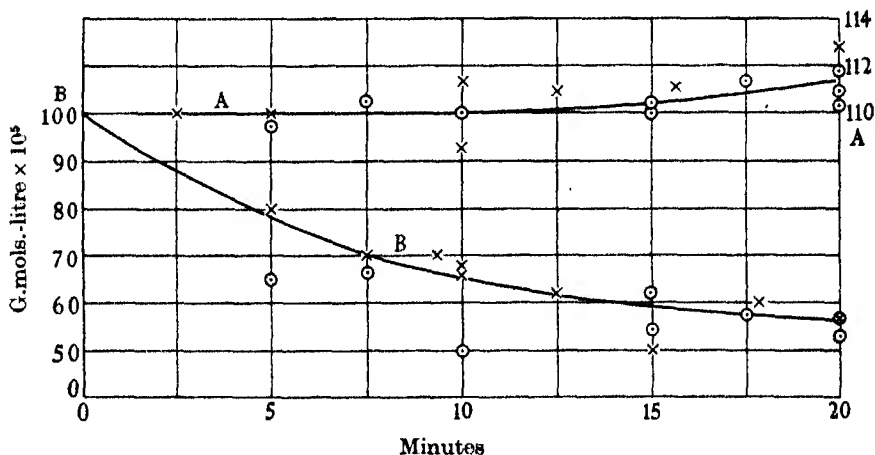
Fig. 2. NO experiments. A, change in volume; B, NO in gas.
Tube 1, ⊙. Tube 2, ×.

The process of analysis of the fractions proceeded as follows. In the case of the $-180°$ fraction the operations were:

(*a*) Absorption of nitric oxide by chromous chloride (Gay and Travers 1937, p. 768).

(*b*) Oxidation of hydrogen and carbon monoxide by copper oxide at 290°, observation of reduction in volume, and absorption by alkali.

(*c*) Oxidation of methane by copper oxide at 600° and absorption by alkali.

(*d*) Nitrogen by difference.

In the case of the −80° fraction the operations were:

(*a*) Treatment with bromine, and observation of reduction in volume.

(*b*) Oxidation by copper oxide at 600°, and absorption by alkali.

(*c*) Nitrogen by difference.

The amounts of nitric oxide remaining are set down in Table III and are shown by the graph in fig. 2 B. Fig. 3 shows the quantities of hydrogen produced. The quantities of carbon monoxide and methane are also given together in Table III. They are small, and show no tendency to increase regularly. These gases are probably the products of reactions taking place at the surface during the first short time interval.
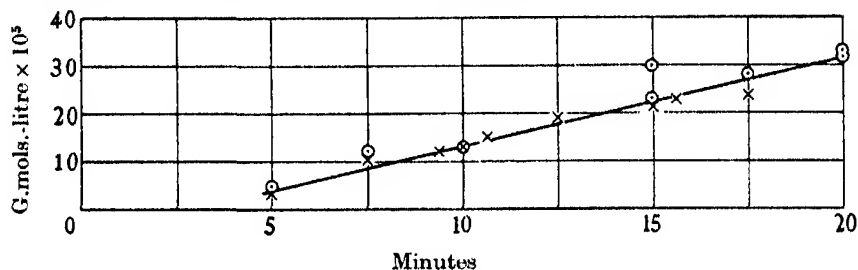
FIG. 3. Hydrogen in NO experiments. Tube 1, ⊙; Tube 2, ×.

The amounts of nitrogen present in the −180° fractions, less 0·00005 g.mol.-litre, the quantity which, as the ethane experiments show, may accumulate in one fraction in the process of analysis, increase fairly regularly with time (Table III, fig. 4). These quantities represent nitric oxide, or some product of its reaction with ethane, reduced to nitrogen. The quantities of gas absorbed by bromine, and the residues from the −80° fraction, the latter less 0·00005 g.mol.-litre, are also set down in Table III. The latter are irregular, and the quantities show no relation to the time interval. It was thought that they might represent quantities of nitrous oxide. However, it is probable that the nitrogen is derived from some carbon-nitrogen compound, which is incompletely removed by the bromine. The sum of the quantities of gas absorbed by bromine, plus twice

that of the nitrogen in the $-80°$ fraction (less 0·00005 g.mol.-litre) are plotted against the time in fig. 4. This graph shows the rate of increase in the ethylene and nitrogen-containing compound, formed by the reaction of nitric oxide and ethane, and also possibly ethylene oxide or a peroxide. It shows that some change is proceeding with accelerated velocity.

TABLE III

(G.mol.-litre × 10⁵)

Tube 1

(a)	Time	10	5	15	20	20	15	17·5	7·5
(b)	NO	50	65	54	57	51	62	57	66
(c)	CH₄+CO	—	11	—	21	16	8	24	15
(d)	N₂, −180° fr.*	—	2	10	10	17	12	11	4
(e)	Absorbed Br	29	14	32	83	80	34	48	31
(f)	N₂, −80° fr.*	6	10	8	3	8	3	11	13

Tube 2

(a)	Time	10	5	7·5	12·5	10	8·75	11·25	15	20	16·25
(b)	NO	66	80	70	62	67	70	—	50	57	60
(c)	CH₄+CO	17	10	13	12	7	11	11	11	20	15
(d)	N₂, −180° fr.*	3	3	3	7	1	3	6	12	13	13
(e)	Absorbed Br	—	8	17	37	16	—	—	—	95	43
(f)	N₂, −80° fr.*	—	3	1	5	2	—	—	—	8	1

* Observed values less 0·00005 g.mol.-litre.
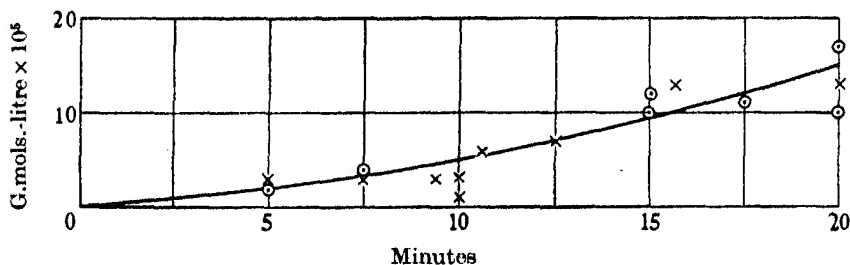
FIG. 4. NO experiments: N₂ in −180° fraction less 0·00005 g.mols-litre. Tube 1, ⊙; Tube 2, ×.

The disappearance of the ethane (fig. 6) is at first rapid, then slow, and then again rapid.

DISCUSSION OF THE EXPERIMENTAL RESULTS

A difficulty in the way of the quantitative treatment of this problem is the fact that surface is not without influence on the primary decomposition of ethane, and the effects observed are particularly marked in the early stages of the process, which is the region in which the results of such
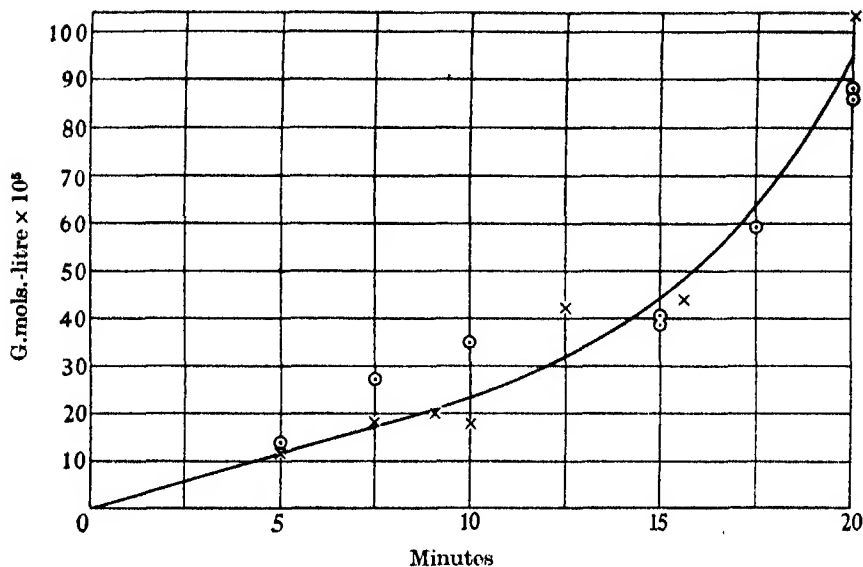
Fig. 5. NO experiments, gas absorbed by bromine. Tube 1, ⊙ ; Tube 2, ×.
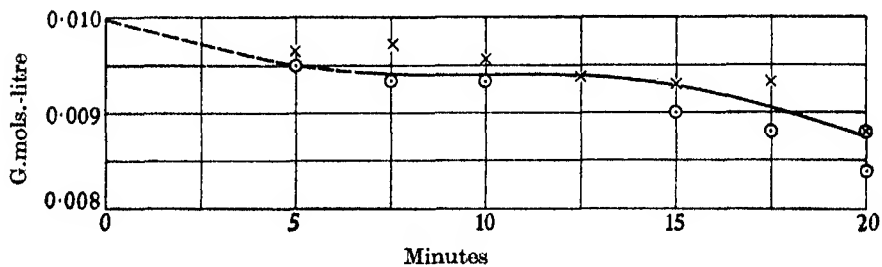
Fig. 6. NO experiments, C_2H_6 in gas. Tube 1, ⊙ ; Tube 2, ×.
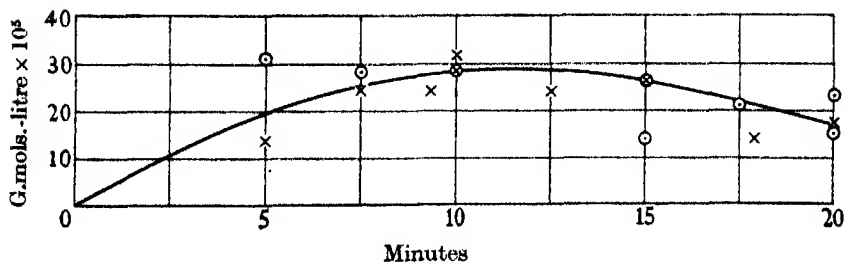
Fig. 7. Value of [0·001—NO in gas $+2(N_2$ in -180_c Fraction $-0·00005)$] as NO. Tube 1, ⊙ ; Tube 2, ×.

investigation are of particular interest. Though Staveley (1937) found the effect to be small, Travers and Pearce (1934, p. 532) found it to be considerable, and the present investigation confirms their conclusion. It may be observed that it is frequently stated in the literature that Marek and McCluer (1931) proved that the reaction is homogeneous. They did not do so, but accepted the statement of Frey and Smith (1928) that a copper surface had little influence on the process between 200 and 400°, and assumed that it would be without influence at 600°. An attempt to determine the rate of the primary process in silica apparatus at temperatures near to 600° in this laboratory was abandoned on account of the difficulties associated with surface effects.

The first conclusion arrived at from these experiments is that while the rate of the primary decomposition of ethane is reduced by addition of nitric oxide, that gas enters into rapid reaction with ethane. As the primary decomposition process still proceeds to some extent, the reaction between ethane and nitric oxide must take place with diminution of volume. From the outset some nitrogen (appearing in the $-180°$ fraction) is formed (fig. 4), so that the quantity of the nitrogen-carbon compound present at any moment in the gas phase, estimated as NO, is given by [0.001—NO in gas $+ 2$ (N_2 in $-180°$ fraction $- 0.00005$)] in g.mol.-litre. The concentration appears to increase to a maximum at 12.5 min., and then to diminish (fig. 7). This diminution of the concentration of the nitrogen-carbon compound, which indicates an acceleration of the rate at which it disappears, is accompanied by marked acceleration of one of the processes which give rise to the products which are absorbed by bromine.

If the formation of hydrogen from the nitric oxide-ethane mixture represents the primary decomposition of ethane, direct inspection of the graphs shows that the initial rate of this process, and the initial rate of disappearance of nitric oxide, together represent a rate of chemical change not far different from the initial rate of the primary decomposition of the ethane in absence of nitric oxide. However, while the rate of formation of hydrogen remains sensibly constant (fig. 3), the rate of disappearance of nitric oxide diminishes (fig. 2B), and the concentration of the carbon-nitrogen compound reaches a maximum, and then diminishes, while the rate of formation of the constituents absorbed by bromine tends, ultimately, to accelerate very rapidly, indicating that a third process is developing. This is probably initiated by the interaction of ethane, either with the carbon-nitrogen compound, or with some oxy-compound derived from it, and gives rise to ethylene.

It was not expected that the rate of disappearance of nitric oxide would

bear any simple relationship to the concentration of the nitric oxide, alone or in association with that of the ethane. The following figures confirm this.

TABLE IV

G.mol.-litre × 10^5, min.

Time	0		5		10		15		20
C_2H_6	1000		950		940		920		880
NO	100		78		65		60		57
Δ NO		22		13		5		3	
K bimol.		5·2		3·85		1·7		1·45	
K unimol.		0·0495		0·0365		0·0160		0·0105	

The theory of free radicals offers no explanation of the phenomena which we have described since they would have to be present in sufficient quantity to account for the rapid reaction between nitric oxide and ethane.

The explanation which we put forward to account for the retardation of the primary decomposition of ethane in association with the development of the reaction between ethane and nitric oxide is as follows. It is generally admitted that in certain cases, particularly those in which a unimolecular reaction requiring a high activation energy is proceeding, the Maxwell-Boltzmann energy distribution is not maintained, and the rate of the reaction may fall off owing to the concentration of *hot* molecules falling below the equilibrium concentration. In the case of the primary decomposition of ethane, it is generally agreed that the process is unimolecular with an activation energy of about 75 kcal., so that this might be a case in which this particular condition obtained. The bimolecular reaction between ethane and nitric oxide certainly requires a lower activation energy, and tends, therefore, to depress the concentration of the *hot* ethane molecules capable of taking part in the changes involved in the primary decomposition process.

It appears that the reaction involving the ethane and nitric oxide is itself slowed down owing to the operation of a tertiary process, which involves reaction of ethane with the product of the ethane-nitric oxide reaction. This compound is doubtless complex, and the tertiary change probably proceeds with lower activation energy than either the primary or secondary reaction, and though the latter is bimolecular, the slowing down of it is still due to further disturbance of the energy distribution amongst the ethane molecules. We may represent the three processes by:

(1) $(C_2H_6)'$, $E_1 = 75$ kcal. $\rightarrow C_2H_4 + H_2$,

(2) $(C_2H_6)' + NO$, $E_2 < E_1 \rightarrow (C.H.N.O$ compound$)$,

(3) $(C_2H_6)' + (C.H.N.O$ compound$)$ $E_3 < E_2 \rightarrow C_2H_4 + ?$

One can regard reaction (2) as being substituted for reaction (1), and reaction (3) as being substituted for reactions (1) and (2).

SUMMARY

The thermal decomposition of pure ethane, and of a mixture of ethane and nitric oxide have been studied at 590° in silica apparatus by the method of detailed analyses.

The observation of Staveley (1937) that the addition of nitric oxide to ethane reduces the rate of primary decomposition is confirmed. However, it is shown that a rapid reaction takes place between ethane and nitric oxide, without apparent increase in volume; wherefore the reaction could not have been detected by the pressure measurement method which Staveley employed. The product of the ethane-nitric oxide reaction at first increases in concentration in the gas and then diminishes. It has not been isolated.

The ethane-nitric oxide reaction itself slows down after an interval, but as it does so, a reaction which appears to involve ethane and the product of the ethane-nitric oxide reaction develops. One product of this reaction appears to be ethylene.

The theory of free radicals cannot be used to explain the facts now put forward.

It is suggested that the ethane-nitric oxide reaction operating with a lower activation energy than the primary decomposition process, removes *hot* molecules at a rate faster than they can be supplied to maintain the Maxwell-Boltzmann equilibrium. The result is that the former process is to a considerable extent *substituted* for the latter. The ethane-nitric oxide reaction in turn slows down at a rate faster than can be accounted for by the removal of ethane or nitric oxide. This is associated with the operation of a reaction between ethane and a product of the ethane-nitric oxide reaction at an activation energy still lower than the ethane-nitric oxide reaction itself.

REFERENCES

Frey and Smith 1928 *J. Industr. Engng Chem.* p. 948.
Gay and Travers 1937 *Trans. Faraday Soc.* **33**, 756.
Marek and McCluer 1931 *J. Industr. Engng Chem.* p. 878.
Staveley 1937 *Proc. Roy. Soc.* A, **162**, 568.
Travers 1937a *Trans. Faraday Soc.* **33**, 735.
— 1937b *Trans. Faraday Soc.* **33**, 1342.
Travers and Pearce 1934 *J. Soc. Chem. Ind.* p. 321 T.

A high-temperature Debye-Scherrer camera, and its application to the study of the lattice spacing of silver

By William Hume-Rothery, F.R.S., and Peter William Reynolds

Introduction

A Debye-Scherrer camera capable of giving accurate results at high temperatures is of great value in metallurgical research work. In Part I of the present paper a camera is described which has been designed primarily for accurate measurements of lattice spacings at temperatures up to 1000° C. In Part II results are given for the lattice spacing of silver at temperatures up to 943° C., and an equation is described which gives the coefficient of expansion of silver from the absolute zero to the melting-point.

PART I

In a previous publication (Hume-Rothery and Reynolds 1937) the authors have described the precautions which are necessary if the composition of annealed filings is to be determined accurately, and in high-temperature work these difficulties are accentuated. At 1000° C. most metals are volatile to some extent in a vacuum, whilst many are appreciably volatile at atmospheric pressure. For precision work on alloys it is there-fore usually undesirable to use any type of camera in which a small quantity of filings is heated in a relatively large space, particularly if the design is such that distillation from a hot to a cold region can occur. In the present camera these difficulties are avoided by enclosing the filings in a very thin-walled silica capillary tube which may be sealed off in a vacuum, or with an inert gas at a suitable pressure. The preparation and handling of these thin tubes requires special methods which are described on p. 29.

The camera

Figs. 1 and 2 show the construction of the camera which is essentially of the type developed by Bradley and Jay (1932) with the addition of a central heating chamber. The camera was machined from castings of

Admiralty bronze, and apart from the detachable cover C consists principally of three members, the upper and lower disks and the connecting central ring, which are securely dowelled and screwed together. The central ring member is formed of two rings AA', machined in one piece with the connecting V-block V, which contains the internal collimating system formed by two tubes M, M_1 of 2 mm. internal diameter inserted tightly into the 3 mm. diameter hole in the V-block. The water channel DP in the upper disk is interrupted by a plate inserted at P, and the inlet and outlet water tubes pass from each side of this plate, down through the V-block to connexions underneath the camera. The lower water channel D_1 is closed by similar plates on each side of the V-block, and the inlet and outlet tubes from this system also pass to connexions below the camera.

The film, covered with black paper, is located by means of the stud B, a small hole being punched in the film for this purpose. The film is held in close contact with the surfaces by means of rubber bands X, and the ends of the film are slipped under the retaining shield P' which ensures intimate contact between the film and the shadow knife edges. In order to protect the film from heat and light radiation from the furnaces, the width of the exposed portion is reduced to 5 mm., and a screening cylinder of thick black paper inserted as shown at E with its ends running into vertical slots in the V-block to prevent possible fogging near the knife edges. For temperatures below 600° C. this screen is sufficient, but at higher temperatures it is necessary to use a second screen of aluminium foil 0·0075 mm. thick inserted as shown at Al, and provided with holes for the entrance and exit of the X-ray beam. This very thin screen does not affect the intensities appreciably, but completely protects the film from damage by heat, and greatly improves the constancy of the temperature in the furnaces (see p. 28). The camera is supported by insulated pins on a levelling stand which carries the external slit system consisting of a $\frac{1}{2}$ mm. vertical slit.

Furnace design and temperature measurement

The temperatures are measured by means of the specially designed thermocouple shown in fig. 1. This consists of a 3 mm. diameter platinum ring welded to 32 s.w.g. platinum and platinum 13 % rhodium wires passing down through quartz insulation in the sindanyo stem K to the cold junctions in ice. The sindanyo support is held by spring clips to the brass holder H, which slides freely in its housing, and thus permits the
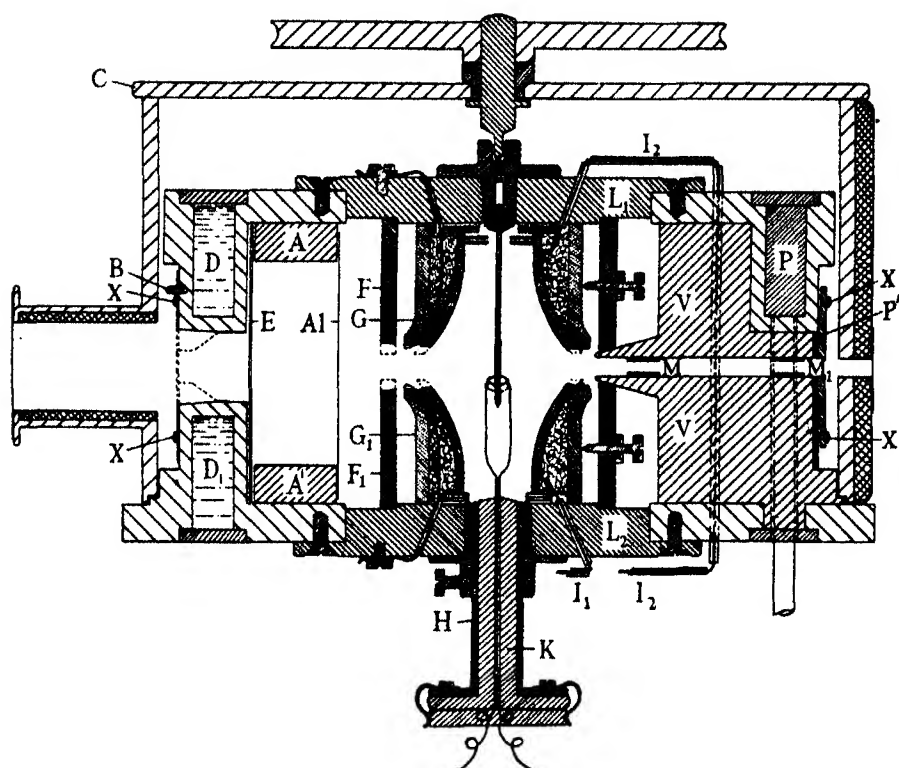
Fig. 1. Vertical section through the camera in the line of the X-ray beam.
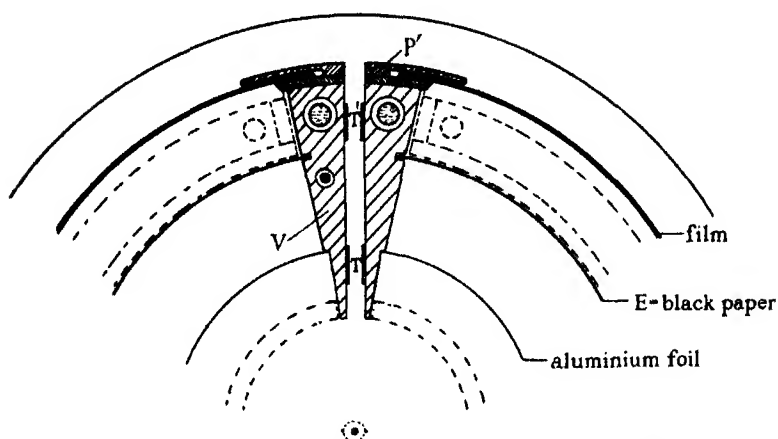
Fig. 2. Horizontal section showing the construction of the V-block and knife edges.

temperature variation in the furnace gap to be measured; for convenience marks are made on the stem to indicate known positions of the thermocouple.

The furnace members L_1, L_2 are detachable, and may be removed without affecting the standard angle of the camera. It is essential to avoid any marked fluctuation of temperature across the gap between the two furnace members, and for this purpose bell-shaped furnaces of the type shown in fig. 1 are by far the most satisfactory. The heating elements consist of No. 26 s.w.g. Brightray wire closely wound on silica formers of the type shown, and held in place by a thin layer of alundum cement. The furnaces are fixed in the outer quartz tubes G, G_1 by tightly packed lagging, and the whole is centred and secured by three screws in each of the brass guard rings F, F_1 which minimize the heating of the camera. The electrical circuit is made through the camera body, and the two insulated leads I_1, I_2 passing to insulated terminals on the camera base. The furnaces may be run in series or in parallel, and the best results were obtained by the series arrangement with an adjustable high resistance in parallel with the otherwise hotter furnace. In an experiment the temperature is measured at the mouth of each furnace by moving the thermocouple to the appropriate position, and the high resistance is then adjusted so that the two temperatures are equal. The thermocouple is then moved to the centre of the furnace gap, and the fall in temperature noted, giving the so-called "centre-point drop". For bell-shaped furnaces with a 3 mm. gap, the maximum centre-point drop was only 2·7° C., and this was reduced to 0·7° C. by the insertion of the cylindrical aluminium screen.

The temperature of the specimen was assumed to be that of the thermocouple junction when the ring was in the middle of the furnace gap, and in view of the thinness of the thermocouple wires it is improbable that the temperatures of the specimen and thermocouple differed by more than 1° C. During the X-ray exposure, the thermocouple was withdrawn to the edge of the furnace gap, out of the X-ray beam, and the temperature was controlled to within ±0·5° C. by hand adjustment of resistances. The mean temperature recorded during the exposure was determined, and when corrected for the centre-point drop gave the mean temperature of the specimen.

The thermocouple was calibrated against a standard platinum-platinum rhodium thermocouple. For this purpose the two thermocouples were placed in adjacent holes in a solid cylinder of copper which was heated electrically by a nichrome winding, and thoroughly lagged in asbestos. The standard thermocouple was calibrated against the melting-points of silver (960·5),

silver-copper eutectic (778·8), aluminium (659), zinc (419), lead (327), and tin (232).

Preparation and mounting of the specimen

The filings for the specimen are contained in a short sealed capillary tube of silica, the wall thickness being from 0·007 to 0·02 mm. These capillaries are best prepared by blowing a small bulb in a clear quartz tube, heating the bulb to the softening point in an oxy-coal-gas flame, and rapidly extending the tube under slight internal air pressure. Using copper $K\alpha$ radiation for the study of copper and silver alloys, it was found that capillaries with a wall thickness of 0·01 mm. produce only a very slight background on the film. The mounting of the specimen is shown in fig. 1. The capillary is first sealed to a thin silica rod, which serves as a convenient handle for subsequent operations and for holding it in the camera. The filings are then introduced to a depth of about 5 mm., after which a short silica plug is introduced. This plug enables the filings to be pressed into a compact specimen, and also prevents the existence of any considerable empty space in the specimen tube, so that volatilization errors on subsequent heating are reduced to a minimum. The silica capillary is connected by a wax joint to a vacuum pump or gas system, and is sealed off by fusing the wall of the capillary to the top of the plug. Specimens of this type can safely be quenched in water.

For insertion in the camera the specimen tube is pushed into the hole drilled in the rotating holder, and a small amount of plasticine placed round the rod, which secures it in position and enables it to be accurately centred by gentle manipulation from outside the camera. The rotating holder has a wide bearing flange to provide heat transfer to the cooled camera body, and is lubricated by vaseline or Apiezon "L" grease according to the operating temperature.

20° C.

846° C.
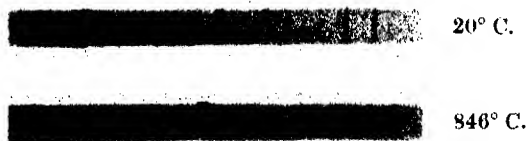
Fig. 3. Debye-Scherrer films for silver using copper $K\alpha$ radiation.
The outermost line is (511).

The camera as described above has given satisfactory results with silver up to 943° C., and with copper alloys at temperatures up to 700° C. Fig. 3 shows the critical ends of films for silver at room temperature and at

846° C. respectively using copper $K\alpha$ radiation. At 943° C. the general scattering was relatively much more intense, but no difficulty was found in measuring the positions of the lines. For lattice-spacing work the best results are obtained by slight or considerable over exposure, followed by development, and later reduction with a reducing agent such as "Farmer's solution", which increases the contrast. Previous experiments, using Bradley and Jay's (1932) $\cos^2\theta$ extrapolation method, have shown that the results are unaffected by the reduction process.*

PART II

The lattice spacing of pure silver

The lattice spacing of silver has been measured at temperatures up to 600° C. by Owen and Yates (1934) whose maximum temperature error above 500° C. was $\pm 10°$ C., the accuracy being subsequently increased. Measurements of the thermal expansion of bars of silver at temperatures up to 500° C. have been made by Scheel (1921). Accurate data at higher temperatures† do not seem to be available, and in the present work we have succeeded in carrying the measurements up to 943° C.

The silver used in the present work was chemically pure assay silver supplied by Messrs Johnson, Matthey and Co., Ltd. Clean filings were prepared by the methods previously described (Hume-Rothery and Reynolds 1937), and were sieved through 250-mesh copper gauze. After sealing in the evacuated specimen tube, the filings were annealed, and a Debye-Scherrer photograph was taken at 19·6° C. using copper radiation, with a nickel screen to eliminate the β lines, the screen forming the window of the Metropolitan Vickers Demountable X-Ray Tube. This photograph was used to calibrate the camera, the value of the lattice spacing of silver being assumed to be 4·07750 A at 19·6°C. Previous experiments by different workers (see Hume-Rothery, Lewin and Reynolds 1936) have established this value to within 0·0001 A and as it was clearly desirable to standardize the camera with a specimen contained in a silica capillary, it appeared better to use silver than quartz for the calibration, since the silver gives much stronger diffraction lines.

---

* Where accurate intensity measurements are required a comparison scale must be photographed on the same film, and developed and reduced under identical conditions.

† Jay (1933) has also published Debye-Scherrer photographs of silver at temperatures up to about 620° C. In this work the temperatures were not measured, and the lattice spacings deduced from the films were used to calibrate the temperature of the camera in terms of the electrical power input to the furnaces.

After being used to calibrate the camera, the specimen was taken through the series of ten experiments, the results of which are summarized in Table I. In this series, Debye-Scherrer photographs were taken at six temperatures up to 943° C., whilst after every one or two high-temperature photographs, a photograph was taken at room temperature to ensure that no change in the specimen had taken place during the high temperature treatment.* At the end of the series, the value of the lattice spacing was

TABLE I

Serial no. of experiment	Temperature ° C.	Lattice spacing in A	Lattice spacing calculated from equation (1)	Lattice spacing calculated by Scheel's equation	Remarks
10	+ 943	4·1656	4·1654	—	
8	+ 846	4·1542	4·1543	—	
2	+ 724	4·1407	4·1411	—	
4	+ 596	4·1278	4·1280	—	
5	+ 459	4·1149	4·1148	4·1148	
7	+ 337·5	4·1040	4·1038	4·1040	
1	+ 19·6	4·0775(0)	4·0774	4·0775	Value assumed for calibration of camera and for calculation by Scheel's equation, and Keesom and Jansen's tables.
3	+ 19·9	4·0774(5)	—	—	Check at room temperature after heating to 724° C. in Exp. 2.
6	+ 20·1	4·0775(7)	—	—	Check at room temperature after the specimen had been used in Exps. 1–5.
9	+ 20·1	4·0773(8)	—	—	Check at room temperature after the specimen had been used in Exps. 1–8.
11	+ 20·0	4·0774(3)	—	—	Final check after Exps. 1–10.
	− 100	4·0687(7)	4·0686	—	The experimental values here are calculated from the tables given by Keesom and Jansen as expressing their results from + 100 to − 253° C.
	− 180	4·0635(6)	4·0635	—	
	− 253	4·0606	4·0606	—	

determined as 4·0774(3) A at 20° C., which is equivalent to 4·0774(1) A at 19·6° C. as compared with the value of 4·0775(0) A assumed for the calibration, so that the change is of the order 0·00009 A, which is within the experimental error. In the five photographs at room temperature the maximum spread of the results (after correcting to a constant temperature) is equivalent to 0·00019 A. As regards reproducibility therefore, the results are probably accurate to within 0·0001 A, and certainly to within 0·0002 A.

The films were measured by eye on a travelling microscope specially calibrated at the National Physical Laboratory. The lattice spacings were

---

* This precaution is often essential, since if accidental oxidation occurs in the preparation of the filings (e.g. if too vigorous filing warms the particles) considerable changes may occur on annealing.

determined from the 511, 422 and 024 reflexions using the Bradley and Jay (1932) $\cos^2 \theta$ extrapolation method. These reflexions give rise to strong well-resolved doublets, the Bragg angle for the 511 line being approximately 78–79° at room temperature. As in the work of Bradley and Jay (1932) the results from the α_1 and α_2 components of the doublets* were averaged in the ratio $2\alpha_1 : 1\alpha_2$. It is thought that even at the highest temperatures the results, so far as X-ray technique is concerned, are accurate to 0·0002 A.

In the course of the development of the camera a number of additional results were obtained of differing degrees of accuracy varying from 0·0001 to 0·0005 A. These confirm the results shown in Table I, but the latter alone are published since they are the most accurate.

DISCUSSION

In Table I columns 2 and 3 give the results of the present investigation, whilst column 5 gives the values calculated for the same temperatures by means of the equation of Scheel deduced for the expansion of massive bars in the range 0–500° C. It will be seen that up to 500° C. the two sets of values agree to within 0·0001 A, so that the coefficients of expansion of the lattice and of the massive bars are identical in this range. Above 500° C. the expansion is greater than that obtained from Scheel's equation, but unfortunately accurate data on massive bars do not appear to exist for the higher temperatures.

The exact agreement of the coefficient of expansion of the lattice and the solid metal in the range 0–500° C. suggests that at low temperatures the two coefficients will also be identical. If this assumption is accepted, the data of Keesom and Jansen (1928) for the expansion of bars of silver in the range −253 to +101° C. may be used to calculate the lattice spacing of silver at low temperatures, and some results obtained in this way are included in the lower half of Table I which thus gives the lattice spacing of silver from 20° above the absolute zero to 18° below the melting-point.

It is naturally of interest to see whether the experimental data can be expressed in the form of a simple equation, since the usual empirical relations are very complicated. We have succeeded in expressing the data in the form of an equation which gives the coefficient of expansion over the

---

* The usual tendency is to measure the lines of the doublet too close together owing to an optical illusion. Experience shows that the Bradley and Jay extrapolation method, with the $2\alpha_1 : 1\alpha_2$ averaging, overcomes this source of error almost entirely. Actually in the present work it was only above 800° C. that the α_1 and α_2 values from the 511 line differed by more than 0·0001 A from the extrapolation curve.

whole range of temperature in terms of only four constants, whilst above
0° C. one term in the equation becomes negligibly small, and the coefficient
of expansion in the range 0–943° C. involves two constants only. This
equation is of the form

$$\log \frac{a}{a_0} = \frac{c\theta}{\theta_0 - \theta} + xe^{-y''},$$ (1)

where the constants have the following values when ordinary logarithms
to the base 10 are used:

$$a_0 = 0.608079, \qquad\qquad x = 0.0004898,$$
$$C = 4.1614 \times 10^{-2}, \qquad\qquad y = 1.5208 \times 10^{-2}.$$
$$\theta_0 = 5586.6,$$

These constants have values such that $da/d\theta = 0$ when $\theta = 0$, so that the
theoretical condition that the coefficient of expansion is zero at the absolute
zero of temperature is satisfied. The second term in this equation is less
than 0.0001 A at temperatures above 273° abs., and the high-temperature
results are thus expressed in the very simple form

$$\log \frac{a}{a_0} = \frac{c\theta}{\theta_0 - \theta}.$$ (2)

The values calculated by equation (1) are given in column 4 of Table I,
and it will be seen that the agreement between the calculated and experi-
mental values is very satisfactory. We have also found that the high-
temperature data for the expansion of zinc and quartz can be expressed
in the form of equation (2), which is very convenient for calculation, since
only one term involving θ is present.

Mr F. J. March for his great skill in making the camera, and for much useful assistance.

REFERENCES

Bradley, A. J. and Jay, A. H. 1932 *Proc. Phys. Soc.* **44**, 563.
Hume-Rothery, W., Lewin, G. F. and Reynolds, P. W. 1936 *Proc. Roy. Soc.* A, **157**, 167.
Hume-Rothery, W. and Reynolds, P. W. 1937 *J. Inst. Metals*, **60**, 303.
Jay, A. H. 1933 *Proc. Phys. Soc.* **45**, 635.
Keesom, W. H. and Jansen, A. F. J. 1928 *Commun. Phys. Lab. Univ. Leiden*, No. 185 C.
Owen, E. A. and Yates, E. L. 1934 *Phil. Mag.* (vii), **17**, 113.
Scheel, K. 1921 *Z. Phys.* **5**, 167.

Resolution and interpretation of the luminescent spectra of some solids at low temperatures

By J. Ewles, M.A.

Physical Laboratories, The University of Leeds

[Plates 3, 4]

1. INTRODUCTION

Luminescent inorganic solids may be divided into a number of classes. Some, like the uranyl salts and rare earth salts, show luminescence in the pure state, and some, like the Lenard and Klatt sulphides, seem to require a small trace of impurity. The alkali halides, which may be rendered luminescent by prolonged heating in the vapour of the alkali metal, by electrolysis, or by exposure to short waves, may possibly be regarded as belonging to the second class, since it is generally recognized that the luminescence is connected with the presence of neutral atoms which must be considered as impurities in the ionic lattice. The chromium-activated substances studied so extensively by Deutschbein (1932) appear to belong to a third class.

The intimate relations which have been found between the line-like emission and absorption spectra of the first class suggests that their luminescence may be quite simply explained as a kind of resonance phenomenon. Indeed, in the case of the rare earths the spectra appear to have been satis-

factorily interpreted in terms of electronic transitions of the metallic ion. But, in spite of the very large amount of work on the second class of luminescent substances, a satisfactory explanation of their luminescence is still lacking. This is chiefly due to the fact that their spectra generally consist of broad and featureless bands. Various workers have claimed to have resolved these very broad bands into a number of partial bands, and Schmidt (1932) and Schellenberg (1932) have attempted to establish general series relationships among the partial band maxima. The resolution, however, has been obtained partly by visual observations and partly by reconstruction of the broad bands from a number of assumed partial bands. Howes (1928) obtained by visual spectrophotometry distinct structure in the bands of some of the alkali earth sulphides. His results will be referred to later in this paper. Tanaka (1921) carried out an extensive series of observations on the cathodo-luminescence of a large number of substances activated by various impurities and deduced the existence of a frequency interval characteristic of the activator. But as many of his numbers are the result of rearranging the slight fluctuations which appear on the visually observed spectrophotometric curves, the validity of his deductions is very doubtful.

In the case of the alkali halides Perrine (1928), Northrop (1928), Hilsch and Pohl (1933) and Roos (1934) have each obtained spectra consisting of a number of quite narrow bands. Von Hippel (1936) has given an ingenious explanation of the absorption spectra of these substances in terms of the energy changes involved in the transfer of an electron from a halogen ion to an alkali ion. His explanation of the phosphorescent spectra, however, is hardly quantitative.

It therefore appeared desirable to make a further attempt to obtain resolution of the luminescent spectra of the second class of luminescent solids. It is the object of this paper to report that certain bands of this type have been resolved and the frequencies of the components determined with a precision which enables suggestions to be made as to the origin of the luminescence. These conclusions are then shown to apply to the results of other workers, and a suggestion is made as to a possible explanation of some cases of phosphorescence.

2. CATHODO-LUMINESCENCE OF CALCIUM OXIDE.
EXPERIMENTAL ARRANGEMENTS AND RESULTS

In order to reduce the problem to its simplest terms it was decided to begin with a substance of simple structure, and for the same reason no flux was used in the preparation. A start was made with calcium oxide, since

this could be obtained in a very pure state (Hilger Specpure), has a simple crystal structure (rock salt) and can easily be rendered luminescent by intimate mixture with a trace of impurity and subsequent heating. The mode of excitation was by cathode-rays generated under a tension of about 20,000 V from a Mercedes electrostatic machine. This mode was adopted for a number of reasons. In the first place it is far more efficient than any other means, and in the second place excitation by light has the disadvantage that unless the luminescence is extremely bright the luminescent spectrum tends to be confused by the strongly scattered exciting lines. Schellenberg (1928, 1932) attempted to get over the latter difficulty by the use of a phosphoroscope, but this has the disadvantage of eliminating all emission of a vanishingly short life. The possible objection that the excitation by cathode-rays involves a special process which would not operate under optical excitation is met by the fact that the cathodo- and photo-luminescent spectra of a given substance are, as far as they have been investigated, identical except as regards relative intensity of the different bands. This point, moreover, has been tested and confirmed by the writer in the case of two samples of calcium oxide and with zinc sulphide (§ 4). The final form of the apparatus is shown in fig. 1.

The sample in the form of a powder was deposited in a very thin layer in the depression in the rustless steel plug, P, which was hard soldered into the end of the hollow brass tube, T. The latter was flanged so as to give a vacuum-tight joint against the flanged end of the side tube, S, of the main discharge vessel, V. C is the cathode, while T itself serves also as the anode. The light from the specimen was led out by a quartz rod, Q, to the slit of a Hilger quartz spectrograph. Liquid air could be poured into T and the temperature watched by means of a thermocouple pushed into T and touching the back of the sample holder, P. The spectrograms were photometered on a Cambridge recording photoelectric photometer. A mercury spectrum was superimposed for calibration purposes.

Experiments were carried out with fourteen different samples of calcium oxide; one spectroscopically pure and the rest containing each a trace of an added metal.

It was found at first that although the spectra could be resolved into separate bands, these could not be further resolved with any certainty in the photometer curves. When, however, the exciting cathode-ray current was cut down to a fraction of a microampere by running the machine very slowly or by putting a spark gap in parallel with the tube, the most remarkable resolution of the ultra-violet bands into almost line like components could be obtained (figs. 3, 4, Pl. 3; fig. 5, Pl. 4). The results are given below.
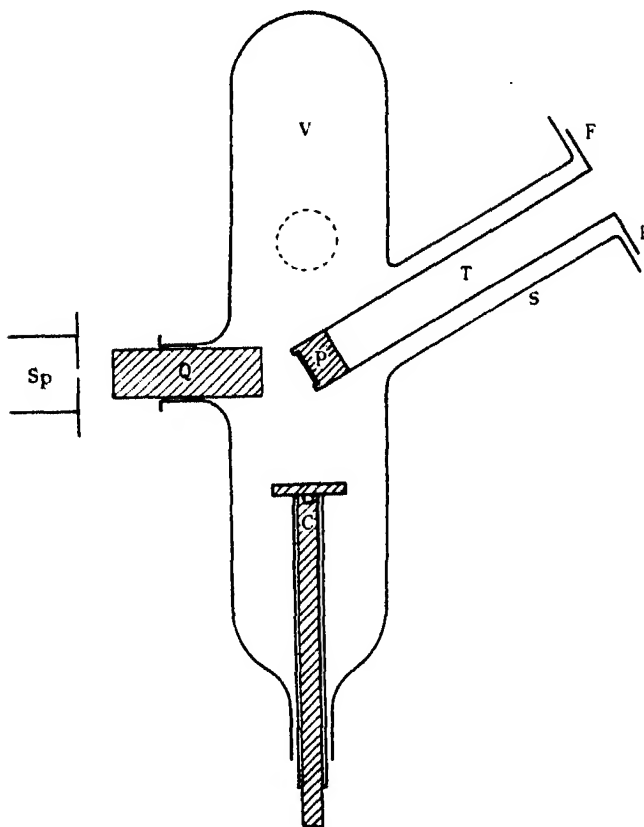
Fɪɢ. 1

CaO. *Hilger Specpure*

Ultra-violet

	ν (air) in cm.$^{-1}$	λ (air) in A	Description
A	28706	3483	Group of broadened lines
B	28203	3546	
C	27988	3572	
F	27397	3650	Group of broadened lines of alternating intensities
G	27155	3682	
F_1	26889	3719	
G_1	26654	3751	F lines stronger than following G lines. Strongest = F
F_2	26396	3788	

Visible

There is a very faint luminescence in the visible which is too weak to be photographed in a reasonable time.

CaO (Bi). *Atomic concentration* Bi/Ca $= 10^{-4}$

Ultra-violet

Designation	ν (air) cm.$^{-1}$	λ (air) in A	Description
A	28716	3479 ⎫	Group of broadened lines on
B	28206	3545 ⎬	partially resolved band
C	28000	3571 ⎭	
F	27404	3650 ⎫	
G	27166	3681 ⎪	Group of broadened lines of
F_1	26891	3718 ⎪	alternating intensities
G_1	26647	3752 ⎬	F lines stronger than following
F_2	26385	3790 ⎪	G lines
G_2	26142	3825 ⎪	F = strongest
F_3	25886	3863 ⎭	
H	26322	3799 ⎫	Faint broadened lines
H_1	25848	3868 ⎭	
L	26023	3843 ⎫	
K	25719	3888 ⎪	Group of broadened lines of
L_1	25525	3918 ⎪	alternating intensities
K_1	25231	3963 ⎪	K lines stronger than following
L_2	25017	3997 ⎬	L lines
K_2	24732	4044 ⎪	K = sharpest
L_3	24521	4079 ⎪	K and K_1 of approximately
K_3	24245	4124 ⎪	equal intensity
K_4	23758	4209 ⎭	
D	24322	4112	Faint broad line

Visible

Only one band was strong enough to be measured. This is broad with the peak at 6200.

CaO. *Activated with various impurities*

(Sn, Sb, Zn, Mn, Pb, Co, As, Ni, W, Cu, Cd, Fe)

Ultra-violet

All samples gave broadened lines whose position agree within experimental errors with those of A, B, C, F, G, F_1, G_1, F_2, G_2, ... above.

Visible

Very broad and unresolved bands were obtained in the visible region. The values given below are those of the peaks of the photometer curves. These curves are generally symmetrical and it is probable that the values given for the peak wave-lengths are not in error by more than about 20 A.

CaO. *Various impurities*

Impurity		Bands. Wave-lengths of peaks in A		
Sn		4650	—	6200
Sb		4700	5570	—
Zn		4660	—	6200
Mn		4650	5560	6210
Pb		4730	—	6180
Co	4460	—	—	6180
As		4650	—	6180
Ni		4650	—	6150
W		4710	—	6150
Cu				
Cd			Visible luminescence very faint	
Fe				

3. DISCUSSION OF ABOVE RESULTS

The ultra-violet region appears to be divided into a number of groups of broadened lines each suggesting a band group. It has been pointed out to me by Professor A. C. Menzies of University College, Southampton, that the F, G and H, K, L groups may be numerically represented by electron vibration band-head formulae of the type

$$\nu = \nu_e + (v' + \tfrac{1}{2})\,\omega' - (v'' + \tfrac{1}{2})\,\omega'',$$

leaving out the anharmonic terms, since the possible accuracy of measurement due to the broadness of the lines does not justify their inclusion. The formal comparison between the lines so calculated from an appropriate choice of ν_e, ω' and ω'' and those observed in the CaO (Bi) spectrum is given below.

In both systems the strong lines (i.e. F lines and K lines respectively) are those with $v' = 0$, while the fainter lines (G, L and H lines) correspond to $v' = 1$ or 2.

This formal representation still leaves open the question as to the origin of the electronic jumps. A number of possibilities have been considered. Taking first the F, G group, which appears in all the CaO spectra including that of the Hilger spectroscopically pure sample, there can be little doubt that this group is *not* due to an impurity. The most obvious suggestion is that it is an electron vibration band of the crystalline oxide. Mahanti (1932) has obtained bands with calcium salts in the carbon arc which he attributes to CaO molecules but, although it is possible to find in his bands a correspondence to every line found here, his electronic jump (28849) and vibrational frequencies ($\omega' = 726\cdot5$, $\omega'' = 811\cdot3$) are very different. Moreover, as

will be seen later in this paper, nothing corresponding to Mahanti's bands for SrO and MgO has been found in the cathodo-luminescent spectra of these substances. Nor does it appear possible to attribute the electron jump to Ca III, Ca II, or to oxygen.

F, G group

$$\nu = 27526 + (v' + \tfrac{1}{2})\,264 - (v'' + \tfrac{1}{2})\,508 \text{ cm.}^{-1}$$

Designation	Obs.	Calc.	v', v''
F	27404	27404	0, 0
G	27166	27160	1, 1
F_1	26891	26896	0, 1
G_1	26647	26652	1, 2
F_2	26385	26388	0, 2
G_2	26142	26144	1, 3
F_3	25886	25880	0, 3

H, K, L group

$$\nu = 25816 + (v' + \tfrac{1}{2})\,298 - (v'' + \tfrac{1}{2})\,493 \text{ cm.}^{-1}$$

Designation	Obs.	Calc.	v', v''
H	26322	26314	2, 0
H_1	25848	25821	2, 1
L	26023	26016	1, 0
K	25719	25718	0, 0
L_1	25525	25523	1, 1
K_1	25231	25225	0, 1
L_2	25017	25030	1, 2
K_2	24732	24732	0, 2
L_3	24521	24537	1, 3
K_3	24245	24239	0, 3
K_4	23758	23746	0, 4

Ca I, however, has a line just in the required region (27526 cm.$^{-1}$), namely,

$$4s4p\,{}^3P^\circ - 4s5d\,{}^3D = 27586 \text{ to } 27419 \text{ cm.}^{-1}.$$

The maximum vibration frequency of the CaO lattice has been given by Tolksdorf (1928) as 453 cm.$^{-1}$. It seems therefore not unreasonable to suppose that the frequency difference of 508 cm.$^{-1}$ appearing in this group is that of the CaO lattice.

Since the H, K, L group appears only when Bi is present it would seem natural to attribute this to some association of Bi or one of its oxides with the CaO crystal. But with an atomic concentration Bi/Ca of only 10^{-6} this group appears with an intensity as great as that of the F, G group and when the atomic concentration of Bi/Ca is still only as small as 10^{-4} the intensity

of the H, K, L group is actually greater. It does not appear in the spectra of the similar oxides SrO and BaO or in any other oxide investigated when Bi is incorporated in them. These facts, together with the recurrence of the frequency difference close to 500 cm.$^{-1}$, suggests that here again the CaO crystal plays the predominant part in the emission of H, K group. Although Mahanti's bands for CaO molecules again have components which correspond to every one of this group there is no correspondence of the electronic jump or vibration frequencies. No bismuth oxide bands appear to have been reported in this region though it is remarkable that the $A \to X$ BiO bands in the red found by Ghosh (1932) have the same vibrational frequencies of 493 and 298 cm.$^{-1}$ in the lower and upper states. There is, however, a close agreement between the electronic jump of this group (25816) and the $4s3d\,^3D\text{--}4s6f\,^3F°$ ($\nu = 25829$ to 25793) of Ca I. Moreover, the next Ca I transition in this series $4s3d\,^3D\text{--}4s5f\,^3F°$ ($\nu = 24426$ to 24392) would account for the line D ($\nu = 24322$) which appears along with the H, K, L group only when Bi is present.

The region of the spectra to the short-wave side of 3650 A appears to consist of a number of broadened lines on an otherwise unresolved background ending sharply with the broad line A at 3479 A. Only three of these lines can be determined with any certainty.

Although these coincide approximately with Ca I lines

$$A \quad 3479 \quad \text{Ca I} \quad 4s3d\,^3D\text{--}4smf\,^3F° = 3452 \text{ to } 3456$$
$$\underset{m\to\infty}{}$$

$$B \quad 3545 \quad \text{Ca I} \quad 4s3d\,^3D\text{--}4smf\,^3F° = 3552 \text{ to } 3533$$
$$\underset{m=12,\,13}{}$$

$$C \quad 3571 \quad \text{Ca I} \quad 4s3d\,^3D\text{--}4smf\,^3F° = 3565 \text{ to } 3595$$
$$\underset{m=11,\,10}{}$$

such interpretations do not appear probable since in such a case one would expect the lines 3871 to 3876 to appear strongly in all the spectra ($4s3d\,^3D\text{--}4s6f\,^3F°$). Actually only in the Bi activated sample does the line $K = 3888$ A appear in this region.

It is observed that the frequency difference of $A - B$ is again about 500 cm.$^{-1}$.

It is obviously not possible to draw any definite conclusions as to the origin of the broad unresolved bands in the visible. It is notable, however, that within the possibility of the measurements these bands are not characteristic of the particular impurity but are common to many different ones. The effect of the "activators" appears to be merely to determine the relative intensities of a set of bands whose positions are determined by the calcium oxide itself.

Similar results have been noted by other observers (e.g. Schellenberg 1928, 1932). The positions of the peaks of these bands are, at any rate, not inconsistent with the possibility that their emission is associated with Ca I transitions. Thus

Observed band A	Ca I transitions (A)
4460	$4s4p\ ^3P^o$–$4s4d\ ^3D$ = 4426 to 4456
4650–4730	$4s3d\ ^3D$–$4s4f\ ^3F^o$ = 4579 to 4585
5560–5570	$4s3d\ ^3D$–$3d4p\ ^3D^o$ = 5591 to 5607
6100–6200	$4s4p\ ^3P^o$–$4s5s\ ^3S$ = 6104 to 6165
	$4s3d\ ^3D$–$4s5p\ ^3P^o$ = 6173 to 6159

4. PHOTO-LUMINESCENCE OF CALCIUM OXIDE

A possible objection to the bearing of the above results on the general phenomenon of luminescence is that under excitation by fast electrons some process might be involved (such as local dissociation of the CaO by the temporarily high local concentration of energy) which would not operate under excitation by light. This objection has now been met, since it has been found possible to obtain, with calcium oxide, under excitation by ultra-violet light, similar resolved bands to those obtained under cathode-ray excitation. So far, only two samples have been investigated by ultra-violet light excitation—the Hilger "Specpure" and the bismuth "activated" sample. The specimens were cooled to liquid air temperature and excited by filtered light from a quartz mercury vapour lamp. One of the very efficient filters described by Bowen (1935) was employed to exclude effectively all mercury lines of wave-length longer than 3341·5 A. (There is a slight transmission of the yellow lines.) A comparison of the wave-lengths and frequencies of the resolved components of the luminescent bands, obtained in the ultra-violet by this method, with the corresponding components of the cathodo-luminescent spectra is given below. There is a shift towards the red in the optically excited spectra of 6–17 A in the "Specpure" and 16–20 A in the bismuth activated sample. No explanation can be offered at present for this shift.

In the bismuth activated sample, with atomic concentration Bi/Ca of 10^{-4}, the L lines observed in the cathodo-luminescent spectra are too faint in the optically excited spectra to be measured accurately. The effect of the bismuth of producing a transference of the region of maximum emission from the F, G group to the K group is very striking (see fig. 4, Pl. 3). With an atomic concentration of Bi/Ca of 10^{-4}, and an exposure long enough to bring out the K lines distinctly (about one hour), the F, G group is quite

indetectable; while with an atomic concentration of Bi/Ca of 10^{-6} the two groups are about equally intense. The A, B, C, F, G, F_1, G_1, F_2, G_2, F_3 lines in the latter sample are in the same position, within the limits of measurement, as the corresponding lines in the Specpure sample.

The mean vibration frequencies of the lower state, appearing in the bands of the optically excited spectra, are 511 cm.$^{-1}$ for the F, G group and 489 cm.$^{-1}$ for the K group, which compare closely with the 508 and 493 cm.$^{-1}$ found for the corresponding groups in the cathodo-luminescent spectra.

Comparisons of cathodo-luminescent and photo-luminescent spectra
CaO *"specpure"*

	Cathode-ray excitation		Ultra-violet light excitation	
	λ (A)	ν (cm.$^{-1}$)	λ (A)	ν (cm.$^{-1}$)
A	3483	28706	3491	28651
B	3546	28203	3552	28155
C	3572	27988	3579	27936
F	3650	27397	3660	27323
G	3682	27155	3694	27074
F_1	3719	26889	3732	26784
G_1	3751	26654	3768	26539
F_2	3788	26396	3805	26285
G_2	Too faint to measure		3839	26052
F_3	Too faint to measure		3877	25790

CaO . (Bi). *Atomic concentration* Bi/Ca $= 10^{-6}$

	Cathode-ray excitation		Ultra-violet light excitation	
	λ (A)	ν (cm.$^{-1}$)	λ (A)	ν (cm.$^{-1}$)
K	3888	25719	3904	25612
K_1	3963	25231	3981	25115
K_2	4044	24732	4064	24596
K_3	4124	24245	4142	24145

5. EXPERIMENTAL RESULTS FOR OTHER SUBSTANCES

The suggestions that some luminescent bands of solids "activated" with an impurity are electron vibration bands associated with the parent lattice and that the electron jump may possibly be attributed to neutral atoms of the metal of the crystal obviously require confirmatory evidence from the luminescent spectra of substances other than calcium oxide.

Some results of investigations on the cathodo-luminescent spectra of various substances at the temperature of liquid air, by the same method as described in § 2, will now be given.

Strontium oxide

This shows, in the ultra-violet, a set of four broadened lines which appear to form a band-like group showing an approximately constant frequency difference of about 404 cm.$^{-1}$. These lines are too faint to be measured very accurately (the probable error is about 30 cm.$^{-1}$). The estimated values are:

Wave-length (A)	Frequency (cm.$^{-1}$)	$\partial\nu$
3787	26410	
		410
3845	26000	
		410
3909	25590 .	
		400
3970	25190	

Regarding this as an electron vibration band of the form

$$\nu_c + (v' + \tfrac{1}{2})\,\omega' - (v'' + \tfrac{1}{2})\,404 \text{ cm.}^{-1},$$

it is required to account for an electron jump in the neighbourhood of 26400 cm.$^{-1}$ and a vibration frequency in the lower state of about 404 cm.$^{-1}$. There is no experimental data available for the vibration frequency of the SrO lattice, but Dr M. L. Huggins who has already published calculations (1937) on the alkali halides based on the Born-Mayer Method and giving excellent agreement with experiment in these cases, has very kindly worked out for me the vibration frequency of the alkaline earth oxides. His value for SrO comes out at 438 cm.$^{-1}$, which suggests that the vibration frequency of 404 cm.$^{-1}$ found in the SrO spectrum may not unreasonably be identified with the SrO lattice frequency. The electron jump in the region of 26410 is quite near to the Sr I transitions:

$$5s5p\,^3\text{P}° - 5s8s\,^3\text{S} = 26445,\ 26258.$$

The bands in the visible are again broad and unresolved. Their peaks were estimated to be at 4600, 5600 and 6450 A respectively. Although these bands are too broad to offer any very positive evidence as to the origin of the electronic jump associated with them, the position of the peaks is not inconsistent with the view that they may be derived from Sr I transitions.

Barium compounds

It was found impossible to resolve any bands of barium oxide. The position of the peaks of the bands obtained with barium oxide, sulphide and carbonate are given below, in Angstroms.

Barium oxide	4650	5620	5970
Barium sulphide	4300	5910	
Barium carbonate	4070	5560	5870

The band peaks 5970 for BaO, 5910 for BaS, and 5870 A for $BaCO_3$, and the band peaks 5620 for BaO and 5560 A for barium carbonate are respectively sufficiently close together in each case to suggest common origins for the electronic jumps. There are Ba I lines in the neighbourhood of all the peaks.

Zinc compounds

Zinc oxide. In one sample only (Kahlbaum A.R.) a band-like structure was seen in the ultra-violet. A reproduction of this is shown in No. 8, fig. 5 (Plate 4).

The wave-lengths, frequencies and frequency differences are:

	Wave-length (A)	Frequency (cm.$^{-1}$)	Frequency difference (cm.$^{-1}$)
A	3708	26962	
B	3754	26640	322
C	3837	26064	576
D	3925	25475	589
E	4011	24926	549

The strongest component is B. This suggests a band group of the form

$$\nu = \nu_e + (v' + \tfrac{1}{2})\,322 - (v'' + \tfrac{1}{2})\,571 \text{ cm.}^{-1},$$

where ν_e is in the neighbourhood of 26764. There are no prominent Zn I lines in this neighbourhood. The 322 cm.$^{-1}$ may possibly correspond to Tolksdorf's (1928) $\nu_2 = 357$ cm.$^{-1}$ for ZnO infra-red frequencies, but the 578 cm.$^{-1}$ does not appear to correspond with any of the values given by Tolksdorf for ZnO, although $B - D = 1165$ cm.$^{-1}$ is close to the 1156 cm.$^{-1}$ given as $\nu_1 + 2\nu_2$ and $B - E = 1714$ cm.$^{-1}$ fairly near to the value 1667 cm.$^{-1}$ given as $\nu_1 + 4\nu_2$. On the whole the evidence is against this group being associated directly with the ZnO. As it only appears in one sample it may possibly be a "solution" spectrum of some impurity present only in this sample. There are two broad bands in the visible region—common to a number of samples—with peaks at 5350 and 4700. There are a number of Zn I lines in the neighbourhood of each peak.

Zinc sulphides

In the case of the very brilliant sulphides of which a number of samples were tried from different sources and containing various impurities, it was found that most of the bands were too broad to give reliable values for the peaks to be regarded with any certainty as simple bands. Three bands appear to be symmetrical on the photometer curves and may possibly be regarded

as single bands. Their peaks are at 6590, 5980 and 4800 A. There are Zn I lines reasonably near to all these peaks.

Zinc silicate

A zinc silicate "activated" with copper gave two bands in the visible with peaks at 5350 and 4650. Both of these are quite close to the peak values found for the visible bands of ZnO, again suggesting, as in the case of the barium compounds, a common origin for the electronic jumps. As indicated above there are Zn I lines in the neighbourhood of both peaks.

Magnesium oxide

This substance appears to give spectra belonging to two classes, since besides two broad bands which are alike in samples activated with Mn, Sn and Bi and whose peaks are near to Mg I lines, the Mn activated sample shows a number of broadened lines and very narrow bands which cannot be compared with Mg I lines but all of which are in the neighbourhood of Mn I lines. There does not appear to be any band like arrangement among these lines and bands. The details are given below.

MgO *activated with* Mn *or* Bi *or* Sn

Broad bands with peaks at 4690 and 3860 A.

MgO . Mn

Wave-length (A)	Description
6710	Strong and very narrow band
6435	Weak narrow band
6030	Strong narrow band
4848	Weak broadened line
4806	Weak broadened line
3665	Weak broadened line
3571	Strong broadened line
3588	Weak broadened line

6. RESULTS OF OTHER OBSERVERS

Howes (1928) carried out a study of the luminescent spectra of three alkaline earth sulphides. He obtained by visual spectrophotometry curves showing a number of peaks and inflexions. His estimated values for the positions of these in the case of CaS activated with bismuth are shown below.

CaS (Bi). *Howes* (1928)

Wave-length (A)	Frequency (cm.$^{-1}$)	Frequency difference (cm.$^{-1}$)
5300	18868	
		387
5411	18481	
		391
5528	18090	
		391
5650	17699	
		401
5781	17298	
		378
5910	16920	
		389
6049	16531	
		402
6200	16129	

Howes does not give the photometer curve or a reproduction of the spectrum, but taking his remark that the spectra "yielded a curve upon the red flank of which eight crests could be located" together with the assumption that this set represents a band of the same type as obtained by the present writer for CaO, then the approximately constant frequency difference of mean value 394 cm.$^{-1}$ would be the vibration frequency of the lower state and the component $\nu = 18868$ cm.$^{-1}$, $\lambda = 5300$ A would be the 0, 0 component.

No measurements appear to be recorded for the lattice frequency of CaS. This substance is of course a cubic lattice of the same type as CaO, so that one may extrapolate by the Huggins formula. Taking the Tolksdorf value of 453 cm.$^{-1}$ for CaO, a value of 369 cm.$^{-1}$ is obtained for CaS, or taking the 500 cm.$^{-1}$ obtained by the present writer in the CaO spectrum a value of 405 cm.$^{-1}$ is obtained for CaS. Either of these values is sufficiently near to the frequency difference of mean value 394 cm.$^{-1}$ which appears in the above spectrum to make it reasonable to suppose that this frequency difference again represents the vibration frequency of the CaS lattice.

There are a number of Ca I lines in the neighbourhood of the supposed electronic transitions (18868 cm.$^{-1}$)

$$4s3d\,^3D - 3d4p\,^3P^\circ = 5262 \text{ to } 5270\,A,$$

and $$4s3d\,^1D - 3d4p\,^1F^\circ = 5349\,A,$$

the mean frequency of these transitions being 18946 cm.$^{-1}$.

BaS (Cu). *Howes* (1928)

Howes gives a curve for BaS activated with copper showing a number of peaks and inflexions. Of these all the well marked peaks are near to Ba I lines. There also appears to be constant frequency differences present of 340 and 680 cm.$^{-1}$ respectively. Taking the Tolksdorf value of 453 cm.$^{-1}$ for

the CaO lattice frequency and extrapolating by Huggins method a value of 306 cm.$^{-1}$ is obtained for the BaS lattice frequency, or using the value of 500 cm.$^{-1}$ for the CaO lattice a value of 348 cm.$^{-1}$ is obtained for the BaS lattice frequency.

SrS (Bi). *Howes* (1928)

Here the photometer curve shows one strong peak at 4800 A flanked on each side by a number of somewhat indefinite inflexions, from which Howes deduces constant frequency intervals of 580 and 1160 cm.$^{-1}$. While there are a number of Sr I in the neighbourhood of 3800 A, including the strong lines 4832, 4872 A, the frequency intervals do not appear to be anywhere near the calculated vibration frequency of the SrS lattice (376 cm.$^{-1}$ taking 500 cm.$^{-1}$ for CaO and 341 cm.$^{-1}$ taking 453 cm.$^{-1}$ for CaO).

CaO *and* CaS (*Schellenberg* 1928, 1932)

Schellenberg has analysed the photometric curves obtained by himself and others from the blue and ultra-violet luminescence of CaO and CaS excited by the zinc spark. Although he did not obtain, except in a few cases, resolution into separate bands, he adopted a method of analysis based on the experimentally alleged assumption that the individual bands are of the form of error curves. By an adjustment of constants the experimental curves were built up from individual bands. A collection of his results are given below. It is seen that all the supposed individual bands are in the region of Ca I lines.

It is striking (1) that all the members of the series

$$4s4p \, ^3P^\circ - 4s \, . \, md \, ^3D \quad \text{and} \quad 4s3d \, ^3D - 4s \, . \, mf \, ^3F^\circ,$$

within the range investigated are represented, (2) that many of the bands are not only common to different impurities but are common (within the limits of measurement) to both CaO and CaS—again suggesting a common origin.

CaO *and* CaS (*Schellenberg* 1928, 1932)

Wave-lengths (Schellenberg) (A)

CaO	CaS	Comparison with Ca I lines (A)
	2600 (Ag)	$4s4p \, ^3P^\circ - 3d4d \, ^3P = 2556$ to 2565
2700 (Cu)⎱	2780 (Fe, Zn)	$4s^2 \, ^1S - 4s5p \, ^1P^\circ = 2722$
2720 (Fe)⎰		$4s^2 \, ^1S - 4s5p \, ^3P^\circ = 2735$
3020 (Cu)		$4s4p \, ^3P^\circ - 4smd \, ^3D = 2929$ to 3151
		$m = 8$ to ∞
3260 (Cu)⎱	3220 (Fe) ⎱	$4s4p \, ^3P^\circ - 4s7d \, ^3D = 3210$ to 3226
3250 (Ag)⎰	3200 (Zn, Ag)⎰	
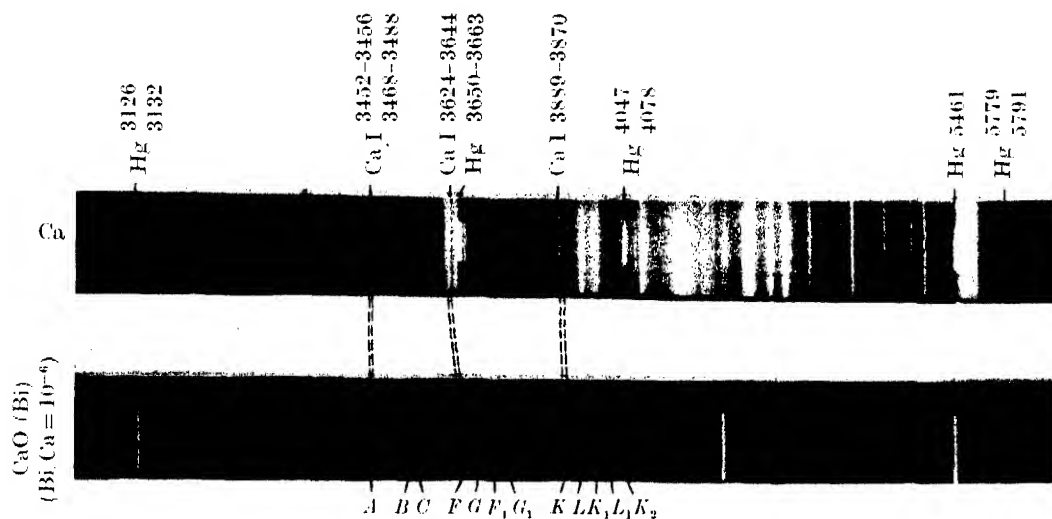
Fig. 3
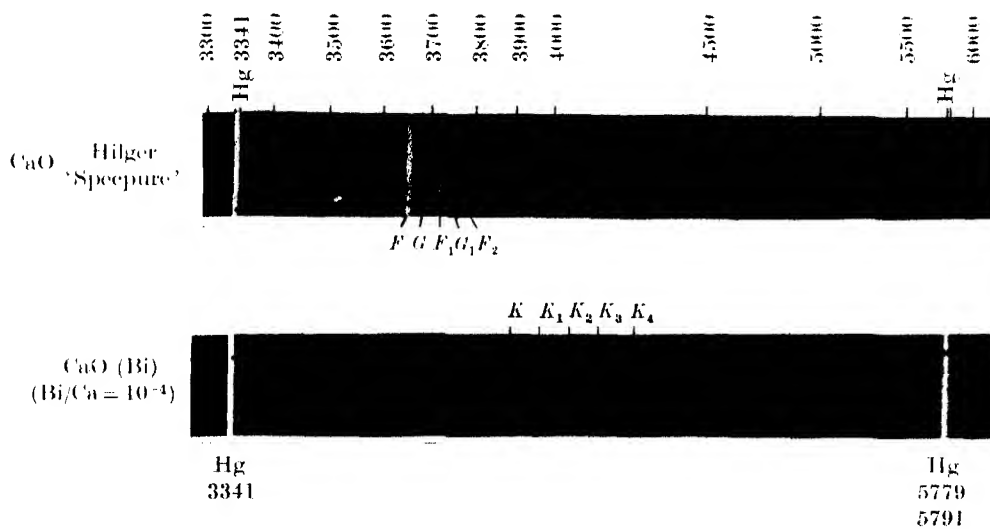
Fig. 4
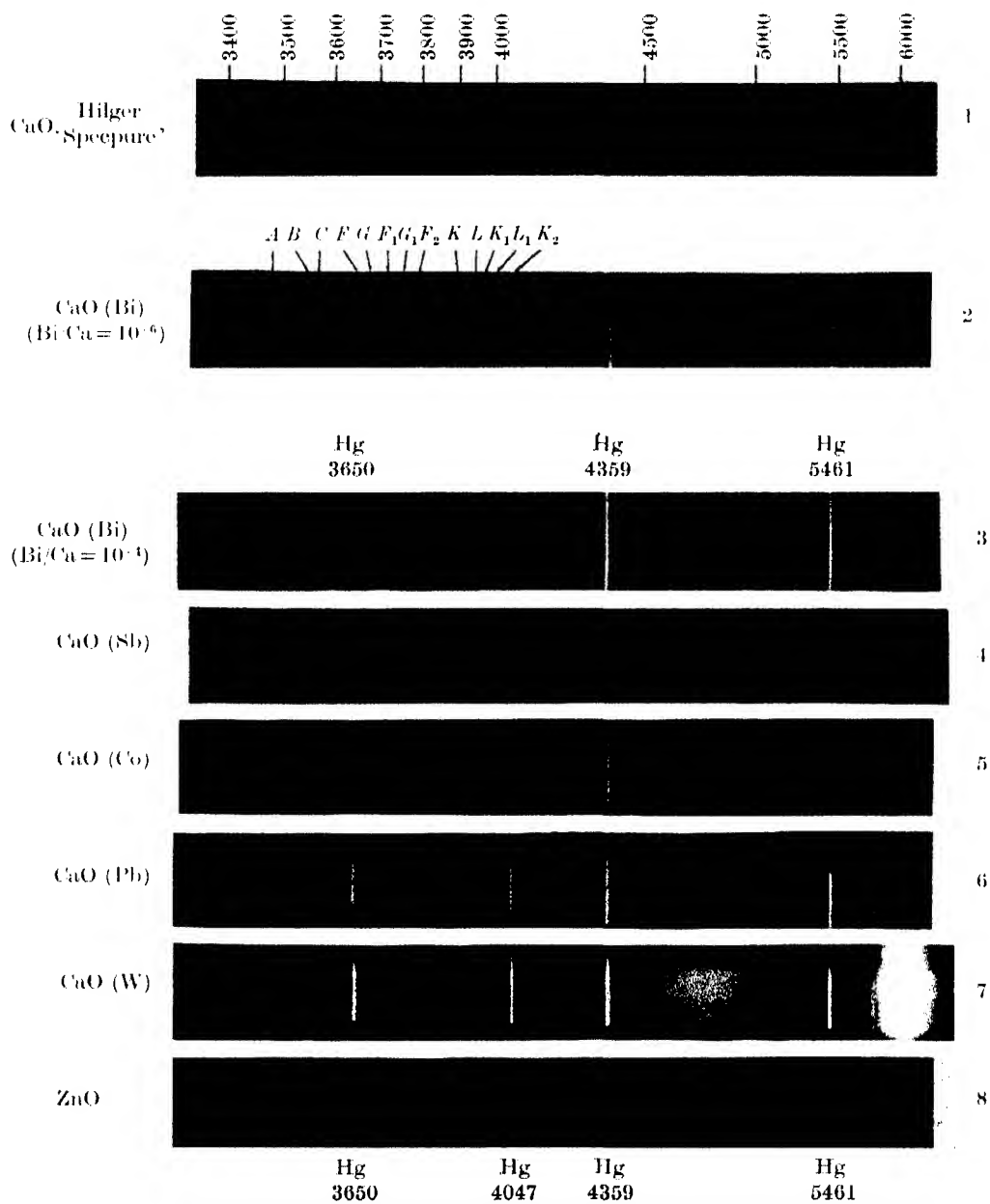
Fig. 5

CaO *and* CaS (*continued*)

Wave-lengths (Schellenberg) (A)

CaO	CaS	Comparison with Ca I lines (A)
3300 (Zn)	3350 (Fe, Ag)	$4s4p$ $^3P°–4s6d$ ^3D = 3344 to 3362
	3500 (Fe)⎫ 3520 (Zn)⎭	$4s3d$ $^3D –4smf$ $^3F°$ = 3451 to 3547 m = 12 to ∞
3600 (Ag)	3600 (Pb)⎫ 3660 (Sb)⎭	$4s3d$ $^3D –4smf$ $^3F°$ = 3547 to 3680 m = 12, 11, 10, 9, 8
3700 (Fe)⎫ 3780 (Bi)⎭	3680 (Fe, Ag)	$4s4p$ $^3P°–4s5d$ ^3D = 3624 to 3646
	3820 (Zn)⎫ 3840 (Pb)⎬ 3860 (Fe, Sb)⎭	$\begin{cases} 4s3d\ ^3D\ –4s6f\ \ ^3F° \\ 4s3d\ ^3D\ –4s7f\ \ ^3F° \end{cases}$ = 3748 to 3876
4000 (Ag)		$4s4p$ $^3P°–4s6s$ ^3S = 3973 to 3949
4140 (Bi)	4150 (Fe, Zn, Ag, Sb)⎫ 4100 (Pb)⎭	$\begin{cases} 4s3d\ ^3D\ –4s5f\ \ ^3P° \\ 4s4p\ ^1P°–4s^2\ \ \ \ ^1S \end{cases}$ = 4094 to 4100 = 4227
4350 (Fe)⎫ 4380 (Cu)⎬ 4400 (Fe)⎭	4380 (Ag)⎫ 4400 (Sb, Pb)⎭ ·	$4s4p$ $^3P°–4s4d$ ^3D = 4426 to 4457
4650 (Cu)	4540 (Fe, Zn, Sb)	$\begin{cases} 4s3d\ ^3D\ –4s4f\ \ ^3F° \\ 4s4p\ ^1P°–4s6d\ \ ^1D_2 \end{cases}$ = 4586 to 4579 = 4685

SrS (*Schellenberg* 1928, 1932)

Schellenberg deduces a number of individual bands in the blue and ultra-violet for SrS activated with Fe, Ag and Pb. Here again, not only are many of the bands similar in position with different impurities but a comparison with Sr I lines shows that the whole of the series $5s5p$ $^3P°–5sms$ ^3S and the series $5s5p$ $^3P°–5smd$ ^3D, within the range studied, are represented.

Zinc sulphides (*Riehl* 1937)

Riehl (1937) has recently confirmed a number of earlier claims that absolutely pure zinc sulphide is not only fluorescent but also phosphorescent. He also points out that the high efficiency of the excitation by x-rays or by ultra-violet light indicates that the whole of the lattice must be taking part in the process.

7. General discussion. Possible explanation
of some types of phosphorescence

The part apparently played by impurities in the conductivity of some semi-conductors on the one hand and the luminescence and photoconductivity of solids on the other, together with the parallelism which has been alleged to exist in some cases between excitation of photoconductivity and of luminescence has naturally led to attempts to explain the luminescence of

crystals containing impurities in terms of the Wilson semi-conductor model. Such theories, in common with the earlier ones, have hitherto assumed that the emission is directly associated with the impurity. The foregoing analyses of experimental observations on luminescent spectra indicate that there is a class of luminescent solids for which such a direct role cannot be assigned to the impurity. Indeed the evidence goes to show that in these cases the emission is characteristic of the parent crystal rather than the impurity.

It has been suggested above that the luminescent bands in such cases are electron vibration bands associated with the parent lattice. Constant frequency intervals have been shown to appear in these spectra which have values quite near to the vibration frequencies of the crystal. A comparison has been drawn between the electron jumps associated with these bands and those of neutral atoms of the metal of the crystal.
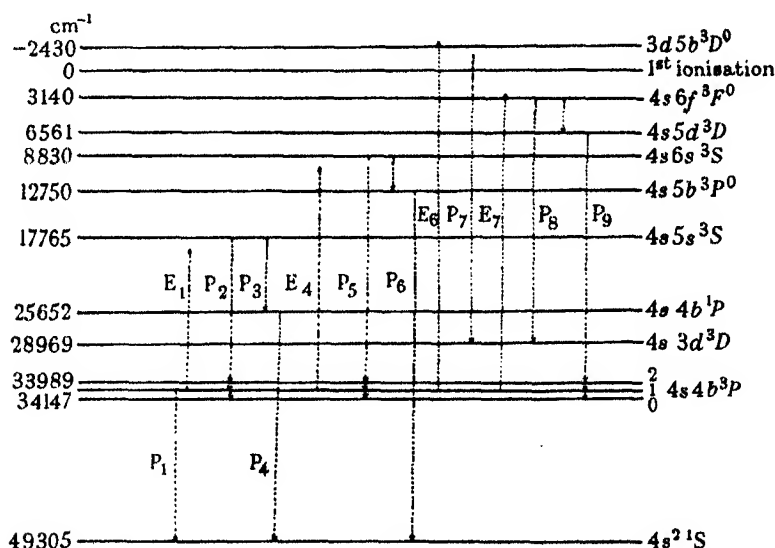
FIG. 2. Suggested mechanism of phosphorescence. $P_1, P_2, \ldots$ Phosphorescent emission. $E_1, E_2, \ldots$ Excitation of metastable atoms by $P_1, P_2, \ldots$. $h\nu_{E_1} = h\nu_{P_1}$, $h\nu_{E_4} = h\nu_{P_4}$, etc.

The striking recurrence of the metastable level of the neutral atom in this comparison suggests a possible explanation of some types of phosphorescence. This is that the atoms are first raised to higher levels by suitable excitation, whence some of them return to the metastable levels either directly or indirectly, and some to other levels. Most of these transitions result in fluorescence. But some of those atoms which have returned to the metastable states may remain there long enough to be re-excited. In the

case of such atoms in a crystal we may expect, however, continual disturbances from the metastable states to occur if there is a nearby state within a few vibration levels. If this nearby state is not metastable, transition will occur to a lower state. The energy thus released may appear directly as phosphorescence or *may be used to excite other atoms to a higher level whence return may again occur either to the metastable states* or to another level, again with emission of phosphorescent light. Phosphorescence thus goes on as long as there are any atoms left in the metastable state. Although, of course, the normal duration of the metastable state in an atom associated with a crystal lattice would not be anything like long enough to account for phosphorescence of long duration it is to be remembered that the metastable state is, according to this scheme, continually being restored by the luminescence itself. That such processes are numerically possible is shown in fig. 2 for the case of Ca I, where the levels are drawn to scale for Ca I.

The scheme, of course, does not exclude the possibility that some types of phosphorescent emission are due to the return of more or less free electrons to an ion. Indeed such a possibility is almost implicit in the suggested mechanism and is indicated in fig. 2.

Such a scheme would account for:

(1) The fact that the phosphorescent spectra are similar to the fluorescent spectra.

(2) The holding up of phosphorescence by cooling, since the chances of vibrational transitions from the metastable state to a nearby non-metastable state are decreased.

(3) The speeding up of phosphorescent emission by infra-red radiation.

Summary

Well-defined resolution of the ultra-violet bands in the cathodo-luminescent spectra of some inorganic solids, activated by various added impurities, has been obtained at the temperature of liquid air. For calcium oxide and strontium oxide constant frequency differences appear which are close to the vibrational frequencies of the crystal lattices.

Optically excited luminescent spectra of spectroscopically pure calcium oxide and of calcium oxide activated with bismuth show resolved bands in

the ultra-violet which are identical with the cathodo-luminescent bands except for a slight shift towards the red.

In general, the bands in the visible are not resolved. In many cases the positions of these bands are determined by the crystal and not by the impurity added.

These observations are shown to be in agreement with those of other workers in a number of cases where the partial resolution obtained by them justifies an analysis of their results.

It is therefore suggested that the luminescent spectra of certain luminescent solids, notably the alkaline earth oxides and sulphides, may be regarded as electron vibration bands associated with the crystal lattice.

In an attempt to interpret the electronic terms of such bands, a certain agreement is shown to exist between the values of these terms and those of electronic transitions of neutral atoms of the metal of the crystal. In this comparison, the striking recurrence of the metastable levels of the neutral atoms suggests a possible mechanism for short duration phosphorescence.

REFERENCES

Bowen 1935 *J. Chem. Soc.* p. 76.
Deutschbein 1932 *Ann. Phys., Lpz.*, **14**, 7.
Fock 1928 *Z. phys. Chem.* **132**, 161.
Ghosh 1932 *Z. Phys.* **78**, 521.
Hippel 1936 *Z. Phys.* **101**, 680–720.
Hilsch and Pohl 1933 *Nachr. Ges. Wiss. Göttingen*, Kl. II. No. 46.
Howes 1928 *Carneg. Inst. Washington Report*, No. 384.
Huggins 1937 *J. Chem. Phys.* **5**, 2.
Mahanti 1932 *Phys. Rev.* **42**, 609.
Northrop 1928 *Carneg. Inst. Washington Report*, No. 384, 105–106.
Perrine 1928 *Carneg. Inst. Washington Report*, No. 384, 93–4.
Riehl 1937 *Ann. Phys., Lpz.*, **29**, 636.
Roos 1934 *Ann. Phys., Lpz.*, **20**, 783.
Schellenberg 1928 *Ann. Phys., Lpz.*, **87**, 677–715.
—— 1932 *Ann. Phys., Lpz.*, **13**, 249–64.
Schmidt 1932 *Ann. Phys., Lpz.*, **12**, 211–38.
Tanaka 1921 *J. Opt. Soc. Amer.* **8**, 287.
Tolksdorf 1928 *Z. Phys. Chem.* **132**, 161.

DESCRIPTION OF PLATES

PLATE 3

Fig. 3. Comparison of Ca spectrum with cathodo-luminescent spectrum of CaO activated with bismuth, showing suggested correspondences.

Fig. 4. Photo-luminescent spectra of calcium oxide showing effect of addition of trace of bismuth.

PLATE 4

Fig. 5. Cathodo-luminescent spectra of calcium oxide and zinc oxide.

The probability of annihilation of positrons without emission of radiation

By H. S. W. MASSEY, PH.D.

Independent Lecturer in Math.-Physics, Queen's University, Belfast

AND E. H. S. BURHOP, PH.D.

Natural Philosophy Laboratory, University of Melbourne

There are two distinct processes by means of which a positron may be annihilated and the excess energy liberated in the form of radiation. These are:

(1) Annihilation by a free electron. Here the energy must reappear in the form of at least two quanta to satisfy the conservation laws.

(2) Annihilation by a bound electron. In this case the energy may appear in the form of a single quantum since the nucleus of the atom in which the electron is bound is available to take up excess momentum.

Calculations of the cross-section for annihilation by the first process have been carried out by Dirac (1930), while Fermi and Uhlenbeck (1933), Hulme and Bhabha (1934) and Nishina, Tomonaga and Tamaki (1934) have dealt with the second process. The two-quantum process is much more probable, yielding for lead a cross-section of 3.8×10^{-22} cm.^{2} compared with 1.93×10^{-23} cm.^{2} for the single quantum process. These values are for positrons of 500,000 e-volts energy for which the cross-sections have their maximum values.

Closely connected with the second process is a type of annihilation in which the positron collides with a bound electron with mutual annihilation but the energy liberated, instead of being radiated as a single quantum, is used to eject another electron from the atom. An estimate of the cross-section for this radiationless annihilation, where the two electrons concerned are K electrons, has been made by Brunings (1934). His calculations, involving a number of approximations, led to the conclusion that the cross-section would reach a value of about 5×10^{-26} cm.^{2} for positrons of 100,000 e-volts energy. This value, though small, would indicate that the process is observable, particularly when account is taken of transitions involving other pairs of bound electrons. In view of this possibility it was thought desirable to calculate the cross-section without making drastic approxi-

mations, taking account of retardation effects and spin-spin interaction in the usual manner (Møller 1931). This has been carried out and, although the more accurate calculation gives rather different results from those obtained by Brunings, it still appears that the process, though rare, should be observable. We now proceed to the detailed account of the method and results.

<div align="center">GENERAL METHOD AND FORMULAE</div>

The annihilation process with which we are concerned is essentially an Auger transition involving the two atomic electrons. One of the electrons jumps to the state of negative kinetic energy made available in the form of the incident positron while the other, receiving the energy liberated in this way, undergoes a transition to a state of positive energy, involving its ejection from the atom. If E_α, E_β are the total energies (including the mass term mc^2) of the electrons before the transition, E_+ that of the positron, and E_- that of the electron after ejection, then

$$E_\alpha + E_\beta = E_- - E_+.$$

To calculate the probability cross-section we may use the method introduced by Møller (1931) for dealing, in a manner consistent with relativistic invariance, with two electron transitions. Let ψ_α, ψ_β be the respective wave functions of the electronic states with energies E_α, E_β respectively, ϕ_- that of the positive energy state occupied by the ejected electron and ϕ_+ that of the negative kinetic energy state. Then the cross-section for the annihilation of a positron incident with momentum $k_+ h/2\pi$, energy E_+ and velocity v_+, by the two electrons considered, is

$$Q = \frac{4\pi^2}{v_+ h} \tfrac{1}{2} \mathbf{s} \, \Sigma \iint \delta(E_\alpha + E_\beta + E_+ - E_-) \, |A|^2 \frac{k_-^2 \, dk_-}{(2\pi)^3} \, d\Omega. \tag{1}$$

Here $d\Omega$ is the element of solid angle into which the electron is ejected, $\mathbf{s}$ and Σ denote summation over the spin directions of positron and ejected electron respectively and $\delta(E_\alpha + E_\beta + E_+ - E_-)$ is the usual δ-function. The matrix element A is given by

$$A = B - C,$$

where

$$
\left.
\begin{aligned}
B &= \iint \left(\rho_1 \rho_2 - \frac{1}{c^2} \mathbf{j}_1 \cdot \mathbf{j}_2\right) \exp(2\pi i \nu r_{12}/c) \, r_{12}^{-1} \, d\tau_1 d\tau_2, \\
C &= \iint \left(\rho_1' \rho_2' - \frac{1}{c^2} \mathbf{j}_1' \cdot \mathbf{j}_2'\right) \exp(2\pi i \nu r_{12}/c) \, r_{12}^{-1} \, d\tau_1 d\tau_2.
\end{aligned}
\right\} \tag{2}
$$

$\rho_1(\mathbf{r}_1)$, $\mathbf{j}_1(\mathbf{r}_1)$ are the respective charge and current densities corresponding to the transition $\psi_\alpha(\mathbf{r}_1) \to \phi_+(\mathbf{r}_1)$; $\rho_2(\mathbf{r}_2)$, $\mathbf{j}_2(\mathbf{r}_2)$ are the corresponding quantities for the transition $\psi_\beta(\mathbf{r}_2) \to \phi_-(\mathbf{r}_2)$; ρ_1', ρ_2' and $\mathbf{j}_1'$, $\mathbf{j}_2'$ refer respectively to the "exchange" transition $\psi_\beta(\mathbf{r}_1) \to \phi_+(\mathbf{r}_1)$, $\psi_\alpha(\mathbf{r}_2) \to \phi_-(\mathbf{r}_2)$; $h\nu = E_\alpha + E_+ = E_- - E_\beta$ and the suffixes 1, 2 distinguish the two electrons.

This formula takes account of spin-spin interaction, retardation and electron exchange. The functions ψ_α, ψ_β are normalized to unit volume as usual, while ϕ_+, ϕ_- must have the asymptotic forms of plane waves of unit amplitude together with the corresponding spherical waves.

DETAILED EVALUATION OF CROSS-SECTION FOR ANNIHILATION BY K-ELECTRONS

We first assume that the energy of the incident positron is so high that the wave function ϕ_+ is adequately represented by a plane wave. Since the ejected electron has a kinetic energy of over 2×10^6 e-volts, in all cases the wave function ϕ_- can always be taken as a plane wave.

Choosing the polar axis along the direction of motion of the incident positron we have, for a chosen spin direction of the positron,

$$\left.\begin{aligned} \phi_+ &= (1 + \Delta_+^2)^{-\frac{1}{2}} e^{-ik_+ z}(1, 0, -\Delta_+, 0), \\ \Delta_+ &= ck_+/(E_+ + mc^2). \end{aligned}\right\} \tag{3}$$

For the ejected electron we have, for the two possible spin orientations

$$\left.\begin{aligned} \phi_-^{\uparrow} &= (1 + \Delta_-^2)^{-\frac{1}{2}} e^{ik_- \mathbf{n} \cdot \mathbf{r}}\{-\Delta_- \cos\vartheta, -\Delta_- \sin\vartheta e^{i\phi}, 1, 0\}, \\ \phi_-^{\downarrow} &= (1 + \Delta_-^2)^{-\frac{1}{2}} e^{ik_- \mathbf{n} \cdot \mathbf{r}}\{-\Delta_- \sin\vartheta e^{i\phi}, \Delta_- \cos\vartheta, 0, 1\}, \\ \Delta_- &= ck_-/(E_- + mc^2). \end{aligned}\right\} \tag{4}$$

$\mathbf{n}(\vartheta, \phi)$ is a unit vector in the direction of ejection of the electron.

The K wave functions are as usual,

$$\left.\begin{aligned} \psi_\alpha &= N_K g(r)\{-i\Delta_0 \cos\theta, -i\Delta_0 \sin\theta e^{i\phi}, 1, 0\}, \\ \psi_\beta &= N_K g(r)\{i\Delta_0 \sin\theta e^{-i\phi}, -i\Delta_0 \cos\theta, 0, -1\}, \end{aligned}\right\} \tag{5}$$

with
$$g(r) = e^{-Zr/a_0} r^{\sqrt{(1-\gamma^2)}-1}$$

$$\Delta_0 = \gamma(1 + \sqrt{(1-\gamma^2)})^{-1}$$

$$N_K = \left\{\left(\frac{2Z}{a_0}\right)^{1+2\sqrt{(1-\gamma^2)}} \frac{(1+\sqrt{(1-\gamma^2)})}{8\pi\Gamma(1+2\sqrt{(1-\gamma^2)})}\right\}^{\frac{1}{2}}$$

$$\gamma = 2\pi Ze^2/hc.$$

Z is the effective nuclear charge and a_0 the radius of the first Bohr orbit of hydrogen.

Using these wave functions the charge and current densities $\rho_1, \rho_2, \rho_1', \rho_2'$; j_1, j_2, j_1', j_2' may be calculated without difficulty. It is then found that integrals of the type

$$\iint \exp\{i(k_+ z_1 - k_1 \mathbf{n}.\mathbf{r}_2 + 2\pi\nu r_{12} + m\phi_1 - m'\phi_2) - Z(r_1 + r_2)/a_0\}$$
$$\times P_l^m(\cos\theta_1) P_{l'}^{m'}(\cos\theta_2) (r_1 r_2)^{\sqrt{(1-\gamma^2)}-1} r_{12}^{-1} d\tau_1 d\tau_2, \quad (6)$$

with $l, l' = 0$ or 1, occur in the matrix elements. These may be evaluated by using the expansions:

$$\left.\begin{array}{l} e^{ik_+ z} = \Sigma (2n+1) \alpha_n(r) P_n(\cos\theta), \\[4pt] e^{ik_- \mathbf{n}.\mathbf{r}} = \Sigma (2n+1) \beta_n(r) P_n(\cos\Theta), \\[4pt] r_{12}^{-1} e^{2\pi i\nu r_{12}/c} = \Sigma (2n+1) \delta_n(r_1, r_2) P_n\left(\dfrac{\mathbf{r}_1.\mathbf{r}_2}{r_1 r_2}\right), \end{array}\right\} \quad (7)$$

where

$$\left.\begin{array}{l} \cos\Theta = r^{-1}\mathbf{n}.\mathbf{r}, \\[4pt] \alpha_n = (\pi/2k_+ r)^{\frac{1}{2}} i^n J_{n+\frac{1}{2}}(k_+ r), \\[4pt] \beta_n = (\pi/2k_- r)^{\frac{1}{2}} (-i)^n J_{n+\frac{1}{2}}(k_- r), \\[4pt] \delta_n(r_1, r_2) = \frac{1}{2}\pi(r_1 r_2)^{-\frac{1}{2}} J_{n+\frac{1}{2}}(2\pi\nu r_1/c)\{i J_{n+\frac{1}{2}}(2\pi\nu r_2/c) \\[4pt] \qquad + J_{-n-\frac{1}{2}}(2\pi\nu r_2/c)\}, r_1 < r_2, \end{array}\right\} \quad (8)$$

together with the integral and addition formulae for spherical harmonics. On carrying out these calculations we obtain, for the matrix elements A_1, A_2 corresponding to the two final states of the ejected electron which differ in spin orientation:

$$\left.\begin{array}{l} A_1 \\ A_2 \end{array}\right\} = 16\pi^2 N_k^2 (1+\Delta_+^2)^{-\frac{1}{2}} (1+\Delta_-^2)^{-\frac{1}{2}} \Sigma_n \left\{\begin{array}{l} P_n^1(\cos\vartheta) e^{-i\phi} A_{1n}, \\ P_n(\cos\vartheta) A_{2n}, \end{array}\right. \quad (9)$$

where

$$\begin{aligned} A_{1n} = {} & 3\Delta_-(\alpha_{n-1}\delta_{n-1}\beta_{n-1} - \alpha_{n+1}\delta_{n+1}\beta_{n+1}) \\ & + i\Delta_0(\alpha_{n+1}\delta_{n+1}\beta_n - \alpha_{n-1}\delta_{n-1}\beta_n - \alpha_{n-1}\delta_n\beta_n + \alpha_{n+1}\delta_n\beta_n) \\ & - i\Delta_0\Delta_+\Delta_-(\alpha_n\delta_n\beta_{n-1} - \alpha_n\delta_n\beta_{n+1} + \alpha_n\delta_{n-1}\beta_{n-1} - \alpha_n\delta_{n+1}\beta_{n+1}) \\ & + \Delta_0^2\Delta_-(\alpha_{n-1}\delta_n\beta_{n-1} - \alpha_{n+1}\delta_n\beta_{n+1}) - \dot{\Delta}_0^2\Delta_+(\alpha_n\delta_{n+1}\beta_n - \alpha_n\delta_{n-1}\beta_n); \end{aligned}$$

$$(10)$$

$$A_{2n} = (2n+1)\Delta_+ \alpha_n \delta_n \beta_n - 3\Delta_-(n\alpha_{n-1}\delta_{n-1}\beta_{n-1} + \overline{n+1}\,\alpha_{n+1}\delta_{n+1}\beta_{n+1})$$

$$+ i\Delta_0(n\alpha_{n-1}\delta_{n-1}\beta_n + \overline{n+1}\,\alpha_{n+1}\delta_{n+1}\beta_n + n\alpha_{n-1}\delta_n\beta_n + \overline{n+1}\,\alpha_{n+1}\delta_n\beta_n)$$

$$+ i\Delta_0\Delta_+\Delta_-(n\alpha_n\delta_{n-1}\beta_{n-1} + \overline{n+1}\,\alpha_n\delta_{n+1}\beta_{n+1} + n\alpha_n\delta_n\beta_{n-1}$$

$$+ \overline{n+1}\,\alpha_n\delta_n\beta_{n+1}) + 3\Delta_0^2\Delta_+(\overline{n+1}\,\alpha_n\delta_{n+1}\beta_n + n\alpha_n\delta_{n-1}\beta_n)$$

$$- \Delta_0^2\Delta_-(\overline{n+1}\,\alpha_{n+1}\delta_n\beta_{n+1} + n\alpha_{n-1}\delta_n\beta_{n-1}). \tag{11}$$

Here we have written for brevity

$$\alpha_u\delta_v\beta_w = \iint g(r_1)\,\alpha_u(r_1)\,\delta_v(r_1,r_2)\,\beta_w(r_2)\,g(r_2)\,r_1^2 r_2^2\,dr_1\,dr_2. \tag{12}$$

Integrating over the angles of ejection one obtains for the total cross-section for this annihilation process

$$Q = r_0^2 \frac{256\pi^3 N_K^2 k_-(1+k_+^2)^{\frac{1}{2}}(1+k_-^2)^{\frac{1}{2}}}{(1+\Delta_+^2)(1+\Delta_-^2)k_+} \, \Sigma_n \frac{1}{2n+1}\{n(n+1)\,|A_{1n}|^2 + |A_{2n}|^2\}, \tag{13}$$

where $h/2\pi mc$, c and m have been taken as units of length, velocity and mass respectively, and $r_0 = e^2/mc^2$.

As far as can be ascertained from his paper,* Brunings makes the approximation of neglecting Δ_+, Δ_0, all retarding effects and all terms in the series excepting those involving $\alpha_0\delta_0\beta_0$. With these approximations

$$\alpha_0\delta_0\beta_0 = \frac{2\gamma(10\gamma^2 + k_+^2 + k_-^2)}{(k_-^2+\gamma^2)(k_+^2+\gamma^2)\{4\gamma^2+(k_+-k_-^2)\}\{4\gamma^2+(k_++k_-)^2\}}, \tag{14}$$

or, neglecting further k_+, γ in comparison with k_-,

$$\alpha_0\delta_0\beta_0 = \frac{2\gamma}{k_-^4}(k_+^2+\gamma^2)^{-1}. \tag{15}$$

Substituting in (13) gives us an expression for Q which we call the "non-relativistic" approximation.

Numerical calculations were carried out for positrons of energies 10^5, 3×10^5 and 5×10^5 e-volts using formula (13) and also the "non-relativistic" approximation. In evaluating (13), the integrals $\alpha_v\delta_u\beta_w$ were calculated by double numerical integration as it is not possible to obtain closed

---

* It would seem from Bruning's paper that he neglects spin-spin interaction as well as retardation. To his approximation this would give a vanishing cross-section but he obtains our non-relativistic approximation, apart from a factor of 9, by using wave functions for the K-shell corresponding to positive electrons in the field of a negative charge.

expressions for them. The convergence of the series in (13) arises from the decrease of $J_{u+\frac{1}{2}}(k_+r)$ at small r with increase of u, so terms involving values of u greater than 3 were unimportant in all cases. Results of the calculations for lead are given in Table I, rows II (formula (13)) and III ("non-relativistic" approximation).

EFFECT OF REPULSION OF POSITRONS BY THE ATOMIC NUCLEUS

In deriving the formula (13) the distortion of the incident positron wave functions by the atomic nucleus was ignored but for the lower energies this becomes important. To allow for this we replace the expression (3) by the following which represents the wave function of an electron in a state of negative kinetic energy* moving in the Coulomb field of a charge Ze:

$$\phi_+ = (1 + \Lambda^2_+)^{-\frac{1}{2}} (1, 0, -\Delta_+, 0) \chi_+(r) \dagger$$

$$\chi_+(r) = i\Sigma[n\zeta'_n + (n+1)\zeta'_{n+1} + nB_n\zeta_n + (n+1)B_{-n-1}\zeta_{n+1}](-1)^n P_n(\cos\theta),$$

where
$$\zeta_n = \frac{\Gamma(\rho + 1 - iq)}{\Gamma(2\rho + 1)}(2k_+r)^{\rho-1}e^{-ik_+r}\exp(-\tfrac{1}{2}\pi q + \tfrac{1}{2}\pi i\rho)$$
$$\times {}_1F_1(\rho + 1 - iq; \; 2\rho + 1; \; 2ik_+r).$$

$$\zeta'_n = \frac{\Gamma(\rho + 1 + iq)}{\Gamma(2\rho + 1)}(2k_+r)^{\rho-1}e^{-ik_+r}\exp(-\tfrac{1}{2}\pi q - \tfrac{1}{2}\pi i\rho)$$
$$\times {}_1F_1(\rho - iq; \; 2\rho + 1; \; 2ik_+r);$$

$$B_n = \exp(2i\eta_{-n-1}) = -\frac{n + iq'}{\rho + iq}\frac{\Gamma(\rho + 1 + iq)}{\Gamma(\rho + 1 - iq)}e^{-\pi i\rho},$$

$$\rho = (n^2 - \gamma^2)^{\frac{1}{2}},$$

$$q = \frac{\gamma c}{v_+}, \quad q' = q(1 - v^2_+/c^2)^{\frac{1}{2}}.$$

Equations (10) and (11) for the matrix elements then remain unaltered provided equation (8) for α is replaced by the expression:

$$\alpha_n = \frac{i}{2n + 1}\{n\zeta'_n + (n+1)\zeta'_{n+1} + nB_n\zeta_n + (n+1)B_{-n-1}\zeta_{n+1}\}.$$

* This may be obtained from the corresponding wave function for an electron of positive kinetic energy given by Mott (1932).

† It is, of course, not strictly correct to write ϕ_+ in this form when dealing with a Coulomb field. The second and fourth components do not vanish completely nor is the third component exactly Δ_+ times the first, as would be the case for plane waves. However, the effect of these modifications will be slight compared with the distortion of the plane waves by the nucleus.

TABLE I. CROSS-SECTIONS FOR ANNIHILATION OF POSITRONS BY THE K-ELECTRONS OF LEAD

Energy of incident positron in e-volts	10^5	3×10^5	5×10^5
Cross-section in 10^{-26} cm.^{2}:			
I. Allowing for repulsive effect of the nucleus	0·1	0·35	0·2
II. Using plane waves for positron wave functions	1·6	1·4	0·9
III. "Non-relativistic" approximation	6·7	0·4	0·05

To obtain numerical values for the new integrals $\alpha_u \delta_v \beta_w$, the distorted wave functions (17), for the positron energies considered, were evaluated numerically from the series for the hypergeometric functions involved. In fig. 1 a typical wave function is illustrated. The effect of the nuclear repulsion is clearly revealed in the reduced amplitude of the function at small r. Having obtained the values of the distorted wave function at a sufficient number of points the calculation of the double integrals proceeded as before. The distortion was only taken into account for the first two terms of the series (17), its effect on higher terms being unimportant. Values obtained in this way for lead are given in the first row of Table I where they may be compared with those obtained without allowing for the nuclear repulsion.
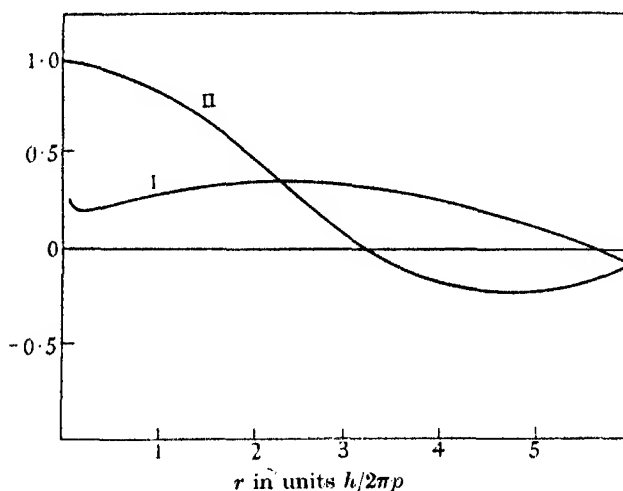
FIG. 1. Wave-function for a position of 100,000 e-volts energy and zero angular momentum in the field of the lead nucleus (curve I). Curve II represents the plane wave function for this case. Both functions are normalized to unit amplitude at infinity. p is the momentum of the positron.

Neglect of the influence of retardation is mainly responsible for the difference between the values in the second and third rows of Table I for

low positron energies. At higher energies the chief defect of the "non-relativistic" approximation is that it neglects the higher terms of the series in (13). Comparison of the values in the first and second rows shows that the repulsive effect of the nucleus is less pronounced as the positron energy increases, in accordance with expectation.

TABLE II. CROSS-SECTIONS FOR ANNIHILATION OF POSITRONS OF 10^5 E-VOLTS ENERGY BY VARIOUS PAIRS OF ELECTRONS IN THE LEAD ATOM, CALCULATED TO THE "NON-RELATIVISTIC" APPROXIMATION

Electrons concerned	Cross-section (in 10^{-26} cm.^{2})
K, K	6·7
L_1, K	2·5
M_1, K	0·6
L_1, L_1	0·1
$L_{\text{II, III}}, K$	4·1
$L_{\text{II, III}}, L_1$	1·5
$L_{\text{II, III}}, L_{\text{II III}}$	Very small

ANNIHILATION BY ELECTRONS IN OTHER ATOMIC SHELLS

Exact calculations for annihilation by other pairs of atomic electrons would involve prohibitive labour so an estimate was made of the probable contribution from such processes by making the same approximations as those employed in deriving the "non-relativistic" formula for the K-electrons. Although the absolute values obtained in this way will be far from correct it is likely that the relative values will be sufficiently correct for our purpose. The results obtained in this way for lead are given in Table II. These show that it is reasonable to conclude that the contribution to the total radiationless annihilation cross-section from other pairs of atomic electrons is not likely to be much greater than twice that from the two K-electrons alone.

CONCLUDING REMARKS

It appears then that the total cross-section for radiationless annihilation involving pairs of electrons within lead atoms has a maximum value of between 1 and $1·5 \times 10^{-26}$ cm.^{2} for incident positrons of energy 3×10^5 e-volts. This is to be compared with the value $1·9 \times 10^{-23}$ cm.^{2} for the one-quantum radiative annihilation by electrons of the same atom. As remarked earlier the radiationless process bears the same relation to the radiative one as Auger transitions between the L and K shells of heavy atom do to

emission of $K \cdot X$-radiation. The ratio of the Auger to radiative transition probability decreases with increase in the energy change of either electron involved and is about 5×10^{-2} for the heaviest atom (in which the energy change is greatest) (Massey and Burhop 1936). A ratio of 10^{-3} is therefore not unexpected for the case we have been considering for here the energy change, being about 2×10^6 e-volts, is much greater still.

It appears, by comparison with the cross-section for radiative annihilation that about one positron in 10,000 would be annihilated by a radiationless process. As strong positron sources are now available from artificially radioactive sodium it should be possible to observe the process in a cloud chamber. It would give rise to quite a characteristic appearance in the chamber, a slow positron entering a thin sheet of lead and emerging as an electron of energy greater than 10^6 e-volts.

SUMMARY

When mutual annihilation occurs on collision of an atomic electron and a positron the energy liberated, instead of appearing as radiation, may be absorbed by a second atomic electron, resulting in its ejection from the atom. In this paper the probability cross-section for this radiationless annihilation process involving the K-electrons of a lead atom is calculated with accuracy, account being taken of the repulsive influence of the nucleus, retardation, spin-spin interaction and electron exchange. Estimates are also made of the contributions from other pairs of electrons and the conclusion is finally reached that the total cross-section for radiationless annihilation by lead electrons attains a maximum value of between 1 and 1.5×10^{-26} cm. for positrons with energy 300,000 e-volts. The possibility of observing the phenomenon is briefly discussed.

REFERENCES

Brunings, J. 1934 *Physica*, **1**, 996.
Dirac, P. A. M. 1930 *Proc. Camb. Phil. Soc.* **26**, 361.
Fermi, E. and Uhlenbeck, G. 1933 *Phys. Rev.* **44**, 510.
Hulme, H. R. and Bhabha, H. J. 1934 *Proc. Roy. Soc.* A, **146**, 723.
Massey, H. S. W. and Burhop, E. H. S. 1936 *Proc. Roy. Soc.* A, **153**, 661.
Møller, C. 1931 *Z. Phys.* **70**, 686.
Mott, N. F. 1932 *Proc. Roy. Soc.* A, **135**, 429.
Nishina, Y., Tomonaga, S. and Tamaki, H. 1934 *Sci. Pap. Inst. Phys. Chem. Res.*, *Tokyo*, **24**, 18.

The two-stage auto-ignition of hydrocarbons and "knock"

By G. P. KANE, PH.D.

(*Communicated by A. C. G. Egerton, F.R.S.—Received* 17 *March* 1938)

INTRODUCTION

The investigations of Townend and co-workers (1934) have revealed that the spontaneous ignition of higher paraffins in admixture with air consists in certain temperature ranges usually between 270 and 400° C., of a two-stage process, preceded by a time interval t_1 prior to the appearance of a cool flame, and a subsequent interval t_2 before the occurrence of normal ignition. The reactions involved may be indicated as proceeding from $A \to B \to C$, where B denotes the rapid formation of intermediate products by the passage of a cool flame. Above and below this temperature range the ignitions are no longer composite and after a time interval t appear to result directly from the process $A \to C$.

Apart from their intrinsic interest, these results have a practical bearing on the problem of "knock" in internal combustion engines. For, whereas the minimum pressures for ignition in the cool flame region of the paraffins and olefins containing more than three carbon atoms have been shown to be related to their knocking propensities in engine practice, non-knocking fuels such as methane have failed to reveal any cool flame systems at all, even at pressures up to 30 atm. While the precise mechanism of "knock" is as yet not entirely understood, it is generally recognized that the phenomenon arises as the outcome of the passage of an explosion flame through a fuel-air mixture which has attained a state of enhanced chemical reactivity (cf. Egerton and co-authors 1938).

Although, in laboratory experiments upon spontaneous ignition, a variable interval usually of a few seconds or more precedes the appearance of flame, increased initial pressure progressively shortens such induction lags; and it appears very probable that at the pressures attained in an internal combustion engine a very high degree of chemical reactivity bordering on spontaneous ignition would be attained in the medium ahead of the flame within the maximum available time interval of approximately 0·005 sec. The apparatus employed by Townend and co-workers, however, precluded attempts at any measurements of induction lags much less than 1 sec., and

[62]

the present paper embodies an account of a further investigation of the matter.

With regard to the kinetic aspect of the subject, it may be recalled that Neumann and Egorow (1932) showed that in the spontaneous ignition of a $CH_4 + O_2$ mixture at a constant temperature of *ca.* 700° C., the relation between the induction lag t and the pressure P (combustible + oxygen) could be expressed by the relation $tP^n = $ constant, the value of n being 1·8.

As the reaction obeys the law $w = Ne^{\phi T}$, the approximate condition for explosion is given by $\phi t = $ constant. Taking into consideration the kinetics of the reaction, the relation should read as $tp^{1·6} e^{-46000/T} = $ constant, and this gave results differing little from those found by experiment.

Neumann and Aivazov (1936) have recently extended these investigations to the induction lags for cool flames in pentane-oxygen mixtures, and have derived the following expression to account for the influence of factors such as temperature, increased initial pressure, nitrogen dilution and vessel diameter

$$t = Ae^{r/T}\left(\frac{a + b/d^2}{1 + (N_2)/P}\right)^2 \cdot \frac{1}{(P - P_0)^2},$$

in which A, a, b and r are constants, P is the total pressure and P_0 the minimum pressure for the propagation of a cool flame.

When the pressure (P) and the induction lag (t) were the only variables, the relation $t(P - P_0)^n = $ constant was found to hold and the value of n for pentane was equal to 2. When P exceeded a certain critical value, the cool flame gave rise to a normal ignition following a second time interval.

Neumann and Tutakin (1936) and Andreev (1937) have studied the transition of cool flames into normal flames in equimolecular butane-oxygen mixtures by means of pressure-time records obtained with a low-pressure silica bourdon gauge. They confirmed that over the temperature range 287–441° C., the process of inflammation is characterized by two stages; a cool flame being first formed which gave rise to a number of intermediate products, the secondary oxidation of which leads to the normal flame. It was also claimed that the second induction period increased with temperature, this being ascribed to thermal instability of an intermediate product. At 461° C., the cool flame disappeared entirely, and it was also very feeble below 279° C. At 321° C. the induction lags decreased progressively with increasing initial pressure, and at the same time the cool-flame intensity became greater. It was concluded that chain reactions played an important part in the subsequent ignition with chain breaking at the walls of the vessel, although there was also evidence of some self-heating of the mixture.

Prettre (1936) has recently studied in some detail the influence of variations of pressure, temperature and mixture composition on the lags prior to cool-flame formation during the combustion of pentane-oxygen mixtures. Between 260 and 300° C., at any given temperature, the variation of the induction lag was expressed by the equation $tPcPt^2 =$ constant, where $t =$ induction lag, $Pc =$ partial pressure of combustible and $Pt =$ the total pressure. This expression was assumed to apply whether the reaction led to a cool flame or to normal ignition, and also when nitrogen was added as a diluent (Pt in this case being equal to the sum of the partial pressures of combustible and oxygen). The experiments were restricted to pressures below 1 atm., and the induction lags to those greater than 1 sec.; but the general applicability of the expression led Prettre to conclude that by extrapolating to higher pressures in the region of 10–15 atm., ignition lags at 350° C. would be reduced to less than $\frac{1}{100}$ sec. for pentane-air mixtures and he agreed that "knock can logically be attributed as if it is an instantaneous spontaneous ignition which is imposed under the conditions of temperature and pressure obtainable in the engine cylinder".

Some recent experiments in these laboratories (as yet unpublished) by Dr M. S. Hsieh upon the propagation of cool flames initiated by a heated wire in cold tubes through ether or higher hydrocarbon-air/oxygen media, have also shown that under conditions where a normal flame results in the products left by the passage of a cool flame, increase of pressure favours a progressive shortening of the interval necessary for its initiation.

While the investigations referred to have indicated the general influence of increased initial pressure in shortening the induction lags prior to the initiation of both cool flames and the ignitions to which they give rise, the extreme violence associated with ignitions at pressures much exceeding the minimum ignition pressure has precluded any extended examination of the matter in the direction of the compression pressures attained in engine practice. It was therefore a matter of importance to devise means by which it would be possible to study how far kinetic interpretations such as have been proposed, are applicable to the two-stage auto-ignition of higher hydrocarbons, over adequate ranges of initial pressures.

In order to attain this end an optical device operating in conjunction with a disk manometer was developed, with which it is possible to obtain records of the induction lags prior to ignition with an accuracy of $\frac{1}{100}$ sec. and relating to explosive media at pressures up to 15 atm. The present paper describes the apparatus employed and the results obtained with propane and propylene at temperatures between 330 and 440° C. These materials were studied in the first place because the induction lags associated with

their ignitions are longer than those with higher hydrocarbons, and it was therefore possible to measure them over adequate pressure ranges.

EXPERIMENTAL

Apparatus. The filling system employed was similar to that used in previous work on this subject in these laboratories (cf. Kane, Chamberlain and Townend 1937). To facilitate rapid filling, however, the length of all capillary connexions was reduced to a minimum.

The recording mechanism was similar to that described by Crowe and Grimshaw (1931) for measuring the pressures developed in explosions of propellants. The principal working member was a light piston made from brass tube 0·20 in. in diameter, one end being tapered to a point which rested at the centre of the disk *d* (fig. 1). Any pressure exerted on the disk caused a small movement of the piston which was magnified optically in the usual way by means of the angular movement imparted to a mirror *M*, suspended by two (one being divided) flat spring steel strips. One end of each strip was fixed to a projection from the mirror holder and the other to the base *B* in such a way that the two springs were set in a plane at right angles to one another, to give a cross-spring suspension. A third short strip connected the mirror holder with the piston head so that any movement of the piston forced the holder to rotate through an arc of a circle.

1 2 3 4 5 6 7 cms
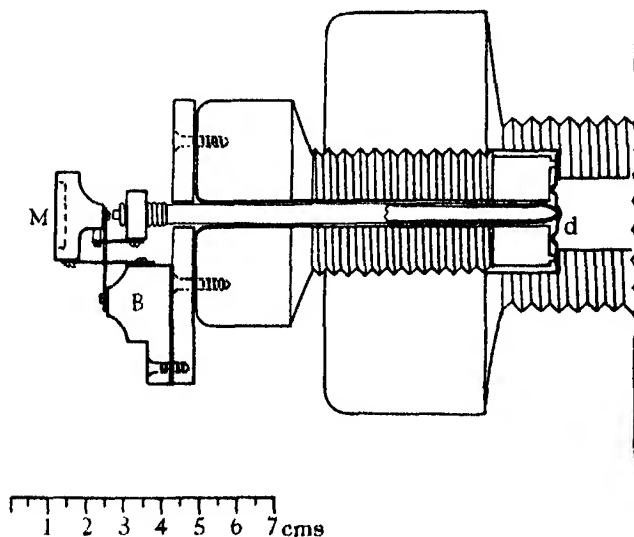
FIG. 1. The mirror system and disk manometer.

A steel mirror, 40 cm. focal length and platinized to avoid corrosion, was mounted in the holder, and the light from a pointolite source reflected from it as a sharp vertical line on the recording paper fastened to the drum of the camera (fig. 2); the distance between the mirror and the camera being about 80 cm.
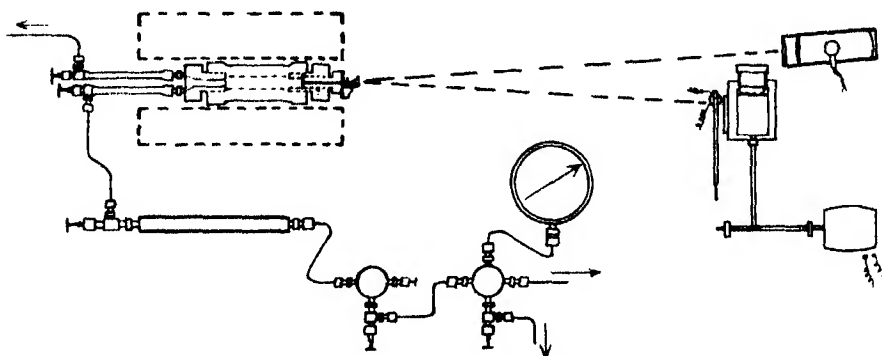
FIG. 2. The filling system and the pressure-recording mechanism.

An electrically controlled tuning fork of a frequency of 100 per sec. intercepted the path of the beam and served as a measure of time, the pressure-time records being obtained in the form of a dotted line. The thickness of the disk was such that a change in pressure of 0·05 atm. produced a visible deflexion of the beam; when the ignitions were violent, however, the reflected beam was deflected beyond the width of the recording paper. Systematic calibration of the disks was not attempted, the purpose of the present investigation being primarily to detect the moments of initiation of cool and normal flames and to estimate the induction lags with accuracy.

The explosion vessel was mounted in such a way that the mirror fitting and its supports just projected from the furnace in order to maintain them at a temperature considerably lower than that of the furnace. By so doing the mirror retained its polish and the springs their elasticity throughout the experiments.

Liners of mild steel (3·2 × 15 cm.) were employed in the explosion vessel. The ignitions at higher pressures being very violent and of the detonating type, particularly when undiluted combustion-oxygen media were employed, gave rise to pressure waves in the elongated chamber and caused a permanent set in the recording disk. In many of the experiments the disk was therefore protected by a blank steel plug which restricted the explosion chamber to a length of 3·5 cm.

Ilford Recorder Cine Bromide paper was employed for the photographic work.

Proceedure. The propane and propylene used in the experiments were obtained from cylinders supplied by the Ohio Chemical Company, U.S.A., and were of purity 99·9 and 99·5 %, respectively. When oxygen alone was employed for the explosive mixtures the latter were made up for each experiment by the method of partial pressures, while when air was used the mixtures were made up and stored under pressure. All observations relate to mixtures in which the ratio between the combustible and oxygen was in the proportion 1 : 3. This ratio was selected in order to avoid the violence of the ignitions of mixtures containing more oxygen, as well as the deposition of carbon associated with mixtures containing a greater defect of oxygen.

The object of the investigation being a study of the influence of increasing pressure on the two-stage auto-ignition of higher hydrocarbons, the temperature of the experiments was usually between 330 and 400° C., but some records were obtained above this range to compare the influence of initial pressure on the single stage normal ignition.
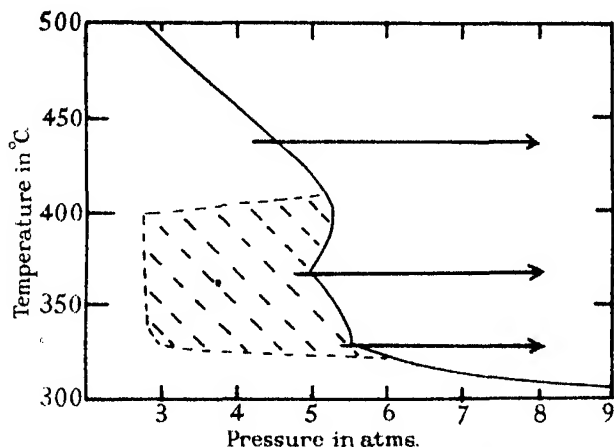
Fig. 3. Spontaneous ignition temperature curve for the 6·5 % propane-air mixture in the shorter cavity. Arrows illustrate where the variation of induction lag with increasing pressure has been studied. Shaded area denotes the region where cool flames only are observed.

In fig. 3 a curve has been drawn showing the variation with temperature of the minimum pressure requisite for the normal ignition of the propane-air mixture. At any selected constant temperature a series of experiments was carried out, beginning at the minimum pressure indicated on the curve; in subsequent experiments the initial pressures were gradually raised to a

degree when the ignitions were either dangerously violent or the lags too short for accurate recording.

Before carrying out an experiment the explosion vessel was first of all evacuated by means of an Hyvac pump for 15 min. The time requisite for filling usually amounted to 0·20 sec. with the shorter and 0·45 sec. in the case of the less frequently employed longer cavity; this time varied slightly with pressure. The records showed that thermal equilibrium had been established in the mixture at the end of the filling operation.
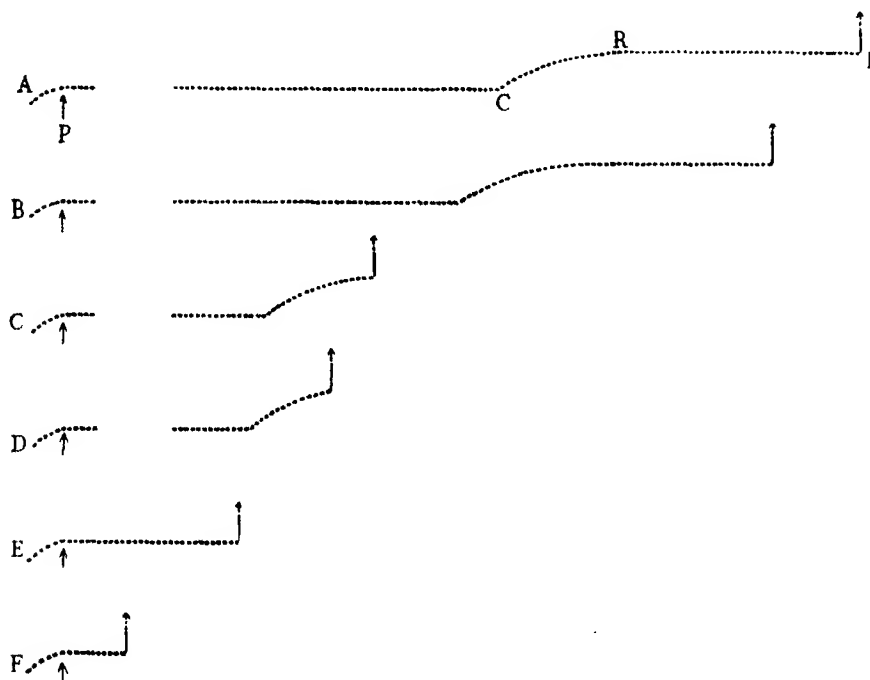
FIG. 4. A reconstruction of pressure-time records obtained with the propane-air mixture at 360° C., indicating the decrease of induction lags with pressure.

Curve	Pressure in atm.	t_1 sec.	t_2 sec.	Total time lag sec.
A	5·25	1·75	0·61	2·36
B	5·55	1·68	0·50	2·18
C	6·80	1·36	0·19	1·55
D	7·45	1·34	0·14	1·48
E	9·30	—	—	0·29
F	11·00	—	—	0·10

RESULTS

The curves A to F, fig. 4, illustrate records obtained of ignitions of a propane-air mixture in the cool-flame temperature range. The time interval from the moment P on the curve to the point C measures the induction lag prior to the formation of a cool flame and will be referred to as t_1. During t_1 pressure increase is not appreciable, and that accompanying the cool flame is indicated by the sloping part of the curve CR. A subsequent slow increase in pressure preceded true ignition, which occurred at I. The induction lag between the cool-flame formation C and the occurrence of true ignition at I is denoted by t_2. The curves have been reconstructed on the same scale in fig. 4 to show the decrease in t_1 and t_2 with increasing pressure for the propane-air mixture at $360°$ C. A record as actually obtained for the type of ignition illustrated by curves A and B, fig. 4, is reproduced in fig. $4a$; it should be understood that this record was originally fastened to the camera drum and that the curve is continuous as indicated by the asterisks. The period of interruption is $\frac{1}{100}$ sec.
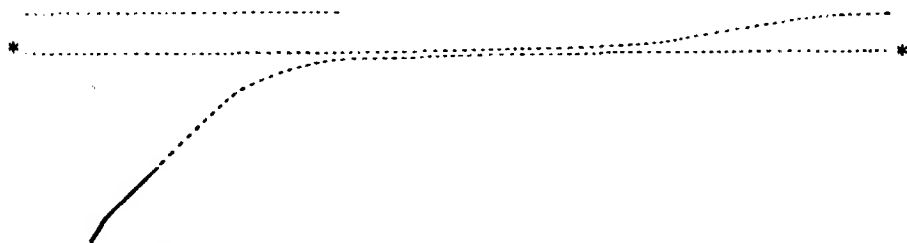
Fig. $4\,a$. Reproduction of an actual pressure-time record.

As the initial pressure was raised the intensity of ignition became greater; also, its influence was more marked in reducing t_2 than t_1, and on the attainment of a critical pressure this eventually resulted in the occurrence of true ignition apparently without the prior separate formation of a cool flame. The elimination of t_2 also corresponded with a sharp acceleration of the pre-ignition reactions, the induction lag now diminishing with surprising rapidity even for very small further pressure increments, so that at pressures above 12 atm. the explosive mixtures ignited before the filling operation was complete. Reference to Tables I and II show this behaviour to be quite general with the propane-air mixture, irrespective of the experimental conditions, although the actual pressure in any particular case, at which the transition from a two- to a single-stage process occurred, varied. If t_1, t_2 and $t_1 + t_2$ are plotted against pressure, curves as illustrated in fig. 5A (cf. a temperature of $352°$ C., Table II) are obtained.

TABLE I. INFLUENCE OF PRESSURE ON INDUCTION LAGS WITH A
6·5% PROPANE-AIR MIXTURE. EXPLOSION CAVITY $3\cdot2 \times 3\cdot5$ CM.

Temp. °C.	Pressure in atm. Propane + oxygen Pt	Total P	Induction lags in sec. t_1	t_2	$t_1 + t_2$	$t_1 Pt$	$(t_1 + t_2) Pt$
335	1·47	5·65	8·92	0·78	9·70	13·12	14·28
	1·60	6·15	8·66	0·44	9·10	13·85	14·56
	1·82	7·00	8·30	0·20	8·50	15·14	15·50
	2·03	7·80	8·05	0·05	8·10	16·30	16·40←
	2·31	8·90			$t = 0\cdot39$		$tPt = (0\cdot90)$←
					Mean 14·60		15·46
348	1·35	5·20	3·46	0·95	4·41	4·68	5·96
	1·44	5·55	3·36	0·60	3·96	4·85	5·72
	1·61	6·20	2·86	0·35	3·21	4·61	5·17
	1·83	7·05	2·54	0·24	2·78	4·66	5·09
	2·08	8·00	2·41	0·14	2·55	5·00	5·31←
	2·68	10·30			$t = 0\cdot12$		$tPt = (0\cdot889)$←
	2·88	11·10			0·04		(0·333)
					Mean 4·76		5·45
353	1·37	5·28	3·30	0·48	3·78	4·53	5·18
	1·42	5·45	3·20	0·33	3·53	4·53	5·00
	1·63	6·25	2·90	0·20	3·10	4·73	5·05
	1·85	7·10	2·62	0·08	2·70	4·66	4·98
	2·05	7·90	2·53	0·03	2·56	5·18	5·25←
	2·28	8·75			$t = 0\cdot32$		$tPt = (1\cdot16)$←
	2·38	9·16			0·30		(1·70)
					Mean 4·73		5·09
360	1·36	5·25	1·75	0·61	2·36	2·38	3·22
	1·44	5·55	1·68	0·50	2·18	2·43	3·14
	1·60	6·15	1·33	0·32	1·65	2·13	2·64
	1·77	6·80	1·36	0·19	1·55	2·41	2·74
	1·94	7·45	1·34	0·14	1·48	2·59	2·87←
	2·42	9·30			$t = 0\cdot29$		$tPt = (0\cdot70)$←
	3·02	11·00			0·10		(0·30)
					Mean 2·39		2·92
367	1·32	5·08	1·34	0·75	2·09	1·77	(2·76)
	1·42	5·45	1·17	0·51	1·68	1·66	2·38
	1·56	6·00	1·08	0·31	1·39	1·69	2·17
	1·74	6·70	0·92	0·17	1·09	1·61	1·90
	1·95	7·50	0·72	0·13	0·85	1·41	1·66←
	2·42	9·30			$t = 0\cdot09$		$tPt = (0\cdot22)$←
					Mean 1·59		1·95
				t		tPt^4	
437	1·35	5·20		4·84		16·26	
	1·43	5·50		3·24		13·48	
	1·58	6·10		1·90		12·07	
	1·74	6·70		1·21		11·1	
	1·93	7·45		0·78		10·9	
	2·12	8·15		0·49		9·83	
	2·37	9·10		0·33		8·66	
	2·48	9·55		0·24		9·65	
	2·91	11·20		0·10		7·23	

← Indicates the pressures between which the two stages are replaced by
a single-stage process.

TABLE II. INFLUENCE OF PRESSURE ON INDUCTION LAGS WITH A 6·5% PROPANE-AIR MIXTURE. EXPLOSION CAVITY 3·2 × 15 CM.

Temp. °C.	Pressure in atm.		Induction lags in sec.				
	Propane + oxygen Pt	Total P	t_1	t_2	$t_1 + t_2$	$t_1 Pt$	$(t_1 + t_2) Pt$
347	1·22	4·70	3·58	0·93	4·51	4·38	(5·52)
	1·29	4·97	3·46	0·66	4·12	4·47	5·32
	1·44	5·53	3·15	0·41	3·56	4·53	5·11
	1·63	6·28	2·80	0·24	3·04	4·57	(5·41)
	1·78	6·85	2·49	0·20	2·69	4·43	4·78
	1·99	7·65	2·19	0·11	2·30	4·17	4·58
	2·26	8·70	1·84	0·10	1·94	4·17	4·39←
	2·76	10·60			$t = 1·35←$		$tPt = (3·72)←$
	3·09	11·90			0·74		(2·29)
						Mean 4·39	4·75
352	1·18	4·55	2·23	0·88	3·11	2·64	(3·68)
	1·29	4·95	2·08	0·49	2·57	2·68	3·31
	1·44	5·55	1·68	0·38	2·06	2·42	2·98
	1·57	6·05	1·47	0·22	1·69	2·31	2·66
	1·78	6·85	1·49	0·08	1·57	2·66	2·80
	1·81	7·12	1·34	0·11	1·45	2·43	2·63
	1·99	7·65	1·44	0·08	1·52	2·86	3·20
	2·52	9·70	1·18	0·05	1·23	2·98	3·10←
	2·75	10·60			$t = 0·34$		$tPt = (1·78)←$
	3·07	11·80			0·22		(0·68)
						Mean 2·62	2·95
374	1·22	4·67	0·96	0·81	1·77	1·166	(2·17)
	1·29	4·95	0·85	0·63	1·48	1·096	1·91
	1·42	5·45	0·71	0·38	1·09	1·006	1·54
	1·66	6·40	0·70	0·17	0·87	1·165	1·45
	2·10	8·07	0·50	0·14	0·64	1·048	1·342
	2·52	9·70	0·35	0·09	0·44	0·883	1·11←
	2·86	11·00			$t = 0·17$		$tPt = (0·49)←$
	3·04	11·70			0·13		(0·42)
	3·28	12·60			0·04		(0·13)
						Mean 1·061	1·47

TABLE III. INFLUENCE OF PRESSURE ON INDUCTION LAGS WITH A 6·5% PROPYLENE-AIR MIXTURE. EXPLOSION CAVITY $3·2 \times 3·5$ CM.

Temp. °C.	Pressure in atm. Propylene + oxygen Pt	Total P	Induction lags in sec. t_1	t_2	$t_1 + t_2$	$t_1 Pt^2$	$(t_1 + t_2) Pt^2$
351	1·06	4·07	28·97	0·73	29·70	(33·0)	(33·9)
	1·13	4·36	18·70	0·51	19·21	24·0	24·6
	1·29	4·96	12·70	0·19	12·89	21·1	21·4
	1·47	5·65	9·01	0·09	9·10	19·4	19·6
	1·61	6·20	7·04	0·06	7·10	18·3	18·5
	1·93	7·05	5·35	0·05	5·40	19·95	20·3
	2·09	8·06	4·08	0·05	4·13	17·9	18·1
	2·40	9·24	3·22	0·04	3·26	18·6	18·85
	2·81	10·80	2·88	0·05	2·93	22·7	23·1
	2·99	11·50	2·51	0·06	2·57	22·5	22·9
					Mean	20·5	20·8
368	1·04	4·00	12·64	0·66	13·30	(13·66)	(14·38)
	1·13	4·33	9·01	0·49	9·50	(11·46)	(12·07)
	1·26	4·87	6·70	0·55	7·25	10·72	11·58
	1·43	5·50	4·91	0·19	5·10	10·00	10·41
	1·61	6·20	3·37	0·29	3·66	8·76	9·52
	1·85	7·10	2·57	0·23	2·80	8·78	9·56
	2·11	8·10	2·01	0·17	2·18	8·86	9·62
	2·41	9·25	1·66	0·12	1·78	9·62	10·32
					Mean	9·46	10·17
380	1·05	4·04			12·10		(13·36)
	1·13	4·33	7·90	1·77	9·67	(10·04)	(12·28)
	1·26	4·85	5·05	0·65	5·70	8·02	9·06
	1·42	5·45	3·80	0·41	4·21	7·62	8·43
	1·63	6·25	2·73	0·22	2·95	7·24	7·82
	1·93	7·05	2·12	0·13	2·25	7·92	8·40
	2·11	8·10	1·56	0·17	1·73	6·93	7·70
	2·42	9·30	1·21	0·14	1·35	7·07	7·88
					Mean	7·47	8·20
					t		$t Pt^2$
437	0·99	4·20			6·02		(5·92)
	1·21	4·65			3·67		5·36
	1·31	5·05			2·97		5·09
	1·54	5·90			1·94		4·57
	1·75	6·72			1·38		4·22
	1·97	7·57			1·08		4·15
	2·18	8·40			0·91		4·32
	2·47	9·50			0·69		4·17
	2·83	10·90			0·61		4·94
	3·23	12·80			0·34		(3·55)
	3·80	14·60			0·17		(2·46)
						Mean	4·72

TABLE IV. INFLUENCE OF PRESSURE ON INDUCTION LAGS WITH A
6·5% PROPYLENE-AIR MIXTURE. EXPLOSION CAVITY 3·2 × 15 CM.

Temp. °C.	Propylene + oxygen Pt	Total P	t_1	t_2	$t_1 + t_2$	$t_1 Pt^2$	$(t_1 + t_2) Pt^2$
366	0·78	3·00	33·69	5·31	39·00	(20·50)	(23·72)
	0·83	3·18	29·07	2·93	32·00	(19·94)	(21·95)
	0·94	3·60			19·60		(17·16)
	0·98	3·78	14·79	2·21	17·00	(14·30)	(16·46)
	1·09	4·20	11·11	1·89	13·00	13·25	15·50
	1·24	4·77	7·47	1·53	9·00	11·49	14·00
	1·35	5·20	6·02	1·01	7·03	11·00	12·86
	1·54	5·90	4·29	0·81	5·10	10·14	12·04
	1·77	6·78	3·23	0·44	3·67	10·10	11·42
	1·99	7·66	2·47	0·23	2·70	9·81	(10·72)
	2·39	9·20	1·99	0·19	2·18	11·38	12·47
	2·76	10·60	1·53	0·15	1·68	11·63	12·75
	3·28	12·60	1·17	0·07	1·24	12·58	13·34
	3·82	14·70	0·94	0·04	0·98	13·72	14·30
						Mean 11·49	13·19
380	0·81	3·10	30·97	2·83	33·80	(20·18)	(22·02)
	0·87	3·33	19·67	2·13	21·80	(14·75)	(16·35)
	0·99	3·82	12·95	2·05	15·00	(12·76)	(14·78)
	1·24	4·75	6·24	0·79	7·03	9·53	10·74
	1·46	5·60	3·82	0·52	4·34	8·10	9·20
	1·72	6·60	2·58	0·22	2·80	7·55	8·19
	2·02	7·77	1·72	0·18	1·90	7·02	7·76
	2·47	9·50	1·36	0·11	1·47	8·31	8·98
	2·99	11·50	0·82	0·06	0·88	7·73	7·88
	3·51	13·50	0·62	0·04	0·66	7·63	8·12
						Mean 7·98	8·90

TABLE V. INFLUENCE OF PRESSURE ON INDUCTION LAGS WITH A
25% PROPANE-OXYGEN MIXTURE. EXPLOSION CAVITY 3·2 × 3·5 CM.

Temp. °C.	Pressure in atm. total Pt	t_1	t_2	$t_1 + t_2$
378	1·70	0·40	0·66	1·06
	1·76	0·42	0·44	0·86
	1·92	0·35	0·24	0·59
	2·03	0·30	0·23	0·53
	2·10	0·25	0·16	0·41
	2·24	0·17	0·13	0·30
402	1·68			$t = 1·45$
	1·77			1·09
	1·92			0·59
	2·14			0·34
	2·30			0·17
434	1·66			3·29
	1·73			2·83
	1·80			1·45
	1·97			0·64

TABLE VI. INFLUENCE OF PRESSURE ON INDUCTION LAGS WITH A 25% PROPYLENE-OXYGEN MIXTURE. EXPLOSION CAVITY $3 \cdot 2 \times 3 \cdot 5$ CM.

Temp. °C.	Pressure in atm. total Pt	Induction in lags sec.				
		t_1	t_2	$t_1 + t_2$	$t_1 Pt^2$	$(t_1 + t_2) Pt^2$
376	0·90			14·00		11·3
	0·99			10·00		9·8
	1·17	7·05	0·55	7·60	9·66	10·4
	1·48	4·70	0·33	5·03	10·3	11·0
	1·64	4·31	0·25	4·56	11·6	12·25
					Mean 10·52	10·95
407	0·93			7·45		6·41
	1·09	5·43	0·62	6·05	6·41	7·41
	1·25	5·30	0·68	5·98	(8·27)	(9·33)
	1·50	3·32	0·53	3·85	7·47	8·66
	1·64	2·20	0·44	2·64	5·92	7·10
					Mean 6·60	8·30

The behaviour of the propylene-air mixture (Tables III and IV) differed somewhat from that of the propane-air mixture, for an increase in pressure was recorded before the appearance of a cool flame; moreover, the cool flames were so feeble that t_1 and t_2 could not be separately measured at the lowest pressures. The curve for $t_1 + t_2$ (fig. 5B) was also quite smooth, and not only were the lags very much longer but there was no indication of any rapid decrease in the induction lags at a critical pressure over the range studied as had been observed with the propane-air mixture.

At temperatures above 410° C., with both propane and propylene ignition was always preceded by a gradual pressure rise indicative of a slow reaction, and the induction lags decreased quite regularly.

So long as the two-stage process was operative the relation between induction lags and initial pressure was found in all cases to obey the general expression tPt^n = constant, where Pt = the sum of the partial pressures of combustible and oxygen. Thus, between 330 and 400° C. the relationships $t_1 Pt$ = constant and $(t_1 + t_2) Pt$ = constant held satisfactorily in the case of propane. When the two-stage was replaced by the single-stage process $t Pt$ ceased to be a constant and had a rapidly diminishing value. Above the cool-flame temperature range, e.g. at 437° C., the expression $t Pt^n$ = constant was found to hold best when n is between 4 and 5.

In the case of propylene, the relation $(t_1 + t_2) Pt^2$ = constant was found to hold over the whole temperature range investigated, a similar relation $t_1 Pt^2$ = constant being also applicable in respect of the cool-flame lags whenever they could be separately estimated.

With propane, t_2 was initially sometimes as long as t_1 (cf. Table I), though

it always decreased more rapidly with increase in pressure; and, although the minimum ignition pressure was greater by about 0·6 atm. when the shorter cavity was in use, the two-stage gave place to the single-stage process at a pressure lower than that found with the longer cavity.

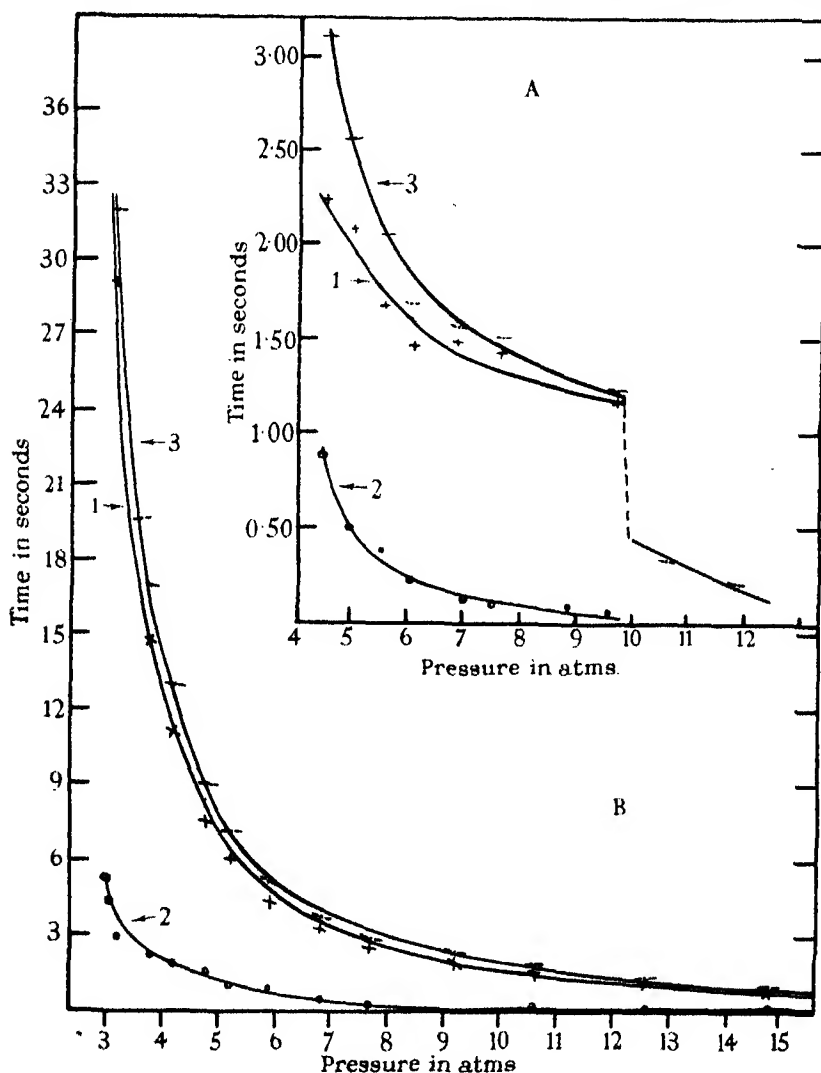With regard to the relationship between the spontaneous ignition experi-

FIG. 5. Variation of induction lags with pressure. A. Propane-air mixture at 352° C. Curves 1, 2 and 3 represent the variation of t_1, t_2 and t_1+t_2, respectively. B. Propylene-air mixtures at 366° C. Curves 1, 2 and 3 represent the variation of t_1, t_2 and t_1+t_2, respectively.

ments under pressure and "knock", it is important to note that with both propane and propylene at pressures much above the minimum required for spontaneous ignition, the latter were accompanied by a sharp metallic "knock" and were so rapid and violent that the manometer disk was frequently subjected to permanent deformation. In the case of propane this was first observed at pressures corresponding with the transition from the two- to the single-stage ignition and with propylene above 10 atm.

When hydrocarbon-oxygen mixtures undiluted with nitrogen were used, the ignitions were so sensitive to shock effects that reproducible results could not be obtained unless the filling time was increased almost to 1 sec. Under conditions where the induction lags were of the order of 2 sec. or more, as was the case with propylene over the pressure range covered, the slower rate of filling had no appreciable influence and the previously determined relationships were found to hold (see Table VI). With propane, however, the subsequent reaction rate was so rapid that it was considered *inadmissible in most cases to calculate in detail numerical constants and derive expressions for the variation of induction lags with pressure. Still it can be seen from Table V that the general influence of pressure is similar to that observed with propane-air mixtures.

DISCUSSION

The work as a whole has directed attention to the difference between the relative influence of the cool flame reactions on the auto-ignition of propane and propylene respectively (cf. Kane and Townend 1937). To compare the change in their reaction velocities with rising temperature, in fig. 6, the induction lags for the two-stage ignitions $(t_1 + t_2)$, at constant pressures of 5·7 and 7·1 atm., have been plotted against temperature. With propane the resulting curves have a minimum at *ca.* 400° C., corresponding with a maximum speed of reaction near the upper temperature limit for cool flames and agreeing with similar observations relating to a negative temperature coefficient of reaction velocity (cf. Newitt and Thornes 1937). With propylene, however, the curve exhibits no irregularity and the reaction velocity as indicated by the induction lags rises regularly with temperature. It appears likely, therefore, that in the case of propane, the cool flames arise as an outcome of a primary oxidation, but with propylene only from a slower secondary process less likely to influence the main reaction. In neither case do the results agree with the observation of Andreev with butane-oxygen mixtures (loc. cit.), that the sum of $t_1 + t_2$ is practically a constant over the temperature range 333–461° C.

It has also been discovered that at a critical pressure, in any particular case, the reactions involving a two-stage process abruptly cease to function. Moreover, they become so rapid that a kinetic interpretation based on the lines suggested by Neumann or Prettre (cf. Introduction) and derived from experiments carried out at low pressures, is no longer tenable.

The oxidation of the higher paraffin hydrocarbons may be regarded as involving two co-existent processes involving chain reactions, such as

$$A \xrightarrow{\quad k_1 \quad} (B) \xrightarrow{\quad k_2 \quad} C \tag{1}$$

and

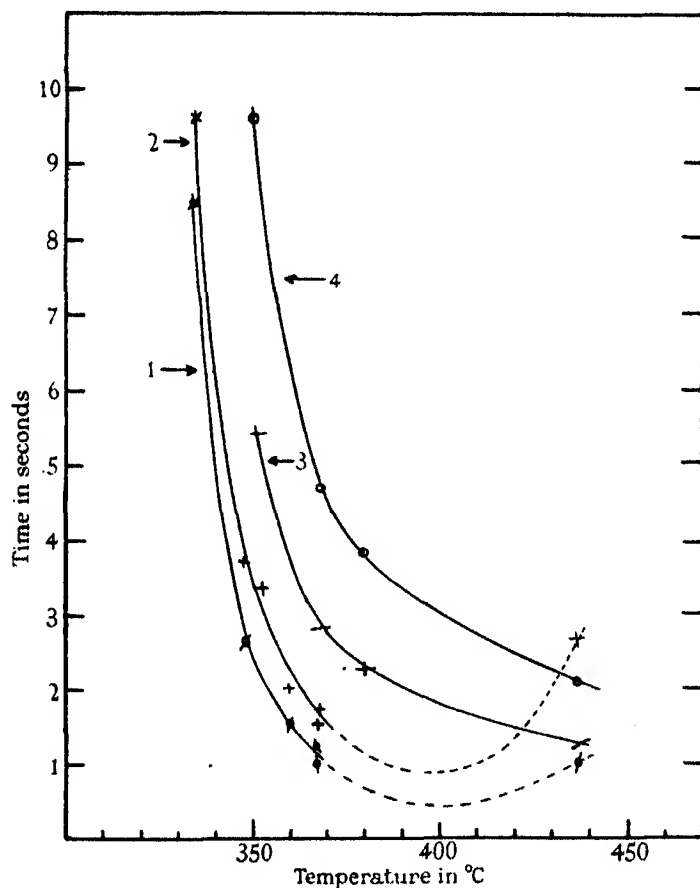$$A \xrightarrow{\quad k_3 \quad} C, \tag{2}$$
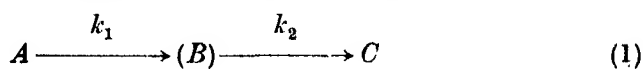
Fig. 6. The variation of induction lag with temperature, for constant pressures. Propane: curves 1 and 2, at 7·1 and 5·7 atm. respectively. Propylene: curves 3 and 4 at 7·1 and 5·7 atm. respectively.

where (1) denotes the two-stage process with a comparatively stable active intermediate compound B, and (2) a direct oxidation which may consist of several transitory stages. The process $B \longrightarrow C$ is apparently sensitive to rise in temperature or pressure, both of which favour an acceleration of k_2 and a rapid diminution of the induction lag t_2. The overall rate of reaction from $A \longrightarrow C$ in (1) likewise depends upon the ratio k_2/k_1, the two velocity constants, and will generally increase with temperature. But the stability of B has a dominating influence on the processes giving rise to cool flames, and at *ca.* 400° C., when the rate of its decomposition is presumably faster than that of its formation, there is a limit to cool-flame initiation. The reaction centres arising from the oxidation of B appear to be also capable of directly inducing the reaction $A \longrightarrow C$ and thus of accelerating k_3, with the result that at sufficiently high pressure reaction (2) will become dominant and the slower two-stage process eliminated. With the propane-air mixture, a pressure of about 8 atm. conditions such a transition and the subsequent induction lags decrease very rapidly with further increase in initial pressure. Above 400° C., owing to the rapid decomposition of B, the acceleration of the process indicated by k_3 by mutual interaction becomes less with rise in temperature, thus accounting for the observed decrease in reaction velocity in this region.

In the case of propylene the ignition seems to be mainly the outcome of (2), for the cool flames giving rise to B appear only as the outcome of a later stage in the oxidation process. Consequently its concentration is never large enough seriously to influence the velocity of reaction k_3 until very much higher pressures are reached than in the case of propane.

It is also now clear that under the conditions prevailing in internal combustion engines the slow-combustion processes would lead to a single-stage ignition and that cool flames would have no measurable separate existence. The present investigation has also shown that if induced by the spontaneous reactivity of the charge ahead of the flame, the ultimate explosion will always be of a knocking type, provided a critical pressure characteristic of the mixture has been attained. Moreover, it can now be seen that the conditions referred to would occur at pressures lower than those which could hitherto have been predicted from determinations of the lags at pressures not greatly exceeding the minimum ignition pressures.

No attempt has yet been made to study the influence of pressure on the induction lags of hydrocarbons containing more than three carbon atoms; for, while much the same behaviour might be predicted as has been found with propane and propylene, the rate of reduction of lag with pressure would

probably be so rapid as to render impossible such a detailed study of the processes operative as has now been made.

It is also a matter of interest to observe that extrapolations from the figures given in Tables II and IV would indicate that for ignition to occur at say 360° C., within a time interval of 0·005 sec. the pressures necessary would exceed 12 atm. for the propane- and 15 for the propylene-air mixture, respectively. In order to attain such pressures adiabatically the compression temperatures would no doubt exceed the upper cool flame limits (fig. 3) as may be seen from the following approximate figures due to Pye (1931):

Compression ratio	Max. compression pressure (lb. per sq. in.)	Max. compression temperature ° C.
4	92·5	313
5	125	362
6	159	399
7	195	434

Beyond the cool-flame limit the reaction velocity for propylene continues to increase while that for propane temporarily decreases (cf. fig. 6). This accounts for the apparent anomaly of the knock-rating for propane (12) being greater than that for propylene (8·4). With all higher hydrocarbons the pressures and temperatures required for the attainment of similar conditions would probably fall within the cool-flame ignition range, and the requisite pressures would probably be much lower than for propane, as is indicated by the difference in the critical compression ratios for "knock".

SUMMARY

Previous investigations into the spontaneous ignition under pressure of the higher paraffins and olefins containing more than three carbon atoms have shown that in the temperature range between *ca.* 270 and 400° C., ignition occurs by a two-stage process preceded by an induction lag t_1 before the formation of a cool flame and a second lag t_2 before the subsequent ignition of the cool-flame products; increasing pressure shortens both these lags, and although kinetic relationships have been developed it has not been

possible adequately to test them hitherto, owing to the extreme violence of the ignitions at pressures much above the minimum ignition pressure.

An optical recording manometer is described whereby it has been possible to measure t_1 and t_2 at pressures up to 15 atm. with an accuracy of $\frac{1}{100}$ sec.

With propane t_2 decreases more rapidly than t_1 with increasing initial pressure, and at a critical pressure (about 8 atm.) the two-stage is replaced by a single-stage process; the induction lag then decreases very rapidly with pressure. With propylene, where the induction lags are much greater, no such transition had occurred at pressures up to 12 atm.

The bearing of these results, both on the nature of the kinetic processes operative and on the problem of "knock", is briefly discussed.

REFERENCES

Andreev 1937 *Acta Phys. chim. U.S.S.R.* **6**, 57.
Crowe and Grimshaw 1931 *Philos. Trans.* A, **230**, 39.
Egerton and co-authors 1938 "The Science of Petroleum", **4**.
Kane, Chamberlain and Townend 1937 *J. Chem. Soc.* p. 436.
Kane and Townend 1937 *Proc. Roy. Soc.* A, **160**, 174.
Neumann and Aivazov 1936 *Z. Phys. Chem.* B, **33**, 349.
Neumann and Egorow 1932 *Phys. Z. Sowjet.* **1**, 700.
Neumann and Tutakin 1936 *C.R. Acad. Sci. U.R.S.S.* **4**, 127.
Newitt and Thornes 1937 *J. Chem. Soc.* p. 1669.
Pye 1931 "Internal Combustion Engine", p. 115.
Prettre 1936 *Ann. Comb. Liquides*, **11**, 669.
Townend and co-workers 1934 *Proc. Roy. Soc.* A, **146**, 113 et seq.

The disintegration of boron by slow neutrons

By C. O'Ceallaigh*, M.Sc., *Trinity College* and

W. T. Davies, M.A., *Selwyn College, Cambridge*†

[Plates 5–7]

The distintegration of boron by neutrons has been studied by a number of workers, and it has been established that it may take place in accordance with two equations

$$_5\text{B}^{10} + {_0}n^1 \rightarrow {_3}\text{Li}^7 + {_2}\text{He}^4 + Q_1, \tag{1}$$

$$\rightarrow {_1}\text{H}^3 + {_2}\text{He}^4 + {_2}\text{He}^4 + Q_2. \tag{2}$$
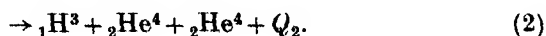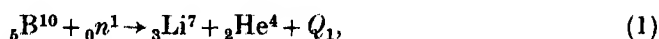
From the values of the nuclear masses at present accepted, it may be calculated that the energy release Q_1 is $2\cdot99 \times 10^6$ e-volts, while Q_2 is only about $0\cdot4 \times 10^6$ e-volts. Observed disintegrations, if caused by slow neutrons, must therefore be of the two-particle type described by equation (1).

The results of experiments carried out by different methods are not in very good agreement. More especially are previous range determinations in the cloud chamber open to very serious objections. For these reasons it was felt that the existing situation might be clarified by a more extended study of the ranges of the disintegration products in a cloud chamber.

The experiments now to be described were begun in the early summer of 1936. When about 500 photographs had been taken one of us (W. T. D.) left Cambridge. The measurements and subsequent work were carried out by the other author. The yield from the first source not being satisfactory, it was decided to make a fresh determination using a much stronger source. The published curves are based entirely on this second series of photographs.

Previous methods of investigation

Five distinct methods of investigation have been brought to bear on this problem:

(1) Ionization chamber coupled to a linear amplifier (Chadwick and Goldhaber 1935; Amaldi, d'Agostino, Fermi, Pontecorvo, Rasetti and Segré 1935; Wahlen 1936).

(2) Ionization chamber and Hoffmann electrometer (Rotblat 1936).

* 1851 Exhibition Scholar, National University of Ireland.
† At present at Bedford College, London.

(3) Proportional Geiger-Müller counter (Haxel 1937; Fünfer 1937).

(4) Impregnated photographic emulsion (Taylor and Goldhaber 1935).

(5) Range determinations in cloud chamber (Kurtschatow, Kurtschatow and Latychew 1935; Roaf 1936).

As we have observed, the agreement between these independent determinations is not satisfactory. The electrical counting methods agree in assigning to the lithium particle a range lying between 3 and 4 mm., and to the α-particle a range between 8 and 9 mm. Haxel (1937), however, finds three distinct ranges (4·1, 6·4, 9·4 mm.). The first of these he attributes to the lithium particle, and the others to α-particles of which, presumably, that having a range of 6·4 mm. would correspond to the formation of the lithium nucleus in an excited state. The results of the expansion chamber and photographic emulsion experiments are inherently much less conclusive. In either method the same difficulty arises. Owing to the negligible momentum of the incident neutron, the conservation laws require that the lithium and helium nuclei be emitted in opposite directions. While, therefore, the sum of the ranges may be measured with reasonable accuracy, the calculation of the fraction of the total length due to each is subject to great uncertainty. An attempt to deduce this ratio from theoretical considerations has been made by Roaf (1936), but the result for R_α/R_{Li} of 0·915 may be shown to proceed from false assumptions. Kurtschatow and others (1935) arrived at an estimate of the partition ratio by measuring the lengths of the particles in disintegrations caused by neutrons of appreciable momentum. In such cases the nuclei will be emitted at an angle to each other which is different from 180°, thus rendering the point of origin clearly visible. This procedure is obviously unsatisfactory, and also leads to values for the ranges which are too high. Two methods remain which are free from objection. According to the measurements of Fünfer (1937) the density of ionization along the track of a lithium nucleus of 4 mm. range is about twice that of an α-particle of the same range. Although, apparently, this difference cannot be appreciated by eye, it should be quite feasible to arrive at an accurate estimate by photometry of the combined track.* The other method is the one which we have used and will now describe.

EXPERIMENTAL METHOD

It will be clear that to calculate the total energy release in any two-particle reaction, it is necessary only to determine the range of one particle, if for that

* This is the experimental method used by Bower, Bretscher and Gilbert as described on p. 94.

particle the law connecting range with energy is known. In the case under discussion it is a consequence of the conservation laws that the total energy release Q_1 is $\frac{14}{3}$ times that of the α-particle. This may be calculated from its range using the range-energy relations. It is unfortunate that the range of the α-particle lies in just that region for which the range-energy relations are most in doubt. Recently, however, a redetermination has been carried out in this laboratory by Blewett and Blewett.* As we shall see later there is considerable ground for the belief that their results may be more reliable in the region of ranges less than 1 cm. than others hitherto proposed.

In our experiments the boron, instead of being present in the chamber in the form of a gaseous compound, was spread in an even layer on the surface of a thin copper foil. The foil extended diametrically across the chamber and was stretched tightly between glass supports so that its plane was accurately at right angles to that of the chamber which was horizontal. The appearance of the foil as viewed by the cameras may be judged from fig. 5, Plate 5. It is visible as a thin white line extending across the chamber and joining the two circular supporting buttons. The origin of any track arising in the boron layer could be fixed to better than 0·2 mm.

Amorphous boron was finely powdered and mixed with distilled water. The suspension so formed was painted on to the copper using a camel-hair brush. In the first series of experiments an attempt was made to spread a layer of negligible stopping power (1/100 mg. boron per cm.²), and although this appeared fairly even when examined under a low-power microscope, it is believed that it is practically impossible to spread a really uniform thin layer using such methods. On the other side of the foil a much thicker layer was painted, the stopping power of which was in excess of a centimetre of air.

In the second series of experiments one side of the foil was left free from boron, while a thick layer was applied to the other. The advantage of the thick layer is that no difficulty can arise owing to slight inequalities in thickness, and the larger yield of particles allows of an accurate measurement of the ranges by inspection of the shape of the number-range curves.

The chamber

The chamber was of a standard piston design 17 cm. in diameter and 5 cm. in depth. The cycle of operations was controlled by an automatic drive of the type described by Blackett (1929). No new feature was incorporated. In order to minimize the heavy background caused by electron recoils from the γ-radiation from the Ra–Be source a difference of potential

* In course of publication.

of about 250 V was maintained continuously across the chamber. This also aided the selection of tracks of a suitable age for measurement. Tracks of particles which had entered the chamber before the completion of the expansion, and for which, in consequence, the stopping power of the chamber gas could not be calculated, are separated into two parallel lines of droplets.

Stopping power of chamber gases

The gas in the chamber consisted of a mixture of about 80 % helium, 20 % air and water vapour, and had a stopping power for 8 mm. α-particles which varied between 0·241 and 0·269 in different runs. In no single run, however, was the variation between the initial and final values greater than 0·5 %. The helium used to fill the chamber was 99·9 % pure and was made available through the courtesy of the Director of the Royal Society's Mond Laboratory. It was collected and stored over water. At each filling this stored helium was fed into the chamber through an absorption system consisting of a P_2O_5 drying tube in series with a tube filled with animal charcoal and immersed in liquid air. Thus, since the constitution of the chamber gases was known with great accuracy, and since the stopping power of helium for α-particles at various portions of the range has been carefully measured by Gurney (1925), it was not deemed necessary to calibrate the chamber at intervals by means of α-particles of known range. Instead, the pressure of the chamber gases with the piston in the "expanded" position, and the room temperature, were read at the beginning, middle, and end of every run.

From these observations, and the value of the barometric pressure, the stopping power of the gas at the instant of track formation could readily be calculated. Correction was made for the fact that the final pressure as recorded by the chamber manometer was slightly lower than that at which the tracks were formed. This is due to the deceleration of the piston at the end of its range of travel by a leather washer which served to seal the chamber. Details of such calculations have been given by Nimmo and Feather (1929).

The source

In the first series of experiments, the source consisted of a radium-beryllium "standard", the effective strength of which, in respect of neutron emission, was 66 millicuries of radon. Owing to the poor yield, the second series was carried out with a radon-beryllium source of initial strength 300 millicuries. Fig. 1 shows the experimental disposition. The source (S) was surrounded by a lead cylinder 2 cm. in thickness and supported centrally

in a paraffin block 22 cm. in diameter. The chamber was screened from the direct γ-radiation of the source by a wedge of lead 10 cm. in length and 8 cm. in depth, which was incorporated in the paraffin. In order further to increase the concentration of slow neutrons in the chamber, paraffin castings were supported in the positions shown in the diagram.
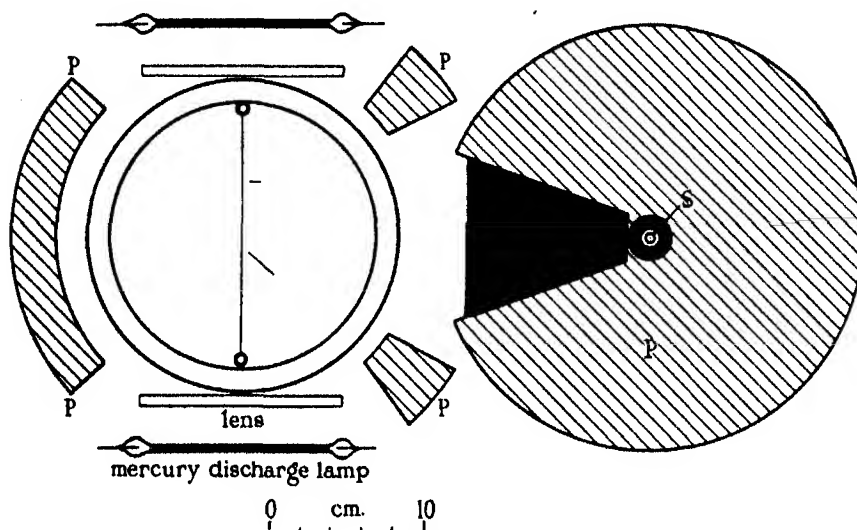
FIG. 1

Photographic arrangements

The tracks were photographed by means of a pair of cameras, the axis of one being at right angles, and that of the other at an angle of 70° to the horizontal plane of the chamber. The lenses were by Taylor Hobson and had a focal length of 35 mm. They could be worked at a maximum aperture of $f/2\cdot5$. The photographs were taken on 35 mm. standard ciné film (Ilford fine-grain Ortho). The magnification was about 1/10.

Appearance of tracks

The appearance of the photographs may be seen from fig. 5, Plate 5, which shows two typical disintegration particles together with the track of a proton recoil which passes through the thin copper foil (stopping power for α-particles 4·5 cm.). It will be noticed that the tracks are not visible right up to their points of origin, but that the foil is surrounded on each side by a dark region in which no condensation takes place. This is to be attributed, among other things, to the heat capacity of the foil which prevents the surrounding air being sufficiently cooled by the expansion to produce

supersaturation. Heavy particles are of course visible in other regions of the chamber and are of two types: (a) fine tracks of proton recoils, (b) denser tracks of helium recoils, both being produced by elastic collisions with neutrons which have escaped slowing down in the paraffin. It is therefore conceivable that such particles may be produced not far from the foil, and passing into the region of no condensation be mistaken for disintegration particles. The total number of these recoil particles was small, and the number traversing planes parallel to the foil in different regions of the chamber was quite negligible in comparison with the total number of disintegrations observed. Furthermore, when the lengths of such tracks were measured from their origins to the points of intersection with the reference lines, they were not found to fall into any particular range group. Thus, even if such recoils are included in the measurements, they cannot influence the form of the range-number curves. The elimination of protons causes no difficulty, both on account of their distinctive appearance, and of the fact that a proton recoil produced near the foil is, in most cases, visible on the other side (fig. 5, Plate 5). The precaution was taken in the second series of mounting the foil so that the boron-coated side faced the direction of the source. In this way it was hoped to diminish the possibility of including in the measurements particles resulting from disintegrations caused by neutrons of appreciable momentum.

Measurement of tracks

In all about 2000 stereoscopic pairs of photographs were taken, 500 in the first series, and 1500 in the second series. About 250 cases of disintegration were suitable for measurement. The measurement of the ranges was carried out in two ways in order to obtain the maximum of information. A large number, 180 in all, were measured by stereoscopic reprojection through the cameras, using the method described by Nuttall and Williams (1930). (In brief, a movable set of pins is adjusted so that each pin occupies the same position on both the direct and oblique images.) In this series each track was examined to see if the line of the track passed through the foil. As a precaution those tracks were rejected as suspect, of which the origins appeared to be very near the top edge of the foil. Actually, as we have seen, the number of recoils which would pass through the plane of the foil was negligibly small. This method was not very suitable for the measurement of short-range particles owing to the fact that the ends of many were obscured by patches of cloud due to the diffusion out from the region of no condensation of ions which had not been fixed by water droplets. This diffuseness rendered setting of the pins a matter of some difficulty. For these

reasons no evidence was found here for the existence of the 4 mm. group of lithium particles. Each track which was examined by reprojection was measured by three separate settings of the pins. In the majority of cases the range values so obtained were consistent to 5 %, and in the most favourable (small obliquity freedom from stray cloud, etc.) to as good as 2 %. Owing to the large number of tracks available no attempt was made to increase the accuracy of the individual measurements beyond these figures, since the dependence of the shape of the range-number curves on small errors in the ranges is slight, if a sufficient number of tracks be measured to satisfy the limitations imposed by statistical fluctuations.

Measurements were also made of the projected lengths of the tracks in the object planes both of the direct and oblique cameras. The photographs were printed on to photographic paper. The magnification was determined by printing, at the same setting of the projector, negatives of a scale photographed in the object planes of the cameras. Direct comparison of the print with the original scale gave the appropriate magnification.* These measurements were checked by comparison with those of tracks which had previously been shown by reprojection to lie in a horizontal plane. The agreement was very satisfactory. Some 230 tracks were measured in this way.

<div align="center">DISCUSSION OF RESULTS</div>

Fig. 2 shows the averaged results of the enlarger measurements on the separate direct and oblique images. Below is the range-number histogram, and above the integrated curve, i.e. the number of tracks greater than a given range plotted as a function of range. Fig. 3 gives the integrated curve for the reprojection measurements.

Before proceeding to interpret these figures we may discuss briefly the type of range-distribution curves to be expected on theoretical grounds for particles arising from neutron disintegrations in thick layers of the target substances. A thick layer is here understood to be one which has a stopping power in excess of the range of the most energetic particle produced. Neglecting effects due to straggling and scattering, and assuming (a) that the spatial distribution of the disintegration particles is isotropic,

---

* Owing to the finite depth of focus the value of the magnification μ appropriate to tracks in a plane through the centre of the foil will not hold for those in planes through the top and bottom edges. Calculation showed that μ was 3 % high at the top edge and 4 % low at the bottom, so that errors due to these causes will average out in a large series of observations.

and (b) that the reaction probability is not a function of the depth of penetration into the layer, it may readily be shown that the number of
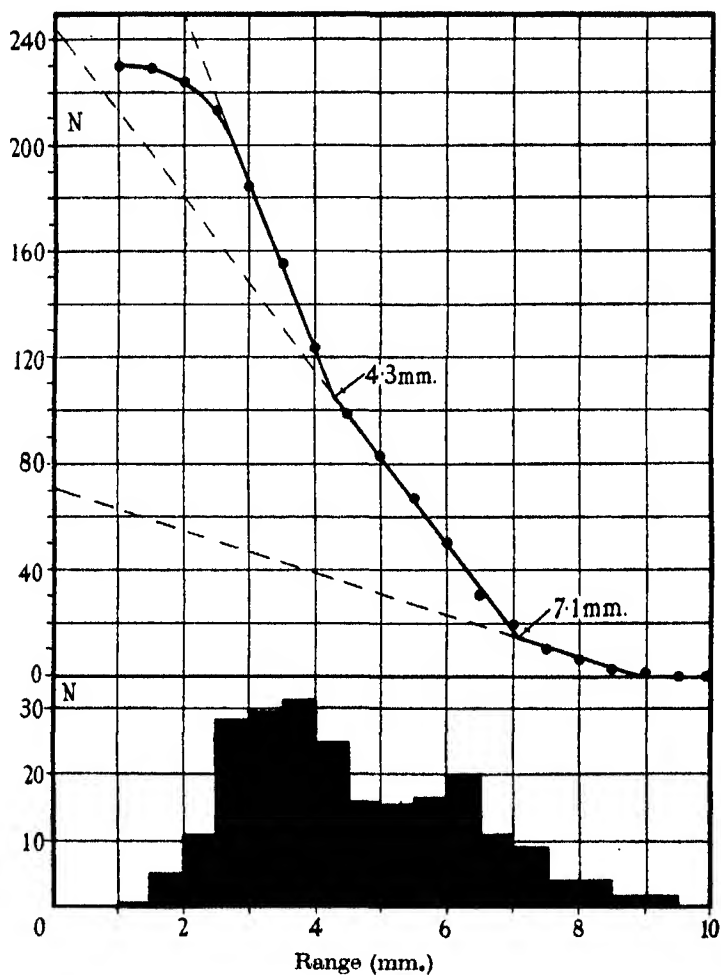
FIG. 2

particles having emergent ranges between r and $r + dr$ is given by a function of the type

$$\left(1 - \frac{s^2}{r^2}\right) dr, \tag{3}$$

where s = depth of the condensation free space already referred to (about 1 mm. in these experiments).

Furthermore, the number of particles having emergent range greater than r will be given by

$$N = \int_r^R \left(1 - \frac{s^2}{r^2}\right) dr = (R-r)\left(1 - \frac{s^2}{Rr}\right), \qquad (4)$$

where $R =$ the unretarded range of the group of particles under consideration.
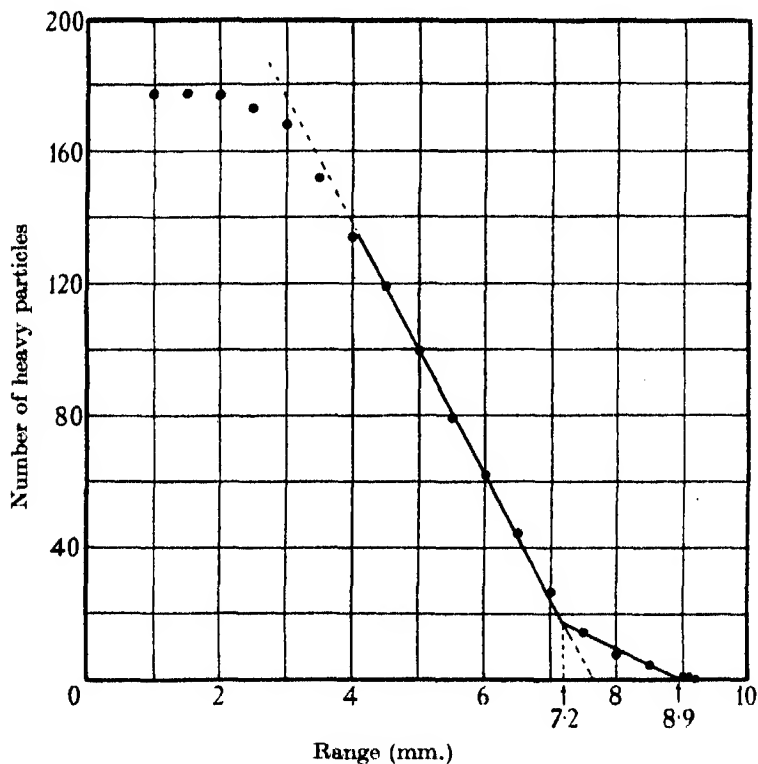
FIG. 3

It follows from (3) that the slope of the integrated curve is independent of r for values of r which are great compared to s, so that the curve is a straight line which cuts the axis at $r = R$. A more rigorous calculation which takes account of straggling has been given by Livingston and Bethe (1937a). For disintegrations caused by neutrons where the energy of the disintegration products is not a function of the depth in the layer of their points of origin, they show that the integrated curve is a straight line which gives directly on extrapolation, the *mean* ranges of the particles coming from the top layer. For comparison with the

experimental results fig. 4 shows (A) the range-number curve and (B) the integrated range-number curve plotted for four groups of particles of ranges 4·1, 5·0, 7·1 and 8·8 mm., the respective relative intensities 1·0, 0·25, 1·0 and 0·25. (A) is drawn from equation (3) and (B) from equation (4) above.
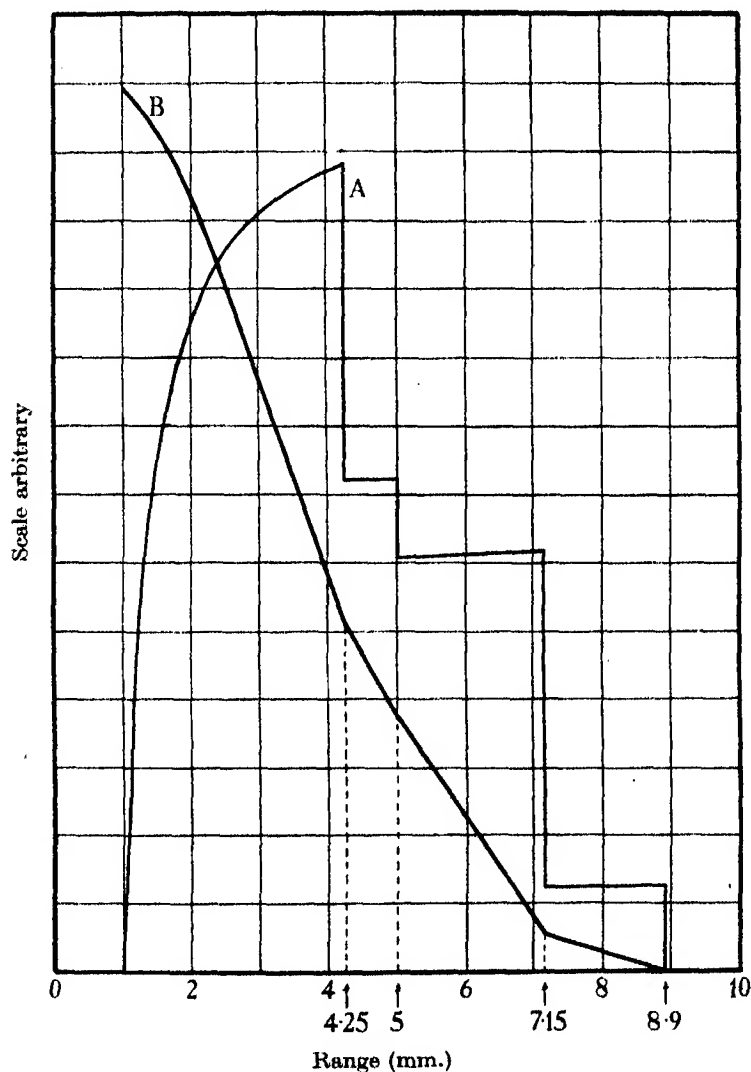
Fig. 4. Number of heavy particles.

It will be seen that the range values may be deduced from the position of the points of inflexion. In virtue of Livingston and Bethe's calculations

the ranges so obtained will be mean ranges, and the corresponding particle energy may be obtained without further correction from the range energy relations.

Bearing these facts in mind, the interpretation of the curves is clear. In fig. 2 three separate breaks occur in the integrated curve. These correspond to ranges of 4·25, 7·1 and about 8·9 mm. The 4·25 mm. range corresponds to the lithium nucleus, but the others must be due to α-particles. In fig. 3 (reprojection measurements) groups are again in evidence at 7·2 and 8·9 mm., while the 4·3 mm. group does not appear for reasons already discussed. The agreement between the results of the reprojection and enlarger determinations is satisfactory. The points of inflexion correspond, as we have noted, to mean ranges, and hence the energy releases may be calculated directly from the range-energy relations.

Owing to the small numbers involved, the determination of the exact point of intersection with the N-axis of the long-range curve is a matter of some difficulty, and in consequence the relative intensity of the two α-particle groups cannot be fixed with any precision. The total number of particles which had ranges greater than 7·3 mm. was 15. Each one of these tracks was very carefully measured by reprojection and its general appearance examined with a view to deciding its direction and whether or not it was a proton. In at least thirteen cases the question could be answered with certainty, and in the two remaining cases the general appearance strongly favoured the belief that they were α-particles. The "tail" on the curve cannot be ascribed to straggling of particles from the 7 mm. group. For particles of this range the straggling is less than 2 % = 0·15 mm. These longer range particles cannot be helium recoils passing into the condensation free space surrounding the foil, since their number was about equal to the average number of recoils of whatever range passing through planes drawn at random in the chamber. We must therefore conclude that the longer range group has a real existence. Fig. 7, Plate 7 shows one of these long-range particles. Its range was found by reprojection to be 9·2 mm. in normal air. The ratio of the intensities of the 9 and 7 mm. groups would appear from fig. 2 to be about 1 : 3, but may easily be less. The ratio cannot well be less than 1 : 6, since it could scarcely be hoped to detect so weak a group of longer range particles. Comparison of fig. 2 with fig. 4 drawn for a ratio of 1 : 4 will serve to illustrate this point.

It will also be seen that it is very difficult to detect the longer (5 mm.) group of lithium particles which should accompany the 8·9 mm. group of α-particles.

The accuracy of the measurements.

The main sources of error in the present investigation are uncertainties in the values of the stopping power of the chamber gases, and of the magnifications in the projection measurements. These are in the nature of systematic errors and cannot be expected to cancel out in a large series of observations. Owing to the precautions taken the stopping powers were probably known to 1 %. The magnifications may be in error by 2 %. Owing to the fact that the shape of the integral curves is known to be linear, errors due to faulty extrapolation may be expected to be less than those arising from the sources just discussed.

The range of the 7 mm. α-group was found to be 7·2 mm. from fig. 3 and 7·1 mm. from fig. 2. That of the longer range α-group was 8·95 mm. from fig. 3 and about the same from fig. 2. The lithium group had a range of 4·25 mm. We may therefore write, allowing for the greater uncertainty in the longer α-group:

$$R_{\text{Li}} = 4\cdot25 \pm 0\cdot2 \quad \text{mm.},$$
$$R_{\alpha_1} = 7\cdot15 \pm 0\cdot25 \text{ mm.},$$
$$R_{\alpha_2} = 8\cdot9 \ \pm 0\cdot4 \quad \text{mm.}$$

Energy release in the reaction

Two sets of range-energy data have been used to calculate the energy release in the reaction. The first (B_1) are obtained from recent curves given by Livingston and Bethe (1937b)—and the second (B_2) from curves embodying the results of Blewett and Blewett (1937) which have been privately communicated by Professor Bethe. In the region with which we are concerned, the latter data predict an energy release some 15 % higher for a given range than those formerly accepted. Table I gives a synopsis of known evidence on this reaction. The ranges of the particles found by each author are given, together with the total energy releases (E_T) calculated as $\frac{11}{7}$ that of the α-particle E_α. The difference between the total energy release observed and the value of Q_1 calculated from the mass values are listed under the headings Δ. The value of each of these quantities has been calculated from each of the two range-energy relations.

DISCUSSION

Reference to Table I shows that the majority of previous workers are agreed on the question of the range of the lithium, and of the more energetic α-particles. With the exception of Haxel, however, no worker

TABLE I

Author	Ranges mm. air 15° C. 760 mm.			E_α		E_r		Δ	
	R_α	R_{Li}	R_r	B_1	B_2	B_1	B_2	B_1	B_2
Fünfer	8·6	4·0	12·6	1·63	1·85	2·56	2·90	− 0·43	− 0·09
Rotblat	8·2	3·6	11·8	1·54	1·77	2·41	2·78	− 0·06	− 0·21
Haxel	9·4	—	—	1·80	1·98	2·83	3·11	− 0·16	+ 0·12
	6·4	4·1	10·5	1·17	1·39	1·82	2·19	− 1·17	− 0·80
Present work	8·9	—	—	1·70	1·91	2·66	3·00	− 0·33	+ 0·01
	7·15	4·25	11·4	1·32	1·56	2·08	2·45	− 0·91	− 0·54
Wahlen	8·5	—	—	1·62	1·83	2·55	2·87	− 0·44	− 0·12
	Max. range								
Kurtschatow, etc.	(9·3)	(3·0)	(12·3)						
Fermi group	7–8	—	—						
Chadwick and Goldhaber	> 5	—	—						
Taylor and Goldhaber	—	—	11·5 ± 0·5						
Roaf	5·5	6·0	11·5						

$Q_1 = 2·99 \times 10^6$ e-volts, $B^{10} = 10·0163$, $He^4 = 4·0039$, $Li^7 = 7·0182$, $n^1 = 1·0090$.

has reported the existence of a group of α-particles of shorter range. For this reason a careful examination was made of the range-number curves given by Haxel and Fünfer. It was found that by redrawing their curves it was possible to bring their results more into agreement with ours. In particular, some evidence was found in Fünfer's curve for the existence of two groups of α-particles having ranges about 7 and 8·8 mm. By neglecting the "tail" in the distribution curve he was led to a figure of 8·6 mm. obtained by extrapolation of a straight line drawn evenly between all the points. It also seemed as if Haxel's extrapolation led to too low a value for the shorter and too high a value for the longer α-particle groups. The fact that Rotblat finds a lower value both for the lithium and the maximum α-particle ranges, is possibly due to a doubtful method of calibration of his ionization chamber. The range of the lithium particle has been found by most workers to lie between 4·0 and 4·3 mm. It is reasonable to suppose that the true value is not far from 4·2 mm. The total length of the lithium-α-particle recoil has been found in three independent determinations (Roaf; Taylor and Goldhaber; Taylor and Dabholkar) to be about 11·5 mm. and 11·4 mm. respectively. (The value (12·3 mm.) found by Kurtschatow, etc., is almost certainly too high for reasons which we have already discussed

(p. 82).) Within the limits of error this figure is equal to $(4\cdot2 + 7\cdot2)$ mm. This would constitute additional evidence for the existence of a strong group of α-particles of about 7 mm. range. We are therefore driven to conclude both from our own experiments and those of other investigators, that the α-particles produced in the reaction are emitted in at least two range groups.* Weaker groups of shorter range may, of course, exist but it cannot be hoped to resolve them by methods such as we have adopted. As already mentioned it would be difficult to resolve the two close lying lithium groups which would correspond to the two α-particle ranges. The agreement between our maximum range 8·9 mm. with that reported by Fünfer (8·6 mm.) and by Wahlen (8·5 mm.) is noteworthy, and lends considerable support to our belief that these authors failed to resolve the two α-particle groups.

When this paper was in preparation for publication, the boron slow neutron disintegration was repeated in this laboratory by Bower, Bretscher and Gilbert. Using a boron rich gas in the expansion chamber they deduced the ratio R_α/R_{Li} by the method of track photometry already mentioned. Their result for the lithium range was $4\cdot3 \pm 0\cdot3$ mm. and for the α-particle group $7\cdot0 \pm 0\cdot3$ mm. both in excellent agreement with ours. They do not find any clear evidence for the existence of a longer α-particle group, and conclude that if such exists it must form less than 10 % of the stronger (7 mm.) group.†

Energy levels of Li⁷

The values of 8·9 mm. and 7·15 mm. for the α-particle ranges receive further confirmation from independent evidence for the existence of discrete energy levels of the Li⁷ nucleus. Bothe (1936) has examined the energy spectrum of the electrons produced in a thin lead plate by the γ-radiation

* It might be thought that the 8·9 mm. group of α-particles could correspond to cases of disintegration by neutrons of appreciable momentum. Assuming an energy release in the reaction of $2\cdot45 \times 10^6$ e-volts (7·15 mm. range on the B_2 relations), it may be shown that in order to project 9 mm. particles backwards, the energy of the neutron must be about 2×10^6 e-volts. The reaction cross-section is extremely small for neutrons of this energy, so that this explanation of the origin of the longer range α-particles must be rejected.

[† *Note added in proof*, 15 *May* 1938. It has been suggested to us that the particles forming the longer range group may be protons from the reaction $_5\mathrm{B}^{10} + _0n^1 \rightarrow _4\mathrm{Be}^{10} + _1\mathrm{H}^1$. The balance of energy in this reaction would result in a value for the proton range of 6·5 mm. It is just possible that errors in the values of the masses or in the range-energy relations may be sufficiently large to justify the identification of these protons with the observed 8·9 mm. group. They cannot be identified with the 7·2 mm. group for the reason that the length of the Be recoil track would be much less than the value of 4·2 mm. found for the tracks associated with this group.]

arising from the excitation without capture of lithium by α-particles. He reports two strong lines at 0.39 and 0.59×10^6 e-volts with, possibly, a weak combination line at 0.2×10^6 e-volts. Absorption measurements of this γ-radiation have been made by Webster (1932), Savel (1935), Schnetzler (1935) and Speh (1936). Their values for the γ-ray energies lie between 0.5 and 0.7×10^6 e-volts.

The reaction $_3\mathrm{Li}^6 + _1\mathrm{D}^2 \rightarrow _3\mathrm{Li}^7 + _1\mathrm{H}^1$ has been very carefully studied by Rumbaugh and Hafstad (1936)—and again by Williams, Shepherd and Haxby (1937). Two groups of protons are emitted. The energy difference corresponding to the difference in range is found to be about 0.4×10^6 e-volts. The latter authors also measured the energy of the γ-ray by absorption and arrived at a value of $0.4 \pm 0.025 \times 10^6$ e-volts. A recalculation of the figure given by Rumbaugh and Hafstad using amended range-energy relations and taking account of the energy of recoil of the lithium particle leads to a value for the excitation energy of 0.44×10^6 e-volts.

Thus, no evidence has been advanced by these authors for the existence of the higher excitation level of Li^7 of 0.6×10^6 e-volts reported by Bothe although a careful search was made for a third group of protons in the reaction quoted above. It is still a moot point, therefore, whether the Li^7 nucleus has one or two low-lying excitation levels. Indeed it would appear as if one low-lying level only is theoretically possible. The next highest level would require to be at least 2×10^6 e-volts above the ground state. (Livingston and Bethe 1937c). It is also possible, however, that transitions to the 0.6×10^6 e-volts level are forbidden in the nuclear reactions under consideration.

The present results are in agreement with these observations. The energy difference corresponding to α-particles of 8.9 and 7.15 mm. range is 0.58×10^6 e-volts on the older (B_1), and 0.55×10^6 e-volts on the newer (B_2) range-energy relations. The values of Δ (Table I) calculated directly from masses are 0.91 (B_1) and 0.54 (B_2). It is probable that the value of $Q = 2.99 \times 10^6$ e-volts calculated from the masses is not seriously in error. It has been found by Savel (1935) and by Schnetzler (1936) that the emission of neutrons in the reverse reaction, $_3\mathrm{Li}^7 + _2\mathrm{He}^4 \rightarrow _5\mathrm{B}^{10} + _0n^1 + Q_1'$, does not begin until the energy of the α-particles is 4.7×10^6 e-volts. This would make $Q_1' = -Q_1 = -2.99 \times 10^6$ e-volts in exact agreement with that deduced from the masses. We may therefore conclude that Q_1 (above) is probably not far from 2.99×10^6 e-volts, and is certainly not greater. This seems to confirm the newer B_2 range-energy relations so that we may perhaps reject the value 0.91×10^6 e-volts for the excitation energy calculated from the earlier B_1 relations.

To sum up, the present experiment leads to values for the excitation energy of the Li^7 nucleus of

(a) $0.55 \pm 0.15 \times 10^6$ e-volts from the range difference of the α-particle groups.

(b) 0.54×10^6 e-volts from the difference $\varDelta$ between Q_1 the energy release calculated from the accepted masses, and the energy release corresponding to the 7.15 mm. α-particles, the newer range energy relations of Blewett and Blewett being assumed throughout to be correct.

The limits of error given above are those deduced from the experimental uncertainties only.

Within these limits the results of the present investigation are in good agreement with the value 0.44×10^6 e-volts predicted by the ranges of the proton groups emitted in the reaction $_3Li^6 + _1D^2 \rightarrow _3Li^7 + _1H^1$. At first sight it seems difficult to reconcile with our conclusion that in at least two-thirds of the disintegrations the Li is formed in an excited state, the observation of Kikuchi, Aoki and Husimi (1936) that the intensity of the radiation emitted by boron under slow neutron bombardment is only about 5 % of that emitted by cadmium under the same conditions. If it is remembered, however, that cadmium emits a number of γ-ray groups per disintegration (probably greater than 7; cf. Griffiths and Szilard (1937), Fleischmann (1936), Kikuchi, Husimi and Aoki (1936)), and that, on the average, a Geiger-Müller counter will be about twice as sensitive to the γ-rays from cadmium as to the softer radiation from boron, this difficulty of interpretation largely disappears.*

SUMMARY

The disintegration of boron by slow neutrons—$_5B^{10} + _0n^1 \rightarrow _3Li^7 + _2He^4 + Q_1$ —has been studied in an expansion chamber. Evidence has been found for

* This suggestion has been put forward by Dr M. Goldhaber.
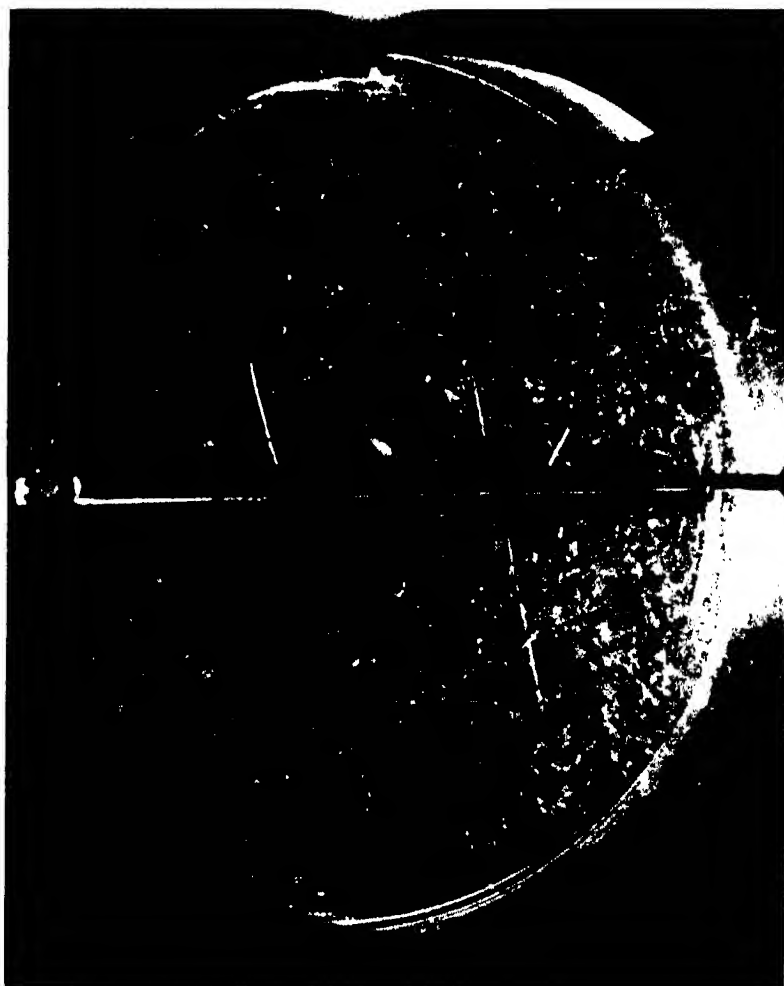
Fig. 5
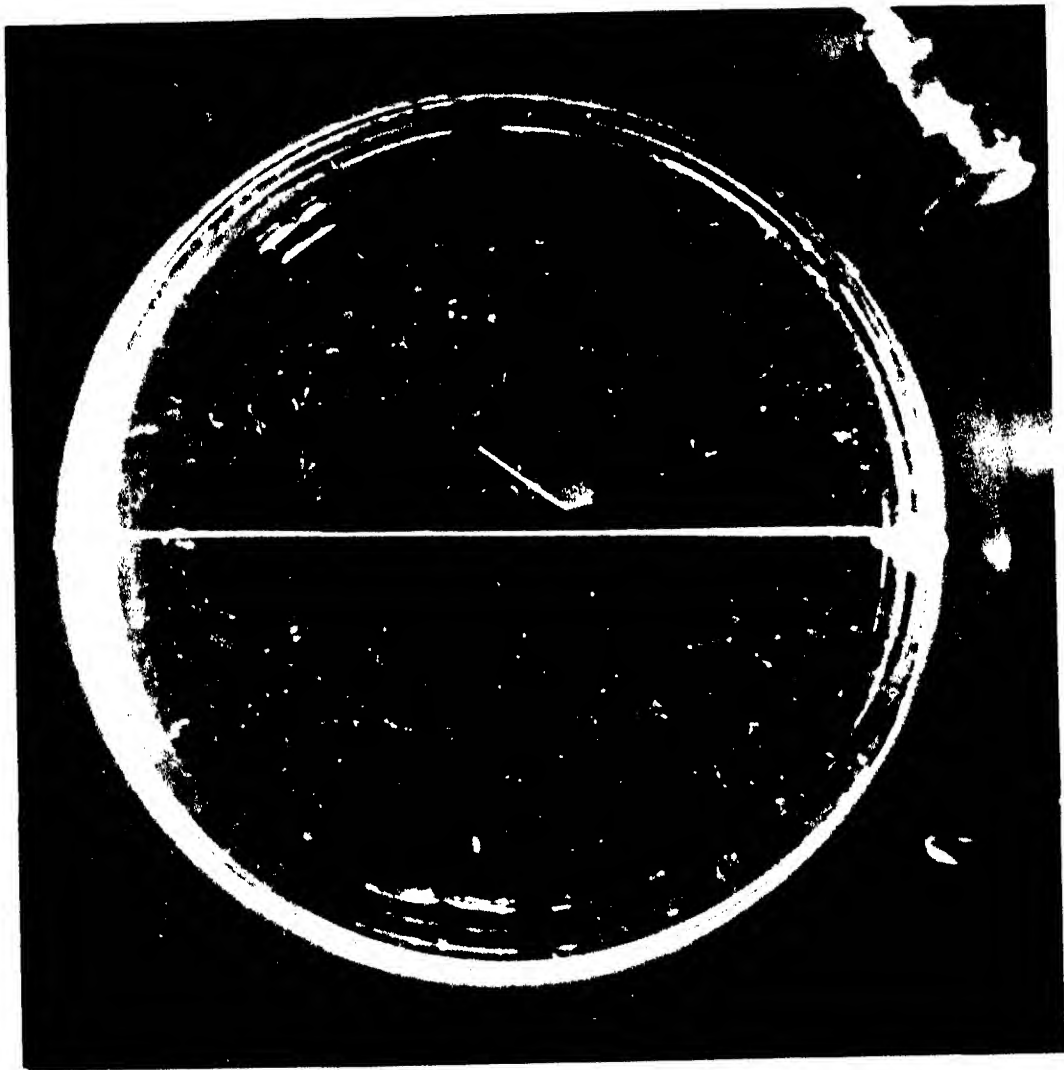
Fig. 6

FIG. 7

the emission of three groups of heavy particles of ranges $4\cdot25 \pm 0\cdot2$ mm. $7\cdot15 \pm 0\cdot25$ and $8\cdot9 \pm 0\cdot4$ mm. in air at $15°$ C. and 760 mm. The $4\cdot25$ mm. group is clearly due to the lithium nucleus. On the basis of the recent range-energy determinations of Blewett and Blewett, the $7\cdot15$ and $8\cdot9$ mm. groups, which consist of α-particles, would lead, respectively, to energy releases of $2\cdot45 \times 10^6$ e-volts and about 3×10^6 e-volts. Substitution in the equation of reaction of the values for the masses at present accepted, leads to a value for Q_1 of $2\cdot99 \times 10^6$ e-volts. The $8\cdot9$ mm. α-particles would correspond, therefore, to the production of the Li^7 nucleus in the ground state, and the $7\cdot15$ mm. particles to an excited nucleus having an energy of $0\cdot55 \pm 0\cdot15 \times 10^6$ e-volts above the ground state.

Evidence based on the emission of two groups of protons in the reaction

$$_3\mathrm{Li}^6 + {}_1\mathrm{D}^2 \rightarrow {}_3\mathrm{Li}^7 + {}_1\mathrm{H}^1$$
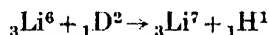
leads to the prediction of one low-lying excited state of the Li^7 nucleus of $0\cdot44 \times 10^6$ e-volts. This is confirmed by absorption measurements on the γ-radiation accompanying this disintegration. The value $0\cdot55 \pm 0\cdot15 \times 10^6$ e-volts is in satisfactory agreement with the above figure. A study of the γ-radiation arising from the non-capture excitation of the Li^7 by α-particles would seem to indicate the presence of two low-lying excitation levels of $0\cdot4$ and $0\cdot6 \times 10^6$ e-volts, but it is possible that transitions to the $0\cdot6 \times 10^6$ e-volts level are not allowed in the above reactions.

REFERENCES

Amaldi, d'Agostino, Fermi, Pontecorvo, Rasetti and Segré 1935 *Proc. Roy. Soc. A,* **149**, 542.
Amaldi 1935 *Nuovo Cim.* **12**, 223.
Blackett 1929 *Jour. Sci. Inst.* **6**, 184.
Blewett and Blewett (in publication).
Bothe 1936 *Z. Phys.* **100**, 273.
Chadwick and Goldhaber 1935 *Proc. Camb. Phil. Soc.* **31**, 612.
Curie and Joliot 1933 *J. Phys. Radium,* **4**, 278.
Fermi 1935 *Ric. Sci.* vi, **1**, 123.
Fleischmann 1936 *Z. Phys.* **100**, 307.
Fünfer 1937 *Ann. Phys., Lpz.,* **29**, 1.
Griffiths and Szilard 1937 *Nature, Lond.,* **139**, 323.
Gurney 1925 *Proc. Roy. Soc. A,* **107**, 340.
Haxel 1937 *Z. Phys.* **104**, 540.
Kikuchi, Aoki and Husimi 1936 *Nature, Lond.,* **137**, 745.
Kikuchi, Husimi and Aoki 1936 *Proc. Phys. Math. Soc. Japan,* **18**, 188.
Kurtschatow, Kurtschatow and Latychew 1935 *C.R. Acad. Sci., Paris,* **200**, 1199.
Livingston and Bethe 1937a *Rev. Mod. Phys.* **9**, 284.
—— 1937b *Rev. Mod. Phys.* **9**, 266.
—— 1937c *Rev. Mod. Phys.* **9**, 341.

Nimmo and Feather 1929 *Proc. Roy. Soc.* A, **122**, 668.
Nuttall and Williams 1930 *Proc. Phys. Soc.* **42**, 212.
Roaf 1936 *Proc. Roy. Soc.* A, **153**, 568.
Rotblat 1936 *Nature, Lond.*, **138**, 202.
Rumbaugh and Hafstad 1936 *Phys. Rev.* **50**, 689.
Savel 1934 *C.R. Acad. Sci., Paris*, **198**, 1404.
— 1935 *Ann. Phys., Lpz.*, **4**, 88.
Schnetzler 1935 *Z. Phys.* **95**, 302.
Speh 1936 *Phys. Rev.* **50**, 689.
Taylor 1935 *Proc. Phys. Soc.* **47**, 873.
Taylor and Dabholkar 1936 *Proc. Phys. Soc.* **48**, 285.
Taylor and Goldhaber 1935 *Nature, Lond.*, **135**, 341.
Wahlen 1936 *C.R. Acad. Sci., Paris*, **202**, 1500.
Webster 1932 *Proc. Roy. Soc.* A, **136**, 428.
Williams, Shepherd and Haxby 1937 *Phys. Rev.* **52**, 390.

DESCRIPTION OF PLATES

PLATE 5

Fig. 5. Two disintegration α-particles issuing from the foil, the longer having a range of 6·2 mm., and the shorter a range of 5·2 mm. A fast proton is seen to pass through the foil (stopping power for α-particles about 4·5 cm.). The heavy background is due to recoil electrons produced by the strong γ-radiation from the source.

PLATE 6

Fig. 6. From the first series of photographs. A 6·8 mm. α-particle produced in a layer of boron of negligible stopping power.

PLATE 7

Fig. 7. Two α-particles from a thick boron layer (second series). The shorter particle has a range 4·8 mm. The longer (range = 9·2 mm.) is typical of the longer range group of α-particles. The dark region within which no condensation takes place is clearly visible.

The photochemical polymerization of methyl acrylate vapour

By H. W. Melville

Colloid Science Laboratory, Cambridge

The investigation of the polymerization reactions of ethylene derivatives has defined fairly clearly the nature of the substituents most likely to favour such a reaction. For instance, it is absolutely essential to have a $=CH_2$ group at one end of the molecule, while the substituent attached to the other carbon atom at the end of the double bond may consist of a large variety of groups such as CH_3, $COOCH_3$, CN, halogen, $CH=CH_2$, etc. In the methyl methacrylate molecule, $CH_2=C(CH_3)COOCH_3$, both groups attached to the α-carbon atom are separately capable of favouring the tendency to form polymers, the methyl group probably making a contribution small compared with that of the carboxyl group since propylene is rather difficult to polymerize. Consequently, if the methyl group is replaced by a hydrogen atom the ability of the molecule to polymerize should not be greatly altered. The experiments on the photo-polymerization of methyl methacrylate vapour (Melville 1937) have shown, however, that this methyl group may play an important part in determining what type of reaction stops the growth of the polymer and thereby limits its molecular weight. Indeed, it was suggested that the long life of the growing methacrylate polymer is entirely due to the immobility of the methyl group. This has the further consequence that the cross-linking of polymers, if branching could occur, should for the same reason be practically impossible—a suggestion compatible with the straight-chain characteristics of the methacrylate polymer. The question then arises as to what will happen when the methyl group is replaced by a relatively more mobile hydrogen atom. This paper is therefore concerned with the photo-polymerization of methyl acrylate vapour which has been carried out under similar conditions to those obtaining with the methacrylate.

Experimental

The apparatus for the experiments at room temperature was identical with that used for the methacrylate vapour, while that for work at higher

temperatures consisted of a reaction vessel and a high-voltage mercury-neon lamp both enclosed in a suitable furnace (Melville 1936; Farkas and Melville 1936). The methyl acrylate as received contained 0·1 % hydroquinone as a stabilizer. This was removed by repeated distillation of the liquid *in vacuo*. Particular care was taken to free the liquid from dissolved oxygen, since this gas is a strong inhibitor for polymerization.
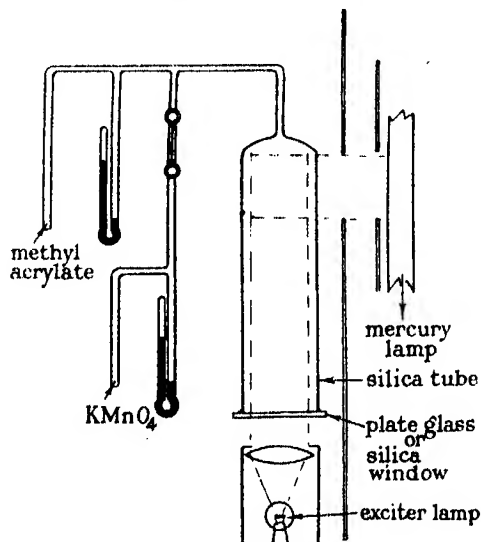
Fig. 1

Methyl acrylate polymerizes exceedingly rapidly when exposed to light of wave-length shorter than about 2700 A. With a mercury lamp yielding some 10^{16} quanta/sec. at 2537 A incident on the reaction vessel of 100 c.c., half the vapour is polymerized in about 1 min., the initial pressure being 50 mm., with the production of a dense cloud of solid polymer. In fact, the rapidity of the reaction makes it eminently suitable for demonstrating the photochemical polymerization of vapours to large audiences. The arrangement of the apparatus is shown in fig. 1. A high-voltage cold cathode mercury lamp is most suitable, as the visible radiation is not very intense. The lamp is situated a few cm. from the cylindrical reaction vessel into which a parallel beam of light is projected from an arc or metal filament lamp. This serves to show up the formation of the cloud of polymer as it settles out of the gas phase. The liquid acrylate is distilled into a side tube to which is attached a U-tube manometer, so that the experiment can be repeated several times. The inhibition by oxygen can also be shown by admitting 0·1 mm. of O_2 from a pipette. As soon as the oxygen is con-

sumed, polymerization starts immediately. The liquid acrylate in absence of oxygen and of hydroquinone polymerizes in about a day or two, and hence the apparatus is best prepared for the demonstration a few hours beforehand. Alternatively, the acrylate may be preserved in a bath of solid carbon dioxide.

If the reaction vessel is put into communication with a reservoir of liquid acrylate several c.c. of liquid may be polymerized per hour. The greater part of the polymer can be removed from the reaction vessel by washing in benzene, and the insoluble residue is best burnt off the surface of the vessel in a current of air. It is important to note that the acrylate polymer is much more stable than the methacrylate polymer, which is completely depolymerized to the monomer at $300°$ C. The acrylate polymer, on the other hand, can be partly distilled as an oil at temperatures approaching a red heat, though a considerable amount of charring also occurs.

As with the methacrylate polymerization, there is the difficulty of determining whether or not the reaction is mercury sensitized. On account of the rapidity of the acrylate polymerization a hydrogen lamp sufficed to give enough radiation to demonstrate that the polymerization is certainly a direct photochemical reaction, as the following run indicates:

Vol. of system 170 c.c. Input between 2000 and 2300 A $0·8 \times 10^{14}$ $h\nu$ sec.$^{-1}$ (estimated by the ammonia photometer). Temp. $23°$ C.

Time (min.)	0	8	12	18	24	31
Press.	50·2	47·8	46·0	43·4	41·1	39·1

Quantum yield of polymerization 5×10^3.

(The quantum yield is an upper estimate as the acrylate vapour exhibits absorption up to 2500 A.)

Employing the mercury lamp, Table I gives the details of a typical run. The fourth and sixth columns contain velocity constants calculated on the assumption that the reaction is of the second and first order respectively. Whereas the first order constants decrease rapidly as the reaction proceeds, the second order constants remain at a fairly steady value. The order of the reaction therefore approaches two. A direct comparison of the initial rates of reaction shows that the rate varies approximately as the 1·6th power of the pressure over the range 10–50 mm.

In view of the fact that the pressure does not decrease to zero on prolonged irradiation, an analysis of the products of the reaction was carried out in the following way. Methyl acrylate was illuminated with 2537 radiation for such a time that about one-half the vapour was poly-

merized. The vapour was withdrawn with liquid air and the pressure of the residual gas measured by a Pirani gauge. This procedure was repeated a number of times until 95 % of the vapour was polymerized. The residual gas, non-condensable in liquid air, proved to be hydrogen as indicated by simultaneous readings on a McLeod and a Pirani gauge. Similar behaviour was observed with the methacrylate except that the non-condensable gas was methane. It appears, therefore, that when the acrylate molecule is broken up, a hydrogen atom attached to each carbon atom is split off.

TABLE I

Input $10^{16} \, h\nu$ sec.$^{-1}$. Vol. of system 100 c.c. Temp. 20° C.

Time min.	p (M.A.) mm.	$1/p - 1/p_0$	$\dfrac{1/p - 1/p_0}{t}$	$\log p_0/p$	$\dfrac{\log p_0/p}{t}$
0	55·0	—	—	—	—
0·5	41·0	0·0062	0·0124	0·127	0·254
1·0	32·0	0·0130	0·0130	0·235	0·235
1·5	24·0	0·0236	0·0157	0·360	0·240
2·5	16·0	0·0444	0·0178	0·438	0·175
3·5	13·0	0·0588	0·0168	0·626	0·178
5·5	9·6	0·0862	0·0157	0·768	0·139
9·5	7·6	0·1136	0·0119	0·859	0·090

Temp. 33° C.

Initial press.	Initial rate mm./min.
47·6	4·4
14·0	0·66

The following figures show the relative rates of polymerization and decomposition.

TABLE II

Temp. 20° C.   Input $10^{16} \, h\nu$ sec.$^{-1}$

Time (min.)	M.A. press.	Hydrogen press.
0	45·8	—
1	35·8	—
2	26·8	—
4	20·0	0·0180
6	17·2	—
8	13·7	0·0470
12	9·0	0·069
16	7·0	0·098

The initial rate of polymerization is 9·8 mm./min.$^{-1}$ and the initial rate of production of hydrogen 0·005 mm./min.$^{-1}$, that is, a ratio of 2000 : 1. Since

the quantum yield for polymerization is about 10^2, the quantum yield for decomposition is 0·05, if the decomposition is due to 2537 radiation, suggesting therefore that the decomposition is a secondary reaction. If light of shorter wave-length is absorbed by the acrylate, the decomposition is more marked. For example, by removing the acetic acid filter and substituting a water filter, the half life time for polymerization changes from 2·9 to 2·3 min. while the rate of production of hydrogen is more than doubled, namely from 0·04 to 0·1 mm./min.$^{-1}$. By employing smaller intensities the decomposition reaction would become much less important as this is proportional to the first power of the intensity and the polymerization to the square root (see below).

Since the $COOCH_3$ group is the effective chromophore in starting polymerization, it was also essential to find if any carbon dioxide was eliminated such as occurs with the COOH group. Using the acetic acid filter 11 mm. of acrylate were exposed for 42 min. when the pressure fell to 4·4 mm. The acrylate was removed with liquid air leaving 1 mm. of hydrogen. Next a CO_2-ether bath at $-80°$ replaced the liquid air, but no increase in pressure resulted which showed that CO_2 was not produced in appreciable quantities.

Finally there is the possible complication that the polymer itself is photochemically decomposed on continued irradiation—a reaction which might contribute to the volume of non-condensable gas. Starting with a clean tube, 38 mm. of acrylate were polymerized. The remainder of the gas mixture was completely removed and the polymer irradiated with 2537 radiation for 5 min. 5×10^{-4} mm. of hydrogen were produced compared with 260×10^{-4} mm. when the vapour was illuminated under the same conditions. The photo-decomposition of the polymer can thus be neglected. While the photo-decomposition of liquid acrylate has not yet been investigated, it is worth noting that although the solid polymer may absorb as much light as the monomeric vapour, the change in structure from $CH_2 = CH.COOCH_3$ to $—CH_2—CH(COOCH_3)—$ prevents the removal of the hydrogen atoms attached to the carbon atoms.

The next question is whether there is a slow continuous growth of the polymer in the dark such as has been observed with methacrylate. Table III shows an experiment with a clean tube in which successive short periods of illumination were followed by long periods of darkness. It will be seen that after the third period of illumination at 15 min., 1 mm. of acrylate polymerized in 5 min. compared with about 6 mm. in 1 min. in the light. After the fourth period, however, the dark rate is much faster but soon decays. The dark rate subsequent to the next period is again very small.

TABLE III

Conditions as in Table I

Time (min.)	M.A. press. (mm.)	Light	Δp in the light	Δp in the dark	$\Sigma\Delta p$ in the light	$\Sigma\Delta p$ in the dark
0·0	57·0	On	2·2	—	2·2	—
0·5	55·8	Off				
1·0	55·8		—	0·0	—	0·0
2·0	55·8					
5·0	55·8	On	3·6	—	5·8	—
5·5	52·2	Off				
7·0	52·2		—	0·0	—	0·0
10·5	52·2	On	4·4	—	10·2	—
11·0	47·8	Off				
12·0	47·6		—	0·2	—	0·2
15·0	47·6	On	5·6	—	15·8	—
15·5	42·0	Off				
17·0	41·4		—	1·0	—	1·2
20·0	41·0	On	5·6	—	21·4	—
20·5	35·4	Off				
21·0	34·2		—	—	—	—
23·0	32·0		—	6·4	—	7·6
25·0	31·0					
27·0	30·0		—	—	—	—
30·0	29·0	On	3·4	—	24·8	—
30·5	25·6	Off				
31·0	24·6		—	1·6	—	9·2
32·0	24·4					
35·0	24·0	On	3·8	—	28·6	—
35·5	20·2	Off				
37·0	19·0		—	6·8	—	16·0
58·0	13·4					

In another experiment 280 mm. of acrylate were polymerized, the vapour being continuously supplied from a graduated capillary tube, and the rate of polymerization being about 10 mm./min.$^{-1}$. When the light was switched off, the rate immediately decreased as is shown by the following figures:

Time (min.)	0	2	7	12	17	27	42	950
p (M.A.)	41·0	38·8	36·0	34·4	34·0	33·0	31·2	23·0
Rate, mm./min.$^{-1}$	1·7	0·7	0·4	0·3	0·1	0·1	0·1	0·01

One simple explanation would be that the dark rate is due to absorption of the monomer by the polymer as the latter accumulates in the vessel. This was tested by polymerizing a suitable amount of acrylate and withdrawing the vapour into a liquid air trap until a Pirani gauge registered a constant pressure—a process which required 15–20 min. The acrylate was then quickly vaporized and its pressure determined. A number of

experiments, recorded below, show that the pressure after evaporation is actually slightly less instead of greater than that before. The pressure decrease is probably due to some polymerization during the evaporation of the acrylate:

M.A. polymerized	31·8	36·6	38·6	6·4
Press. before	13·8	9·0	7·0	47·0
Press. after	12·0	7·2	6·8	46·0

It would appear then that the slow disappearance of acrylate in the dark is really a true polymerization. It will be shown later that oxygen is a powerful inhibitor of the normal gas-phase polymerization, and hence it was necessary to see whether oxygen would also inhibit the dark polymerization. First a normal polymerization run was made, the reaction being allowed to continue in the dark for 67 min. during which 14·4 mm. of acrylate polymerized. The reaction vessel was then pumped out and 50 mm. of oxygen kept in contact with the polymer for 10 mm. On readmitting acrylate vapour polymerization occurred at approximately the same rate as that to be expected after a decay period of 10 min. The growth in the dark occurs at the surface of the vessel, since no cloud of polymer is formed in the gas phase and is therefore a concurrent reaction to that in the gas.

Effect of intensity. As has been pointed out previously the variation of rate of polymerization with intensity of incident light immediately indicates the type of collision which terminates the growth of the polymer. In these experiments the velocity was altered by interposing screens of aluminium foil perforated with holes of known dimensions. The transmission was measured by a photoelectric photometer. As is evident from the following figures the rate is proportional to the square root of the intensity:

<div align="center">Transmission of filter 36 %</div>

Press. of M.A. (mm.)	54·0	51·4	53·4
Filter	Out	In	Out
$\tau_{\frac{1}{2}}$ (min.)	2·85	4·50	2·50
$\tau_{\frac{1}{2}}$ (in)/$\tau_{\frac{1}{2}}$ (out)	——	1·68	——
$\dfrac{\tau_{\frac{1}{2}} \text{ (in)}}{\tau_{\frac{1}{2}} \text{ (out)}}$ (calc.)	—	1·63	—

Even at very low intensities—about 0·005 of that used above—the rate is reduced by a factor of 17, which is just what would be expected from a square root dependence on intensity. These experiments show that the polymer stops growing by the mutual destruction of two growing polymers.

Effect of temperature. This effect was investigated with the high-voltage

mercury lamp, the intensity being adjusted so that it was comparable
with that employed at room temperature, namely, 10^{16} quanta/sec.:

Effect of temperature

Temp. °C.	20	30	42	100	102
Initial press.	39·8	40·8	42·6	45·2	39·8
$\tau_{\frac{1}{2}}$ (min.)	1·1	1·9	3·2	37·5	28·0

Energy of activation $-8\cdot9$ kcal.

At 158° polymerization could not be measured, i.e. less than 0·02 mm./min.
Moreover, at this temperature there was no appreciable thermal depoly-
merization of previously deposited photo-polymer which immediately
demonstrates that the negative temperature coefficient of the photo rate
is not due to a progressively increasing rate of thermal depolymerization.
Since the absorption coefficient of the acrylate vapour and the efficiency
of the primary photoreaction is certainly almost independent of tempera-
ture, the negative coefficient might be due to the occurrence of a new type
of inhibition reaction, negligible at room temperature. First, then, the
intensity exponent was determined at 100°, where the rate of polymerization
is 30–40 times smaller than that at room temperature and therefore under
conditions where any new chain-terminating mechanism is the predominant
reaction. It will be seen from the results in Table IV that the intensity

TABLE IV. EFFECT OF INTENSITY AT HIGH TEMPERATURES

Transmission of filter 36 %

Initial press.	Filter	Temp. °C.	$\tau_{\frac{1}{2}}$	$\dfrac{\tau_{\frac{1}{2}}\text{ (out)}}{\tau_{\frac{1}{2}}\text{ (in)}}$
41·6	Out	26	1·45	1·41
41·8	In	28	2·05	1·57
41·0	Out	30	1·30	1·54
41·4	In	29	2·00	
41·8	In	89	20·6	1·51
42·0	Out	89	13·6	

exponent remains at 0·5 as is shown by the fact that the ratio of rates with
the filter in and out is independent of temperature. The growth of the
polymer is therefore limited by essentially the same type of reaction as
occurs at 20°. The terminating collision must therefore require considerable
energy of activation, the value of 9 kcal. calculated from the above results
being only a minimum estimate. This evidence is supported too by the
fact that the variation of rates with pressure is similar at different tem-

peratures. Here it is rather difficult to obtain accurate measurements of the rate at high temperatures and low initial pressures:

Initial press. mm.	Temp. ° C.	Initial rate mm./min.$^{-1}$	Order
47·6	32	4·4	1·6
14·0	34	0·66	
49·4	100	0·59	1·2
13·0	102	0·12	

Having thus determined the type of collision process responsible for the cessation of growth of the polymer, the appropriate kinetic equation may be worked out so that the relationship between propagation and termination coefficients may be obtained. Denoting by P an active polymer and by k_p the velocity coefficient for the reaction with the monomer (M) and k_m the termination coefficient, then the concentrations of the various growing polymers are represented by

$$\frac{d(P_1)}{dt} = f(I) - k_{p_1}(P_1)(M) - k_{m_1}(P_1)\{k_{m_1}(P_1) + k_{m_2}(P_2) + \dots k_{m_r}(P_r) + \dots\} = 0,$$

$$\frac{d(P_2)}{dt} = k_{p_1}(P_1)(M) - k_{p_2}(P_2)(M) - k_{m_2}(P_2)\{k_{m_1}(P_1) + \dots k_{m_r}(P_r) + \dots\} = 0,$$

or in general

$$\frac{d(P_r)}{dt} = k_{p_{r-1}}(P_{r-1})(M) - k_{p_r}(P_r)(M) - k_{m_r}(P_r)\{k_{m_1}(P_1) + \dots\} = 0.$$

On substituting $k_{m_r}/k_{p_r} = \delta$, which is assumed independent of r, then

$$\delta\{k_{p_1}(P_1) + k_{p_2}(P_2) + \dots k_{m_r}(P_r) + \dots\} = f(I)^{\frac{1}{2}}.$$

Hence the rate of polymerization is given by

$$-\frac{d(M)}{dt} = f(I) + (M)\sum_{r=1}^{r=\infty} k_{p_r}(P_r)$$

$$= \frac{(M)}{\delta}\{f(I)\}^{\frac{1}{2}},$$

since the chains are long. Since the light is not completely absorbed by the methyl acrylate vapour $f(I)$ will be a function (M), thus making the order of the reaction with respect to (M) between 1·0 and 1·5 as is found. On account of the overall temperature coefficient of $-d(M)/dt$ being negative,

the energy of activation of the termination reaction, defined in the above manner, must exceed that of propagation by 8 kcal.

Effect of oxygen. Oxygen is a most powerful inhibitor of the gas and even the liquid phase polymerization. In the gas phase, induction periods were at first observed, but on freeing the vapour from oxygen by repeated condensation in liquid air the induction period disappears. The results are best shown graphically in fig. 2. By adding only 0·18 mm. of oxygen, the half life of the reaction is increased from 2·5 to 11·1 min. 1·66 mm. of oxygen increased $\tau_{\frac{1}{2}}$ to 41 min. It is evident that the kinetics of the oxygen-inhibited reaction are entirely changed. This can be seen by comparing the ratio of the times required for the pressure to drop to different values. From the
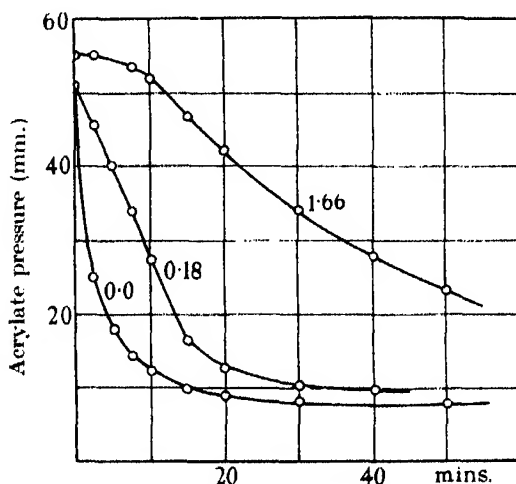
Fig. 2. Effect of oxygen pressure at 20° C.

fact that the ratio decreases, the order of the oxygen-inhibited reaction must therefore be considerably lower than that of the normal reaction, although the order should actually be greater (see p. 111). This decrease in order is, however, due to two partially compensating factors. As the oxygen-inhibited reaction progresses, the oxygen disappears and hence the velocity should increase. Such an increase is balanced by the decrease in the concentration of the acrylate. There is another remarkable effect only observed in presence of oxygen. Fig. 3 shows three experiments made with nearly the same initial pressure of acrylate and exactly the same pressure of oxygen, viz. 1·66 mm. The first was done in a clean tube where it will be observed that there is a long induction period terminated by a slow polymerization. The second experiment exhibits a much shorter induction period followed

by a steady reaction, succeeded by a much faster reaction with the production of a cloud of polymer in the gas. It should be mentioned that in the oxygen-inhibited reaction, the visible formation of polymer cannot be detected. In the third experiment, however, the polymerization starts immediately and continues with the same speed as that in the second experiment. The explanation would appear to be that the growing polymer is deactivated in some way in so far as further growth is concerned by collision with a "clean" silica surface. When this surface is covered with polymer, the growing polymer must be elastically reflected back into the gas phase to be stopped growing by collision with an oxygen molecule. The most curious fact is that the normal photo-polymerization is not affected whether
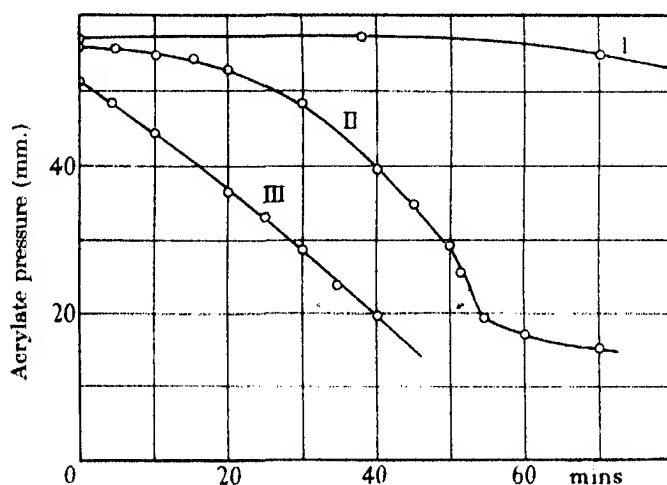
Fig. 3. Effect of tube surface on velocity of oxygen-inhibited reaction.

a clean or a polymer-covered tube is employed, which would suggest that adsorbed oxygen may also terminate growth at the walls. As a matter of fact the different behaviour of clean and of polymer-covered tubes has already been observed in the methacrylate reaction in which the deposition of the requisite number of centres on the walls for continual growth of the polymer in absence of light is not only inhibited by oxygen, but is much hindered if the experiment is made with a clean tube.

If oxygen does inhibit the polymerization by reaction with the growing polymer before such molecules have an opportunity of interacting with each other, then it is evident that the rate of termination of growth will be proportional to the first power of their concentration. The rate of reaction should therefore become proportional to the first power of the intensity of

the light. The two experiments recorded below indicate that the value of the exponent of the intensity factor is increased towards unity.

Initial pressure 49·8 mm.   Temp. 20° C.   1·5 mm. O_2 added.

Intensity	Rate mm./min.	Ratio	Ratio calc.	
			$R \sim I$	$R \sim I^{\frac{1}{2}}$
1·00	1·28	0·45	0·60	0·36
0·36	0·58			

The next problem is to obtain a quantitative measure of oxygen inhibition. This may be done by the introduction of a term containing (O_2) into the expressions used for the normal reaction as follows:

$$\frac{d(P_1)}{dt} = f(I) - k_{p_1}(P_1)(M) - k_{d_1}(P_1)(O_2)$$
$$- k_{m_1}(P_1)\{k_{m_1}(P_1) + \ldots k_{m_r}(P_r) + \ldots\} = 0,$$

and in general

$$\frac{d(P_r)}{dt} = k_{p_{r-1}}(P_{r-1})(M) - k_{p_r}(P_r)(M) - k_{d_r}(P_r)(O_2)$$
$$- k_{m_r}(P_r)\{k_{m_1}(P_1) + \ldots k_{m_l}(P_l) + \ldots\} = 0.$$

By addition
$$f(I) = \sum_{r=1}^{r=\infty} k_{d_r}(P_r)(O_2) + \{\Sigma k_{m_r}(P_r)\}^2$$

$$= \beta(O_2)\Sigma k_{p_r}(P_r) + \delta^2\{\Sigma k_{p_r}(P_r)\}^2,$$

where $\beta = k_{d_r}/k_{p_r}$. Hence

$$\Sigma k_{p_r}(P_r) = \frac{-\beta(O_2) + \{\beta^2(O_2)^2 + 4\delta^2 f(I)\}^{\frac{1}{2}}}{2\delta^2}.$$

When the concentration of oxygen is small compared with the acrylate, expansion of the term under the root sign gives

$$\Sigma k_{p_r}(P_r) = \frac{f(I)^{\frac{1}{2}}}{\delta} - \frac{\beta(O_2)}{2\delta^2}\left(1 - \frac{\beta(O_2)}{4\delta f(I)^{\frac{1}{2}}}\right)$$

or
$$-\frac{d(M)}{dt} = \frac{f(I)^{\frac{1}{2}}(M)}{\delta} - \frac{\beta(O_2)(M)}{2\delta^2}\left\{1 - \frac{\beta(O_2)}{4\delta f(I)^{\frac{1}{2}}}\right\}.$$

The rate of polymerization should therefore decrease at first linearly with increasing oxygen pressure. At high enough oxygen pressures mutual

destruction of growing polymers may be neglected and the general stationary state equation will assume the simple form

$$\frac{d(P_r)}{dt} = k_{p_{r-1}}(P_{r-1})(M) - k_{p_r}(P_r)(M) - k_{d_r}(P_r)(O_2) = 0$$

and

$$\Sigma k_{p_r}(P_r) = f(I)/\beta(O_2)$$

or

$$-\frac{d(M)}{dt} = \frac{f(I)(M)}{\beta(O_2)},$$

which is in agreement with the fact that the intensity exponent increases from 0·5 towards unity. The reciprocal of the rate of polymerization should also be proportional to (O_2), whereas it is unchanged with respect to the acrylate concentration. The data are summarized in Table V.

TABLE V. EFFECT OF OXYGEN AT 20° C.

p_{O_2}	t in min. for $-\Delta p = 6$ mm.	$p_{M.A.}$	t corr. to 40 mm. M.A.	t^{-1}
		Series I		
0·0	0·77	40·0	0·77	1·30
0·68	5·9	36·8	5·2	0·192
0·41	4·8	39·0	4·7	0·213
1·45	8·0	36·4	7·0	0·143
0·23	3·6	34·4	2·9	0·34
0·0	1·5	32·4	1·1	0·91
		Series II		
0·0	1·2	41·2	0·78	1·28
2·12	7·8	38·0	7·3	0·137
0·0	1·5	34·6	1·20	0·83
0·52	3·2	40·2	3·2	0·313
0·20	2·9	36·8	2·6	0·384
0·0	1·2	36·4	0·95	1·05
0·8	5·3	36·6	5·0	0·2

When the times for the pressure to fall 6 mm. are plotted against oxygen pressure, i.e. the times for 15% reaction (fig. 4), the line is straight until the reaction velocity has fallen to one-fifth of its normal value, then the line bends round towards the oxygen axis showing that oxygen ceases to exert as strong an inhibiting influence as that indicated by the low-pressure experiments. This may be due to (a) another type of initiation reaction coming into play, (b) the fact that β is not independent of r. At present there is no evidence for the second alternative, but there is evidence from another reaction that oxygen can function in this twofold manner if mercury vapour is present, as happens in these experiments. In the direct and mercury photosensitized

photo-oxidation of phosphine (Melville and Roxburgh 1934) the initial
process is the dissociation of PH_3 to PH_2 and H. The chain length of the
reaction is thus easily calculated from the ratio of rate of oxidation to that
of decomposition. At high oxygen pressures in the sensitized reaction, the
chain length so computed is much shorter than that in the direct reaction,
although propagation and termination reactions are identical. The reason
is that excited mercury atoms generate oxygen atoms which in turn initiate
oxidation. It is probable therefore that the same type of reaction occurs
in this polymerization.
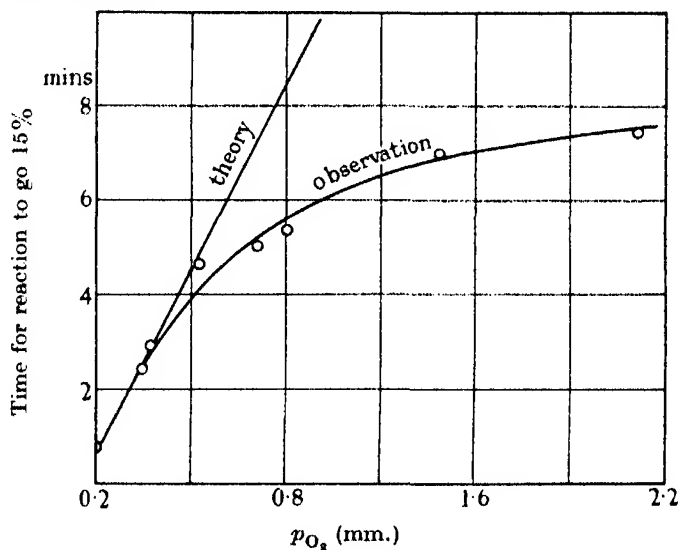
FIG. 4. Effect of oxygen pressure at 20° C.

Owing to the destruction of growing polymers by mutual interaction it
is rather difficult to compute the exact value of the ratio of propagation to
oxygen termination coefficients. An approximate estimate may be made
in the following manner. 0·1 mm. of oxygen in 40 mm. of acrylate reduces
the rate of polymerization by one-half, hence an oxygen molecule reacts
with a growing polymer 400 times more readily than a monomer molecule.
If these collisions are of a simple bimolecular type, this would correspond
to a difference in 3·6 kcal. for the energies of activation of the two reactions.
Since there is reason to believe that the energy of activation for propagation
of the chain is in the neighbourhood of 5 kcal., then the energy of activation
for the reaction of oxygen is only 1·4 kcal. Hence it would be expected that
if the temperature coefficient of the oxygen-inhibited reaction is measured
it should have a *positive* value. On the other hand, at high temperatures

where the mutual destruction reaction has become more efficient, oxygen inhibition ought to disappear entirely. These anticipations are fully realized by the data plotted in fig. 5 in which $\log_{10} t^{-1}(\Delta p = -6 \text{ mm.})$ is plotted against $10^3/T$ for various oxygen pressures. Unfortunately, the acceleration brought about by oxygen at high pressures prevents the true state of affairs being realized. If, however, the $1/R - p_{O_2}$ curve is extrapolated, the full lines exhibit an opposite slope to that of the uninhibited reaction. Hence the negative temperature coefficient is certainly due to the termination process. These results also indicate that the energy of activation for growth of the polymer is about 4 kcal.
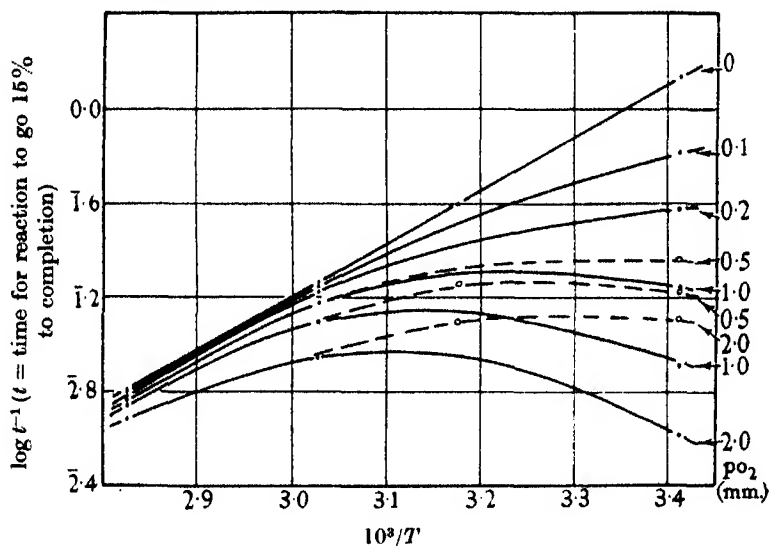
FIG. 5. Effect of oxygen pressure as a function of temperature. The dotted lines show the effect of oxygen when oxygen initiation has become important.

Effect of butadiene. As part of another series of experiments on inter-polymerization of molecules, an attempt was made to incorporate butadiene in the acrylate polymer. The most surprising fact emerged that, although butadiene may be polymerized photochemically, it acted as a strong inhibitor for the acrylate reaction. The following figures show the magnitude of the effect:

Effect of butadiene at 20° C.

M.A. press. (mm.)	44·0	40·0	38·0
Butadiene press. (mm.)	—	2·4	15·0
Initial rate (mm./min.)	4·0	1·5	0·2

In these experiments matters are more complicated than those with oxygen, for there are now two possibilities. The first is that the butadiene

molecule adds on to the growing acrylate polymer, but no further molecules of acrylate or butadiene add on, the structure of the polymer being $AAAAAAAB$. The second is that butadiene readily adds on to the acrylate polymer, but the addition of acrylate to the butadiene end of the polymer is somewhat slower than that to a pure acrylate polymer. Provided the time which elapses during the process is not greater than the lifetime of the reaction chain, the chain will be terminated in the usual way by the interaction of two acrylate ends. The structure of the growing polymer is therefore $AAAABAAAAABA$. This latter process is therefore really an interpolymerization, although the butadiene cuts down the overall velocity of polymerization. A choice between the two may be made by measuring the intensity exponent in the rate equation. The first type of interaction will be analogous to that obtained in the oxygen-inhibited reaction, that is, $R \sim I$, whereas in the second type the rate will remain proportional to the square root of the intensity. The following results show that the intensity exponent is increased from 0·5 to 0·6. Unfortunately, in carrying out this

TABLE VI. EFFECT OF INTENSITY ON BUTADIENE
INHIBITED REACTION. M.A. 40 mm.

Butadiene press.	Intensity	Time for Δp − 4 mm. (min.)	Intensity exponent
0·0	1·00	0·5	
3·6	1·00	4·0	
3·6	0·35	7·7	0·62
3·6	1·00	4·2	
3·6	0·36	8·0	0·62

kind of experiment the butadiene is used up during the reaction so that the ratio of rates at the two intensities is soon given by the square root law. For example, this is shown by the fact that the ratio of times for the pressure to fall to the same value in the inhibited and uninhibited reactions decreases during the course of the reaction.

Press. of M.A. 40 mm.   Press. of butadiene 3·6 mm.

Δp (mm.)	2	4	6	8	10	12	14
t_1/t_2	2·3	1·9	1·60	1·58	1·58	1·58	1·50

In view of the complicated behaviour of oxygen, the effect of butadiene was studied at different temperatures in order to obtain another independent estimate of the energy of activation for growth of the polymer. The results at 18° C. are shown in fig. 6, where R and $1/R$ are plotted against butadiene pressure. At low butadiene pressures, the linear decrease of R with p is obtained, while at high pressures $1/R$ is proportional to pressure as is

required by theory. Even at pressures in excess of 20 mm. there is no deviation from linearity as was found with oxygen. From the slope of this
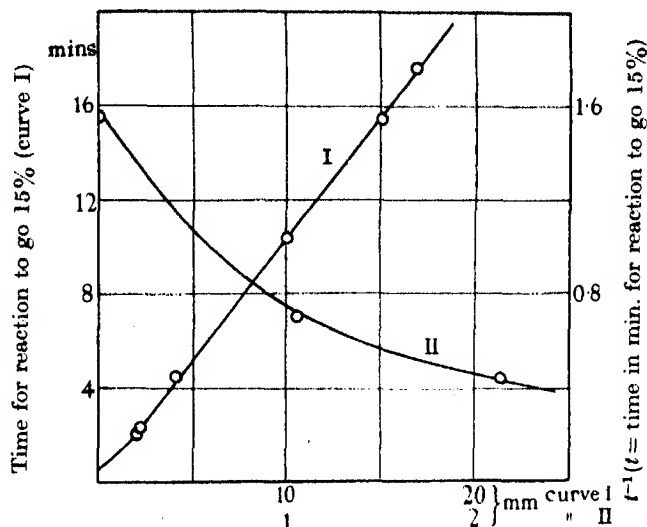

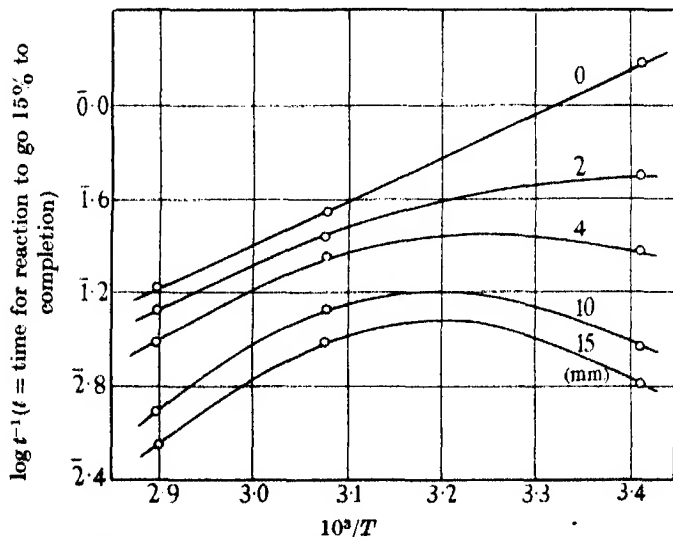Fig. 6. Effect of butadiene pressure at 20° C.

Fig. 7. Effect of butadiene pressure as a function of temperature.

curve and that for oxygen, the relative values of the efficiencies of these molecules in terminating chains is, butadiene : oxygen 8 : 1. Experimental data at 52° and 72° are plotted in fig. 7 for different butadiene pressures.

Again the same phenomena makes its appearance. Below 52° there is complete inversion of the temperature coefficient, since the normal termination reaction has been replaced by one of small energy of activation. The measured value of the positive coefficient is 2·8 kcal. If it is assumed that the energy of activation for oxygen inhibition is zero, then this value of 2·8 must be increased by the energy of activation for butadiene inhibition which amounts to 1·2 kcal. calculated from the relative efficiencies of the two inhibitors. This figure of 4·0 agrees with the estimate made by extrapolation of the oxygen results.

At 72°, however, butadiene behaves differently from oxygen. It exerts an inhibitory reaction once more. The nature of this second type of inhibition will be considered in a subsequent paper.

TABLE VII

Input 2×10^{16} $h\nu$ sec.$^{-1}$ to 80 c.c.   50 % light absorbed.   Temp. 52° C.

Distillation data

| | Pressure | | Polymerization | |
Time (min.)	Before	After	t (min.)	Total press.
1	4·0	1·2	0	56·4
2	6·2	1·8	2	55·4
3	9·8	—	5	53·0
4	—	5·4	10	49·6
5	14·0	—	20	43·4
7	15·8	—	30	38·6
10	16·8	15·0	40	35·2
12	—	15·0	—	—
14	16·8	15·0	—	—

Butadiene inhibition may be used to obtain a measure of the chain length of the polymer. The average value is the number of acrylate molecules polymerized divided by the number of butadiene molecules which disappear. The analysis of the mixture is easily made by condensing it in a side tube of small volume and allowing it to evaporate slowly. Owing to the fact that butadiene boils at −5° and acrylate at 70°, the separation is adequate. The following experiment was carried out at a sufficiently high temperature (52°) so that the chain was short enough for a measurable amount of butadiene to disappear and with a butadiene pressure (16·8 mm.) such that the velocity of polymerization was cut down by a factor of 3. Thus about 70 % of the chains started are terminated by butadiene. The following figures show the distillation data before and after the polymerization run which is also included in Table VII.

Since $21 \cdot 2 - 1 \cdot 8 = 19 \cdot 4$ mm. of acrylate disappear for $1 \cdot 8$ mm. of butadiene used up, the chain length of the inhibited reaction is $19 \cdot 4 / 1 \cdot 8 \times 0 \cdot 7 = 7 \cdot 6$. The chain length of the uninhibited reaction is therefore 23 and at $20°$, 101, at a pressure of $16 \cdot 8$ mm.*

Effect of methyl methacrylate. As might be expected the acrylate polymerization is not appreciably affected by 25 % of methacrylate vapour.

Effect of hydrogen. From the kinetics described in the previous pages there is no unambiguous evidence to indicate whether the acrylate polymer grows by the free-radical or double-bond mechanism. In the methacrylate polymerization the curious accelerating effect of hydrogen at once gave a means of saying which mechanism operated in this particular reaction. On the other hand, there is very little acceleration in the acrylate polymerization as may be seen from the following figures:

	Series I			Series II	
M.A. press.	59·8	62·6	55·0	53·4	60·8
Hydrogen press.	12·0	1·0	0·1	—	9·4
$\tau_{\frac{1}{2}}$ (min.)	1·3	1·6	1·6	2·5	2·7

These results do not imply that there is no hydrogen atom-sensitized reaction, they merely show that this reaction is not faster than the ordinary photoreaction. If it so happens that the hydrogen-sensitized polymerization is faster than the normal polymerization, as occurs with methyl methacrylate, then the reaction may be detected and its kinetics examined: if it is slower, other methods must be adopted to study and characterize the free radical polymerization of the molecule concerned.

Hydrogen does, however, have an appreciable effect if oxygen is already present with the acrylate vapour as is shown by fig. 8. In presence of oxygen in a clean tube there is a very long induction period (curve 1). When the tube is covered with polymer this induction period disappears (curve 2), but the rate of polymerization is much less than that of the reaction in absence of oxygen (curve 4). When hydrogen is added to the oxygen, again starting with a clean tube, there is still an induction period but of much shorter duration than in Exp. 1. Moreover, the velocity of the succeeding reaction is nearly equal to that of the uninhibited reaction (curve 4), thus showing

* [*Note added in proof,* 12 *May* 1938.] The average quantum yield of the polymerization is 2·5. Hence the efficiency of the primary process, that is, the number of chains started per quantum absorbed by acrylate is therefore $2 \cdot 5 / 7 \cdot 6 = 0 \cdot 33$. In this reaction then, the molecular weight of the product is given by multiplying the molecular weight of the monomer by three times the quantum yield of the photoreaction.

that at the end of the induction period nearly all the oxygen has been reduced by the atomic hydrogen. This experiment also demonstrates that hydrogen atoms react more readily with oxygen than with acrylate molecules or growing polymers.
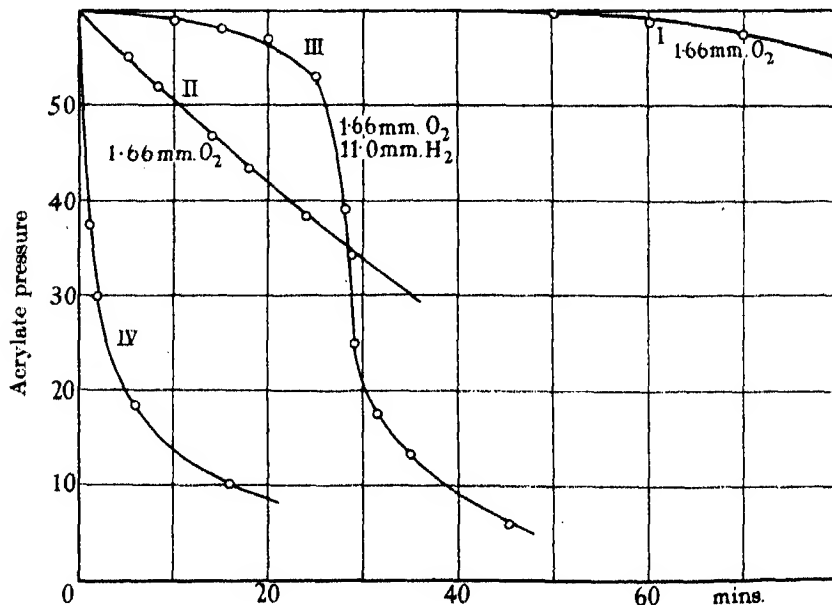
FIG. 8. Effect of hydrogen on the oxygen-inhibited reaction.

Properties of the polymer. Unlike the methacrylate polymer the acrylate polymer does not easily depolymerize on heating. It invariably chars, breaking up into complex products. Neither is it completely soluble in benzene though it swells to many times its original volume. Considering these results in relation to the behaviour of the methacrylate, it would appear that the acrylate is to some extent cross-linked. The essential reaction for the production of cross-linking is that (*a*) the chains shall branch, (*b*) that the ends of the growing polymer should be able to react and mutually saturate each other. The occurrence of the second type of reaction has already been established. The first reaction may occur in the following manner. On p. 102 it was noted that a small quantity of hydrogen is produced during polymerization apparently by the photo-decomposition of acrylate, thus: $CH_2=CH.COOCH_3=H_2+CH:C.COOCH_3$. Assuming that the normal polymerization reaction is of the double-bond type, the branching by means of propiolic ester could occur in the following manner. First a molecule of propiolic ester reacts with the end of the acrylate polymer, thus producing

two potentially reactive groups, each of which grows by the addition of monomer. When two such ends react the two-branched chains cross-link:

$$
\begin{array}{cccc}
\text{CH} & \text{CH} & \text{CH} & \text{CH} \\
\parallel & \parallel\parallel & \parallel\parallel\parallel & \parallel \\
\text{H.C.COOCH}_3 & \text{C.COOCH}_3 & \text{C.COOCH}_3 & (\text{COOCH}_3).\text{C.H}
\end{array}
$$

$$
\begin{array}{cc}
\text{C}-\text{CH}{=}\text{CH.COOCH}_3 & \text{COOCH}_3{=}\text{CH}-\text{C} \\
\parallel & \parallel \\
\text{H.C.COOCH}_3 & \text{H.C.COOCH}
\end{array}
$$

$$
\begin{array}{cc}
\text{COOCH}_3 \ \ \text{H} \ \ \text{COOCH}_3 & \text{COOCH}_3 \ \ \text{H} \ \ \text{COOCH}_3 \\
\text{C}-\text{CH}_2-\text{C}\!-\!\!-\!\!-\!\text{C}{=}\text{C} & \text{C}{=\!\!=\!\!=}\text{C}-\text{C}\!-\!\!-\!\!-\text{CH}_2-\text{C} \\
\quad \text{H} \qquad \text{H} & \quad \text{H} \qquad \text{H}
\end{array}
$$

$$
\begin{array}{cc}
\text{COOCH}_3 \ \ \text{H} \ \ \text{COOCH}_3 \ \ \text{COOCH}_3 \ \ \text{H} \ \ \text{COOCH}_3 \\
\text{C}-\text{CH}_2\!-\!\!-\!\!\text{C}\cdots\cdots\text{C}-\text{C}{=\!\!=\!\!=}\text{C}\cdots\cdots\text{C}-\text{C}\!-\!\!-\!\!\text{CH}_2-\text{C} \\
\parallel \qquad\quad\ \ \text{H} \qquad\qquad\quad\ \ \text{H} \qquad\ \ \parallel \\
\text{H.C.COOCH}_3 \ \text{H} \qquad \text{H} \qquad\qquad\qquad\quad \text{H} \ \ \text{H} \qquad\quad \text{H.C.COOCH}_3
\end{array}
$$
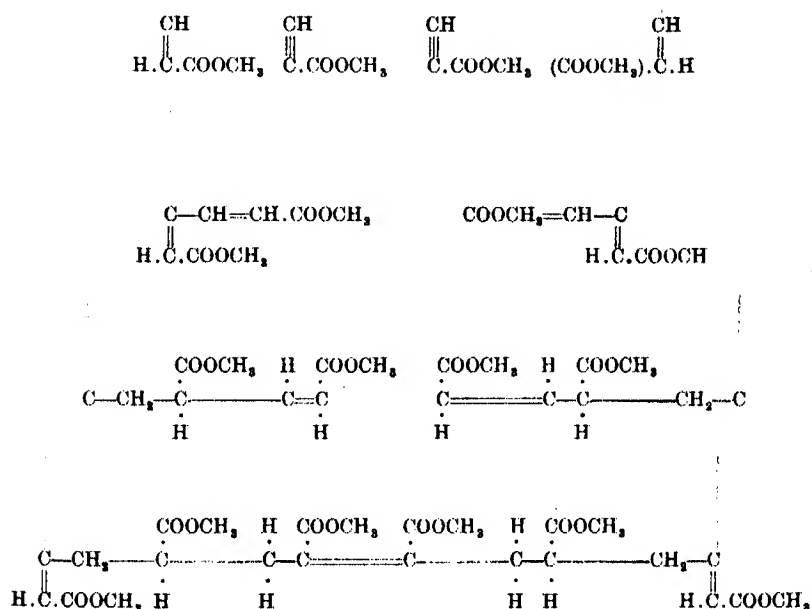
In a normal chain reaction such branching of chains leads to indefinitely long chains, that is, explosion, under suitable conditions, except when the chains mutually destroy each other. This latter type of reaction always keeps the velocity of the reaction under control since the rate of branching is proportional to the first power of the concentration of the chain carrier, whereas the rate of termination is proportional to the second power. In this polymer reaction where these conditions of branching and termination must be simultaneously fulfilled in order to obtain a cross-linked polymer, branching has therefore no appreciable effect in augmenting reaction velocity. Hence by kinetic methods alone the estimation of the extent of cross-linking is impossible.

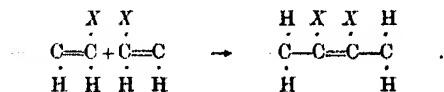### Comparison of acrylate and methacrylate reactions

The most important difference in behaviour is the fact that under identical conditions of photo-initiation one molecule grows indefinitely, the other is soon made inactive by a collision with another of its kind. Since the meth-

acrylate polymerization is of the double bond type then it is very probable that a similar mechanism is operative with the acrylate. But it is evident that the substitution of a hydrogen atom for a methyl group increases the efficiency of the reaction of the monomer with the growing polymer. On the other hand if a methyl group is substituted for one of the hydrogen atoms of the CH_2 group giving methyl crotonate, then no polymerization can be detected at all even although this molecule absorbs the same number of quanta as the acrylate or methacrylate. Thus in these three examples, the differences in polymerizability is certainly due to the different efficiencies and probably energies of activation for the addition of monomer to a molecule of monomer activated photochemically.

CONCLUSIONS

From these experiments the following conclusions may be drawn. In the photo-polymerization of methyl acrylate with light at 2500 A, the double bond of the molecule is activated in such a way that further molecules of the monomer add on to the growing polymer with the production of a double bond at the end of the molecule, the mean energy of activation of the addition reaction being 4 kcal. In the absence of inhibitors, the growth is stopped when two active polymers collide, the reaction comprising the simultaneous migration of two hydrogen atoms thus ($X = COOCH_3$):

$$\begin{array}{ccc} X\ \ X & & H\ \ X\ \ X\ \ H \\ C{=}C + C{=}C & \longrightarrow & C{-}C{=}C{-}C \\ H\ \ H\ \ H\ \ H & & H\quad\quad H \end{array}\ .$$

This reaction possesses a high energy of activation > 10 kcal., which makes the overall energy of activation of the polymerization reaction negative in sign. Since the termination process is not very much slower than the growth of the polymer itself, the concentration of the growing molecule must be very much greater than that of the chain carriers normally encountered, namely of the order of 10^{-3} mm. and of a life time *ca.* 10^{-2} sec. under similar intensities of absorbed radiation. This in turn suggests that although the energy of activation for growth of the polymer is comparatively small, the efficiency of the reaction must be low, implying therefore that a large steric factor is operative.

ACKNOWLEDGEMENTS

SUMMARY

The photo-polymerization of methyl acrylate vapour has been studied at pressures up to 60 mm. and at temperatures between 20 and 150° C. Polymerization occurs almost quantitatively, giving a dense cloud of polymer in the gas phase when about 10^{14} quanta are absorbed per c.c. per sec. at 2537 Å, the quantum yield ranging from unity to 5000 depending on the temperature and intensity. At shorter wave-lengths the molecule is dissociated to hydrogen and propiolic ester. Growth of the polymer ceases when two growing polymers interact with each other. The temperature coefficient of this latter process is so large that the polymerization has a negative temperature coefficient. The reaction is very sensitive to inhibitors especially to oxygen and to a lesser extent butadiene. By controlled use of inhibitors a direct measure of the energy of activation of the propagation reaction has been made: it amounts to 4 kcal. At high oxygen pressures, oxygen exerts a positive catalytic effect believed to be due to the mercury sensitized production of O atoms.

The molecular weight of the polymer has been estimated by measuring the ratio of acrylate to butadiene molecules used up in the inhibited reaction under a given intensity of illumination. Hence by calculation the molecular weight of the product in the normal reaction is easily found.

This behaviour of acrylate is in marked contrast with that exhibited by methyl methacrylate, the long life time of the latter polymer being completely absent in the acrylate. Like the methacrylate, the acrylate grows by the double-bond mechanism and the differences in behaviour of these two similar molecules is accounted for by the theories advanced in this and previous papers.

REFERENCES

Farkas, A. and Melville, H. W. 1936 *Proc. Roy. Soc.* A, **157**, 625–51.
Melville, H. W. 1936 *Trans. Faraday Soc.* **32**, 1525–31.
— 1937 *Proc. Roy. Soc.* A, **163**, 511–42.
Melville, H. W. and Roxburgh, H. L. 1934 *J. Chem. Phys.* **2**, 739–52.

A new form of resorcinol

I. Structure determination by X-rays

By J. Monteath Robertson and A. R. Ubbelohde

At about 74° C. ordinary resorcinol (α-resorcinol) undergoes a transformation into a denser crystalline modification, called β-resorcinol (Ubbelohde and Robertson 1937), and a comparison of these two structures is of considerable general interest for the problem of intermolecular bonding in hydroxylic compounds. The crystalline structure of α-resorcinol has already been fully determined (Robertson 1936), and the present paper gives a corresponding X-ray determination of the structure of β-resorcinol. The comparatively open structure of α-resorcinol, which is apparently maintained by the directive power of the hydroxyl bonds, is replaced in β-resorcinol by a more parallel and compact arrangement of the molecules, reminiscent of many hydrocarbon structures. Several different factors are involved in this transformation, and it is accompanied by some deformation of the resorcinol molecule. The results are discussed more fully in relation to the thermodynamic properties of resorcinol in the following paper (Part II).

Crystal data

β-*Resorcinol*: $C_6H_6O_2$; $M = 110$; melting-point 109–110° C.; density, calculated, 1·327; orthorhombic pyramidal, $a = 7\cdot91 \pm 0\cdot01$, $b = 12\cdot57 \pm 0\cdot02$, $c = 5\cdot50 \pm 0\cdot01$ A. Space group, $C_{2v}^9 (Pna)$. Four molecules per unit cell. No molecular symmetry. Volume of the unit cell $= 547$ A^3. Absorption coefficient for X-rays, $\lambda = 1\cdot54$, $\mu = 9\cdot68$ per cm. Total number of electrons per unit cell $= F(000) = 232$. The space group is the same as for α-resorcinol (loc. cit.), and hence the same structure factor and electron density formulae are applicable. (For α-resorcinol, $a = 10\cdot53$, $b = 9\cdot53$, $c = 5\cdot66$ A.)

Experimental measurements and structure analysis

The habit of β-resorcinol is quite different from that of α-resorcinol (see Part II, fig. 4, Plate 8), and even when they are crystallized together there is no difficulty in picking out the long thin plates, or laths, which are characteristic of the β-form. These are elongated in the c axis direction, and

the large face of the lath is the (100). Small (*hk*0) side faces are frequently observed, but no well-developed end-faces were noted.

The X-ray work was carried out in a manner similar to that described for α-resorcinol (Robertson 1936), with copper *K*α radiation and photographic methods. Owing to the shape of the β-crystals, however, the path of the X-ray beam through the specimen is not the same for all the reflexions in a given zone, and it was necessary to calculate correction factors for the intensities. These were obtained roughly by evaluating a mean path for the beam through the crystal in each different reflecting position and applying the calculated absorption coefficient. Uncertainties remain owing to the divergence of the beam, and to some of the crystal specimens being slightly bent, but as the specimens employed were small (e.g. 0·091 and 0·0585 mg.) the final results should be of about the same accuracy as those obtained for α-resorcinol.

The structure factors, *F*, in absolute units, were calculated from the intensity measurements by the usual formulae, and the results are given in Table I under " *F* measured ".

In the analysis of the structure it was necessary in the first place to obtain an approximate solution by trial. Comparing the cell dimensions with those of α-resorcinol, we observe that while the *c* axes remain of nearly the same length, the *b* axis in β-resorcinol has increased by 3·0 A., and the *a* axis has diminished by 2·6 A. This suggests that in the two crystals the molecules may be inclined at similar angles to the *c* axes, but that in the β-crystals they have turned round to align themselves more nearly in the *b*-axis direction. This is confirmed by the intensities of the principal reflexions, the (200) being much the strongest reflexion in the (*hk*0) zone of β-resorcinol, while (020) is comparatively weak.

Beyond these preliminary indications there are very few outstanding features in the spectra of β-resorcinol, and the exact analysis proved to be a difficult matter. We can assume, for the trial structures, a rigid molecular model of dimensions similar to those already found in the case of α-resorcinol. It then remains to find the orientation of this model with respect to the crystal axes, and also its position with respect to the dyad screw axis of symmetry, which introduces two further parameters. It was hoped that measurements of the diamagnetic susceptibilities would help to define the orientation, but the first results proved to be ambiguous, and only confirmed the preliminary indications noted above. The latest magnetic results which have been obtained by Mrs Lonsdale, however, are now sufficiently accurate to confirm the orientation derived from this analysis.

It is perhaps unnecessary to describe the details of the trial analysis.

Various possibilities were eliminated, and finally sufficient accuracy was obtained to enable the phase constants of about 50 reflexions in the (hk0) zone to be calculated with reasonable certainty. From this stage the co-ordinate values were refined in a straightforward manner by the application of two successive double Fourier syntheses to the (hk0) structure factors.
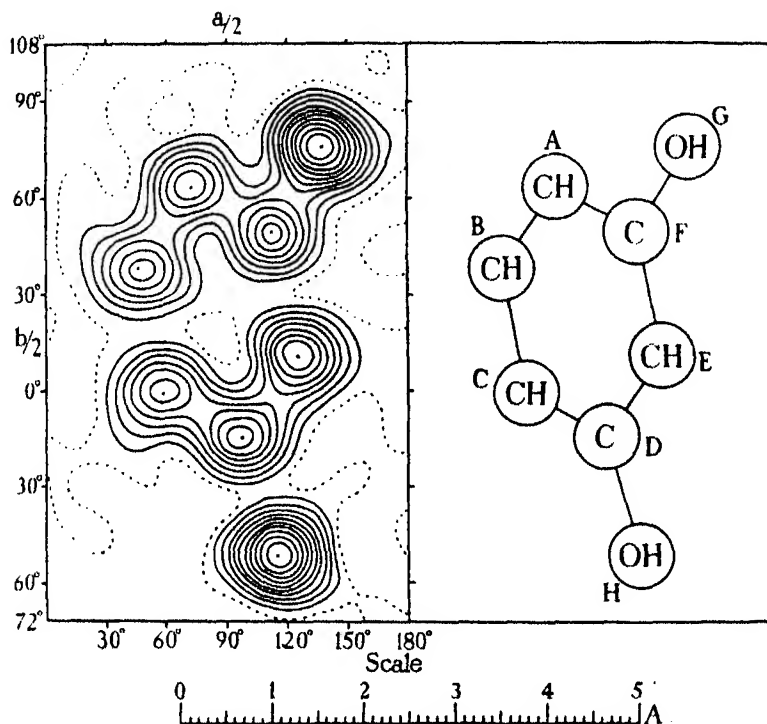
Fig. 1. β-Resorcinol in the c-axis projection on (001). Each contour line represents a density increment of approximately one electron per A^2, the one electron line being dotted. The plane of the benzene ring is inclined at 51° to the plane of this projection.

The results of the final Fourier synthesis are represented by the electron density contours of fig. 1, which cover the asymmetric unit of the crystal (one chemical molecule). In this projection, along the c-axis, the dyad screw axis is equivalent to a centre of symmetry. The complete unit cell contains four molecules, and their relative arrangement is shown in figs. 2 and 4. These diagrams should be compared with figs. 1, 2 and 8 for α-resorcinol (Robertson 1936). The final synthesis included all the observed (hk0) structure factors, listed in Table I, and the phase constants employed (α)

were subsequently verified by recalculation from the co-ordinates finally assigned to the atoms (Table II). The Fourier series for the electron density

$$\rho(x,y) = \frac{1}{ab} \sum_{-\infty}^{+\infty} \sum_{-\infty}^{+\infty} F(hk0) \cos 2\pi(hx + ky)$$

Fig. 2. Group of resorcinol molecules in the c-axis projection. Each line approximately two electrons per A².

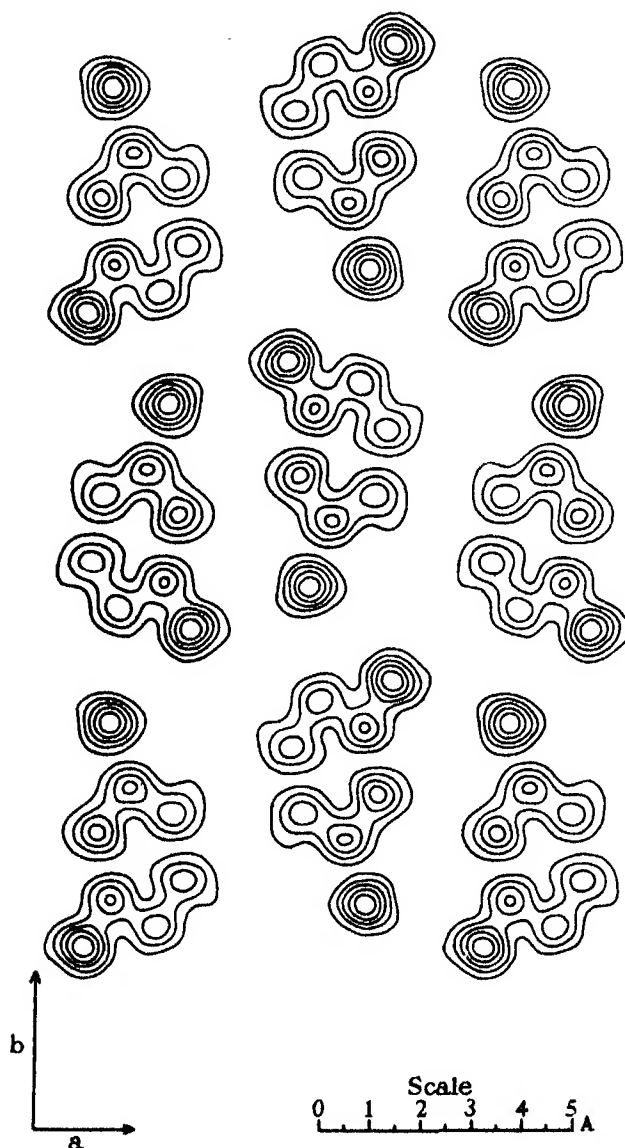was summed at 450 points on the asymmetric unit, at intervals of 12° or 0·264 A on the *a*-axis, and 6° or 0·209 A on the *b*-axis, and the maps were prepared by graphical interpolation from these summation totals.

TABLE I. MEASURED AND CALCULATED VALUES OF THE
STRUCTURE FACTOR

hkl	$\sin\theta$ $\lambda = 1\cdot 54$	$\alpha°$ calc.	*F* calc.	*F* measured
200	0·195	180	63	60
400	0·389	180	25	32
600	0·584	0	15	21
800	0·778	180	1	< 5
020	0·123	0	13	14
040	0·245	180	7	< 3
060	0·367	0	30	36
080	0·490	0	10	14
0, 10, 0	0·612	0	1	< 5
0, 12, 0	0·735	180	7	11
0, 14, 0	0·857	0	2	< 4
002	0·280	65	9	10
004	0·559	295	14	13
006	0·839	357	18	18
011	0·153	344	24	23
031	0·231	187	15	16
051	0·337	323	10	16
071	0·451	350	13	17
091	0·569	301	9	11
0, 11, 1	0·688	359	5	7
0, 13, 1	0·808	126	8	11
022	0·305	248	9	15
042	0·372	139	18	23
062	0·462	336	10	15
082	0·564	192	7	9
0, 10, 2	0·675	131	18	22
0, 12, 2	0·786	53	3	< 9
013	0·424	221	11	11
033	0·458	270	34	33
053	0·519	78	7	< 8
073	0·600	178	4	< 9
093	0·693	262	16	22
0, 11, 3	0·793	—	0	< 9
201	0·240	181	63	63
202	0·341	154	23	25
203	0·462	268	17	19
401	0·414	35	22	28
402	0·479	329	24	26
403	0·572	345	6	<12

TABLE I (*continued*)

hkl	sin θ λ = 1·54	α° calc.	F calc.	F measured
110	0·115	180	6	10
120	0·157	180	22	23
130	0·208	0	14	16
140	0·264	0	19	22
150	0·321	180	12	19
160	0·380	180	7	10
170	0·440	0	4	5
180	0·499	0	11	16
190	0·560	0	2	< 4
1, 10, 0	0·620	180	1	< 5
1, 11, 0	0·680	0	10	14
1, 12, 0	0·741	180	7	8
1, 13, 0	0·802	—	0	< 4
1, 14, 0	0·863	—	0	< 4
210	0·204	0	1	< 2
220	0·230	180	13	14
230	0·268	180	21	24
240	0·313	0	8	8
250	0·363	0	19	28
260	0·416	180	19	24
270	0·471	0	9	13
280	0·527	180	3	7
290	0·585	180	1	< 4
2, 10, 0	0·643	0	7	11
2, 11, 0	0·701	0	7	11
2, 12, 0	0·760	0	2	< 5
2, 13, 0	0·819	180	4	7
310	0·298	0	12	18
320	0·317	180	14	17
330	0·345	180	15	21
340	0·381	180	7	7
350	0·423	—	0	< 4
360	0·469	180	12	17
370	0·518	0	4	7
380	0·570	0	4	< 4
390	0·624	180	4	5
3, 10, 0	0·678	180	8	14
3, 11, 0	0·734	180	16	23
3, 12, 0	0·791	180	1	< 5
410	0·394	0	14	19
420	0·408	0	3	4
430	0·430	180	2	< 3
440	0·459	180	3	6
450	0·495	180	7	8
460	0·535	—	0	< 4
470	0·579	0	5	4
480	0·626	180	6	7
490	0·675	180	2	< 5

TABLE I (*continued*)

hkl	sin θ λ = 1·54	α° calc.	F calc.	F measured
4, 10, 0	0·725	180	9	10
4, 11, 0	0·777	180	3	< 5
4, 12, 0	0·832	0	2	< 4
510	0·490	180	10	14
520	0·502	0	8	10
530	0·520	0	1	< 4
540	0·545	0	7	9
550	0·575	0	17	20
560	0·610	0	10	14
570	0·648	180	11	15
580	0·690	180	1	< 5
590	0·735	0	1	< 5
5, 10, 0	0·782	0	5	8
5, 11, 0	0·830	0	8	11
610	0·587	180	10	12
620	0·597	0	5	7
630	0·612	0	7	6
640	0·633	180	4	6
650	0·659	180	4	7
660	0·689	0	9	10
670	0·724	180	11	13
680	0·762	0	8	10
690	0·803	0	1	< 4
6, 10, 0	0·846	180	1	< 4
710	0·684	0	4	< 5
720	0·692	0	4	< 5
730	0·706	0	3	5
740	0·724	180	5	5
750	0·747	180	5	7
760	0·774	180	2	< 5
770	0·805	0	3	< 4
780	0·839	180	5	7
810	0·780	—	0	< 5
820	0·788	—	0	< 5
830	0·800	0	3	< 5
840	0·816	0	6	8
850	0·836	0	4	7
860	0·860	180	6	6

DIMENSIONS AND ORIENTATION OF THE MOLECULE. CO-ORDINATES

All the atoms in the molecule are resolved in fig. 1, and the positions of their centres can be determined with accuracy. It is found that the projection of a regular plane hexagon can be inscribed on the benzene ring, and the corners are indicated by crosses in fig. 1. The true positions of the carbon atoms may depart from these regular points by amounts varying from

0·02 to 0·05 A (at atom *B*), but these apparent departures from regularity can probably be ascribed to experimental errors in determining the structure factors and to imperfect convergence of the Fourier series.

We assume the carbon atoms to be at the marked points, and we further assume that the regular hexagon of which this is a projection has the usual benzene ring carbon-carbon distance of 1·39 A. It is then easy to obtain the complete orientation of the molecule, which can be described by giving the angles which the lines *L* and *M* and their normal *N* (fig. 3) make with the three crystallographic axes. The notation and calculations are similar to those previously used (Robertson 1936), and the results are given below:

$$\chi_L = 51·2° \cos\chi_L = 0·6260 \qquad \chi_M = 82·4° \cos\chi_M = 0·1323$$
$$\psi_L = 110·3° \cos\psi_L = -0·3469 \qquad \psi_M = 21·6° \cos\psi_M = 0·9296$$
$$\omega_L = 134·3° \cos\omega_L = -0·6984 \qquad \omega_M = 110·1° \cos\omega_M = -0·3431$$
$$\chi_N = 39·8° \cos\chi_N = 0·7685$$
$$\psi_N = 82·8° \cos\psi_N = 0·1249$$
$$\omega_N = 51·1° \cos\omega_N = 0·6281$$

The positions of the hydroxyl groups, *G* and *H*, are also marked in fig. 1. These are found to depart from the symmetrically disposed positions by small but apparently definite amounts, as can readily be seen by producing the lines *AD* and *CF*. Instead of lying on the extensions of these lines, *G* and *H* are both found to be displaced in an anticlockwise direction.

The projection of the structure in fig. 1 gives no information as to whether the hydroxyl groups are also displaced out of the plane of the benzene ring, and this matter must now be examined by means of the structure factors from other zones of planes. The displacement of the group *G* from the symmetrical position is small (< 3°), and we may assume it to lie in the plane of the ring without serious error. With regard to the group *H*, two positions were tested. (1) It was assumed to remain in the plane of the ring. (2) It was displaced out of the plane of the ring in a direction which would decrease the intermolecular approach distances of neighbouring hydroxyl groups, and also give a minimum total displacement from the symmetrical position. This movement requires the oxygen atom *H* to lie at 0·08 A above the plane of the benzene ring. The co-ordinates were calculated for these two positions, and the resulting structure factors for the (00*l*) series of planes are compared below.

These results are strongly in favour of the second alternative. Further calculations of the (0*kl*) and (*h0l*) structure factors (Table I) are also slightly in favour of the second alternative, but the difference for the two positions

is small. In calculating the remainder of the structure we assume the second alternative (H at 0·08 A above plane of ring), but it should be noted that the z co-ordinates of the oxygen atoms are uncertain to about $\pm$ 0·04 A. A second Fourier projection along the a crystal axis might settle the positions more definitely, but the experimental measurements at present available do not justify this course, and as such a projection would display no centre of symmetry, the work would be extremely tedious.

	F calculated		
	H in plane of ring	H above ring by 0·08 A	F measured
002	3	9	10
004	16	14	13
006	15	18	18

The orientations of the lines FG and DH are now as follows:

$$\chi_{FG} = 66\cdot0° \quad \cos\chi_{FG} = 0\cdot4064 \qquad \chi_{DH} = 73\cdot7° \quad \cos\chi_{DH} = 0\cdot2806$$

$$\psi_{FG} = 48\cdot4° \quad \cos\psi_{FG} = 0\cdot6631 \qquad \psi_{DH} = 163\cdot5° \quad \cos\psi_{DH} = -0\cdot9586$$

$$\omega_{FG} = 128\cdot9° \quad \cos\omega_{FG} = -0\cdot6287 \qquad \omega_{DH} = 93\cdot1° \quad \cos\omega_{DH} = -0\cdot0532$$

The real angle between L (BE) and FG becomes 62·4°, and between L and DH, 57·0°. The actual dimensions of the molecule, with the benzene ring assumed planar, are summarized in fig. 3.
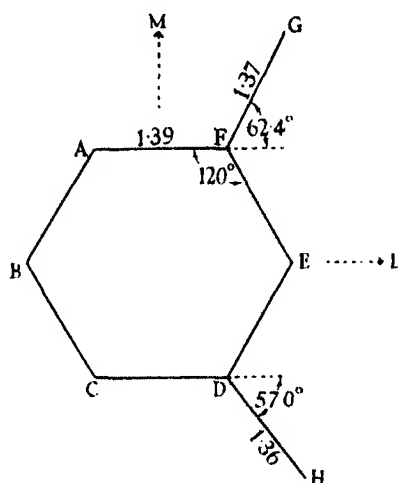

FIG. 3. Dimensions of β-resorcinol molecule. Atom H (oxygen) is 0·08 A above the plane of the ring.

It will be noted that for the two carbon-oxygen distances we obtain almost the same result as was found for α-resorcinol, viz. 1·36 A. These results are expressed in Table II, where the co-ordinates of the atoms are referred to the molecular axes and the centre of the benzene ring as origin. From fig. 1, the co-ordinates of the centre of the benzene ring with respect to the dyad screw axis are given by

$$x_0 = 1·874 \text{ A}, \qquad y_0 = 0·856 \text{ A}.$$

TABLE II. CO-ORDINATES REFERRED TO MOLECULAR AXES

Atom ...	A	B	C	D	E	F	G	H
L co-ordinate (A)	−0·695	−1·39	−0·695	0·695	1·39	0·695	1·33	1·435
M co-ordinate (A)	1·203	0	−1·203	−1·203	0	1·203	2·416	−2·337
N co-ordinate (A)	0	0	0	0	0	0	0	0·084

The atomic co-ordinates referred to the crystal axes are given in Table III. The origin of the x and y co-ordinates is taken on a dyad screw axis, while the z co-ordinates are referred to an arbitrary origin at the centre of the benzene ring.

TABLE III. CO-ORDINATES* REFERRED TO CRYSTAL AXES.
ORIGIN ON DYAD SCREW AXIS

Atom		x A	$2\pi x/a$	y A	$2\pi y/b$	z A	$2\pi z/c$
A	CH	1·60	72·7	2·215	63·5	0·07	4·7
B	CH	1·005	45·7	1·34	38·3	0·97	63·5
C	CH	1·28	58·3	−0·02	− 0·6	0·90	58·8
D	C	2·15	97·8	−0·505	−14·4	−0·07	− 4·7
E	CH	2·745	124·8	0·375	10·7	−0·97	− 63·5
F	C	2·47	112·3	1·735	49·6	−0·90	− 58·8
G	OH	3·025	137·7	2·64	75·7	−1·76	−115·0
H	OH	2·53	115·2	−1·80	−51·6	−0·145	− 9·4

* Erratum. In α-resorcinol (Robertson 1936) the x co-ordinate of atom C should read 1·855 instead of 1·185.

It will be noted that while the x and y co-ordinates can be obtained by direct measurement of the Fourier projection diagram, the z co-ordinates can only be obtained from the calculated orientation discussed above. The agreements obtained between the calculated and observed structure factors, however, are quite satisfactory, showing that the whole structure is essentially correct.

The calculated F values are based on an average hydrocarbon f-curve (Robertson 1935), the scattering power of the hydroxyl groups being weighted with respect to that of the carbon atoms in the ratio of 3:2. This is an

approximate treatment only, and of course it has no effect on the Fourier projection, which is based on the measured F values. It will be noted, however, that the calculated F values tend to be lower than the measured values, especially for the small spacing planes (large $\sin\theta$), and, in fact, to obtain the best average correlation the calculated values must be increased by a factor of about 1·3. It does not seem likely that the absolute scale of the measured values can be in error by as much as this, and the result is probably due to the temperature factor being abnormally low for β-resorcinol, which is in keeping with the relatively high density of the structure (1·327). Similar results have previously been obtained for other compounds (Robertson 1935).

In Table I the average correlating factor of 1·3 has not been applied to the calculated F values. When this is done, the average discrepancy between the measured and calculated F values for the $(hk0)$ reflexions, expressed as a sum of the individual discrepancies divided by the sum of the measured values, is only 11·3 %, rather better than is ususally obtained in work of this kind.

As a matter of interest, the oxygen atom H was now moved to the symmetrical position, i.e. on to the extension of the line AD, and the $(hk0)$ structure factors were recalculated on this basis. The discrepancies were found to increase to 17·5 %, thus showing in a very definite manner that the distortion of the molcule is a real effect.

INTERMOLECULAR DISTANCES AND ARRANGEMENT
OF MOLECULES IN THE CRYSTAL

The way in which the molecules are grouped together in the crystal will be clear from figs. 4, 5 and 6, which are projections of the structure along the three crystallographic axes. In these diagrams the atoms are indicated by letters (in conformity with figs. 1 and 3 and Table III), while the numbers on the molecules indicate the four asymmetric units in the structure which have the equivalent points: (1) x, y, z; (2) $-x, -y, \frac{1}{2}+z$; (3) $\frac{1}{2}-x, \frac{1}{2}+y, \frac{1}{2}+z$; (4) $\frac{1}{2}+x, \frac{1}{2}-y, z$.

The shortest distances between the hydroxyl groups on neighbouring molecules are indicated by dotted lines. These represent the "hydroxyl bonds", and their lengths, 2·75 and 2·70 A, appear to be slightly greater than the corresponding distances in α-resorcinol (mean 2·70 A), and slightly less than the bonds in ice (2·76 A). The angles between the hydroxyl bonds in β-resorcinol, however, are 97 and 123° compared with 102 and 106° in α-resorcinol. This greater distortion from the tetrahedral value is significant,

and is discussed in the following paper. The magnitudes of all the angles are indicated in fig. 4.

The projections are rather deceptive with regard to the disposition of the bonds in space. In fig. 4, the G---H bonds of 2·75 A between molecules 1 and 2 do not form a closed circuit, but return to a molecule one translation
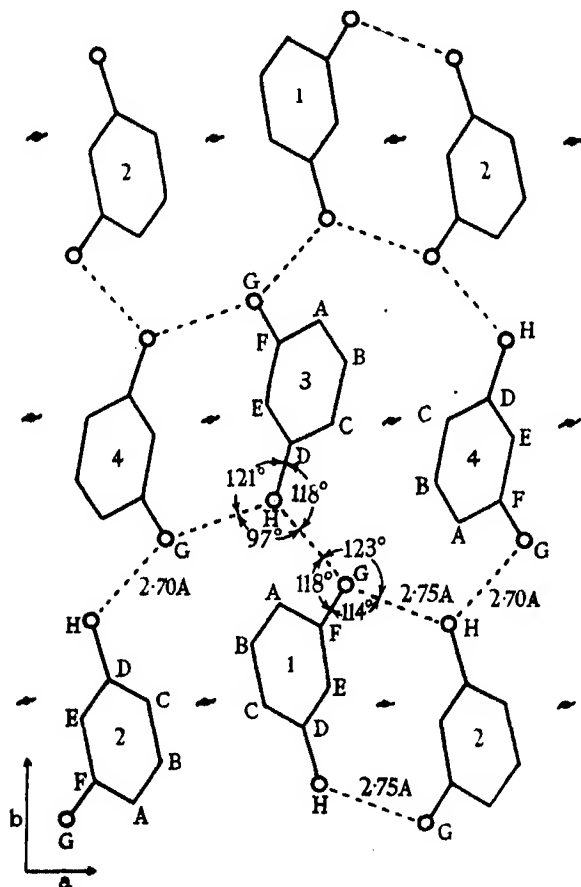

FIG. 4. *c*-axis projection on (001) showing hydroxyl bonds.

farther along the *c* axis, thus forming a staggered array which extends throughout the crystal. The relations will be clear by comparison with fig. 5.

The greatest difference between the structures of α- and β-resorcinol lies in the more parallel and compact arrangement of the molecules in the β-crystal, resulting in a higher density (1·327 instead of 1·278 in α-resorcinol).

The packing in β-resorcinol is, in fact, more typical of a hydrocarbon than of a hydroxylic compound. This is shown most clearly in fig. 6, where the molecules are viewed nearly end on, and are seen to approximate to a layer structure.
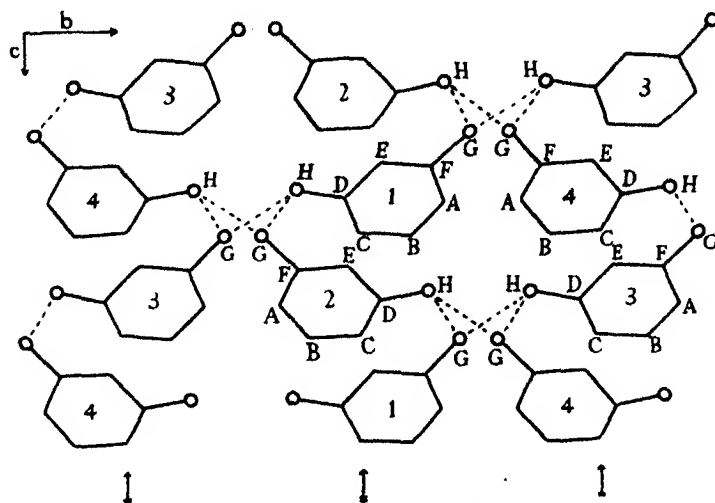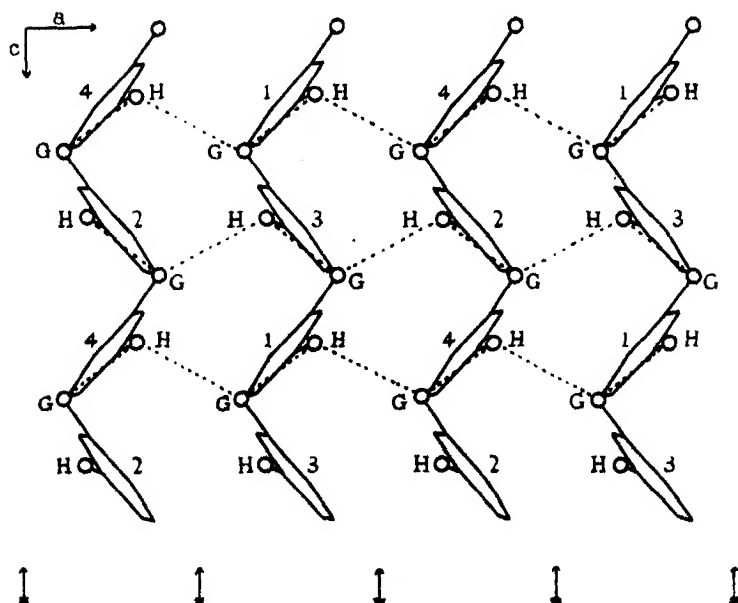

FIG. 5. *a*-axis projection on (100).

FIG. 6. *b*-axis projection on (010).

As in the case of α-resorcinol, it is found that there are two distinct types of intermolecular approach. There are the hydroxyl bonds of 2·70–2·75 A, and the ordinary van der Waals approaches of 3·4 A and upwards, but no intermediate distances. All the intermolecular distances below 4 A have been calculated from the co-ordinates, and are given in Table IV. Letters indicate atoms, suffixes the molecule, and an *accent indicates a molecule one translation further along the c-axis (which cannot be shown in fig. 4).

TABLE IV. INTERMOLECULAR DISTANCES

Oxygen-oxygen:		Carbon-carbon:	
$G_1H_3' = 2·70$ A		$D_1E_2 = 3·54$ A	
$H_1G_2 = 2·75$		$B_1D_2 = 3·68$	
Oxygen-carbon:	$A_1H_3 = 3·41$	$E_1E_2 = 3·74$	
	$A_1G_4 = 3·43$	$B_1C_2 = 3·76$	
	$D_1G_3 = 3·53$	$C_1C_2 = 3·76$	
	$F_1H_2' = 3·53$	$C_1B_2 = 3·86$	
	$E_1H_2' = 3·56$	$C_1D_2 = 3·90$	
	$F_1H_3' = 3·56$	$C_1E_1' = 3·94$	
	$B_1H_3 = 3·57$	$B_1F_1' = 3·94$	
	$D_1G_2 = 3·63$	$A_1F_4 = 3·99$	
	$B_1G_1' = 3·67$		
	$A_1H_3' = 3·74$		
	$B_1H_2 = 3·92$		
	$F_1G_4 = 3·99$		

SUMMARY

The structure of the dense, high temperature modification of resorcinol has been fully determined by means of a quantitative X-ray investigation. The structure is characterized by a more compact and parallel arrangement of the molecules than in ordinary resorcinol, which is a rather open arrangement. The benzene rings are apparently regular hexagons to within 0·05 A, but the OH groups are definitely displaced from the symmetrical positions, and one of them at least is also displaced out of the plane of the ring. The carbon-oxygen distances are 1·36–1·37 A, as in ordinary resorcinol. The orientation of the molecule in the crystal and the atomic co-ordinates are given. Hydroxyl bonds of length 2·70 and 2·75 A connect neighbouring molecules in the crystal, but the angles between these bonds are further distorted from the tetrahedral value than in ordinary resorcinol. All other intermolecular distances are greater than 3·4 A.

REFERENCES

Robertson 1935 *Proc. Roy. Soc.* A, **150**, 106, 110.
— 1936 *Proc. Roy. Soc.* A, **157**, 79.
Robertson and Woodward 1937 *J. Chem. Soc.* pp. 219, 226.
Ubbelohde and Robertson 1937 *Nature, Lond.*, **140**, 239.

A new form of resorcinol

II. Thermodynamic properties in relation to structure

By J. Monteath Robertson and A. R. Ubbelohde

[Plates 8, 9]

As is discussed below, resorcinol is one of a limited number of substances for which the denser polymorph is stable at higher temperatures. It is also one of the limited number of substances for which the detailed structure has been worked out for both forms. The correlation of thermodynamic properties with structure is thus of particular interest, and is discussed in the first part of this paper. This discussion is followed by a description of experiments on the heat of transition between the two polymorphs, on the specific volume of liquid resorcinol, and on the relative stabilities of α- and β-resorcinol in the compounds $C_6H_4(OH)_2$ and $C_6H_4(OD)_2$. Brief reference is also made to experiments on the polymorphism of pentaerythritol.

The relation between enantiotropy and structure in resorcinol

When two polymorphs can exist in thermodynamic equilibrium, it becomes possible to correlate the statistical and metrical factors which determine crystal structure. The most compact formulation of the statistical factors is obtained by using the thermodynamic functions of the solid. By definition, the free energy G_1 of a solid may be written

$$G_1 = H_1 - TS_1,$$

where H_1 is the heat content and S_1 the entropy of the solid. The dependence of H_1 and S_1 on the structure of two polymorphs can be inferred when these have a transition point. At absolute zero the crystalline structure with the lowest heat content $(H_1)_0$ will also have the lowest free energy, and will therefore be the stable form. Equilibrium with a second crystal structure of free energy G_2 will only be possible at a transition temperature θ such that

$$G_2 - G_1 = 0 = (H_2 - H_1) - \theta(S_2 - S_1). \tag{A}$$

[136]

One condition for enantiotropy is that θ must lie below the melting-point of the form stable at low temperatures. Furthermore, above the transition point $G_1 > G_2$, so that in the neighbourhood of this temperature

$$dG_1/dT > dG_2/dT.$$

From the Gibbs-Helmholtz equation

$$G_1 - H_1 = T\frac{dG_1}{dT} \quad \text{and} \quad G_2 - H_2 = T\frac{dG_2}{dT}.$$

Combining this information, $H_2 > H_1$, i.e. heat must always be absorbed in passing into the polymorph stable at higher temperatures. From equation (A) it follows that θ can only be positive, i.e. have a physical meaning if S_2 is likewise greater than S_1.

The condition $H_2 > H_1$, $S_2 > S_1$ can be satisfied by quite large differences of heat content between the two crystal structures, provided there is a corresponding increase in entropy. One molecular mechanism corresponding with a polymorphism of this type can be readily visualized, viz. when the increase in heat content is due to a weakened binding and an expansion in volume of the crystal, and the increase in entropy is due to the consequent increase in thermal motion of the molecules, and in many cases to an increase in crystal symmetry. A typical example in a crystal which involves only van der Waals forces is the transition in solid long-chain paraffins (Garner, van Bibber & King 1931; other references are in Ubbelohde 1937 b). In such cases the heat of transition is of the same order of magnitude of the heat of melting. A survey of the enantiotropic structures described by Groth (1906-19) suggests that even when forces other than van der Waals attractions contribute to the crystal structure, the majority of polymorphs at ordinary pressures show the general behaviour described in this paragraph. Amongst the very limited number of exceptions is the change from hexagonal to cubic silver iodide at 146°, and from grey to white tin at 18°, both of which involve a contraction of volume with rise in temperature. At higher pressures (P. W. Bridgman 1937) exceptions are more common.

From what is stated in Part I, and from the experimental details given below, it is clear that the behaviour of resorcinol likewise departs from the general rule. On changing to the high temperature polymorph, there is (a) a contraction in volume (cf. fig. 1); (b) no change in crystal symmetry (Part I, p. 122); (c) a heat of transition which does not exceed 5 % of the heat of fusion (p. 145); (d) the temperature factors for the intensities of

reflexion (Part I, p. 132) show that there is no great increase in thermal motion of the atoms in β-resorcinol.

A comparison of the structure of the two forms can most readily be made by inspecting figs. 8 and 9 of the paper on α-resorcinol (Robertson 1936) and figs. 4, 5 and 6 of Part I (p. 134), and throws considerable light on the change of structure with temperature. The unusually open structure of α-resorcinol (cf. Robertson 1936, fig. 8) is apparently conditioned by two factors:

(1) The arrangement of hydroxyl bonds about the oxygen atoms at approximately the tetrahedral angle. In α-resorcinol the angle between the two hydroxyl bonds is $102°$ for one oxygen atom and $106°$ for the other.
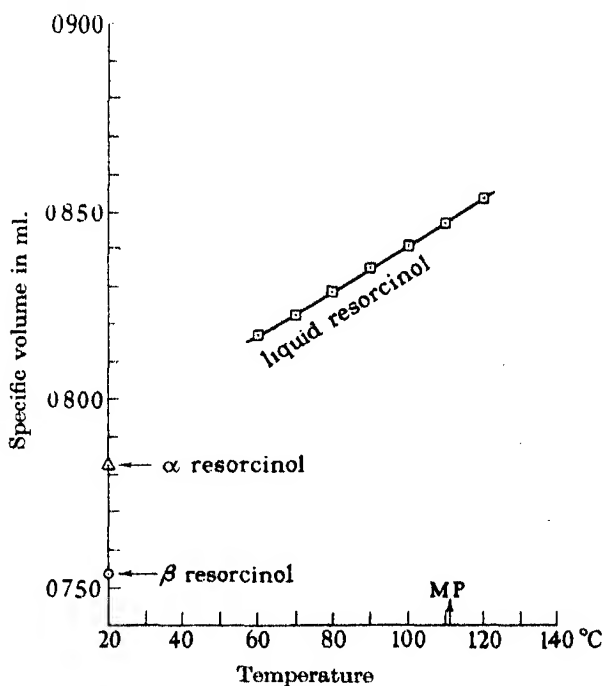

FIG. 1. Specific volumes of resorcinol in different arrangements of molecules.

(2) The rigidity of the resorcinol molecule, in which the six carbon atoms and the two oxygen atoms lie in one plane. Such an open structure will not as a rule have the minimum van der Waals energy, nor will the dipoles be surrounded by the maximum amount of polarizable material, but the contribution of these energy factors to the lattice structure is outweighed by the energy contribution made by the hydroxyl bonds.
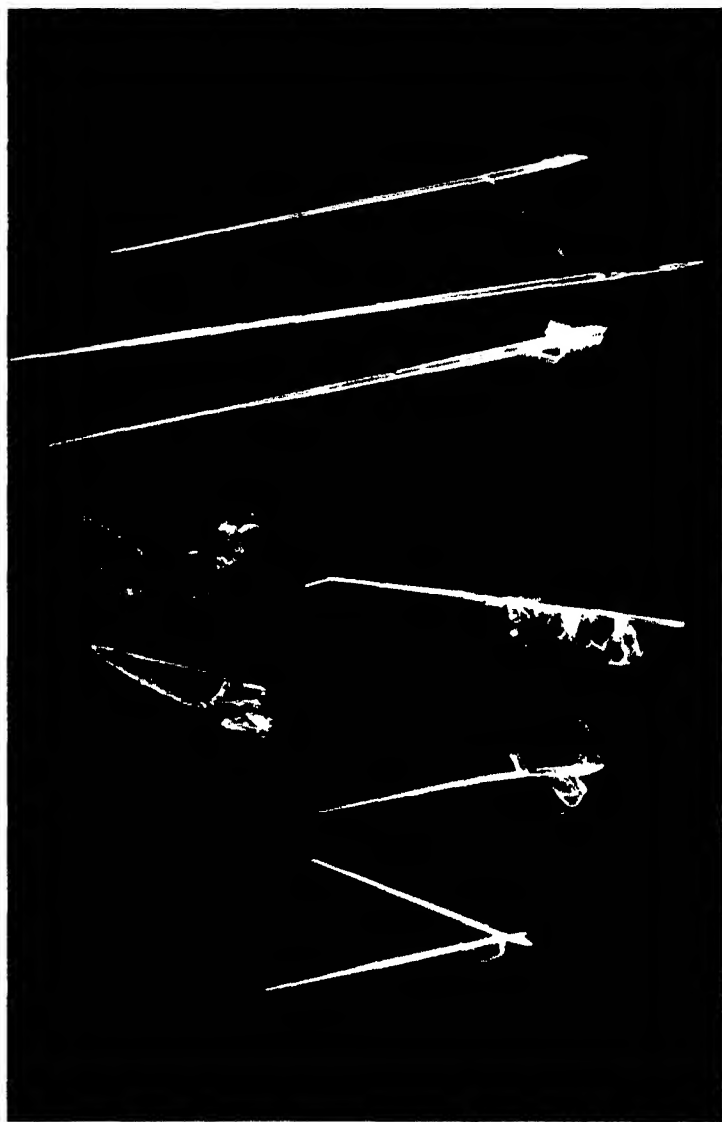
Fig. 4. Crystals of α and β resorcinol. α (needles). β (plates).
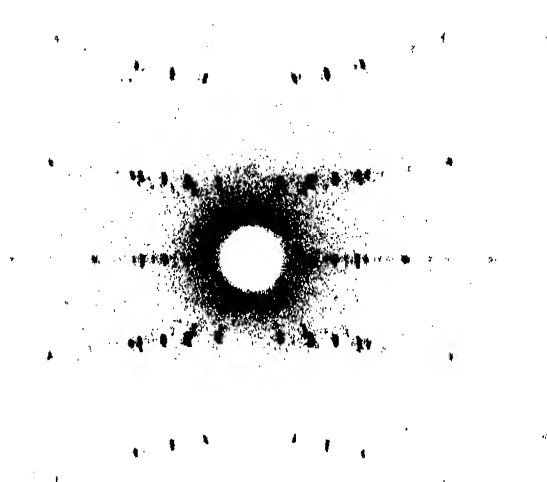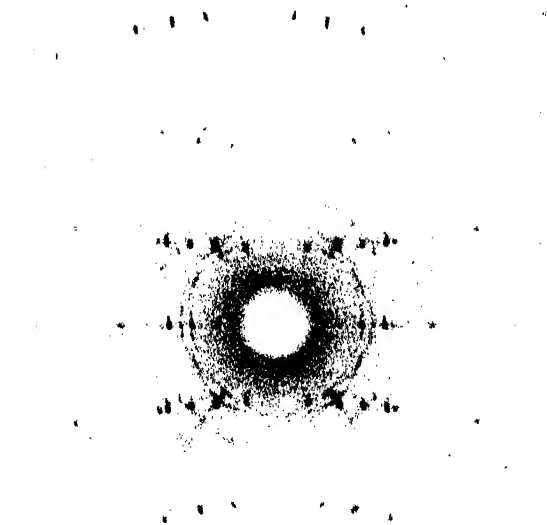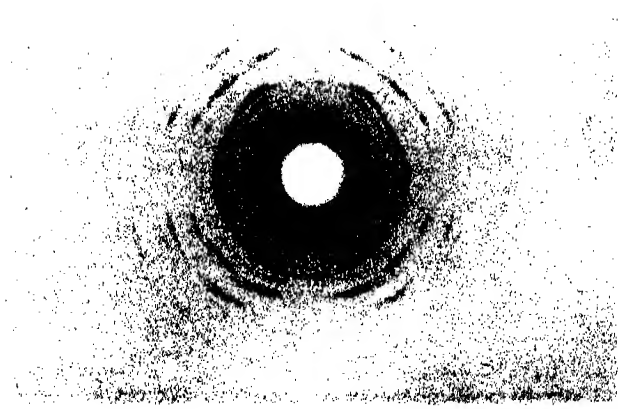
Fig. 5

Fig. 6

Fig. 7

As the temperature is raised, either of the factors (1) or (2) may be upset. For example, in the case of H_2O the open structure maintained by the hydroxyl bonds in ice I changes to a more compact arrangement of molecules when these bonds are broken by melting, i.e. when factor (1) ceases to be operative. Inspection of the structure of β-resorcinol shows that the *minimum* distance of approach between two oxygen atoms has increased, but only from 2·66 to 2·70 A. Furthermore, the angle between the two hydroxyl bonds has been considerably distorted, and is now 97° for one oxygen atom and 123° for the other. The hydroxyl bonds in the high-temperature polymorph are thus both stretched and distorted, but do not disappear. The structures suggest that the reason for the transition is connected with a breakdown of the planar resorcinol molecule, i.e. with factor (2). Details of the deformation which this molecule undergoes in β-resorcinol are given in Part I (p. 129). The experimental evidence is against the assumption that this decrease in rigidity of resorcinol is due to a large increase in thermal motion of the atoms. Rise in temperature may change the resorcinol molecule into an excited structure with slightly higher energy. Two structures which may be considered in this connexion are:
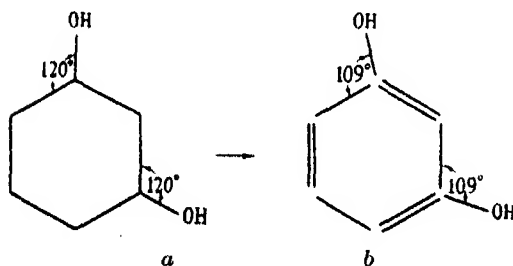

FIG. 2. Normal resorcinol molecule (*a*) compared with the Kekulé structure (*b*).
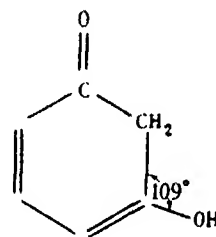
FIG. 3. One of the possible keto forms of resorcinol.

(1) A stabilization of one of the Kekulé forms, with consequent departure from the hexagon valency angle (cf. fig. 2). The direction of the distortion agrees with that observed in β-resorcinol (cf. fig. 3, Part I), but the assumption of such a structural change would not account for the fact that the oxygen atom is pulled out of the plane of the ring.

(2) A change of resorcinol into a keto form is suggested by the substitution experiments of Munzberg (1936), but a consideration of fig. 3 makes it clear that this assumption would not account for the fact that the C—O distances are practically unchanged in β-resorcinol, and that the hydroxyl bonds are somewhat longer. Although neither of these structures

for the distorted resorcinol molecules is in complete accord with experiment, it seems desirable to mention them in order to emphasize that an organic molecule, with a number of possible arrangements of valency bonds of practically the same energy, may pass from the ground structure into one of the excited structures if the resulting crystal has a lower free energy. Such a behaviour would be analogous to the Mills-Nixon effect of neighbouring groups on the benzene nucleus.

The small heat of transition between the polymorphs might be ascribed to the fact that (using the acquisitive convention for signs) the lower van der Waals and polarization energy of the denser crystals compensates almost completely for the higher strain energy of the bonds. These sources of crystal energy could in principle be calculated by summing the mutual potential energy of all the atoms, but it is found that the summation series converge too slowly to make such a calculation at all informative. It is, however, significant that the roughly parallel arrangement of molecules in β-resorcinol closely resembles that of many hydrocarbons, in which the structure is determined solely by van der Waals forces. A further point of interest is that the deformation of the hydroxyl bonds which takes place when ice I changes into the denser ice III (cf. W. H. Bragg 1938) likewise involves only a small heat of transition (0·17 kcal./mol.), presumably because the strain energy is again nearly compensated by increased van der Waals and polarization effects in the denser structure.

The conclusion from this discussion is that the anomalous change of structure with rise in temperature shown by resorcinol is due to the unusually open structure of the low-temperature form, which results from the orienting influence of hydroxyl bonds on rigid resorcinol molecules. As the temperature is raised this rigidity breaks down, and since the deformation of hydroxyl bonds apparently takes place without much increase in energy, the molecules rearrange into a structure resembling many hydrocarbons, so as to achieve a lower van der Waals and polarization potential.

EXPERIMENTS ON THE THERMODYNAMIC PROPERTIES OF RESORCINOL

Preparation of α- and β-resorcinol

In view of the complete determination of structure of α-resorcinol (Robertson 1936), this compound was included in a series of investigations on the isotope effect in solids (Ubbelohde 1936, 1937c; Robertson and Ubbelohde 1937). The effect of substitution of hydrogen by deuterium on the lattice spacing is small, and will not be discussed in the present paper. The

effect on certain other properties of the crystal is, however, rather striking. For example, when a compound with the approximate composition $C_6H_4(OD)_2$ is crystallized from boiling benzene, the bulk of the crystals belong to a new form, which has been termed β-resorcinol.

Crystals of β-resorcinol obtained in this way from the deuterium compound are, however, poor and feathery, and unsuitable for accurate determinations of the structure. Repeated attempts to obtain this form by crystallizing $C_6H_4(OH)_2$ from boiling benzene were unsuccessful, but the possibility that it was identical with the high-temperature polymorph (H. Lautz 1913) suggested an application of Ostwald's rule of successive states (cf. Ubbelohde 1937a). By evaporating a dilute solution of resorcinol in benzene at ordinary temperatures, the bulk of the spontaneously formed crystallization nuclei were in fact found to grow into crystals of the new form. In order to avoid the presence of air-borne nuclei of α-resorcinol, and also in order to avoid traces of water, the current of air used in evaporating the benzene solution was filtered through glass-wool cooled in liquid air (cf. Ubbelohde 1933). Crystals of β-resorcinol prepared in this way were used in the bulk of the X-ray measurements described in Part I.

A second method of preparing β-resorcinol, by sublimation *in vacuo*, brings out a further striking difference between $C_6H_4(OH)_2$ and $C_6H_4(OD)_2$. Using a vacuum of about $\frac{1}{2}$ mm. and a sublimation path of about 3 cm., $C_6H_4(OH)_2$ gives about equal numbers of long α-crystals and of β-crystals in the shape of large irregular plates (cf. fig. 4, Plate 8). Under the same conditions of sublimation $C_6H_4(OD)_2$ gives almost exclusively α-crystals. β-crystals are only obtained at much higher pressures, when the sublimed crystals are deposited in regions of comparatively high temperature.

The origin of these differences between $C_6H_4(OH)_2$ and $C_6H_4(OD)_2$ is discussed below.

Transition between α- and β-resorcinol

The identity of β-resorcinol with the high-temperature polymorph described by Lautz (1913) was established by taking X-ray powder photographs of ground-up β-crystals, and comparing these with photographs of powdered α-resorcinol, and with the high-temperature polymorph prepared as is described below (p. 145). In order to investigate the origin of the differences between $C_6H_4(OH)_2$ and $C_6H_4(OD)_2$ dideutero resorcinol was prepared by dissolving 10 g. resorcinol (B.D.H. A.R.) in 8·5 g. of 99·6 % D_2O, standing 1 hr., evaporating the D_2O *in vacuo*, and repeating the process with three fresh samples of 4 g. D_2O. The final purification was carried out by sublimation *in vacuo*. Microcombustions of about 3 mg. of the product

were made by Dr Weiler, and showed a carbon content of $63 \cdot 87 \pm 0 \cdot 05 \%$. This compares with the theoretical values of $65 \cdot 45 \%$ for $C_6H_4(OH_2)$, $64 \cdot 26 \%$ for $C_6H_4(OD)_2$, and $62 \cdot 07 \%$ for $C_6D_4(OD)_2$, and suggests in agreement with Munzberg (1936) that in addition to the rapid replacement of hydrogen in the hydroxyl groups, substitution in the nucleus has taken place by a much slower process.

The melting-point of resublimed A.R. resorcinol was 109–110°. When long single α-crystals were placed in the melting-point tube the breaking up of the crystals on changing to β-resorcinol was clearly visible below the melting-point. The deuterium compound appears to melt at a slightly lower temperature, but the difference is within experimental error. The transition into the denser polymorph was determined by a method similar to that used by Lautz. About 5 g. of resublimed resorcinol was weighed into a special pyknometer, and covered with xylol (previously shaken with strong sulphuric acid, distilled and dried over solid KOH), taking care to avoid air bubbles by repeatedly evacuating the apparatus. A comparison pyknometer was filled with crystals of $C_6H_4(OD)_2$ prepared by sublimation under similar conditions.

Although the volume contraction on changing from α- to β-resorcinol is as much as $0 \cdot 100$ c.c./4 g., the hysteresis observed for both $C_6H_4(OH)_2$ and $C_6H_4(OD)_2$ made it difficult to determine the true equilibrium temperature between the polymorphs. The results of a large number of experiments can be summed up by the statement that for $C_6H_4(OH)_2$ no transition into the denser polymorph was ever observed below $74 \cdot 2°$ C., even when the crystals were nucleated by heating for a short time up to 85° C. to initiate the change. For $C_6H_4(OD)_2$ the corresponding temperature was $76 \cdot 0°$ C. The change from one polymorph into the other was always more rapid for the deuterium compound; for example, on storing the β-crystals under xylol for 12 hr. at 20° C., complete reversion to the α form was observed for $C_6H_4(OD)_2$ and only a small change for $C_6H_4(OH)_2$. Large single crystals of β-$C_6H_4(OH)_2$ show the same transition even more slowly. Figs. 5, 6, 7, Plate 9 show a series of rotation photographs of such a crystal taken at intervals of 14, 25, and 48 days after its preparation. It will be noticed that in addition to the spots due to the single β-crystal, powder streaks corresponding with crystallites of α-resorcinol gradually appear. The fact that these streaks do not form complete rings indicates that these crystallites are formed preferentially in certain directions, with respect to the original β-crystal. Under the same conditions of observation an α-crystal shows no change at ordinary temperatures.

These results suggest that the differences in behaviour between $C_6H_4(OD)_2$

and $C_6H_4(OH)_2$ are due to the fact that the deuterium compound adjusts itself more rapidly to the equilibrium conditions prevailing at the moment of crystal formation, so that the rule of successive states holds for $C_6H_4(OH)_2$ whereas for $C_6H_4(OD)_2$ the most stable modification is obtained.

The heat of transition from α- to β-resorcinol

Measurements of the specific heat of resorcinol (Andrews, Lynn and Johnston 1926) apparently show no anomaly in the specific heat in the neighbourhood of the transition point. From this it could be inferred that the heat of transition is small compared with experimental error. The heat of transition from α- to β-resorcinol might, however, have been missed in the above measurements, on account of the hysteresis, so that an independent estimate of the heat of transition was obtained from a comparison of the heats of solution of α- and β-resorcinol in water.

A simple calorimeter which was quite satisfactory for this purpose was made from a 500 c.c. thermos flask, selected for its good heat insulation. This was filled with about 200 c.c. of distilled water, and the neck was fitted with apertures for inserting a stirrer, a calibrated constantan heating coil of about 37 ohms, a wide tube for the rapid addition of weighed amounts of resorcinol, and a thermometer. The temperature could be estimated to 1/100th of a degree with a reading microscope. The heat capacity of the system was measured before and after each addition of resorcinol by passing a current, measured with a calibrated ammeter, for a measured time through the heating coil. Temperature equilibrium was very rapid, and since the heat of solution of resorcinol is positive (see below) it was possible to maintain the contents of the calorimeter approximately at room temperature, by balancing this heat of solution with the electrical heat input. In this way the correction for temperature drift which has to be considered in all calorimetric experiments (cf. Eucken 1929) was negligible in practically all cases.

Using the acquisitive convention for signs, the heat quantities measured in these experiments are the heats of solution Q_1 and Q_2, where $XQ_1 = -$ (heat content of X g. α-resorcinol at $0°$ C.) $-$ (heat content of water at $18°$ C.) $+$ (heat content of solution at $18°$ C.), and Q_2 is the corresponding quantity for β-resorcinol. Q_1 and Q_2 were found to show only a slight drift with increasing concentration, up to 4 % by weight of resorcinol, so that the average heat of solution per g. was calulated irrespective of concentration.

The experimental results may be described by giving an extract from a

typical series of observations, together with the average values of Q_1 and Q_2.

Time in min.	Temp.
0	18·77
$\frac{1}{2}$	18·77
1	18·77
$1\frac{1}{2}$	18·77
2	18·77
$2\frac{1}{2}$	18·77
3	18·77

3 min. 15·0 sec. to 4 min. 15·0 sec.

642 mA passed through the heating coil

$4\frac{1}{2}$	19·70
5	19·74
$5\frac{1}{2}$	19·75
6	19·75
$6\frac{1}{2}$	19·75

Add 3·536 g. resorcinol

$8\frac{1}{2}$	19·20
9	19·20
$9\frac{1}{2}$	19·20
10	19·20
$10\frac{1}{2}$	19·20

The average of seven complete experiments on resorcinol gave a value

$$Q_1 = +37 \cdot 5 \pm 0 \cdot 5 \, \text{cal./g.,}$$

and on β-resorcinol

$$Q_2 = +35 \cdot 5 \pm 0 \cdot 4 \, \text{cal./g.}$$

The average value of $Q_2 - Q_1$ for all the experiments was

$$Q_2 - Q_1 = -2 \cdot 0 \pm 0 \cdot 25 \, \text{cal./g.} = -220 \pm 28 \, \text{cal./mol.}$$

This difference is equal to the difference in heat contents of the α and β forms at $0°$ C. Since there is no large difference between the specific heats of chemically similar solids (Andrews and others 1926) the heat change at the transition point will be about the same, i.e.

$$\Delta H(\alpha \to \beta) = 220 \pm 28 \, \text{cal./mol.}$$

In this result the random errors are as given. The chief systematic errors would arise from a heating up of the powdered resorcinol during transfer from a bath at $0°$ C. to the calorimeter, and from the fact that the powders used may not have contained exclusively α- and β-crystals respectively. The first source of error would tend to cancel in the difference $Q_2 - Q_1$ since

the conditions were kept closely similar. The source of resorcinol was a finely crystalline sample (B.D.H. A.R.). A powder of β-crystals was obtained by heating this sample to 100° C. for 1 hr., and rapidly plunging into ice water, and was kept at 0° C. till introduced into the calorimeter. The change in texture of the powder as a result of this treatment is readily observed. No evidence of the alternative form could be observed in either of these samples by X-ray powder photographs, even after the β sample had been stored for 24 hr. at 20° C.

This method of analysis would however fail to detect 10 % of the alternative form in the samples used. In order to give a margin for systematic errors, the heat of transition should be taken as

$$\Delta H(\alpha \to \beta) = 220 \pm 50 \, \text{cal./mol. at } 0° C.$$

Since the heat of fusion is 5090 cal./mol. (Andrews and others 1926), the heat of transition does not exceed 5 % of the heat of fusion; this probably explains why it has been missed in specific heat measurements.

THE SPECIFIC VOLUME OF LIQUID RESORCINOL

As is discussed above, the molecules in α-resorcinol are arranged in an unusually open structure. The analogy of ice suggests that such a structure might melt to a more compact liquid. It is not possible to make direct observations of the volume change on melting α-resorcinol, but some information is available from measurements on the supercooled liquid. By using a calibrated pyknometer carefully protected from dust etc., it was possible to measure the specific volume of liquid resorcinol some 60° below the melting-point and 16° below the transition point. These specific volumes are given in the diagram (fig. 1), together with the values for crystals of α- and β-resorcinol at 20° C., as calculated from X-ray measurements. Although the curve for the supercooled liquid could not be prolonged down to this temperature, it shows quite clearly that there is only a small expansion in changing from the arrangement of molecules in α-resorcinol to the arrangement in the liquid.

THE TRANSITION IN PENTAERYTHRITOL

A preliminary investigation of the transition from a tetragonal to a cubic structure in pentaerythritol (Ebert 1931) was made in order to verify whether the large number of hydroxyl bonds in the low-temperature polymorph might lead to an anomaly similar to that of resorcinol. The transition

however appears to be of the normal kind. The heat of transition is large compared with the heat of fusion (Ebert 1931). The volume change was measured in a pyknometer, using a high-boiling paraffin as indicator liquid. Great difficulty was experienced in freeing the crystals from traces of air, and especially from traces of water. Even with crystals dried at 150° in air, bubbles of steam are evolved in the pyknometer near the transition point. These bubbles appear to be resorbed by the pentaerythritol when it passes into the cubic structure at 180° C., and are not reevolved till 210°. In consequence, there is a contraction in volume on passing through the transition point. If the pyknometer and contents are, however, first evacuated for several hours at 210° C. till practically no more H_2O is evolved, and cooling curves are then plotted of volume against temperature, there is a more rapid decrease in volume when the tetragonal crystals begin to appear. This point (about 176° C.) can be readily observed by the change from translucent to opaque crystals in the pyknometer. The conclusion from these preliminary experiments is that pentaerythritol shows the normal volume and heat changes on transition. The molecule is of course much less rigid than H_2O or $C_6H_4(OH)_2$ so that this result might have been expected.

[*Note added in proof.* This conclusion is confirmed by the X-ray investigation of Nitta and Watanabe (1938).]

In conclusion, we wish to thank Sir William Bragg, O.M., P.R.S., and the Managers of the Royal Institution for their interest in this work. We are also indebted to Miss Woodward for assistance in preparing the diagrams.

SUMMARY

The anomalous temperature relationship between the polymorphs of resorcinol is discussed in the light of the crystal structures. The open α-structure is maintained by hydroxyl bonds orienting the rigid resorcinol molecules. Transition to the denser β-structure, which resembles that of many hydrocarbons, is associated with a distortion of the hydroxyl bonds, and a deformation of the resorcinol molecule which may involve a Mills-Nixon effect.

Experiments are described on the preparation of α- and β- resorcinol, on the transition between the two forms, and on the heat of transition. The transition point of $C_6H_4(OH)_2$ is about 2° lower than that of $C_6H_4(OD)_2$, and the change from one form to the other is considerably more rapid in the deuterium compound. The heat of transition from α- to β-resorcinol is 220 ± 50 cal./mol. Experiments on the volume change from (supercooled) liquid resorcinol to either crystal structure show that there is only a small

expansion on passing from the open α-structure to the liquid. Experiments on the transition between two polymorphs of pentaerythritol show a normal temperature relationship for this substance.

REFERENCES

Andrews, Lynn and Johnston 1926 *J. Amer. Chem. Soc.* **48**, 1274.
Bragg, Sir W. H. 1938 *Not. Proc. Roy. Instn.* **30**, 283.
Bridgman, P. W. 1937 *Proc. Amer. Acad.* **72**, 133, 227.
Ebert, L. 1931 *Ber. dtsch. chem. Ges.* **64B**, 114.
Eucken, A. 1929 "Energie und Warmeinhalt", p. 47. Leipzig.
Garner, van Bibber and King 1931 *J. Chem. Soc.* p. 1533.
Groth 1906–19 "Chemische Kristallographie." Leipzig.
Lautz, H. 1913 *Z. phys. Chem.* **84**, 611.
Munzberg, F. 1936 *Z. phys. Chem.* B, **33**, 23.
Nitta, I. and Watanabe, T. 1938 *Bull. Chem. Soc. Japan*, **13**, 28.
Robertson, J. M. 1936 *Proc. Roy. Soc.* A, **157**, 79.
Robertson, J. M. and Ubbelohde, A. R. 1937 *Nature, Lond.*, **139**, 504.
Ubbelohde, A. R. 1933 *J. Chem. Soc.* p. 972.
—— 1936 *Trans. Faraday Soc.* **32**, 525.
—— 1937a *Trans. Faraday Soc.* **33**, 1203.
—— 1937b *Trans. Faraday Soc.* **34**, 289.
—— 1937c *Proc. Roy. Soc.* A, **159**, 295.

DESCRIPTION OF PLATES

PLATE 8

FIG. 4. It will be seen from the crystals photographed that two α-crystals are frequently found joined at a definite angle, and that crystals of β-resorcinol can apparently grow out of crystals of α-resorcinol, presumably because in either case the two crystals have approximately the same arrangement of molecules at the plane of contact.

PLATE 9

FIGS. 5–7. Rotation X-ray photographs of a crystal of β resorcinol gradually reverting to α resorcinol, showing the preferential orientation of the α crystallites.

expansion on passing from the open α-structure to the liquid. Experiments on the transition between two polymorphs of pentaerythritol show a normal temperature relationship for this substance.

REFERENCES

Andrews, Lynn and Johnston 1926 *J. Amer. Chem. Soc.* **48**, 1274.
Bragg, Sir W. H. 1938 *Not. Proc. Roy. Instn.* **30**, 283.
Bridgman, P. W. 1937 *Proc. Amer. Acad.* **72**, 133, 227.
Ebert, L. 1931 *Ber. dtsch. chem. Ges.* **64B**, 114.
Eucken, A. 1929 "Energie und Warmeinhalt", p. 47. Leipzig.
Garner, van Bibber and King 1931 *J. Chem. Soc.* p. 1533.
Groth 1906–19 "Chemische Kristallographie." Leipzig.
Lautz, H. 1913 *Z. phys. Chem.* **84**, 611.
Munzberg, F. 1936 *Z. phys. Chem.* B, **33**, 23.
Nitta, I. and Watanabe, T. 1938 *Bull. Chem. Soc. Japan,* **13**, 28.
Robertson, J. M. 1936 *Proc. Roy. Soc.* A, **157**, 79.
Robertson, J. M. and Ubbelohde, A. R. 1937 *Nature, Lond.,* **139**, 504.
Ubbelohde, A. R. 1933 *J. Chem. Soc.* p. 972.
— 1936 *Trans. Faraday Soc.* **32**, 525.
— 1937a *Trans. Faraday Soc.* **33**, 1203.
— 1937b *Trans. Faraday Soc.* **34**, 289.
— 1937c *Proc. Roy. Soc.* A, **159**, 295.

DESCRIPTION OF PLATES

PLATE 8

FIG. 4. It will be seen from the crystals photographed that two α-crystals are frequently found joined at a definite angle, and that crystals of β-resorcinol can apparently grow out of crystals of α-resorcinol, presumably because in either case the two crystals have approximately the same arrangement of molecules at the plane of contact.

PLATE 9

FIGS. 5–7. Rotation X-ray photographs of a crystal of β resorcinol gradually reverting to α resorcinol, showing the preferential orientation of the α crystallites.

Classical theory of radiating electrons

BY P. A. M. DIRAC, F.R.S., *St John's College, Cambridge*

(*Received* 15 *March* 1938)

INTRODUCTION

The Lorentz model of the electron as a small sphere charged with electricity, possessing mass on account of the energy of the electric field around it, has proved very valuable in accounting for the motion and radiation of electrons in a certain domain of problems, in which the electromagnetic field does not vary too rapidly and the accelerations of the electrons are not too great. Beyond this domain it will not go unless supplemented by further assumptions about the forces that hold the charge on an electron together. No natural way of introducing such further assumptions has been discovered, and it seems that the Lorentz model has reached the limit of its usefulness and must be abandoned before we can make further progress.

One of the most attractive ideas in the Lorentz model of the electron, the idea that all mass is of electromagnetic origin, appears at the present time to be wrong, for two separate reasons. First, the discovery of the neutron has provided us with a form of mass which it is very hard to believe could be of electromagnetic nature. Secondly, we have the theory of the positron—a theory in agreement with experiment so far as is known—in which positive and negative values for the mass of an electron play symmetrical roles. This cannot be fitted in with the electromagnetic idea of mass, which insists on all mass being positive, even in abstract theory.

The departure from the electromagnetic theory of the nature of mass removes the main reason we have for believing in the finite size of the electron. It seems now an unnecessary complication not to have the field equations holding all the way up to the electron's centre, which would then appear as a point of singularity. In this way we are led to consider a point model for the electron. Further reasons for preferring the point-electron have been given by Frenkel (1925).*

We are now faced with the difficulty that, if we accept Maxwell's theory, the field in the immediate neighbourhood of the electron has an infinite mass. This difficulty has recently received much prominence in quantum mechanics (which uses a point model of the electron), where it appears as

* See pp. 526 and 527 of Frenkel's paper. The reason on p. 518 is not valid according to present-day knowledge.

[148]

a divergence in the solution of the equations that describe the interaction of an electron with an electromagnetic field and prevents one from applying quantum mechanics to high-energy radiative processes. One may think that this difficulty will be solved only by a better understanding of the structure of the electron according to quantum laws. However, it seems more reasonable to suppose that the electron is too simple a thing for the question of the laws governing its structure to arise, and thus quantum mechanics should not be needed for the solution of the difficulty. Some new physical idea is now required, an idea which should be intelligible both in the classical theory and in the quantum theory, and our easiest path of approach to it is to keep within the confines of the classical theory.

A possible line of attack is to modify Maxwell's theory so as to make the energy of the field around the singularity that represents an electron finite. This method has been tried by Born, but it leads to great complexity, and its present outlook is not very hopeful.

We shall here proceed from the opposite point of view. We shall retain Maxwell's theory to describe the field right up to the point-singularity which represents our electron and shall try to get over the difficulties associated with the infinite energy by a process of direct omission or subtraction of unwanted terms, somewhat similar to what has been used in the theory of the positron. Our aim will be not so much to get a model of the electron as to get a simple scheme of equations which can be used to calculate all the results that can be obtained from experiment. The scheme must be mathematically well-defined and self-consistent, and in agreement with well-established principles, such as the principle of relativity and the conservation of energy and momentum. Provided these conditions are satisfied, it should not be considered an objection to the theory that it is not based on a model conforming to current physical ideas.

We shall be working all the time with the ordinary Maxwell theory, and thus we shall not be led to any essentially new equations. We shall be concerned rather with getting a satisfactory physical interpretation for equations which are already well known. It may be wondered why this problem was not solved long ago. A great deal of work has been done in the past in examining the general implications of Maxwell's theory, but it was nearly all done before the discovery of quantum mechanics in 1925, when people gave all their attention to the question of how an electron could remain in an atomic orbit without radiating—a question we now know can be answered only by going outside classical theory—and were thus not interested in simply looking for the most natural interpretation their equations will allow.

The fields associated with an electron

We shall deal first with the problem of a single electron moving in an electromagnetic field. We shall use relativistic notation throughout, taking the velocity of light to be unity. When we want to pass from the contravariant form K_μ to the covariant form K^μ of a vector, we shall use the fundamental tensor $g^{\mu\nu}$ appropriate for flat space-time, with components $g^{00} = 1$, $g^{11} = g^{22} = g^{33} = -1$, the other components vanishing. We shall also sometimes use the scalar product notation

$$(\mathbf{K}, \mathbf{L}) = K_\mu L^\mu = K_0 L_0 - K_1 L_1 - K_2 L_2 - K_3 L_3. \tag{1}$$

Let us suppose the world-line of our electron in space-time to be known and to be described by the equations

$$z_\mu = z_\mu(s), \tag{2}$$

where the $z_\mu(s)$ are given functions of the proper-time s. We have, of course, $dz_0/ds > 0$. The electromagnetic potentials A_μ at the point x_μ satisfy the equations

$$\frac{\partial A_\mu}{\partial x_\mu} = 0, \tag{3}$$

$$\Box A_\mu = 4\pi j_\mu, \tag{4}$$

where j_μ is the charge-current density vector. With our present model of the electron, j_μ vanishes everywhere except on the world-line of the electron, where it is infinitely great. The singularity in j_μ may conveniently be expressed in terms of δ-functions, and is easily seen to be

$$j_\mu = e \int \frac{dz_\mu}{ds} \delta(x_0 - z_0)\, \delta(x_1 - z_1)\, \delta(x_2 - z_2)\, \delta(x_3 - z_3)\, ds \tag{5}$$

for an electron of charge e. From the potentials A_μ the field quantities $F^{\mu\nu}$ can be derived according to

$$F^{\mu\nu} = \frac{\partial A^\nu}{\partial x_\mu} - \frac{\partial A^\mu}{\partial x_\nu}. \tag{6}$$

Equations (3) and (4) have many solutions and thus do not suffice to fix the field. One solution is provided by the well-known retarded potentials of Liénard and Wiechert. We shall call the field derived from these potentials $F^{\mu\nu}_{\text{ret}}$. We can obtain other solutions by adding to this one any solution of (3) and

$$\Box A_\mu = 0, \tag{7}$$

representing a field of radiation. The particular solution that represents the actual conditions in our one-electron problem will be the sum of the retarded potentials and the potentials satisfying (7) that represent the incoming *electromagnetic waves incident on our electron. Thus, calling the actual* field $F_{\text{act}}^{\mu\nu}$ and the incident field $F_{\text{in}}^{\mu\nu}$, we have

$$F_{\text{act}}^{\mu\nu} = F_{\text{ret}}^{\mu\nu} + F_{\text{in}}^{\mu\nu}. \tag{8}$$

Another important solution of (3) and (4) is that provided by the advanced potentials. We call the field derived from it $F_{\text{adv}}^{\mu\nu}$. We should expect $F_{\text{adv}}^{\mu\nu}$ to play a symmetrical role to $F_{\text{ret}}^{\mu\nu}$ in all questions of general theory. Let us therefore put, corresponding to (8),

$$F_{\text{act}}^{\mu\nu} = F_{\text{adv}}^{\mu\nu} + F_{\text{out}}^{\mu\nu}, \tag{9}$$

defining in this way a new field $F_{\text{out}}^{\mu\nu}$. This field is derivable from potentials satisfying·(7) and thus represents some field of radiation, and we should expect it to play a symmetrical role in general theory to $F_{\text{in}}^{\mu\nu}$, so that it should be interpretable as the field of outgoing radiation leaving the neighbourhood of the electron. The difference

$$F_{\text{rad}}^{\mu\nu} = F_{\text{out}}^{\mu\nu} - F_{\text{in}}^{\mu\nu} \tag{10}$$

would then be the field of radiation produced by the electron. This difference may, from (8) and (9), be expressed as

$$F_{\text{rad}}^{\mu\nu} = F_{\text{ret}}^{\mu\nu} - F_{\text{adv}}^{\mu\nu}, \tag{11}$$

which shows that it is completely determined by the world-line of the electron. In the appendix it is calculated near the world-line and found to be free from singularity and to have the value on the world-line

$$F_{\mu\nu\,\text{rad}} = \frac{4e}{3}\left(\frac{d^3z_\mu}{ds^3}\frac{dz_\nu}{ds} - \frac{d^3z_\nu}{ds^3}\frac{dz_\mu}{ds}\right). \tag{12}$$

Let us compare our result (11) with the usual one for the radiation produced by an accelerating electron. For definiteness, suppose we have an electron initially moving with constant velocity, then undergoing an acceleration and finally getting again into a state of constant velocity. According to the usual theory, the radiation emitted by the electron while it is accelerating will be given by the value of $F_{\text{ret}}^{\mu\nu}$ at great distances from the electron and at correspondingly great times after the time of the acceleration. This will be equal to the value of the right-hand side of (11) at these distances and times, since $F_{\text{adv}}^{\mu\nu}$ will be zero in this part of space-time. *Thus our result* (11) *for the radiation produced by an accelerating electron is*

in agreement with the usual one in that region of space-time where the usual one is defined. Our result goes beyond the usual one in providing a definite value for the field of radiation throughout space-time, which is an advantage in giving us a meaning for the radiation field close to the electron. (The usual theory gives this field inextricably mixed up with the Coulomb field.) Our result also gives a meaning for the radiation field before its time of emission, when it can have no physical significance. This, however, is unavoidable if we are to have the radiation field well defined near the electron.

Our theory has attained symmetry between the use of retarded and advanced potentials. This symmetry will be maintained in all general theoretical discussions, but it will not apply to practical applications, since we then have $F_{\text{in}}^{\mu\nu}$ given (very often it is zero), while its counterpart $F_{\text{out}}^{\mu\nu}$ is unknown.

A field that we shall need in the future is $f^{\mu\nu}$, defined as the actual field minus the mean of the advanced and retarded fields,

$$f^{\mu\nu} = F_{\text{act}}^{\mu\nu} - \tfrac{1}{2}(F_{\text{ret}}^{\mu\nu} + F_{\text{adv}}^{\mu\nu}). \tag{13}$$

It is derivable from potentials satisfying (7) and is free from singularity on the world-line of the electron. It is, in fact, from (8) and (9), just the mean of the ingoing and outgoing fields of radiation,

$$f^{\mu\nu} = \tfrac{1}{2}(F_{\text{in}}^{\mu\nu} + F_{\text{out}}^{\mu\nu}).$$

The equations of motion of an electron

To complete our theory of the interaction between an electron and the electromagnetic field we require equations of motion for the electron—equations to determine the world-line which we assumed known in the preceding section. We can get information on this question from the laws of conservation of energy and momentum. We surround the singular world-line in space-time by a thin tube, whose radius is much smaller than any length of physical importance in our one-electron problem, and we calculate the flow of energy and momentum across the (three-dimensional) surface of this tube, using the stress tensor $T_{\mu\rho}$ of Maxwell's theory, calculated from the actual field $F_{\text{act}}^{\mu\nu}$ according to the formula*

$$4\pi T_{\mu\rho} = F_{\mu\nu}F_{\rho}^{\ \nu} + \tfrac{1}{4}g_{\mu\rho}F_{\alpha\beta}F^{\alpha\beta}. \tag{14}$$

* The usual derivation of the stress-tensor is valid only for continuous charge distributions and we are here using it for point charges. This involves adopting as a fundamental assumption the point of view that energy and momentum are localized in the field in accordance with Maxwell's and Poynting's ideas.

We then have the information that the total flow of energy (or momentum) out from the surface of any finite length of tube must equal the difference in the energy (or momentum) residing within the tube at the two ends of this length, and must thus depend only on conditions at the two ends of this length. In mathematical language, the rate of flow of energy (or momentum) out from the surface of the tube must be a perfect differential.

It is easily seen that the information obtained in this way is independent of what shape and size we give to our tube (provided it is sufficiently small for the Taylor expansions used in the calculations to be valid). If we take two tubes surrounding the singular world-line, the divergence of the stress tensor $\partial T_{\mu\rho}/\partial x_{\rho}$ will vanish everywhere in the region of space-time between them, since there are no singularities in this region and (7) is satisfied throughout it. Expressing the integral

$$\iiint \partial T_{\mu\rho}/\partial x_{\rho} \,.\, dx_0\, dx_1\, dx_2\, dx_3$$

over the region of space-time between a certain length of the two tubes as a surface integral over the (three-dimensional) surface of this region, we obtain immediately that the difference in the flows of energy (or momentum) across the surfaces of the two tubes depends only on conditions at the two ends of the length considered. Thus the information provided by the conservation laws is well defined.

The calculations involved in getting this information are rather long and are given in the appendix. We choose the simplest shape of tube, a tube which is spherical, of constant radius ϵ, for each value of the proper-time, in that Lorentz frame of reference in which the electron is then at rest. To save writing we put v_{μ} for dz_{μ}/ds and use dots to denote differentiations with respect to s. We note for future use the elementary equations

$$\mathbf{v}^2 = 1 \tag{15}$$

$$(\mathbf{v}\dot{\mathbf{v}}) = 0 \tag{16}$$

$$(\mathbf{v}\ddot{\mathbf{v}}) + \dot{\mathbf{v}}^2 = 0 \tag{17}$$

in the vector notation (1).

The result of the appendix is now that, with $f^{\mu\nu}$ defined by (13), the flow of energy and momentum out from the surface of any length of tube is given by the vector

$$\int [\tfrac{1}{2} e^2 \epsilon^{-1} \dot{v}_{\mu} - e v_{\nu} f_{\mu}{}^{\nu}]\, ds,$$

integrated over the length of tube, where terms that vanish with ϵ are

neglected. This must depend only on conditions at the two ends of the length of tube, so that the integrand must be a perfect differential, i.e.

$$\tfrac{1}{2}e^2\epsilon^{-1}\dot{v}_\mu - ev_\nu f_\mu{}^\nu = \dot{B}_\mu. \tag{18}$$

This is as far as we can get from the laws of conservation of energy and momentum. To fix our equations of motion for the electron, we must make some further assumption to fix the vector B_μ. From (18) we see that

$$(\mathbf{v}\dot{\mathbf{B}}) = \tfrac{1}{2}e^2\epsilon^{-1}(\mathbf{v}\dot{\mathbf{v}}) = 0, \tag{19}$$

with the help of (16), which restricts our choice of B_μ. Apart from this, B_μ may be any vector function of v_μ and its derivatives. The simplest B_μ satisfying the restriction (19) is

$$B_\mu = kv_\mu, \tag{20}$$

where k is a constant. There are other possible expressions for B_μ satisfying (19), for example,

$$B_\mu = k'[\dot{\mathbf{v}}^4 v_\mu + 4(\dot{\mathbf{v}}\dot{\mathbf{v}})\dot{v}_\mu],$$

k' being another constant, but they are all much more complicated than (20), so that one would hardly expect them to apply to a simple thing like an electron. We therefore assume (20).

Substituting (20) into the right-hand side of (18), we see that the constant k must be of the form

$$k = \tfrac{1}{2}e^2\epsilon^{-1} - m, \tag{21}$$

where m is another constant independent of ϵ, in order that our equations may have a definite limiting form when ϵ tends to zero. We then get

$$m\dot{v}_\mu = ev_\nu f_\mu{}^\nu, \tag{22}$$

as our equations of motion for the electron. They are of the usual form of the equations of motion of an electron in an external electromagnetic field, with m playing the part of the rest-mass of the electron and $f_\mu{}^\nu$, the actual field minus the mean of the advanced and retarded fields, playing the part of the external field.

Equations (22) are not in a form suitable for application to practical problems where we are given, not $f_\mu{}^\nu$, but the incident field $F_\mu{}^\nu{}_{\text{in}}$. The connexion between these two fields is, from (13), (8) and (11),

$$f_\mu{}^\nu = F_\mu{}^\nu{}_{\text{in}} + \tfrac{1}{2}F_\mu{}^\nu{}_{\text{rad}}$$

$$= F_\mu{}^\nu{}_{\text{in}} + \tfrac{2}{3}e(\ddot{v}_\mu v^\nu - \ddot{v}^\nu v_\mu) \tag{23}$$

with the help of (12). Substituting this into (22) and using (15) and (17), we get

$$mv_\mu - \tfrac{2}{3}e^2\ddot{v}_\mu - \tfrac{2}{3}e^2\dot{v}^2 v_\mu = ev_\nu F_{\mu\,\text{in}}^{\ \nu}. \tag{24}$$

These are the same as the equations of motion obtained from the Lorentz theory of the extended electron by equating the total force on the electron to zero, if one neglects terms involving higher derivatives of v_μ than the second. But whereas these equations, as derived from the Lorentz theory, are only approximate, we now see that *there is good reason for believing them to be exact, within the limits of the classical theory.*

To discuss the significance of equations (24), let us take the equation with $\mu = 0$, describing the energy balance. The right-hand side, which gives the rate at which the incident field does work on the electron, is equated to the sum of the three terms $m\dot{v}_0$, $-\tfrac{2}{3}e^2\ddot{v}_0$ and $-\tfrac{2}{3}e^2\dot{v}^2 v_0$. The first two of these are perfect differentials and the things they are the differentials of, namely mv_0 and $-\tfrac{2}{3}e^2\dot{v}_0$, may be considered as intrinsic energies of the electron. The former is just the usual expression for the kinetic energy of a particle of rest-mass m, while the latter is what is called the "acceleration energy" of the electron (Schott 1915). Changes in the acceleration energy correspond to a reversible form of emission or absorption of field energy, which never gets very far from the electron. The third term $-\tfrac{2}{3}e^2\dot{v}^2 v_0$ corresponds to irreversible emission of radiation and gives the effect of radiation damping on the motion of the electron. It is necessarily positive, since, according to (16), $\dot{v}_\mu$ is orthogonal to the time-like vector v_μ and is thus a space-like vector, and hence its square is negative.

Let us see how the kinetic energy term arises. The B_μ introduced in (18) can be interpreted as minus the vector of energy and momentum residing within the tube at any value of the proper-time. Thus, from (20) and (21), the energy within the tube must be negative and must tend to $-\infty$ as ϵ tends to zero. This negative energy is needed to compensate for the large positive energy of the Coulomb field just outside the tube, to keep the total energy down to the value appropriate to the rest-mass m. If we want a model of the electron, we must suppose that there is an infinite negative mass at its centre such that, when subtracted from the infinite positive mass of the surrounding Coulomb field, the difference is well defined and is just equal to m. Such a model is hardly a plausible one according to current physical ideas but, as discussed in the Introduction, this is not an objection to the theory provided we have a reasonable mathematical scheme.

APPLICATION OF THE EQUATIONS OF MOTION

Let us now accept equations (24) as giving an exact description of the motion of an electron in a specified incident field and investigate some of their consequences. The equations involve $\ddot{v}_\mu$, which means that the motion will not be determined if we are given only the position and velocity of the electron at one instant of time. We must also be given its acceleration. The equations can then be used to determine the rate of change of the acceleration and the whole motion will then be fixed.

As an interesting special case let us suppose there is no incident field, so that we have the equations of motion

$$a\dot{v}_\mu - \ddot{v}_\mu - \dot{\mathbf{v}}^2 v_\mu = 0, \tag{25}$$

where $a = 3m/2e^2$. In general the electron will not now be moving with constant velocity, as it would according to ordinary ideas, since we may suppose it to be started off with a non-zero acceleration and it cannot then suddenly lose its acceleration. Let us pass over to the notation x, y, z, t instead of z_1, z_2, z_3, z_0 and choose a system of co-ordinates so that the initial velocity and acceleration are in the direction of the x-axis, or, in relativistic language, the initial velocity and acceleration four-vectors lie in the (xt) plane. Then from symmetry considerations the motion must lie entirely in this plane.

The equations (25) now become

$$a\dddot{x} - \dddot{x} - \dot{x}(\ddot{t}^2 - \ddot{x}^2) = 0, \tag{26}$$

$$a\dddot{t} - \dddot{t} - \dot{t}(\ddot{t}^2 - \ddot{x}^2) = 0. \tag{27}$$

Equations (15), (16) and (17) give

$$\dot{t}^2 - \dot{x}^2 = 1, \tag{28}$$

$$\dot{t}\ddot{t} - \dot{x}\ddot{x} = 0, \tag{29}$$

$$(\dot{t}\dddot{t} - \dot{x}\dddot{x}) + (\ddot{t}^2 - \ddot{x}^2) = 0,$$

from which we see that $\dot{x}$ times equation (26) minus $\dot{t}$ times equation (27) vanishes identically, so that either of these equations is equivalent to the other. Eliminating $\dot{t}$ from (28) and (29), we get

$$\ddot{t} = \ddot{x}\frac{\dot{x}}{(1 + \dot{x}^2)^{\frac{1}{2}}},$$

which gives, on being substituted into (26),

$$a\dddot{x} - \dddot{x} + \frac{\dot{x}\ddot{x}^2}{1 + \dot{x}^2} = 0.$$

If $\ddot{x}$ does not vanish, we may write this as

$$a - \frac{\dddot{x}}{\ddot{x}} + \frac{\dot{x}\ddot{x}}{1 + \dot{x}^2} = 0,$$

and integrate immediately, to get

$$as - \log \ddot{x} + \tfrac{1}{2} \log (1 + \dot{x}^2) = c,$$

where c is a constant of integration. It is convenient to choose the origin from which s is measured to make $c = -\log a$. We then have

$$\frac{\ddot{x}}{(1 + \dot{x}^2)^{\frac{3}{2}}} = ae^{as},$$

which can be integrated again, to give

$$\log [\dot{x} + (1 + \dot{x}^2)^{\frac{1}{2}}] = e^{as} + b,$$

where b is another constant of integration. We may write this result as

$$\left. \begin{aligned} \dot{x} &= \sinh (e^{as} + b), \\ \dot{t} &= \cosh (e^{as} + b). \end{aligned} \right\} \tag{30}$$

We now have that, as s tends to $-\infty$, the velocity tends to a constant value, given by $\dot{x} = \sinh b$ or $dx/dt = \tanh b$. As s increases from $-\infty$, the motion departs from the asymptotic motion of constant velocity, and the velocity steadily increases. For large values of s the velocity tends to the velocity of light according to an extremely rapid law.

At this stage one would be inclined to say that there is a mistake in sign in our equations and that we ought to have e^{-as} instead of e^{as} in (30). With this alteration we should have a theory in which, if an electron is disturbed in any way and then left alone, it would rapidly settle down into a state of constant velocity, with emission of radiation while it is settling down. This would be a reasonable behaviour for an electron according to our present-day physical ideas. However, it is not possible to tamper with the signs in our theory in any relativistic way to obtain this result, without getting equations of motion which would make the electron in the hydrogen atom spiral outwards, instead of spiralling inwards and ultimately falling into the nucleus, as it should in the classical theory. We are therefore forced to keep the signs in (30) as they are and to see what interpretation we can give to the equations as they stand. This will lead us to the most beautiful feature of the theory.

The motion (30) is certainly never observed for an electron in the absence of incident radiation. This does not give a contradiction between our theory

and observation, however, since our equations of motion (25) admit of alternative solutions, namely $v_\mu =$ constant, which are in agreement with observation. We must merely impose the condition that these solutions are the ones that occur in Nature. Let us see how this condition works in a practical problem.

Suppose we have an electron which is disturbed by some electromagnetic radiation incident on it and is then left alone. We may use our general equations of motion (24) and must restrict ourselves to those solutions for which the velocity is constant during the final period when the electron is left alone. This will in general prevent us from having the velocity exactly constant during the initial period before the disturbance has arrived and will compel us then to have a motion of the form (30), with the electron gradually building up a small acceleration. The difference of such a motion from one of constant velocity is too small to show itself as a contradiction with observation, so that we can get agreement between the solutions of our equations and observed motions on these lines.

• We now have a striking departure from the usual ideas of mechanics. *We must obtain solutions of our equations of motion for which the initial position and velocity of the electron are prescribed, together with its final acceleration, instead of solutions with all the initial conditions prescribed.*

MOTION OF AN ELECTRON DISTURBED BY A PULSE

To study the rather unexpected results of the preceding section more closely, let us take a typical special case, which is sufficiently simple to be worked out completely. Suppose we have an electron initially at rest, disturbed by a pulse of electromagnetic radiation passing over it. To simplify the mathematics as much as possible, let us suppose the duration of the pulse to be infinitely short, so that the electric force is represented by a δ-function, say

$$\mathscr{E}_x = k\,\delta(t-y) \quad \mathscr{E}_y = \mathscr{E}_z = 0, \tag{31}$$

in the $xyzt$ notation, where k is a constant, giving us a pulse polarized in the direction of the x-axis and moving in the direction of the y-axis. We shall consider a motion for which the electron remains always in the plane $y = 0$, $z = 0$ in space-time (neglecting the magnetic effects of the pulse).

Substituting (31) into our equations of motion (24), we get

$$a\ddot{x} - \dddot{x} - \dot{x}(\ddot{t}^2 - \ddot{x}^2) = \kappa\,\delta(t)\,\dot{t}, \tag{32}$$

where $\kappa = 3k/2e$. The equation involving $\ddot{t}$ is not independent of this one and may be ignored. Let us now suppose k to be sufficiently small for the

velocity acquired by the electron to be small compared with the velocity of light, so that we may neglect relativistic effects. Equation (32) then reduces to

$$a\ddot{x} - \ddot{x} = \kappa\,\delta(t), \tag{33}$$

in which we may take the dot to denote differentiation with respect to t. Equation (33) shows that, at the time $t = 0$, $\ddot{x}$ increases discontinuously by an amount $-\kappa$, and before and after this time we have

$$a\ddot{x} - \ddot{x} = 0. \tag{34}$$

According to the conclusions of the preceding section, we must take a motion for which, after $t = 0$, $\dot{x}$ is a constant, q say. We now have $\ddot{x}$ zero just after $t = 0$, so it must have the value κ just before. The general solution of (34) is

$$\dot{x} = c_1 e^{at} + c_2,$$

where c_1 and c_2 are constants of integration. To obtain the motion of our electron before $t = 0$, we must choose these constants of integration so that $\dot{x} = 0$ for $t = -\infty$ and $\ddot{x} = \kappa$ for $t = 0$, the former condition taking into account that the electron is initially at rest. This fixes $c_2 = 0$ and $c_1 = \kappa/a$. Finally, we have the condition that $\dot{x}$ must be continuous at $t = 0$ (since there is no δ-function in $\ddot{x}$), which gives us $q = c_1$. Thus the solution of our equations of motion is

$$\begin{aligned}
\dot{x} &= \kappa/a \,.\, e^{at}, \quad t < 0, \\
&= \kappa/a, \qquad t > 0.
\end{aligned} \tag{35}$$

We can describe the motion by saying that the electron is, to a high approximation, at rest for large negative values of t, but as t approaches zero it acquires a velocity and acceleration, in accordance with equations (30), of such amounts that just before $t = 0$ the acceleration has the right value to be exactly cancelled by the effect of the pulse, so that after $t = 0$ the electron is left moving with constant velocity. It would appear here that we have a contradiction with elementary ideas of causality. The electron seems to know about the pulse before it arrives and to get up an acceleration (as the equations of motion allow it to do), just sufficient to balance the effect of the pulse when it does arrive. The electron will, of course, radiate all the time it is accelerating and will thus be radiating before $t = 0$.

The behaviour of our electron can be interpreted in a natural way, however, if we suppose the electron to have a finite size. There is then no need for the pulse to reach the centre of the electron before it starts to accelerate. It starts to accelerate and radiate as soon as the pulse meets

its outside. Mathematically, the electron has no sharp boundary and must be considered as extending to infinity, but for practical purposes it may be considered to have a radius of order a^{-1}, this being the distance within which the pulse must arrive before the acceleration and radiation are appreciable.

The above interpretation leaves one further point to be examined. Suppose we have a pulse sent out from a place A and a receiving apparatus for electromagnetic waves set up at a place B, and suppose there is an electron on the straight line joining A to B. Then the electron will be radiating appreciably at a time a^{-1} before the pulse has reached its centre and this emitted radiation will be detectable at B at a time a^{-1} earlier than when the pulse, which travels from A to B with the velocity of light, arrives. In this way a signal can be sent from A to B faster than light. This is a fundamental departure from the ordinary ideas of relativity and is to be interpreted by saying that *it is possible for a signal to be transmitted faster than light through the interior of an electron. The finite size of the electron now reappears in a new sense, the interior of the electron being a region of failure, not of the field equations of electromagnetic theory, but of some of the elementary properties of space-time.* In spite of this departure from ordinary relativistic ideas, our whole theory is the Lorentz invariant.

Some interesting points about the solution (35) of our problem may be noted. In the first place, the total momentum acquired by the electron is

$$m\kappa/a = ek.$$

This is precisely the same as the momentum the electron would acquire on an elementary theory which ignores the radiation damping completely.

Secondly, let us determine the spectral distribution of the radiation emitted by the electron. The rate of emission of energy is $\frac{2}{3}e^2\ddot{x}^2$ and its spectral distribution is given by the Fourier resolution of $\ddot{x}$. Thus the energy emitted per unit frequency range will be

$$E_\nu = \frac{2}{3}e^2 \left| \int_{-\infty}^{\infty} \ddot{x} e^{2\pi i\nu t} dt \right|^2$$

$$= \frac{2}{3}e^2\kappa^2 \left| \int_{-\infty}^{0} e^{(a+2\pi i\nu)t} dt \right|^2$$

$$= \frac{2e^2\kappa^2}{3(a^2 + 4\pi^2\nu^2)} = \frac{2e^4 k^2}{3m^2(1 + 4\pi^2\nu^2/a^2)}. \tag{36}$$

If we resolve the incident pulse into its Fourier components and suppose each component to be scattered in accordance with Thomson's formula, we should obtain for the energy scattered per unit frequency range the

value $2e^4k^2/3m^2$. This is the same as (36) for values of ν small compared with a.

It has been suggested by Oppenheimer (1935), as a possible escape from the discrepancy between theory and cosmic ray observations for the penetrating power of fast electrons, that it may not be permissible to calculate the scattering of the various Fourier components of the radiation incident on an electron independently, but that the presence of the high-frequency components may reduce the scattering of the low-frequency components. We now see that this suggestion is not supported by our theory and some other explanation of the discrepancy, such as the recently proposed heavy electron, is needed.

EXTENSION TO SEVERAL ELECTRONS

The foregoing theory may easily be extended to apply to any number of electrons interacting with each other and with a field of radiation. Let us label the electrons by a suffix n or m. The nth electron will have its own retarded field $F_{n,\,\mathrm{ret}}^{\mu\nu}$ and advanced field $F_{n,\,\mathrm{adv}}^{\mu\nu}$, determined by its world-line, and the difference

$$F_{n,\,\mathrm{rad}}^{\mu\nu} = F_{n,\,\mathrm{ret}}^{\mu\nu} - F_{n,\,\mathrm{adv}}^{\mu\nu} \qquad (37)$$

may be considered as the radiation field produced by the nth electron. Equation (12) will still apply for the value of this field on the world-line of the electron producing it.

Generalizing (8), we have that the actual field is equal to the incident field plus the sum of the retarded fields of all the electrons,

$$F_{\mathrm{act}}^{\mu\nu} = F_{\mathrm{in}}^{\mu\nu} + \Sigma_n F_{n,\,\mathrm{ret}}^{\mu\nu}. \qquad (38)$$

Similarly, generalizing (9), we have

$$F_{\mathrm{act}}^{\mu\nu} = F_{\mathrm{out}}^{\mu\nu} + \Sigma_n F_{n,\,\mathrm{adv}}^{\mu\nu}. \qquad (39)$$

Subtracting, we find that the total radiation field produced by the assembly of electrons is

$$F_{\mathrm{rad}}^{\mu\nu} = F_{\mathrm{out}}^{\mu\nu} - F_{\mathrm{in}}^{\mu\nu} = \Sigma_n (F_{n,\,\mathrm{ret}}^{\mu\nu} - F_{n,\,\mathrm{adv}}^{\mu\nu}),$$

which is thus the sum of all the above-defined radiation fields produced by the electrons individually. Of course only the total radiation field is observable, that for an individual electron being merely a mathematical concept.

To get the field $f_n^{\mu\nu}$ which must be inserted into the equations of motion (22)

for the nth electron we must, generalizing (13), subtract the mean of the retarded and advanced fields of this electron from the actual field, thus

$$f_n^{\mu\nu} = F_{\text{act}}^{\mu\nu} - \tfrac{1}{2}(F_{n,\text{ret}}^{\mu\nu} + F_{n,\text{adv}}^{\mu\nu}). \tag{40}$$

With the help of (38) we may write this as

$$f_n^{\mu\nu} = F_{\text{in}}^{\mu\nu} + \Sigma_{m \neq n} F_{m,\text{ret}}^{\mu\nu} + \tfrac{1}{2}(F_{n,\text{ret}}^{\mu\nu} - F_{n,\text{adv}}^{\mu\nu}).$$

Substituting this into (22) and proceeding along the same lines as those which led to (24), we get the final equations of motion

$$m\dot{v}_{\mu n} - \tfrac{2}{3}e^2 \ddot{v}_{\mu n} - \tfrac{2}{3}e^2 \dot{v}_n^2 v_{\mu n} = ev_{\nu n}\{F_{\mu,\text{in}}^{\ \nu} + \Sigma_{m \neq n} F_{\mu m,\text{ret}}^{\ \nu}\}. \tag{41}$$

The field on the right-hand side here is just the incident field plus the retarded fields of all the other electrons, which is in agreement with current practice. It is interesting to remember that this result has been obtained in a theory which is fundamentally symmetrical between retarded and advanced potentials.

From (40), (38) and (39) we have

$$f_n^{\mu\nu} = \tfrac{1}{2}(F_{\text{in}}^{\mu\nu} + F_{\text{out}}^{\mu\nu}) + \tfrac{1}{2}\Sigma_{m \neq n}(F_{m,\text{ret}}^{\mu\nu} + F_{m,\text{adv}}^{\mu\nu}). \tag{42}$$

Suppose now we are concerned with a problem in which

$$F_{\text{in}}^{\mu\nu} + F_{\text{out}}^{\mu\nu} = 0. \tag{43}$$

Then the field $f_n^{\mu\nu}$ to be used in the equations of motion (22) for the nth electron is just the sum of the mean of the retarded and advanced fields of all the other electrons. The interaction of the electrons for this case has been studied by Fokker (1929), who finds that the motion of all the electrons may now be described by a variation principle

$$\delta I = 0. \tag{44}$$

In our present notation I would have the form

$$I = \Sigma_n \int m\, ds_n + \tfrac{1}{2}\Sigma_n \Sigma_{m \neq n} \int \frac{e^2(\mathbf{v}_m, \mathbf{v}_n)}{(\mathbf{z}_n - \mathbf{z}_m, \mathbf{v}_m)}\, ds_n + \tfrac{1}{2}\Sigma_n \Sigma_{m \neq n} \int \frac{e^2(\mathbf{v}_m, \mathbf{v}_n)}{(\mathbf{z}_m - \mathbf{z}_n, \mathbf{v}_m)}\, ds_n, \tag{45}$$

where the two double sums are to be taken over all pairs of electrons, and in the first we must take for $\mathbf{z}_m$ and $\mathbf{v}_m$ their retarded values (with respect

to the point on s_n considered), and in the second we must take their advanced values.

When the condition (43) does not apply, Fokker's variation principle (44) will still hold provided we add on to I the terms

$$\Sigma_n e \int \tfrac{1}{2}(A_{\text{in}}^\mu + A_{\text{out}}^\mu)\, v_{\mu n}\, ds_n, \tag{46}$$

involving the potentials of the mean of the ingoing and outgoing fields. The variation principle will not be of much use in practical problems, where this mean field is unknown, but it may be of value in suggesting how the quantum generalization of our theory is to be made.

Appendix

We shall consider an electron whose world-line is given by equations (2) and shall evaluate field quantities at the point x_μ. The retarded potentials at this point are, in the scalar product notation (1),

$$A_{\mu,\,\text{ret}} = \frac{e\dot{z}_\mu}{(\dot{z}, \mathbf{x} - \mathbf{z})}, \tag{47}$$

taken at the retarded proper-time, namely that value of s for which

$$(\mathbf{x} - \mathbf{z}, \mathbf{x} - \mathbf{z}) = 0 \tag{48}$$

with $x_0 - z_0$ positive. We can get $A_{\mu,\,\text{ret}}$ in a form suitable for deriving the field quantities (6) from it with the help of the δ-function. Using the general property of the δ-function, that with $f(s)$ and $g(s)$ any two continuous functions of s and $\dot{g}(s) > 0$,

$$\int f(s)\, \delta\{g(s)\}\, ds = \int \frac{f(s)}{\dot{g}(s)}\, \delta\{g(s)\}\, dg(s) = \frac{f(s)}{\dot{g}(s)}, \tag{49}$$

taken at the value of s in the range of integration that satisfies $g(s) = 0$, we can express (47) in the form

$$A_{\mu,\,\text{ret}} = 2e \int \dot{z}_\mu\, \delta(\mathbf{x} - \mathbf{z}, \mathbf{x} - \mathbf{z})\, ds, \tag{50}$$

where the range of integration is from $-\infty$ to some value of s intermediate between the retarded and advanced times. We now have

$$\frac{\partial A_{\mu,\,\mathrm{ret}}}{\partial x_{\nu}} = 4e\int \dot{z}_{\mu}\{x^{\nu}-z^{\nu}\}\,\delta'(\mathbf{x}-\mathbf{z},\,\mathbf{x}-\mathbf{z})\,ds$$

$$= -2e\int \frac{\dot{z}_{\mu}\{x^{\nu}-z^{\nu}\}}{(\dot{z},\,\mathbf{x}-\mathbf{z})}\frac{d}{ds}\,\delta(\mathbf{x}-\mathbf{z},\,\mathbf{x}-\mathbf{z})\,ds$$

$$= 2e\int \frac{d}{ds}\left[\frac{\dot{z}_{\mu}\{x^{\nu}-z^{\nu}\}}{(\dot{z},\,\mathbf{x}-\mathbf{z})}\right]\delta(\mathbf{x}-\mathbf{z},\,\mathbf{x}-\mathbf{z})\,ds,$$

so that $\qquad F_{\mu\nu,\,\mathrm{ret}} = -2e\int \frac{d}{ds}\left[\frac{\dot{z}_{\mu}\{x_{\nu}-z_{\nu}\}-\dot{z}_{\nu}\{x_{\mu}-z_{\mu}\}}{(\dot{z},\,\mathbf{x}-\mathbf{z})}\right]\delta(\mathbf{x}-\mathbf{z},\,\mathbf{x}-\mathbf{z})\,ds.$ (51)

In the form of (47), this result becomes

$$F_{\mu\nu,\,\mathrm{ret}} = -\frac{e}{(\dot{z},\,\mathbf{x}-\mathbf{z})}\frac{d}{ds}\frac{\dot{z}_{\mu}\{x_{\nu}-z_{\nu}\}-\dot{z}_{\nu}\{x_{\mu}-z_{\mu}\}}{(\dot{z},\,\mathbf{x}-\mathbf{z})}$$ (52)

taken at the retarded proper-time.

Let us now suppose the field point x_{μ} to lie very close to the world-line of the electron, so that we can put

$$x_{\mu} = z_{\mu}(s_0) + \gamma_{\mu},$$ (53)

where the γ_{μ}'s are very small. We shall evaluate the field quantities by means of Taylor expansions in which the coefficients depend on z_{μ} and its successive derivatives with respect to s, namely $v_{\mu}, \dot{v}_{\mu}, \ldots$, taken at the proper-time s_0. Similar expansions have already been made by Page (1918, 1924), working with the Lorentz model, but the coefficients in his expansions involve the d/dt derivatives instead of the d/ds ones, which is not so convenient for a relativistic theory. For brevity, the value s_0 of the proper-time will not be mentioned explicitly in the coefficients, but will be understood.

Without loss of generality we may assume the point s_0 to be chosen so that

$$(\gamma v) = 0$$ (54)

for the value of $\mathbf{v}$ at the proper-time s_0. This equation will be much used in the future, together with the equations (15), (16) and (17).

Let the retarded proper-time, to be used in the right-hand side of (47) or (52), be $s_0 - \sigma$, σ being a small positive quantity of the same order as the γ_{μ}. We shall obtain expansions for the retarded field quantities, given by the right-hand side of (52), in powers of σ. These field quantities are of the order σ^{-2} and we shall need to have them correctly to the order of terms independent of σ, so we must retain terms of the first three orders in all

our expansions. To make the calculations clearer, commas will be inserted to separate terms of different orders of magnitude.

We have the Taylor expansions

$$x_\mu - z_\mu(s_0 - \sigma) = \gamma_\mu + \sigma v_\mu, \quad -\tfrac{1}{2}\sigma^2 \dot{v}_\mu, \quad +\tfrac{1}{6}\sigma^3 \ddot{v}_\mu, \tag{55}$$

$$\dot{z}_\mu(s_0 - \sigma) = v_\mu, \quad -\sigma \dot{v}_\mu, \quad +\tfrac{1}{2}\sigma^2 \ddot{v}_\mu. \tag{56}$$

These give, with the help of (15), (16), (17) and (54),

$$(\dot{z}, \mathbf{x} - \mathbf{z}) = \sigma, \quad -\sigma(\gamma \dot{v}), \quad +\tfrac{1}{2}\sigma^2(\gamma \ddot{v}) - \tfrac{1}{6}\sigma^3 \dot{v}^2,$$

and hence $(\dot{z}, \mathbf{x} - \mathbf{z})^{-1} = \sigma^{-1}[1 - (\gamma \dot{v})]^{-1}[1,, \ -\tfrac{1}{2}\sigma(\gamma \ddot{v}) + \tfrac{1}{6}\sigma^2 \dot{v}^2].$

It saves a little writing if we do not expand the factor $[1 - (\gamma \dot{v})]^{-1}$. We have again from (55) and (56)

$$\dot{z}_\mu \{x_\nu - z_\nu\} - \dot{z}_\nu \{x_\mu - z_\mu\}$$
$$= v_\mu \gamma_\nu, \quad -\sigma \dot{v}_\mu \gamma_\nu - \tfrac{1}{2}\sigma^2 \dot{v}_\mu v_\nu, \quad +\tfrac{1}{2}\sigma^2 \ddot{v}_\mu \gamma_\nu + \tfrac{1}{6}\sigma^3 \ddot{v}_\mu v_\nu -,$$

where the minus sign at the end indicates that we must subtract the terms obtained by interchanging μ and ν, so as to make the whole expression antisymmetrical in μ and ν. We now get

$$\frac{\dot{z}_\mu \{x_\nu - z_\nu\} - \dot{z}_\nu \{x_\mu - z_\mu\}}{(\dot{z}, \mathbf{x} - \mathbf{z})}$$
$$= [1 - (\gamma \dot{v})]^{-1} [\sigma^{-1} v_\mu \gamma_\nu, \quad -\dot{v}_\mu \gamma_\nu - \tfrac{1}{2}\sigma \dot{v}_\mu v_\nu, \quad -\tfrac{1}{2}(\gamma \ddot{v}) v_\mu \gamma_\nu$$
$$+ \tfrac{1}{6}\sigma \dot{v}^2 v_\mu \gamma_\nu + \tfrac{1}{2}\sigma \ddot{v}_\mu \gamma_\nu + \tfrac{1}{3}\sigma^2 \ddot{v}_\mu v_\nu -].$$

We have to differentiate this expression with respect to s. This is equivalent to differentiating with respect to σ and changing the sign, as we have not yet used the condition that fixes σ. Thus

$$\frac{d}{ds} \frac{\dot{z}_\mu \{x_\nu - z_\nu\} - \dot{z}_\nu \{x_\mu - z_\mu\}}{(\dot{z}, \mathbf{x} - \mathbf{z})}$$
$$= -[1 - (\gamma \dot{v})]^{-1} [-\sigma^{-2} v_\mu \gamma_\nu, \quad -\tfrac{1}{2} \dot{v}_\mu v_\nu, \quad +\tfrac{1}{6} \dot{v}^2 v_\mu \gamma_\nu + \tfrac{1}{2} \ddot{v}_\mu \gamma_\nu + \tfrac{2}{3}\sigma \ddot{v}_\mu v_\nu -],$$

and hence

$$F_{\mu\nu,\,\text{ret}} = e[1 - (\gamma \dot{v})]^{-2} [-\sigma^{-3} v_\mu \gamma_\nu, \quad -\tfrac{1}{2}\sigma^{-1} \dot{v}_\mu v_\nu, \quad +\tfrac{1}{2}\sigma^{-2}(\gamma \dot{v}) v_\mu \gamma_\nu$$
$$+ \tfrac{1}{2}\sigma^{-1} \ddot{v}_\mu \gamma_\nu + \tfrac{2}{3} \ddot{v}_\mu v_\nu -]. \tag{57}$$

We must now determine the value of σ. From (48) and (55)

$$\gamma^2 + \sigma^2, \quad -\sigma^2(\gamma \dot{v}), \quad +\tfrac{1}{3}\sigma^3(\gamma \ddot{v}) - \tfrac{1}{12}\sigma^4 \dot{v}^2 = 0. \tag{58}$$

Since γ is a space-like vector, γ^2 is negative. We put it equal to $-\epsilon^2$, ϵ being a positive number. To solve equation (58) for σ, we note that $\sigma = \epsilon$ to the first order, so that, without spoiling the accuracy of the equation, we may rewrite it

$$-\epsilon^2 + \sigma^2, \; -\sigma^2(\gamma\dot{v}), \; +\tfrac{1}{3}\epsilon^3(\gamma\dot{v}) - \tfrac{1}{12}\epsilon^4\dot{v}^2 = 0.$$

Hence
$$\sigma^2 = [1 - (\gamma\dot{v})]^{-1}[\epsilon^2,, \; -\tfrac{1}{3}\epsilon^3(\gamma\dot{v}) + \tfrac{1}{12}\epsilon^4\dot{v}^2],$$

so that
$$\sigma = \epsilon[1 - (\gamma\dot{v})]^{-\frac{1}{2}}[1,, \; -\tfrac{1}{6}\epsilon(\gamma\dot{v}) + \tfrac{1}{24}\epsilon^2\dot{v}^2]. \tag{59}$$

Substituting this expression for σ in (57), we get

$$F_{\mu\nu,\,\mathrm{ret}} = e[1 - (\gamma\dot{v})]^{-\frac{1}{2}}\{-\epsilon^{-3}v_\mu\gamma_\nu, \; -\tfrac{1}{2}\epsilon^{-1}\dot{v}_\mu v_\nu[1, + (\gamma\dot{v})]$$
$$+ \tfrac{1}{8}\epsilon^{-1}\dot{v}^2 v_\mu\gamma_\nu + \tfrac{1}{2}\epsilon^{-1}\ddot{v}_\mu\gamma_\nu + \tfrac{2}{3}\ddot{v}_\mu v_\nu -\}. \tag{60}$$

This gives us the retarded field close to the world-line of the electron. To obtain the advanced field at the same field point, it is easily seen that we must change the sign of ϵ in the right-hand side of (60) and also change the sign of the whole expression. Thus the mean of $F_{\mu\nu,\,\mathrm{ret}}$ and $F_{\mu\nu,\,\mathrm{adv}}$ will be given by the terms of odd powers of ϵ in (60), and half their difference, $\tfrac{1}{2}(F_{\mu\nu,\,\mathrm{ret}} - F_{\mu\nu,\,\mathrm{adv}})$, will be given by the terms of even powers of ϵ. The only terms of even powers are the last term written down explicitly and the term obtained from it by interchanging μ and ν. These remain finite on the world-line of the electron and give the result (12) for the value of $F_{\mu\nu,\,\mathrm{ret}} - F_{\mu\nu,\,\mathrm{adv}}$ on the world-line.

With $f_{\mu\nu}$ defined by (13), we now have for the actual field close to the world-line

$$F_{\mu\nu} = e[1 - (\gamma\dot{v})]^{-\frac{1}{2}}\{[\epsilon^{-3} - \tfrac{1}{8}\epsilon^{-1}\dot{v}^2][\gamma_\mu v_\nu - \gamma_\nu v_\mu],$$
$$+ \tfrac{1}{2}\epsilon^{-1}[1 + (\gamma\dot{v})][v_\mu\dot{v}_\nu - v_\nu\dot{v}_\mu], + \tfrac{1}{2}\epsilon^{-1}[\ddot{v}_\mu\gamma_\nu - \ddot{v}_\nu\gamma_\mu]\} + f_{\mu\nu}.$$

We shall evaluate $F_{\mu\nu}F^\nu_\rho$ to the accuracy of ϵ^{-2}. We note first that

$$[\gamma_\mu v_\nu - \gamma_\nu v_\mu][\gamma^\nu v_\rho - \gamma_\rho v^\nu] = -\gamma_\mu\gamma_\rho + \epsilon^2 v_\mu v_\rho$$
$$[\gamma_\mu v_\nu - \gamma_\nu v_\mu][v^\nu\dot{v}_\rho - v_\rho\dot{v}^\nu] = \gamma_\mu\dot{v}_\rho + (\gamma\dot{v})v_\mu v_\rho$$
$$[\gamma_\mu v_\nu - \gamma_\nu v_\mu][\ddot{v}^\nu\gamma_\rho - \ddot{v}_\rho\gamma^\nu] = -\dot{v}^2\gamma_\mu\gamma_\rho - (\gamma\dot{v})v_\mu\gamma_\rho - \epsilon^2 v_\mu\ddot{v}_\rho$$
$$[v_\mu\dot{v}_\nu - v_\nu\dot{v}_\mu][v^\nu\dot{v}_\rho - v_\rho\dot{v}^\nu] = -\dot{v}^2 v_\mu v_\rho - \dot{v}_\mu\dot{v}_\rho.$$

With the help of these results we obtain

$$F_{\mu\nu}F^\nu_\rho = e^2[1 - (\gamma\dot{v})]^{-1}\{[\epsilon^{-6} - \tfrac{1}{4}\epsilon^{-4}\dot{v}^2][-\gamma_\mu\gamma_\rho + \epsilon^2 v_\mu v_\rho]$$
$$+ \tfrac{1}{2}\epsilon^{-4}[1 + (\gamma\dot{v})][\gamma_\mu\dot{v}_\rho + \gamma_\rho\dot{v}_\mu + 2(\gamma\dot{v})v_\mu v_\rho] - \tfrac{1}{2}\epsilon^{-4}[2\dot{v}^2\gamma_\mu\gamma_\rho$$
$$+ (\gamma\dot{v})(v_\mu\gamma_\rho + v_\rho\gamma_\mu) + \epsilon^2(v_\mu\ddot{v}_\rho + v_\rho\ddot{v}_\mu)] - \tfrac{1}{4}\epsilon^{-2}[\dot{v}^2 v_\mu v_\rho + \dot{v}_\mu\dot{v}_\rho]\}$$
$$+ e\epsilon^{-3}\{[\gamma_\mu v_\nu - \gamma_\nu v_\mu]f^\nu_\rho + [\gamma^\nu v_\rho - \gamma_\rho v^\nu]f_{\mu\nu}\}.$$

Contracting, we find

$$
\begin{aligned}
F_{\mu\nu}F^{\nu\mu} &= e^2[1-(\boldsymbol{\gamma}\dot{\mathbf{v}})]^{-1}\left\{[\epsilon^{-6}-\tfrac14\epsilon^{-4}\dot{\mathbf{v}}^2]\,2\epsilon^2+\tfrac12\epsilon^{-4}[1+(\boldsymbol{\gamma}\dot{\mathbf{v}})]\,4(\boldsymbol{\gamma}\dot{\mathbf{v}})\right. \\
&\quad \left.-\tfrac12\epsilon^{-4}[-2\epsilon^2\dot{\mathbf{v}}^2+2\epsilon^2(\mathbf{v}\dot{\mathbf{v}})]-\tfrac12\epsilon^{-2}\dot{\mathbf{v}}^2\right\}+2e\epsilon^{-3}[\gamma_\mu v_\nu-\gamma_\nu v_\mu]f^{\nu\mu} \\
&= e^2[1-(\boldsymbol{\gamma}\dot{\mathbf{v}})]^{-1}\left\{2\epsilon^{-4}[1+(\boldsymbol{\gamma}\dot{\mathbf{v}})+(\boldsymbol{\gamma}\dot{\mathbf{v}})^2]+\epsilon^{-2}\dot{\mathbf{v}}^2\right\}+4e\epsilon^{-3}\gamma_\mu v_\nu f^{\nu\mu}.
\end{aligned}
$$

We can now get the stress tensor $T_{\mu\rho}$ defined by (14). However, we shall not require the complete tensor, but only its component in the direction of $\boldsymbol{\gamma}$, namely $-\epsilon^{-1}T_{\mu\rho}\gamma^\rho$. We have

$$
\begin{aligned}
4\pi T_{\mu\rho}\gamma^\rho &= F_{\mu\nu}F^\nu{}_\rho\gamma^\rho-\tfrac14 F_{\alpha\beta}F^{\beta\alpha}\gamma_\mu \\
&= e^2[1-(\boldsymbol{\gamma}\dot{\mathbf{v}})]^{-1}\left\{[\epsilon^{-4}-\tfrac14\epsilon^{-2}\dot{\mathbf{v}}^2]\gamma_\mu+\tfrac12\epsilon^{-4}[1+(\boldsymbol{\gamma}\dot{\mathbf{v}})]\,[(\boldsymbol{\gamma}\dot{\mathbf{v}})\,\gamma_\mu-\epsilon^2\dot{v}_\mu]\right. \\
&\quad \left.+\epsilon^{-2}\dot{\mathbf{v}}^2\gamma_\mu-\tfrac14\epsilon^{-2}(\boldsymbol{\gamma}\dot{\mathbf{v}})\,\dot{v}_\mu-[\tfrac12\epsilon^{-4}+\tfrac12\epsilon^{-4}(\boldsymbol{\gamma}\dot{\mathbf{v}})+\tfrac12\epsilon^{-4}(\boldsymbol{\gamma}\dot{\mathbf{v}})^2+\tfrac14\epsilon^{-2}\dot{\mathbf{v}}^2]\,\gamma_\mu\right\} \\
&\quad +e\epsilon^{-3}\left\{\gamma_\mu v_\nu f^\nu{}_\rho\gamma^\rho+\epsilon^2 v^\nu f_{\mu\nu}-\gamma_\rho v_\nu f^{\nu\rho}\gamma_\mu\right\} \\
&= e^2[1-(\boldsymbol{\gamma}\dot{\mathbf{v}})]^{-1}\left\{[\tfrac12\epsilon^{-4}+\tfrac12\epsilon^{-2}\dot{\mathbf{v}}^2]\gamma_\mu-\tfrac12\epsilon^{-2}[1+\tfrac32(\boldsymbol{\gamma}\dot{\mathbf{v}})]\,\dot{v}_\mu\right\}+e\epsilon^{-1}v^\nu f_{\mu\nu}.
\end{aligned}
$$

$$(61)$$

We must now determine the flow of energy and momentum out from the tube introduced on page 153. The surface of this tube is described by that equation which is the result of eliminating s from the two equations

$$(\mathbf{x}-\mathbf{z},\mathbf{x}-\mathbf{z})=-\epsilon^2 \qquad (62)$$

$$(\mathbf{x}-\mathbf{z},\mathbf{v})=0, \qquad (63)$$

in which $\mathbf{z}$ and $\mathbf{v}$ are considered as functions of s. Let us make a variation of the point x_μ on the surface to the point $x_\mu+dx_\mu$, also on the surface, and let us suppose this corresponds to s varying by an amount ds. We then have, varying (62) and (63),

$$(\mathbf{x}-\mathbf{z},d\mathbf{x}-\mathbf{v}\,ds)=0,$$

$$(d\mathbf{x}-\mathbf{v}\,ds,\mathbf{v})+(\mathbf{x}-\mathbf{z},\dot{\mathbf{v}}\,ds)=0,$$

which reduce, with the help of (63) and (15), to

$$(\mathbf{x}-\mathbf{z},d\mathbf{x})=0$$

$$(d\mathbf{x},\mathbf{v})=[1-(\mathbf{x}-\mathbf{z},\dot{\mathbf{v}})]\,ds.$$

Putting the $\mathbf{x}-\mathbf{z}$ here equal to $\boldsymbol{\gamma}$, in agreement with equation (53), we have

$$(\boldsymbol{\gamma},d\mathbf{x})=0 \qquad (64)$$

$$(d\mathbf{x},\mathbf{v})=[1-(\boldsymbol{\gamma}\dot{\mathbf{v}})]\,ds. \qquad (65)$$

Equation (64) shows that the normal to the surface is in the direction of the vector $\boldsymbol{\gamma}$, and equation (65) shows that if we split up $\mathbf{dx}$ into a part $\mathbf{d_1 x}$ orthogonal to $\mathbf{v}$ and a part $\mathbf{d_2 x}$ parallel to $\mathbf{v}$, then the magnitude of $\mathbf{d_2 x}$ is

$$| \mathbf{d_2 x} | = [1 - (\boldsymbol{\gamma}\dot{\mathbf{v}})]\,ds. \tag{66}$$

Now the three-dimensional "area" of an element of the surface is equal to the two-dimensional area, dS say, of an element of a section of the surface by a three-dimensional plane orthogonal to $\mathbf{v}$, multiplied by the element $| \mathbf{d_2 x} |$ parallel to $\mathbf{v}$. Hence the flow of energy and momentum out through the surface is

$$\iint -\epsilon^{-1} T_{\mu\rho} \gamma^\mu \, dS \, | \mathbf{d_2 x} |$$

$$= -(4\pi)^{-1} \iint [e^2\{(\tfrac{1}{2}\epsilon^{-5} + \tfrac{1}{2}\epsilon^{-3}\dot{\mathbf{v}}^2)\gamma_\mu - \tfrac{1}{2}\epsilon^{-3}[1 + \tfrac{3}{2}(\boldsymbol{\gamma}\dot{\mathbf{v}})]\dot{v}_\mu\} + e\epsilon^{-2}v^\nu f_{\mu\nu}]\,dS\,ds, \tag{67}$$

from (61) and (66), with neglect of terms that vanish with ϵ. The integration with respect to dS here is just integration over the surface of the sphere in three-dimensional space given by (62) and (63) for a particular s. The terms linear in γ in the integrand will contribute nothing to the integral, while the remaining terms will get multiplied by the area of the sphere, namely $4\pi\epsilon^2$. Thus (67) becomes

$$\int \{\tfrac{1}{2}e^2\epsilon^{-1}\dot{v}_\mu - ev^\nu f_{\mu\nu}\}\,ds, \tag{68}$$

which is the result used on page 153.

Summary

The object of the paper is to set up in the classical theory a self-consistent scheme of equations which may be used to calculate all the results that can be obtained from experiment about the interaction of electrons and radiation. The electron is treated as a point charge and the difficulties of the infinite Coulomb energy are avoided by a procedure of direct omission or subtraction of unwanted terms, somewhat similar to what has been used in the theory of the positron. The equations obtained are of the same form as those already in current use, but in their physical interpretation the finite size of the electron reappears in a new sense, the interior of the electron being a region of space through which signals can be transmitted faster than light.

REFERENCES

Fokker, A. D. 1929 *Z. Phys.* **58**, 386–93.
Frenkel, J. 1925 *Z. Phys.* **32**, 518–34.
Oppenheimer, J. R. 1935 *Phys. Rev.* **47**, 44–52.
Page, L. 1918 *Phys. Rev.* **11**, 376–400.
— 1924 *Phys. Rev.* **24**, 296–305.
Schott, G. A. 1915 *Phil. Mag.* **29**, 49–62.

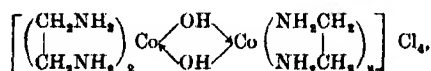# The crystal structure of certain bridged palladium compounds

BY A. F. WELLS

Crystallographic Laboratory, Cambridge

INTRODUCTION

Many compounds have been formulated with metal atoms "bridged" by non-metallic atoms or groups such as halogen or hydroxyl. The polynuclear cobaltammines provide many examples, e.g.
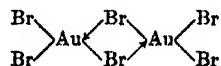
$$\left[\left(\begin{matrix} CH_2NH_2 \\ | \\ CH_2NH_2 \end{matrix} \right)_2 Co \left\langle \begin{matrix} OH \\ OH \end{matrix} \right\rangle Co \left(\begin{matrix} NH_2CH_2 \\ | \\ NH_2CH_2 \end{matrix} \right)_2 \right] Cl_4,$$

and many years ago the phosphite ester derivatives of palladous and platinous chlorides, $(RO)_3P.Pd(Pt)Cl_2$, were shown to have molecular weights twice those of the empirical formulae. This led to their formulation (Werner and Pfeiffer 1923) as bridged derivatives with possible isomerism:

$$(RO)_3P \diagdown \underset{Cl}{\overset{Cl}{Pt}} \diagdown \underset{Cl}{\overset{Cl}{Pt}} \diagdown \begin{matrix} Cl \\ Cl \end{matrix} \qquad (RO)_3P \diagdown \underset{Cl}{\overset{Cl}{Pt}} \diagdown \underset{Cl}{\overset{Cl}{Pt}} \diagdown \begin{matrix} Cl \\ P(OR)_3 \end{matrix}.$$

Such molecules have a definite existence in the dissolved state and undergo substitution in much the same way as mononuclear cobaltammines. There also exist salts of the type of caesium thallic enneachloride $Cs_3Tl_2Cl_9$ and the corresponding $K_3W_2Cl_9$, and here it is found that a complex ion $(Tl_2Cl_9^{3-}$

or $W_2Cl_9^{3-}$) exists in the crystal and there is also some evidence for its existence in solution (Collenberg and Sandved 1923). It is necessary, however, to distinguish two types of bridged compounds, the classification depending on the nature of the chemical bonding between the metal and the bridging atom. The first type is essentially a covalent molecule involving electron-pair bonds, and the second is essentially ionic. This is shown by the interatomic distances and by the general nature of the compounds in the crystalline state. The structure to be described below is typical of the first type. The X-ray examination of $Cs_3Tl_2Cl_9$, however, shows it to consist (Hoard and Goldstein 1935; Powell and Wells 1935) of a simple hexagonal close-packing of the large caesium and chlorine ions with thallium ions occupying two-thirds of the interstices. Along the trigonal axis the arrangement is

$$\begin{array}{c} \begin{array}{c}{>}Tl{<} \end{array} \end{array} \quad \text{etc.}$$

the complex ion consisting of a pair of octahedra of chlorine ions sharing one face.

The development of the electronic theory of valency systematized the formulation of co-ordination compounds, and the dotted lines in the formulae given above become co-ordinate links. The formulation (Burawoy and Gibson 1935) of $AuBr_3$ as

at the same time removes the anomaly of its double molecular weight and is consistent with the stereochemistry of 4-covalent auric compounds. The analogous compound $[(C_2H_5)_2AuBr]_2$ has recently been shown (Burawoy and others 1937) to have the configuration
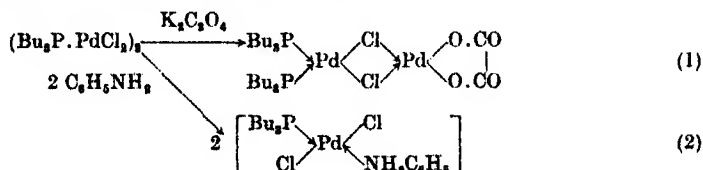
The present paper describes the results of a crystallographic study of di-chlorobis (trimethylarsine)-μ-dichlorodipalladium and its bromine analogue, viz. $[(CH_3)_3As . PdCl_2]_2$ and $[(CH_3)_3As . PdBr_2]_2$, hereafter referred to as the tetrachloride and tetrabromide respectively. These compounds show in all solvents molecular weights twice those of the simplest empirical formulae and are therefore similar in type to the phosphite esters already mentioned. Their crystal structure has been studied first, to establish the existence of the bridged molecule, and secondly, to determine the configuration of the

molecule. Assuming that the eight bonds from the palladium atoms all lie in one plane, then there are three isomeric forms of such a molecule:

$$
\begin{array}{c}
(CH_3)_3As\!\!\diagdown \\
(CH_3)_3As\!\!\diagup
\end{array}\!\!Pd\!\!\diagup^{\displaystyle Cl}_{\displaystyle Cl}\!\!\diagdown Pd\!\!\diagup^{\displaystyle Cl}_{\displaystyle Cl}
\qquad\qquad
\begin{array}{c}
(CH_3)_3As\!\!\diagdown \\
Cl\!\!\diagup
\end{array}\!\!Pd\!\!\diagup^{\displaystyle Cl}_{\displaystyle Cl}\!\!\diagdown Pd\!\!\diagup^{\displaystyle As(CH_3)_3}_{\displaystyle Cl}
$$

I   II

$$
\begin{array}{c}
(CH_3)_3As\!\!\diagdown \\
Cl\!\!\diagup
\end{array}\!\!Pd\!\!\diagup^{\displaystyle Cl}_{\displaystyle Cl}\!\!\diagdown Pd\!\!\diagup^{\displaystyle Cl}_{\displaystyle As(CH_3)_3}
$$

III
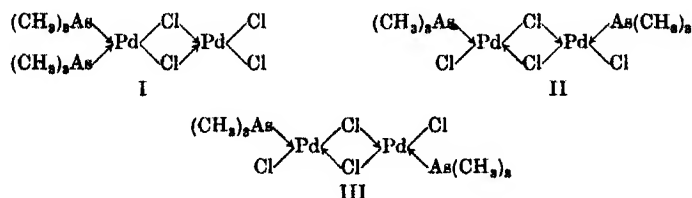
Only one crystalline form of the tetrachloride and tetrabromide is obtainable. From its chemical reactions* it is not possible to deduce its configuration, for a careful chemical study (Mann and Purdie 1936) of such compounds provides evidence in favour of both formula 1 and of formula II or III. The forms II and III cannot, of course, be distinguished chemically, since they are *cis-trans* isomers. In order to account for these facts we may assume either that the various forms of the complex exist together in solution and that the most stable form crystallizes out, or that only the one form exists in the solution as in the solid but that change of configuration accompanies chemical reaction. It has long been known that inversion sometimes occurs during chemical reaction both of organic and inorganic compounds. Werner, for example, studied a large number of reactions of cobaltammines in which change of configuration occurred (Werner 1912), and the present author has shown by X-ray methods that the ion $[Co(NH_3)_2(NO_2)_4]^-$ has, in the silver salt, the *trans* configuration (Wells 1936), whereas the *cis* configuration had been assigned to the ion on chemical grounds (Thomas 1922, 1923). It is not proposed to discuss this problem at length in the present paper, but it will be seen that although the crystallographer is necessarily concerned with the configuration of a complex in the crystal only, the results he obtains may have considerable bearing on problems which are at first sight specifically chemical.

* For the analogous tributylphosphino compound, e.g.

$$
(Bu_3P.PdCl_2)_2 \xrightarrow[]{K_2C_2O_4} Bu_3P\!\!\diagdown Pd\!\!\diagup^{\displaystyle Cl}_{\displaystyle Cl}\!\!\diagdown Pd\!\!\diagup^{\displaystyle O.CO}_{\displaystyle O.CO}
\tag{1}
$$

$$
2 C_6H_5NH_2 \searrow
$$

$$
2\left[Bu_3P\!\!\diagdown_{\displaystyle Cl}\!\!Pd\!\!\diagup^{\displaystyle Cl}_{\displaystyle NH_2C_6H_5} \right]
\tag{2}
$$

The first reaction would suggest that both phosphine groups are attached to the same palladium atom (formula I above), whereas the second would indicated that one phosphine group is attached to each palladium atom in the original compound (formula II or III).

THE UNIT CELLS AND SPACE-GROUP OF $[(CH_3)_3As \cdot PdCl_2]_2$
AND $[(CH_3)_3As \cdot PdBr_2]_2$

The tetrachloride crystallizes from organic solvents as tetragonal prisms {110}, usually in hair-like needles. Crystals from alcohol were first examined, but later it was found that larger crystals could be obtained by slow deposition from dioxane. Comparison of X-ray photographs of crystals from the two solvents showed that the cell dimensions of the dioxane crystals were about $1\frac{1}{2}$ % larger than those of the alcohol crystals, and the two forms are isomorphous. Crystals of the tetrabromide from *dioxane* are strictly isomorphous with the tetrachloride, but those from alcohol show slight departures from tetragonal symmetry, though the general nature of the structure of these crystals must be very similar to that of the tetragonal crystals. This form of the tetrabromide will not be further discussed here. The cell dimensions of the tetragonal crystals are:

	a	c
Tetrachloride (alcohol)	16·00 A	7·22 A
,, (dioxane)	16·25	7·31
Tetrabromide (dioxane)	16·6	7·48

These crystals show high negative birefringence and marked pleochroism: pale yellow for vibrations along the needle axis and orange red at right angles to the axis. They exhibit no signs of pyroelectricity when tested in liquid air. Oscillation and Weissenberg photographs were taken about the [100], [110] and [001] axes with Cu K_α radiation. The cell dimensions and densities indicate that there are four molecules in the unit cell. The approximate density of the crystals of the tetrabromide (from dioxane) was determined by flotation, 2·5 g./c.c.—the density calculated for 4 molecules per unit cell is 2·48 g./c.c. The absences are those due to a body-centred lattice only, and this together with the fact that $F_{hk0} \neq F_{kh0}$ limits the possible space-groups to I 4, I $\bar{4}$ or I 4/m.

Since the crystals have a common structure, differing only in detail in the three compounds, the next section deals with the approximate structure of all three.

THE MOLECULAR SYMMETRY AND THE APPROXIMATE STRUCTURE

In the space-groups I 4, I $\bar{4}$ and I 4/m the twofold positions have point-symmetries 4, $\bar{4}$ and 4/m respectively, which are impossible for a molecule of this type. The point-symmetries of the various fourfold positions are:[*]

* Space-group nomenclature is that of the "International Tables".

I 4:   (b) 2,

I $\overline{4}$:   (e) and (f) 2,

I 4/m: (c) 2/m, (d) $\overline{4}$, (e) 4.

The positions (d) and (e) in I 4/m are excluded for the reason already given, so that the molecular symmetry is either 2 or 2/m. All the three structural formulae given above could possess a diad axis of symmetry, but in these space-groups the diad axes lie parallel to the c axis. Moreover, the optical properties and cell dimensions suggest flat molecules lying in planes parallel to (001). If, therefore, the plane of the molecule is (001), then the *trans* form III must be that found in the crystal, and an elegant structure immediately suggests itself. If the molecules are stacked along the $\overline{4}$ axes in I $\overline{4}$ or along the 4_2 axes in I 4 or I 4/m, then each molecule will be related to those above and below by a rotation through 90° and each palladium atom will be in six-co-ordination, considering the central portion of a molecule to be approximately a square. The spacing of the molecules along the c axis will be determined by the choice of space-group; in I $\overline{4}$ the molecules would lie in planes 2z apart, where z is a variable parameter, and in I 4 or I 4/m in planes c/2 apart. The points to be established are therefore:

(1) the planar nature of the molecule and the separation of the molecules along the c axis, and

(2) the orientation of the molecules with respect to the axes in the plane (001).

(1) The regular falling off in intensity of the orders 00l and the fact that the variation in intensity of a series of h0l reflexions (h constant) is similar for different values of h suggest planar molecules in planes c/2 apart. This was confirmed by making an F^2 projection on the ac plane, using the values of F'_{h0l} obtained from intensities estimated visually on a Weissenberg photograph about the [100] axis of a crystal of the tetrachloride from dioxane. If I is the estimated intensity on an arbitrary intensity scale, then

$$F' = \left[\frac{I \sin 2\theta}{1 + \cos^2 2\theta}\right]^{\frac{1}{2}},$$

the intensity scale being adjusted to make the values of $F'_{obs.}$ comparable with $F_{calc.}$ for the low orders h00, since this facilitates comparison of the two sets of values. The data for the projection are given in Table I, the values of $F_{calc.}$ being calculated from the parameters on page 180.

The resulting projection is shown in fig. 1. All the peaks lie at heights $z = 0$ or $\frac{1}{2}$, indicating planar molecules lying in planes c/2 apart. Some or all of the carbon atoms will lie between these planes but produce very little effect on

TABLE I. OBSERVED AND CALCULATED F_{h0l}—TETRACHLORIDE
(DIOXANE)—IN ORDER OF INCREASING $\sin \theta/\lambda$

hkl	F'_{obs}	F_{calc}	hkl	F'_{obs}	F_{calc}
200	14	+ 13	802	17	+ 24
101	11	+ 13	901	< 7	+ 3
301	20	+ 22	204	15	+ 11
400	< 4	− 1	703	11	+ 18
002	67	+ 73	404	< 8	0
202	19	+ 16	10 0 0	56	+ 52
501	5	− 9	604	< 8	− 3
402	< 5	0	10 0 2	42	+ 45
600	8	− 7	11 0 1	9	+ 16
103	6	+ 8	903	< 9	0
701	15	+ 19	105	< 9	+ 9
303	20	+ 20	305	10	+ 15
602	< 6	0	804	10	+ 22
800	22	+ 27	505	< 9	− 4
503	< 7	− 6	006	28	+ 48
004	57	+ 64	10 0 4	25	+ 44
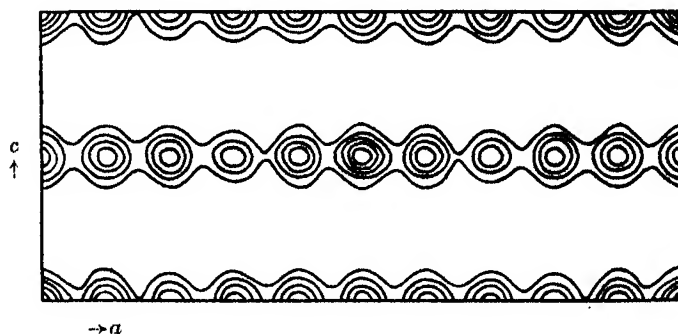
FIG. 1. F^2—Fourier projection on ac plane—tetrachloride from dioxane.

such a projection. At this point the space-group $I\bar{4}$ may be discarded since in this the heights of atoms in the eightfold positions are $\mp z$ and $\frac{1}{2} \mp z$, and there are 8 Pd, 8 As and 16 Cl (Br) in the cell.* We should therefore have to assign the special value $\frac{1}{4}$ to the z co-ordinates of all the atoms. Assuming the molecule to be strictly planar, the choice between $I4$ and $I4/m$ merely determines the positions of the carbon atoms and in so doing makes the point-symmetry of the whole molecule either 2 or $2/m$. In $I4$ the heights

* It should perhaps be pointed out here that the rejection of $I\bar{4}$ is justified only if the alternative space-group chosen accounts satisfactorily for all the observations. Even then there may be slight distortions of the molecule which, though too small to be detected in the present structure determination, would require the space-group to be $I\bar{4}$. This, however, is a matter of formal rather than practical importance.

of the atoms in the eightfold positions are z and $\frac{1}{2}+z$; in I $4/m$, 0 and $\frac{1}{2}$. In I 4 the 24 carbon atoms would occupy three eightfold positions, the point-symmetry of the molecule being 2. In I $4/m$ the carbon atoms must occupy one sixteenfold (i) and one eightfold position (h), since three eightfold positions would place them all in the plane of the arsenic atom and the eightfold positions (f) and (g) are impossible for reasons of interatomic distances. The trimethylarsine group then has a plane of symmetry and the whole molecule point-symmetry $2/m$.

(2) Having demonstrated that the molecules are planar, or very nearly so, and lie parallel to (001), it is justifiable to adopt a molecular model in order to determine the signs of F_{hk0} and to project the structure on that plane. The following interatomic distances were assumed: Pd–Cl, 2·30; Pd–As, 2·50 A; and angles of 90° between the palladium bonds. The method adopted was to draw the molecule to scale on tracing-paper and to use the Bragg structure factor curves (Bragg and Lipson 1936) to find the contributions of the atoms to a given F_{hk0} for various orientations of the molecule with respect to the cell side (a axis). The molecule was first placed with the Pd–Pd axis parallel to the cell side and rotated through a total of 90°. Curves were drawn for the orders $h00$ showing the variation in F (with sign) with the orientation of the molecule, and comparison with the observed intensities of these reflexions showed that the axis of the molecule must lie approximately parallel to the cell side. The signs of the stronger $hk0$ reflexions were now computed and an F-projection on (001) made, using estimated intensities as before (fig. 2). In this figure and fig. 5 the origin of co-ordinates is at $x = \frac{1}{2}$, $y = 0$. The positions of Pd, As and Cl^2 are shown* but Cl^1 is superimposed on Pd in this projection.

The structure is shown diagrammatically in fig. 3, where the molecules are represented by lines, full at $z = 0$ and dotted at $z = \frac{1}{2}$. It will be seen that if the layers can be separated, then we can obtain a picture of a single molecule. This can be done by making a section of the three-dimensional electron density distribution at the height $z = 0$ or $\frac{1}{2}$. Normally this involves the determination of the magnitude and sign of the structure-factors of all the general planes. In this particular structure, however, the problem may be greatly simplified. The summation of the series

$$\sum_h \sum_k F_{hk0} e^{i(hx+ky)}$$

gives a projection of the contents of the unit cell on (001). If instead of

* There are two types of halogen atom in the molecule; one attached to two palladium atoms, the other to one palladium atom. These will be distinguished as Cl^1(Br^1) and Cl^2(Br^2) respectively.

F_{hk0} we use as coefficients of the double Fourier series $\phi_{hk} = \sum_l F_{hkl}$, then

we obtain a section at $z = 0$ of the three-dimensional distribution of electron density. Since all the heavy atoms lie in planes at $z = 0$ or $\frac{1}{2}$, the geometrical
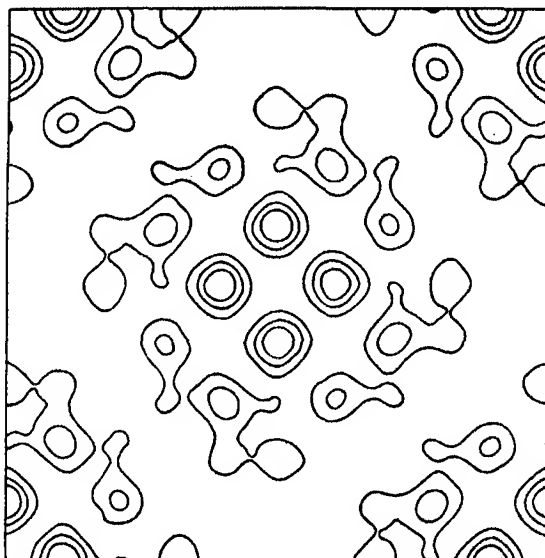

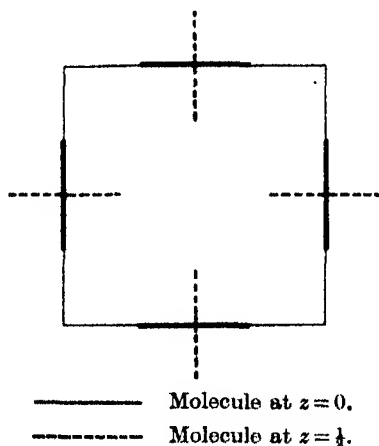FIG. 2. Fourier projection on (001)—tetrachloride from dioxane.

——————— Molecule at $z = 0$.
– – – – – – Molecule at $z = \frac{1}{2}$.

FIG. 3. Diagrammatic representation of the structure.

structure-factors of hkl orders are functions of h and k only, apart from the contributions from the carbon atoms. For a given series of hkl orders (keeping h and k constant) the sum $\sum_l F_{hkl}$ would be proportional to the

first member F_{hk0} or F_{hk1}, neglecting the change in atomic scattering power (f), so that for $\sum_l F_{hkl}$ we may write

$$F_{hk0} \text{ when } h+k \text{ is even,}$$

$$F_{hk1} \text{ when } h+k \text{ is odd.}$$

Actually the decrease in atomic scattering power with angle precludes a strict proportionality between $\sum_l F_{hkl}$ and F_{hk0} or F_{hk1}, but it will be safe to assume that the sums will be in the same relative order as their first terms. The required section is therefore obtained by proceeding as in the case of the two-dimensional projection except that we insert the values of F_{hk1} as well as those of F_{hk0} in the above summation. This method is applied in the next section, which deals with the detailed structure of the tetra-bromide. This compound was chosen in preference to the tetrachloride on account of the greater scattering power of bromine compared with chlorine which should make possible a more precise location of the halogen atoms.

THE DETAILED STRUCTURE OF THE TETRABROMIDE FROM DIOXANE

The determination of the precise structure implies the evaluation of the x and y co-ordinates of Pd, As, Br^1 and Br^2, i.e. of eight parameters neglecting the carbon atoms. The most satisfactory method was found to be as follows. If the exact configuration of the molecules were known, then the only variable would be the inclination of the molecule to the axes in the basal plane. Accordingly, various molecular models were tested and for each the variation in F of certain high-order reflexions with rotation of the molecule was plotted. The labour is reduced by working first with four reflexions, the relative intensities of which are

$$8\,10\,0 > 9\,11\,0 \geqslant 11\,9\,0 > 10\,8\,0.$$

Starting from a standard molecule (having Pd–Br, 2·43; Pd–As, 2·50 A; and Pd bond angles of 90°), various distortions were tested out. Fig. 4 shows the variation in the structure factor of these reflexions as the molecule is rotated through a small angle, and such curves exclude a large number of possible molecular models, e.g. (a) and (b) in fig. 4. Finally a model was found which accounted for all the major intensity relationships between the high-order reflexions. The carbon atoms were then placed in the most probable positions and the structure factors of all the $hk0$ and $hk1$ reflexions calculated. The intensity data were obtained from equatorial and first layer line Weissenberg photographs, taken with Cu K_α radiation using

a very thin needle of approximately square cross-section. The observed values are denoted by F' since they are not absolute, and for the projection they were reduced by an artificial temperature factor $e^{-4\sin^2\theta}$. A section
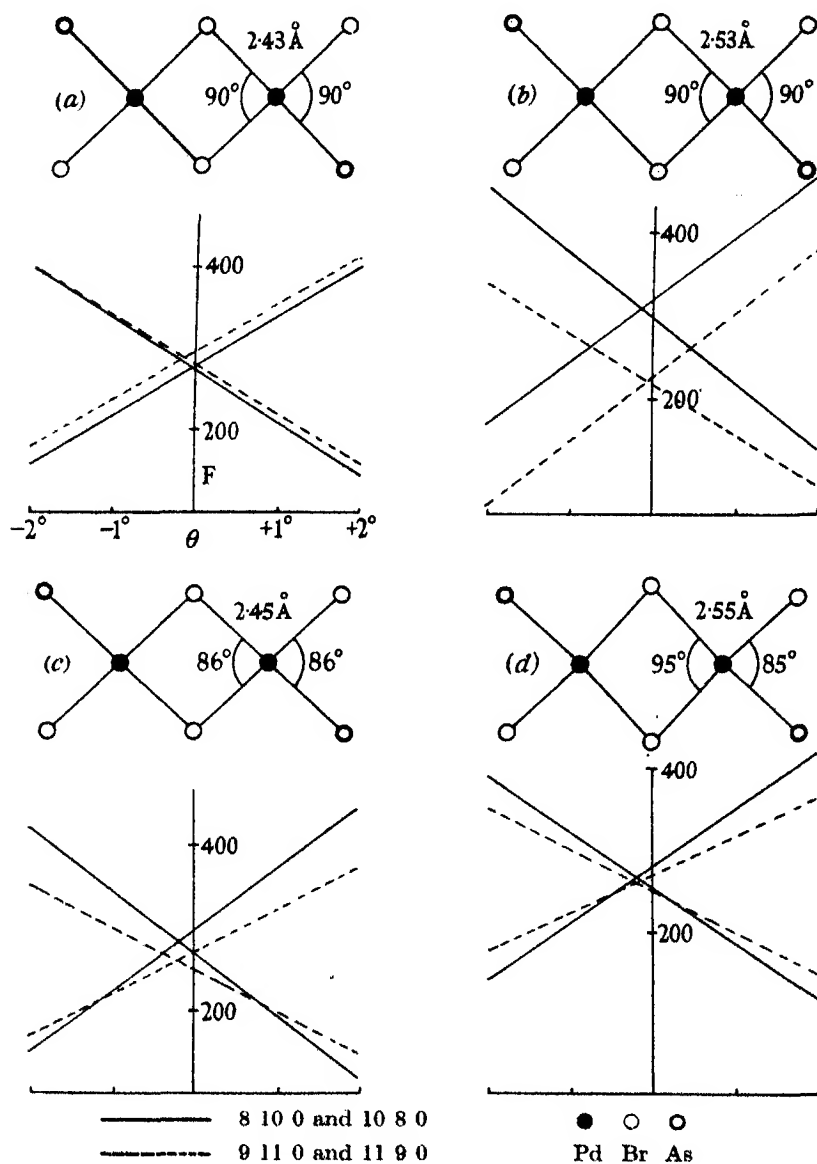

FIG. 4. Curves showing the variation in the structure factors of the reflexions 8 10 0, 10 8 0, 9 11 0 and 11 9 0 with rotation of the molecule for different molecular models.

at $z = 0$ of the three-dimensional electron-density distribution was made as described in the previous section and is shown in fig. 5. The molecular model arrived at by the "trial and error" method is shown in fig. 4(*d*), and this model was used to determine the signs of the structure factors, an inclination to the axis of $+1\frac{1}{2}°$ giving the best agreement with the
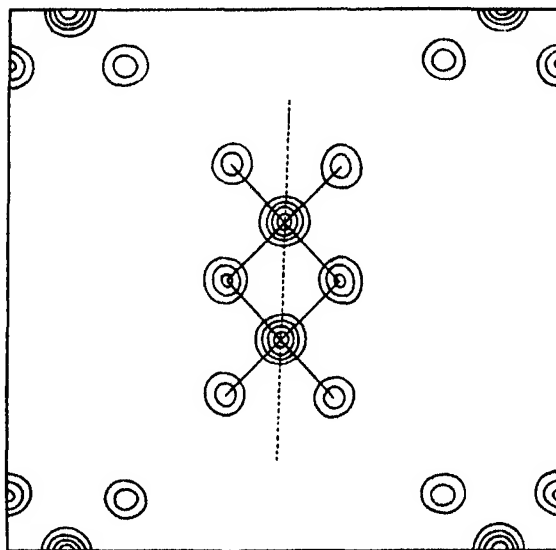
FIG. 5. Section at $z = 0$ of three-dimensional electron density distribution (tetrabromide from dioxane).

high-order reflexions. The molecule shown by the Fourier projection is that of fig. 4(*c*) and the angle between the Pd–Br[2] and Pd–As bonds is within 1° of that found by the "trial and error" determination, but the angle between the Pd–Br[1] bonds and also the distance apart of the palladium atoms have changed from
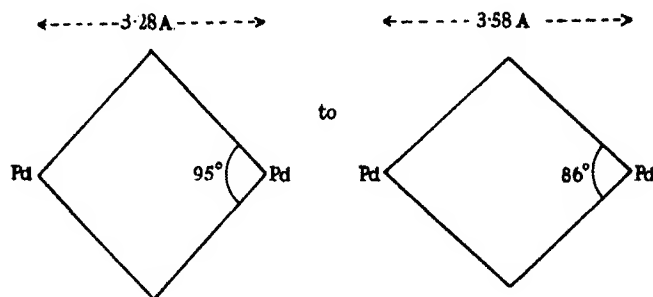
Both models give equally good agreement between calculated and observed values of F_{hk0} and the reason for this is apparent from the structure. The fact that alternate molecules along the c axis are rotated through 90° relative to one another causes the two changes—(1) reduction of the angle between the Pd–Br^1 bonds and (2) increase in the Pd–Pd separation—to neutralize one another. This illustrates a limitation of the "trial and error" method of determining such a structure, for the curves in fig. 4(c) and (d) for the two different molecular models are almost identical. Since, however, the projection incorporated the observed structure factors of some 130 planes, the general shape of the molecule as determined from that projection must be accepted.

The interpretation of Fourier projections of complex metallic compounds is rather different from that of projections of purely organic compounds. The fact that high-order reflexions often have large structure factors owing to the presence of heavy atoms necessitates the introduction of an artificial temperature factor to avoid spurious diffraction effects which can alter both the volumes and positions of peaks. This leads to loss of detail in the projection, but the differences in the intensities of high-order reflexions may still be used to refine the parameters obtained from the projections. For this reason such projections are not necessarily final as in the case of purely organic compounds. The better definition of Br^2 than Br^1 in fig. 6 may be due to the greater rigidity of the central portion of the molecule as compared with the outer parts.

The parameters finally adopted are:

	x	y	z
8 Pd (h)	0·608	0·003	0
8 As (h)	0·715	0·109	0
8 Br^1 (h)	0·497	0·101	0
8 Br^2 (h)	0·717	−0·094	0
16 C (i)	0·783	0·100	0·212
8 C (h)	0·669	0·219	0

These define a molecule inclined at an angle of $1\frac{1}{2}$° to the a axis. The carbon atoms in such a compound cannot be located by X-ray methods on account of their small scattering power compared with palladium, bromine and arsenic. The above parameters for carbon are based on considerations of packing, assuming tetrahedral disposition of the arsenic bonds and an As–C bond-length of 1·95 A, and the horizontal plane of symmetry through the molecule has been retained. Tables II and III contain the observed structure factors and those calculated from the above parameters.

TABLE II. OBSERVED AND CALCULATED VALUES OF F_{hk0}—TETRABROMIDE (DIOXANE)

hkl	F'_{obs}	F_{calc}	hkl	F'_{obs}	F_{calc}	hkl	F'_{obs}	F_{calc}	hkl	F'_{obs}	F_{calc}
200	26	+18	150	<5	− 7	2 10 0	<7	0	13 1 0	<8	− 5
400	<4	0	510	<5	− 3	10 2 0	19	+22	7 11 0	<8	− 5
600	16	−16	350	45	+38	590	<7	+ 7	11 7 0	<8	+ 2
800	33	+44	530	38	+27	950	<7	+ 3	3 13 0	16	+24
10 0 0	59	+67	260	<5	− 3	4 10 0	<7	+ 6	13 3 0	<8	+ 9
12 0 0	<7	+ 7	620	10	+ 8	10 4 0	<7	+ 2	6 12 0	<8	+ 1
14 0 0	<8	+ 5	170	5	− 4	1 11 0	14	−11	12 6 0	<8	− 10
16 0 0	<8	−14	710	<4	+ 1	11 1 0	25	− 28	5 13 0	17	+29
110	53	−57	460	53	− 51	790	<7	− 7	13 5 0	30	+42
220	<3	+ 2	640	45	− 34	970	<7	+ 2	2 14 0	<8	0
330	17	+16	370	5	+ 9	3 11 0	<7	− 5	14 2 0	<8	+ 5
440	63	−73	730	<5	− 4	11 3 0	<7	+ 3	9 11 0	24	−35
550	73	+80	280	14	+ 9	6 10 0	<7	−12	11 9 0	17	−18
660	26	−23	820	14	+14	10 6 0	<7	0	4 14 0	42	− 60
770	<6	+ 2	570	14	+14	5 11 0	<7	− 6	14 4 0	30	−41
880	15	+19	750	12	+12	11 5 0	<7	−12	1 15 0	<8	− 3
990	41	−50	480	<6	+ 2	2 12 0	<7	− 5	15 1 0	<8	+ 8
10 10 0	38	+46	840	<6	− 4	12 2 0	<7	− 4	6 14 0	12	−21
130	12	+ 4	190	47	−44	4 12 0	<8	− 1	14 6 0	33	−46
310	<3	− 1	910	51	− 61	12 4 0	<8	− 3	3 15 0	17	+26
240	11	+11	390	<7	+ 2	8 10 0	29	+41	15 3 0	<8	+ 4
420	4	− 5	930	<7	+ 2	10 8 0	11	+13	5 15 0	30	+37
			680	<7	0	1 13 0	<8	− 5	15 5 0	30	+39
			860	<7	− 2						

TABLE III. OBSERVED AND CALCULATED VALUES OF F_{hk1}—TETRABROMIDE (DIOXANE)

hkl	F'_{obs}	F_{calc}	hkl	F'_{obs}	F_{calc}
101	11	+16	271	10	+ 7
301	15	+15	721	22	+ 8
501	33	−33	561	12	+14
701	18	+12	651	27	+28
901	<7	− 2	181	<7	+ 1
11 0 1	19	+25	811	10	− 4
			471	26	−26
121	25	− 19	741	23	− 26
211	30	− 26	381	15	+13
231	13	+15	831	10	+13
321	14	+10	671	10	− 16
141	<5	+ 3	761	21	− 17
411	14	+14	291	17	− 22
341	10	− 12	921	19	− 21
431	23	− 21	1 10 1	10	− 5
251	21	+19	10 1 1	<8	− 3
521	20	+16	3 10 1	8	+ 4
161	<6	− 7	10 3 1	12	+17
611	<6	− 2	2 11 1	14	− 9
451	<6	− 3	11 2 1	<9	+ 1
541	<6	+ 2	1 12 1	<9	− 16
361	10	− 4	12 1 1	20	− 21
631	14	− 8			

THE TETRACHLORIDE—FROM ALCOHOL AND FROM DIOXANE

The c-axis Weissenberg photographs of the crystals of the tetrachloride obtained from alcohol and from dioxane are very similar in general appearance but there are differences in the intensities of a number of reflexions, chiefly of high order. Now alterations in the intensities of high-order reflexions indicate a shift of heavy atoms, and since there is no reason to assume any change in the molecule itself, these alterations must be accounted for by a change in the orientation of the molecules. Low-order reflexions, on the other hand, are very insensitive to a small change of this sort, but may be appreciably affected by the presence of dioxane. For these reasons the high and low order reflexions must be treated separately and in that order.

As in the case of the tetrabromide, the relative intensities of the reflexions 10 8 0, 8 10 0, 11 9 0 and 9 11 0 may be used first to determine approximately the orientation of the molecule, and for this purpose the molecule will be assumed to have a configuration analogous to that of the tetrabromide, allowing for the difference in size of chlorine and bromine. The observed intensities of these reflexions are:

Tetrachloride from dioxane: $9\,11\,0 > 11\,9\,0 \approx 10\,8\,0 \approx 8\,10\,0$

Tetrachloride from alcohol: $9\,11\,0 \approx 8\,10\,0 \gg 11\,9\,0 \approx 10\,8\,0$

and curves were drawn similar to those in fig. 4 showing the variation in the structure factors of these reflexions with rotation of the molecule in the basal plane. The most satisfactory agreement with high-order reflexions was obtained with the molecule inclined at $2°$ to the a axis in the crystals from alcohol and parallel to the axis in the crystals from dioxane, giving the parameters:

	From alcohol		From dioxane	
	x	y	x	y
Pd	0·606	0·004	0·604	0·000
As	0·716	0·114	0·716	0·106
Cl^1	0·496	0·098	0·500	0·097
Cl^2	0·716	$-0·091$	0·708	$-0·096$

The c-axis Weissenberg photographs show two isolated groups of four high-order reflexions, viz. 15 5 0, 14 4 0, 14 6 0, 13 5 0 and 5 15 0, 4 14 0, 6 14 0, 5 13 0, and their intensities form a convenient check on the structures, as seen from the following comparison of the observed intensities and calculated structure factors:

| From alcohol			From dioxane	
	F_{calc}			F_{calc}
4 14 0 > 14 4 0	41 > 28		4 14 0 ≈ 14 4 0	35 ≈ 35
5 15 0 ≈ 15 5 0	26 ≈ 26		5 15 0 ≈ 15 5 0	35 ≈ 34
6 14 0 < 14 6 0	15 < 33		6 14 0 < 14 6 0	24 < 26
5 13 0 < 13 5 0	22 < 34		5 13 0 ≈ 13 5 0	25 ≈ 25

It is seen that the slight change in the orientation of the molecules gives quite a satisfactory explanation of the alterations in the intensities of these high-order reflexions.

The small changes in intensity of low-order reflexions are not amenable to such treatment, since they are presumably due either to the scattering by the dioxane itself or to rearrangements of the methyl groups caused by the introduction of the solvent molecules. The dioxane of crystallization is further discussed below. The following parameters for carbon were used in calculating the values given in Table I of F_{h0l} for the tetrachloride from dioxane:

	x	y	z
Sixteenfold (*i*)	0·785	0·100	0·217
Eightfold (*h*)	0·669	0·218	0·000

DESCRIPTION OF THE STRUCTURE

The structure of the tetrabromide is illustrated in fig. 6. It consists of two interpenetrating body-centred lattices related to one another by the operation of 4_2 axes. The units in the structure are molecules of $[(CH_3)_3As]_2Pd_2Br_4$ having the *trans* configuration. Within the limits of experimental error the molecule is planar apart from four methyl groups and has the structure
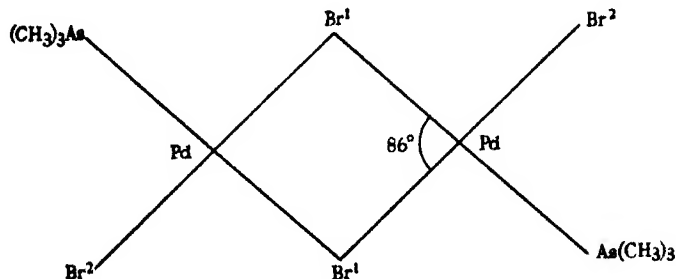
The probable error in the lengths of the bonds is not greater than 0·05 A, though from the nature of the structure this is difficult to estimate. The bond lengths are normal: Pd–As, 2·50 and Pd–Br, 2·45 A, ±0·05 A, and

there is no appreciable difference* between the lengths of the bonds $Pd-Br^1$ and $Pd-Br^2$. The general distortion of the molecule from the "ideal" (i.e. with the interbond angles of 90°) results from the repulsion of the palladium atoms to a distance of 3·58 A compared with 3·44 A for the "ideal" molecule, leading to a contraction of the angle between the $Pd-Br^1$ bonds to 86°.
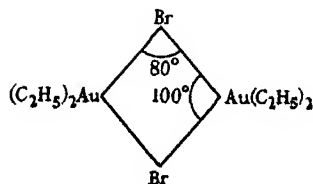

Pd   Br   As CH_3
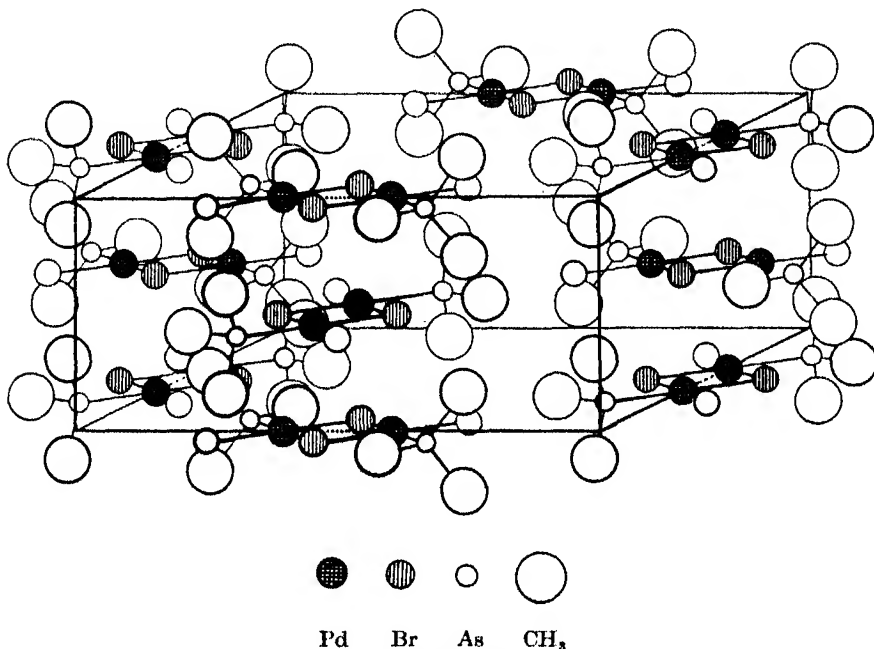
Fig. 6. The crystal structure of $[(CH_3)_3As]_2Pd_2Br_4$. (For the sake of clarity two molecules at the back of the cell are omitted.)

* Mention must be made here of the structure of diethylmonobromogold recently published. The structure is admittedly only approximate and gives the dimensions shown for the molecule

According to Pauling (Pauling and Huggins 1934) the covalent radii for Pd^{II} and Au^{III} in square co-ordination are 1·32 and 1·31 A, respectively, so that the distances $Pd-Br^1$ and Au–Br should be very nearly the same. The value 2·65 ± 0·1 A for Au–Br therefore appears rather too large, and the distortion of the interbond angles is in the opposite sense to that found here.

This may be compared with the reduction in length of shared edges of co-ordination polyhedra which occurs in ionic compounds if we regard the bridged molecule as two $(CH_3)_3AsPdBr_3$ groups having one edge (Br^1–Br^1) in common. Here, however, the bonds are all covalent and such distortion is very much less than in the case of ionic compounds. It is interesting to compare with this the very much greater repulsion of thallic ions in the complex ion $Tl_2Cl_9^{3-}$, formed by two $TlCl_6$ octahedra having one face in common. The observed distance Tl–Tl within the complex ion is 3·65 A compared with only 3·04 A for the "ideal" (i.e. Tl^{3+} ions at the centres of the octahedra).

The molecules are stacked with their planes parallel to one another along the 4_2 axes at intervals of 3·74 A, so that in this direction neighbouring molecules are related by a rotation through 90°. Consequently each palladium atom is surrounded by 1 As and 5 Br atoms at the apices of an elongated octahedron, neglecting the CH_3 groups of its own molecule, at distances

$$\text{Pd} \begin{cases} \text{intramolecular} \begin{cases} 2\ Br^1,\ 2\text{·}45\ A, \\ 1\ As,\ \ \ 2\text{·}50 \\ 1\ Br^2,\ 2\text{·}45 \end{cases} \\ \text{intermolecular} \quad 2\ Br^1,\ 3\text{·}74 \end{cases}$$

All other intermolecular contacts are between bromine atoms and methyl groups and range from 3·94 to 4·07 A.

A projection of the structure on (001) shows two interesting features. First the molecules are arranged in columns along the 4_2 axes (perpendicular to the plane of the paper), and it will be seen that the separate columns of molecules are held together only by van der Waals forces between bromine atoms and methyl groups of different molecules. These cohesive forces must be very weak since the distances between bromine and carbon atoms are almost exactly 4 A. This feeble cohesion is shown by the easy (110) cleavage of the tetrachloride and tetrabromide, but crystals of the intermediate dichloro-dibromide illustrate this point in a very striking way. One form of this compound is monoclinic (pseudo-tetragonal), being a slightly distorted form of the tetragonal structure of the tetrabromide, and forms long flattened needles. When one of these needles is touched with the point of a pin it disintegrates along the needle axis into a number of fine fibres. In fig. 7 (a) the centres of the carbon and Br^2 atoms are accentuated in order to illustrate this. Secondly the packing of the molecules in this way leaves tunnels through the structure, and the axes of these tunnels are [00z] and $[\frac{1}{2}\frac{1}{2}z]$ which are fourfold axes. Crystals of the tetrachloride
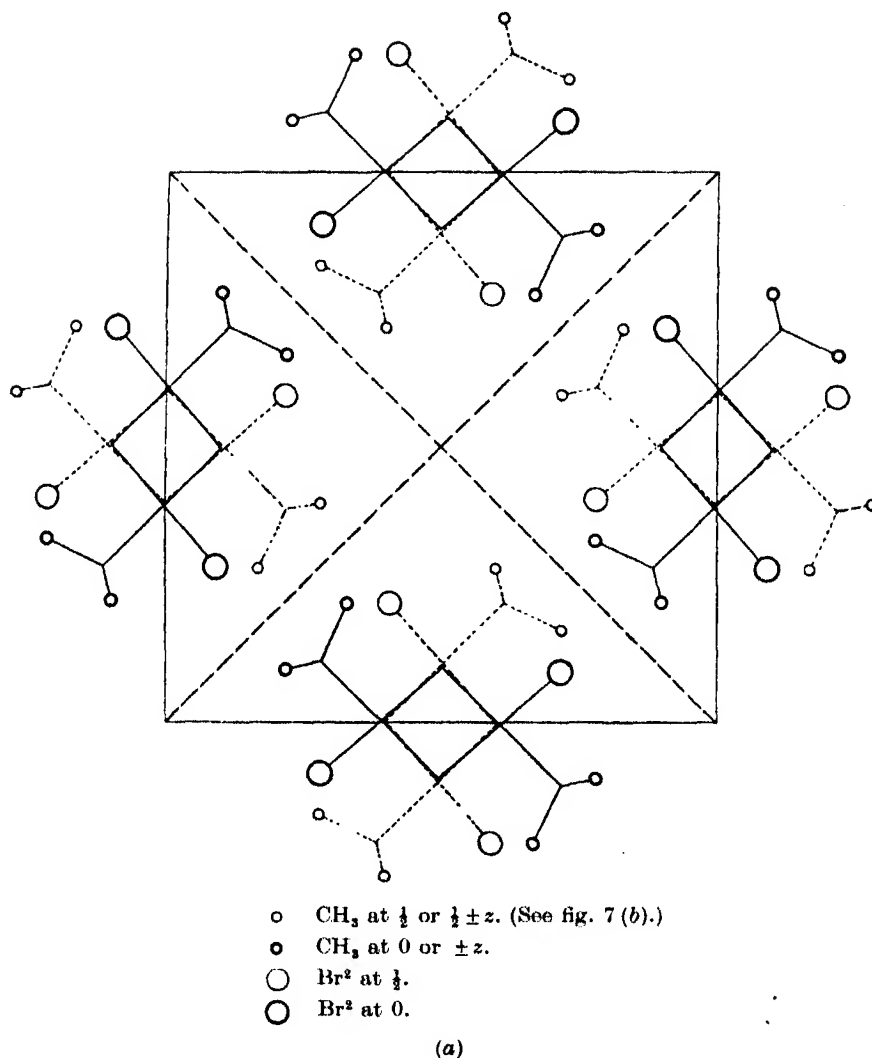
o CH_3 at $\frac{1}{4}$ or $\frac{1}{4} \pm z$. (See fig. 7 (b).)

o CH_3 at 0 or $\pm z$.

◯ Br^2 at $\frac{1}{4}$.

◯ Br^2 at 0.

(a)

FIG. 7. (a) Projection of the structure of $[(CH_3)_3As]_2Pd_2Br_4$ on (001) to illustrate the arrangement of the molecules in columns in the direction of the c axis. The diagonal dotted lines indicate the (110) cleavages. Molecules at $z = 0$ and $\frac{1}{2}$ are drawn with full and dotted lines (compare fig. 3).

(b) Projection of the structure of $[(CH_3)_3As]_2Pd_2Br_4$ on (001). The small circles represent methyl groups at the heights indicated. Molecules at $z = 0$ and $\frac{1}{4}$ are drawn with full and dotted lines. The dioxane is represented in this projection as a circle of radius 3·45 A.

are similar in this respect. Now when one of these compounds crystallizes from alcohol these cylindrical holes remain empty, presumably because the molecules of ethyl alcohol do not fit snugly into them. The diameter of a molecule of dioxane however, is almost exactly that of the holes (fig. 7 (b)), and the introduction of the solvent takes place with only a slight
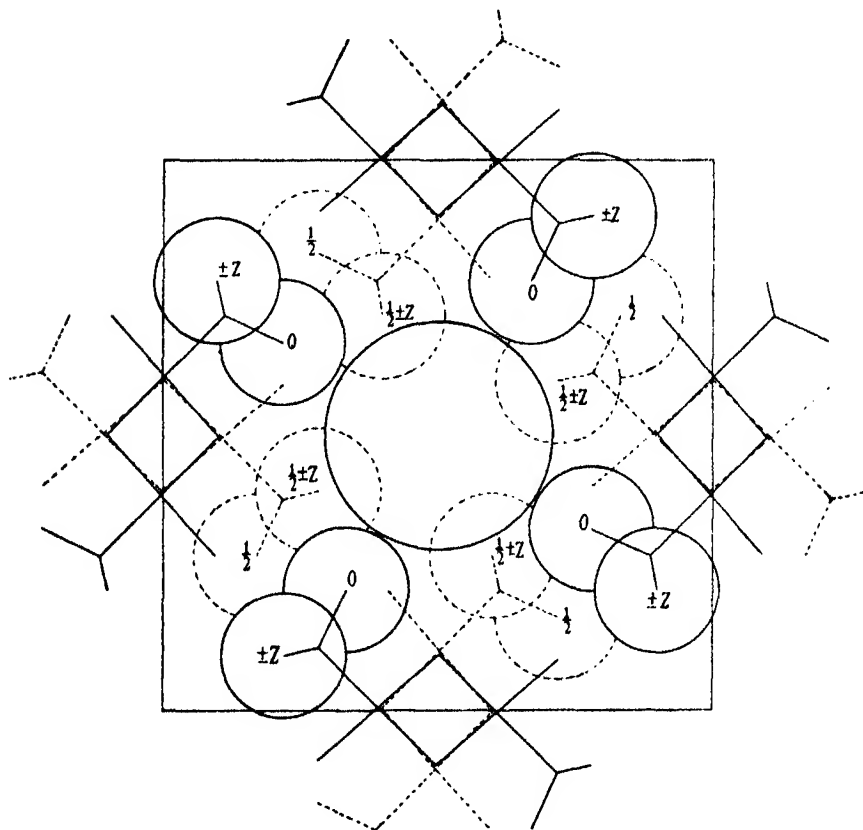
FIG. 7 (b)

increase in cell size ($1\frac{1}{2}$ %) and a slight change in orientation of the molecules of the palladium compound. From the fact that the dioxane molecules are situated along fourfold axes of symmetry it must be concluded that they are rotating in the crystal. There is room for four molecules of dioxane in the unit cell, considering them to be oblate spheroids of effective thickness *ca.* 3·7 A. It is not certain, however, that the full complement of dioxane is ever taken up, and it is possible that a smaller proportion of solvent

of crystallization is statistically distributed throughout the crystals. For these reasons no account has been taken of the dioxane in calculating the structure factors given in the tables above.

SUMMARY

The crystal structures of the bridged compounds $[(CH_3)_3As]_2Pd_2Cl_4$ and its bromine analogue have been determined. The crystals of the tetrachloride from alcohol and from dioxane and those of the tetrabromide from dioxane are all isomorphous. A probable structure deduced from the optical properties, cell dimensions and symmetry was confirmed by Fourier projections using visually estimated intensities. The structure of the tetrabromide was investigated in detail, the configuration of the molecule being finally obtained from a section of the three-dimensional electron density distribution. The bridged molecule is found to be planar with the configuration:
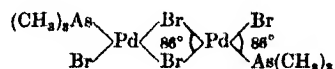
The interatomic distances are: Pd–Br, 2·45 and Pd–As, $2·50 \mp 0·05$ A. The molecules are stacked in columns along 4_2 axes in the space group $I 4/m$, and the columns of molecules are held together by very weak van der Waals forces. The packing of the molecules in this way leaves tunnels through the structure. These remain empty in certain circumstances, as for example when the tetrachloride crystallizes from alcohol. On crystallizing from dioxane, however, this compound takes up dioxane of crystallization presumably owing to the fact that the diameter of the dioxane molecules is approximately the same as that of the holes in the structure. The introduction of the solvent is accompanied by a small increase in the cell size and a slight reorientation of the molecules of the palladium compound.

REFERENCES

Bragg and Lipson 1936 *Z. Kristallogr.* **95**, 323.
Burawoy and Gibson 1935 *J. Chem. Soc.* p. 217.
Burawoy, Gibson, Hampson and Powell 1937 *J. Chem. Soc.* p. 1690.
Collenberg and Sandved 1923 *Z. anorg. Chem.* **130**, 1.
Hoard and Goldstein 1935 *J. Chem. Phys.* p. 199.
Mann and Purdie 1936 *J. Chem. Soc.* p. 873.
Pauling and Huggins 1934 *Z. Kristallogr.* **87**, 228.
Powell and Wells 1935 *J. Chem. Soc.* p. 1008.
Thomas 1922 *J. Chem. Soc.* p. 2069.
—— 1923 *J. Chem. Soc.* p. 617.
Wells 1936 *Z. Kristallogr.* **95**, 74.
Werner 1912 *Liebigs Ann.* **386**, 1.
Werner and Pfeiffer 1923 "Anorganische Chemie," 5th ed., pp. 56, 170.

The paramagnetism of the ferromagnetic elements

By W. Sucksmith and R. R. Pearce

H. H. Wills Physical Laboratory, University of Bristol

Introduction

The theory of paramagnetism, originally developed by Langevin (1905) and extended by Weiss (1907) to include ferromagnetics, led to expressions giving the variation of magnetization with temperature above and below the Curie point. These proved of great value in correlating experimental results, and the general agreement between theory and experiment leaves no doubt of the essential correctness of the ideas involved. However, with the introduction of the quantum theory, the nature of the elementary carriers of magnetic moment became apparent, and new values of atomic moments were calculated from the variation of susceptibility with temperature above the Curie point. The chief problem has been to reconcile these with the values more directly measured at low temperatures. Whilst the saturation intensities of the three ferromagnetics—iron, cobalt and nickel—are known with reasonable certainty, the susceptibility measurements of several workers on iron and cobalt show such large discrepancies that, except

for nickel, the theoretical development has been considerably hampered by lack of sufficiently accurate data.

The present work was undertaken to measure accurately the variation of susceptibility with temperature above the Curie point, for iron and cobalt, and to extend the range of the measurement on nickel.

EARLIER RESULTS

The variation of susceptibility with temperature for many paramagnetics and for the ferromagnetics above the Curie temperature is found to conform to the law

$$\chi = \frac{C}{T - \theta},$$

in which C is the Curie constant and θ the paramagnetic Curie point, being the intercept of the extrapolated $1/\chi$, T curve on the temperature axis. The significance of the quantity C will be discussed later in the light of recent theoretical developments. From it the atomic moment is calculable, but for the present, values of C and θ only will be given.

The earliest systematic investigation of the variation of susceptibility with temperature above the Curie point for all three ferromagnetics was by Weiss and Foëx (1911). Their measurements, however, only extended to 1050° C. for nickel and 1300° C. for cobalt. Honda and Takagi (1913) repeated this work with a slightly larger temperature range, but Terry (1917) traced the $1/\chi$, T curves of the three metals up to their respective melting points. Nickel especially has been extensively investigated up to about 950° C., and many results agree in giving $C = 0.323$ per g. atom. Honda and Takagi, however, found $C = 0.412$ per g. atom up to 1060° C., whilst Terry's results give $C = 0.293$ for the Curie constant below about 950° C., the curve being concave to the temperature axis from this temperature up to the melting point (1450° C.). Bloch (1912), on the other hand, reports two straight lines on the $1/\chi$, T graph sharply intersecting at 927° C., and for two different samples of nickel the slopes above this temperature differ by some 10 %.

For iron the sudden decrease in χ at 920° C. corresponding to the β-γ transition considerably limits experiments. Below this temperature and above 1390° C. (the γ-δ transition), iron is body-centred cubic, the intervening γ phase being face-centred cubic. Weiss and Foëx found the linear law to hold in all phases, and further split the β phase into two linear segments β_1 and β_2 sharply intersecting at 828° C. Their C values were 2·24, 1·52, 4·0, 0·25 per g. atom for β_1, β_2, γ, and δ respectively, but the δ value

is very uncertain. No values could be deduced from Terry's curve, as all phases showed curvature convex to the temperature axis. In the β region Honda and Takagi obtained similar curvature, but in the γ phase the susceptibility appeared independent of temperature. Other results over special regions show similar inconsistencies.

Work on cobalt is difficult on account of the high Curie point ($\sim 1100°$ C.). The results of Weiss and Foëx showing two linear portions on the $1/\chi$, T graph sharply intersecting at $1241°$ C. were not confirmed by Honda and Takagi nor by Terry, both of these researches showing smooth curves even up to the melting point ($1485°$ C.). The C values given by Weiss were $1\cdot28$ and $1\cdot07$ per g. atom below and above $1241°$ C., but the temperature was limited to $1300°$ C.

Surveying these results we see considerable discrepancies between workers except on nickel below about $950°$ C. The only available values for the Curie constant for nickel above $950°$ C. are those of Bloch, and for cobalt that of Wiess and Foëx up to $1300°$ C., neither of which were confirmed by Terry.

No special precautions appear to have been taken by Weiss and Foëx to prevent oxidation of their specimens, while Terry worked in a vacuum of $0\cdot001$ mm. of mercury. Now it is known that the vapour pressures of iron, cobalt and nickel at $1250°$ C. are about $0\cdot001$ mm. of mercury, so that at these temperatures appreciable evaporation must occur. Also experiment showed that mutual contamination of the specimen and carrier takes place by solid diffusion, both of these phenomena being considerably accelerated at higher temperatures. Preliminary experiments showed the importance of these factors and that consistent results would only be obtained if precautions to minimize these effects were adopted.

Accordingly, the final apparatus was designed so as to reduce these sources of error to a minimum, it being considered extremely difficult, if at all possible, to eliminate them entirely. By working in an atmosphere of argon at a low pressure and adopting a specially designed specimen carrier, it was found possible to prevent a great deal of the evaporation and at the same time eliminate the effects of solid diffusion of the specimen and carrier. Repeatable measurements of susceptibility could be made in some cases up to $1500°$ C., this being the highest temperature used during the work.

THE APPARATUS

The magnetic balance employed was based on a previous apparatus designed by one of us (Sucksmith 1929) but adapted for high temperature

measurements. The force on a specimen of mass m and susceptibility χ placed in an inhomogeneous magnetic field is

$$F_x = \chi m H \frac{dH}{dx},$$

where dH/dx is the field gradient in the direction of the force. As $H\,dH/dx$ varies fairly rapidly, F_x is usually measured by applying a compensating force of known magnitude to restore the system to its original position in the field. In this method, however, the deflexions are kept extremely small, one scale division representing a displacement of the specimen of 7×10^{-6} cm.; as the largest deflexion used was about 10^{-2} cm., $H\,dH/dx$ can be assumed to remain constant and equal to that at the undeflected position, which was the maximum value at which the gradient of $H\,dH/dx$ is zero. The force is measured by the deformation of a ring of strip phosphor bronze fixed at the top in a vertical plane, and subjected to the downward magnetic force at the lowest point. Fig. 1 shows the essential parts of the arrangement approximately to scale.

The ring R was attached at the top to a three-dimensional screw adjustment. To the lowest point of the ring, a thin quartz rod was fixed. Two flat spiral springs of thin phosphor bronze S_1 and S_2 fixed to this rod with shellac and clamped on their outer edges to the case prevent lateral motion of the suspended system while causing only a small reduction of vertical sensitivity. A second quartz rod was joined on at B by means of a brass sleeve attached with de Khotinsky cement. This rod was sealed on to a tungsten wire which carries the specimen. To prevent softening of the cement joint due to radiation from the furnace, a quartz shield Q was fitted and the sleeve itself adjusted so that the greater part of its length was inside the water jacket W. The small hole in W at B also served to prevent radiation from reaching the lower flat spiral.

The ring carried two small plane mirrors M_1 and M_2 which were sputtered on the front surface with aluminium. Light from a straight filament lamp about one metre distant passed through the lens L, was reflected by the mirrors in turn and passed out through the plane glass window P, converging to a point, about one metre away from the mirrors, on which was focused a microscope with vertical screw motion. The linear magnification of the system was then about 150 times, and with a little practice the position of the image could be read to 0.01 mm., which corresponds to a displacement of the specimen of 7×10^{-6} cm.

The small electromagnet E operated from the observer's table was used to add or remove a steel ball of known weight, so the mechanical sensitivity

of the system by means of a weight calibration could be followed throughout a temperature run. Deflexions were always read with the ball clear of the system. The increase of the sensitivity of the system between room temperature and 1500° C. was about 1 %.
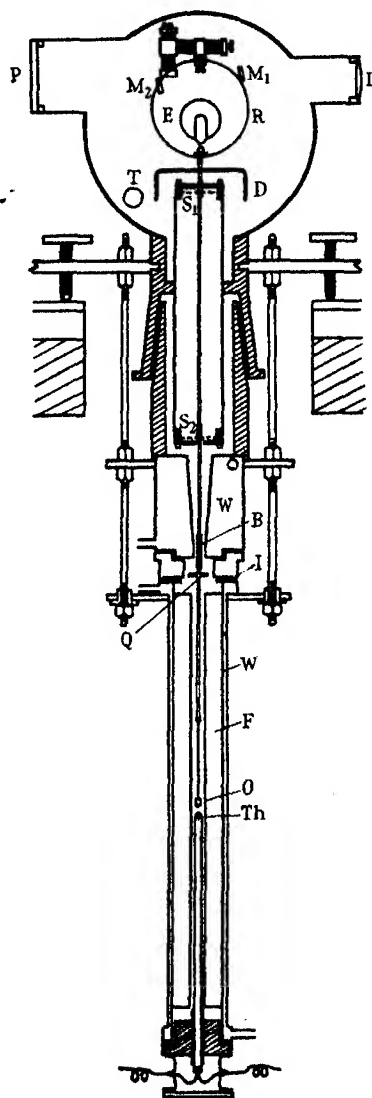

FIG. 1.

The inhomogeneous field was provided by an electromagnet with horizontal traverse and provided with adjustment in three directions at right

angles. Using plane pole pieces 10 cm. diameter and 3·2 cm. apart, the value of $H\,dH/dx$ was about $6·5 \times 10^7$, and to avoid inconveniently large deflexions with iron a 3·9 cm. gap was used giving $H\,dH/dx = 4·5 \times 10^7$. Tests showed that $H\,dH/dx$ was uniform over the volume occupied by the specimen, within the limits of experimental error.

THE FURNACE

The furnace unit, F, was attached to the apparatus through a disk of bakelite, I. The ends of the furnace winding were brought to the case above and below this disk so obviating leads through the vacuum jacket. After considerable investigation the furnace finally adopted was uniformly wound with 0·6 mm. diameter molybdenum wire on an "alundum" tube ($9 \times \frac{1}{8} \times \frac{1}{4}$ in. bore). This was cemented inside a larger "alundum" tube and the unit centrally fixed in a double walled cylindrical brass water jacket with $\frac{1}{32}$ in. annular space. The jacket was baffled spirally to ensure adequate circulation of the water. 1450° C. was maintained in this furnace for long periods using only 800 W. In the early stages of the work non-inductively wound furnaces were used but, besides shortening the life of the furnace, this precaution was proved unnecessary. The furnace was always centred over the specimen with the help of a mirror suitably placed to reflect the inside, the necessary adjustments being made on the picein joint at I.

MEASUREMENT OF TEMPERATURE

Temperatures were measured with a platinum-platinum rhodium thermocouple (30 s.w.g.) placed as closely as possible below the specimen; the e.m.f. developed being measured on a potentiometer. Considerable difficulty was experienced with this couple in the presence of metallic vapours. It was found necessary to sheath the wires completely, the most suitable covering being alundum tubing sealed at one end. The constancy of the calibration was further improved by annealing the wires at red heat in air for a long period before use. Even so it was found necessary to calibrate each couple used before and after a run.

The following *in situ* method of calibration of the thermocouple was therefore adopted. Short lengths of nickel, copper, silver and lead wires were in turn used as fuses in a low current circuit. The fuses were placed in the position normally occupied by the specimen. On increasing the furnace temperature slowly in the neighbourhood of the melting point, the fuse wire was eventually melted and the temperature at which the circuit broke was

assumed to represent the melting point. Calibrations in this manner agreed amongst themselves and with that of the manufacturer to a few degrees even at the nickel point. Outside the furnace, the thermocouple wires were soldered to a long piece of flex leading to the potentiometer, and the joints surrounded with melting ice in a vacuum flask.

Technique

The specimens were right circular cylinders with a central hole and in the case of iron were 2×2 mm. Larger specimens of nickel were used to obtain the same order of deflexions, but in all cases the proportionality between force and weight for a given value of χ was maintained. The electromagnet was adjusted so that the specimen was symmetrical between the poles in the y and z axes, but at the position of maximum inhomogeneity (i.e. $H\,dH/dx$ maximum) along the vertical x axis.

Final adjustment to this position was made magnetically by raising or lowering the magnet on its adjustable screw feet until the deflexion for a fixed temperature was a maximum. This condition ensured that all specimens including the calibrating phial were in exactly the same position for which $H\,dH/dx$ was constant and maximum. This quantity was not directly measured, but absolute results were obtained from a small pyrex calibrating phial containing recrystallized $MnSO_4.4H_2O$, of which the susceptibility is known, suspended on a pyrex rod in the position occupied by the specimens. The small deflexion (~ 1 division) due to the empty phial was measured and allowed for. The susceptibility of the manganous sulphate was taken as $66\cdot1 \times 10^{-6}$ per unit mass at $16\cdot2°$ C.

The specimen carrier was the subject of considerable investigation. Several refractories, tungsten and molybdenum, were used, but always a certain amount of ferromagnetic contamination was detected after a high temperature run. Whilst this is partly due to solid diffusion between the specimen and the immediate parts of the carrier in contact, evaporation of the ferromagnetic is continually occurring. It seems impossible to eliminate this source of error entirely at high temperatures, but it was considerably reduced by designing the specimen and carrier so that the area of contact was as small as possible. However, a temperature run was always performed on the carrier only after a run and suitable correction (~ 2 divisions) made for its deflexion. The same carrier was never used more than once and they were always cleaned before use, and magnetically tested.

As was mentioned earlier, on account of the relatively high vapour pressures of iron, cobalt and nickel, considerable evaporation would be

experienced at high temperatures. For testing purposes hydrogen at various small pressures was used, but whilst the rate of evaporation was reduced, the thermal conductivity is so great that the efficiency of the furnace was considerably reduced. Accordingly argon, the thermal conductivity of which is one-tenth that of hydrogen, was employed. The optimum pressure was found to be at about 5 mm. of mercury and this was kept constant by pumping off and refilling when it increased due to degassing of the hot parts after exposure to prolonged high temperatures.

RESULTS

The results of these measurements are best expressed by means of the $1/\chi, T$ curves. In general the Curie-Weiss law is followed, but iron and nickel exhibit more than one magnetic state for which different values of C and θ are obtained. For some 50° immediately above the Curie point, all three ferromagnetics show curvature convex to the axis of temperature. The deduction of atomic moments is deferred until the theory is considered, so only the directly measured quantities C and θ will be given here.

(a) Nickel

The results for this metal are given in Table I and plotted in fig. 2. The paramagnetic Curie point obtained by extrapolation of the linear portion below 950° C. is 377° C. and the value of C is 0·322 per g. atom, in
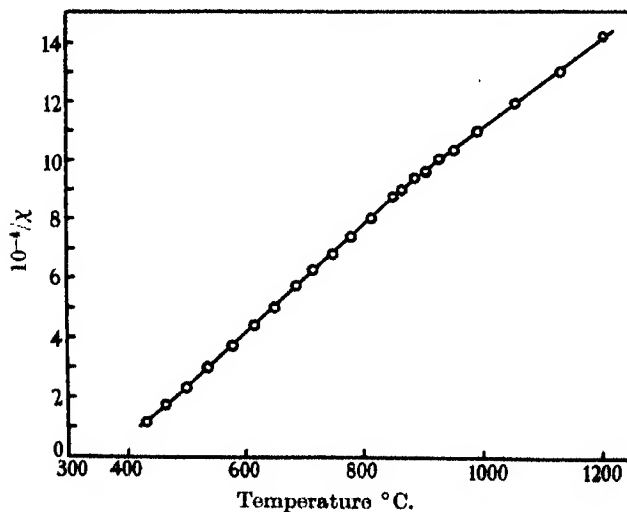

FIG. 2

agreement with the generally accepted value. Above 950° C. the slope decreases, giving $C = 0.402$ per g. atom. Although close observation at small temperature intervals was kept, the change of slope was not sudden as was observed by Bloch, although our value of C coincides with that for one of his samples. The nickel used was 99·98 % pure, obtained from the International Nickel Co.*

TABLE I. NICKEL

Temp. ° C.	$1/\chi \times 10^{-4}$	Temp. ° C.	$1/\chi \times 10^{-4}$	Temp. ° C.	$1/\chi \times 10^{-4}$
433	1·115	651	4·94	887	9·34
457	1·550	688	5·69	906	9·54
465	1·683	716	6·21	927	9·94
490	2·040	740	6·63	993	10·94
501	2·280	781	7·34	1055	11·83
537	2·980	815	7·97	1130	12·90
580	3·680	851	8·67	1201	14·10
616	4·360	865	8·95	—	—

(b) *Iron*

Table II and fig. 3D show the results on Hilger H.S. iron of 99·96 % purity. The curve consists of three linear portions separated discontinuously. Below 920° (the β-phase) and above 1390° C. (the δ-phase), iron is body-centred cubic as it is at ordinary temperatures and the intervening γ-phase is face-centred. The transformations are of the ordinary type, taking some hours for completion, and no close study of the magnetic changes accompanying them was attempted, especially the γ-δ change, as the prolonged heating necessary would have impaired the accuracy so as to make the curve

TABLE II. IRON

Temp. ° C.	$1/\chi \times 10^{-3}$	Temp. ° C.	$1/\chi \times 10^{-3}$	Temp. ° C.	$1/\chi \times 10^{-3}$
824	1·125	915	26·50	1164	36·73
838	1·650	936	33·35	1200	37·40
846	1·910	959	35·30	1238	37·78
860	2·430	962	33·55	1253	37·80
872	2·860	940	28·80	1315	38·30
875	3·030	928	24·44	1362	38·75
884	3·390	918	4·61	1385	37·20
894	3·680	1012	35·60	1395	26·10
904	3·970	1049	36·12	1415	27·30
909	4·260	1094	36·55	1480	29·70
—	—	—	—	1507	30·95

almost valueless. However, a large irreversibility is seen at the β-γ change extending over some 50°, the lower limit corresponding to increasing temperatures. This phenomenon had previously been studied by Terry. The C values obtained are 6·45 and 1·23 per g. atom for the γ- and δ-phases respectively.
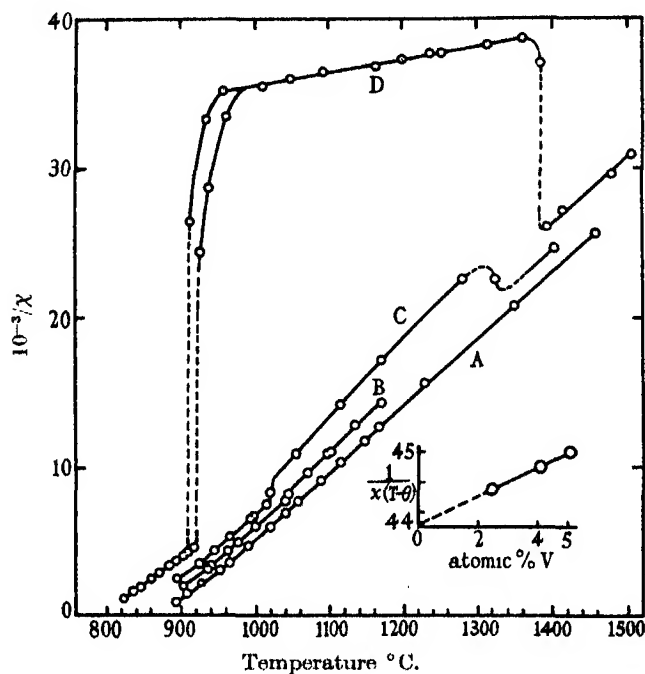

FIG. 3. A, 5 % vanadium-iron. B, 4·1 % vanadium-iron.
C, 2·3 % vanadium-iron. D, pure iron.

(c) *Iron-vanadium alloys*

The existence of the γ-phase in iron extending over some 470° limits the practical range for investigation to the short β-region. Obviously for accurate results a much longer linear range is required, so that elimination of the γ-phase becomes necessary. As is well known, this can be achieved by alloying iron with certain soluble non-magnetic metals. It is desirable to use as small percentages of the foreign metal as possible, and for this reason the iron-vanadium system was chosen. Three alloys with a maximum of 5 atomic % vanadium were made by diluting commercial ferro-vanadium (50 %) with Armco iron in a vacuum induction furnace. Chemical tests showed these to be free from cobalt and nickel. In fig. 3 the curves A, B and C, representing 5·0, 4·1 and 2·3 atomic % vanadium respectively, are staggered

on the temperature scale for clarity. It will be seen that 5 atomic % is sufficient to remove completely the γ-phase, leaving a linear graph from about 900° C. to the highest temperature. Alloys B and C both show the γ-phase but it extends over a smaller range, leaving longer linear portions than in iron from which more accurate slopes can be obtained. Table V below gives the values of C per gram so derived, and the extrapolated value for iron (i.e. zero % vanadium) is 1·27 per g. atom. The uncertainties of extrapolation were minimized, as fig. 3 (inset) shows, by using these very small quantities of foreign metal.

TABLE III. THE ALLOYS

A		B		C	
Temp. ° C.	$1/\chi \times 10^{-3}$	Temp. ° C.	$1/\chi \times 10^{-3}$	Temp. ° C.	$1/\chi \times 10^{-3}$
834	0·920	863	1·89	875	2·44
848	1·482	897	3·12	904	3·49
868	2·130	900	3·28	925	4·36
893	3·020	923	4·32$_5$	945	5·29
905	3·545	937	4·93	972	6·53
930	4·690	961	6·01	978	6·71
960	6·000	1000	7·75	995	7·49
980	6·950	1004	8·18	1000	8·29
997	7·720	1030	9·63	1035	10·85
1028	9·080	1057	10·85	1095	14·17
1055	10·320	1062	11·05	1150	17·17
1088	11·750	1095	12·81	1260	22·60
1107	12·700	1131	14·25	1304	22·60
1169	15·650			1383	24·70
1290	20·800				
1398	25·720				

Néel (1932) has performed similar experiments on the iron-tin and iron-silicon systems. The temperature range he employed was, however, smaller than ours, i.e. 80–160° C., but the extrapolated value of C (1·26) agrees. It is to be noted that the paramagnetic Curie points from curves A, B and C are identical at 828° C. Reverting to fig. 3D, it will be seen that the extrapolated $1/\chi$, T line for δ iron joins on to β iron at the discontinuity (contrary to the result of Weiss and Foëx), and as might be expected the value of the Curie constant so deduced is in good accord with that obtained from the alloys.

(d) *Cobalt.*

This metal is unique amongst the ferromagnetics in showing a marked dependence of susceptibility on previous heat treatment.

Fig. 4 shows a selection of the $1/\chi$, T curves obtained for 99·8 % pure electrolytic cobalt* subjected to different heat treatment, whilst Table IV gives an average set of results obtained after considerable annealing at temperatures up to 1440° C. Being parallel on their linear portions, the
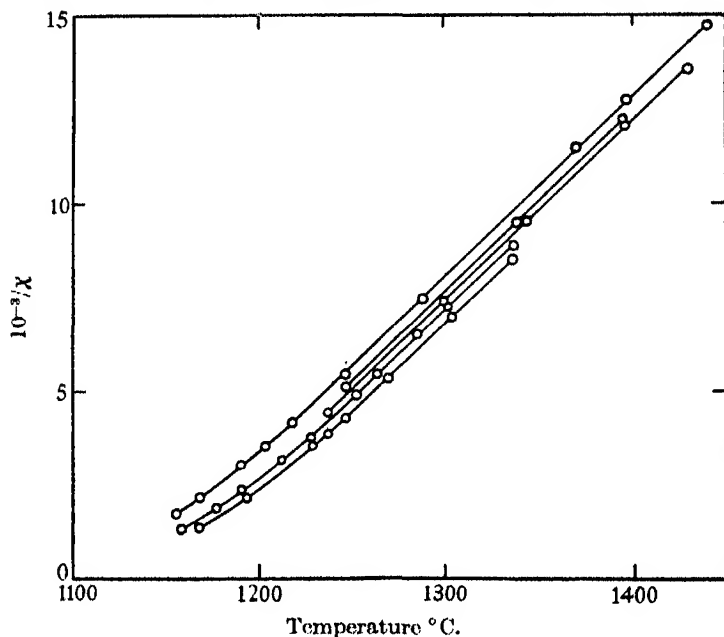

Fig. 4

TABLE IV. COBALT

Temp. ° C.	$1/\chi \times 10^{-3}$	Temp. ° C.	$1/\chi \times 10^{-3}$
1156	1·74	1247	5·49
1168	2·19	1288	7·46
1191	3·02	1370	11·50
1204	3·51	1397	12·75
1218	4·18	1440	14·75

curves all give the same value of the Curie constant, namely, 2·23 per g. atom, although the Curie point extends from about 1130 to about 1155° C. Near 400° C. cobalt suffers a transformation from a close-packed hexagonal lattice below to a face-centred lattice above this temperature. At ordinary temperatures the α cobalt is stable, but it appears that both forms may exist together in the metal (Mellor *1935*). At higher temperatures, trans-

* We are indebted to L'Union Minière du Haut-Katanga for a gift of the electrolytic cobalt.

formations have been reported, but there appears to be considerable divergence of opinion on the existence of any further phase change.

Density measurements of the various specimens showed the pronounced effect of heat treatment. On quenching from about 1200° C. the density decreased some 7 % whilst high temperature annealing caused a 3 % change, but it appeared that continued annealing tended to stabilize the susceptibility. It is known that the density of packing is the same for both crystal structures, so the large change in volume could not arise from a rearrangement of the lattice. Further, Hull (1922) reports that it is not possible to complete the change from hexagonal to cubic by annealing. In the absence of an explanation of this phenomenon the curves of fig. 4 must be regarded as representative of cobalt of different densities. The original electrolytic cobalt had the highest density (8·8). Each high temperature run, it must be remembered, is equivalent to annealing the specimen, although the precise conditions are not known, and often it was found that the plotted points began to follow a parallel curve always towards smaller susceptibility values. Only after prolonged annealing at about 1400° C. was it possible to obtain a stable and complete $1/\chi, T$ curve. These changes of density are of the same order as those given in Mellor, from which it will be seen that the magnetic constants of cobalt generally are uncertain. The phenomenon, however, does not invalidate the Curie constant which is quite definite, but the Curie point is rather variable.

TABLE V

	θ	$C = \chi(T - \theta)$	$p_{par} = \sqrt{3kC/N\mu^2}$
Nickel 500–850° C.	377° C.	0·00548	1·61
925–1200° C.	265° C.	0·00685	1·78
Cobalt 1230–1450° C.	1130–1155° C.	0·02080	3·15
Iron-Vanadium 5 %	828° C.	0·02220	3·16
4·1 %	828° C.	0·02240	3·17
2·5 %	828° C.	0·02250	3·18
(extrapolated) 0 %	——	0·02270	3·20
Iron from δ-phase	820° C.	0·02200	3·15

TABLE VI

Element	σ_0	$p = \sigma_0/N$	C_A
Ni	3,370	0·606	0·322
Co	9,500	1·710	1·228
Fe	12,230	2·220	1·265

The summarized results are shown in Table V, and Table VI includes other relevant data. The values of the saturation intensity per gram atom are given in the second column of Table VI, whilst the third gives the

intensity expressed in Bohr magnetons per atom. In the fourth column are the products $\chi M(T - \theta) = C_A$, where M is the atomic weight and C_A the Curie constant per gram atom deduced from the experimental data.

The general quantum theory of paramagnetism leads to the equation (Stoner 1934; Mott and Jones 1936)

$$\chi M(T - \theta) = C_A = \frac{j+1}{3j} \frac{N g^2 j^2 \mu^2}{k}, \tag{1}$$

where N is the number of elementary magnets per gram atom, g the Landé splitting factor, μ the Bohr magneton and k the Boltzmann constant.

Comparison of the above equation with the experimental results shows that the deduced values of C_A are higher than those predicted theoretically, assuming the spins to be uncoupled, whilst the curvature of the $1/\chi, T$ curves near the Curie point is not accounted for. Attempts have been made (Mott and Jones 1936) to explain the observed results in nickel by assuming that the metal contains a mixture of ions with different j values, electrons in ions with $j > \frac{1}{2}$ being coupled. Thus if A_j is the fraction of the lattice points occupied by ions with a given j value, equation (1) can be generalized to

$$p_{\text{par}}^2 = \frac{3kC}{N\mu^2} = \Sigma g^2 j(j+1) A_j, \tag{2}$$

where p_{par} is the paramagnetic magneton number. The summation extends over all the relevant j values.

The observed values of p_{par} are given in the last column of Table V. Experimental work on the gyromagnetic effect for the three ferromagnetics gives $g = 2$, whilst for normal ferromagnetics above the Curie point there is some evidence that a similar value obtains (Sucksmith 1935). For nickel

$$\frac{kC}{N\mu^2} = 0 \cdot 862 = \Sigma \frac{g^2 j(j+1) A_j}{3}.$$

We have from the ferromagnetic number for this element

$$g \, \Sigma j A_j = 0 \cdot 606,$$

and finally
$$\Sigma A_j = 1.$$

The possible states for the nickel atom deduced from spectroscopic data are $d^8 s^2$, $d^9 s^1$ and d^{10}, with 2, 1 or 0 positive holes respectively, giving j values for the ions 1, $\frac{1}{2}$ or 0. Solving the above equations, excluding negative values for A_j, the best solution is given by $A_0 = 0 \cdot 70$, $A_1 = 0$ and $A_2 = 0 \cdot 30$, giving $0 \cdot 81$ for $kC/N\mu^2$ instead of the experimental value $0 \cdot 87$.

For cobalt and iron analogous calculations lead to even less satisfactory conclusions.

In the case of atomic iron, the lowest levels are d^6s^2 and d^7s^1, corresponding to $j = 2$ or $1\frac{1}{2}$. Hence

$$\frac{kC}{N\mu^2} = 5A_3 + 8A_4 = 3\cdot40,$$

$$3A_3 + 4A_4 = 2\cdot2,$$

and

$$A_3 + A_4 = 1.$$

These equations do not, of course, admit of a solution. If we make the assumption that the level d^8 is possible, extending the calculation to include A_2, we get

$$A_2 = 0\cdot85, \quad A_3 = 0, \quad A_4 = 0\cdot15,$$

i.e. the largest proportion of atoms have two parallel spins and a small fraction four.

For cobalt the levels are analogous to those found in nickel, i.e. d^7s^2, d^8s^1 and d^9, i.e. $j = 1\frac{1}{2}$, 1 or $\frac{1}{2}$. The corresponding equations for this element are

$$A_1 + \tfrac{8}{3}A_2 + 5A_3 = 3\cdot40,$$

$$A_1 + 2A_2 + 3A_3 = 1\cdot71,$$

$$A_1 + A_2 + A_3 = 1.$$

Inspection shows that there is no solution even approximating to the above conditions.

It does not then appear possible to account for the ferromagnetic *and* paramagnetic magneton numbers by assuming that the metal is a mixture of ions, having the j values that the ions have in the lower states of the free atoms.

It may be that the difficulty of securing even an approximate explanation for the case of cobalt is in some way connected with its abnormal density variation or its hexagonal crystal structure. In connexion with the latter, the law of corresponding states, i.e. the variation of the ratio of the saturation intensity at a temperature T to that at absolute zero (σ/σ_0) with θ/T, has been investigated closely only for nickel. For cobalt and iron, no results of comparable accuracy are available. The theoretical shape of the curve depends upon the j value assumed for the ferromagnetic state, $j = \frac{1}{2}$ giving the best fit for nickel. It is necessary to establish whether or not the variation is of the same type for all three ferromagnetics. Experiments

on the saturation intensity of cobalt and iron at different temperatures up to the Curie point are at present in progress in these laboratories.

Our thanks are due to Professor N. F. Mott for discussion and advice on the theoretical aspects of the work, and also to the Colston Research Society of the University of Bristol for a grant towards the expenses of the investigation.

SUMMARY

A method is described for measuring magnetic susceptibilities in a controlled atmosphere or *in vacuo* at temperatures up to 1500° C. The special precautions required to prevent solid diffusion and minimize evaporation in measurements on metals are discussed. Accurate measurements on the susceptibilities of the ferromagnetic elements, hitherto confined to nickel, are extended to cobalt and iron. The magneton numbers for both these elements are deduced to an estimated accuracy of 1–2 % from the experimental data. It is shown that the existing theory is inadequate to explain the new results obtained.

REFERENCES

Bloch, O. 1912 *Arch. Sci. phys. nat.* **33**, 293–308.
Honda, K. and Takagi, H. 1913 *Sci. Rep. Tôhoku Univ.* **1**, 229–42.
Hull, A. W. 1922 *J. Franklin Inst.* **193**, 189–216.
Langevin, P. 1905 *Ann. Chim. (Phys.)*, **5**, 70–127.
Mellor, J. W. 1935 "A Treatise on Inorganic Chemistry," pp. 14, 459, 1st ed. London, New York, Toronto: Longmans Green and Co.
Mott, N. F. and Jones, H. 1936 "The Theory of the Properties of Metals and Alloys," 1st ed. Oxford: Clarendon Press.
Néel, L. 1932 *Ann. Phys., Lpz.*, **17**, 5–110.
Stoner, E. C. 1934 "Magnetism and Matter." London: Methuen.
Sucksmith, W. 1929 *Phil. Mag.* **8**, 158–65.
— 1935 *Helv. Phys. Acta*, **8**, 205–10.
Terry, E. M. 1917 *Phys. Rev.* **9**, 394–413.
Weiss, P. 1907 *J. Phys. Radium* (4), **6**, 661–90.
Weiss, P. and Foëx, G. 1911 *Arch. Sci. phys. nat.* **31**, 5–19, 89–117.

The hyperfine structure of the Zeeman components of the resonance lines of sodium

By D. A. Jackson and H. Kuhn

[Plate 10]

Introduction

The existence of a nuclear spin, which is responsible for the hyperfine structure of spectral lines, also causes the components of the Zeeman pattern to have a hyperfine structure of a similar width of splitting. In order to find the value I of the nuclear spin from the normal hyperfine structure, accurate measurements of intensity ratios or interval ratios are in general necessary. The magnetic hyperfine structure however yields the value of I in a more direct and certain way. In a sufficiently strong field, each Zeeman component consists of $2I + 1$ hyperfine structure lines of fairly uniform spacings and intensities. If it is possible to resolve this structure, the value of the nuclear spin can be established with absolute certainty from the number of lines.

. If the magnetic field is decreased, the relative position of the hyperfine structure lines changes, as a result of the change in the relative coupling between the field and the angular moments J and I of the electrons and of the nucleus. Quantum mechanics gives a complete quantitative description of this change of the pattern in intermediate fields.

In four instances only—Bi (Back and Goudsmit 1928; Zeeman, Back and Goudsmit 1930), Tl (Back and Wulff 1930), Cs (Kopfermann and Krüger 1936), and K (Jackson and Kuhn 1938)—has the hyperfine structure of the Zeeman effect been resolved, and only in the case of Tl ($I = \frac{1}{2}$) was a systematic study made of the variation of the pattern with varying field strength.

The main difficulties in observing magnetic hyperfine structures are the closeness of the lines and the great range of wave-lengths which has to be observed.

In the following experiments, the hyperfine structure in the Zeeman components of the two resonance lines of sodium has been investigated. By the method of absorption in an atomic beam, the Doppler width was reduced to one-tenth of the normal value. To overcome the second of the two difficulties just mentioned, two etalons in series were used.

[205]

In agreement with intensity measurements (Atta and Granath 1933) and magnetic deflexion experiments (Rabi and Cohen 1932), the value $I = \frac{3}{2}$ of the nuclear spin of Na was established. The position of the lines as given by quantum mechanical theory was compared with the measured values. The agreement was perfect up to the limit of experimental accuracy. On account of the very high resolving power used, the accuracy of the experimental test of the theory was very much greater than that in the case of thallium; also it was possible to test the theory over a greater range of field strengths.

Exposures without magnetic field, using a collimation of 1/20 of the atomic beam, showed the hyperfine structure due to the $3\,^2P_{\frac{1}{2}}$ term resolved.

LIGHT SOURCE, ATOMIC BEAM AND ELECTROMAGNET

The light source was a commercial sodium lamp. With a current of about 0·7 amp. the resonance lines were emitted with little self-reversal but considerable broadening, the width being about 0·2 cm.$^{-1}$.

The atomic beam producing the absorption was similar to that used by the authors in the investigations of the hyperfine structure in the spectrum of potassium (Jackson and Kuhn 1935, 1938). The collimation was 1/10 for the magnetic experiments, giving a half-value width of 0·006 cm.$^{-1}$. For resolving the $^2P_{\frac{1}{2}}$ structure without magnetic fields, a collimation of 1/20 of the atomic beam was used, giving a half-value width of 0·003 cm.$^{-1}$.

The magnet used was that described in the work on potassium; the field strengths were determined ballistically by comparison with a standard solenoid to an accuracy of about 0·5 %. On account of the relatively small field strength, there was no difficulty in obtaining a uniform field.

THE SPECTROGRAPH AND INTERFEROMETER

The spectrograph used was of 1·5 m. focal length, the prism being of very dense glass ($\mu_D = 1\cdot78$) with an angle of 65°. The prism was displaced 6° from the position of minimum deviation, the dispersion thus being increased to about twice the normal, the separation of the sodium D lines being 0·7 mm.

In order to obtain the necessary high resolving power (0·003 cm.$^{-1}$), together with the relatively great spectral range (0·2–0·25 cm.$^{-1}$), it was necessary to use two etalons in series. An arrangement similar to this has been used by Houston (1927) and by Gehrcke and Lau (1927). Two etalons are so arranged that the centres of their fringe systems exactly coincide, and

the ratio of their plate separations is made equal to a whole number. Now the scale of wave-lengths, measuring from the centre of the fringe system, is independent of the thickness of the etalon and depends only on the wave-length of the light and the focal length of the lens used. In the present work a 2 cm. etalon was used in conjunction with an 8 cm. etalon; under these conditions the fringes of the nth order of the 2 cm. etalon exactly overlap those of the $4n$th order of the 8 cm. etalon; while the fringes of order $4n+1$, $4n+2$ and $4n+3$ of the 8 cm. etalon are no longer visible, as these correspond to the orders $n+\frac{1}{4}$, $n+\frac{1}{2}$ and $n+\frac{3}{4}$ of the 2 cm. etalon. This is shown diagrammatically in fig. 4.

	n+2				n+1			n
2 cm. etalon								

8 cm. etalon   4n+8   4n+7   4n+6   4n+5   4n+4   4n+2   4n
              4n+3   4n+1
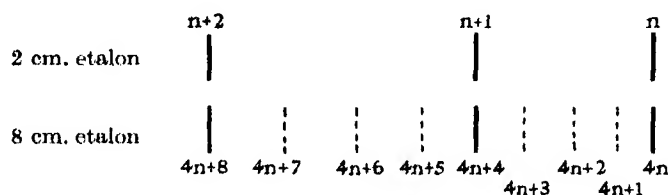
FIG. 4

This arrangement gives a spectral range of 0·25 cm.$^{-1}$, corresponding to that of a 2 cm. etalon, and a resolving power of about 0·003 cm.$^{-1}$, equal to that of the 8 cm. etalon. The plates of the 2 cm. etalon were silvered to about 20 % transmission, giving a sufficiently high resolving power to reduce the light of the orders $4n+1$ or $4n+3$ of the 8 cm. etalon to a small fraction of its value at the maximum; heavier silvering would have caused great loss of intensity, without any advantage. The 8 cm. etalon was silvered to about 5 % transmission, giving the necessary resolving power of 1/20 order (0·003 cm.$^{-1}$). The two etalons were placed between the collimator and the prism, that of smaller plate separation being nearer to the collimator.

In practice it is impossible to make the plate separation of the one etalon exactly four times greater than that of the other. However, this difficulty can be overcome if a small adjustment in the path difference of one etalon can be made so that the nth order of one exactly coincides with the $(4n+a)$th order of the other, where a is a whole number, small compared with n. The alteration in path necessary for this is between 0 and $\frac{1}{2}$ wave-length; this was achieved by Burger and van Cittert (1935) by heating one of the etalons; in this work it was achieved by adjusting the air pressure in the 8 cm. etalon.*

* Gehrcke and Lau obtained coincidence by tilting one etalon relative to the other, a method which can only be used when the fringes are observed at a point considerably removed from the centre, where the scale is nearly linear, but too small for the resolution of the very small differences of wave-lengths observed here.

Accordingly, both of the etalons were enclosed in airtight boxes; the box containing the etalon of 2 cm. plate separation being fitted with a mercury manometer, and the other with an oil manometer. The length of slit used was 15 mm., and the two etalons were adjusted so that the centre of the fringe system coincided with a cross-wire fitted to one end of the slit.

ADJUSTMENT OF THE DOUBLE ETALON

First the plates of both of the etalons were adjusted parallel in the usual manner, by means of the cadmium red ray. The angle of the 2 cm. etalon was then adjusted so that the centre of the fringe system coincided with the cross-wire on the slit. The angle of the 8 cm. etalon was then adjusted by observing the slit through the two etalons with a telescope; when the two etalons were not parallel, a multiple image of the slit was observed.

The pressure in the box containing the 2 cm. etalon was set so that the fringe nearest the centre of the system (in either the line 5896 or 5890, according to which was to be observed) was approximately in the centre of the image of the slit, this fringe then occupying the central 7 mm. of the image. The air pressure in the box containing the 8 cm. etalon was then adjusted for coincidence. The D lines of sodium were observed through the etalons and spectrograph, with the atomic beam of sodium at sufficient intensity to give a good absorption. It was seen that at two pressures separated by about 16 cm. of oil, instead of the normal doublet hyperfine structure, there were observed three components, while at a point midway between these the normal structure was observed. The pressure giving three apparent components corresponded to the two fringe systems being exactly out of phase, the nth order of the one etalon overlapping the $(4n + a + \frac{1}{2})$ order of the other. The "doubling" due to this resulted in three apparent lines instead of four, because the separation of the hyperfine structure doublet happens to be almost exactly equal to one order of the 8 cm. etalon, resulting in the overlapping of two of the four lines. The pressure midway between those required for doubling gave the condition for coincidence of the two fringe systems, and was determined to an accuracy of about 1/15 order of the 8 cm. etalon, or 1/60 order of the 2 cm. etalon.

OBSERVATIONS OF ZEEMAN EFFECT

The line 5890 was observed at eleven different field strengths varying between 1060 and 3060 gauss, and the line 5896 at nine different field strengths between 790 and 2090 gauss, three or four independent photo-

graphs being made at each field strength. In both series of observations the π components only were photographed, a Nicol prism being placed before the slit of the spectrograph. It was considered unnecessary to observe the σ components because the hyperfine structure of the Zeeman effect arises almost entirely from the level $3S_\frac{1}{2}$; the σ components would therefore possess almost the same structure as the π components, but the separation of the groups would be greater and thus require a greater spectral range.

The exposure needed was 1 min.; on each plate four (or five) exposures were made, one of the absorption without magnetic field and three (or four) of the absorption at different magnetic fields. Three such plates were made at short intervals. The positions of the simple hyperfine structure lines were measured in all three plates; the variation was never greater than 0·0005 cm.$^{-1}$; this was a reliable test of the constancy of the thickness of the etalon during the course of a series of exposures. The temperature of the sodium was 250 and 285° C. without and with magnetic field for the line 5890; and 270 and 305° C. for the line 5896.

The plates were measured by finding the distance of the observed lines from the cross-wire on the slit. For the calculation of the wave-lengths the distances from the centre of the fringe system are needed. The coincidence of the centre with the cross-wire was, however, not accurate enough to be relied on. Therefore the exact position of the centre was found from measurements of the same line in several orders and the value of the scale constant $F^2 \times \lambda$, calculated from the focal length F and the wave-length λ. It was found that the probable error of this determination of the centre gives rise to errors of not more than about 0·0002 cm.$^{-1}$.

The centre of gravity of the hyperfine structure doublet was determined from the measurements of the photographs of the absorption without magnetic field, and the wave numbers of the measured Zeeman components were calculated as displacements from this.

RESULTS

Enlargements and photometer tracings of some of the plates are shown in figs. 1 and 2, Plate 10. They are so arranged that the centres of gravity of the patterns are on a vertical line, marked c.g. The last photograph shows the line without field. It appears as a doublet, the splitting being mainly due to the $3S_\frac{1}{2}$ term. The finer structure due to the splitting of the $^2P_{\frac{1}{2},\frac{3}{2}}$ terms is not resolved here (see last paragraph).

In the stronger fields, two groups of lines are visible, each group repre-

senting one π component of the anomalous Zeeman effect. The fact that each group consists of four lines proves that $2I + 1 = 4$, or $I = \frac{3}{2}$.

The complete structure could easily be observed visually. With decreasing field strength at first the distance between the two groups decreases, but at lower fields also the distances within each group change. Most conspicuous is the displacement of the line most to the left of the right group away from this group, while the remaining three lines approach each other.

The results of the measurements are given in ordinary type in Tables I and II. Each figure is the mean of three or four independent determinations; the average departure from the mean was 0.001 cm.$^{-1}$. Below 790 gauss the lines were too indistinct to be measured with certainty. This is partly due to their closeness, but mainly to the appearance of new lines at very low fields, as a result of the breakdown of the transition rules for m_I and m_J.

TABLE I. OBSERVED AND CALCULATED
π COMPONENTS OF $\lambda\,5890$, $3S_{\frac{1}{2}}$–$3\,{}^2P_{\frac{1}{2}}$

Field	Displacements of components from centre of gravity of normal h.f.s. doublet, in cm.$^{-1}$							
1060	-0.038	-0.028	-0.016	-0.003		0.019	0.033	0.045
	-0.038	-0.029	-0.018	-0.005	-0.003	0.018	0.032	0.043
1200	-0.041	-0.029	-0.017	-0.002		0.020	0.035	0.047
	-0.040	-0.030	-0.019	-0.005	-0.002	0.019	0.033	0.045
1330	-0.042	-0.029	-0.018	-0.004	0.002	0.020	0.036	0.048
	-0.042	-0.032	-0.020	-0.006	0.000	0.021	0.035	0.047
1450	-0.044	-0.033	-0.018	-0.006	0.003	0.022	0.038	0.050
	-0.044	-0.034	-0.022	-0.007	0.001	0.022	0.036	0.048
1570	-0.046	-0.035	-0.022	-0.009	0.004	0.023	0.038	0.051
	-0.046	-0.036	-0.023	-0.009	0.003	0.023	0.038	0.050
1840	-0.051	-0.038	-0.025	-0.011	0.007	0.026	0.041	0.054
	-0.050	-0.039	-0.027	-0.012	0.007	0.026	0.041	0.054
2090	-0.054	-0.043	-0.030	-0.015	0.011	0.030	0.045	0.058
	-0.054	-0.043	-0.030	-0.015	0.011	0.029	0.045	0.057
2320	-0.059	-0.046	-0.033	-0.018	0.015	0.032	0.048	0.061
	-0.058	-0.046	-0.033	-0.018	0.015	0.033	0.048	0.061
2560	-0.061	-0.050	-0.037	-0.022	0.019	0.037	0.052	0.065
	-0.062	-0.050	-0.037	-0.022	0.018	0.036	0.051	0.064
2800	-0.065	-0.053	-0.040	-0.024	0.023	0.040	0.056	0.070
	-0.066	-0.054	-0.040	-0.025	0.022	0.040	0.055	0.068
3060	-0.069	-0.057	-0.044	-0.029	0.028	0.045	0.060	0.074
	-0.070	-0.057	-0.044	-0.030	0.026	0.044	0.060	0.072

Fig. 1.　$3S_{\frac{1}{2}}$–$3^2P_{\frac{1}{2}}$, 5890 A.
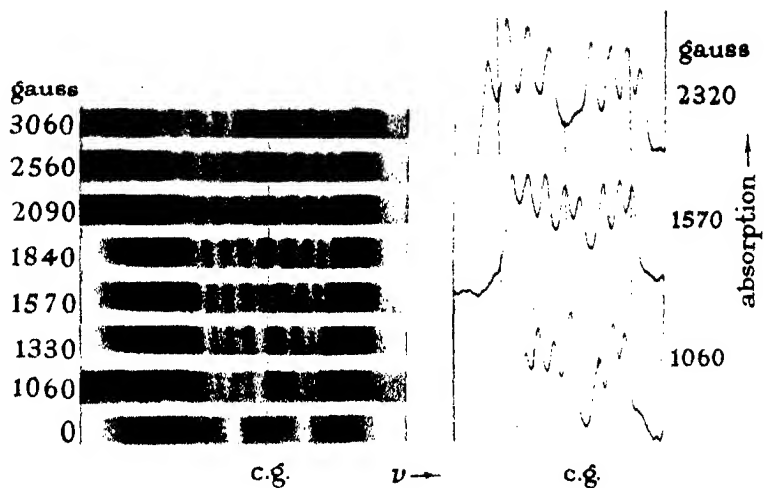
Fig. 2.　$3S_{\frac{1}{2}}$–$3^2P_{\frac{1}{2}}$, 5896 A.
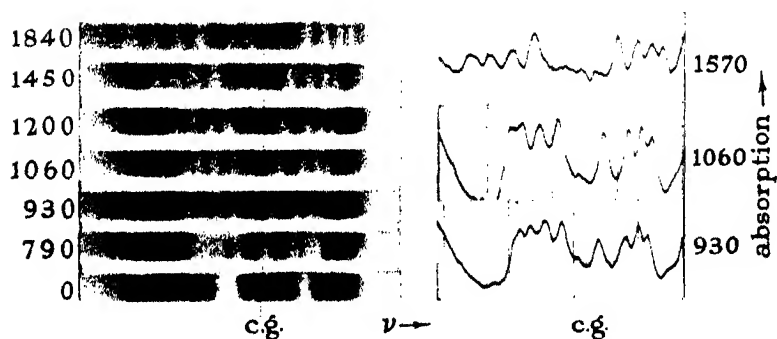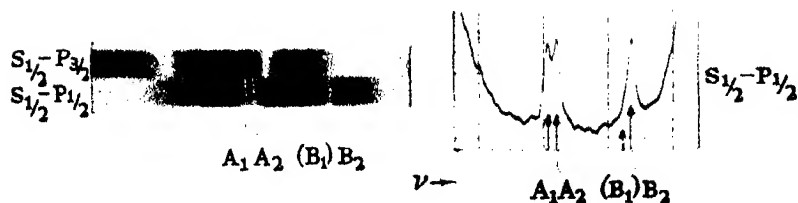
Fig. 3

Figs. 1 and 2.　Atomic beam of collimation 1 : 10.
Fig. 3.　　　　Atomic beam of collimation 1 : 20.

NOTE.　*The left edge of the photographs is very near the centre of the fringe system; the scale therefore increases rapidly towards this edge*

TABLE II. OBSERVED AND CALCULATED
π COMPONENTS OF $\lambda 5896$, $3S_{\frac{1}{2}}-3\,^2P_{\frac{1}{2}}$

Field	Displacements of components from centre of gravity of normal h.f.s. doublet, in cm.$^{-1}$							
790	−0·045	−0·038	−0·029	−0·016	0·005	0·029	0·043	0·051
	−0·045	−0·038	−0·029	−0·017	0·005	0·030	0·042	0·051
930	−0·049	−0·041	−0·031	−0·018	0·011	0·032	0·046	0·057
	−0·049	−0·041	−0·032	−0·019	0·009	0·032	0·045	0·055
1060	−0·053	−0·045	−0·034	−0·021	0·015	0·035	0·049	0·059
	−0·053	−0·045	−0·035	−0·022	0·014	0·035	0·048	0·058
1200	−0·058	−0·049	−0·038	−0·026	0·017	0·038	0·052	0·062
	−0·058	−0·049	−0·039	−0·025	0·018	0·038	0·052	0·062
1330	−0·062	−0·052	−0·041	−0·028	0·022	0·041	0·054	0·066
	−0·062	−0·052	−0·042	−0·029	0·022	0·042	0·055	0·066
1450	−0·066	−0·056	−0·045	−0·032	0·025	0·044	0·058	0·069
	−0·065	−0·056	−0·045	−0·032	0·026	0·045	0·058	0·069
1570	−0·071	−0·060	−0·049	−0·035	0·029	0·047	0·061	0·073
	−0·069	−0·060	−0·049	−0·035	0·029	0·048	0·062	0·073
1840	−0·079	−0·068	−0·057	−0·043	0·038	0·055	0·069	0·081
	−0·078	−0·068	−0·056	−0·042	0·038	0·056	0·069	0·081
2090	−0·086	−0·076	−0·064	−0·051	0·045	0·062	0·076	0·088
	−0·085	−0·075	−0·063	−0·050	0·046	0·063	0·077	0·088

Comparison with theory

The complete quantum mechanical theory of the anomalous Zeeman effect for fields of any strength has been given by Heisenberg and Jordan (1926) and by Darwin (1927). It has been applied to the hyperfine structure of the Zeeman effect by Goudsmit and Bacher (1930).

Fig. 5 gives the term diagram of the Zeeman effect of the line $3S_{\frac{1}{2}}-3\,^2P_{\frac{1}{2}}$ of sodium. The very narrow hyperfine structure of the term $3\,^2P_{\frac{1}{2}}$ is omitted, and the π components only are shown. In the left part of the diagram the calculated transition into the terms in a weak field is plotted.

The following expression gives the distances of the eight π components from the centre of gravity of the pattern.

$$\Delta\nu = \frac{\Delta S_{\frac{1}{2}}}{2(2I+1)} - \frac{\Delta S_{\frac{1}{2}}}{2}\sqrt{\left(1+\frac{4m}{2I+1}x+x^2\right)} \pm \tfrac{1}{2}g(J)\frac{\mu_0 H}{h} \pm m_I m_J \times \frac{\Delta^2 P_{\frac{1}{2},\frac{1}{2}}}{2J(I+\frac{1}{2})},$$

where $x = \dfrac{\mu_0 g(J) H}{h\Delta S_{\frac{1}{2}}}$, μ_0 being the Bohr magneton, $g(J)$ the Landé g-value of the term. $\Delta S_{\frac{1}{2}}$, $\Delta^2 P_{\frac{1}{2}}$ and $\Delta^2 P_{\frac{1}{2}}$ are the widths of the ordinary hyperfine

structure splittings of the corresponding levels. The first two terms of the right side of the equation represent the structure of the level $3S_{\frac{1}{2}}$, the last two terms that of the levels $3\,{}^2P_{\frac{1}{2},\frac{3}{2}}$.

Seven of the eight lines are found by putting $m = 2, 1, 0$ and -1 and using the positive value of the root, and $1, 0$ and -1 with the negative value of the root. The eighth line is given by $m = -2$, the value of the root being made
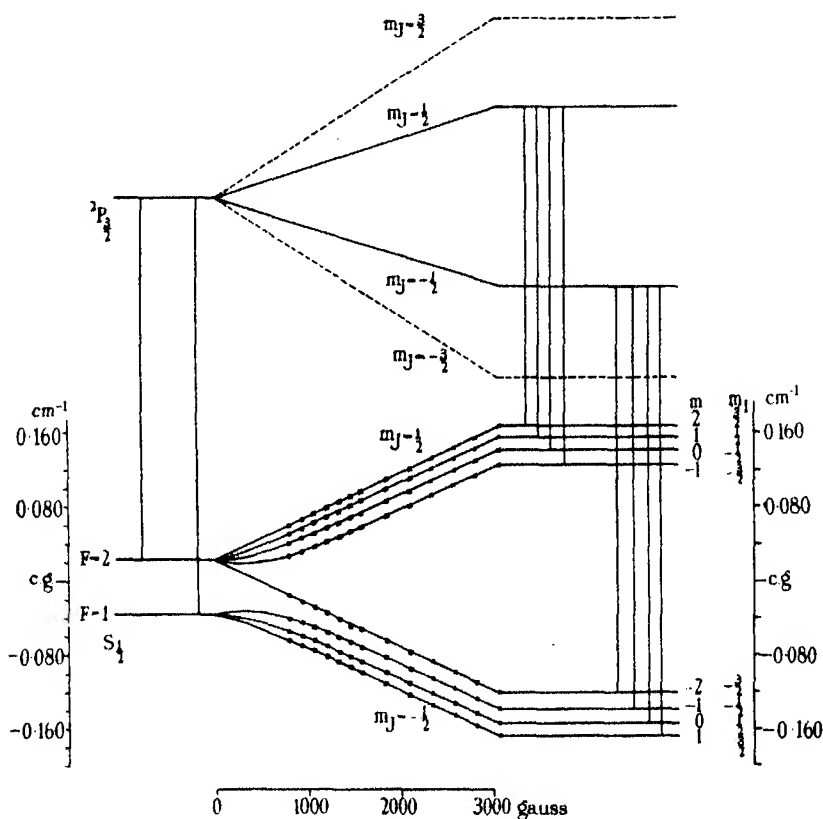

FIG. 5

equal to $1 - x$. For great values of x (strong fields) this is negative and makes the corresponding spectral line join the group with positive values of $\Delta\nu$; for $x < 1$, however, it joins the other group, forming a set of five lines which pass into the stronger of the two hyperfine structure lines without magnetic field.

The simple form of the last two terms of the equations is made possible by the smallness of the $^2P_{\frac{1}{2},\frac{3}{2}}$ structures compared with the Lorentz splitting.

It is an expression of the "Paschen-Back effect" of the hyperfine structure of the $^2P_{\frac{1}{2},\frac{3}{2}}$ terms, causing a pattern of equidistant fine structure terms superimposed on the ordinary anomalous Zeeman shift of the term, the distance between each two terms being $\Delta^2P_{\frac{1}{2},\frac{3}{2}} \times \dfrac{m_J}{2J(J+\frac{1}{2})}$. It does not depend on the field strength. This fine structure of the $^2P_{\frac{1}{2},\frac{3}{2}}$ terms as expressed in the last term of the equations is a small correction only, for the $3\,^2P_{\frac{1}{2}}$ term it is within the limits of error of the experiment.

Using the experimental values

$$\Delta S_{\frac{1}{2}} = 0.0592, \quad \Delta^2P_{\frac{3}{2}} = 0.0064 \text{ and } \Delta^2P_{\frac{1}{2}} = 0.004 \text{ cm.}^{-1}$$

(see last paragraph), the above formula gives for the line $3S_{\frac{1}{2}}-3\,^2P_{\frac{3}{2}}$

$$\Delta \nu = 0.0074 - 0.0297 \sqrt{(1+mx+x^2)}$$
$$\pm \tfrac{2}{3} \times 4.7 \times 10^{-5}H \pm m_I m_J \times 0.001 \text{ cm.}^{-1},$$

and for the line $3S_{\frac{1}{2}}-3\,^2P_{\frac{1}{2}}$

$$\Delta \nu = 0.0074 - 0.0297 \sqrt{(1+mx+x^2)}$$
$$\pm \tfrac{1}{3} \times 4.7 \times 10^{-5}H \pm m_I m_J \times 0.003 \text{ cm.}^{-1}.$$

These formula give the results printed in italics in Tables I and II.

In figs. 6 and 7 the curves give the calculated positions of the spectral lines and the crosses or circles the experimental values. The agreement is well within the experimental errors. In particular the displacement of the line mentioned before (arising from the level $m = -2$) shows directly the change in arrangement of the levels with changing field.

In fig. 5 the term values derived from direct observations of the lines $3S_{\frac{1}{2}}-3\,^2P_{\frac{3}{2}}$ and $3S_{\frac{1}{2}}-3\,^2P_{\frac{1}{2}}$ are marked by crosses and circles respectively. They are obtained from the measured frequencies by subtracting the last two terms of the equation.

For the strongest fields used, the Paschen-Back effect of the hyperfine structure is very nearly complete even for the $3S_{\frac{1}{2}}$ term, the distances between the four lines of each group and also their intensities being almost equal.

The hyperfine structure of the $3\,^2P_{\frac{1}{2}}$ term

In order to determine accurately the values $\Delta S_{\frac{1}{2}}$ and $\Delta P_{\frac{1}{2},\frac{3}{2}}$ used above, it seemed desirable to resolve the structure of the line $3S_{\frac{1}{2}}-3\,^2P_{\frac{1}{2}}$ completely. This line was therefore investigated without magnetic field, by means of an atomic beam of collimation 1/20 and the same set of etalons. The enlargement and photometer tracing in fig. 3, Plate 10 show the long wave-length
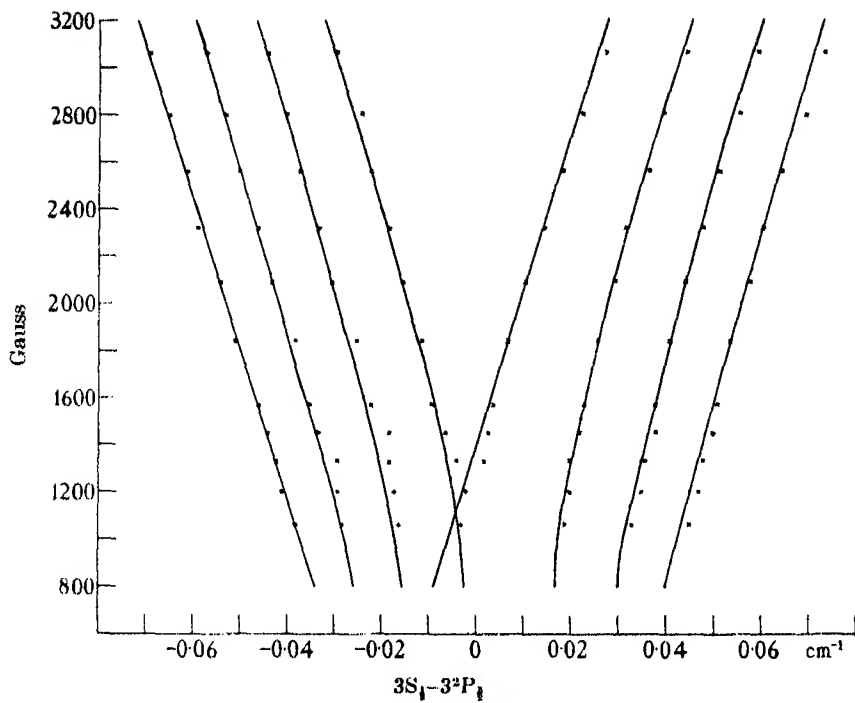
$3S_{\frac{1}{2}}-3^2P_{\frac{1}{2}}$
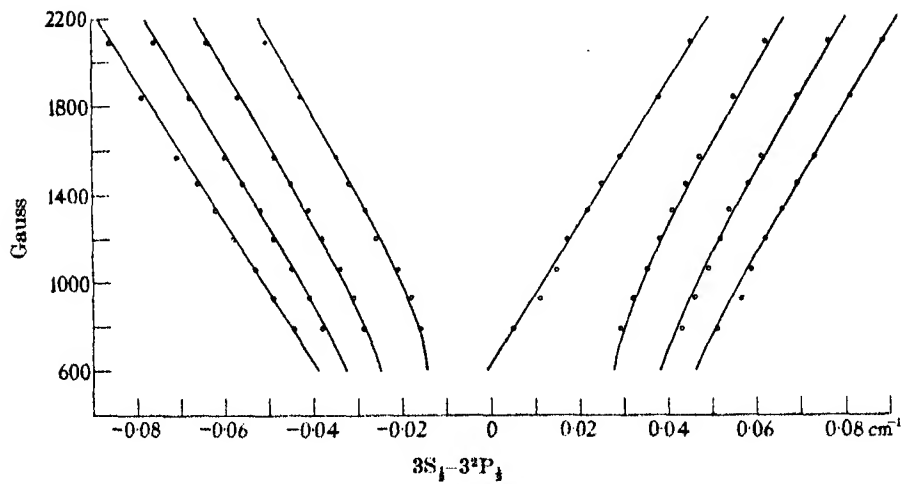
Fig. 6

$3S_{\frac{1}{2}}-3^2P_{\frac{3}{2}}$

Fig. 7

component of the doublet resolved into two lines A_1 and A_2, and a very weak line B_1 (hardly visible in the reproduction) appears close to the short wave-length component B_2. The results of the measurements of the lines are

A_1	A_2	B_1	B_2
0·0000	0·0064	—	0·0656 ± 0·0003 cm.$^{-1}$

The position of the component B_1 was not measured on account of its weakness; the separation between B_1 and B_2 must be equal to that between A_1 and A_2.

From the measurements it follows directly that the doublet splitting of the term $3\,^2P_{\frac{1}{2}}$ is equal to $0·0064 \pm 0·0003$ cm.$^{-1}$, and that of the term $3S_{\frac{1}{2}}$ is $0·0592 \pm 0·0003$ cm.$^{-1}$.

The separation of the hyperfine structure doublet of the line $3S_{\frac{1}{2}}$–$3\,^2P_{\frac{3}{2}}$, 5890, was also measured and found to be $0·0575 + 0·0003$ cm.$^{-1}$. This gives, when allowance is made for the unresolved $^2P_{\frac{3}{2}}$ structure, the value $0·0596 \pm 0·0003$ cm.$^{-1}$.

Previous measurements by the authors, where the $3\,^2P_{\frac{1}{2}}$ structure was not resolved, gave the values 0·059 and 0·007 cm.$^{-1}$ for the $3S_{\frac{1}{2}}$ and $3\,^2P_{\frac{1}{2}}$ splittings, in very good agreement with the new measurements. The value of the splitting of the $3S_{\frac{1}{2}}$ term from magnetic deflexion experiments is $0·0596 \pm 0·0006$, while Meissner and Luft (1937), using an excited atomic beam, found the value $0·0594 \pm 0·0003$ cm.$^{-1}$ and for the term $3\,^2P_{\frac{1}{2}}$, $0·0058 \pm 0·0003$ cm.$^{-1}$.

The authors take this opportunity of thanking Professor Plaskett for placing at their disposal his excellent photometer, and Professor Lindemann for his continued interest in the research; and also Queen's College and St John's College, Oxford for the stipends granted to one of them.

SUMMARY

The hyperfine structure of the Zeeman π components of the two resonance lines of sodium was observed by means of the absorption in an atomic beam, the high resolving power instrument being a double etalon with separations of 2 and 8 cm. In strong fields, each Zeeman component was found to possess four hyperfine structure components, proving with certainty that the nuclear spin of sodium is $\frac{3}{2}$.

The alteration in the spacings of the lines as the field strength was changed from 3060 to 790 gauss was found to be in excellent agreement with that predicted by quantum mechanics.

A direct determination of the hyperfine structures of the terms $3S_{\frac{1}{2}}$ and $3\,^2P_{\frac{1}{2}}$ was made from the complete resolution of the line 5896.

REFERENCES

Van Atta, G. M. and Granath, L. P. 1933 *Phys. Rev.* **44**, 60–1.
Back, E. and Goudsmit, S. 1928 *Z. Phys.* **47**, 174–83.
Back, E. and Wulff, J. 1930 *Z. Phys.* **66**, 31–48.
Burger, H. C. and van Cittert, P. H. 1935 *Physica*, **2**, 87–96.
Darwin, C. G. 1927 *Proc. Roy. Soc.* A, **115**, 1–19.
Gehrcke, E. and Lau, E. 1927 *Z. techn. Phys.* **8**, 157.
Goudsmit, S. and Bacher, R. F. 1930 *Z. Phys.* **66**, 13–30.
Heisenberg, W. and Jordan, P. 1926 *Z. Phys.* **37**, 263–77.
Houston, W. V. 1927 *Phys. Rev.* **29**, 475–484.
Jackson, D. A. and Kuhn, H. 1938 *Proc. Roy. Soc.* A, **165**, 303–312.
Kopfermann, H. and Krüger, H. 1936 *Z. Phys.* **102**, 527–33.
Meissner, K. W. and Luft, K. F. 1937 *Ann. Phys.*, *Lpz.*, **28**, 667–72.
Rabi, I. I. and Cohen, V. W. 1932 *Phys. Rev.* **43**, 582–3.
Zeeman, P., Back, E. and Goudsmit, S. 1930 *Z. Phys.* **66**, 1–12.

The absorption spectra of the halogen acids in the vacuum ultra-violet

By W. C. Price

The Physical Chemistry Laboratory, Cambridge

[Plate 11]

Although the halogen acids have long been known to possess regions of continuous absorption, no discrete electronic spectra have previously been reported for the neutral molecules. Their emission spectra occurring between 2800 and 4000 A really belong to the molecular ions. In the work to be described here, new absorption spectra of the halogen acids, which consist of very intense systems of relatively discrete bands, have been discovered in the Schumann region. The spectra are essentially in the nature of strong resonance bands and are very similar in this respect to corresponding bands of the alkyl halides (Price 1936). Extensive absorption systems of I_2, Br_2 and Cl_2 have also been found in the same region. These

will be described in a later publication. The continuous background against which the bands were observed was provided by the Lyman continuum. Other experimental details have been reported previously (Collins and Price 1934).

The absorption spectrum of hydrogen iodide is shown in fig. 1 *a* (Plate 11). This particular photograph corresponds to a pressure of about 0·01 mm. in a path length of 50 cm. The most striking feature of the spectrum is the presence of a large number of bands with strong sharp *Q* branches accompanied on either side by weaker *P* and *R* branches (fig. 1 *a*, *b*, *c*), the rotational structures of which are only slightly degraded. This indicates that a relatively non-bonding electron is being excited, a fact which is also substantiated by the absence of any pronounced vibrational progressions. For example, the first strong band at 1762 A is unaccompanied by any vibrational bands, there being a transparent region more than 5000 cm.$^{-1}$ wide to the short wave-length side of it. Though the rotational structures of the *P* and *R* branches of this band are diffuse, the sharp nature of the *Q* branch is easily discernible (see fig. 1 *a*, *c*). The spectra of HBr and HCl each begin with a very similar band occurring at 1491 A for HBr (fig. 1 *d*) and at 1331 A for HCl (fig. 1 *e*). It will be shown that these bands are related to one another and are analogous to the *B* bands of the alkyl halides. The next strong bands on the short wave-length side of them can further be linked with the *C* bands of the alkyl halides. Because of certain peculiarities which the above bands of the halogen acids (fig. 1 *c*, *d*, *e*) exhibit, they will be discussed together in a later paragraph.

In going to shorter wave-lengths, the general tendency of the bands is to diminish in intensity and to crowd more closely together in the manner characteristic of bands approaching an ionization potential. In fact, below 1200 A a well-developed "Rydberg head" of bands can be observed. This consists of successive groups of rather diffuse bands converging to a limit around 1122 A. The contours of successive bands resemble one another, and the intensities of the bands diminish regularly in the manner expected for the electronic bands of a Rydberg series. The strongest peaks of the contours conform quite well to the following Rydberg formula:

$$\nu = 89{,}130 - R/(n + 0{\cdot}70)^2 \quad n = 2,\ 3,\ 4,\ \text{etc.} \quad \text{(i)}$$

About eleven members of this series were found, and their observed and calculated frequencies are given in Table I. Subsidiary peaks in the contours can be represented by changing the Rydberg denominator in (i) to $(n + 0{\cdot}93)^2$ (ii), and $(n + 1{\cdot}25)^2$ (iii).

TABLE I. OBSERVED AND CALCULATED FREQUENCIES FOR SERIES (1)
OF HYDROGEN IODIDE

n	$\lambda_{obs.}$	$\nu_{obs.}$	$\nu_{calc.}$	$\nu_{obs.-calc.}$
2	1346·1	74,290	74,067	213
3	1232·8	81,115	81,114	1
4	1187·6	84,200	84,162	38
5	1165·8	85,770	85,752	18
6	1153·4	86,700	86,685	15
7	1145·6	87,285	87,269	16
8	1140·3	87,700	87,680	20
9	1136·9	87,960	87,964	− 4
10	1134·2	88,170	88,172	− 2
11	1132·2	88,325	88,328	− 3
12	1130·5	88,454	88,450	+ 4
13	1129·4	88,540	88,545	− 5

The convergence limit of the Rydberg series is equivalent to an ionization potential of 10·990 V, the maximum error in its determination being about ± 0·005 V. The state of the molecular ion to which it belongs is undoubtedly $(p\sigma)^2 (p\pi)^3$, $^2II_{\frac{1}{2}}$. That the non-bonding $p\pi$ electron is the one which has been removed is indicated by the absence of vibrational structure among the bands which converge to this limit. The correspondence of the limit to the upper and not the lower component of ^2II of HI$^+$ is revealed by the fact that in the region from 0·60 V below the limit to 0·60 V above the limit no bands are found which cannot be fitted into Rydberg series converging to 10·99 V. Now the spectroscopically determined doublet separations of the ^2II states of HCl$^+$ and HBr$^+$ (Kulp 1931; Norling 1935) are approximately equal to the spin-orbit coupling coefficients of the respective halogen atoms, a result which is to be expected theoretically (Mulliken 1932). In fact, the actual separations exceed the theoretical values by 10 % for HCl$^+$ (643 : 588) and by 8 % for HBr$^+$ (2653 : 2448). Thus the doublet width in HI$^+$ might be expected to be about 5 % greater than the value of the spin-orbit coupling coefficient of I(I) (5066 cm.$^{-1}$) and therefore about 5320 cm.$^{-1}$ or 0·66 V. The lower ionization potential should thus be 10·99−0·66 = 10·33 V, and a convergence limit of Rydberg series ought to occur around 1200 A. The overlapping of stronger bands going to the upper limit and the presence of a number of emission lines superimposed on the continuum, together with the intrinsic weakness of these particular series, prevents the lower limit from being apparent in the spectrum. A further difficulty might possibly be the mutual perturbation of the two overlapping sets of Rydberg series (White 1934). Although two plausible series were found to converge to 83,560 cm.$^{-1}$ (10·31 V), they could

not, because of the above difficulties, be established in a really satisfactory way. It is quite sure, however, that the lower ionization potential does not differ from the suggested value of 10·33 V by more than a few hundredths of a volt. This is indicated by the following considerations. The strong bands at 1762·1 and 1604·7 A almost certainly correspond to configurations $(^2\Pi_{1\frac{1}{2}})nx$ and $(^2\Pi_{\frac{1}{2}})nx$ and are analogous to the B and C bands of the alkyl halides.* Now the separation of the B and C bands of methyl iodide is 0·61 V, a value which is very close to the doublet separation in the molecular ion, 0·625 V (Price 1936). The corresponding bands in hydrogen iodide are separated by 5570 cm.$^{-1}$ (0·69 V), and this should therefore correspond fairly closely to the doublet separation of HI$^+$, thus indicating a value of 10·3 V for the minimum ionization potential. Further support for the existence of this ionization potential comes from the diffuseness of the bands below 1200 A (10·3 V). This is most probably due to auto-ionization and is to be expected for all bands lying above the minimum ionization potential. A determination of the doublet separation of $^2\Pi$ of HI$^+$ from emission data is most desirable in order to obtain this ionization potential exactly.

The values of the ionization potentials predicted theoretically by Mulliken are 10·85 and 11·47 V. Those obtained here, namely, 10·3 and 10·99 V, are in good agreement with the predicted values. It should be mentioned that the lack of complete data on the iodine atom gives rise to an uncertainty of a few tenths of a volt in the predicted potentials. The small discrepancies of the observed values from those predicted are to be attributed partly to the charge transfer effect resulting from the dipole (0·38D) associated with the molecule and partly due to a departure from ideal non-bonding conditions. The electron impact values for the ionization potential of hydrogen iodide are $\sim$ 12·8 V (Knipping 1921; Mackay 1924). This is considerably too high and is incompatible both with the spectroscopic data and the theoretical expectations.

Although a large number of the bands of hydrogen iodide are diffuse, many are sharp and show fairly well-resolved rotational structure. The photo-micrographs given in fig. 1 b are typical examples of these latter bands. It is obvious from the sharpness of the Q branches and the lack of very pro-nounced shading, that the moments of inertia in the various excited states differ little from that of the ground state. The structure of the 1449 and the 1442 A bands is particularly simple. Assuming the value of 6·555 cm.$^{-1}$ for the B_e of hydrogen iodide in the ground state (A. H. and H. H. Nielsen 1935), the value in the upper state works out to be between 6·2 and

* Term value considerations given later establish this definitely.

6·4 cm.⁻¹. The dispersion is not great enough to permit a more exact analysis to be made. This might be done on a 21 ft. vacuum spectrograph using a fluorite cell. Of all the bands present in the spectrum only one or two bands appear to be vibrational bands accompanying the main electronic transitions. This is a further indication of the non-bonding character of the excited electron, since it means that the potential energy curve of the excited state of the molecule resembles so closely that of the ground state *that the vibrational wave functions of both states are nearly orthogonal. Thus the probability of any transition involving change of vibrational quantum number is almost zero and the bands all correspond to vibration-less electronic transitions.* This is particularly true of the first strong band *at 1762 A. The second strong band at 1605 A apparently has a diffuse vibrational band roughly 1970 cm.⁻¹ on its high-frequency side.*

The absorption spectra of HBr and HCl

The first strong resonance bands of HBr and HCl are shifted by increasing amounts to shorter wave-lengths relative to those of HI. This indicates successively greater ionization potentials, as might also be expected from the well-known increase in ionization potential in going to the lighter halogen atoms. The very short wave-length bands analogous to the bands forming the Rydberg series in HI are rather weak in the spectra of HBr and HCl, and not enough bands of this type could be obtained with sufficient distinctness and certainty to enable Rydberg series to be established. Thus spectroscopic values of the ionization potentials of these molecules could not be derived directly. In what follows we shall be concerned with the longest wave-length bands and in correlating them with certain bands in the spectra of the methyl halides. This enables approximate term values of the bands to be deduced. From these the ionization potentials of the molecules may be inferred.

Because of the analogous character of the longest wave-length sets of bands in HI, HBr and HCl they are shown together in fig. 1 *c, d, e*. The first band in each set is strikingly similar. It consists of a remarkably sharp *Q* branch not in any case wider than 10–15 cm.⁻¹, with diffuse rotational structure on either side.* No vibrational band is found to accompany this main electronic band in either the iodide, the bromide or the chloride.

---

* In the case of HBr and HCl part of this structure is resolvable. Four lines in the *P* branch of HBr showed an average spacing of about 20 cm.⁻¹. Five similar lines in HCl had a mean spacing of 25 cm.⁻¹.

(The weak satellites which accompany all the bands of HCl lying a few Ångströms towards the shorter wave-lengths will be disregarded for the moment.) The second bands appearing at 1605 A for HI, at 1417·5 A for HBr and at 1390 A for HCl, differ considerably from the first bands. Their structure, though somewhat diffuse (except in the case of HCl), is shaded towards the red, thus indicating an appreciable change in the dimensions of the molecule as a result of the excitation. This is also in harmony with the fact that vibrational bands now appear accompanying the main band. These increase in intensity and number in going from HI to HCl. The values obtained for the vibration frequencies are 1970, 2440 and 2670 cm.$^{-1}$ for HI, HBr and HCl respectively. The determinations are rather rough because of the diffuseness of the bands. In the case of hydrogen chloride it should be noticed that the frequency has been almost completely reduced from its value in the ground state (2989 cm.$^{-1}$) to its value in the $^2\Pi$ state of HCl$^+$ (2608 cm.$^{-1}$). The rough value of $x_e\omega_e = 20$ obtained for this state is quite different from the ground state ($x_e\omega_e = 51\cdot65$), but agrees well with the value ~ 20 found for HCl$^+$. While similar remarks are probably also true of the bromide and the iodide, the emission data on HBr$^+$ and HI$^+$ are not yet available, so that the comparisons cannot be made. It must be recorded that the higher lines of the P branches of the 1290 and the 1248 A bands of hydrogen chloride are sufficiently discrete to be measured. Eight lines of the 1290 A band gave differences which increased uniformly from 30 to 40 cm.$^{-1}$, and six lines of the 1248 A band gave differences increasing from 31 to 37 cm.$^{-1}$. The R and Q branches of both these bands are diffuse or at least unresolvable, so that values of the molecular constants cannot be derived from an analysis of the rotational structure. However, from a consideration of the rather sharp R head it can be shown that these spacings are not inconsistent with a slight increase in the moment of inertia of the molecule resulting from the electronic excitation, supplemented by a further increase in the case of the 1248 A band due to its vibrational energy. These facts leave little doubt that the non-bonding "$p\pi$" electron has been excited.

It is now desired to show that the above analogous systems in the halogen acids correspond to systems in the methyl halides known as the B and C systems (Herzberg and Schiebe 1930; Henrici 1932; Price 1936). The B, C bands of the different methyl halides have been related because their term values are similar (Price 1936). The two bands in hydrogen iodide occurring at 1762 and 1605 A have term values of 32,380 and 26,810 cm.$^{-1}$ respectively with reference to the $^2\Pi_{\frac{3}{2}}$ state of HI$^+$. The states B and C of methyl iodide are 32,280 and 27,365 cm.$^{-1}$ below the

upper component of the doublet state of CH_3I^+.* The close agreement of the two sets of term values in hydrogen iodide and methyl iodide leaves little doubt as to the relatedness of the respective bands. This is especially so in view of the expected theoretical similarity of the iodine in the two molecules (Mulliken 1935 a). Since it has not been possible to determine the ionization potentials of hydrogen bromide and hydrogen chloride spectroscopically, the term values cannot be used to correlate the bands of these molecules with the B and C bands of methyl bromide and chloride. However, it is possible to make this correlation by virtue of a certain peculiarity which they exhibit and by the fact that they are the first strong resonance bands of the molecules. The electronic terms of the halogen acids are derived from the doublet states of the molecular ions by adding an electron in an excited orbital with Ω–s coupling (Mulliken 1934) in a similar way to that in which the excited states of the corresponding united (rare gas) atom are obtained from the atomic ion. Thus the electronic states which we are considering here are of the type $(^2\Pi_{1\frac{1}{2}})nx$ and $(^2\Pi_{\frac{1}{2}})nx$. On consulting the data on the rare gas atoms (Bacher and Goudsmit 1932), it will be found that when nx is ns, the separations of the excited states agree very closely with the doublet separation of the ion. However, when nx is np or nd the separations tend to be considerably larger. Now in the alkyl halides although C–B for the iodide is 4915 cm.$^{-1}$ (i.e. 54,625–49,710), agreeing fairly well with the doublet separation 5060 cm.$^{-1}$ of CH_3I^+, it is found that for the bromide the value is 3070 cm.$^{-1}$ (59,100–56,030) against 2540 cm.$^{-1}$ for CH_3Br^+ and for the chloride $\sim$1200 cm.$^{-1}$ (63,700–62,500) against 680 cm.$^{-1}$ for CH_3Cl^+. The increase of these separations for the bromide and the chloride over the doublet separation of the molecular ions is strange, especially in view of the fact that all the shorter wave-length pairs of bands of these molecules seem to have closely the ionic separation. This peculiarity was not stressed in the article on the alkyl halides (Price 1936) because the bands were diffuse and it was thought that the factor producing this diffuseness might also be responsible for their deviations from normal doublet separations. Mulliken (1935 b) states that the excited orbitals of these particular bands are probably $6d\pi$ iodine orbitals, an interpretation which seems likely, since the separation of the excited states of the united atom would in such a case tend to be considerably greater than the doublet separation of the ion. The bands of the halogen acids which we have been considering in the previous paragraphs show deviations similar to those discussed for the B and C bands of the methyl

* All term values are with respect to ionization potentials based upon firmly established Rydberg series limits in CH_3I and HI.

halides only to a somewhat greater extent. The separation of the bands of hydrogen bromide is 3455 cm.$^{-1}$ (70,540–67,085) as compared with 2653 cm.$^{-1}$ for $^2\Pi$ of HBr$^+$ (Norling 1935). For hydrogen chloride the separation is 2345 cm.$^{-1}$ (77,480–75,135) as against 644 cm.$^{-1}$ for the ion (Norling 1937). The doublet separation of HI$^+$ is unfortunately not known with great accuracy, but it is certain that it is not very much different from the separation of the hydrogen iodide bands at 1762 and 1605 A (i.e. 5570 cm.$^{-1}$). Thus, in addition to being the first strong absorption bands of the molecules, these halogen acid bands show similar peculiarities to the B and C bands of the methyl halides in deviating from the doublet separations of the molecular ions, and there can be little doubt that they correspond to very similar excited orbitals.

It is possible to obtain quite close estimates of the ionization potentials of hydrogen bromide and hydrogen chloride by adding the term values of the B and C bands of methyl bromide and chloride to the frequencies of the corresponding bands of the halogen acids. This procedure, applied, for example, to hydrogen iodide, gives 11·06 V for its upper ionization potential, a value which differs from that determined from Rydberg series by only 0·07 V. The underlying reason for this agreement is that for the substances considered big changes are only expected to occur in the lowest orbitals. The outer orbitals are likely to be essentially the same and to have the same term values in both the methyl halides and the halogen acids. Thus almost the same order of accuracy is to be expected for predictions of the ionization potentials of the other acids obtained by adding the term value of the methyl halide band to the corresponding band of the halogen acid. Taking mean-term values of the B and C bands of the methyl halides referred respectively to the lower and upper components of the doublet state of the molecular ion and adding these to the mean frequencies of the corresponding bands of the halogen acids, we should obtain very good approximations to the mean ionization potentials of the $^2\Pi$ states of the molecular ions. For hydrogen iodide the value obtained by this method is 10·71 V. This is to be compared with the value 11·16 V predicted theoretically by Mulliken on the assumption of ideal non-bonding conditions, i.e. the predicted energy separation of the iodine atom in its appropriate "valence" state from the corresponding "valence" state in the molecular ion. For hydrogen bromide we get 12·04 V as compared with 12·44 V predicted, and for hydrogen chloride 12·84 V against 13·66 V predicted. The value of the ionization potential of hydrogen iodide is of course strongly supported from the Rydberg series limit. The most recent electron impact determination of the ionization potential of hydrogen

chloride has been made by Nier and Hanson (1935). These measurements have been carried out with considerably improved technique and the results quoted in their paper are unusually self-consistent. The value they obtain is $12 \cdot 9 \pm 0 \cdot 2$ V, in very good agreement with the value we have deduced from spectroscopic evidence. The older electron impact potentials which are around $13 \cdot 8$ V thus seem to be definitely ruled out.

The ionization potentials given are in all cases only very slightly less than those predicted. The discrepancies are chiefly due to the presence of the well-known dipole moments associated with the molecules and are of the same order of magnitude as those found in molecules having comparable dipole moments (e.g. H_2S, predicted I − observed $I = 10 \cdot 83 - 10 \cdot 42 = 0 \cdot 41$ V, dipole moment $= 1 \cdot 1$ D). There is evidence for certain small changes in the shape of the potential energy curve of the ion relative to that of the neutral molecule which might also have some small influence on the ionization potential. This is most marked for HCl, becoming less so for HI. The latter molecule conforms most closely of all to the theoretical requirements by virtue of its very low dipole moment, and the almost complete covalent nature of the bond as judged by its negligible departure from the additivity law of bond energies (Pauling 1932). This is supported by the close proximity of the first strong resonance bands of I_2 ($\nu_e = 57,517$ cm.$^{-1}$) to the HI band at 56,750, as the spectra of both molecules are expected to be similar to a limited extent. The other halogen molecules have bands which lie very near to the bands of the corresponding halogen acids and consequently must have ionization potentials which are close to those given above for the acids. This is confirmed by the rough electron impact values 10, $12 \cdot 8$ and $13 \cdot 2$ V for the ionization potentials of I_2, Br_2 and Cl_2 respectively.

The closeness of the ionization potentials of HI, HBr and HCl to the values $I(I) = 10 \cdot 44$, $Br(I) = 11 \cdot 80$ and $Cl(I) = 12 \cdot 96$ V indicates very little difference between the heats of dissociation of the normal molecule and the molecular ions. The fact that in the molecular ions the internuclear distance is slightly increased and the vibration frequency somewhat diminished does not necessarily imply a diminution in the heat of dissociation. It is interesting to note that the relative displacements of the first long wave-length bands of the halogen acids are fairly close to the relative displacements of the ionization potentials of the corresponding halogen atoms, i.e. 10,334 : 8050 cm.$^{-1}$ as against 11,050 : 9441 cm.$^{-1}$. The same displacements for the methyl halides are considerably less, being 5400 : 5535 cm.$^{-1}$. This is to be expected as much larger charge transfer effects influence the term value of the ground states of the methyl halides,

a fact which is indicated from their greater bond moments and the larger diminutions of their ionization potentials with respect to the predicted values.

With regard to the exact nature of the excited states of the bands reported here, it may be remarked that it is clear from the spectrum that strong absorption only occurs to comparatively few of the very many excited states which can be formed from a normal hydrogen and an excited halogen atom. It has not yet been found possible to come to any definite conclusion for a particular band in the face of so many possibilities. Comparison with the rare gases indicates coupling practically completely of the Ω-s (J-J like) type for HI and HBr, while slight deviations are expected to occur for HCl. Possibly the tendency towards Λ-Σ coupling in HCl accounts for the presence of the weak satellite band situated a few Ångströms to the short wave-length side of all the strong bands. The appearance of these bands suggests a partially forbidden transition. They duplicate all the stronger bands at slightly shorter wave-lengths. The vibrational frequency in the subsidiary set is less than that for the strong main system, and the bands rapidly approach one another with increase in vibrational quantum number. This makes it highly probable that both the main and the subsidiary systems have the same products of dissociation. The frequencies of the (Q) centres of the B and C bands of the halogen acids are given in Table II. The possible error of the measurements is probably about 5 cm.$^{-1}$.

TABLE II. FREQUENCIES OF THE (Q) CENTRES OF THE BANDS OF THE
HALOGEN ACIDS BELONGING TO STATES PROVISIONALLY
DESIGNATED AS B AND C

State	HCl (m)*	HCl (s)†	HBr	HI
B	75,134	75,483	67,084	56,750
C	77,480	77,856	70,542	62,320
$C + \omega$	80,150	80,420	72,990	64,290
$C + 2\omega$	82,780	82,965	75,380	—

* $m \equiv$ main.   † $s \equiv$ subsidiary.

The predicted value of the ionization potential of HI rests upon an assumed value of $\sim 10 \cdot 5$ V for the ionization potential of I(I) ($^2P_{1\frac{1}{2}} \rightarrow {}^3P_2$). It is supported to some extent by the approximate value $10 \cdot 44$ V, which Evans (1931) obtained by a rather big extrapolation. The good agreement obtained here between the observed and the predicted ionization potential of HI must also be regarded as supporting this value. It rules out quite

definitely the value $8 \cdot 9 \pm 0 \cdot 2$ V suggested by Cordes (1936) which is based upon an extrapolation of the $^1\Sigma_u^+$ state of I_2 to its limit and on the assumption that the products of dissociation of this state are I^- and I^+. The pictures we have obtained of this somewhat diffuse system indicate the extreme difficulty and uncertainty of such an extrapolation. Mulliken's suggestion (Mulliken 1934, p. 567) that this $^1\Sigma_u^+$ state really dissociates into neutral atoms, one normal and one excited, in a similar fashion to the analogous state of H_2 seems much more likely.

SUMMARY

The absorption spectra of hydrogen iodide, bromide and chloride have been investigated in the vacuum ultra-violet. The bands observed are due to the excitation of a non-bonding $np\pi$ electron and are the strong resonance bands approaching the $^2\Pi_{1\frac{1}{2},\frac{1}{2}}$ states of the molecular ion. They start at 1762, 1491 and 1331 A for hydrogen iodide, bromide and chloride respectively. In the case of hydrogen iodide a well-developed Rydberg series of bands was found approaching the $^2\Pi_{\frac{1}{2}}$ state of HI^+, the limit of which corresponded to $10 \cdot 990 \pm 0 \cdot 005$ V. It was not possible to establish with certainty Rydberg series going to $^2\Pi_{1\frac{1}{2}}$ of HI^+ or to any of the $^2\Pi$ states of HBr^+ or HCl^+. However, from correlations made amongst the bands of the different acids and with the corresponding transitions in the methyl halides, the mean ionization potentials (i.e. $HX : {}^1\Sigma \rightarrow HX^+ : {}^2\Pi$) are determined to be $10 \cdot 71$, $12 \cdot 04$ and $12 \cdot 84$ V for hydrogen iodide, bromide and chloride respectively, the probable error being about a tenth of a volt.

REFERENCES

Bacher and Goudsmit 1932 "Atomic Energy States." New York: McGraw Hill.
Collins and Price 1934 *Rev. Sci. Instrum.* **5**, 423–5.
Cordes, H. 1936 *Z. Phys.* **97**, 603–24.
Evans, S. F. 1931 *Proc. Roy. Soc.* A, **133**, 417–30.
Henrici, A. 1932 *Z. Phys.* **77**, 35–57.
Herzberg and Scheibe 1930 *Z. phys. Chem.* B, **7**, 390–406.
Knipping, H. 1921 *Z. Phys.* **7**, 328–40.
Kulp, M. 1931 *Z. Phys.* **67**, 7–23.
Mackay, C. A. 1924 *Phys. Rev.* **24**, 319–29.
Mulliken, R. S. 1932 *Rev. Mod. Phys.* **4**, 34–8.
— 1934 *Phys. Rev.* **46**, 549–71.
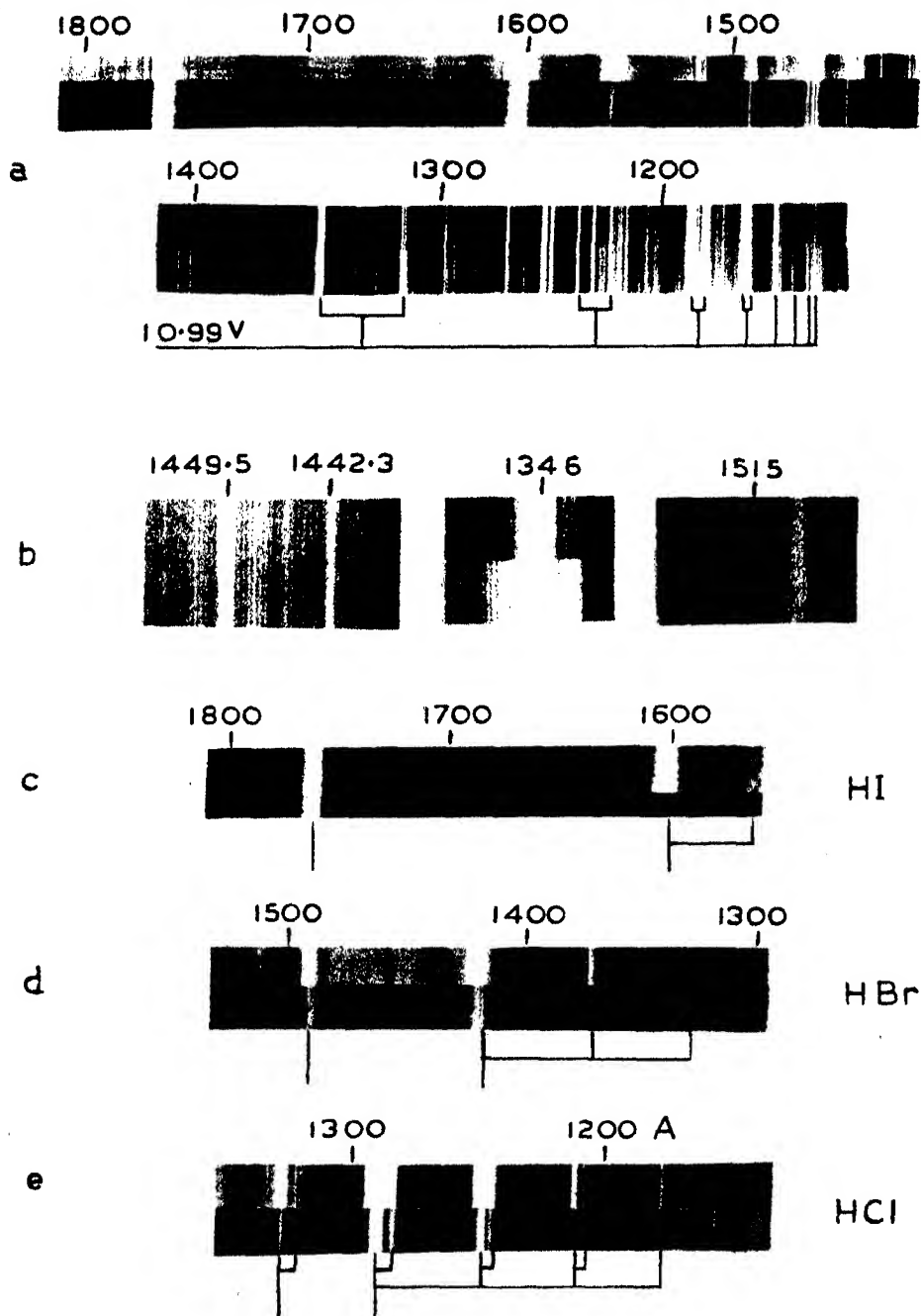
FIG. 1. The absorption spectra of the halogen acids.

Mulliken, R. S. *1935 a Phys. Rev.* **47**, 413–15.
—— *1935 b J. Chem. Phys.* **3**, 506–14.
Nielsen, A. H. and Nielsen, H. H. *1935 Phys. Rev.* **47**, 585–6.
Nier, A. O. and Hanson, E. E. *1935 Phys. Rev.* **50**, 722–6.
Norling, F. *1935 Z. Phys.* **95**, 179–88.
—— *1937 Z. Phys.* **104**, 638–52.
Pauling, L. *1932 J. Amer. Chem. Soc.* **54**, 3570–82.
Price, W. C. *1936 J. Chem. Phys.* **4**, 539–47.
White, H. E. *1934* "Introduction to Atomic Spectra," Chapter XIX. New York: McGraw Hill.

The determination of the meteorological conditions of the atmosphere by the use of radio-sounding balloons

By H. A. Thomas, D.Sc., M.I.E.E.

Radio Department, National Physical Laboratory

1. Introduction

Radio-signalling methods are sometimes applied to indicate or record temperature, pressure, humidity, and wind velocity, where the installation of an ordinary meteorological observing station would present difficulties due to the inaccessibility of the desired observing point. Such methods may also be applied to free balloon ascents for sounding the atmosphere, in which case the use of radio-signalling gives rise to three great advantages over the self-recording type of meteorograph. First, a record is obtained during the ascent of the balloon and consequently the ultimate loss of the apparatus is of no importance; secondly, a large amount of aerological data can be obtained at a cost far less than that required for aeroplane observations; thirdly, information can be obtained at altitudes considerably greater than those given by aeroplane instruments. For these various reasons considerable attention has been given in certain European countries and in America to radio-sounding methods of exploring the atmosphere.

The collection of reliable aerological data is now a matter of prime importance for a variety of purposes. Since a large number of ascents are necessary to obtain an adequate knowledge of conditions over a large area, and since many of the instruments will be lost or returned in a damaged

condition, it is important to keep as low as possible the cost of the apparatus. In the present paper a description is given of a satisfactory radio transmitter equipped with meteorological instruments to give instantaneous indication of the pressure and temperature of the atmosphere.

The general scheme by which aerological data are obtained with sounding balloons is as follows. A balloon of the necessary lifting capacity is attached to a parachute which in turn is tied to a radiating aerial supplied with current by a radio transmitter. Signals are emitted in a manner which is controlled by the meteorological instruments, and reception of these signals during ascent enables a knowledge of the aerological conditions to be obtained. The function of the parachute is to allow the apparatus to descend safely after the balloon has burst. The determination of wind velocity and direction is accomplished by observing the movement of the balloon by means of directional receivers situated on the ground.

It is essential in this method of exploration to reduce as far as possible the weight of the apparatus so that comparatively small and cheap balloons may be employed to reach high altitudes. Furthermore, to obtain a large range with small power it has been found advisable to use very high radio frequencies.

2. BRIEF REVIEW OF EXISTING METHODS

There are four ways in which the emission from a radio transmitter can be controlled by meteorological instruments. These are as follows:

(a) Variation of signal intensity.

(b) Variation of signal frequency.

(c) Variation of modulation frequency.

(d) Interruption of signal.

The first method is impracticable, due to variation of intensity of the received signal with distance between the transmitter and receiver. Methods involving variation of frequency or interruption of the signal have been explored to a considerable extent, but a method making use of variation of modulation frequency has, so far as is known, not been attempted previously.

Existing radio-meteorographs may be divided into two groups. One group makes use of interrupted signals at a constant radio frequency, the interruptions being produced and controlled by the meteorological instruments. The signals emitted are received at the ground station, and a succession of known instrumental values is obtained at irregular time in-

tervals. On this principle radio-meteorographs have been built by Molt-chanoff (1931), Bureau (1929) and Lange (1935). Some of these instruments make use of a code of signal interruptions to give the desired information, while others adopt what is known as the "Olland" principle, in which a uniformly rotating arm makes contact successively with fingers attached to the meteorological instruments, the time intervals between the impulses being used to give the desired information. This method does not give continuous observation of the desired parameters.

The other group of instruments makes use of a variable radio-frequency signal to transmit the setting of one meteorological element. In this way a continuous record at the ground station can be obtained for one meteorological parameter. The other meteorological elements provide additional signals by the use of a switching device which operates only at certain selected points during the ascent. This principle of operation does not provide a continuous record of all the changing meteorological conditions, although in the case of the Väisälä instrument, the sequence of observations is sufficiently rapid for most purposes.
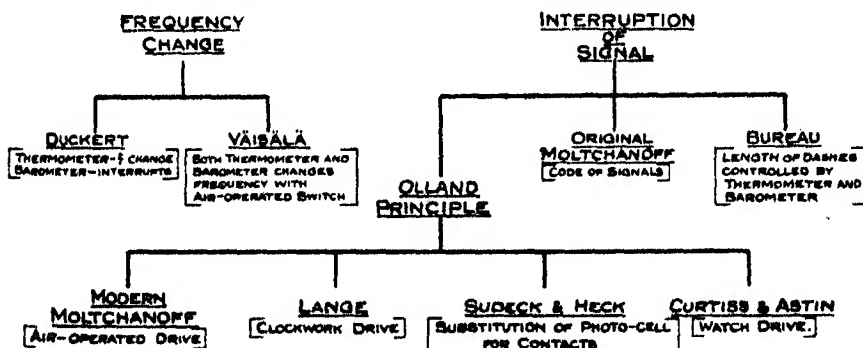
Fig. 1. Classification of existing types of radio-sounding transmitters.

The various existing methods of operation are tabulated in schematic form in fig. 1. In comparing the variable-frequency and constant-frequency types of radio-meteorographs with one another, it is obvious that one disadvantage of instruments of the constant-frequency type is that none of those at present available permit both extreme accuracy and rapid sequence of individual readings. Most instruments using a variable radio-frequency emission for indicating temperature furnish a continuous record of this parameter except for the occasional short intervals during which the pressure is being transmitted. In the Väisälä instrument (Väisälä 1935), a rapid sequence of observations of both temperature and pressure is given

by means of an air-operated switch. Although neither of these types gives a continuous record of temperature and pressure, the sequence of observations is often sufficiently rapid for most practical purposes.

A more serious objection to variable-frequency instruments is that the frequency band required to obtain the required instrumental accuracy is usually of the order of 1000 kc./sec. Tests made in America have shown that over this frequency range it is quite usual to find as many as fifty interfering stations, and consequently a considerable part of the record is missed. Difficulties are likely to arise.in obtaining permission to use such a wide frequency band permanently for meteorological purposes. A further serious objection arises with variable-frequency instruments due to the necessity of calibrating the meteorological elements with the aerial system in position. When the transmitter leaves the ground, there is an appreciable change of radio frequency due to the sudden change of the aerial constants, and correction for this change is very difficult. Also, the reception of signals of variable frequency is not easy and adds considerably to the complexity of the receiving arrangements.

Constant-frequency instruments possess the great advantage that only a small frequency band is necessary and reception is extremely easy. In addition, the meteorological instruments can be calibrated independently before assembly in the transmitter. On the other hand, with instruments employing moving contacts, the meteorological elements themselves are more complicated and expensive, and the accuracy is critically dependent on the uniformity of rotation of some clock or air-operated driving mechanism and on the constancy of the friction introduced by the contacts. Tests made on a "Duckert" instrument (Duckert 1933), in which the pressure element operates a light rolling contact to interrupt the anode circuit of the radio-frequency oscillator, revealed the presence of considerable hysteresis; the accuracy of the pressure determination was not better than 2 in. of mercury and was critically dependent on the contact pressure. The delicacy of meteorological instruments is such that no appreciable work can be performed by the moving parts, and the greatest objection to the use of devices employing rollers, fingers or similar contacting devices is the serious inaccuracy which is introduced inevitably by their presence.

3. General Principle of New Method of Exploration

Consideration of the various existing methods of operation indicated that a satisfactory instrument could not be designed by further development

along such lines. The following characteristics appear to be desirable in any radio-sounding method of exploring the atmosphere:

(*a*) The radio frequency of the signal emitted by the apparatus should be independent of the parameters to be measured.

(*b*) Continuous recording of both pressure and temperature should be possible.

(*c*) The meteorological instruments should not be called upon to operate any mechanism involving frictional members.

(*d*) It should be possible to calibrate the meteorological instruments independently of the radio transmitter and such calibration should also be independent of the radio-frequency conditions.

It appeared that the most promising means of attaining these characteristics was to make use of a modulated radio-frequency transmitter in which the modulation frequencies were controlled by the meteorological instruments. Hitherto such a method has received practically no attention, due no doubt to the difficulty of obtaining audio-frequency oscillators of sufficient frequency stability and also to the difficulty of devising a satisfactory scheme of modulation. Recent improvement in the design of constant-frequency oscillators has made the first difficulty less serious, while the development of a satisfactory means of modulation presents no serious objections.

In the present system, both the barometer and thermometer units contain an iron-cored coil and a small iron plate. A change of inductance is produced by variation of the air gap between the plate and coil, and this inductance variation is converted into a change of modulation frequency by using the iron-cored coil as the inductance in the tuned circuit of an audio-frequency oscillator. Very little mechanical work is done by the meteorological instruments when operated in this manner, and consequently a great advantage is obtained over instruments employing linkage systems. The output from the two oscillators, the frequencies of which are controlled by the barometer and thermometer units respectively, is used to modulate the radio transmitter. By the use of correct circuit values, it can be arranged that the modulating system imposes no load on the audio-frequency oscillators, and thus the modulation frequencies can be made to depend only on the meteorological instruments.

A conventional system is employed for the generation of the radio-frequency energy, the aerial being connected directly to the oscillatory circuit. The two audio-frequency oscillators, modulator and radio-frequency

oscillator are all energized by primary batteries situated in the base of the apparatus.

Any standard radio receiver may be used for the reception of the modulated signal, and the two audio frequencies produced in the output circuit may be measured by calibrated oscillators. This procedure enables a continuous measurement of both temperature and pressure to be made. Reception of the signal by two loop or spaced aerial direction finders situated at the extremities of a known base line enables a knowledge of the air velocity and direction to be obtained during the ascent of the apparatus.

4. ARRANGEMENT OF APPARATUS

(a) Electrical circuit

The radio frequency selected to give satisfactory reception with a minimum of atmospheric interference is 35 Mc./sec. (wave-length 8·6 m.). The value of this frequency is not critical, but at frequencies much in excess of this value difficulties arise due to the necessity of using a special valve for the radio-frequency oscillator, while at frequencies much below this value the aerial system becomes large.
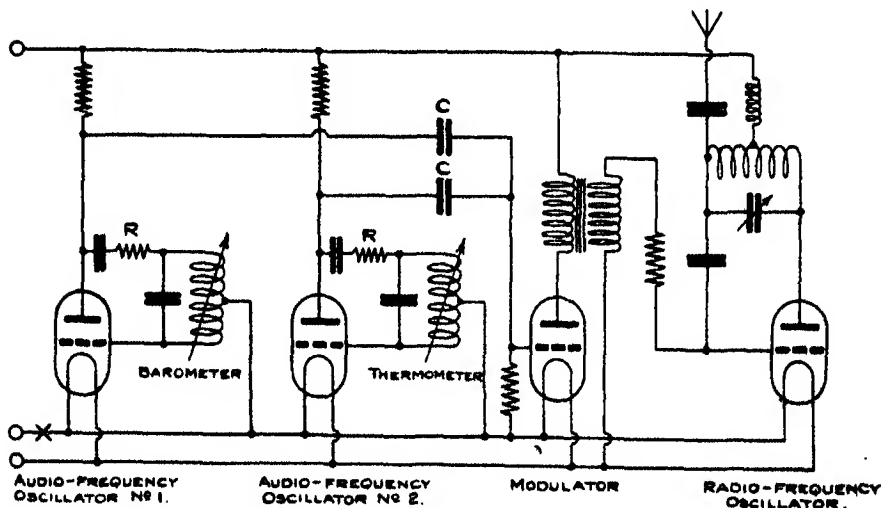
FIG. 2. Schematic winding diagram.

The electrical circuit is illustrated schematically in fig. 2. Reading from left to right, the frequencies of the first and second audio-frequency oscillators are controlled by the barometer and thermometer units respectively; the audio-frequency voltages generated by these oscillators are applied to

the modulator which in turn controls the output of the radio-frequency oscillator.

It is desirable that the frequencies of the two audio-frequency oscillators shall be as independent as possible of changes in battery voltage. This can best be accomplished by the use of the special stabilizing circuit shown in the figure. In this circuit, connexion is made between the anode and the oscillation circuit by a condenser and a resistance in series. The frequency stability is controlled by the values of these resistances R which can be adjusted by trial to give a very high degree of stability. The two oscillator circuits are adjusted by their respective tuning condensers to cover the two frequency bands 700–1000 c./sec. for the barometer, and 1400–1700 c./sec. for the thermometer. Experience has shown that these two frequency bands are satisfactory for telephonic reception.

Modulation of the radio-frequency oscillator is accomplished in the following manner. The primary circuit of a small audio-frequency transformer is supplied by the modulator valve with the two audio-frequency currents, while the secondary winding is connected in series with the grid-circuit resistance of the radio-frequency oscillator. The transformer circuit is working almost under open-circuit conditions, a very small output voltage being sufficient to produce 100 % modulation. The modulator valve can be quite small, and the audio-frequency voltages required to give the necessary output is exceedingly small. The great advantage of this system is that the coupling condensers C required to produce the input voltage to the modulator are so small that no variation of audio frequency is produced by the load of the modulator circuit. Consequently the frequencies of the two oscillators controlled by the meteorological instruments are entirely unaffected by the presence of either the modulator or radio-frequency oscillator systems.

The radio-frequency oscillator consists of a simple series-fed Hartley circuit coupled to a half-wave aerial. Experiments with both current-fed and voltage-fed aerial systems have shown that the latter are superior for the present purpose. The current-fed arrangement in which two quarter-wave-length aerials are arranged with the transmitter at the centre possesses the disadvantage that during ascent the lower aerial swings excessively. On the other hand, the voltage-fed system in which a half-wave-length aerial is coupled to the oscillation circuit has the advantage that the aerial remains practically straight during ascent and consequently the frequency stability is of a high order. Reduction of aerial swinging is a matter of prime importance, particularly for direction-finding purposes, since errors in the determination of the bearing are intimately associated with the angular

displacement of the aerial from the vertical position. Further reduction of the angle of swing can be obtained by inserting a considerable length of cord between the balloon and the transmitter.

Current is supplied to the transmitter by dry batteries housed in an aluminium container. Although the weight for a given capacity is about double that of secondary batteries, the advantages of dry batteries are considerable. In the first place, the shelf life is at least 3 months, and consequently the transmitters can be equipped with their batteries many weeks before use. In the second place, the reliability of operation is superior to that obtained with very small secondary batteries; and thirdly, no acid is spilt during transport and consequently no damage can be done to the components in the transmitter. The battery is arranged to be near the valves so that the heat produced in these may assist in preventing freezing of the electrolyte. Experience shows that the heat produced by the battery action together with that developed by the valves is sufficient to prevent freezing for a considerable time period. Although thermal lagging was not utilized, no case has arisen where a transmission has failed through freezing of the battery. Several ascents to heights of 15 k. have been made, and the signal has been received continuously throughout the ascent and descent. The current at the centre of the aerial is about 50 mA, and this current is maintained nearly constant for a period of about 120 min.

(b) Barometer unit

The simplest means of converting pressure variation into change of modulation frequency without the use of moving parts consists of a variable inductance coil arranged in an audio-frequency oscillator so that change of inductance varies the frequency. The barometer unit consists of an evacuated aneroid box and a small iron-cored coil arranged so that contraction of the box increases the air gap in the magnetic circuit. Experiments have shown that the most satisfactory performance is obtained with an aneroid box in which the expanding element consists of a thin-walled seamless bellows made of phosphor-bronze. Such bellows are now used commercially in thermostatic-control apparatus and packless glands. By choosing an appropriate thickness of metal and evacuating the bellows, it has been found that good sensitivity can be obtained and that the performance with repeated pressure cycles approximates very nearly to true elastic behaviour.

The general arrangement of the unit is illustrated in fig. 3. The bellows 1 are soldered to a brass bottom plate 2 and are sealed with a brass top plate 3 which has a small thin strip of "Stalloy" iron sweated to its surface. A thin metal tube 4 is fitted to the bottom plate for connexion to an exhaust-

ing pump, this tube being sealed off on completion of evacuation. The laminated iron-cored coil 5 is mounted above the top plate of the bellows by means of brass bracket 6. The thickness of the metal and diameter of the bellows has been selected to give a movement of about one-tenth of an inch for a pressure change of 1000 mb. This movement gives rise to a frequency change of about 250 c./sec.

The unit is provided with a three-pin base 7 to facilitate removal from the transmitter during calibration. The weight of the complete unit is 105 g., and the instrument is extremely robust. Several units have been transferred from transmitters that have been returned after flight to transmitters under construction and in every case the performance was satisfactory, while the calibration was not altered appreciably by the shocks encountered on landing.

A typical calibration curve is shown in fig. 4. Since the frequency can be measured to an accuracy of half a cycle per second, the possible observational error in the de-

Fig. 3. Assembly of barometer unit.

termination of pressure is 8 mb. in the neighbourhood of atmospheric pressure, while at pressures of about 200 mb., the possible error is less than 1 mb. Hysteresis effects are quite small; at a pressure of 500 mb. the difference in pressure between ascending and descending readings is 15 mb., while the return frequency for atmospheric pressure is exactly the same as the starting value. Experience has shown that hysteresis and "ageing" effects can be reduced appreciably by the application to the bellows of successive pressure cycles before assembly. If the unit is calibrated just prior to a flight, "ageing" effects would be of negligible importance.

A complete examination of the effect of temperature on the calibration of the unit has not yet been made, but indirect evidence suggests that errors in the determination of pressure due to temperature change are likely to be very small. Tests on a punctured barometer unit have shown that the contraction of the bellows due to temperature change produces a negligible frequency variation, while the change of elastic modulus of the metal with temperature is inappreciable. Care has been taken in the disposition of the

unit in the transmitter assembly to ensure that the full external temperature change is not applied to the bellows.
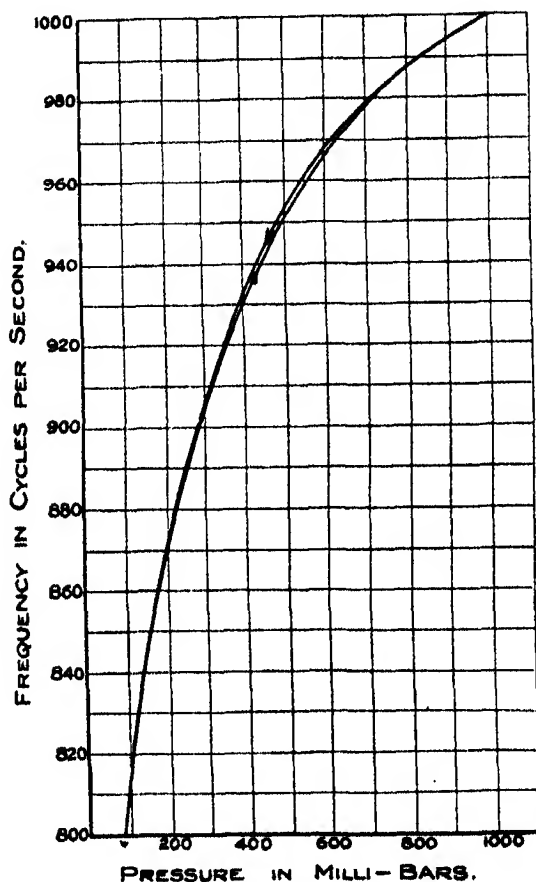
FIG. 4. Typical barometer calibration.

(c) *Thermometer unit*

The most important practical difficulty in the production of a satisfactory thermometer unit is the avoidance of time lag between the actual temperature change and the observation of this change. At a rate of ascent of 4 m./sec., the temperature is changing at about 2° C./min. Accordingly, for an accurate observation of temperature, the thermal capacity of the instrument must be very small; many instruments used at present are deficient in this respect.

Tests on bimetallic elements have revealed the difficulty of producing

strips of sufficient rigidity and stability which at the same time have a small enough thermal capacity; furthermore, it has been found that such strips possess appreciable mechanical hysteresis.

The most satisfactory method of converting temperature change into variation of modulation frequency makes use of the expansion of a fine wire in conjunction with an iron-cored inductance whose air gap is controlled by the length of the wire. A good sensitivity can be obtained by adopting the system of mounting commonly used in hot-wire ammeters, and the thermal lag of a fine wire is very small.
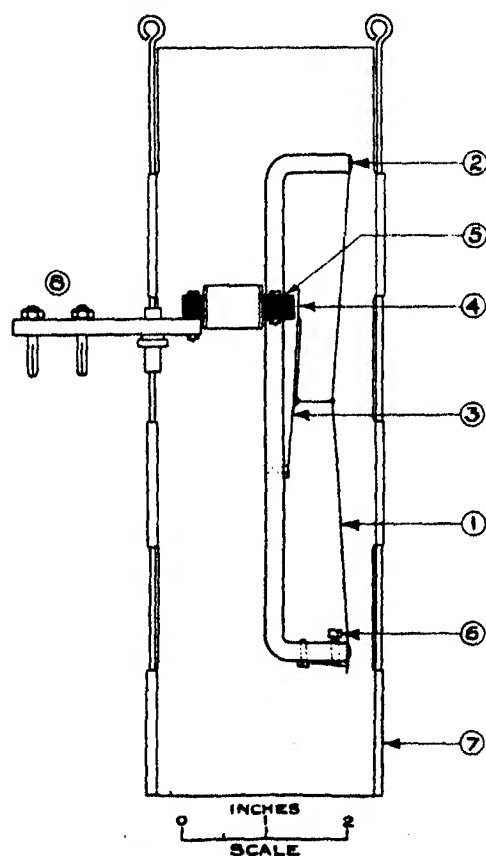
FIG. 5. Assembly of thermometer unit.

The general arrangement of the unit is illustrated in fig. 5. A brass wire 1 of No. 38 gauge is stretched on an invar frame 2 and is kept under slight tension by an invar spring 3 supporting a moving "Stalloy" iron plate 4. Movement of this plate varies the air gap of an iron-cored coil 5, so changing

its inductance. The initial sag of the wire is adjusted at atmospheric temperature so that the wire becomes taut at $-80°$ C., an adjusting screw 6 being provided for this purpose. After adjustment of the initial sag, the wire is soldered at both ends, great care being taken not to overheat the wire. The movement of the iron plate over the range $+20$ to $-80°$ C. is about one-tenth of an inch; this movement gives rise to a frequency change of about 200 c./sec.
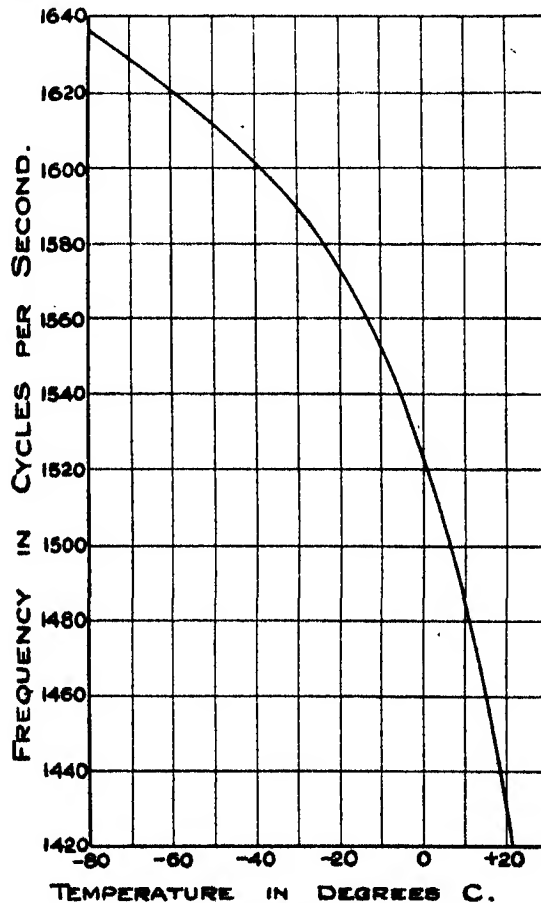
FIG. 6. Typical thermometer calibration.

The complete assembly is shielded from direct solar radiation by a detachable cylindrical aluminium shield 7 and the unit is fitted with a three-pin plug 8 so that it may be removed from the transmitter for calibration. A small celluloid cover is provided to shield the moving plate from air currents during ascent. The weight of the unit complete with shield is 170 g.

A typical thermometer calibration is shown in fig. 6, from which it is seen that over the temperature range $+20$ to $-80°$ C. the corresponding frequency change is 220 c./sec. Since the accuracy of measurement is half a cycle per second, the temperature can be measured to an accuracy of about $0.1°$ C. in the neighbourhood of $+20°$ C. and about $0.6°$ C. in the neighbourhood of $-80°$ C.

No definite evidence of hysteresis has been observed. The effect on the calibration of successive repetitions of a large thermal excursion has not yet been made, but frequent measurements taken over a period of 7 days within the temperature range 18–40° C. have shown that the calibration can be relied on to an accuracy of about $\pm 0.5°$ C.

(d) Assembly of transmitter

The general arrangement of the transmitter, battery, barometer and thermometer units, protection covers, and aerial, is shown in fig. 7. The
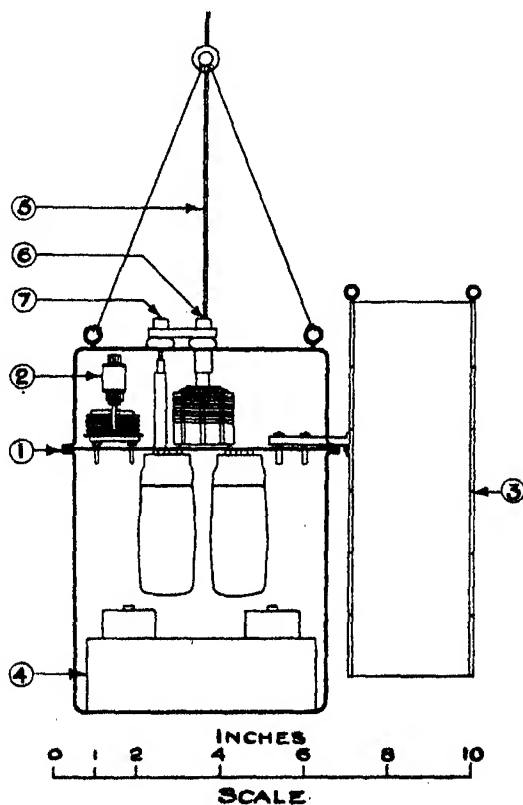
Fig. 7. Assembly of transmitter.

circuit components are all mounted on one side of a circular sheet of bakelite 1, the grade of which has been selected to give good electrical properties at radio frequencies and at the same time reasonable mechanical strength. The barometer unit 2 is mounted on the top side of the panel, a hole being cut below the instrument to permit the warm rising air from the valves to reduce temperature changes. The thermometer unit 3 is also mounted by means of a bracket on the same panel, so that the complete transmitter including instruments can be assembled and tested as a unit.
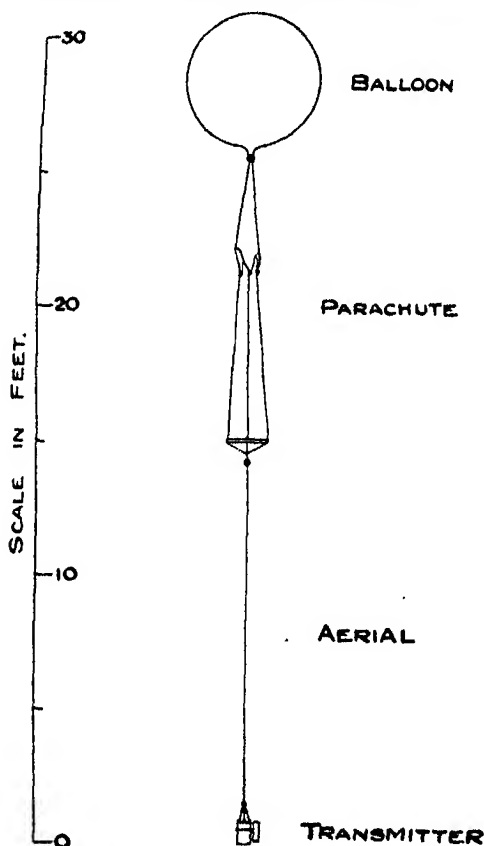
Fɪɢ. 8. Assembly of balloon, parachute and transmitter.

The aluminium protecting covers comprise a battery container and a transmitter cover, the two being hinged at one point; the bakelite panel supporting the transmitter components is held between the two flanges as shown in fig. 7. The 86 V H.T. battery 4 is tied down to the bottom of the lower can, and three leads are connected to a plug for insertion in a socket

completing the supply circuit to the transmitter. The copper-cord aerial 5 is 4 m. long and is connected by a waterproof plug 6; another plug 7 closes the filament circuit and so energizes the transmitter at the same time as the aerial is connected; this double plug is inserted just before the launch.

(e) *Balloon and parachute*

The rubber balloon is inflated until it is just buoyant when loaded with a weight of 2·89 kg. and its diameter is then about 4 ft.; this degree of inflation requires about 120 cu. ft. of hydrogen and gives a free lift of 500 g. and a rate of ascent of between 3 and 4 m./sec.

The parachute necessary to ensure a safe descent of the apparatus at a rate about equal to that of ascent consists of a sheet of cotton fabric 6 ft. square tied to the balloon at its centre and fitted with four strings tied between the corners and a wooden hoop; this hoop keeps open the folds of the cloth during ascent.

The assembly of the balloon, parachute, aerial and transmitter is shown in fig. 8. For direction-finding purposes, swinging of the apparatus leads to errors in the determination of the bearing, and consequently a length of about 30 ft. of string is sometimes inserted between the parachute and the aerial to lengthen the system and so reduce angular swing.

The launching of the apparatus presents no difficulties except in a strong wind. In such circumstances, launching from an elevated point is advisable, or alternatively a 20 ft. length of string attached to the transmitter may be payed out before release. The following table summarizes the weight of the components of the transmitter:

	g.
Circuit components and panel	355
Barometer unit	105
Thermometer unit with solar shield ...	170
Valves	175
Battery	935
Aluminium container	230
Aerial, insulators, plugs, etc.	70
Parachute	350
Total weight	2390

The weight of the transmitter alone is 2040 g., and it will be noted that the battery accounts for nearly half this weight; this proportion cannot be reduced appreciably without sacrificing the advantages outlined on p. 234 for the particular dry battery employed.

5. Method of reception

Satisfactory reception of the signals emitted from the transmitter can be obtained with any sensitive short-wave receiver. Since a fixed radio frequency is used, the tuning range need only be sufficient to cover small frequency differences between individual transmitters incidental to constructional variations. Experience has shown that if automatic volume control is employed, the telephone output varies very little from the launch of the apparatus to the cessation of the signal when the balloon is possibly 100 miles away. Furthermore, the frequency stability of the transmitter is so high that normally no retuning is necessary during the ascent or descent.

The two modulation frequencies are measured by the utilization of two audio-frequency oscillators, the output from which can be inserted in series with the receiver telephones. The frequencies of the measuring oscillators are adjusted by the zero beat method to synchronize in turn with the incoming modulation frequencies. The two oscillators are arranged to cover the frequency ranges 700–1000 and 1400–1700 c./sec. The frequency variation is obtained by varying the air gap of a small inductance coil by means of a cam mechanism operated by a slow-motion drive. The scale attached to this drive has a discrimination of less than 0·25 c./sec., and the calibration of these oscillators remains constant with reasonable precision.

As indicated above, the measurement of audio frequency is made by adjusting the amplitude of the oscillator signal to give beats with the telephone signal and then, when the beat frequency is zero, to read the corresponding frequency on the scale. An accuracy of half a cycle per second is readily obtained by this method, and a little practice is sufficient to enable an operator to obtain reliable results. The rapidity with which observations can be taken is dependent on the skill of the operator. There is no difficulty in taking readings of both pressure and temperature every half minute, and it is possible that four sets of readings a minute could be obtained if required. The value of an automatic recording arrangement is of course very considerable, and the construction of such an apparatus is now well advanced.

6. Calibration of barometer and thermometer

The general arrangement of the measuring and calibrating apparatus is illustrated schematically in fig. 9. A number of pressure elements are arranged in a testing chamber with an external switch or plug to connect

each unit in turn to the calibrating oscillator, this oscillator being an exact replica of the one used in the transmitter. The frequency corresponding to any known pressure is measured by beating the audio-frequency output with the signal given by the pressure-measuring oscillator. In a similar manner, a number of thermometer units may be arranged in a testing chamber with another calibrating oscillator. The fixed value of the capacitance used in conjunction with either unit during calibration may not be exactly the same as that used in the transmitter, since the manufacturing tolerance is not greater than 1 %. The calibration law is inappreciably affected, however, by small variations of capacitance, so that if one calibrating point of temperature and pressure is obtained accurately prior to launch, the chamber calibration may be corrected for small capacitance differences.
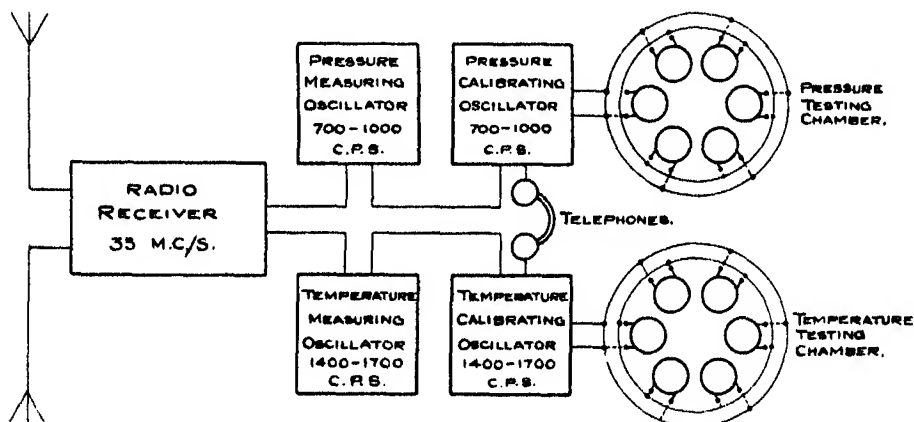
Fig. 9. General arrangement of measuring and calibrating apparatus.

For measurement of the frequencies during ascent, the output from either the pressure or temperature-measuring oscillator is applied in series with the telephone output from the radio receiver. Since the output circuits of the four oscillators and the receiver are all connected in series, switching is avoided, it being necessary only to switch on the appropriate pair of audio-frequency sources to obtain a frequency measurement of the unit either when undergoing calibration or during an ascent.

One considerable advantage of this method is that a number of units may be calibrated simultaneously and the pressure and temperature units may then be plugged into the transmitter, the two starting frequencies being sufficient to enable the true calibration to be determined.

7. RELIABILITY OF PERFORMANCE AND ACCURACY OF PRESSURE, TEMPERATURE AND ALTITUDE DETERMINATION

Data obtained from a number of ascents are given in Table I. Some of the transmitters were used purely for direction-finding purposes and consequently were not equipped with meteorological instruments, while others fitted with barometers only were used in the development of the pressure-measuring apparatus. Measurements on transmitters working at radio frequencies of 7 and 35 Mc./sec. (wave-lengths 43 and 8·6 m.) are included, since these alternative frequencies were sometimes employed in the original experiments.

It is seen that in no single case has a failure of a transmitter been observed during ascent due to the circuit or the valves. The valve damage produced by the crashing of the apparatus is, in fact, almost negligible; certainly not more than 5 % of the valves have suffered the slightest damage and so far no instance of a broken filament has occurred.

No case has yet arisen where the signal was too weak to be observed due to the distance of the transmitter from the receiver. In one case the distance was 170 km. and perfect reception was maintained, from which fact it is certain that the aerial current and receiver sensitivity are adequate for reception up to distances considerably in excess of those observed in the experimental ascents. In the great majority of cases, the signal ceased only when the transmitter was nearing the earth due to ground attenuation. In those cases where battery failure may have occurred, the batteries had been in stock for nearly three months before being used; with new batteries there is no danger of failure due to freezing at high altitudes. The average duration of an ascent and descent is between 60 and 100 min., and in many flights the signal was received continuously from the moment of launching to the time of landing; in one case the signal was received 150 min. after the launch of the apparatus. Therefore it appears that the capacity of the battery is sufficient for satisfactory reception over such long time periods.

The height normally attained by the instrument is about 10 km., while the maximum height so far recorded is 14 km. The rather scanty information available for determining the rate of ascent and descent suggests that the former lies between 2 and 4·5 m./sec., while the latter lies between 2·5 and 6 m./sec.; the parachute used at present appears therefore to be adequate to ensure a landing without appreciable damage. The condition in which most of the sets are returned is such that they are frequently used several times. Although the weight of the apparatus is rather high, a satisfactory altitude is obtained, and although every effort will be made in future development

TABLE I. DATA OBTAINED FROM EXPERIMENTAL ASCENTS

Transmitter no.	Radio frequency (Mc./sec.) (wave-length in m.)	Duration in minutes of				Maximum altitude km.	Horizontal distance traversed km.	Transmitter equipped with		Probable cause of signal termination
		Ascent and descent	Satisfactory reception	Ascent	Descent			Barometer	Thermometer	
1	7 (43)	98	94	57	41	13·0	20	Yes	No	Transmitter reaching ground
2	35 (8)	—	75	—	—	—	40	No	No	,,
3	35 (8)	—	63	—	—	—	56	No	No	,,
4	35 (8)	—	45	—	—	—	38	No	No	Not known
5	35 (8)	—	74	—	—	—	112	No	No	Transmitter reaching ground
6	7 (43)	—	67	—	—	—	33	No	No	,,
7	7 (43)	—	91	—	—	—	37	No	No	,,
8	35 (8)	—	7	—	—	—	11	No	No	Balloon leaking
9	35 (8)	101	94	78	23	8·8	45	Yes	No	Transmitter reaching ground
10	7 (43)	—	86	—	—	—	—	No	No	,,
11	7 (43)	—	54	—	—	7·4	82	Yes	No	Batteries failed after balloon burst
12	7 (43)	—	84	68	—	10·1	—	Yes	No	Transmitter reaching ground
13	7 (43)	—	76	60	—	7·0	62	Yes	No	,,
13a	7 (43)	—	90	—	—	—	170	No	No	,,
15	7 (43)	—	100	—	—	—	160	No	No	,,
16	30 (10)	—	71	—	—	—	78	No	No	,,
17	30 (10)	—	160	—	—	—	—	No	No	,,
18	30 (10)	—	31	—	—	—	13	No	No	Balloon failure
20	35 (8)	—	76	76	—	14·0	—	Yes	Yes	Bursting of balloon
21	35 (8)	135	70	70	65	10·2	37	Yes	No	,,
22	35 (8)	153	102	93	60	10·0	57	Yes	No	Batteries failed after balloon burst
23	35 (8)	153	86	—	—	—	57	Yes	No	,,
24	35 (8)	—	35	35	—	6·7	—	Yes	Yes	Bursting of balloon
26	35 (8)	82	80	43	39	11·7	46	Yes	Yes	Transmitter reaching ground
27	30 (10)	—	95	—	—	—	—	No	No	,,
29	35 (8)	—	88	86	—	11·5	105	Yes	No	Batteries failed after balloon burst

work to reduce weight, there appears to be no reason why the present reliability of operation should be sacrificed by appreciable reduction of weight. If ascents to greater altitudes are required, it would be expedient to employ a slightly larger balloon, since the extra cost entailed would be far less than that necessary to produce special light-weight batteries and circuit components.

The accuracy of measurement of both temperature and pressure during flight would be the same as the calibration accuracy of the separate meteorological instruments if the conditions of oscillation could be maintained constant. This can never be realized in practice, since the modulation frequency is dependent to a slight extent on the battery voltages and also on the stability of the circuit components when subjected to a fall of temperature.

The most important single factor in this respect is the variation of capacitance of the fixed tuning condensers in the audio-frequency oscillator circuits. The temperature coefficient of capacitance of these condensers is about 50 parts in 1 million per ° C., and the temperature change experienced by these condensers during an ascent to an altitude of 10 km. is about 30° C. The frequency change produced by variation of capacitance with temperature is consequently about 0·7 parts in 1000, which corresponds to actual changes of about 0·6 and 1·0 c./sec. for the barometer and thermometer units respectively. Reference to the calibration of these two units shows that the possible error in the measurement of low pressures and temperatures is about 1 mb. and 1° C. respectively. A secondary cause of frequency variation with temperature is the change of inductance of the iron-cored coils. Experiments have shown that this change is negligible.

The drop in high-tension and low-tension battery voltages over a period of 60 min. is about $1\frac{1}{2}$ and 10 % respectively, but these variations do not produce frequency changes greater than 0·5 c./sec. due to the special stabilized circuit employed.

The cumulative effect of the various errors which may arise, together with the variation of instrumental sensitivity over the working range, produces an overall accuracy of measurement which varies with altitude. The accuracy at present obtainable at different altitudes is shown in Table II.

8. Typical results obtained from observation

The particular record of pressure, temperature and altitude shown in fig. 10 may be taken as representative of other ascents. In this case the isothermal region was reached, the lowest temperature recorded being

TABLE II. ACCURACY OF PRESSURE, ALTITUDE
AND TEMPERATURE DETERMINATION

Height km.	Accuracy of pressure determination mb.	Accuracy of altitude determination m.	Accuracy of temperature determination ° C.
2	7	60	0·5
4	5	65	0·5
6	4	55	0·5
8	4	60	0·9
10	3	65	1·5
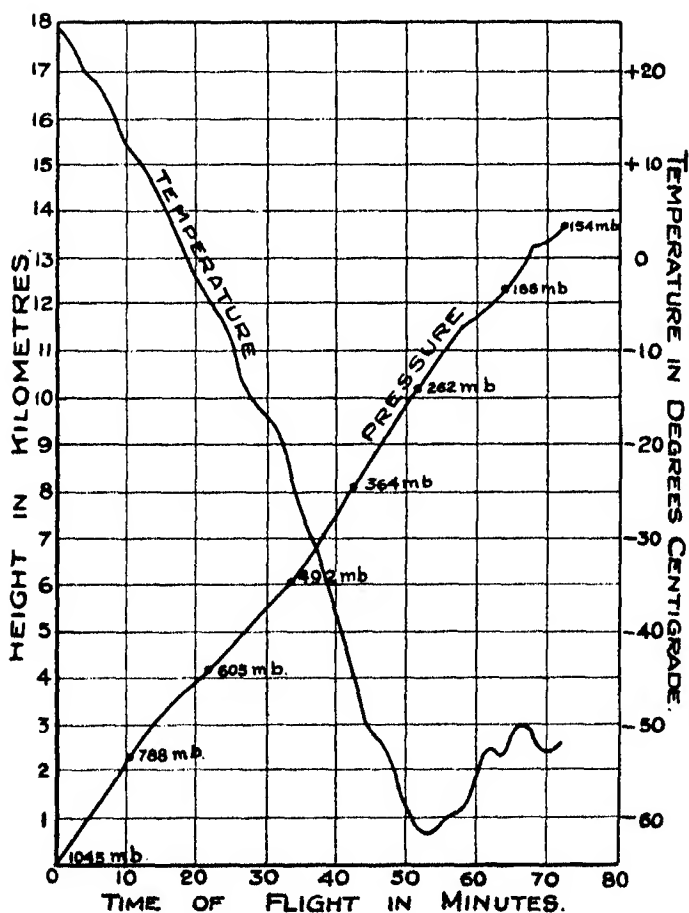
Fig. 10. Typical flight record.

about $-60°$ C. The altitude has been calculated by graphical means from the formula

$$h = 18400 \frac{T}{273} (\log_{10} p_0 - \log_{10} p),$$

where T = mean absolute temperature of air column, h = height in metres, p_0 = pressure at bottom of column in mm. of mercury, p = pressure at top of column in mm. of mercury.
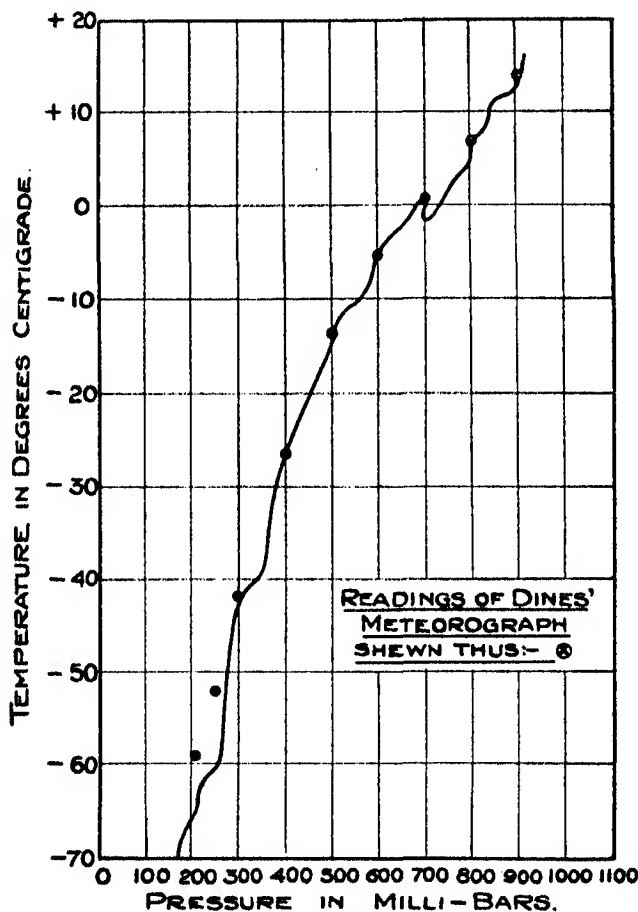
FIG. 11. Test on transmitter and Dines recorder.

In a second test, a Dines recording meteorograph was attached below the radio-sounding transmitter. The result of this test is shown in fig. 11, from which it is seen that good agreement was obtained between the two instruments up to a height of 10 km.

It may be concluded from other experimental ascents that considerable reliance can be placed on the determinations of both pressure and temperature given by the radio-sounding transmitter and that the modulated radio-frequency scheme described in this paper is a cheap and reliable means of exploring the atmosphere. The consistent reliability of operation obtained with the transmitters so far constructed is in fact extremely satisfactory and gives encouragement to the further development of the apparatus.

9. Acknowledgements

10. Summary

Existing methods of exploring the atmosphere by radio-sounding balloons are reviewed briefly, and it is explained that arrangements involving variation of radio frequency are not likely to be satisfactory due to the wide frequency band required and the possibility of appreciable interference. Furthermore, methods involving signalling codes are complex and expensive, and the delineation of the signals at the receiver presents considerable difficulty.

The essential features of an original method of exploration are described; in this method a signal of fixed radio frequency is employed and each meteorological instrument produces a continuous variation of modulation frequency. Calibration of the meteorological parameters in terms of frequency can be made independently of the radio transmitter, and measurement of these audio frequencies at the receiver is comparatively easy. The pressure- and temperature-measuring instruments are both arranged to produce variation of modulation frequency without the use of mechanical linkages. The cost of the apparatus is comparatively low, and reproduction in large quantities is possible.

The results obtained from a number of experimental ascents are analysed and it is shown that a high degree of reliability and accuracy is obtainable.

Using the present balloon, observation of both pressure and temperature up to an altitude of about 10 km. is obtained, the accuracy of the pressure and temperature determinations being about 5 mb. and 1° C. respectively.

REFERENCES

Bureau, R. 1929 *C.R. Acad. Sci., Paris*, **188**, 1565.
Duckert, E. 1933 *Beitr. Phys. frei. Atmos.* **20**, 303.
Lange, K. O. 1935 *Bull. Ann. Met. Soc.* **16**, 233, 267, 297 and **17**, 136.
Moltchanoff, P. 1931 *Beitr. Geophys.* **34**, 36.
Väisälä, V. 1935 *Comment. phys.-math., Helsingf.*, **8**, 14.

On the stability of a viscous liquid between rotating coaxial cylinders

By J. L. Synge

1. From the fullness of G. I. Taylor's theoretical discussion (1923) of the stability of a viscous liquid contained between rotating coaxial cylinders and the remarkable experimental confirmation of his results by himself and by Lewis (1927), it might be thought that the problem has been dealt with completely. However, it must be borne in mind that Taylor's results depend on the solution of an infinite determinantal equation, which presents a problem insoluble from a practical standpoint except when simplifications arise in a limiting case. Taylor's deductions deal only with the case when the distance between the cylinders is small in comparison with the radius of either, and even then the calculations are formidable. General results concerning stability, obtained without heavy calculations and not limited by any approximation, appear worthy of attention. The present paper contains one such result, namely, the proof of stability if

$$\omega_2 r_2^2 > \omega_1 r_1^2, \tag{1.1}$$

where ω_1, r_1 = angular velocity and radius of the inner cylinder,

   ω_2, r_2 = angular velocity and radius of the outer cylinder,

ω_1 being (without loss of generality) assumed to be positive. Stability under

the condition (1·1) was established by Taylor for the limiting case he considered, and has been confirmed by the experiments mentioned.

With regard to the disturbance, Taylor assumed

(i) independence of the azimuthal angle ϕ,

(ii) spatial periodicity in the direction of the generators of the cylinders:

these assumptions are also made in the present paper.

The condition (1·1) (or, more precisely, that the circulation should increase steadily outwards) was given by Rayleigh (1916) as the condition for stability of an inviscid rotating liquid: his argument, based on a minimum of energy, was perhaps not convincing, but the same condition (as a necessary condition for stability of an inviscid liquid between rotating coaxial cylinders) was established by Synge (1933), by the method of characteristic values, with generalization to the case of a heterogeneous liquid.

2. We shall here formulate the characteristic-value problem in a form simpler than Taylor's. Let r, ϕ, z be cylindrical co-ordinates, the cylinders being $r = r_1$ and $r = r_2$ $(r_2 > r_1)$. Let u, v, w be the components of velocity along the parametric lines of r, ϕ, z respectively. Let the body force possess a potential Π independent of ϕ. Then, for any motion possessing rotational symmetry, in the sense that velocity and pressure are independent of ϕ, the equations of motion of a viscous liquid are*

$$\begin{aligned}
\frac{Du}{Dt} - \frac{v^2}{r} &= -\frac{\partial}{\partial r}\left(\Pi + \frac{p}{\rho}\right) + \nu\left(\Delta u - \frac{u}{r^2}\right), \\
\frac{Dv}{Dt} + \frac{uv}{r} &= \nu\left(\Delta v - \frac{v}{r^2}\right), \\
\frac{Dw}{Dt} &= -\frac{\partial}{\partial z}\left(\Pi + \frac{p}{\rho}\right) + \nu\Delta w,
\end{aligned} \qquad (2\cdot1)$$

where p and ρ are pressure and density, ν the kinematical viscosity, and D/Dt, Δ the operators

$$\begin{aligned}
\frac{D}{Dt} &= \frac{\partial}{\partial t} + u\frac{\partial}{\partial r} + w\frac{\partial}{\partial z}, \\
\Delta &= \frac{\partial^2}{\partial r^2} + \frac{1}{r}\frac{\partial}{\partial r} + \frac{\partial^2}{\partial z^2}.
\end{aligned} \qquad (2\cdot2)$$

We have also the equation of continuity,

$$\frac{1}{r}\frac{\partial}{\partial r}(ru) + \frac{\partial w}{\partial z} = 0. \qquad (2\cdot3)$$

*Cf. A. S. Ramsey 1935, p. 372.

Hence there exists a function $\psi(r, z, t)$ such that

$$u = -\frac{1}{r}\frac{\partial}{\partial z}(r\psi), \quad w = \frac{1}{r}\frac{\partial}{\partial r}(r\psi). \tag{2.4}$$

Elimination of $\Pi + p/\rho$ from (2.1) gives two equations for ψ and v,

$$\left.\begin{aligned}\left(\frac{D}{Dt} - \frac{u}{r} - \nu\Theta\right)\Theta\psi + \frac{2v}{r}\frac{\partial v}{\partial z} &= 0,\\ \left(\frac{D}{Dt} + \frac{u}{r} - \nu\Theta\right)v &= 0,\end{aligned}\right\} \tag{2.5}$$

where Θ is the operator

$$\Theta = \Delta - \frac{1}{r^2} = \frac{\partial^2}{\partial r^2} + \frac{1}{r}\frac{\partial}{\partial r} + \frac{\partial^2}{\partial z^2} - \frac{1}{r^2}. \tag{2.6}$$

3. If ω_1, ω_2 ($\omega_1 > 0$) are the angular velocities of the cylinders between which the liquid is contained, we have the familiar steady motion

$$\left.\begin{aligned}u = w = 0, \qquad v &= Ar + B/r,\\ A = \frac{\omega_2 r_2^2 - \omega_1 r_1^2}{r_2^2 - r_1^2}, \quad B &= -\frac{r_1^2 r_2^2(\omega_2 - \omega_1)}{r_2^2 - r_1^2}.\end{aligned}\right\} \tag{3.1}$$

We note that for this steady motion the ψ of (2.4) is zero.

To discuss a small disturbance of this steady motion, we put

$$v = Ar + \frac{B}{r} + \eta, \tag{3.2}$$

and treat η and ψ as small. Thus we obtain from (2.5)

$$\left.\begin{aligned}\left(\frac{\partial}{\partial t} - \nu\Theta\right)\Theta\psi &= -2\left(A + \frac{B}{r^2}\right)\frac{\partial\eta}{\partial z},\\ \left(\frac{\partial}{\partial t} - \nu\Theta\right)\eta &= 2A\frac{\partial\psi}{\partial z},\end{aligned}\right\} \tag{3.3}$$

with boundary conditions

$$\frac{\partial}{\partial r}(r\psi) = \frac{\partial\psi}{\partial z} = \eta = 0 \quad \text{for } r = r_1 \text{ and } r = r_2. \tag{3.4}$$

Let us introduce the dimensionless quantities

$$\left.\begin{aligned}\tau &= \nu t/r_1^2, & \xi &= r/r_1, & \zeta &= z/r_1,\\ \alpha &= r_2/r_1 > 1, & \beta &= \omega_2/\omega_1, & R &= \omega_1 r_1^2/\nu,\\ a &= \frac{\alpha^2\beta - 1}{\alpha^2 - 1}, & b &= -\frac{\alpha^2(\beta - 1)}{\alpha^2 - 1}.\end{aligned}\right\} \tag{3.5}$$

We may call α, β, R respectively the *geometrical ratio*, the *kinematical ratio* and the *Reynolds number* of the steady motion (3·1). Substitution from (3·5) in (3·3) gives

$$\left.\begin{array}{r} \left(\dfrac{\partial}{\partial\tau}-\varPhi\right)\varPhi\psi = -2R\left(a+\dfrac{b}{\xi^2}\right)r_1\dfrac{\partial\eta}{\partial\zeta}, \\[3mm] r_1\left(\dfrac{\partial}{\partial\tau}-\varPhi\right)\eta = 2Ra\dfrac{\partial\psi}{\partial\zeta}, \\[3mm] \varPhi = \dfrac{\partial^2}{\partial\xi^2}+\dfrac{1}{\xi}\dfrac{\partial}{\partial\xi}+\dfrac{\partial^2}{\partial\zeta^2}-\dfrac{1}{\xi^2}. \end{array}\right\} \qquad (3\cdot6)$$

The range of ξ is $1 \leqslant \xi \leqslant \alpha$.

Introducing now periodicity in the z-direction and an exponential time factor in the usual way, we put

$$\psi = r_1 f(\xi)\,e^{\sigma\tau+i\lambda\zeta}, \quad \eta = ig(\xi)\,e^{\sigma\tau+i\lambda\zeta}, \qquad (3\cdot7)$$

where σ, λ are constants, λ being real.

Substitution in (3·6) gives the two ordinary differential equations

$$\left.\begin{array}{r} (L-\lambda^2-\sigma)(L-\lambda^2)f = -2\lambda R(a+b/\xi^2)g, \\[2mm] (L-\lambda^2-\sigma)g = -2\lambda Raf, \\[2mm] L = \dfrac{d^2}{d\xi^2}+\dfrac{1}{\xi}\dfrac{d}{d\xi}-\dfrac{1}{\xi^2}, \end{array}\right\} \qquad (3\cdot8)$$

with the boundary conditions

$$f = df/d\xi = g = 0 \quad \text{for } \xi = 1 \text{ and } \xi = \alpha. \qquad (3\cdot9)$$

The system (3·8), (3·9) contains the characteristic-value problem, this system being consistent only when the constants σ, λ, α, β, R satisfy a characteristic equation. We have here a formulation of the problem equivalent to, but rather simpler than, that of Taylor. Instead of proceeding in the manner of Taylor to obtain an infinite determinantal characteristic equation, we seek a sufficient condition under which the real part of σ is negative, such condition implying stability.

4. We shall now use accents to denote derivations of f and g with respect to ξ: complex conjugates will be denoted by superimposed bars.

Let us multiply the first of (3·8) by $\xi\bar{f}d\xi$ and integrate over the range. Integration by parts and use of the boundary conditions leads to the result

$$\sigma(J_1^2+J_0^2+\lambda^2 K_0^2)+I_2^2+3(I_1^2-I_0^2)+2\lambda^2(J_1^2+J_0^2)+\lambda^4 K_0^2$$
$$= -2\lambda R\int_1^\alpha (a+b/\xi^2)\,\xi\bar{f}g\,d\xi, \quad (4\cdot1)$$

where we have denoted certain positive-definite integrals as follows:

$$I_2^2 = \int_1^\alpha \xi f'' \bar{f}'' \, d\xi, \quad I_1^2 = \int_1^\alpha \xi^{-1} f' \bar{f}' \, d\xi, \quad J_1^2 = \int_1^\alpha \xi f' \bar{f}' \, d\xi,$$
$$I_0^2 = \int_1^\alpha \xi^{-3} f \bar{f} \, d\xi, \quad J_0^2 = \int_1^\alpha \xi^{-1} f \bar{f} \, d\xi, \quad K_0^2 = \int_1^\alpha \xi f \bar{f} \, d\xi. \tag{4.2}$$

Let us multiply the second of (3.8) by $(a + b/\xi^2) \xi \bar{g} \, d\xi$ and integrate over the range: we find, on dividing by a and changing signs,

$$\sigma \int_1^\alpha \left(1 + \frac{b}{a\xi^2}\right) \xi g\bar{g} \, d\xi + \int_1^\alpha \left(1 + \frac{b}{a\xi^2}\right) (\xi g' \bar{g}' + \xi^{-1} g\bar{g} + \lambda^2 \xi g\bar{g}) \, d\xi$$
$$- \frac{2b}{a} \int_1^\alpha \xi^{-2} \bar{g} g' \, d\xi = 2\lambda R \int_1^\alpha \left(a + \frac{b}{\xi^2}\right) \xi f\bar{g} \, d\xi. \tag{4.3}$$

Let us add to (4.1) its complex conjugate. Writing

$$\sigma = p + iq \quad (p, q \text{ real}), \tag{4.4}$$

we obtain

$$p(J_1^2 + J_0^2 + \lambda^2 K_0^2) + I_2^2 + 3(I_1^2 - I_0^2) + 2\lambda^2(J_1^2 + J_0^2) + \lambda^4 K_0^2$$
$$= -\lambda R \int_1^\alpha \left(a + \frac{b}{\xi^2}\right) \xi (f\bar{g} + \bar{f}g) \, d\xi. \tag{4.5}$$

Let us add to (4.3) its complex conjugate. We note that

$$\int_1^\alpha \xi^{-2} (\bar{g} g' + g\bar{g}') \, d\xi = 2 \int_1^\alpha \xi^{-3} g\bar{g} \, d\xi, \tag{4.6}$$

and obtain

$$p \int_1^\alpha \left(1 + \frac{b}{a\xi^2}\right) \xi g\bar{g} \, d\xi + \int_1^\alpha \left(1 + \frac{b}{a\xi^2}\right) (\xi g' \bar{g}' + \xi^{-1} g\bar{g} + \lambda^2 \xi g\bar{g}) \, d\xi$$
$$- \frac{2b}{a} \int_1^\alpha \xi^{-3} g\bar{g} \, d\xi = \lambda R \int_1^\alpha \left(a + \frac{b}{\xi^2}\right) \xi (f\bar{g} + \bar{f}g) \, d\xi. \tag{4.7}$$

Adding (4.5) and (4.7), we have

$$pP + L + M + N = 0, \tag{4.8}$$

where
$$P = J_1^2 + J_0^2 + \lambda^2 K_0^2 + \int_1^\alpha \left(1 + \frac{b}{a\xi^2}\right) \xi g\bar{g} \, d\xi,$$
$$L = I_2^2 + 3(I_1^2 - I_0^2) + 2\lambda^2(J_1^2 + J_0^2) + \lambda^4 K_0^2,$$
$$M = \int_1^\alpha \left(1 + \frac{b}{a\xi^2}\right) (\xi g' \bar{g}' + \xi^{-1} g\bar{g}) \, d\xi - \frac{2b}{a} \int_1^\alpha \xi^{-3} g\bar{g} \, d\xi,$$
$$N = \lambda^2 \int_1^\alpha \left(1 + \frac{b}{a\xi^2}\right) \xi g\bar{g} \, d\xi. \tag{4.9}$$

If χ is any real constant, we have

$$\int_1^\alpha \xi^{-1}(f' + \chi f/\xi)(\bar{f}' + \chi \bar{f}/\xi)\,d\xi \geqslant 0, \qquad (4\cdot10)$$

or

$$I_1^2 + \chi \int_1^\alpha \xi^{-2}(f\bar{f}' + \bar{f}f')\,d\xi + \chi^2 I_0^2 \geqslant 0, \qquad (4\cdot11)$$

or, by ($4\cdot6$) with f instead of g,

$$I_1^2 + 2\chi I_0^2 + \chi^2 I_0^2 \geqslant 0. \qquad (4\cdot12)$$

Putting $\chi = -1$, we get
$$I_1^2 \geqslant I_0^2, \qquad (4\cdot13)$$

and hence by ($4\cdot9$) $L > 0$.

5. We shall now establish the following result:

If the motions of the cylinders satisfy

$$\omega_2 r_2^2 > \omega_1 r_1^2 > 0, \qquad (5\cdot1)$$

the subscript 2 referring to the outer cylinder, then the real parts of all characteristic values σ are negative, and hence the steady motion is stable.

In the notation of ($3\cdot5$), the condition ($5\cdot1$) implies

$$\alpha^2\beta - 1 > 0. \qquad (5\cdot2)$$

Then
$$1 + \frac{b}{a\xi^2} = 1 - \frac{\alpha^2(\beta-1)}{\xi^2(\alpha^2\beta-1)} = \frac{\alpha^2\beta(\xi^2-1) + \alpha^2 - \xi^2}{\xi^2(\alpha^2\beta-1)} > 0, \qquad (5\cdot3)$$

since $1 \leqslant \xi \leqslant \alpha$. Hence
$$P > 0, \quad N > 0. \qquad (5\cdot4)$$

Also, for any real constant χ,

$$\int_1^\alpha \left(\xi + \frac{b}{a\xi}\right)\left(g' + \frac{\chi g}{\xi}\right)\left(\bar{g}' + \frac{\chi\bar{g}}{\xi}\right)d\xi \geqslant 0, \qquad (5\cdot5)$$

or
$$\int_1^\alpha \left(1 + \frac{b}{a\xi^2}\right)\xi g'\bar{g}'\,d\xi + \chi \int_1^\alpha \left(1 + \frac{b}{a\xi^2}\right)(g\bar{g}' + \bar{g}g')\,d\xi$$
$$+ \chi^2 \int_1^\alpha \left(1 + \frac{b}{a\xi^2}\right)\xi^{-1}y\bar{y}\,d\xi \geqslant 0. \quad (5\cdot6)$$

But
$$\int_1^\alpha \left(1 + \frac{b}{a\xi^2}\right)(g\bar{g}' + \bar{g}g')\,d\xi = \frac{2b}{a}\int_1^\alpha \xi^{-3}y\bar{y}\,d\xi; \qquad (5\cdot7)$$

hence putting $\chi = -1$ in ($5\cdot6$), we see that $M \geqslant 0$. Thus we have

$$P > 0, \quad L > 0, \quad M \geqslant 0, \quad N > 0, \qquad (5\cdot8)$$

and so, by ($4\cdot8$), $p < 0$: this establishes the result.

The condition (5·1) may be stated in this form: the circulations at the inner and outer cylinders have the same sense, and that at the outer cylinder is the greater.

SUMMARY

The differential equations of the characteristic-value problem for the small disturbance of a viscous liquid contained between two rotating coaxial cylinders are put into convenient form. From these is deduced an expression for the real part of the characteristic number σ occurring in an exponential time factor, the expression involving integrals in which the integrands contain the product of a characteristic function or one of its derivatives by the complex conjugate. If the circulation at the outer cylinder is greater than that at the inner cylinder and has the same sign ($\omega_2 r_2^2 > \omega_1 r_1^2 > 0$), the signs of these integrals are known without knowledge of the characteristic functions, and it is found that the steady motion is stable under the condition stated. Unlike the work of G. I. Taylor on this problem, the present theory involves no approximations based on the thinness of the layer of liquid, but (as in Taylor's work) the only disturbances considered are those which are independent of the azimuthal angle and periodic in the direction of the generators of the cylinders.

REFERENCES

Lewis, J. W. 1927 *Proc. Roy. Soc.* A, **117**, 388–407.
Ramsey, A. S. 1935 "Treatise on Hydromechanics," part 2, 372.
Rayleigh 1916 *Proc. Roy. Soc.* A, **93**, 148–54.
Synge, J. L. 1933 *Trans. Roy. Soc. Canada*, **27**, iii, 1–18.
Taylor, G. I. 1923 *Philos. Trans.* A, **223**, 289–343.

Investigations of infra-red spectra. Absorption of the CH_2 group in the region of 3μ

BY J. J. FOX AND A. E. MARTIN

INTRODUCTION

We have previously recorded a few observations on the CH vibrations of some organic compounds in the 3μ region (Fox and Martin 1937), and indicated that while in general a CH group gave rise to a single C—H vibration band, and a CH_2 group to two such bands, in many molecules, especially those containing a benzene ring, the C—H units interacted in such a way as to give several bands, and in particular benzene itself and many mono-substituted benzenes gave three strong C—H bands which could be regarded as characteristic of the phenyl group.

Coblentz (1905), in his extensive investigations of infra-red spectra, found that all compounds which contained C—H linkages had strong absorption in the region of 3μ. The persistence of frequencies characteristic of certain groups throughout a wide range of compounds has also been recognized from Raman spectra, and this persistency has received considerable emphasis from the work of Wulf and others (1935, 1936) on the characteristic infra-red bands of OH and NH groups in the region of 1.5μ. The bands observed were the first overtones of the fundamental vibrations, and it was found that the rest of the molecule, however complicated, had surprisingly little effect on the characteristics of the OH and NH bands. In a general way the explanation given was that each molecule contained a number of oscillating units, OH, CH, C=C, all loosely coupled together, the persistence of a given frequency through a variety of compounds indicating the looseness of this coupling.

Bonino (1929) pointed out that "aromatic" and "aliphatic" CH frequencies occurred more or less in the same region of the spectrum for a number of compounds, namely, about 3.4μ for saturated aliphatic compounds and about 3.25μ for benzene derivatives. These results, however, and the discussion thereon depend upon data from unresolved bands obtained with comparatively small dispersion, and also from Raman spectra. In this communication we present results obtained with much higher dispersion, so that details of individual bands now become clear. A large number of

[257]

compounds with CH, CH_2 and CH_3 groups arranged in many different ways has been examined by us, but here we confine ourselves to seven compounds in which the CH_2 groups are attached to the rest of the molecule by single bonds. Compounds containing CH_3 and aliphatic CH groups will be considered in a future communication.

<div align="center">EXPERIMENTAL</div>

The apparatus used was that described previously (Fox and Martin 1937). All the substances used were specially purified and were examined in solution in carbon tetrachloride, this procedure practically eliminating the complication of molecular rotation. Kinsey and Ellis (1937) and Borst, Buswell and Rodebush (1938) have found slight indications of rotational structure for water dissolved in CS_2 and CCl_4. In general, however, the rotational structure appears to be almost entirely suppressed, and our results on such molecules as methane, ethane, and methyl bromide show practically no rotational structure. The sharpness of the bands observed in the 3μ region varied, but in general frequencies could be obtained accurately to 1 cm.$^{-1}$, an accuracy comparable with the best Raman results. In this connexion we propose in this and future work to take account of a small frequency error in infra-red measurements which is generally neglected. When a grating spectrometer is calibrated visually with a mercury line such as λ 5460·7, this wave-length is the value in air, and so a wave-length 3μ measured with the instrument is the wave-length in air. The reciprocal of this wave-length (cm.$^{-1}$) should be corrected to vacuum by dividing by the refractive index of air at 3μ, and the value so obtained then becomes strictly comparable with Raman frequencies which are corrected to vacuum. The correction is small, but in view of the increasing accuracy of infra-red measurements should, in our opinion, be applied in the region here considered. Values of this correction to be deducted over the wave-length range for which the refractive index of air is known are

Wave-length (μ)	1	2	3	4	5	8	13
Correction (cm.$^{-1}$)	2·7	1·3	0·9	0·7	0·5	0·3	0·2

In the course of the present work absorption cells of two different lengths were used. The longer cell, 1 cm. in length, was made of brass tubing $\frac{3}{4}$ in. internal diameter, and fluorite end-plates were cemented on with a trace of fish glue. A side tube fitted with a ground-in stopper was provided for filling the cell. The smaller cell, 1·74 mm. in length, was similarly constructed, but owing to the small bore of the filling tube a second tube was

provided to allow air to escape as liquid was introduced through the other tube.

In assessing molecular extinction coefficients of absorption bands a correction for stray light in the spectrometer was made as described in the earlier communication. The accuracy of the extinction coefficients varies greatly according to the nature of the bands. Where the band is well separated from others an accuracy of 1 or 2 % is attainable, but when the bands overlap, as in the case of the three intense benzene bands in the region of 3.27μ, a graphical method of separation must be employed and the accuracy of the measurement may be much reduced. Illustrations of the graphical method of band separation are shown in figs. 1 and 2, for dioxan in which there are four overlapping bands, and benzyl alcohol with two overlapping bands. It will be noticed, particularly for benzyl alcohol, that the position taken as the maximum of a band may be in error unless the bands are separated (cf. band α). When it is desired to compare the relative intensities of bands which may differ somewhat in sharpness we may consider the total area of a band which has been plotted as molecular extinction coefficient κ against frequency ν, as a measure of the intensity of the band. The area of a band is, however, frequently difficult to measure because of overlap with other bands, and the shape of a band some distance from its peak is generally rather indefinite. In this connexion we may note that Leberknight and Ord (1937) have made measurements on the absorption bands of HCl and HBr in carbon tetrachloride and other solvents, and found that if A denotes twice the area under the curve included between the two points where the extinction has half its maximum value, and f the halfwidth of the band, i.e. the band width in cm.$^{-1}$ at these two points, then

$$\frac{A}{f\kappa\,\mathrm{max}} = \tfrac{1}{2}\pi$$

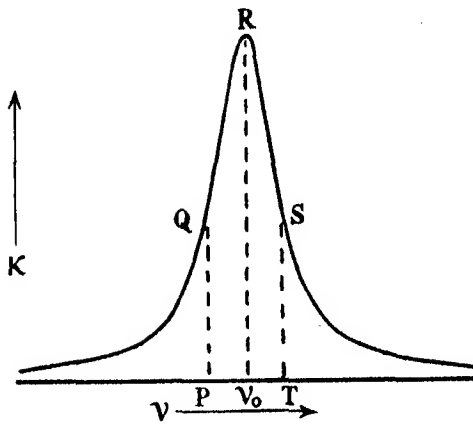very nearly for all the bands examined. This result, however, does not really give much information regarding the frequency function which determines the shape of the absorption band, since $\dfrac{A}{f\kappa\,\mathrm{max}}$ is close to 1·5 for the various shapes of bands shown in fig. 3. Further, if the shape of the extinction curve is that to be expected for damped simple harmonic oscillators with the damping force proportional to the velocity of motion, and the band width is small compared with the frequency of the oscillator, ν_0, then the molecular extinction coefficient at frequency ν is given by

$$\kappa = \frac{\kappa\,\mathrm{max}}{1 + a(\nu - \nu_0)^2},$$

where a is a constant. For a band of this type it is easy to show that the total area is equal to twice the area included between the two points for which κ has half its maximum value, but for the other band shapes
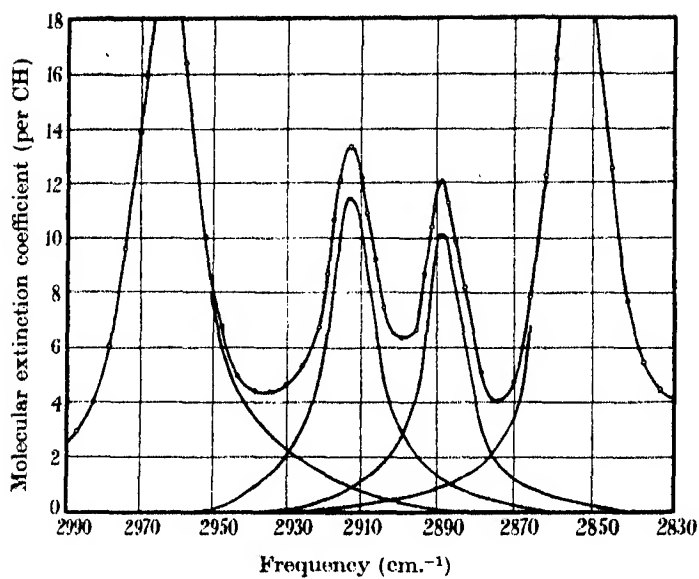
Fig. 1. Graphical separation of CH_2 absorption bands of dioxan.
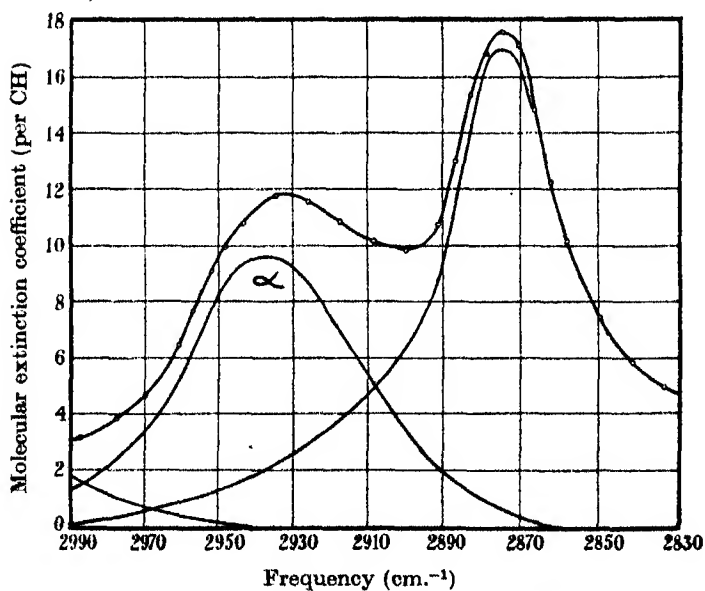
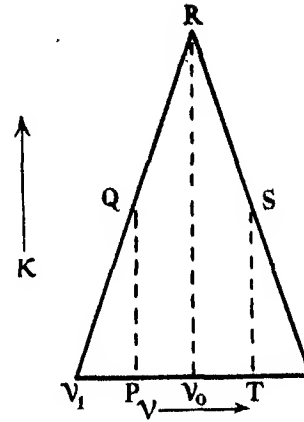Fig. 2. Graphical separation of CH_2 absorption bands of benzyl alcohol.

$$\kappa = \frac{\kappa \max}{1 + a(\nu - \nu_0)^2}; \quad f = QS = \frac{2}{\sqrt{a}}$$

$$\frac{A}{2} = \text{area } PQRST = \frac{\pi}{2\sqrt{a}} \kappa \max$$

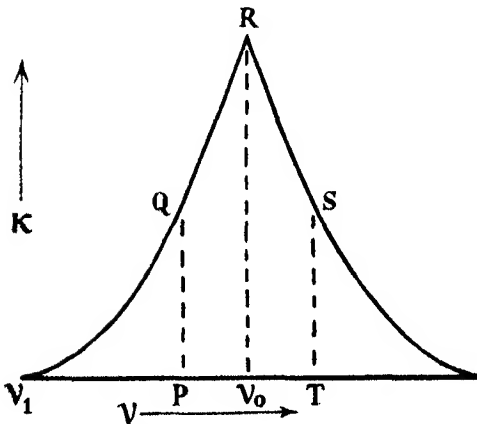$$\frac{A}{f\kappa \max} = \frac{\pi}{2} = 1\cdot571 \text{ and}$$

$$\text{total area} = \frac{\pi}{2} f\kappa \max$$

$$\kappa = \frac{\kappa \max (\nu - \nu_1)}{(\nu_0 - \nu_1)}; \quad f = QS = \nu_0 = \nu_1$$

$$\frac{A}{2} = \text{area } PQRST = \tfrac{3}{4}\kappa \max (\nu_0 - \nu_1)$$

$$\frac{A}{f\kappa \max} = 1\cdot5 \text{ and total area} = f\kappa \max$$

$$\kappa = \frac{\kappa \max (\nu - \nu_1)^2}{(\nu_0 - \nu_1)^2};$$
$$f = QS = (2 - \sqrt{2})(\nu_0 - \nu_1)$$

$$\frac{A}{2} = \text{area } PQRST$$

$$= \frac{1}{3}\left(2 - \frac{1}{\sqrt{2}}\right) \kappa \max (\nu_0 - \nu_1)$$

$$\frac{A}{f\kappa \max} = 1 + \frac{\sqrt{2}}{3} = 1\cdot471 \text{ and}$$
$$\text{total area} = 1\cdot138 f\kappa \max$$
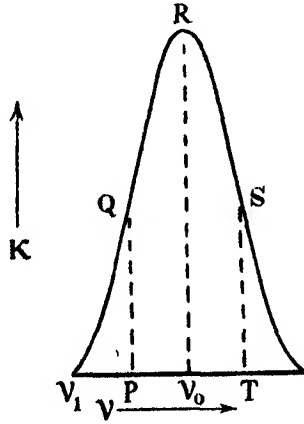
$$\kappa = \kappa \max \sin^2 \frac{\pi}{2}\left(\frac{\nu - \nu_1}{\nu_0 - \nu_1}\right);$$
$$f = QS = \nu_0 - \nu_1$$

$$\frac{A}{2} = \text{area } PQRST$$

$$= \left(\frac{\pi + 2}{2\pi}\right) \kappa \max (\nu_0 - \nu_1)$$

$$\frac{A}{f\kappa \max} = \frac{\pi + 2}{\pi} = 1\cdot637 \text{ and}$$
$$\text{total area} = f\kappa \max$$

Fig. 3. Hypothetical absorption curves.

shown in fig. 3 this is by no means the case. In Tables I, II and III we record values of κ max and f, since these quantities can be measured with fair accuracy. If the area of the band is required, it can be obtained from the relation $cf\kappa$ max = area, where c is a numerical factor dependent on the shape of the band, and as can be seen from fig. 3 may vary between 1 and $\frac{1}{2}\pi$. An examination of some of our own bands which happen to be well separated from others gives values of c close to 1·4, so that the area of any of our bands may be obtained approximately by evaluating the expression 1·4$f\kappa$ max.

Since different compounds are examined at somewhat different molar concentrations, a test experiment was made in which the absorption of a benzene solution was measured first in the short absorption cell and then in the longer one, the concentration being reduced in this case in the ratio of the cell lengths (approximately 6 : 1). The curves obtained are shown in fig. 4, and no difference is observed in percentage absorption or in the positions of the absorption peaks. Small differences in concentration in passing from one compound to another can therefore in general be ignored, except when association occurs. A second experiment was made with the benzene solution heated to 50° C., and again no change in the results was found (fig. 4). This experiment shows that the small changes in room temperature (18–20° C.) arising in the course of the experiments when changing from one compound to another are of no importance, again except for associated substances.

Results

Fig. 5 shows the absorption curves obtained for the compounds benzyl alcohol, diphenyl methane, dibenzyl and cyclohexane in which the CH_2 group is not subject to strain. Two sets of bands will be observed, a group of three intense and some weaker bands in the region of 3·27μ, characteristic of the phenyl group, and a double band about 3·4μ attributable to a CH_2 group or groups. Details of both sets of bands are given in Table I together with relevant details of Raman spectra. Values of the "molecular" extinction coefficients per CH are given for both aromatic and aliphatic CH groups, a CH_2 group for this purpose being regarded as containing two CH units.

Frequencies of the double CH_2 band do not vary much for the four compounds given in Table I, the mean values being 2927 and 2857 cm.$^{-1}$ (about 3·42 and 3·50μ). The band of higher frequency is not strictly single and shows signs of being resolved in diphenyl methane, dibenzyl and cyclohexane. Frequencies and extinction coefficients for these components are given in
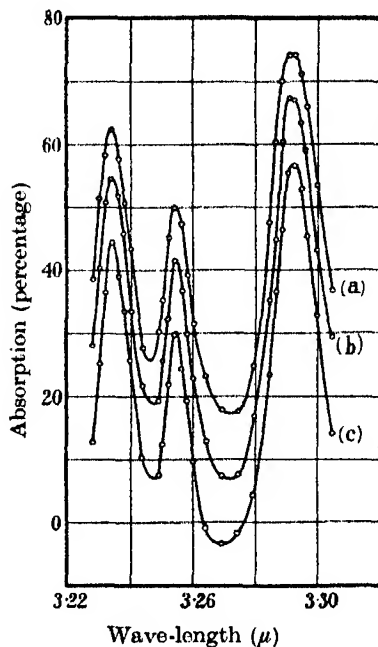
FIG. 4. Absorption of benzene in carbon tetrachloride: (a) 1·74 mm. cell, 50° C., (b) 1·74 mm. cell, 19° C., and (c) 10 mm. cell, 19° C. Curves (b) and (c) are reduced by 10 and 20 % respectively.
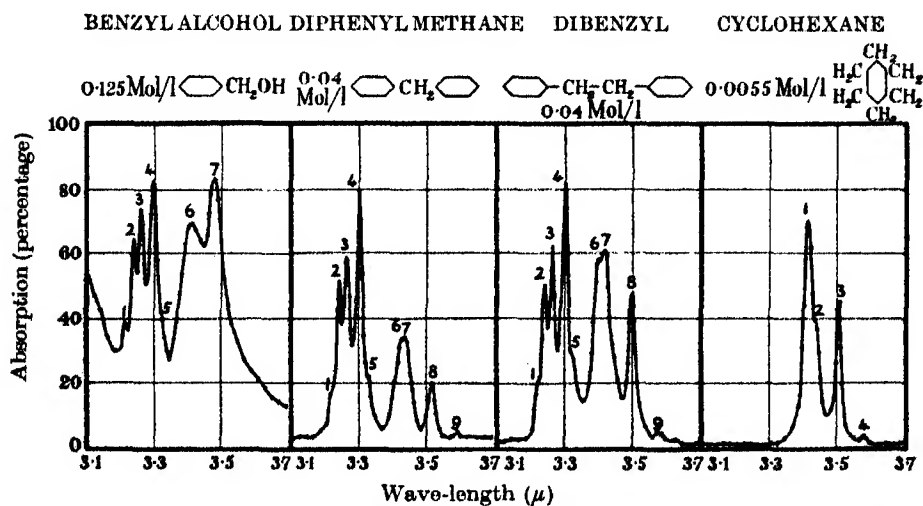

FIG. 5. Absorption in carbon tetrachloride of substances containing CH_2 groups. Cell length 1·74 mm.

Table II; in the subsequent treatment this finer structure will not be considered.

TABLE I. INFRA-RED AND RAMAN CH FREQUENCIES IN THE REGION OF 3000 CM.$^{-1}$

Substance	Band no. in fig. 5	Infra-red frequency (cm.$^{-1}$)	Molecular extinction coefficient (per CH) at band max	Band width, f, at half extinction (cm.$^{-1}$)	Raman frequency (cm.$^{-1}$)	Intensity
Benzyl alcohol	1	3111	0·73	14·6		
	2	3087	3·3	16·2		
	3	3067	3·8	13·3	3050	3
	4	3032	6·8	23·0		
	5	3006	0·29	7·6		
	6	*2937*	9·5	55·0		
	7	*2874*	16·9	38·3		
Diphenyl methane	1	3107	0·68	15·6		
	2	3086	4·0	13·5		
	3	3064	4·8	14·5	3054	4
	4	3029	9·8	15·4		
	5	3002	0·45	6·0		
	6 and 7	*2912*	14·0	—	2909	1
	8	*2844*	7·2	21·6	2855	0
	9	2785	—	—		
Dibenzyl	1	3108	0·47	14·3		
	2	3085	4·0	16·0		
	3	3063	5·2	13·0	3052	4
	4	3028	10·5	15·5		
	5	3003	0·59	11·9		
	6 and 7	*2933*	14·9	—	2928	1
	8	*2857*	11·2	14·9		
	9	2793	—	—		
Cyclohexane					2937	6
	1	*2927*	47·4	21·0	2921	6
					2898	2
					2887	2
	3	*2851*	22·9	13·1	2853	10
	4	2793	—	—		

CH_2 frequencies are given in italic type.

The Raman data are due to the following authors: benzyl alcohol, Kohlrausch (1931); diphenyl methane, Dadieu, Pongratz and Kohlrausch (1931), Crigler (1932), and Donzelot and Chaix (1935), (mean values); dibenzyl, Dadieu, Pongratz and Kohlrausch (1931); cyclohexane, Kohlrausch and Stockmair (1936), and Ananthakrishnan (1936), (mean values).

TABLE II. STRUCTURE OF CH_2 INFRA-RED BAND NEAR 2920 CM.$^{-1}$

Substance	Band no. in fig. 5	Frequency of component (cm.$^{-1}$)	Molecular extinction coefficient (per CH) at band max	Band width, f, at half extinction (cm.$^{-1}$)
Diphenyl methane	6	2919	7·9	42·0
	7	2906	7·9	29·8
Dibenzyl	6	2942	10·4	22·3
	7	2926	11·2	27·7
Cyclohexane	1	2927	47·4	21·0
	2	2904	7·0	14·2
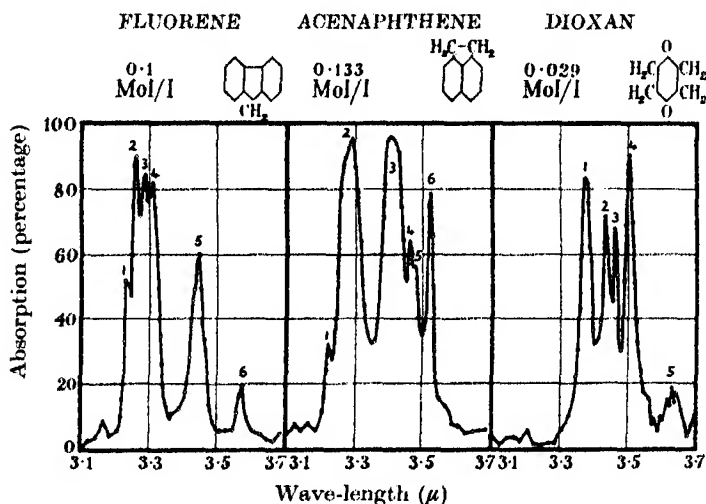
FIG. 6. Absorption in carbon tetrachloride of substances containing CH_2 groups. Cell length 1·74 mm.

Fig. 6 shows the absorption curves obtained for fluorene, acenaphthene and dioxan, where the CH_2 groups are attached to the rest of the molecule in a somewhat different manner from the other four compounds shown in fig. 5. Aromatic bands in the $3·27\mu$ region are still obtained for fluorene and acenaphthene, but the structure is now not so well defined as in compounds containing phenyl groups. Also the CH_2 bands are considerably different, especially for dioxan for which we find four intense bands instead of two as before. Acenaphthene has CH_2 bands intermediate between those for dioxan and the bands shown in fig. 5, for besides the usual pair of strong bands, two weaker ones are also clearly indicated. Fluorene has only two

bands for the CH_2 group but they are greatly altered as regards position and intensity from the normal values in Table I. The details of the various bands are given in Table III together with available Raman data.

From Tables I and III it will be seen that the Raman lines are fewer than the infra-red frequencies, but in most cases for each Raman line there is a corresponding infra-red band within a few cm.$^{-1}$. Generally, in complicated molecules many of the frequencies are likely to be active in both Raman and infra-red. Since, however, highly symmetrical modes of vibration are few, many of the Raman lines may be too weak for recognition.

TABLE III. INFRA-RED AND RAMAN CH FREQUENCIES IN THE REGION OF 3000 CM.$^{-1}$

Substance	Band no. in fig. 6	Infra-red frequency (cm.$^{-1}$)	Molecular extinction coefficient (per CH) at band max	Band width, f, at half extinction (cm.$^{-1}$)	Raman frequency (cm.$^{-1}$)	Intensity
Fluorene	1	3095	1·3	10·9		
	2	3068	6·2	16·0	3064	½
	3	3043	4·1	26·6	3049	2
	4	3019	3·9	19·7		
	5	2901	11·5	32·3	2909	1
					2840	½
	6	2795	2·7	24·5		
Acenaphthene	1	3105	0·52	13·9		
	2	3048	ca. 11	45·6	3058	2
	3	2932	ca. 16	41·3	2924	2
	4	2887	2·9	11·0		
	5	2875	2·2	13·6		
	6	2839	7·2	11·3		
Dioxan					3040	0
	1	2963	20·6	21·7	2965	9
	2	2913	11·5	14·6		
	3	2888	10·1	12·9	2892	4
	4	2854	25·0	17·1	2854	8
	5	2746	—	—		
					2720	3

CH_2 frequencies are given in italic type.

The Raman data are due to the following authors: fluorene and acenaphthene, Manzoni Ansidei (1937); dioxan, Kohlrausch and Stockmair (1936), and Simon and Fehér (1936), (mean values).

Variation of CH *frequency* (3000 cm.$^{-1}$) *in pure liquid, solution and gas.* Dioxan in the liquid and vapour states has recently been investigated in the infra-red by McKinney, Leberknight and Warner (1937) and their

figures are given in Table IV together with those obtained in the present work for comparison. Similar figures are given for benzene, the results for liquid and vapour being due to Leberknight (1933) and for carbon tetrachloride solution, Fox and Martin (1937). For interest a few Raman frequencies taken from collected data by Glockler and Renfrew (1938) for liquid and gaseous ethylene are included. It will be seen that the solution frequencies are in no case more than 3 cm.$^{-1}$ away from the liquid values, but are lower than the vapour frequencies by 10 cm.$^{-1}$ or so. The Raman data for ethylene show about the same difference. We propose to add 6 cm.$^{-1}$ to our measured frequencies in the region of 3000 cm.$^{-1}$ whenever we desire to compare accurately our measurements with gas data and also for calculation of accurate force constants.

TABLE IV. FREQUENCIES ABOUT 3000 CM.$^{-1}$ FOR DIOXAN, BENZENE AND ETHYLENE IN VARIOUS STATES

Vapour	CCl$_4$ solution	Difference from vapour	Liquid	Difference from vapour
		Dioxan—infra-red		
2862	2854	− 8	2854	− 8
2897	2888	− 9	2890	− 7
2920	2913	− 7	2916	− 4
2969	2963	− 6	2960	− 9
		Mean − 7·5		− 7
		Benzene—infra-red		
3099	3093	− 6	3090	− 9
3073	3073	0	3070	− 3
3045	3035	− 10	3032	− 13
		Mean − 5		− 8

Ethylene—Raman

Gas	Liquid	Difference from gas
3272	3264	− 8
3240	3231	− 9
3080(?)	3076	?
3019	3008	− 11
2880	2871	− 9
	Mean	− 9

DISCUSSION

Vibrations of an isolated CH$_2$ *group.* When we consider such a CH$_2$ group we may regard it as possessing three modes of vibration depicted in fig. 7. ν_1 and ν_2 may be taken as essentially CH valency vibrations, out of and in

phase, and will be close to 3000 cm.$^{-1}$, the value associated with such vibrations, while ν_3 is a deformation frequency about 1400 cm.$^{-1}$, i.e. outside the region of the spectrum in which we are at present interested. The CH_2 group can still retain these frequencies when joined to other groups, although in some cases interaction with similar frequencies arising from other parts of the molecule or with harmonics of lower frequencies may modify or increase the number of bands observed.
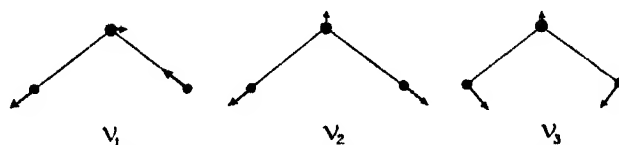

FIG. 7. Modes of vibration of imaginary molecule CH_2.

CH_2 *absorption in compounds shown in figs. 5 and 6.* Our results for benzyl alcohol, diphenyl methane, dibenzyl and cyclohexane (fig. 5) show that CH_2 groups in an ordinary aliphatic straight chain or unstrained ring compound have two intense absorption bands approximately at 3·4 and 3·5μ corresponding to the in and out of phase CH vibrations shown in fig. 7. When, however, the CH_2 group forms part of a strained ring, the two bands occur with somewhat changed frequencies so long as only one CH_2 group is present in the molecule, e.g. fluorene (fig. 6). With two CH_2 groups in a slightly strained condition, acenaphthene (fig. 6), the two normal bands are accompanied by two weaker ones at intermediate frequencies. In dioxan, presumably due to the presence of the oxygen atoms, this effect becomes even more pronounced, four intense and well-separated bands being obtained.

Vibrations of the ethylene molecule. This molecule provides an interesting case of two CH_2 groups coupled together, through the double bond, and we have found it particularly useful in this discussion, because it has been considered theoretically by several workers including Mecke (1932), Sutherland and Dennison (1935), Teller and Topley (1935), Bonner (1936), Manneback and Verleysen (1936, 1937), and Thompson and Linnett (1937). A consideration of the methods used successfully for ethylene and other simple molecules enables us to consider the case of CH_2 groups in more complicated molecules. Ethylene has nine planar vibrations (figs. 8 and 9), seven of which are assigned as follows:

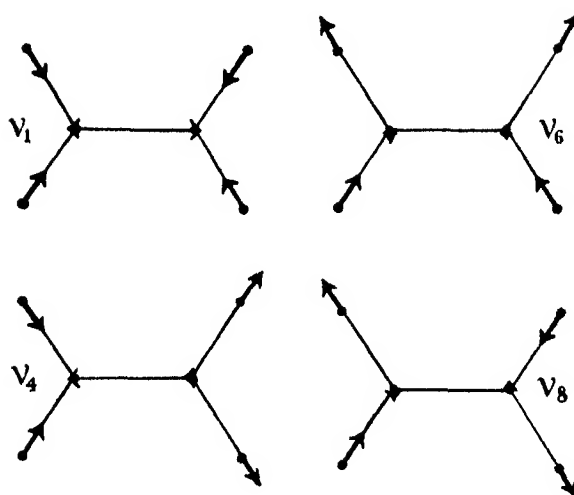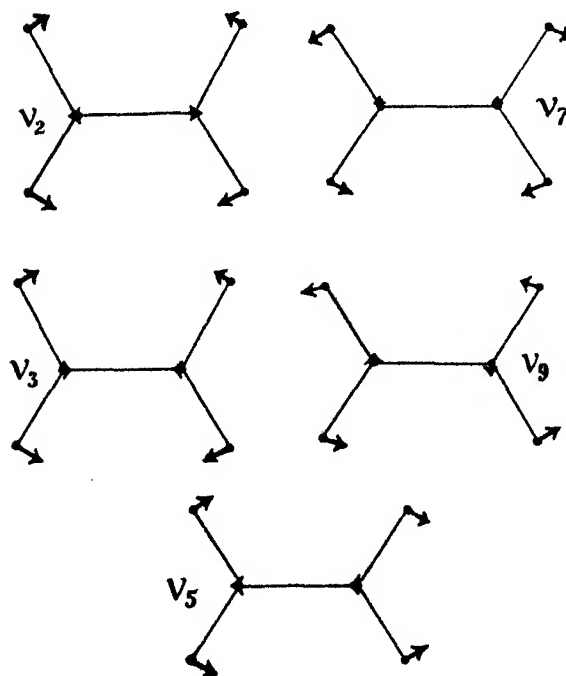|	ν_1	ν_2	ν_3	ν_4	ν_5	ν_6	ν_7
cm.$^{-1}$	3019	1623	1342	2988	1444	3107	950

FIG. 8. CH valency vibrations of ethylene.

FIG. 9. Angular deformation vibrations of ethylene.

The remaining frequencies ν_8 and ν_9 have not been so satisfactorily identified.

Calculation of force constants from ethylene vibrations ν_1 to ν_7. Thompson and Linnett (1937) find that a potential function with only five constants is adequate to reproduce the seven accurately known frequencies. We considered it advisable, however, before attempting to apply the results to more complex molecules, to examine the effect of introducing a further cross term of the type suggested by Thompson and Linnett in the potential function, namely, a term denoting interaction between two CH bonds of the same CH_2 group, since this type of interaction is important in many simple linear molecules, and if of any considerable magnitude will affect the value of the C—H force constant, a magnitude which we are particularly interested in.
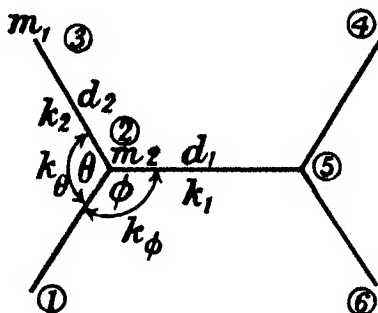
Fig. 10

In fig. 10 we have retained the nomenclature of Thompson and Linnett for the constants of the ethylene molecule. k_1 and k_2 are the stretching constants of the C=C and C—H bonds, and k_θ and k_ϕ the deformation constants of the respective angles.

Introducing two cross-terms into the potential function, $2k_3 \Delta_{25} \Delta\theta$ for the interaction between θ and the bond C=C and $2k_4 \Delta_{12} \Delta_{23}$ for the interaction between the two CH bonds of the same CH_2 group, we have

$$2V = k_1 \Delta_{25}^2 + 4k_2 \Delta_{12}^2 + 2k_\theta \Delta\theta^2 + 4k_\phi \Delta\phi^2 + 2k_3 \Delta_{25} \Delta\theta + 2k_4 \Delta_{12} \Delta_{23}.$$

For the vibrations ν_1 to ν_5 (figs. 8 and 9) assigned by Thompson and Linnett $\Delta_{12} = \Delta_{23}$, so that the term $4k_2 \Delta_{12}^2$ in the potential function (used by these authors) now becomes $4\Delta_{12}^2(k_2 + \frac{1}{2}k_4)$. The quantity $(k_2 + \frac{1}{2}k_4)$ will be denoted by k_2'. For the remaining vibrations ν_6 to ν_9 $\Delta_{12} = -\Delta_{23}$, so that the term

$4k_2\Delta_{12}^2$ now becomes $4\Delta_{12}^2(k_2 - \tfrac{1}{2}k_4)$ and in this case we shall write k_2'' for $(k_2 - \tfrac{1}{2}k_4)$. The appropriate equations can now be written

$$\nu_1^2 + \nu_2^2 + \nu_3^2 \qquad = k_2' P + k_1 R + kQ - k_3' W \qquad\qquad = \alpha, \tag{1}$$

$$\nu_1^2 \nu_2^2 + \nu_2^2 \nu_3^2 + \nu_1^2 \nu_3^2 = k_1 k_2' U + k_1 kU + k_2' kS - k_2' k_3' W/m_1 - k_3'^2 U = \beta, \tag{2}$$

$$\nu_1^2 \nu_2^2 \nu_3^2 \qquad = k_1 k_2' kU/m_1 - k_2' k_3'^2 U/m_1 \qquad\qquad = \gamma, \tag{3}$$

$$\nu_4^2 + \nu_5^2 \qquad = k_2' P + kQ \qquad\qquad\qquad\qquad = a, \tag{4}$$

$$\nu_4^2 \nu_5^2 \qquad = k_2' kS \qquad\qquad\qquad\qquad\qquad = b, \tag{5}$$

$$\nu_6^2 + \nu_7^2 \qquad = k_2'' Q + k_0 P \qquad\qquad\qquad\qquad = c, \tag{6}$$

$$\nu_6^2 \nu_7^2 \qquad = k_2'' k_0 S \qquad\qquad\qquad\qquad\qquad = d, \tag{7}$$

$$\nu_8^2 + \nu_9^2 \qquad = k_2'' Q + k_0 (d_2^2/d_1^2) 4R + k_0 P + k_0 (d_2/d_1) T, \tag{8}$$

$$\nu_8^2 \nu_9^2 \qquad = k_2'' k_0 (d_2^2/d_1^2) 4R/m_1 + k_2'' k_0 S + k_2'' k_0 (d_2/d_1) T/m_1, \tag{9}$$

where $\quad P = (1/m_1 + 2\cos^2 \tfrac{1}{2}\theta/m_2), \qquad Q = (1/m_1 + 2\sin^2 \tfrac{1}{2}\theta/m_2),$

$\qquad\qquad R = 2/m_2, \qquad\qquad\qquad\qquad S = \{(1/m_1)(1/m_1 + 2/m_2)\},$

$\qquad\qquad T = 8\cos \tfrac{1}{2}\theta/m_2, \qquad\qquad\qquad U = 2/m_1 m_2,$

$\qquad\qquad W = 4\sin \tfrac{1}{2}\theta/m_2, \qquad\qquad\qquad k = (2k_\theta + k_\phi)/d_2^2,$

$\qquad\qquad k_0 = k_\phi/d_2^2, \qquad\text{and}\qquad k_3' = k_3/d_2.$

In these equations ν_1 to ν_9 are not observed frequencies in cm.$^{-1}$ but really angular velocities; they are obtained from the observed frequencies by multiplying by the factor $2\pi c$, c being the velocity of light; the force constants k_1, k_2', k_2'', k, k_0, and k_3' are measured in dynes/cm.

From equations (2) and (3) we have

$$k_1 k_2' U + k_1 kU + k_2' kS - k_2' k_3' W/m_1 - (k_1 k_2' kU - \gamma m_1)/k_2' = \beta.$$

Thus $\qquad\qquad k_1 k_2' U + k_2' kS - k_2' k_3' W/m_1 + \gamma m_1/k_2' = \beta,$

i.e. $\qquad\qquad k_2'(k_1 R/m_1 - k_3' W/m_1) + k_2' kS + \gamma m_1/k_2' = \beta.$

Also from (1) $\qquad\qquad k_1 R - k_3' W = \alpha - k_2' P - kQ,$

and making use of equations (4) and (5) we obtain the relation

$$\left(\frac{k_2'}{m_1}\right)^2 - \left(\frac{\beta - b}{\alpha - a}\right)\frac{k_2'}{m_1} + \left(\frac{\gamma}{\alpha - a}\right) = 0.$$

The constants in this equation, apart from m_1, are all obtained from observed frequencies, so that k_2' can be found without requiring any knowledge of the HCH angle, C—H distance or C=C distance in the ethylene molecule. k_2' is found to be $4 \cdot 984 \times 10^5$ dynes/cm. and we can now calculate k

from equation (5), and substituting for k_2' and k in equation (4) obtain a relation between P and Q; but $P + Q = 2(1/m_1 + 1/m_2)$, so that both P and Q can be found. The value of θ can now be obtained since $Q = 1/m_1 + \dfrac{2\sin^2\frac{1}{2}\theta}{m_2}$; it is 110° 23′.* This angle is somewhat different from 118° given by Penney (1937), but it is very sensitive to small changes in the value of k_2', an increase of 0·2 % in this constant increasing θ by 1·5°. k_2'' and k_0 can now be calculated from equations (6) and (7), the values being $5·11 \times 10^5$ and $0·508 \times 10^5$ dynes/cm. Since $k_2' = k_2 + \frac{1}{2}k_4$ and $k_2'' = k_2 - \frac{1}{2}k_4$, we have $k_2 = 5·05 \times 10^5$ and $k_4 = -0·126 \times 10^5$ dynes/cm. The error in the value of θ calculated above, assuming 118° to be the correct angle, would indicate an error of about $0·05 \times 10^5$ in the value of k_2' found from equations (1)–(5), and since $\frac{1}{2}k_4$ is found to be only $-0·06 \times 10^5$, it is impossible to say whether k_4 has real significance, i.e. whether there is any measurable interaction between the CH units of one CH_2 group.

Since we may now without loss of accuracy consider k_4 as zero, we again have the seven equations (1)–(7), but as $k_2 = k_2' = k_2''$ there are only six constants including θ. As already shown k_2 can be calculated from equations (1)–(5) using only observed frequencies and a value for m_1, while a second value can be obtained from equations (4)–(7) which yield the quartic

$$k_2^4 - \left(\frac{a+c}{P+Q}\right)k_2^3 + \frac{ad+bc}{S(P+Q)}k_2 - \frac{bd}{S^2} = 0,$$

where $P + Q = 2(1/m_1 + 1/m_2)$. The constants in this equation depend on observed frequencies, together with the masses m_1 and m_2. These two different methods of calculating k_2 give the values respectively 4·984 and $5·051 \times 10^5$ dynes/cm. The mean value $5·02 \times 10^5$ is as good as we can expect to get from the available data. The method of calculation here displayed has the advantage that no dimensions or angles of the ethylene molecule are required, and the accuracy of the value obtained for k_2 is dependent solely on the accuracy of the observed frequencies which, it must be noted, are uncorrected for anharmonicity. This correction may rise to about 5 %, but since all the frequencies are subject to this error to a greater or less extent, force constants calculated for a given linkage in different molecules may be relatively accurate to about 1 %. This is indicated by agreement of the two values of k_2 above to within nearly 1 %. It will be noted that the value of k_2 ($5·02 \times 10^5$) is but little different from the value of $5·05 \times 10^5$ obtained when k_4 was included.

* It is interesting to note that Pauling and Brockway (1937) gave for θ 110° ± 5°.

Ethylene vibrations ν_8 and ν_9. Substituting for k_2'' and k_0 in equations (8) and (9), and using the dimensions of the ethylene molecule derived by Penney (1937), the frequencies ν_8 and ν_9 are found to be 3119 and 1214 cm.$^{-1}$ respectively, quite close to those given by Thompson and Linnett. It can be seen from equations (1)–(9) that these frequencies alone require a knowledge of the distances d_1 and d_2 or rather their ratio d_2/d_1, and we now proceed to show that the frequencies calculated above are not sensitive to the value taken. If we eliminate d_2/d_1 between equations (8) and (9), and make use of (6) and (7), we find $\nu_8^2 \nu_9^2 = d + \dfrac{k_2}{m_1}(\nu_8^2 + \nu_9^2 - c)$, where $k_2 = k_2''$ and c and d depend only on observed frequencies which are known fairly accurately. In this equation ν_8 is very insensitive to the value of ν_9 as shown below, using $k_2 = 5 \cdot 02 \times 10^5$:

ν_9	0	500	1000	1500
ν_8	3087	3092	3109	3146

The value of 3119 already calculated thus seems to be quite a reasonable value, and further, the following considerations show that ν_8 must be very nearly equal to ν_6, the observed value of which is 3107 cm.$^{-1}$. In ν_1 and ν_4 (fig. 8) we have the CH vibrations of each CH$_2$ group in phase (as in ν_2 of fig. 7), but the CH$_2$ groups themselves are in phase for ν_1 and out of phase for ν_4, the coupling being provided by the large force constant k_1. The frequency difference is, however, small, about 30 cm.$^{-1}$, and the corresponding difference between ν_6 and ν_8 should be even smaller, as in this case we have the CH vibrations of each group out of phase (as in ν_1 of fig. 7), while the CH$_2$ groups are now coupled by means of the relatively weak force constant κ_ϕ. There is an observed frequency which can reasonably be assigned to ν_8. Several investigators have observed a Raman line with about the right frequency, but only one value, 3080 cm.$^{-1}$, due to Daure (1929), has been given for the gas. For the liquid we have the following values: 3069 cm.$^{-1}$, Bonner (1936); 3082 cm.$^{-1}$, Hemptinne, Jungers and Delfosse (1937); 3076 cm.$^{-1}$, Glockler and Renfrew (1938). By comparison with other more accurately known lines (Table IV) it appears that the liquid value is likely to be about 10 cm.$^{-1}$ lower than for the gas, so that 3086 cm.$^{-1}$ is a probable value for ν_8 and may be compared with the calculated value 3119 cm.$^{-1}$ which, however, is certainly too high, since it was calculated from the rather high value of $5 \cdot 11 \times 10^5$ dynes/cm. for k_2''. ν_9 must also be close to the value calculated, since it is insensitive to possible errors in the ratio d_2/d_1. For example, in the extreme case if d_2/d_1 is put equal to zero in equation (9) we have $\nu_8^2 \nu_9^2 = d$, and taking $\nu_8 = 3100$ we find ν_9 is only reduced to 952 from the

calculated value 1214 (vide supra). Professor Manneback in discussion with us has put forward reasons for supposing that the weak Raman frequency 942 cm.$^{-1}$ is to be identified with ν_9, but the foregoing calculation does not accord with this. Further, from equations (7) and (9) we see that

$$\nu_8^2 \nu_9^2 = \nu_6^2 \nu_7^2 \left[1 + \frac{8m_1}{2m_1 + m_2} \cdot \frac{d_2}{d_1} \left(\frac{d_2}{d_1} + \cos \tfrac{1}{2}\theta \right) \right],$$

and taking the values $\nu_6 = 3107$, $\nu_7 = 950$, $\nu_8 = 3086$ cm.$^{-1}$, $\theta = 118°$ and $d_2/d_1 = 0.81$, we find $\nu_9 = 1216$ cm.$^{-1}$, in good agreement with the value previously calculated. Equations (6) and (8) also show that ν_9 is greater than ν_7 (950 cm.$^{-1}$), since ν_8 is smaller than ν_6 and $\nu_8^2 + \nu_9^2 = \nu_6^2 + \nu_7^2 +$ additional terms. We would assign the observed frequency 942 cm.$^{-1}$ to the Raman frequency out of the plane.

Values for the frequencies of an isolated CH_2 *group.* The frequencies ν_1, ν_4, ν_8, and ν_8 of ethylene are the only ones in the region of 3000 cm.$^{-1}$, and it will be seen from fig. 8 that they are all essentially valency vibrations. The two frequencies ν_1 and ν_8 are Raman active and the other two infra-red active, but in general where two CH_2 groups are coupled in a complicated molecule of low symmetry all four frequencies will be infra-red active, and in fact, in such a molecule as acenaphthene four frequencies are observed (fig. 6), although it must be borne in mind that the coupling between the CH_2 groups in this case is different from that obtaining in ethylene.

From fig. 8 it can be seen that all four vibrations can be obtained by combining the frequencies ν_1 and ν_2 of fig. 7, in and out of phase. We can obtain the frequencies of the isolated CH_2 group from the equations derived for ethylene by making k_1, k_3' and k_4 all zero. We then have

$$\nu_1^2 + \nu_2^2 + \nu_3^2 \qquad = \nu_4^2 + \nu_5^2 = k_2 P + kQ,$$

$$\nu_1^2 \nu_2^2 + \nu_2^2 \nu_3^2 + \nu_1^2 \nu_3^2 = \nu_4^2 \nu_5^2 \quad = k_2 kS,$$

$$\nu_6^2 + \nu_7^2 \qquad = \nu_8^2 + \nu_9^2 = k_2 Q,$$

$$\nu_1^2 \nu_2^2 \nu_3^2 \qquad = \nu_6^2 \nu_7^2 \quad = \nu_8^2 \nu_9^2 = 0.$$

It is easy to see from fig. 9 that for this case ν_3, ν_7 and $\nu_9 = 0$. We then have

$$\nu_1^2 + \nu_2^2 = \nu_4^2 + \nu_5^2 = k_2 P + kQ,$$

$$\nu_1^2 \nu_2^2 \quad = \nu_4^2 \nu_5^2 \quad = k_2 kS,$$

and $$\nu_6^2 \quad = \nu_8^2 \quad = k_2 Q.$$

Clearly, $\nu_4 = \nu_1$ and $\nu_5 = \nu_2$ so that only three independent frequencies remain. These we will call ν_1, ν_2 and ν_3, as shown in fig. 7. Since k_ϕ is 0, k in the equations above is to be identified with $k - k_0$ of equations (1)–(9), and using equations (5) and (7) we have for the CH_2 group of fig. 7

$$\nu_2^2 \nu_3^2 = b - d,$$

$$\nu_2^2 + \nu_3^2 = k_2 P + \frac{b-d}{k_2 S} Q,$$

and

$$\nu_1^2 = k_2 Q.$$

Adopting the value of $5 \cdot 02 \times 10^5$ dynes/cm. for k_2 and taking θ as $118°$ (for P and Q), we find

$$\nu_1 = 3092, \quad \nu_2 = 2983, \quad \nu_3 = 1055.$$

Previous estimates of these frequencies have been given by Sutherland and Dennison (1935) and Ta-You Wu (1937). The value for ν_1 is between the ethylene frequencies ν_6 (3107) and ν_8 (3086) as is to be expected, since these vibrations consist of CH_2 units vibrating as in ν_1 of fig. 7, loosely coupled in and out of phase.

The valency vibrations ν_1 and ν_2 are about 150 cm.$^{-1}$ higher in frequency than those observed by us for CH_2 groups in molecules (Table I), but this is not surprising when we remember that the angle HCH in our compounds is probably close to $109°$ instead of $118°$ and that the corresponding k_θ will be different. Another difference is that the CH_2 group is connected by single bonds to other carbon atoms or to oxygen.

CH_2 *groups in complex molecules.* In the compounds here discussed, except dioxan and benzyl alcohol, the carbon atom of the CH_2 group is attached by single bonds to two other carbon atoms, all the bonds being considered as disposed approximately tetrahedrally. The centre of gravity of these two carbon atoms is at P, fig. 11, and the planes HCH and CCC are at right angles to each other. P is in the same plane as the CH_2 group, being situated on the bisector of the angle HCH. To a first approximation our compounds can be represented by the model shown in fig. 12, where, however, the mass m_3 and its distance from m_2 are not known exactly. It will be shown that quite big changes in these values have but little effect on the CH frequencies, and this justifies our procedure. A molecule of the kind depicted in fig. 12 has five planar vibration frequencies, two of which ν_1 and ν_4 will be in the region of 3000 cm.$^{-1}$. Assuming for this type of molecule a potential function

$$2V = k_1 \Delta_{34}^2 + 2k_2 \Delta_{12}^2 + k_\theta \Delta\theta^2 + 2k_\phi \Delta\phi^2 + k_2 \Delta_{24} \Delta\theta,$$

where $k_3 \Delta_{24} \Delta\theta$ denotes an interaction between θ and the linkage m_2—m_3, while the other constants are indicated in fig. 12, equations connecting the
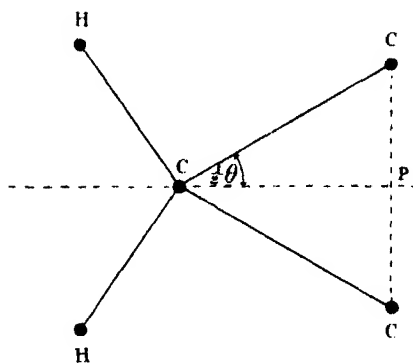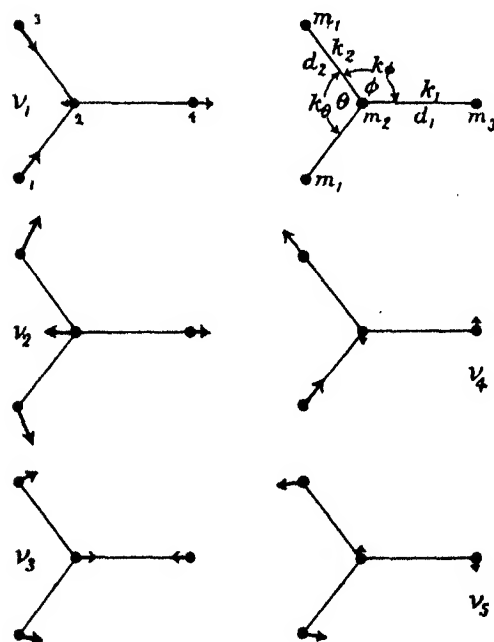

FIG. 11

FIG. 12. Planar vibrations of a formaldehyde type molecule.

frequencies of vibration with the various constants of the molecule can be derived. These equations have been given in a form suitable for our use by

Thompson and Linnett (1937), but as some omissions have been made, we have derived these equations independently and give them as follows:

$$\nu_1^2 + \nu_2^2 + \nu_3^2 \qquad = k_1 A + k_2 B + kC/d_2^2 - k_3 D/d_2, \tag{10}$$

$$\nu_1^2\nu_2^2 + \nu_2^2\nu_3^2 + \nu_1^2\nu_3^2 = k_1 k_2 E + k_1 kF/d_2^2 + k_2 kG/d_2^2 - k_2 k_3 D/d_2 m_1 - k_3^2 F/2d_2^2, \tag{11}$$

$$\nu_1^2\nu_2^2\nu_3^2 \qquad = k_1 k_2 kH/d_2^2 - \tfrac{1}{2}k_2 k_3^2 H/d_2^2, \tag{12}$$

$$\nu_4^2 + \nu_5^2 \qquad = k_2 C + k_\phi B/d_2^2 + 2k_\phi A/d_1^2 + k_\phi J/d_1 d_2, \tag{13}$$

$$\nu_4^2\nu_5^2 \qquad = k_2 k_\phi G/d_2^2 + 2k_2 k_\phi F/d_1^2 + k_2 k_\phi J/d_1 d_2 m_1, \tag{14}$$

where $A = 1/m_2 + 1/m_3,$ $\qquad B = 1/m_1 + 2\cos^2 \tfrac{1}{2}\theta/m_2,$

$\qquad D = 2\sin \tfrac{1}{2}\theta/m_2,$ $\qquad C = 1/m_1 + 2\sin^2 \tfrac{1}{2}\theta/m_2,$

$\qquad E = 1/m_1(1/m_2 + 1/m_3) + 2\cos^2 \tfrac{1}{2}\theta/m_2 m_3,$

$\qquad F = 1/m_1(1/m_2 + 1/m_3) + 2\sin^2 \tfrac{1}{2}\theta/m_2 m_3,$

$\qquad G = 1/m_1^2 + 2/m_1 m_2,$ $\qquad H = \left\{ \dfrac{2}{m_1 m_2 m_3} + \dfrac{m_2 + m_3}{m_1^2 m_2 m_3} \right\},$

$\qquad J = 4\cos \tfrac{1}{2}\theta/m_2,$ and $\qquad k = (2k_\theta + k_\phi).$

CH *force constant calculated from the observed value of one of the* CH *valency vibrations,* ν_4, *in a formaldehyde type molecule.* It will be seen from equations (13) and (14) that ν_4 and ν_5 depend only on k_2 and k_ϕ. We shall first assume that k_2 has the value found for CH in ethylene, i.e. 5×10^5 dynes/cm. very nearly, and try various values of k_ϕ of the order found by Thompson and Linnett for other compounds (0.59×10^{-11} for ethylene and 0.93×10^{-11} for formaldehyde). The distance C—H is taken to be 1.09 A (see p. 280), this value being close to that found for methane and ethylene. The distance d_1 is not greatly different from d_2 and for convenience is taken equal to it. In any case d_1 only occurs in equations (13) and (14) and these are very insensitive to changes in d_1. The values for ν_4 and ν_5 calculated for different values of k_ϕ and of m_3 are given in Table V and it will be seen that for large changes in the values of these constants ν_4 only varies between 3070 and 3083 cm.$^{-1}$, even in the extreme cases when $m_3 = 0$ or ∞. This frequency is however much higher than the value observed by us 2927 (Table I) and the explanation is that k_2 is less than 5×10^5 found for ethylene and should have a value close to 4.50×10^5 dynes/cm. This value of k_2 has been calculated from equations (13) and (14) assuming that $\nu_4 = 2927$, $k_\phi = 1 \times 10^{-11}$ dyne cm./ radian, and $m_3 = 2m_2$. The reduction of k_2 for the CH$_2$ group in the compounds examined, as compared with ethylene, may be due to the closer approach of the H atoms as θ is reduced from 118 to 109°, but more probably

arises from the fact that the carbon atom of the CH_2 group is connected to the rest of the molecule by single bonds instead of the double bond of ethylene. It is significant that if the carbon atom is attached by a triple bond as in acetylene, the C—H bond constant increases to 5.88×10^5 dynes/cm. (Colby (1935) gave 5.85; recalculating we find 5.88), so that the values for single, double and triple bonds are in ascending order of magnitude.

TABLE V. VALUES OF ν_4 AND ν_5 CALCULATED FROM EQUATIONS (13) AND (14) FOR DIFFERENT VALUES OF THE FORCE CONSTANT k_ϕ AND THE MASS m_3 ATTACHED TO THE CH_2 GROUP IN THE FORMALDEHYDE-LIKE MOLECULE OF FIG. 12

k_ϕ (10^{-11} dyne cm./radian)	m_3	ν_4 (cm.$^{-1}$)	ν_5 (cm.$^{-1}$)
Any finite value	0	3070	∞
1	m_1	3083	1478
1	$2m_1$	3083	1438
1	∞	3083	1396
0	Any finite value	3070	0
0.5	m_1	3076	1048
0.5	$2m_1$	3076	1019
0.5	∞	3076	989

k_2 is taken as 5×10^5 dynes/cm. and $d_1 = d_2 = 1.09$ A.

Calculation of the CH *valency vibration* ν_1. Having calculated k_2 from one of the known frequencies of the CH_2 group, we should be able to find the value of the other frequency and compare it with the measured value. We can obtain ν_1, ν_2 and ν_3 from equations (10)–(12) if we assume likely values for the constants involved, and as before we can see just how sensitive these frequencies are to the values chosen for the constants. The results obtained are shown in Table VI and it will be seen that ν_1 comes out close to the observed frequency 2857 cm.$^{-1}$ provided that a value about 10×10^5 dynes/cm. is chosen for k_1, although it is not very sensitive to changes in the value of this constant. The other constants including mass m_3 have scarcely any effect on the value of ν_1. An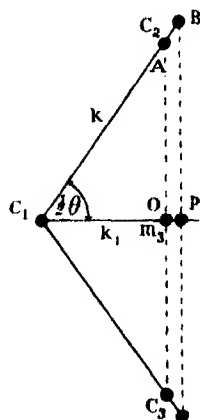 independent rough estimate of k_1 is obtained as follows: If C_1 is the carbon atom of the CH_2 group, fig. 13, while C_2

Fig. 13

and C_3 are the carbon atoms to which it is attached, and C_2 and C_3 are moved equally by the small distance AB, then restoring forces $k \cdot AB$ will act on

C_2 and C_3 towards C_1, where k is the force constant for the C—C bond and may be taken as $4\cdot0 \times 10^5$ dynes/cm. These two forces will be equivalent to $2kAB\cos\frac{1}{2}\theta$ acting in the direction PO, and this force may also be regarded as due to the movement of m_3 from O to P, so that $2kAB\cos\frac{1}{2}\theta = k_1 OP = k_1 AB\cos\frac{1}{2}\theta$. Thus $k_1 = 2k = 8\cdot0 \times 10^5$ dynes/cm., and this value is of the magnitude required for the correct value of ν_1 as shown in Table VI.

TABLE VI. VALUES OF ν_1, ν_2 AND ν_3 CALCULATED FROM EQUATIONS (10), (11) AND (12) FOR DIFFERENT VALUES OF THE FORCE CONSTANTS k_1, $2k_\theta + k_\phi$, k_3, AND THE MASS m_3 ATTACHED TO THE CH_2 GROUP IN THE FORMALDEHYDE-LIKE MOLECULE OF FIG. 12

k_1 (10^5 dynes/ cm.)	$2k_\theta + k_\phi$ 10^{-11} dyne cm./radian	k_3 (10^{-3})	m_3	ν_1 (cm.$^{-1}$)	ν_2 (cm.$^{-1}$)	ν_3 (cm.$^{-1}$)
10	1	1	m_2	2857	1620	1221
20	1	1	m_2	2909	2272	1225
10	2	1	m_2	2861	1758	1610
10	1	1	∞	2854	1090	1234
10	1	0	m_2	2861	1696	1194
10	1	1	$2m_2$	2855	1391	1216

Mean observed value for ν_1 is 2857.

k_2 is taken as $4\cdot50 \times 10^5$ dynes/cm. and $d_2 = 1\cdot09$ A. The value taken for d_2 is unimportant, since $2k_\theta + k_\phi$ and d_2 always occur together as $\dfrac{2k_\theta + k_\phi}{d_2^2}$ and k_3 and d_2 always occur together as k_3/d_2.

The possibility of there being a cross term in the potential function for a formaldehyde-like molecule arising from an interaction between the two C—H bonds of a CH_2 group as considered above for ethylene should not be forgotten. It would have the effect of making k_2 slightly different for the two sets of frequencies, ν_1, ν_2 and ν_3 (symmetrical) and ν_4 and ν_5 (antisymmetrical). Our calculations show, however, that this effect, if it exists at all, must be small. As we have demonstrated for ethylene that the effect of such a cross term on the C—H force constant was negligible, we propose to ignore it in this case too.

Relation between CH force constant and internuclear distance. It becomes apparent that the force constant for the CH linkage depends to some considerable extent on the manner in which the carbon atom is attached to the rest of the molecule. Knowing the force constant for this linkage with considerable accuracy for acetylene ($5\cdot88 \times 10^5$), ethylene ($5\cdot02 \times 10^5$), and the CH_2 groups investigated in this communication ($4\cdot52 \times 10^5$ dynes/cm. after allowing for small frequency shift in passing from solution to vapour), we

may calculate the CH distances from a relation of the type given by Morse (1929) and Clark (1935), namely, $r = 9\cdot63/(k)^{\frac{1}{4}}$, where r is the C—H distance in A, and k the force constant in dynes/cm. We may compare with the values obtained from the fine structure of infra-red bands: acetylene, Herzberg, Patat, and Spinks (1934); ethylene, Penney (1937) from infra-red data of Badger (1934); methane, Ginsburg and Barker (1935). The chief point of interest in this comparison made below is the closeness of the C—H distance calculated from the CH_2 group to the value observed in methane:

	C_2H_2	C_2H_4	$>CH_2$
C—H distance from fine structure	1·057 A	1·08 A	1·093 A (CH_4)
C—H distance calculated from force constant	1·052	1·080	1·099

We desire to thank Mr F. S. Benge of the Government laboratory for his valuable assistance throughout the course of the investigation.

SUMMARY

The absorption of seven substances containing CH_2 groups has been investigated in the region of 3μ. Besides the aromatic CH bands found about $3\cdot27\mu$ when a benzene ring is present, two or more bands near $3\cdot4\mu$ are attributable to the CH_2 groups.

A critical survey of the data available for ethylene enables us to explain the bands observed for CH_2 groups in more complicated molecules. When only one CH_2 group is contained in the molecule, two bands are observed and these are identified as the CH valency vibrations in and out of phase; but when the number of CH_2 groups is increased, the coupling between them may increase the number of bands as in dioxan, for example, where four strong bands are observed.

A satisfactory approximation to the molecules studied by us is found in a model of the formaldehyde type in which the CH_2 group is attached to a mass of similar magnitude. This model enables us to explain the observed frequencies provided that the CH force constant is $4\cdot52 \times 10^5$ dynes/cm., a value considerably lower than $5\cdot02 \times 10^5$ for ethylene and $5\cdot88 \times 10^5$ for acetylene. The important result is obtained that the mass to which the CH_2 group is attached and the various other force constants involved in compounds of the type investigated have very little effect on the positions of the CH_2 absorption bands in the 3μ region, except in rare cases involving strain of the bonds connecting the CH_2 groups to the rest of the molecule, e.g. fluorene.

REFERENCES

Ananthakrishnan, R. 1936 *Proc. Ind. Acad. Sci.* A, 3, 52.

Badger, R. M. 1934 *Phys. Rev.* 45, 648.

Bonino, G. B. 1929 Faraday Soc. General Discussion, p. 879.

Bonner, L. G. 1936 *J. Amer. Chem. Soc.* 58, 34.

Borst, L. B., Buswell, A. M. and Rodebush, W. H. 1938 *J. Chem. Phys.* 6, 61.

Clark, C. H. D. 1935 *Phil. Mag.* 19, 476.

Coblentz, W. W. 1905 "Investigations of Infra-red Spectra," part 1.

Colby, W. F. 1935 *Phys. Rev.* 47, 388.

Crigler, E. A. 1932 *J. Amer. Chem. Soc.* 54, 4199.

Dadieu, A., Pongratz, A. and Kohlrausch, K. W. F. 1931 *S.B. Akad. Wiss. Wien*, 140, 647.

Daure, P. 1929 *Ann. Phys., Paris*, 12, 375.

Donzelot, P. and Chaix, M. 1935 *C.R. Acad. Sci., Paris*, 201, 501.

Fox, J. J. and Martin, A. E. 1937 *Proc. Roy. Soc.* A, 162, 419.

Ginsburg, N. and Barker, E. F. 1935 *J. Chem. Phys.* 3, 668.

Glockler, G. and Renfrew, M. M. 1938 *J. Chem. Phys.* 6, 170.

Hemptinne, M., Jungers, J. C. and Delfosse, J. M. 1937 *Nature, Lond.*, 140, 323.

Herzberg, G., Patat, F. and Spinks, J. W. T. 1934 *Z. Phys.* 92, 87.

Kinsey, E. L. and Ellis, J. W. 1937 *Phys. Rev.* 51, 1074.

Kohlrausch, K. W. F. 1931 "Der Smekal-Raman Effekt", p. 331.

Kohlrausch, K. W. F. and Stockmair, W. 1936 *Z. phys. Chem.* B, 31, 382.

Leberknight, C. E. 1933 *Phys. Rev.* 43, 967.

Leberknight, C. E. and Ord, J. A. 1937 *Phys. Rev.* 51, 430.

McKinney, D. S., Leberknight, C. E. and Warner, J. C. 1937 *J. Amer. Chem. Soc.* 59, 481.

Manneback, C. and Verleysen, A. 1936 *Ann. Soc. Sci. Bruxelles*, 56, 349.

Manzoni Ansidei, R. 1937 *R.C. Accad. Lincei*, 26, 166.

Mecke, R. 1932 *Z. phys. Chem.* B, 17, 1.

Morse, P. M. 1929 *Phys. Rev.* 34, 57.

Pauling, L. and Brockway, L. O. 1937 *J. Amer. Chem. Soc.* 59, 1223.

Penney, W. G. 1937 *Proc. Roy. Soc.* A, 158, 306.

Simon, A. and Fehér, F. 1936 *Ber. dtsch. chem. Ges.* A, 69, 214.

Sutherland, G. B. B. M. and Dennison, D. M. 1935 *Proc. Roy. Soc.* A, 148, 250.

Teller, E. and Topley, B. 1935 *J. Chem. Soc.* p. 885.

Thompson, H. W. and Linnett, J. W. 1937 *J. Chem. Soc.* p. 1376.

Verleysen, A. and Manneback, C. 1937 *Ann. Soc. Sci. Bruxelles*, 57, 31.

Wu, Ta-You 1937 *J. Chem. Phys.* 5, 392.

Wulf, O. R. and Liddel, U. 1935. *J. Amer. Chem. Soc.* 57, 1464.

Wulf, O. R., Liddel, U. and Hendricks, S. B. 1936 *J. Amer. Chem. Soc.* 58, 2287.

The measurement of sand storms

By R. A. Bagnold

[Plate 12]

In earlier papers (Bagnold 1936, 1937*a*) a description was given of experiments made in a wind tunnel 1 ft. sq. in cross-section to examine the conditions of wind and ground surface governing the mass flow q of sand across open country. It was found that:

(*a*) The sand movement over a loose sand surface profoundly modifies the vertical velocity distribution of the wind, and that Prandtl's expression for the velocity distribution over a rough surface of immobile grains

$$v = 5 \cdot 75 \, V_* \log \frac{30z}{k} \tag{1}$$

(where the drag velocity $V_* = \sqrt{(\tau/\rho)}$, z is the height of measurement above the surface, k is the height above the surface at which v is zero—a height of the order of $1/30$ of the dimension of the surface irregularity, i.e. the grain diameter, τ is the surface drag and ρ the air density) becomes

$$v = 5 \cdot 75 \, V_@ \log \frac{z}{k'} + V_t \tag{2}$$

(where $V_@$ is a new drag velocity due to a new surface drag τ' occasioned by the sand movement, k' is a much greater height, of the order of the amplitude of the surface ripples, and V_t is the threshold wind velocity, as measured at the height k', at which the sand movement once started just maintains itself).

(*b*) Over the above type of surface the mass flow q of sand should be given by an expression

$$q = C \sqrt{\frac{d}{D}} \frac{\rho}{g} V_@^3 \tag{3}$$

(where C is an experimental constant ranging from 1·5 for a uniform sand of grain diameter d, to 2·8 for a sand of a very wide range of grain size but having the same mean diameter d, and D is a standard grain diameter 0·025 cm. used for comparison because it is found near the tops of most desert dunes).

Since in the wind tunnel the measured values of the drag velocity $V_@$ were obtained from velocity readings up to a height of only 5 in. above the surface, the results could only be used to predict real conditions in the open air

provided the basic assumption is valid, that the movement of sand (as distinct from dust) is a purely surface phenomenon unaffected to any appreciable extent by circulatory currents within the air stream.

It was important therefore to confirm the laboratory work by observations under natural conditions in the open air. Such observations require continued dry weather and clean sand free of dust and uncontaminated by salt which causes hygroscopic effects. With the aid of a government grant allotted to me by the Royal Society I was able, after having designed and built special apparatus, to carry out such observations in the Egyptian Desert during February and March 1938.

The apparatus consisted of a set of pitot tubes which could be mounted in various combinations on vertical masts, a multiple manometer and sand collectors.

The pitot tubes were of the modified N.P.L. pattern with hemispherical heads. The bore of the pressure orifices was 1·6 mm. and each tube, 16 in. long, could be clipped at its leeward end to a vertical mast of thin golf club steel tubing $\frac{5}{8}$ in. in diameter and 66 in. high. Rubber tubing $\frac{3}{16}$ in. bore led to the manometer which was sometimes 100 ft. away. Usually four pitots were clipped to one mast, at heights of 1, 10, 40 and 160 cm. above the surface.

The design of the manometer had to embody special features. The instrument had to register both velocity and static pressures at at least six points simultaneously, it had to be capable of carriage by car across rough country without requiring readjustment, and to be set up, levelled, zeroed and read rapidly and easily under the unfavourable conditions of an open dune during a violent sand storm.

The manometer is shown in fig. 1, Plate 12 and fig. 2. The heights of the twelve inclined tubes A, each mounted in independent graduated cradles, can be adjusted at each end by the screws B and C. Six tubes were given an inclination of 1/20 for the lower pressures, and the remainder had an inclination of 1/5; but other slopes can be used when desired. Alcohol is stored for travelling in the tank D and thence can be driven up into the gauge tank E by blowing through the cock F, the cock G being closed. The cock H is then closed and G opened, allowing the liquid to rise into the gauge tubes A through the chokes I. The whole gauge can be levelled by the screws J and by theodolite bubbles (not shown) fixed to the base plate. When necessary the inclination of each and every gauge tube can be checked by means of a separate micro-manometer P, shown in fig. 1, Plate 12, embodied in the instrument. This is connected to the tube K and, when it is required, to one of the orifices L.

In order to zero all the gauges during a high wind, it is necessary to short-circuit all the working connexions M of the gauges back to the air space above the gauge tank. This is done by providing special short-circuiting manifolds N which can be clipped rapidly into place. When the zero gauge readings have been recorded, these manifolds and their connecting tubes to L are removed and the manifolds O carrying all the working pitot connexions, both pressure and static, are substituted. One of the orifices L is then closed, and the other connected to a "breather" of wire gauze lightly buried under the flat sand surface of the ground.
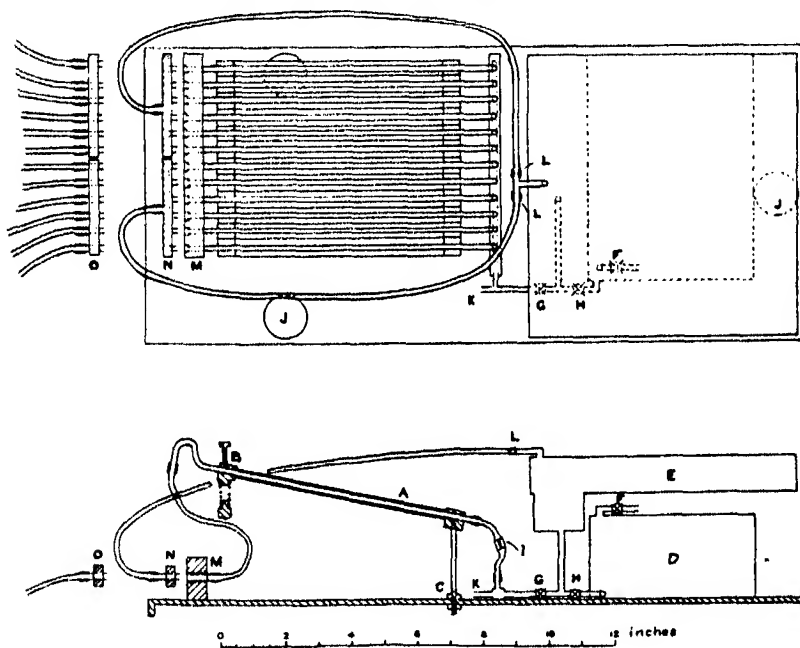
Fig. 2. Details of the manometer.

The instrument can be set up, levelled and zeroed in 6 min. even in bad conditions. The period of measurement varied from 15 to 45 min., and readings of wind velocity were taken at intervals of from 1 to 3 min. The degree of damping provided by the chokes was such that no technical difficulty was found in taking the readings, and no trouble was found to arise from the great lengths (occasionally more than 100 ft.) of connecting tube used.

The measurement of the total sand flow over an open surface can only be approximate, since all known collecting instruments interfere with the air stream. But if the collector is nearly streamlined, and offers but a narrow
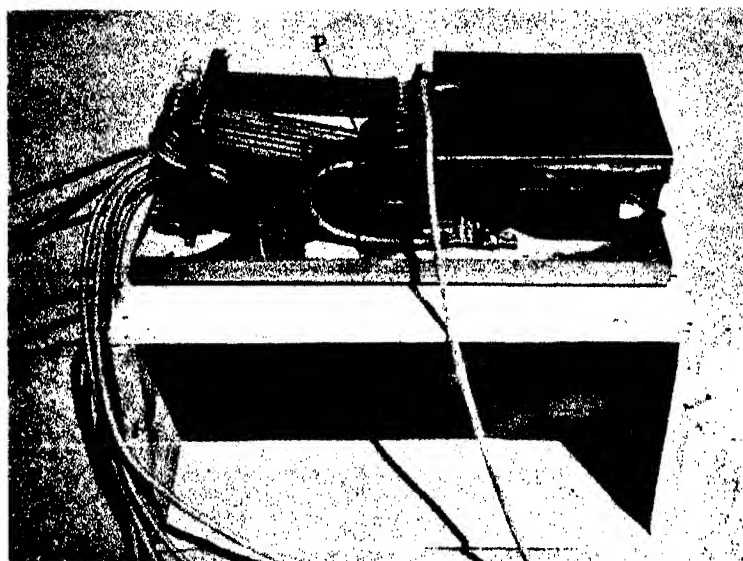
Fig. 1. The portable manometer.

front to the wind, the flying grains (saltation), other than the small pro-
portion of dust with which I was not concerned, are unable to follow the
deflected wind and pass straight into the open mouth of the collector.
This, however, is not the case at the ground surface, for the increased wind
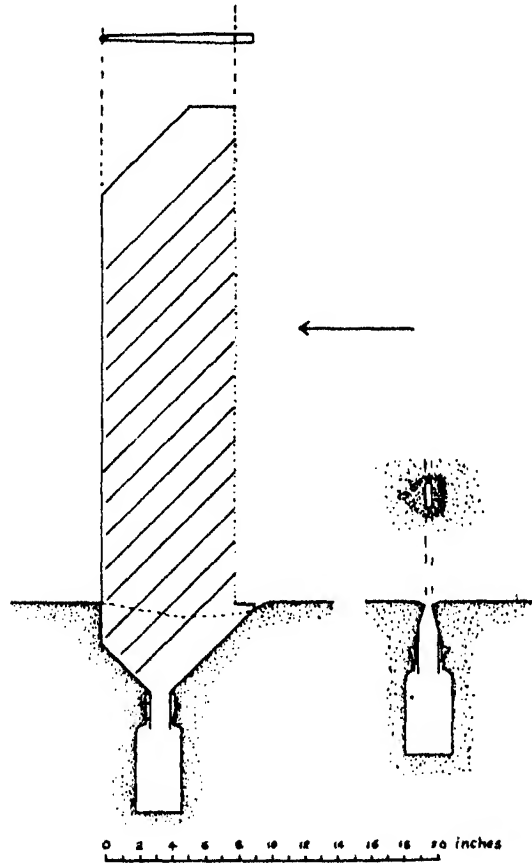velocity along the sides of the vertical collector causes removal of the

FIG. 3. Sand collectors. Left, saltation collector.
Right, ground trap for surface creep.

surface sand with the consequent formation of a hollow. Thus the slow
moving grains in "surface creep" are carried round the sides of the collector
and lost. It was therefore necessary to provide two collectors, as shown in
fig. 3, a tall thin one $\frac{1}{4}$ in. wide and 30 in. high to catch the saltation (the
sand flow above this height even in a bad storm is negligible) and a buried
ground trap for the surface creep. The weight of sand collected in each,

corrected for the differing widths of the orifices exposed, was assumed to give the flow of sand in saltation q_s and in surface creep q_c, and their sum was assumed to be the total sand flow q. The creep q_c was found to be approximately equal to $q_s/4$, which is in agreement with the ratio found in the wind tunnel experiments.

One complete set of observations took an hour. During heavy storms this was about the longest period it was possible for an observer to work efficiently without elaborate protection against the sand blast. As neither the direction nor the date of occurrence of a storm could be foretold, the two collectors, the manometers and pitot tubes had to be erected and removed during the storm.

<div align="center">RESULTS</div>

Full-scale work of this nature is entirely dependent on the weather, which unfortunately was exceptionally calm, although the locality (Western Egypt) and the time of year (Spring) were specially selected for their storminess. Only two real storms occurred in two months, but despite this sufficient data were obtained regarding the relation between wind velocity and sand movement to confirm remarkably the conclusions previously arrived at in the laboratory. The intervening long periods of calm were utilized for other observations whose results will be published separately.

In comparing the laboratory results with those obtained in the field, it must be remembered that (a) the sand used in the wind tunnel experiments was of uniform grain size, whereas the grains of the real dunes, though approximating closely to this in mean size, were not uniform; (b) the observations were all made on different days and the storms came from different directions, so that the grain grading was not quite constant.

A further difficulty, which it was feared might seriously mask the expected linear distribution of wind velocity with the log-height lay in the fact that the surfaces of dunes are always curved, surfaces of any size composed of fine sand and free of a covering layer of grit never being found on the flat desert plains. Measurements had therefore to be made on the surfaces of the flattest barchan dunes available—radius of curvature of the order of 1000 ft.

Typical wind velocity distributions are shown in fig. 4. It will be seen that the manometer readings gave velocities which, when plotted against the log-height of the four pitots above the ground, led to linear distributions. The velocity rays converge to an apparent focus at a height k' and at the velocity of the threshold wind, thus corroborating equation (2).

The height k' is here about 1 cm. above the ground. The corresponding height for the uniform sand used in the wind tunnel was 0·3 cm. If the height k' is to be associated with the ripple amplitude, this increase in height tallies with the greater amplitude of ripples observed with sands of mixed grain size.
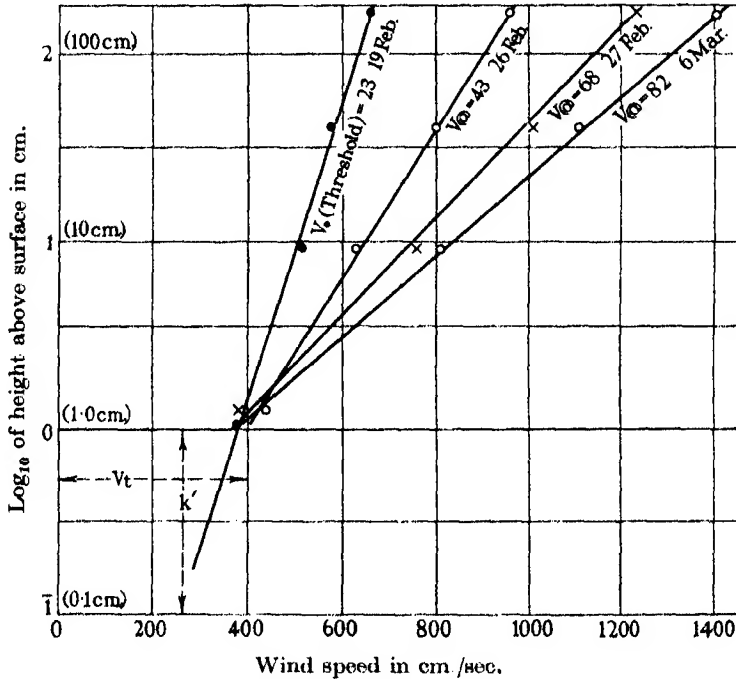

Fig. 4. Observed normal wind velocity distribution over a dune when sand is driving. V_* is the drag velocity $\sqrt{(\tau/\rho)}$ when no sand is moving; $V_{@}$ is the special drag velocity $\sqrt{(\tau'/\rho)}$ due to the sand movement.

A comparison of fig. 4 with the corresponding figure giving the wind velocity distribution in the tunnel (Bagnold 1936, fig. 6) will show that the threshold wind velocity in the former case is somewhat greater than it is in the latter. This is to be expected, since, although the mean grain diameter of the sand of the dunes (fig. 7) is approximately the same as the uniform wind tunnel sand (0·025 cm.), the dune sand contains grains of other sizes of which the largest, collected on the surface, tend to protect the surface from disturbance. The dotted curve of fig. 7 represents a sample of the coarser surface sand which was collected as the "surface creep" in the ground trap. The mean grain diameter of this is 0·033 cm. and the threshold wind velocity for such sand was found in the wind tunnel to have approximately

the value shown in fig. 4. This supports the view that after the wind has blown from the same direction for sufficient time to stabilize the surface by causing the larger grains to collect at the crests of the ripples (Bagnold 1937a, p. 431), the presence of these larger grains, even in very small proportions, appreciably raises the threshold wind velocity.
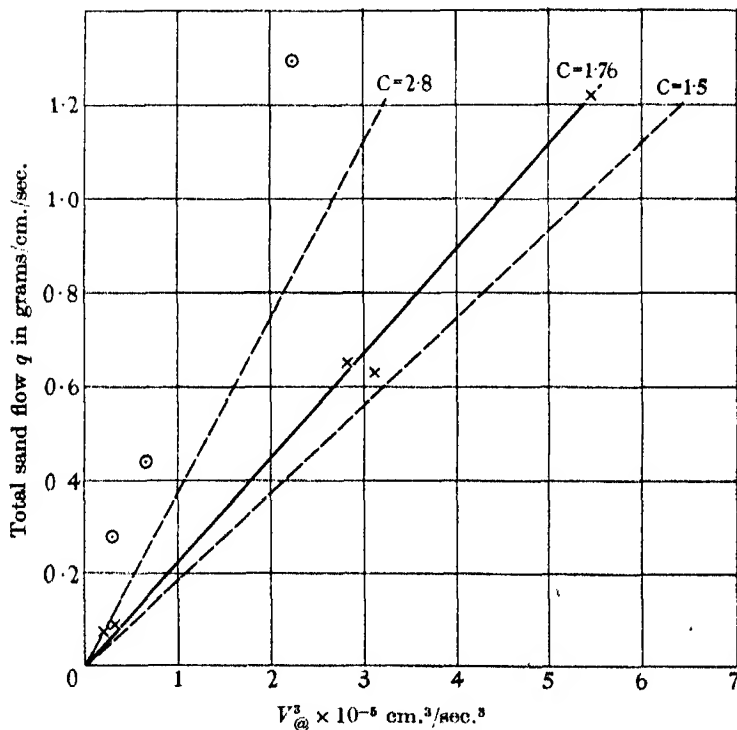

FIG. 5. Comparison of wind tunnel and open-air values of the observed rate of mass flow q of sand, and their proportionality to $V_@^3$ according to equation (3).

Results in open country	Previous wind tunnel results
× Sand over sand surface (fairly uniform dune sand)	Dotted line $C = 1·5$ indicates sand flow for uniform sand of same grain size as ×.
⊙ Sand over grit surface (sand-sheet)	Dotted line $C = 2·8$ indicates sand flow for sand of same mean size but very wide range of size.

In order to check the validity of equation (3), the values of $V_@$ were found from the inclination of the velocity rays of fig. 4, and $V_@^3$ was plotted against the measured values of the sand flow q. The result is shown in fig. 5. d/D was taken as unity and ρ/g as $1·25 \times 10^{-6}$. It will be seen that the points lie well in a straight line and that the value of the constant C is approxi-

mately that which would be predicted from the laboratory results for sand of the degree of uniformity of grain size which is found on the average dune.
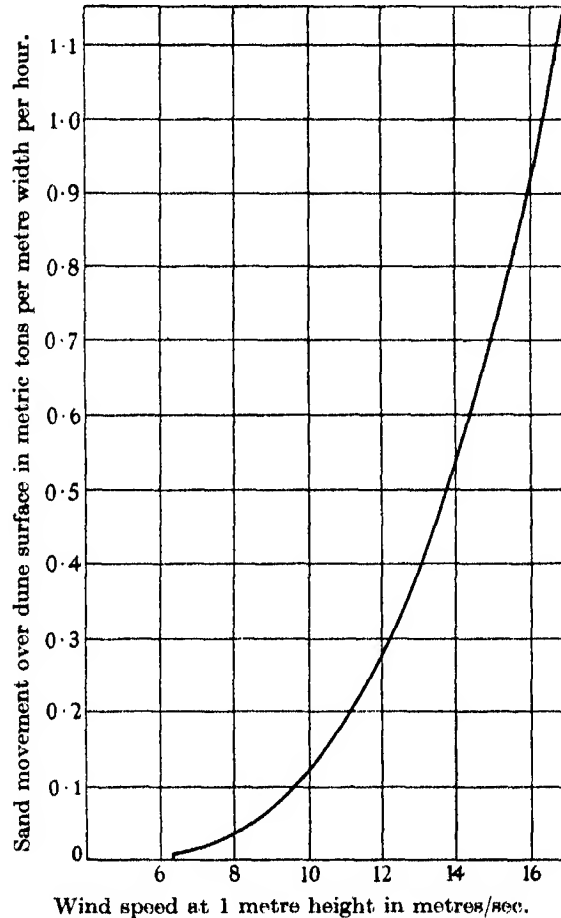

FIG. 6. Relation between the flow of average dune sand and the wind velocity as measured at a standard height of one metre. In the units used $q = 5 \cdot 2 \times 10^{-4}(v - V_t)^3$. This is obtained from equations (1) and (2) from which

$$q = C \frac{\rho}{g} \sqrt{\frac{d}{D}} \frac{(v - V_t)^3}{190 \log^3 z/k'},$$

by taking $C = 1 \cdot 76$, $d/D = 1$, $\rho/g = 1 \cdot 25 \times 10^{-6}$, $k' = 1$ cm., $z = 100$ cm., $V_t = 400$ cm./sec.

It is now possible to give, with some confidence, a curve, fig. 6, showing directly the rate of sand movement over the surface of an eolian sand accumulation, caused by a wind of any velocity as measured at a standard

height of one metre above the surface. The cubic character of the curve emphasizes the fact that more sand is moved by a strong wind in a short time than by a weak wind in a proportionately longer time. From this it is seen that the direction of the "prevailing wind" as defined by mean square values may differ from the direction of sand drift. For the latter the "prevailing wind" should be computed on a mean cube basis (after subtracting the threshold velocity from all wind velocity figures).

Similar measurements of wind gradient and sand movement during storms were made above the grit-covered surfaces of a flat sand-sheet over which the dunes are creeping. Since in this case there is no fixed relation between $V_{@}$ and q (vide the last section of my 1936 paper) but only a maximum value of q for a given value of $V_{@}$, there must be some uncertainty as to whether the wind is sand-saturated or not at the time of measurement. The measurements were, however, made when the sand was drifting heavily over the sand-sheet, and was being temporarily deposited upon the grit floor not far away in long narrow strips 1–2 cm. in thickness. That is, the air was probably very near sand-saturation.

Though the mean grain diameter was here considerably bigger than that of the sand moving over the dune nearby, and the range of grain size was also wider, the values of q given in fig. 5 (dotted circles) are far in excess, for the same values of $V_{@}$, of any found for sand moving over a grit-free sand surface. This is also in accord with the previous laboratory work.

In a paper (Bagnold 1937b) describing experiments on the changes which occur in the size grading of sand when it is transported by wind, a new type of grading diagram was used to express the results. In this the grain diameter, on a log scale, is plotted as abscissa against the logarithm of a quantity ϕ, where ϕ is the percentage weight of sand present per log-cent change of diameter. This form of diagram has the advantage that the proportions in which the extreme grades are present can be clearly seen.

The experiments showed that whatever may be the grading of a bed from which sand is being removed by a wind, the percentage weights of the extreme grades present in the sand transported, and in that subsequently deposited, tend to die away on each side of the mean diameter according to an exponential law (straight line on the diagram). Moreover the exponential coefficient on the large grain side tends to a limiting value of 9.

In fig. 7 I have shown a typical curve giving the grading of a sand in process of transport through the wind tunnel (thin continuous curve). The two heavy curves were similarly obtained from sand actually blowing over the dunes, by adding together the collected saltation and surface creep. It will be seen that the results found in the wind tunnel are again corroborated.

The bi-linear arrangement is clearly shown, and the right-hand sides are exactly parallel to one another and to that of the wind tunnel curve, the coefficient in each case being 9.
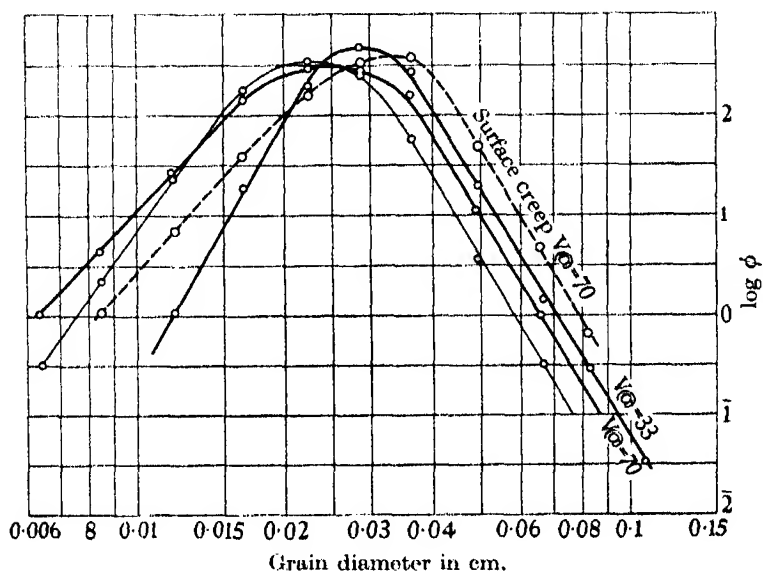

FIG. 7. Grading diagram. The thin curve represents the size-grading of a sand which has been removed by wind from the floor of the wind tunnel and transported through the tunnel. The two heavy curves show the similar grading of sand in motion over two dune surfaces in the desert. Here the saltation and surface creep, collected separately, have been recombined for analysis. The dotted curve shows the grading of the surface creep only. $\phi = dn/d(\log R)$, where n is the percentage weight of the grade, and R is the grain diameter.

REFERENCES

Bagnold, R. A. 1936 *Proc. Roy. Soc.* A, **157**, 594.
— 1937a *Geogr. J.* **89**, 428.
— 1937b *Proc. Roy. Soc.* A, **163**, 250.

The bi-linear arrangement is clearly shown, and the right-hand sides are exactly parallel to one another and to that of the wind tunnel curve, the coefficient in each case being 9.
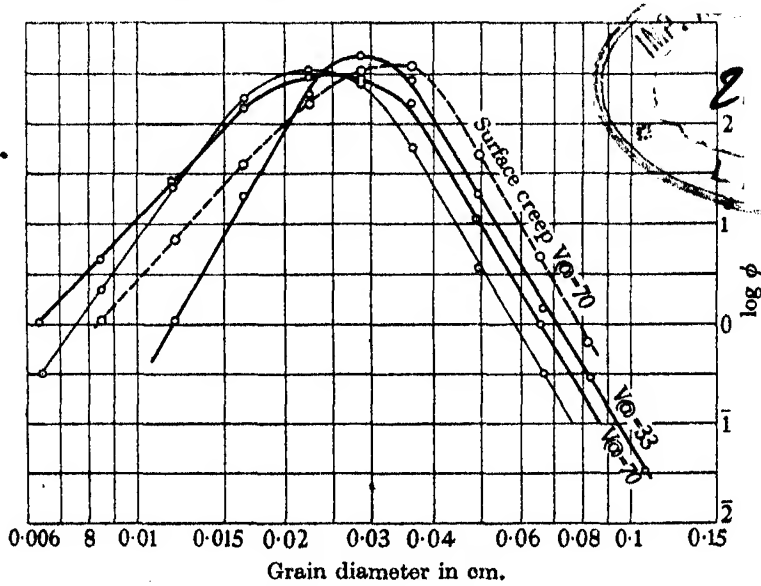

FIG. 7. Grading diagram. The thin curve represents the size-grading of a sand which has been removed by wind from the floor of the wind tunnel and transported through the tunnel. The two heavy curves show the similar grading of sand in motion over two dune surfaces in the desert. Here the saltation and surface creep, collected separately, have been recombined for analysis. The dotted curve shows the grading of the surface creep only. $\phi = dn/d(\log R)$, where n is the percentage weight of the grade, and R is the grain diameter.

REFERENCES

Bagnold, R. A. 1936 *Proc. Roy. Soc.* A, **157**, 594.
—— 1937*a Geogr. J.* **89**, 428.
—— 1937*b Proc. Roy. Soc.* A, **163**, 250.

A study of sensitized explosions
II. Ignition phenomena in mixtures of carbon monoxide and oxygen sensitized by hydrogen

By E. J. Buckler and R. G. W. Norrish, F.R.S.

Laboratory of Physical Chemistry, Free School Lane, Cambridge

Introduction

Not the least important factors affecting the utilization of gaseous fuels are the remarkable effects of small quantities of catalytic substances, the presence of which may initiate or entirely change the nature of a combustion process. A proper understanding of these factors is therefore of great importance in the control of processes which are fundamental to many parts of applied chemistry. Such processes, however, are also intrinsically interesting for the insight they give into the ultimate mechanism of chemical reaction, and as a result of their study in the light of the theory of chain reactions, many empirical facts relating to combustion processes which previously were obscure now acquire a new significance.

Of all these reactions the combustion of hydrogen and carbon monoxide stand in a unique position, for these substances more than any others occur as intermediaries in the burning of gaseous fuels; it is therefore of special interest to realize that the presence of traces of hydrogen may have a profound effect on the combustion of carbon monoxide, not only in lowering the temperature of ignition, but also in influencing the rate of propagation of the flame. This becomes of particular importance when it is remembered that carbon monoxide as used industrially nearly always contains traces of hydrogen.

The extensive researches of Garner and his co-workers (1927–32) on the radiation emitted by the carbon monoxide flame, have shown that the mechanism of oxidation changes completely in the presence of appreciable traces of hydrogen. However, the nature of the catalytic effect of hydrogen has not been completely elucidated, nor has its effect on the limits of ignition been demonstrated. It would appear that the catalytic influence of hydrogen has never been clearly separated from that of water, which in the past has been the subject of many profitable and important observations (Bone 1931;

[292]

Hadman, Thompson and Hinshelwood 1932a; Topley 1930). The view has been expressed by Hadman, Thompson and Hinshelwood (1932a) that the virtue of water in catalysing the combustion of carbon monoxide lay in its property of yielding hydrogen. That this view is in part erroneous, however, becomes at once apparent when the effects of hydrogen and water are contrasted, for with the latter a comparison of the work of Sagulin, Kowalsky, Kopp and Semenoff (1930), Hadman, Thompson and Hinshelwood (1932b), and Cosslett and Garner (1930) shows that the catalytic effect of water is confined only to the propagation of the flame and has no effect on the ignition temperature, while our own preliminary experiments, on the other hand, demonstrated that traces of hydrogen have an enormous effect in depressing the ignition temperature.

It soon became apparent that in the presence of only 1 % of hydrogen, the combustion region for carbon monoxide is transferred to that characteristic of hydrogen, and that the propagation and branching of chains becomes possible at temperatures over 150° lower than with pure carbon monoxide and oxygen. The results of our investigation indicate that the catalytic effect of molecular hydrogen is indeed consequent upon its introducing a new and facile branching process. This is in contrast with the effect of water which, as was first envisaged by Haber, Farkas and Harteck (1930), can facilitate chain propagation by yielding H atoms, but which, as was pointed out by von Elbe and Lewis (1937), leaves the branching process and therefore the ignition temperature unaffected.

The present work is described in two parts; in the first the conditions affecting the ignition of carbon monoxide and oxygen in the presence of small quantities of hydrogen are examined and elucidated; in the second which constitutes the succeeding paper the kinetic study is completed by a comparison of the characteristics of the present reaction with those of the reaction between hydrogen and oxygen, the influence of deuterium also being taken into consideration.

The final conclusion is reached that the combustion of carbon monoxide in the presence of even traces of hydrogen is controlled uniquely by the reactions involving the combustion of the latter gas.

EXPERIMENTAL METHOD

Apparatus. The experimental arrangement shown in fig. 1 was similar to that used by Foord and Norrish (1935). A reaction vessel V of quartz or pyrex, which could be evacuated to $10^{-5} - 10^{-6}$ mm. Hg by "Hyvac" and mercury diffusion pumps, was supported horizontally in an electric furnace

wound to give a constant temperature within 1° C. over 25 cm. of its length. The furnace temperature was maintained constant within 0·5° C. by a Cambridge Instrument Company automatic regulator and chromel-alumel thermocouple previously calibrated at the melting-points of antimony,
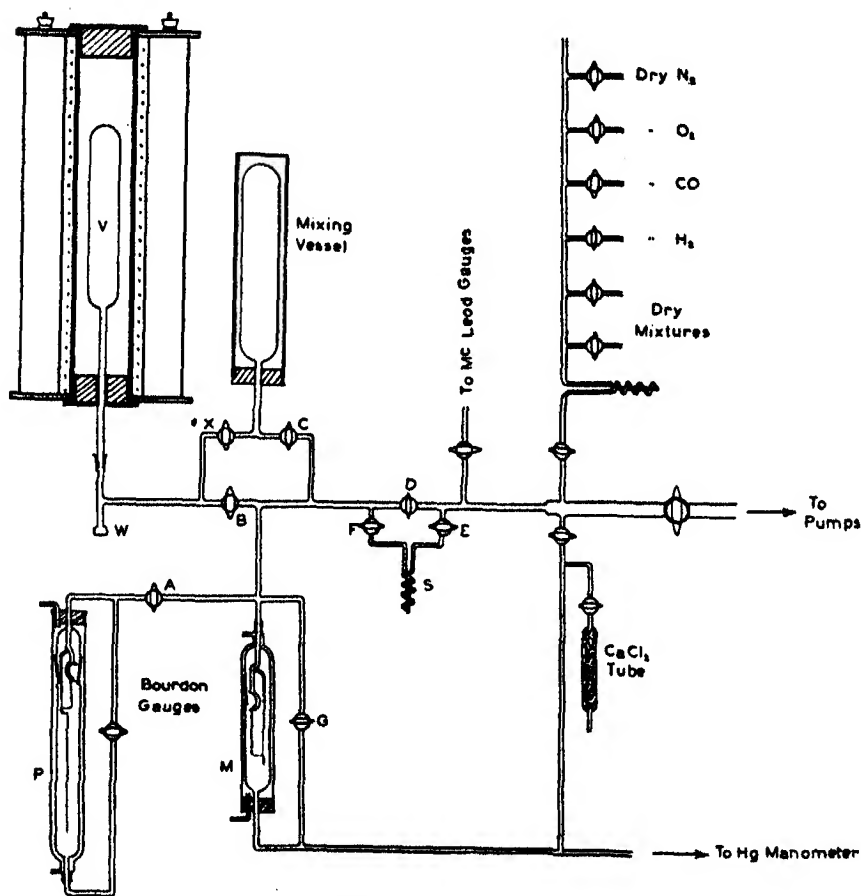

FIG. 1. Diagram of reaction system.

zinc, lead and tin. Gas mixtures could be introduced from a separate mixing vessel through a wide-bore tap X, and subsequent reaction detected visually through a small window W in the entry tube. The pressure measurements involved in making up gas mixtures, observing induction periods and calculating percentage combustion were carried out by the use of two water-jacketed Bourdon gauges of the type described by Foord (1934). The first, in which pressure changes were measured by deflexion of a beam of light,

was used in the determination of ignition limits and as a null instrument in conjunction with a mercury manometer for making up gas mixtures. The second gauge was sufficiently sensitive to enable pressure changes to be estimated within 0·01 mm. Hg by the movement of a pointer observed by a travelling microscope, while both were robust enough to withstand the shock of explosions in the reaction vessel or pressure changes up to one atmosphere across their diaphragms.

The gases required in the experiments were prepared as described below and stored in large soda-glass bulbs which previously had been evacuated and heated with a large luminous flame to remove any surface impurities. Mixtures which would be required for some time were stored in bulbs fitted with mercury seals which could be closed between experiments to remove any possibility of leaks and prevent undue contamination by tap grease. Every permanent gas or mixture was passed through a spiral cooled in liquid air before entering the final mixing vessel to eliminate traces of water vapour and other impurities.

Preparation of gases. Carbon monoxide was prepared by dropping 100 % sulphuric acid on to anhydrous sodium formate warmed to 110° C. in an apparatus which previously had been evacuated with a water pump. The gas was purified by passing through a trap cooled to − 80° C., over soda lime and solid potash, and through a spiral cooled in liquid air, finally being collected in a bulb immersed in liquid nitrogen. Approximately one-third of the product was pumped away, and the remainder taken for storage in a 5 l. glass bulb connected to the main system. Prepared in this way the gas proved to be 100 % pure on analysis, and gave no detectable oxidation when left in the reaction vessel at 540° C. for half an hour.

Oxygen was taken from a commercial cylinder, passed over platinized asbestos heated electrically in a pyrex tube to remove traces of hydrogen and ozone, and collected in a tube cooled in liquid air. About one-half of the condensate was pumped away to remove traces of nitrogen, and the remainder was drawn off when required through a spiral cooled in liquid air. Since all gases were required to contain less than 1 : 5000 of hydrogen, this method was chosen in preference to that of preparing the gas by electrolysis.

Nitrogen, helium, and argon taken from cylinders were freed from traces of hydrogen by treatment with red hot copper oxide in a pyrex tube for 15 min. immediately prior to use, and dried by passing through spirals cooled in solid carbon dioxide or liquid air.

Hydrogen was prepared by the electrolysis of 10 % sodium hydroxide solution saturated with barium peroxide, purified over heated platinized asbestos and dried by passing through spirals cooled in liquid air.

Deuterium was prepared by the electrolysis of 98 % heavy water, stored in a clean glass bulb fitted with a mercury seal, and dried before use by passing through spirals cooled in liquid air.

Practical methods. In the preparation of samples of gas containing accurately known small concentrations of hydrogen, a mixture of oxygen with about 5 % hydrogen was first prepared in a subsidiary bulb, and requisite amounts of this dilute mixture admitted to the main reservoir, followed by extra carbon monoxide and oxygen. After allowing 30 min. for the attainment of uniform composition, samples were withdrawn for use through a spiral cooled in liquid air.

Each complete series of experiments, which often extended over a period of several days, was performed without allowing the furnace to cool, in order to maintain the surface conditions of the reaction vessel as constant as possible.

Two distinct methods were employed for the determination of ignition limits. The first, which may be described as the "withdrawal" method, depended upon the fact that a mixture of carbon monoxide and oxygen sensitized with hydrogen could be introduced into the reaction vessel without inflammation occurring, provided that a sufficiently high pressure of pure gases was first established there. Such mixtures were stable above 200 mm. Hg, but on withdrawal underwent sudden spontaneous ignition at some critical pressure below 100 mm. Hg.

In contrast with the results obtained in this way are those furnished by what may be termed the "admission" method, in which a study was made of the behaviour of sensitized mixtures entering the evacuated reaction vessel through the tap X from the final mixing vessel. The boundary of ignition obtained in this way was defined by the final limiting conditions of composition and pressure in mixtures which could be introduced into the furnace without inflammation occurring. The percentage combustion of an ignited mixture was conveniently determined by withdrawing the residual gases from the furnace through a spiral S cooled in liquid air. The amount of carbon dioxide collected could be estimated from the pressure shown on the mirror gauge when the gas was allowed to expand into the volume occupied by the spiral, the gauge diaphragm and the connecting tubing. From a knowledge of the volume of the bulb of the reaction vessel, as little as 0·1 % combustion could be detected and measured in this way.

Experimental results
Ignition by withdrawal

It has been found that the region of low-pressure explosion of pure carbon monoxide and oxygen is extended over 150° C. towards lower temperatures

in the presence of about 2 % hydrogen. The sensitized mixtures ignite between definite upper and lower pressure limits which vary with hydrogen concentration in the manner shown in fig. 2. These results were obtained in a 27·0 mm. diameter pyrex reaction vessel using the "optimum" mixtures $2CO + O_2$ throughout.

For the determination of the upper pressure limits of spontaneous ignition, mixtures containing hydrogen were added to samples of the pure
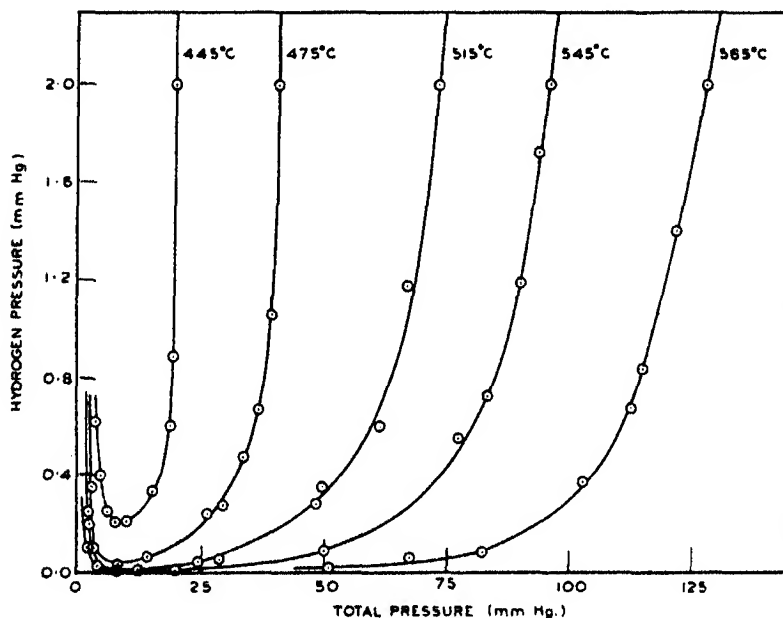

Fig. 2. The variation of ignition limits of $2CO + O_2$ with hydrogen pressure. Pyrex reaction vessel diameter 27·0 mm.

gases previously introduced into the reaction vessel at a pressure greater than the limit value. After allowing 30 sec. for the attainment of uniform composition, the contents of the furnace were withdrawn slowly until the mirror gauge registered the sudden kick followed by decrease of pressure characteristic of explosion.

The values of the lower limit were found by admitting mixtures containing a known amount of hydrogen directly into the reaction vessel, the total pressure being adjusted by trial and error until no faint blue flash could be seen through the window in the entry tube.

The intermediate values of the limit for small hydrogen pressures at the foot of the curve were also determined visually, since in this region the

percentage combustion and pressure change during ignition is small. For this purpose a small quantity of $2CO + O_2$ containing hydrogen was added to a mixture of the pure gases in the reaction vessel at a pressure close to the limit value, and the minimum value of the total pressure required to prevent ignition determined by trial and error within 0·5 mm. Hg.

The curves show that the sensitized ignition of carbon monoxide and oxygen is situated in the same region as that of hydrogen, the curve at 445° C. indicating where the upper and lower limits converge at the low-temperature extremity of the explosion region. The ignition in the neighbourhood of the lower limit and at very small hydrogen pressures was marked by a faint blue flash, and was not investigated in any detail. When the concentration of hydrogen exceeds about 0·2 % the explosions are definite and the combustion almost complete, as shown in Table I which is

TABLE I. THE PERCENTAGE COMBUSTION AFTER IGNITION OF MIXTURES OF $2CO + O_2$ CONTAINING HYDROGEN

Pyrex reaction vessel 27·0 mm. diameter.
Temperature 520° C.

Hydrogen pressure mm. Hg	Total pressure mm. Hg	Percentage combustion
1·580	80·0	100·0
1·220	74·2	99·8
0·880	67·0	100·2
0·590	60·6	97·5
0·400	53·0	95·0
0·220	45·0	81·0
0·100	33·0	60·0
0·075	25·0	40·2
0·040	10·0	3·0

typical of the results obtained. Nevertheless these explosions possess none of the violence associated with the ignition of oxyhydrogen mixtures, and never produce any audible sound. The small degree of combustion at low hydrogen pressures confirms the results of many previous workers that even when flame is initiated in mixtures of carbon monoxide and oxygen, it lacks self-propagating power unless an adequate supply of free radicals containing hydrogen also are present.

Above the upper pressure limit the reaction rate falls abruptly to values which are very small below 540° C., but which at higher temperatures, even in vessels poisoned by treatment with potassium chloride, constitute a source of error by altering the composition of the mixtures in the reaction vessel during the time allowed for the attainment of uniform composition.

For this reason it was difficult to study these curves above 570° C. A detailed examination of the kinetics of the sensitized ignition will be deferred until an account has been given of further phenomena observed in this system of interest in the general theory of gaseous ignition.

Ignition by admission

In contrast with the technique already described for determining ignition limits, a study has been made of the behaviour of sensitized mixtures entering the previously evacuated reaction vessel. When the final values of the hydrogen pressure and total pressure of mixtures shared between the mixing vessel and the furnace lay close to the limits of spontaneous ignition, inflammation occurred while the gases were entering the reaction vessel. As the total pressure of such mixtures was increased by the addition of inert gas or extra carbon monoxide and oxygen, a critical value was reached above which no visible ignition occurred during the sharing process, provided that it was carried out as rapidly as possible. In other words, with a sufficiently rapid flow of gas, mixtures could be established in the furnace at pressures greater than the ignition limit before the reaction had time to develop into explosion. However, the unexpected result was obtained that visible ignition reappeared when the initial total pressure of gases in the mixing vessel was further increased to considerably higher values above 100 mm. Hg. It was decided to investigate this phenomenon in detail, especially as it was found that provided the wide-bore tap X was opened as quickly as possible, the two pressure limits had definite and reproducible values. The relation between final total pressure of mixtures containing fixed concentrations of hydrogen, and the percentage combustion after sudden admission to a 27·0 mm. diameter pyrex reaction vessel at 540° C. is shown in fig. 3. In these experiments the concentration of $2CO + O_2$ was maintained constant at 50·0 mm. Hg and the total pressure varied by addition of purified nitrogen. The diagram shows that for a given suitable pressure of hydrogen there exists two pressure limits between which there is no ignition and outside which inflammation occurs in mixtures admitted to the reaction vessel. The small residual percentage combustion between the limits was due to the spontaneous ignition of a portion of the gases during subsequent withdrawal from the reaction vessel for analysis.

The effects of diluent gases. The results are best expressed as curves showing the relation between hydrogen pressure and final total pressure at which sudden discontinuities occur in the percentage combustion of mixtures entering the reaction vessel. Such curves may be described as the ignition boundaries obtained by the admission method, and are shown in fig. 4 for

mixtures in which argon, oxygen, nitrogen and carbon monoxide were used in turn to augment the total pressure. When the final composition of mixtures is represented by points lying below these curves no ignition occurs during admission of the gases to the furnace. The corresponding results using helium and carbon dioxide as diluent gases are shown in figs. 5 and 6 respectively.
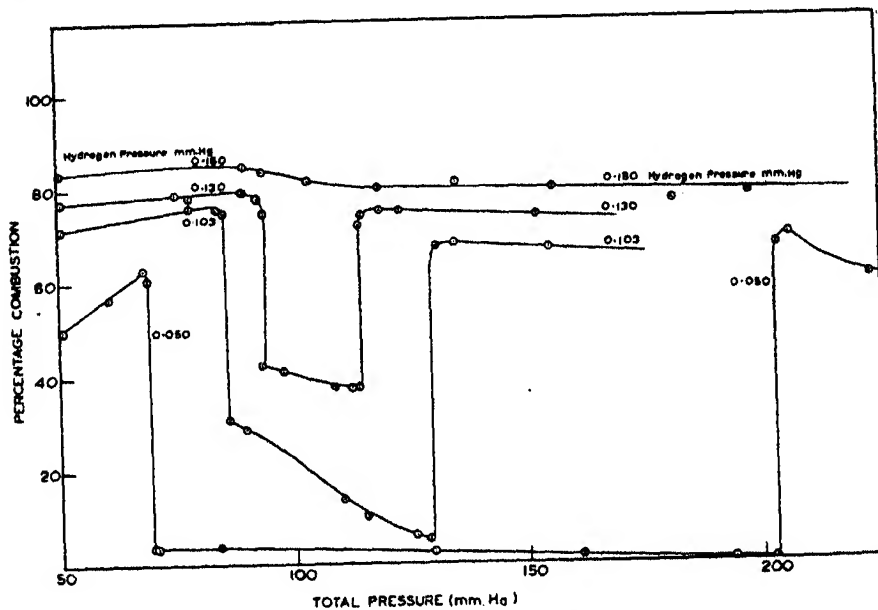

FIG. 3. The relation between final total pressure and percentage combustion of mixtures entering a 27·0 mm. diameter pyrex reaction vessel at 540° C. Pressure of 2CO + O₂ constant at 50·0 mm. Hg. Hydrogen pressures constant along each curve. Nitrogen used as diluent gas to augment the total pressure.

Comment on the extraordinary variation in shape of the curves using different inert gases must be reserved until all the experimental evidence has been presented. For comparison of these curves, however, it should be pointed out that during admission of a mixture to the reaction vessel the hydrogen pressure and total pressure move along a straight line from the origin to a point on the diagram representing the final composition of the mixture, and that providing the slope of this line has an appropriate value, all ignition boundaries except that obtained using helium as a diluent gas will intersect it at two points, representing limits of inflammability. All mixtures except those diluted with helium, therefore, possess upper and lower critical pressure limits of ignition, although the range of hydrogen
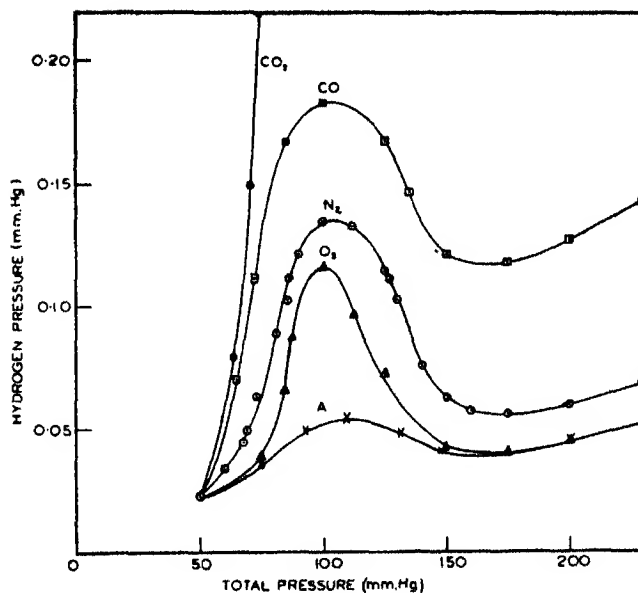
Fig. 4. Ignition boundaries by admission method in mixtures of $2CO + O_2$ with different diluent gases. Temperature $540°$ C. Pressure of $2CO + O_2$ constant at $50\cdot0$ mm. Hg. Pyrex reaction vessel $27\cdot0$ mm. diameter. × Argon. ▵ Oxygen. ⊙ Nitrogen. ▣ Carbon monoxide. ● Carbon dioxide.
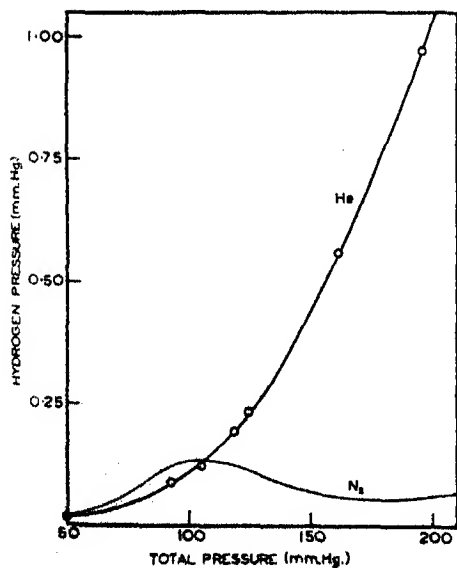

Fig. 5
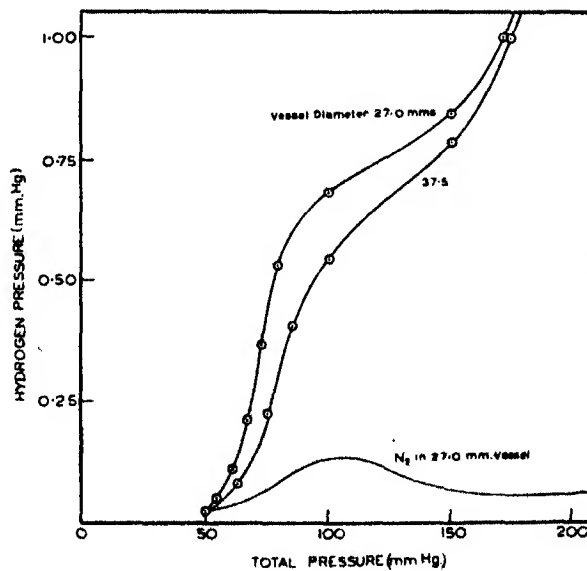

Fig. 6

Ignition limits by admission method in mixtures of $2CO + O_2$ containing helium (fig. 5) and carbon dioxide (fig. 6). (Curve for nitrogen shown for comparison.) Temperature $540°$ C. Pressure of $2CO + O_2$ constant at $50\cdot0$ mm. Hg. Pyrex reaction vessel $27\cdot0$ mm. diameter in fig. 5. Pyrex reaction vessels $27\cdot0$ mm. and $37\cdot5$ mm. diameter in fig. 6.
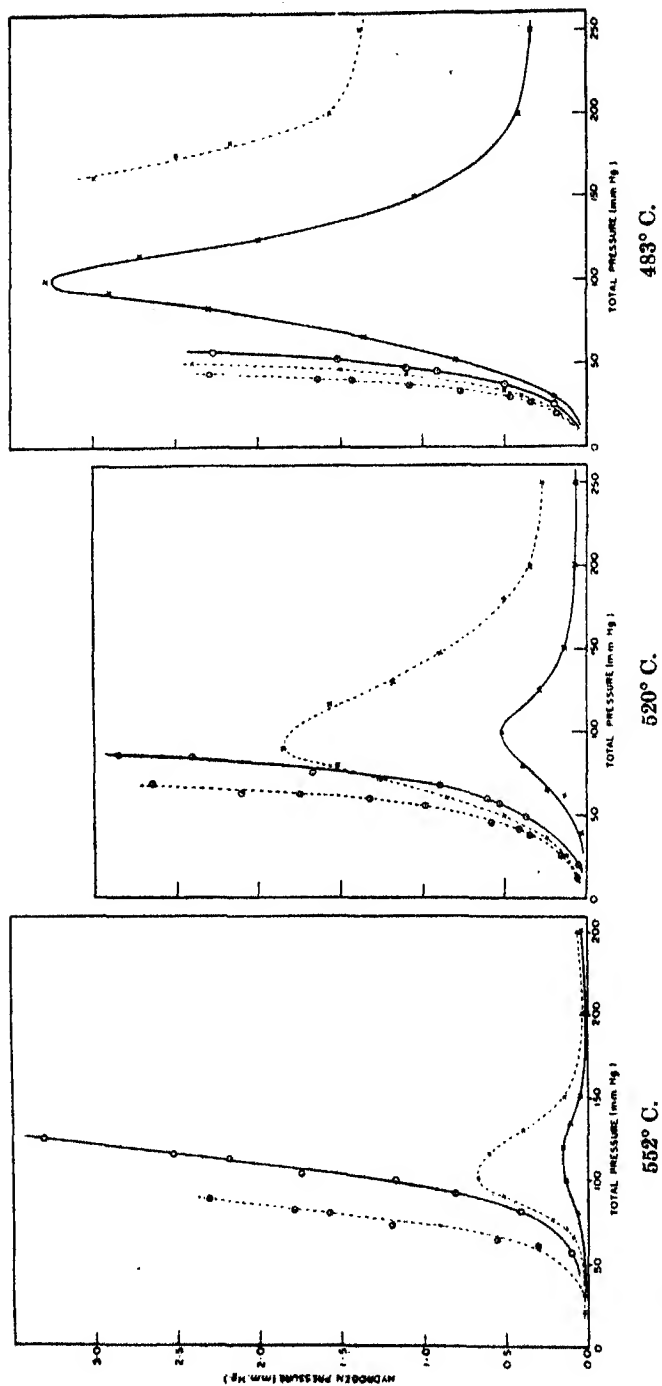
Fig. 7. The boundaries of ignition of $2CO + O_2$ determined by the admission method and the withdrawal method in a 27.0 mm. diameter pyrex reaction vessel. O Withdrawal method. × Admission method. — Sensitization by hydrogen. - - - Sensitization by deuterium.

concentrations in which they may be observed varies considerably in the presence of different inert gases.

Effect of temperature. The region of stability expands considerably at lower temperatures and is related to the region of spontaneous ignition determined by the "withdrawal" method as shown in the three diagrams of fig. 7, which were obtained at 552, 520 and 483° C. respectively, using sensitized mixtures of carbon monoxide and oxygen containing no inert gas.
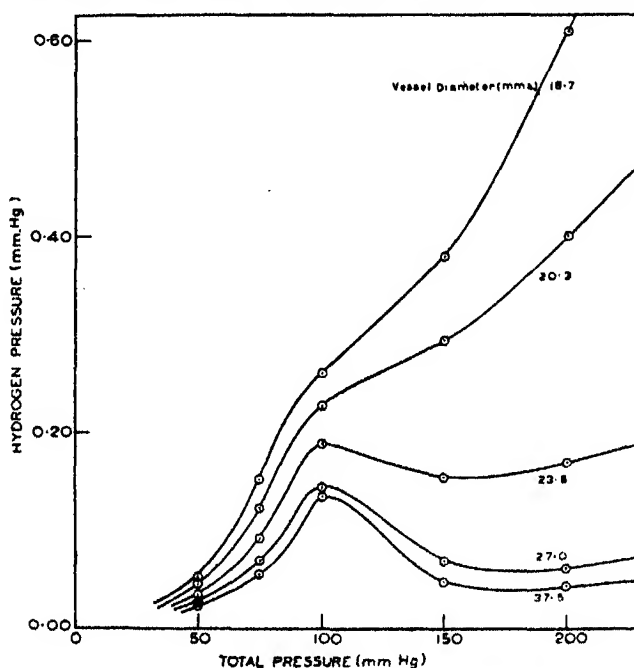

FIG. 8. Ignition boundaries by admission method in pyrex reaction vessels of different diameters. Temperature 540° C. Pressure of $2CO + O_2$ constant at 50·0 mm. Hg. Nitrogen used as inert gas.

Sensitization by deuterium. In fig. 7 are also shown the corresponding results obtained in mixtures sensitized with deuterium. A comparison of the results obtained by the withdrawal method in mixtures containing these two forms of hydrogen are of fundamental importance in connexion with the detailed kinetics of the reaction and will be considered in the succeeding paper, the results obtained by the "admission" method serve to demonstrate that mixtures become generally less inflammable when hydrogen is replaced by the same percentage of deuterium.

Effect of vessel diameter. In fig. 8, which shows the boundary of inflammation of mixtures entering reaction vessels of diameters 37·5, 27·0, 23·6, 20·3

and 16·7 mm., it is seen that a small decrease in vessel diameter has the effect of rotating the ignition boundary about the origin as an axis without affecting its general form. It may be noted at this point that in these and all other curves obtained by the "admission" method, the boundary of inflammation at high total pressures lies approximately along a tangent from the origin to the low pressure portion of the curves below 50 mm. Hg.

Conditions determining ignition by admission. The preceding observation, coupled with the fact that it has already been shown possible to establish
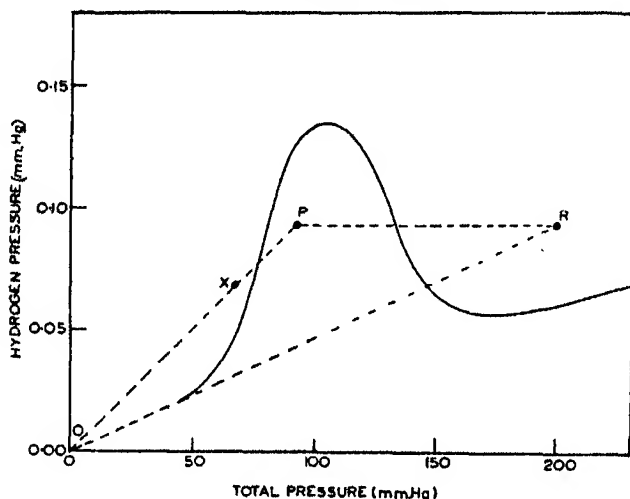

Fig. 9. The behaviour of mixtures at the boundary of ignition obtained by the admission method.

stable sensitized mixtures in the reaction vessel at high total pressures by introducing the components in the correct order, suggests that the region of high pressure inflammation determined by the "admission" method is not limited by a true kinetic boundary, but is conditioned in some way by the pretreatment suffered during entry of the gases into the evacuated vessel. This conclusion could be verified in the following way. In fig. 9 is shown once more the boundary above which inflammation occurs in mixtures of $2CO + O_2$ diluted with nitrogen entering a 27 mm. diameter pyrex reaction vessel at $540°$ C. By adding 42·8 mm. Hg of $2CO + O_2$ containing 0·093 mm. Hg of hydrogen to 50 mm. Hg of $2CO + O_2$ already present in the reaction vessel, it was possible to establish a mixture at the point P in the region of stability without ever having passed through the region of low-pressure explosion. It could be proved that this technique did not entail oxidation of the hydrogen, since on slow withdrawal of the complete mixture, the composition moved

down the line *PO*, and eventually reached the region of spontaneous ignition at *X* where explosion occurred. By the gradual addition of nitrogen to a mixture at *P*, the total pressure could be increased to 200 mm. Hg and the composition moved along the line *PR*, with no signs of inflammation on crossing the boundary obtained by the admission method. It seems that the further the composition of the mixture moves from the boundary of ignition obtained by withdrawal, the more remote become the possibilities of ignition by chain branching processes.

However, in contrast with the effect of gradual dilution of a mixture at P by slow addition of nitrogen, it was found that sudden compression of the gases by the instant admission of a large pressure of nitrogen resulted in visible general ignition.

When it is realized that the first portions of a high pressure mixture to enter an evacuated reaction vessel will be compressed by the rapid influx of the remainder of the gas, it will be seen that whatever be the fundamental cause of ignition by compression, the existence of the phenomenon offers a reason for the region of high pressure ignition obtained by the admission method. A detailed application of this idea will be postponed until the factors controlling ignition by compression have been investigated.

Ignition by compression

The intensity of reactions of the chain type may be raised to the level necessary for ignition by increasing the temperature or altering the composition of the system in such a way as to increase the probability of chain branching. It has been shown by Foord and Norrish (1935), in a study of the hydrogen oxygen reaction sensitized by nitrogen peroxide, that the transition from slow reaction to ignition occurs when the concentration of chain centres exceeds a critical value required to establish adiabatic conditions in some favourable volume element of the reaction vessel. This must be ultimately the fundamental condition for ignition in other chain reactions, but excepting certain special cases is not inconsistent with the view that ignition occurs when the effective branching factor exceeds zero.

A consideration of these ideas leads to the following possible mechanisms by which mixtures undergoing stable reaction may be ignited by compression:

(1) Compression may produce transitory high local concentrations of chain centres by confining into a smaller volume those free radicals present in the initial mixture. The increased number of elementary reactions in unit volume may then be sufficient to establish adiabatic conditions before the chain centre concentration reverts to the equilibrium value proper to the high pressure conditions.

(2) The momentary increase of temperature accompanying sudden compression may be the primary cause of ignition by accelerating the velocity of reaction between molecules and those free radicals present in the gaseous mixture. A sufficient increase in velocity in some favourable volume element of the system may then impose adiabatic conditions before the temperature reverts to its normal value.

If the first mechanism be adopted, the minimum degree of compression required to produce ignition would be given by

$$R = \frac{n_c}{n_e},\tag{1}$$

where n_c is the critical concentration of chain centres required to establish adiabaticity, and n_e is the equilibrium concentration of chain centres existing in the initial mixture. The compression ratio R would be expected to increase by the operation of any factor tending to decrease the equilibrium concentration of chain centres.

On the other hand, if the primary cause of ignition by compression were the momentary rise in temperature produced by adiabatic compression the value of the compression ratio would be determined by the thermal capacity and thermal conductivity of the system as follows.

If a gas is compressed adiabatically from a pressure p_0 to a pressure p the temperature rises from T_0° K. to T° K. given by

$$\log \frac{T}{T_0} = \frac{\gamma - 1}{\gamma} \log \frac{p}{p_0} = \frac{\gamma - 1}{\gamma} \log R,\tag{2}$$

where γ = ratio of specific heat at constant pressure to the specific heat at constant volume. The theoretical rise of temperature will not be realized in a reaction vessel owing to thermal losses during the time required for compression, but it may be expected that the degree of compression required to produce a given rise in temperature will be greater the smaller the value of γ in gases of similar thermal conductivity, and the greater the larger the value of the thermal conductivity in mixtures with similar values of γ.

The following experiments were carried out to distinguish between the two possible mechanisms of ignition by compression. Sensitized mixtures were made directly in the reaction vessel at 480° C. above the upper pressure limit of ignition obtained by the withdrawal method by introducing the components in the correct order. After allowing two minutes for the attainment of uniform composition, the contents of the reaction vessel were compressed by the sudden admission of nitrogen from a large bulb connected to the reaction vessel by a wide bore tap. The tap was closed immediately after

turning, and the final pressure of the mixture determined at leisure. By trial and error the minimum pressure to which a mixture had to be compressed to produce ignition could be determined within about 3 %. The degree of compression was taken as the ratio of the final to the initial pressure of the gaseous mixture.

In fig. 10 is shown the variation of compression ratio with initial total pressure of mixtures containing constant partial pressures of carbon monoxide, oxygen and hydrogen to which purified nitrogen was added as inert gas to augment the initial total pressure. Pyrex reaction vessels of diameters 27·0 and 16·7 mm. were used, and the determinations carried to within 1·5 mm. Hg of the boundary of ignition determined by the withdrawal method.

Using a similar technique the variation of compression ratio with initial total pressure was studied in mixtures containing constant partial pressures of reactants to which the inert gases argon, nitrogen, helium and carbon dioxide were added in turn, with the results shown in fig. 11. The following arguments enable a decision to be made between the two possible mechanisms of ignition by compression.

(1) *The "chain centre" theory.* The equilibrium concentration of free radicals in a reaction of the chain type is determined by the interplay of elementary processes which for convenience may be divided into three main types:

(*a*) Primary processes in which the first centres are produced from which subsequent reaction chains originate.

(*b*) Reactions between free radicals and molecules involving multiplication and destruction of chain centres.

(*c*) Recombination processes between pairs of free radicals in the presence of a third body.

Using this classification the equilibrium concentration of chain centres is given by the following equation, which is based on the original treatment due to Semenoff (1932)

$$\theta + fn_c - gn_e - p\delta n_e^2 = 0, \tag{3}$$

where θ = rate of primary processes, fn_c = rate of chain multiplication, gn_e = rate of destruction of centres exclusive of self-neutralization processes, $p\delta n_e^2$ = rate of recombination reactions where p is the total pressure.

The probability of the chain branching mechanism responsible for the region of ignition obtained by the withdrawal method must of necessity increase with decreasing total pressure. If it were operative above the upper pressure limit of spontaneous ignition, it would be expected that the equilibrium concentration of chain centres would increase as the initial
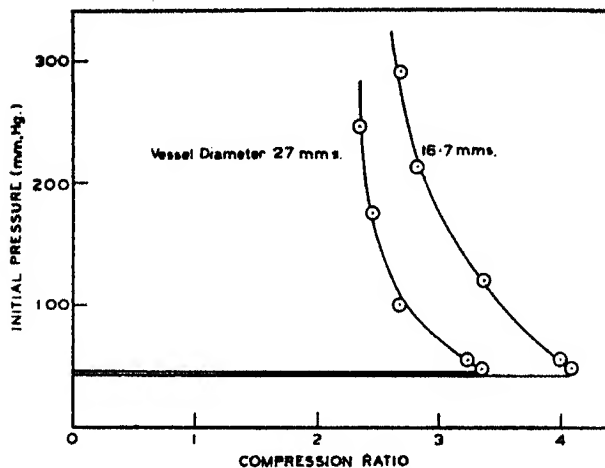
FIG. 10. Variation of compression ratio with initial total pressure of gaseous mixture. Partial pressure of $2CO + O_2$ constant at 48·0 mm. Hg. Hydrogen pressure constant at 1·0 mm. Hg. Temperature 480° C. Nitrogen used to augment the initial total pressure.
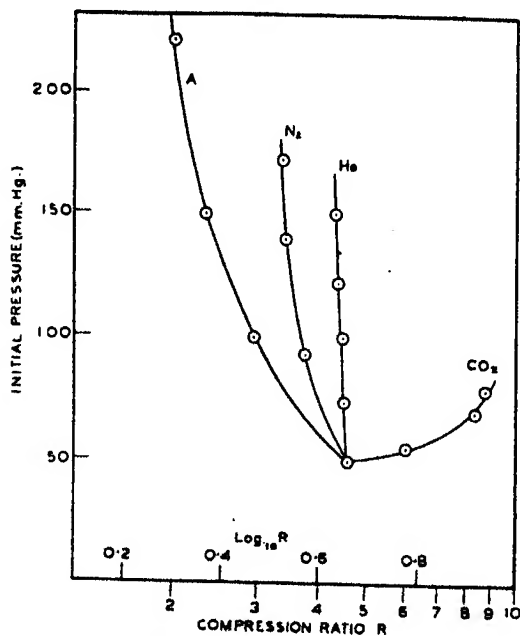

FIG. 11. Variation of compression ratio with initial total pressure of mixtures containing different inert gases. Initial partial pressure of $2CO + O_2$ constant at 50·0 mm. Hg. Hydrogen pressure constant at 0·5 mm. Hg. Pyrex reaction vessel diameter 27·0 mm. Temperature 480° C.

total pressure was reduced, with the result that the compression ratio would show a steady decrease up to the limit of spontaneous ignition. In actual fact the results of fig. 10 show that the compression ratio increases slightly with decreasing initial total pressure, and it must be concluded that the term representing the rate of chain multiplication in equation (3) is negligible above the upper pressure limit of spontaneous ignition.

If the principal method of chain ending involves diffusion of free radicals to the vessel wall the equilibrium concentration will be given by

$$\theta = \frac{kD}{pd} n_e,$$

where D = diffusion coefficient of the gaseous mixture at unit pressure, p = total pressure of mixture, d = vessel diameter and k = a constant depending on the activity of the surface. The compression ratio R then becomes

$$R = \frac{n_c}{n_e} = \frac{kn_c}{\theta pd} D. \tag{4}$$

On the other hand, if recombination processes constitute the principal chain ending mechanism

$$\theta = p\delta n_e^2$$

and

$$R = \frac{n_c}{n_e} = n_c \sqrt{\frac{p\delta}{\theta}}. \tag{5}$$

The results of fig. 10 eliminate this second mechanism since, as p increases, R at first decreases and then tends to a constant value.

On the other hand consideration of equation (4) shows that under conditions in which k, n_c, θ, p and d are constant R should vary directly with the diffusion coefficient of the gaseous mixture. In Table II are given the relative values of the diffusion coefficients calculated from the formula

$$D = \tfrac{1}{3} \lambda \bar{c},$$

where λ = molecular mean free path, and $\bar{c}$ = root mean square velocity. The degrees of compression required to produce ignition in mixtures diluted to the same extent with different inert gases should therefore be in the order

$$R_{He} > R_{N_2} > R_A > R_{CO_2}.$$

This is in entire disagreement with the results of fig. 11 in which the order is

$$R_{CO_2} > R_{He} > R_{N_2} > R_A$$

and on these grounds the theory that ignition by compression is due to a momentary increase in the concentration of chain centres must be rejected.

(2) *The thermal theory.* If the momentary rise of temperature accompanying sudden compression is the fundamental cause of ignition, a consideration of equation (2) shows that the minimum degree of compression required to

TABLE II

Gas	Coefficient of thermal conductivity	Coefficient of gaseous diffusion	Ratio of specific heats
Argon	1·58	2·40	1·667
Nitrogen	2·28	2·63	1·401
Carbon dioxide	1·37	1·42	1·300
Helium	13·90	20·80	1·667
Carbon monoxide	2·15	2·63	1·405
Oxygen	2·33	2·73	1·401

produce ignition in mixtures possessing similar thermal conductivities will increase as the value of γ decreases. The thermal conductivities of all gases except helium employed in these experiments are of the same order of magnitude, as may be seen by reference to Table II which was compiled from values given in *The International Critical Tables*. The following order of compression ratios is to be expected for mixtures diluted to the same extent with carbon dioxide, nitrogen and argon

$$R_{CO_2} > R_{N_2} > R_A,$$

since the values of γ increase in that order.

When a mixture containing argon is replaced by one diluted to the same extent with helium, the value of γ remains unchanged but the thermal conductivity may be increased as much as ninefold. In order to compensate for the increased dissipation of heat in the latter gases during the finite time required for compression, a greater degree of compression will be required to ignite mixtures containing helium than that necessary for similar mixtures diluted with argon.

The verification of these deductions by the results of fig. 11 indicate that the fundamental cause of ignition is the local rise of temperature attending sudden compression.

It will be observed that progressive dilution of a mixture of carbon monoxide and oxygen with nitrogen leaves the values of γ and thermal conductivity practically unchanged, but nevertheless is accompanied by a slight decrease in the degree of compression required for ignition. This would seem to be explained in the following way.

As lower initial pressures of gas are used in the furnace, the excess pressure $p - p_0$ between the compressor bulb and the reaction vessel required to produce a given degree of compression R is also decreased, since

$$p - p_0 = p_0(R - 1).$$

As a result compression will take place more slowly when the initial pressure of the mixture is small and must be carried to a greater degree to compensate for the increased loss of heat during the operation. In a similar way the
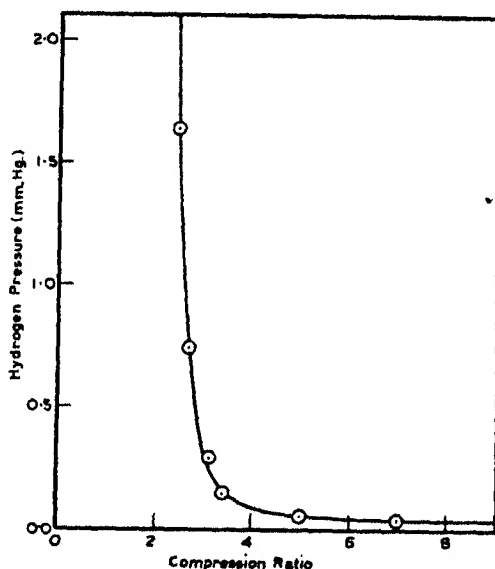
FIG. 12. Variation of compression ratio with hydrogen pressure. Initial pressure of $2CO + O_2$ constant at 100 mm. Hg. Pyrex reaction vessel 27·0 mm. diameter. Temperature 480° C.

increased dissipation of heat in vessels of smaller diameter may account for the results of fig. 10, which show that a greater degree of compression is required for ignition in a 16·7 mm. diameter vessel than in one of 27·0 mm. diameter.

The question arises whether the fluctuation of temperature during sudden compression is sufficient to ignite mixtures of carbon monoxide and oxygen containing no free radical derivatives of hydrogen. A partial answer is provided by the results of fig. 12 which show the variation of R with pressure of hydrogen in mixtures of constant initial total pressure. In mixtures containing no hydrogen—and therefore no free radicals formed from hydrogen—ignition cannot be realized with the degrees of compression experimentally attainable. As the hydrogen concentration rises the compression

ratio decreases rapidly and becomes almost constant for concentrations of hydrogen exceeding 0·5 %. Furthermore, the results obtained by the admission method indicate that self-compression of a mixture containing hydrogen produces ignition only when the initial portions of the gas have passed through the region in which free radicals can be formed rapidly by the low pressure branching mechanism. Unless this condition is fulfilled in the admission experiments the compressed portion of the gas will contain no centres from which reaction chains can start, and the temperature will revert to its normal value before adiabatic conditions can be imposed.

However, as shown by the results of figs. 10, 11 and 12, ignition by compression can be realized in mixtures which have never passed through the region in which chain branching occurs, provided that sufficient time has elapsed for the attainment of a small equilibrium concentration of reaction centres.

Interpretation of results obtained by admission method

We are now in a position to interpret in detail the curves obtained by the admission method.

In fig. 13 is shown in general form the boundaries of ignition obtained by the "admission" and the "withdrawal" methods using mixtures of carbon monoxide and oxygen sensitized with hydrogen. During admission of mixtures containing some fixed percentage of hydrogen, the composition of the contents of the reaction vessel will move along a line OZ, first passing through the region OP in which chain branching is possible by the mechanism responsible for the region of ignition obtained by the withdrawal method. If at the end of the sharing process the final pressure of the mixture is at

X, inflammation occurs,

Y, no ignition takes place,

Z, visible ignition reappears.

While the contents of the furnace lie in the range of pressures from O to P an exponential increase of centres occurs by the chain branching mechanism, and after a time τ the reaction velocity will exceed the critical value required for the establishment of adiabatic conditions. This induction period although too short to be measured by the present apparatus, is finite and of the same order as the time taken to establish the mixture in the reaction vessel. When the final pressure is destined to stop at a point such as X only slightly above P, the reaction chains will have been branching for a time long enough to establish adiabatic conditions. However, as the final pressure to which the mixture tends is increased, the contents of the reaction vessel will pass

through the region OP in a time less than τ, after which chain branching will be suppressed and the concentration of reaction centres will settle down to a steady value below the requirements for ignition. By a further increase in the value of the final total pressure, the initial portions of the mixture containing centres produced during passage from O to P will be compressed at the remote end of the reaction vessel. If the local rise of temperature is sufficient, the intensity of chemical reaction involving those centres already present will be increased to such an extent that adiabatic conditions will be imposed once more, and ignition will spread out from that spot. The three
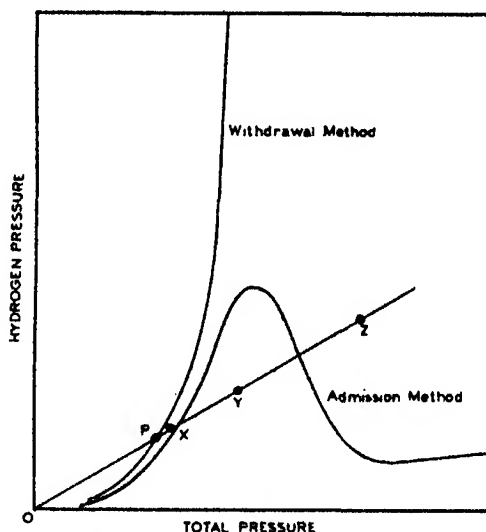
FIG. 13

cycles of low pressure ignition, intermediate stability and high pressure inflammation are depicted in fig. 14 by diagrams A, B and C respectively, in which centres of reaction are represented by dots and the full inking is intended to signify ignition.

The value of the final total pressure at which self-compression first becomes appreciable will depend to some extent on the geometry of the apparatus, and will be made evident by a maximum or point of inflexion in the boundary of inflammation obtained by the admission method. All such curves obtained in the present apparatus which has remained unaltered in design, develop this tendency when the final total pressure of mixtures admitted suddenly to the reaction vessel exceeds about 100 mm. Hg. The higher the final total pressure is made above this value the greater becomes the degree of self-compression and local temperature rise in the compressed

portion of the gases, and the smaller is the number of reaction centres required to establish adiabatic conditions. Accordingly, the minimum percentage of hydrogen required for ignition by self-compression decreases with increasing total pressure, until the line OZ of fig. 13 becomes tangential to the boundary of ignition obtained by the withdrawal method. If the composition of mixtures lies below this tangent no reaction centres will be present in the compressed portion of the issuing gases, and the temperature will revert to its normal value before adiabatic conditions can be imposed by chemical reaction.
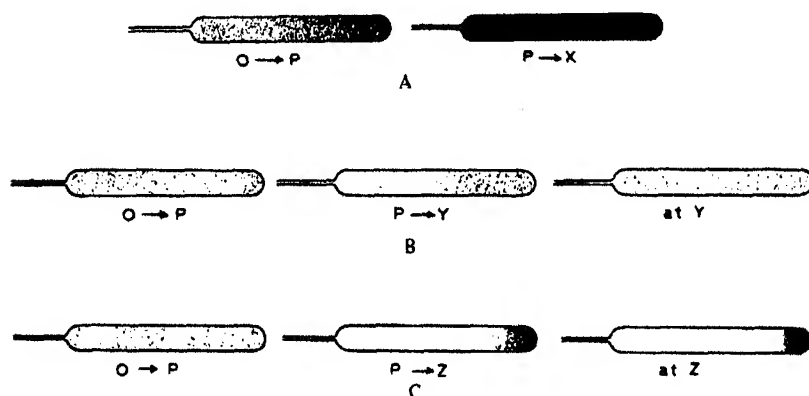
FIG. 14. The behaviour of mixtures of carbon monoxide and oxygen containing hydrogen admitted suddenly to a heated reaction vessel. A. Low-pressure ignition. B. Intermediate stability. C. High-pressure inflammation.

Any factor which contracts the region of low pressure ignition will increase the slope of the tangent and alter the position of the boundary of ignition determined by the admission method. As shown in fig. 8 this may be accomplished by increased surface deactivation in reaction vessels of smaller diameter. Fig. 6 indicates that a similar result may be obtained by using a diluent gas such as carbon dioxide, which is known to be an efficient agent in three-body collisions in the gas phase.

The very similar ignition boundaries represented in fig. 4 for mixtures diluted with nitrogen, oxygen and carbon monoxide respectively are consequent upon the almost identical thermal characteristics of these diatomic gases. Mixtures diluted with argon possess a small thermal conductivity and coefficient of diffusion combined with a large value of γ, and give boundary of ignition situated at very low concentrations of hydrogen.

The only anomalous results are those of fig. 5 provided by mixtures diluted with helium, which show no evidence of self-compression above

100 mm. Hg. Reference to the characteristics of helium given in Table II indicate that the following two factors, of which the second is the more important, may combine to produce this effect:

(1) The rate of diffusion of free radicals to the wall of the reaction vessel through mixtures containing helium may be up to eight times that in similar mixtures diluted with nitrogen.

(2) The thermal conductivity of helium is about six times that of any other gas examined, and will result in very rapid equalization of any fluctuations of temperature produced by self-compression.

The form of the boundary of ignition shown in fig. 5 suggests that ignition in mixtures diluted with helium is obtained only when the initial portions of the gases admitted to the reaction vessel have been situated in the region of chain branching for a time sufficient to establish adiabatic conditions.

It will be recognized that the form of the ignition boundary determined by the admission method is controlled by three factors: the rate of formation of free radicals by isothermal branching chain processes during the early stages of admission of mixtures to the reaction vessel, the extent of the region in which branching chain reactions are possible and the temperature fluctuation accompanying a given degree of self-compression. The three diagrams of fig. 7 indicate that the final total pressure at which the effects of self-compression first become evident, as determined by the maxima in the curves obtained by the admission method, is nearly independent of temperature; on the other hand it will be seen that the minimum hydrogen pressure required to ensure ignition at a given final total pressure increases rapidly with decrease of temperature. In order that a given degree of self-compression should produce ignition it is evident therefore, that the minimum length of the intercept OP of fig. 13 must increase with decrease of temperature, and that a longer time is necessary at lower temperatures for the formation of initial centres which, as explained above, occurs while the composition of the mixture in the reaction vessel is passing through the region to the left of the ignition curve obtained by the withdrawal method. It is concluded therefore, that the expansion of the region of stability observed by the admission method with reduction of temperature must be ascribed principally to decrease in the rate of formation of reaction centres during the early stages of admission of gases to the reaction vessel. This assumption not only explains the increase observed in the minimum hydrogen pressure required for ignition of mixtures admitted to the reaction vessel to values of the final total pressure above 100 mm. Hg as the temperature is reduced, but also would account for the closer approximation observed at lower temperatures between the boundary of

ignition determined by the withdrawal method and that determined by the admission method for values of the final total pressure below 100 mm. Hg.*

CONCLUSION

The results obtained support the view that ignition occurs in reactions of the chain type when chemical change becomes self-heating in a favourable volume element of the reaction vessel. The transition from slow reaction to explosion may be effected by alterations of temperature or composition which increase the probability of chain branching. In the temperature range characteristic of the low pressure explosion of hydrogen and oxygen, mixtures of carbon monoxide and oxygen containing hydrogen ignite by a branching chain mechanism which comes into operation abruptly below a critical pressure, the value of which increases with percentage of hydrogen and temperature. Alternatively, mixtures undergoing stable reaction above the upper pressure limit of explosion can be ignited by sudden compression, which may produce sufficient fluctuations of temperature to establish local branching chain reactions once more. On these assumptions a complete explanation can be given of the unique results obtained by the sudden admission of sensitized mixtures to the heated reaction vessel.

While the exact nature of the branching mechanism is yet to be established, it appears to be similar in characteristics to that responsible for the explosion of hydrogen and oxygen. A further investigation of this matter will be described in the succeeding paper.

SUMMARY

In extending the research of other workers on the catalytic influence of hydrogen on the oxidation of carbon monoxide, it has been found that ignition in mixtures containing hydrogen occurs at temperatures more than 150° C. below those of the pure gases, and is attended by complete combustion when the concentration of hydrogen exceeds about 0·5 %. The region of sensitized ignition is bounded by a lower pressure limit which was

* See additional paragraph at the end of this paper.

not investigated in detail, and an upper pressure limit the dependence of which on temperature and hydrogen concentration was determined by the slow withdrawal of sensitized mixtures from the reaction vessel up to the point of explosion.

Mixtures are stable above the upper pressure limit but may be ignited by sudden compression. A study of the minimum degree of compression required to produce inflammation in mixtures containing different inert gases proved that although the initial presence of free radicals containing hydrogen was essential, the primary cause of ignition was the momentary rise of temperature accompanying sudden compression.

It has also been found that mixtures containing a suitable percentage of hydrogen admitted suddenly to an evacuated reaction vessel ignite when the final pressure is only slightly greater than the upper limit determined by the withdrawal method, but for higher final pressures may be introduced without inflammation occurring. However, ignition reappears when the final pressure is further increased to values above 100 mm. Hg, due to approximately adiabatic compression of the first portions of gas to enter the reaction vessel by the rapid influx of the remainder of the mixture. Owing to the momentary rise of temperature in the compressed portion of the mixture, ignition spreads out from reaction centres formed by chain branching processes operative during the early stages of admission.

[*Added* 25 *July*, 1938. We have to thank Dr D. T. A. Townend for pointing out after completion of the present work, that White and Price (1919) had found that the ignition temperatures of ether-air mixtures and carbon disulphide-air mixtures could be reduced from above 200° C. to room temperatures by admitting the mixed gases as suddenly as possible to an evacuated reaction vessel through a wide-bore tap. The ignition temperatures of acetone-air mixtures and oxy-hydrogen mixtures also were found to be below their normal values when determined by this method, and the authors suggested that ignition was due to the "shock" waves set up by abrupt alterations in the rate of flow of gas entering the reaction vessel. The more detailed experimental results of the present paper provide definite evidence that fluctuation of temperature rather than mechanical shock is the fundamental cause of ignition in experiments of this type.]

REFERENCES

Bone, W. A. 1931 *J. Chem. Soc.* 1, 338–61.
Cosslett, V. E. and Garner, W. E. 1930 *Trans. Faraday Soc.* 26, 190–5.
von Elbe, G. and Lewis, B. 1937 *J. Amer. Chem. Soc.* 59, 2025.

Foord, S. G. 1934 *J. Sci. Instrum.* **2**, 126.

Foord, S. G. and Norrish, R. G. W. 1935 *Proc. Roy. Soc.* A, **152**, 196–220.

Garner, W. E. and Johnson, C. H. 1927 *Phil. Mag.* **3**, 97–110.

Garner, W. E. and Roffey, F. 1929 *J. Chem. Soc.* pp. 1123–40.

Garner, W. E. and Hall, D. A. 1930 *J. Chem. Soc.* pp. 2037–47.

Garner, W. E. and Bawn, C. E. H. 1932 *J. Chem. Soc.* pp. 129–38.

Haber, F., Farkas, L. and Harteck, P. 1930 *Naturwissenschaften*, **18**, 266.

Hadman, G., Thompson, H. W. and Hinshelwood, C. N. 1932 *a Proc. Roy. Soc.* A, **137**, 87.

— — — 1932 *b Proc. Roy. Soc.* A, **138**, 297.

Sagulin, A., Kowalsky, A., Kopp, D. and Semenoff, N. 1930 *Z. phys. Chem.* B, **6**, 307–29.

Semenoff, N. 1932 *Phys. Z. Sowjet.* **1**, 755.

Topley, B. 1930 *Nature, Lond.*, **125**, 560.

White, A. G. and Price, F. W. 1919 *J. Chem. Soc.* p. 1462.

A study of sensitized explosions

III. The kinetics of ignition of carbon monoxide and oxygen sensitized by hydrogen

By E. J. Buckler and R. G. W. Norrish, F.R.S.

Laboratory of Physical Chemistry, Free School Lane, Cambridge

(*Received* 27 *April* 1938)

Introduction

The results of the preceding paper have revealed that in the presence of less than 1 % of hydrogen, mixtures of carbon monoxide and oxygen assume many of the characteristics of oxy-hydrogen mixtures. In both systems ignition is possible over the same range of temperatures, and in each case is confined between upper and lower pressure limits outside which the rate of reaction falls abruptly to small values. It is reasonable to suppose that the catalytic function of hydrogen is primarily to impose a branching mechanism on the carbon monoxide reaction similar to that which operates in the combustion of hydrogen itself, and that since in each case the region of ignition is situated in the same range of temperatures each reaction will be controlled by the same elementary temperature dependent process.

The object of the present work was to investigate the extent to which participation of carbon monoxide in the reaction chains alters the characteristics of the branching mechanism as revealed by a study of the upper pressure limit of ignition.

The existing data on the hydrogen-oxygen reaction indicates that multiplication of chain carriers involves elementary reactions of high energy of activation, which are subject to deactivation in the presence of inert molecules (Sagulin, Kowalsky, Kopp and Semenoff 1930; Grant and Hinshelwood 1933), and it is concluded that ignition is suppressed above the upper pressure limit by a preponderance of ternary deactivating collisions over binary branching collisions. The value of the total pressure at which this occurs is practically independent of the nature and size of the reaction vessel (Thompson and Hinshelwood 1929), being determined only by the speeds and sizes of the various molecules involved in ternary collisions (Grant and Hinshelwood 1933). The value of the upper limit is displaced towards higher pressures as the temperature is increased in a manner given by an Arrhenius equation in which the energy of activation is 26,000 cal. according to Thompson and Hinshelwood (1929), and 24,200 cal. according to Frost and Alyea (1933). A similar value of 25,000 cal. obtained in mixtures of deuterium and oxygen indicates that the elementary reaction associated with this energy of activation does not involve the breaking of an H—H bond (Hinshelwood, Williamson and Wolfenden 1934; Frost and Alyea 1934), although the values of the total pressure required to suppress ignition are generally higher in these mixtures owing to the smaller molecular velocity of deuterium compared with hydrogen.

It has been found that ignition in the present system resembles that obtained in oxy-hydrogen mixtures in that the values of the upper pressure limits of ignition of mixtures of carbon monoxide and oxygen sensitized by hydrogen are not markedly affected by change of vessel diameter, and are displaced by the addition of inert gases to an extent which can be predicted satisfactorily from a knowledge of the velocities and sizes of the molecules involved. On the other hand the relation between the logarithm of the pressure limit and the reciprocal of the absolute temperature is more complex than the corresponding relation in the hydrogen-oxygen reaction, although it becomes linear in mixtures of constant hydrogen/carbon monoxide ratio when the concentration of hydrogen is less than about 2 %. Under these conditions the apparent energy of activation of the branching mechanism, as deduced from the slope of the linear portions of these curves, is only 13,300 cal.—approximately one-half the value obtained by Thompson and Hinshelwood (1929), using mixtures of pure hydrogen and oxygen.

A similar value for the energy of activation is obtained in mixtures sensitized by constant small percentages of deuterium, although in this case the pressure limits of ignition are lower than those obtained in mixtures containing the same percentage of hydrogen.

These results indicate that while ternary collisions undoubtedly control the upper pressure limit of ignition in these mixtures, the presence of carbon monoxide introduces additional chain-ending mechanisms which are not present in the hydrogen-oxygen reaction. Any detailed kinetic mechanism proposed for the ignition of carbon monoxide and oxygen sensitized by hydrogen must be based on the series of elementary reactions adopted to account for the characteristics of mixtures of pure hydrogen and oxygen. The various possible mechanisms for the latter have been exhaustively investigated by Kassel and Storch (1935) and von Elbe and Lewis (1937), who have evolved a self-consistent scheme which has been taken as the basis of the present detailed mechanism.

In the discussion which follows the experimental part of this paper it will be seen that the differences between these two closely related reactions can be satisfactorily explained by one additional chain-ending process introduced by carbon monoxide which competes with a chain-branching reaction involving molecular hydrogen, and that while stable compounds of hydrogen may supply chain carriers necessary for the propagation of reaction chains in carbon monoxide and oxygen, they cannot effect continued branching which is obtained only in the presence of molecular hydrogen. It thus follows that only hydrogen combines the dual function of lowering the temperature of ignition, and catalysing the propagation of the flame.

EXPERIMENTAL METHOD

The apparatus, preparation of gases and experimental procedure were identical with those described in the preceding paper. It was found that precise measurement of ignition limits by the withdrawal method was rendered difficult at the highest temperatures used by an appreciable rate of oxidation prevailing in sensitized mixtures above the upper pressure limit of explosion. Even in vessels "poisoned" by previous rinsing with potassium chloride solution, it was necessary above 550° C. to reduce the time allowed for the attainment of uniform composition to 30 sec., to avoid appreciable reduction in the small percentages of hydrogen during manipulation of the gases. Nevertheless, by this means it was possible to reproduce results within 5 % even at 570° C., giving adequate experimental accuracy for the deductions later to be made.

EXPERIMENTAL RESULTS

Effect of vessel diameter. The limits of ignition of mixtures of $2CO + O_2$ containing different concentrations of hydrogen were determined at 540° C. by the withdrawal method in a number of pyrex reaction vessels each 20 cm. long with diameters ranging from 7·0 to 37·5 mm. The three curves shown in
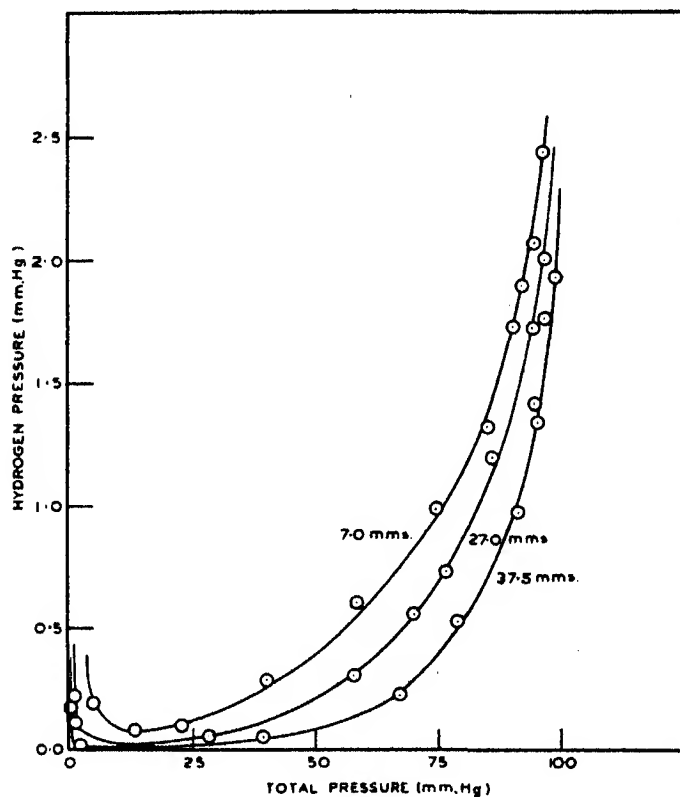
FIG. 1. The variation of ignition limits obtained by the withdrawal method with hydrogen pressure using sensitized mixtures of $2CO + O_2$. Temperature 545° C. Pyrex reaction vessels 20 cm. long and diameters 7·0, 27·0 and 37·5 mm. respectively.

fig. 1 indicate that some lowering of the upper pressure limit to ignition occurs in the smaller vessels, although several factors may contribute to this result. While these curves indicate that the vessel diameter may have some kinetic effect on the upper pressure limit in mixtures containing small quantities of hydrogen, the increased rate of heterogeneous reaction as the surface/volume ratio is increased, and the greater difficulty of attaining

uniform composition, may both combine to reduce the value of the limit in narrow vessels by reducing the hydrogen concentration. The ignition limits in different vessels tend to a constant value when the concentration of hydrogen exceeds 1 %, and the absence of any marked effect of vessel diameter, such as is observed in the combustion of hydrocarbons (Norrish and Foord 1936; Spence 1932), indicates that the branching mechanism is not of the "degenerate" type, and does not depend on the production of stable intermediaries.

The effect of temperature. By adding the components in the correct order, sensitized mixtures of $2CO + O_2$ were made directly in the reaction vessel, to give gases containing concentrations of hydrogen fixed at 10, 2, 1, 0·5 and 0·25 % respectively. The limits of ignition obtained by withdrawing such mixtures to the point of explosion are recorded in Table I for a range of temperatures between 480 and 560° C., each limit representing the mean of three consecutive results differing by not more than 5 %. In mixtures containing 10 % hydrogen the explosions were audible and accompanied by the red flame characteristic of oxy-hydrogen ignition, while in contrast the explosions of mixtures containing 0·25 % hydrogen were very feeble and could not be detected by the withdrawal method below 520° C.

TABLE I. IGNITION LIMITS OBTAINED BY WITHDRAWAL METHOD IN MIXTURES OF $2CO + O_2$ CONTAINING CONSTANT PERCENTAGES OF HYDROGEN

Pyrex reaction vessel 27·0 mm. diameter.

Temperature ° C.	Ignition limits mm. Hg				
	10 %	2 %	1 %	0·5 %	0·25 %
560	—	134·0	108·8	96·6	79·6
550	—	123·0	100·5	85·8	71·2
540	137·7	111·8	89·8	78·6	65·6
530	121·1	100·7	83·9	72·4	54·9
520	109·0	87·7	75·9	63·0	53·5
510	93·1	75·5	67·8	58·3	—
500	75·1	56·9	54·7	47·9	—
490	—	40·2	—	—	—
480	44·3	—	—	—	—

The form of the graph shown in fig. 2 between the reciprocal of the absolute temperature and the logarithm of the pressure limit gives evidence of a kinetic mechanism which is complex in mixtures containing more than 2 % hydrogen, but which simplifies to a linear relation when the concentration of hydrogen is below this value. The apparent energy of activation E of

the branching process may be derived from the slope of these curves by means of the equation

$$\frac{d \log_e P}{d(1/T)} = \frac{E}{R}, \quad \text{(Semenoff 1928)}$$

where P = pressure limit of ignition, T = temperature of ignition limit (°abs.). It is seen that the value of E becomes practically independent of temperature and composition in mixtures containing less than 2 % hydrogen,
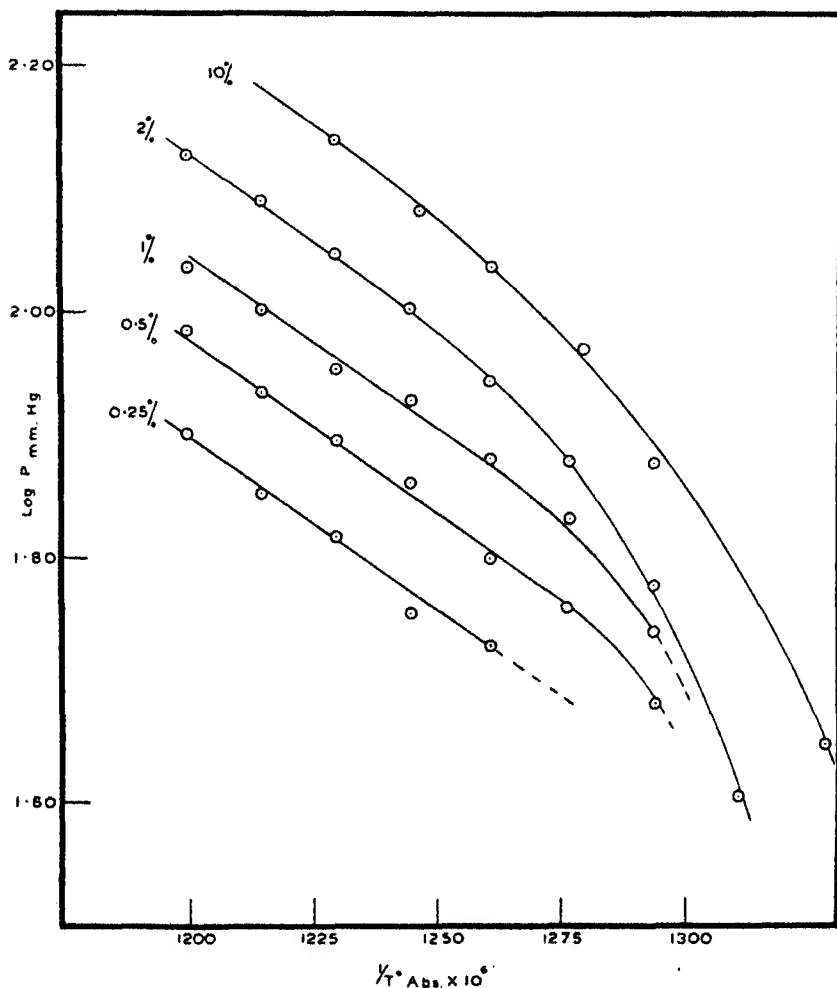

Fig. 2. The temperature coefficient of ignition limits obtained by withdrawal method in mixtures of $2CO + O_2$ containing constant percentages of hydrogen. Pyrex reaction vessel 27·0 mm. diameter.

and possesses a value of 13,100 cal. deduced from the slope of the linear portions of these curves.

Sensitization by deuterium. Two standard mixtures of carbon monoxide and oxygen containing identical concentrations of hydrogen and deuterium respectively were used in conjunction with pure $2CO + O_2$ to compare the values of the ignition limits obtained by the withdrawal method in mixtures containing the same percentage of each form of hydrogen. A number of such limits obtained at 483, 520 and 552° respectively are recorded in order of decreasing percentage of sensitizer in Table II, which shows that the

TABLE II. IGNITION LIMITS OBTAINED BY WITHDRAWAL METHOD IN MIXTURES OF $2CO + O_2$ SENSITIZED BY HYDROGEN AND DEUTERIUM

Pyrex reaction vessel 27·0 mm. diameter.

| | | Ignition limits mm. Hg | | |
Temperature ° C.	Percentage hydrogen or deuterium	Hydrogen sensitized P_1	Deuterium sensitized P_2	P_1/P_2
483	5·22	60·2	44·0	1·37
	4·03	56·3	40·7	1·38
	3·55	56·1	40·3	1·39
	2·87	52·8	37·6	1·40
	2·32	47·4	33·2	1·43
	1·28	37·9	26·5	1·43
520	3·81	94·6	69·3	1·36
	3·32	86·0	63·0	1·37
	2·83	85·0	61·2	1·39
	2·21	82·9	59·6	1·39
	1·10	61·0	43·5	1·40
	0·94	56·5	38·3	1·46
552	2·65	124·5	88·0	1·41
	2·18	114·2	81·6	1·40
	1·95	111·8	79·0	1·41
	1·65	105·5	71·9	1·47
	1·33	101·5	70·0	1·45
	0·87	90·5	63·0	1·43
	0·50	80·0	60·2	1·33

ignition limits of mixtures containing deuterium are definitely lower than those obtained using the same percentage of hydrogen. The ratio of the latter values to the former is approximately constant at 1·42 and shows no systematic variation with temperature, although it decreases slightly when the concentration of sensitizer exceeds about 3 %.

TABLE III. IGNITION LIMITS OBTAINED BY WITHDRAWAL METHOD IN MIX-
TURES OF $2CO + O_2$ CONTAINING 0.5% HYDROGEN AND DEUTERIUM
RESPECTIVELY

Pyrex reaction vessel 27.0 mm. diameter.

Ignition limits mm. Hg

Temperature °C.	Hydrogen sensitized P_1	Deuterium sensitized P_2	P_1/P_2
560	96.6	67.6	1.43
550	85.8	59.5	1.44
540	78.6	54.9	1.43
530	72.4	50.7	1.43
520	63.0	45.0	1.40
510	58.3	41.5	1.41
500	47.9	36.3	1.31
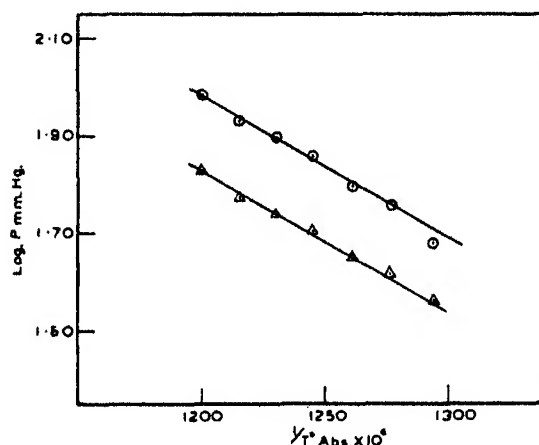
FIG. 3. Temperature coefficient of ignition limits obtained by withdrawal method in
mixtures of $2CO + O_2$ containing 0.5% hydrogen and deuterium respectively. Pyrex
reaction vessel 27.0 mm. diameter. ⊙ Sensitization by hydrogen. ▲ Sensitization by
deuterium.

The relative catalytic effects of hydrogen and deuterium are shown to
greater advantage in Table III, which records the ignition limits of mixtures
containing 0.5% hydrogen and deuterium respectively at a number of
temperatures between 500 and 560°. The relations between the reciprocal of
the absolute temperature and the logarithms of these ignition limits are well
represented by two parallel straight lines, the separation of which confirms
the results of the preceding paragraph in assigning a value 1.42, independent
of temperature, to the ratio of the pressure limits of ignition in mixtures

containing the same percentages of hydrogen and deuterium respectively. The similar gradients of these lines indicate that the apparent energies of activation of the branching mechanisms involving hydrogen and deuterium are identical, and possess the value 13,500 cal., which is in satisfactory agreement with the result 13,100 cal. obtained in the preceding section.

The effect of inert gases. For an accurate comparison of the efficiencies of different inert gases in suppressing the ignition of a complex system of three reactive components it seemed desirable to determine the ignition limits of mixtures containing constant partial pressures of carbon monoxide, oxygen and hydrogen. Since the withdrawal method could not be used for the measurement of ignition limits under these conditions, the following procedure was adopted. Purified inert gas was added to 50·0 mm. Hg of pure $2CO + O_2$ in the reaction vessel until the total pressure approximated to the value of the ignition limit, and after the mixture had attained uniform composition a small extra quantity of inert gas was added containing 2·0 mm. Hg of hydrogen. Addition of the last component was followed after about 5 sec. either by slow reaction or complete ignition, and by repeated experiments the minimum partial pressure of inert gas required to suppress ignition could be determined within 0·5 mm. Hg. The results obtained using argon, helium, nitrogen and carbon dioxide in turn are recorded in Table IV

TABLE IV. EFFECT OF INERT GASES ON THE IGNITION LIMITS

Pyrex reaction vessel 27·0 mm. diameter.
Concentration of $2CO + O_2 = 50·0$ mm. Hg.
Concentration of hydrogen = 2·0 mm. Hg.

Temperature ° C.	Partial pressures of inert gases at limit mm. Hg			
	Argon	Helium	Nitrogen	Carbon dioxide
585	145·0	106·2	103·2	60·1
575	132·8	99·5	94·8	53·9
565	117·5	90·7	86·5	48·3
555	105·1	80·6	76·7	42·9
545	92·6	69·8	66·4	38·2
535	77·4	58·8	54·9	30·9
525	58·3	48·8	42·2	24·0

for a series of temperatures between 585 and 525° C. in a pyrex reaction vessel 27·0 mm. diameter.

The order of effectiveness of these inert gases in suppressing ignition at the upper pressure limit of explosion is therefore

$$CO_2 > N_2 > He > A,$$
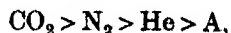
which is similar to the results obtained by van Heiningen (1936) in a study of the influence of A, N_2, He and CO_2 on the limits of inflammability of H_2, CO, CH_4 and butane in air using spark ignition. An analysis of the table reveals that the ratio of the partial pressure of one inert gas to another in the limit mixtures is approximately constant over this temperature range as shown in Table V, in which argon has been taken as the standard with which to compare the effects of helium, nitrogen and carbon dioxide. A further examination of these figures will be made after the kinetic mechanism of the reaction has been developed.

TABLE V

Temperature °C.	P_A/P_{He}	P_A/P_{N_2}	P_A/P_{CO_2}
585	1·36	1·39	2·42
575	1·33	1·40	2·46
565	1·30	1·36	2·43
555	1·30	1·37	2·45
545	1·32	1·39	2·42
535	1·31	1·41	2·50
525	1·20	1·37	2·43
Means	1·30	1·385	2·44

DISCUSSION

The results of the present work and the relevant observations of the preceding paper may be summarized as follows:

(1) The ignition temperatures of carbon monoxide and oxygen are lowered more than 150° C. in the presence of less than 1 % of hydrogen to those characteristic of the explosion of pure hydrogen and oxygen.

(2) Ignition sets in abruptly below a critical pressure and is never preceded by measurable induction periods.

(3) The values of the upper pressure limits of ignition obtained by the withdrawal method are not markedly affected by wide variations in the diameter of the reaction vessel.

(4) In mixtures containing more than 2 % of hydrogen the apparent energy of activation of the upper pressure limit varies in a complex manner with temperature and composition, but when the percentage of hydrogen is below this amount the energy of activation attains a constant value of approximately 13,100 cal.

(5) The apparent energy of activation of the upper pressure limit of ignition of mixtures containing 0·5 % of deuterium is 13,500 cal.

(6) The ratio of the values of the upper pressure limits of ignition of mixtures containing the same percentage concentrations of hydrogen and deuterium respectively is independent of temperature and attains the value 1·42 in mixtures containing less than 2 % of either form of hydrogen.

(7) The effectiveness of different inert gases in suppressing the ignition of mixtures of carbon monoxide and oxygen containing hydrogen is in the order

$$CO_2 > N_2 > He > A,$$
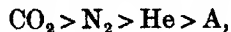
while the ratio of the partial pressures of any pair of inert gases required to prevent ignition of mixtures containing fixed concentrations of reactive gases is approximately constant over the range of temperatures from 525 to 585°.

From the facts enumerated above it may be concluded that molecular hydrogen, besides supplying those free radicals essential for self-propagating reaction chains in mixtures of carbon monoxide and oxygen, also introduces a branching mechanism which operates at temperatures far below those required to maintain the branching chain reactions responsible for the ignition of the pure gases. Since the region of sensitized ignition of carbon monoxide is situated in the same range of temperatures as the explosion of hydrogen and oxygen, the same chain branching processes will occur in both systems, and any kinetic mechanism proposed for the latter must also apply to the present reaction, being modified only to the extent of including additional chain propagating and chain-ending reactions involving carbon monoxide molecules. While the kinetic formulae developed to account for the behaviour of a system of three reactive components will be necessarily complex, the experimental results indicate that a simplification is to be expected when the concentration of hydrogen becomes small.

General conditions of ignition. As has been shown in the previous paper, the general equation representing the rate of increase of centres in a chain reaction is given by

$$\frac{dn}{dt} = \theta + \phi n - \delta n^2,$$

(Semenoff 1932, modified by Foord and Norrish 1935)

where θ = rate of production of chain carriers by primary processes, ϕ = difference between the probabilities of branching and deactivation exclusive of self-neutralization, δn^2 = rate of destruction of chain centres by self-neutralization processes. The transition from slow reaction to ignition in a chain reaction is best studied in a system such as that of hydrogen and oxygen sensitized by nitrogen peroxide (Foord and Norrish 1935) in which the probability of chain branching is small and under precise control. It has
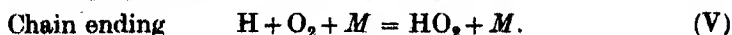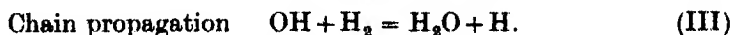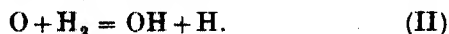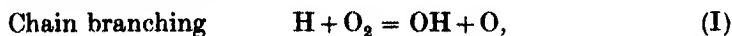
been found by these authors that a positive value of ϕ is not necessarily the general criterion for ignition, since when ϕ is small the initial exponential increase of chain centres may be arrested by self-neutralization processes, and the system may settle down to a stable reaction consequent upon a small equilibrium concentration of chain centres. Ignition sets in when the intensity of reaction exceeds a critical value required to impose adiabatic conditions in some favourable volume element of the reaction vessel, a condition which is attained when $\phi > \phi_c$, where the value of ϕ_c is small, positive and dependent to some extent on the dimensions of the system.

On the other hand, the characteristics of many chain reactions, especially the explosion of unsensitized hydrogen and oxygen, are described by expressions for ϕ which change rapidly from negative to positive values with slight alteration of temperature or composition. In such systems the range of conditions in which ϕ increases from zero to the small positive value required for ignition is so contracted as to be beyond experimental investigation, and although the ultimate cause of ignition may be a disturbance of thermal equilibrium, the formal condition may be given without serious error as
$$\phi > 0.$$

There is every indication that this condition controls ignition in the present reaction. In particular, it has been found impossible to adjust experimental conditions to give any appreciable induction periods; at the upper pressure limit studied by the withdrawal method there is an abrupt transition from slow reaction to immediate ignition with no intervening region in which the velocity of chemical change increases with decrease of pressure.

Chain mechanisms. While the characteristics of many chain reactions can be satisfactorily described by a purely formal treatment without assuming any specific mechanism, an accurate comparison of two systems so closely related as the present one and that of hydrogen and oxygen can be achieved only through a study of the possible elementary reactions involved. A systematic mathematical investigation of the hydrogen-oxygen reaction undertaken by Kassel and Storch (1935), and later completed by von Elbe and Lewis (1937), revealed that the most satisfactory detailed kinetic mechanism capable of accounting for the characteristics both of the slow reaction and the region of low-pressure explosion could be constructed on the following fundamental reactions:

Chain branching	$H + O_2 = OH + O,$	(I)
	$O + H_2 = OH + H.$	(II)
Chain propagation	$OH + H_2 = H_2O + H.$	(III)
Chain ending	$H + O_2 + M = HO_2 + M.$	(V)

The first reaction is endothermic to the extent of about 13,000 cal. and has a high energy of activation, while the second, although not proceeding at every collision (Kistiakowsky 1930), is exothermic and of sufficient efficiency to exclude any other reactions involving O atoms. All OH groups produced by these two reactions undergo reaction III, while the majority of H atoms are removed by the last reaction, which, as has been shown by the work of Cook and Bates (1935), Farkas and Sachsse (1934) and Bodenstein and Schenke (1933), proceeds only by triple collisions. An essential feature of the theory is that HO_2 radicals should possess considerable stability, and at the relatively low pressures of the region of ignition should be destroyed at the vessel wall without continuing the reaction chains. At the higher pressures character- istic of the slow reaction these radicals may exist for a sufficient time in the gas phase to undergo reaction with hydrogen according to one of the equations

$$HO_2 + H_2 = H_2O_2 + H$$
$$\text{or} \quad HO_2 + H_2 = H_2O + OH,$$
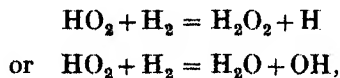
but these chain-propagating reactions need not be considered in a treatment of the region of low-pressure explosion.

Since the only chain carriers involved at these temperatures are O, H and OH, the presence of carbon monoxide can introduce no more than the following two reactions:

$$CO + OH = CO_2 + H, \tag{IV}$$

$$O + CO + M = CO_2 + M. \tag{VI}$$
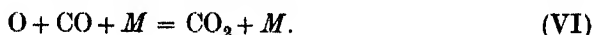
Reaction IV, which was proposed by Haber, Farkas and Harteck (1930) as one of the essential reactions in the oxidation of moist carbon monoxide, is supported by the work of Bonhoeffer and Haber (1928), on the spectrum of the flame of moist carbon monoxide, and constitutes a chain link very similar to reaction III. A study of the photochemical oxidation of carbon monoxide by Harteck and Kopsch (1931), Harteck and Geib (1932), Jackson (1934), and Groth (1937) reveals that reaction VI, which is exothermic to the extent of about 127,000 cal., possesses only a small energy of activation approximating to 1·8 cal. Although the ratio of binary to ternary collisions in a gas at atmospheric pressure is of the order of 10^3, a reaction as efficient as VI will constitute a probable alternative to reaction II when the concentra- tion of hydrogen is small. Chain branching in the present system therefore is controlled by ternary collisions at two separate links in the reaction chain as follows:

$$H + O_2 = OH + O, \quad \text{(I)} \qquad O + H_2 = OH + H, \quad \text{(II)}$$
$$H + O_2 + M = HO_2 + M, \quad \text{(V)} \qquad \text{and} \qquad O + CO + M = CO_2 + M, \quad \text{(VI)}$$
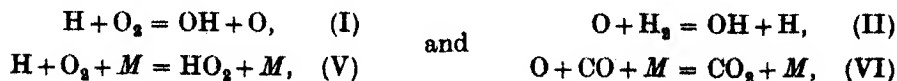
whereas in the hydrogen-oxygen reaction branching is conditioned only by the rates of reactions I and V.

The mathematical theory based on this fundamental distinction between the two reaction mechanisms provides a complete explanation of the experimental results obtained, and reveals important numerical relation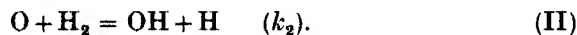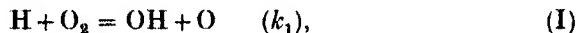s between the apparent energy of activation of the upper limits of ignition in the two systems, and between the relative effects of hydrogen and deuterium in the present reaction.

Theory of reaction kinetics

All the important experimental results of this paper have been concerned with the upper pressure limit of ignition, which is controlled principally by chain-branching and chain-ending reactions in the gas phase. In the first instance, therefore, the destruction of reactive species at the vessel wall, which is responsible for the lower pressure limit of ignition and which may have some kinetic influence on the upper limit in mixtures of small hydrogen concentration at low total pressures, will be neglected in the following treatment. On the basis of the foregoing discussion the following series of reactions are proposed to account for the upper pressure limit of ignition in mixtures of carbon monoxide and oxygen containing hydrogen.

(a) *Chain initiation.* The first chain centres, which may be taken as H atoms, are assumed to be formed by primary processes either in the gas phase or at the surface. Provided such processes are not excluded completely, their mechanism and velocity n_0 are not important in determining the position of the limits of ignition.

(b) *Chain branching.*

$$H + O_2 = OH + O \qquad (k_1), \qquad (I)$$

$$O + H_2 = OH + H \qquad (k_2). \qquad (II)$$

(c) *Chain propagation.*

$$OH + H_2 = H_2O + H \qquad (k_3), \qquad (III)$$

$$OH + CO = CO_2 + H \qquad (k_4). \qquad (IV)$$

(d) *Chain ending.*

$$H + O_2 + M = HO_2 + M \qquad (k_5), \qquad (V)$$

$$O + CO + M = CO_2 + M \qquad (k_6). \qquad (VI)$$
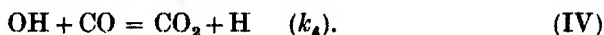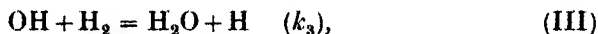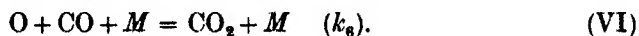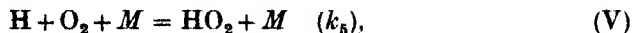
M represents any molecular species in the system and may be O_2, H_2, CO or inert gas molecules. It is assumed that HO_2 is destroyed without continuing the reaction chains.

It is then easy to deduce from this series of reactions that the rate of production of H atoms is given by

$$\frac{d[H]}{dt} = n_0 + \left\{ \frac{2k_1}{1 + \dfrac{k_6[CO]\,M}{k_2[H_2]}} - k_5\,M \right\} [H]\,[O_2], \qquad (VII)$$

which is of the form

$$\frac{dn}{dt} = \theta + \phi n,$$

where ϕ is the effective probability of chain branching.

It may readily be shown that the rate of production of water and carbon dioxide is dependent on the H-atom concentration according to the equation

$$\frac{d}{dt}\{[CO_2] + [H_2O]\} = 2k_1[H]\,[O_2]. \qquad (VIII)$$

It follows that the ignition limits are described by the value of ϕ in equation VII which controls the rate of increase of H-atom concentration. Assuming that the transition from slow reaction to explosion on reduction of pressure occurs when $\phi = 0$, the conditions at the ignition boundary will be given by

$$2k_1 = k_5\,M\left\{ 1 + \frac{k_6[CO]\,M}{k_2[H_2]} \right\}, \qquad (IX)$$

where k_1 is the only quantity subject to considerable variation with temperature.

As $[CO]/[H_2]$ is varied from 0 to ∞, equation IX simplifies to three special cases, each of which has been realized in practice:

(1) The upper pressure limit of mixtures of hydrogen and oxygen containing no carbon dioxide may be described by the equation

$$2k_1 = k_5\,M, \qquad (X)$$

which, as shown by von Elbe and Lewis (1937), is in full agreement with the existing experimental data.

(2) When the percentage of hydrogen is small, the first term on the right-hand side of equation IX is negligible compared with the second, and the boundary of ignition may be described by the equation

$$2k_1 = \frac{k_5 k_6\,M^2[CO]}{k_2[H_2]}. \qquad (XI)$$

(3) When the mixtures contain no hydrogen, the value of the effective branching factor in equation VII is negative for all values of the total

pressure, and ignition becomes impossible. However, equation VIII indicates that slow reaction is still possible in such mixtures if H atoms are supplied through the decomposition of compounds of hydrogen such as water, alcohol, etc.

The effect of concentration of hydrogen. By rearrangement of equation IX it may be shown that the variation in value of the upper pressure limit of ignition with concentration of hydrogen is given by

$$H_2 = \frac{k_5 k_6 [CO] M^2}{k_2 (2k_1 - k_5 M)}. \tag{XII}$$

The quantities $k_5 M$ and $k_6 M$ each represent the sum of separate terms for the various molecular species involved in ternary collisions. For instance,

$$k_5 [H] [O_2] M = [H] [O_2] \{ Z_{O_2} [O_2] + Z_{CO} [CO] + Z_{H_2} [H_2] + Z_X [X] \},$$

where X may be any inert gas molecule, and Z_X, etc., represent the number of ternary collisions per second involving H, O_2 and X at unit partial pressure of X. In the present experiments the variation of the pressure limit of ignition obtained by the withdrawal method with concentration of hydrogen has been studied in mixtures of $2CO + O_2$ containing no inert gas and not more than 3 % of hydrogen. Under these conditions each of the quantities $k_5 M$ and $k_6 M$ will be given by expressions of the form

$$k_5 M = P \{ \tfrac{1}{3} Z_{O_2} + \tfrac{2}{3} Z_{CO} \},$$
$$k_6 M = P \{ \tfrac{1}{3} Z'_{O_2} + \tfrac{2}{3} Z'_{CO} \},$$

where P is the total pressure, and Z'_{O_2}, etc., are quantities similar to Z_{O_2} except that O and CO are involved in the ternary processes in place of H and O_2. Substitution of these expressions in equation XII leads to the following relation between the concentration of hydrogen and the total pressure at the boundary of ignition obtained by the withdrawal method in mixtures of $2CO + O_2$ containing small percentages of hydrogen:

$$H_2 = \frac{k_7 P^3}{k_1 - k_8 P}, \tag{XIIa}$$

where k_7 and k_8 are independent of temperature and pressure, while k_1, as previously mentioned, has a large temperature coefficient. The curves derived from this equation are of the same form as those determined by the withdrawal method for the upper limit of ignition, shown in fig. 2 of the preceding paper. This may be seen by reference to fig. 4 in which experimental values from fig. 2 of the preceding paper for the upper limit of ignition at 545° C. have been plotted beside the curve derived from equation XIIa taking $k_1/k_8 = 120$ and $k_7/k_8 = 4.58 \times 10^{-5}$.

The effect of temperature. The preceding equations lead to the following dependence on temperature of the upper pressure limit of ignition obtained by the withdrawal method in mixtures of $2CO + O_2$ sensitized by hydrogen:

$$k_9 e^{-E/RT} = k_8 P + k_7 \frac{[CO]}{[H_2]} P^2, \text{ where } k_9 e^{-E/RT} = k_1. \qquad \text{(XIII)}$$
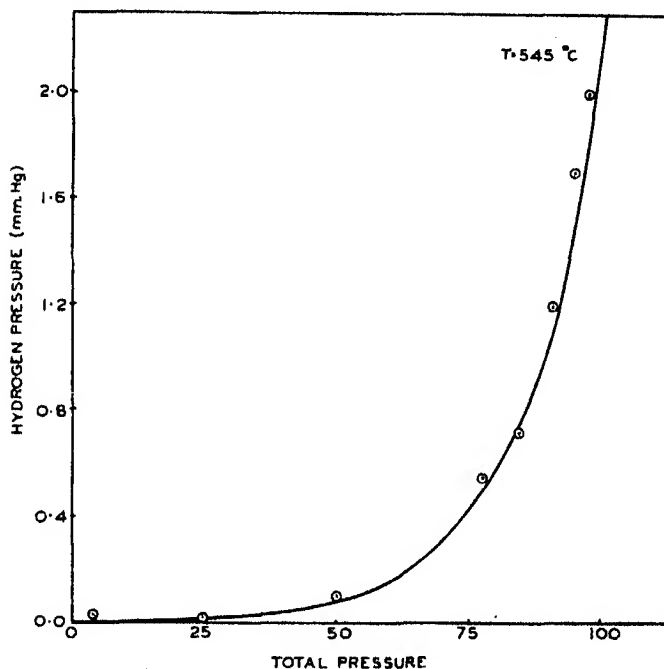
FIG. 4

This equation gives linear relations between $\log P$ and $1/T$ for the limiting cases in which either term of the right-hand side is negligible compared with the other. In mixtures of oxygen and hydrogen containing no carbon monoxide the slope of the line is given by

$$\frac{d \log_e P}{d(1/T)} = \frac{E}{R}.$$

In mixtures of oxygen and carbon monoxide containing constant small percentages of hydrogen the second term of equation XIII becomes the more

important, especially at high total pressures, and the variation of log P and $1/T$ may be written

$$\frac{d \log_e P}{d(1/T)} = \frac{E}{2R}.$$

The apparent energy of activation of the upper pressure limit of ignition may therefore be expected to decrease from E to $\frac{1}{2}E$ as the composition changes from pure oxygen and hydrogen to that of mixtures of carbon monoxide and oxygen containing only very small percentages of hydrogen.

These deductions are confirmed in a striking way by the graphs between log P and $1/T$ shown in fig. 2, in which it is seen that the slope is continuously variable in mixtures containing 10 % of hydrogen, but becomes linear over an increasing range of temperatures as the concentration of hydrogen is reduced from 2 to 0·25 %. Furthermore, the average value of the apparent energy of activation deduced from the linear portions of these curves and that of fig. 3 is 13,300 cal., which is approximately one-half the figures 26,000 cal. given by Thompson and Hinshelwood (1929) and 24,200 cal. obtained by Frost and Alyea (1933) for the energy of activation of the upper pressure limit of ignition of mixtures of oxygen and hydrogen. So close an agreement between theory and experiment confirms the view that carbon monoxide itself does not introduce any chain-branching reactions at these temperatures, but is restricted to the propagation and ending of chains by processes with small temperature coefficients.

Sensitization by deuterium. The velocity constant k of any elementary reaction is given by

$$k = S\sqrt{(2)} \pi\sigma^2 \sqrt{(\bar{u}_1^2 + \bar{u}_2^2)} e^{-E/RT}, \tag{XIV}$$

where σ = collision diameter of the colliding particles, $\bar{u}_1$ and $\bar{u}_2$ = root mean square velocities of reactants, S = steric factor of reaction, E = energy of activation. A comparison of the effects of deuterium and hydrogen in the present reaction involves examination of changes in individual velocity constants brought about by alterations in $\bar{u}_1$ and E; S, σ and $\bar{u}_2$ remaining unchanged.

The limiting cases of equation IX for the limits of ignition in oxy-hydrogen mixtures and mixtures of carbon monoxide and oxygen containing small quantities of hydrogen respectively may be written

$$M = 2\frac{k_1}{k_5} \tag{XV}$$

and

$$M^2 = 2\frac{k_1}{k_5} \cdot \frac{k_2[\text{H}_2]}{k_6[\text{CO}]}. \tag{XVI}$$

It has been assumed that the only elementary reaction with a marked temperature coefficient is

$$H + O_2 = OH + O, \quad (k_1) \tag{I}$$
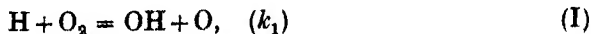
and it is to be expected on theoretical grounds that the corresponding reaction with deuterium atoms should possess a similar energy of activation, since no rupture of H—H or D—D bonds is involved. This is supported both by the results of the present work and those of Frost and Alyea (1934) and Hinshelwood, Williamson and Wolfenden (1934) in which it is seen that the apparent energies of activation of the upper pressure limits of ignition are not affected by substitution of deuterium for hydrogen.

From a study of the photochemical oxidation of hydrogen and deuterium iodides it has been shown by Cook and Bates (1935) that the efficiencies of ternary collisions in the formation of HO_2 and DO_2 are identical, and, in addition, it is to be expected that the ratio of binary collisions in reaction I to ternary collisions of the type

$$H + O_2 + M = HO_2 + M \quad (k_5) \tag{V}$$
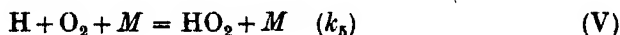
will be the same for deuterium atoms under otherwise identical circumstances, provided that the third bodies represented by M are the same in each case. In mixtures of carbon monoxide and oxygen containing only about 1 % of sensitizer, therefore, the quantity k_1/k_5 is not affected by substitution of deuterium for hydrogen, although this does not apply to mixtures of $2H_2 + O_2$ and $2D_2 + O_2$ owing to the smaller molecular velocities of deuterium molecules entering into ternary collisions in the latter system (Hinshelwood, Williamson and Wolfenden 1934).

The value of k_6 in the reaction

$$O + CO + M = CO_2 + M \quad (k_6) \tag{VI}$$
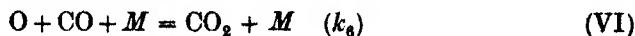
will evidently be the same in mixtures of carbon monoxide and oxygen containing small percentages of hydrogen and deuterium respectively, since the proportion of ternary collisions involving hydrogen or deuterium molecules is negligible.

A comparison of the reactions

$$O + H_2 = OH + H \quad (k_2) \tag{II}$$

and

$$O + D_2 = OD + D \quad (k_2') \tag{IIa}$$
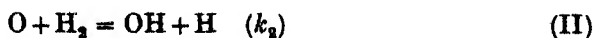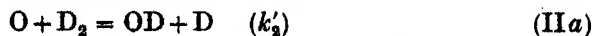
is more difficult owing to scarcity of information on the respective temperature coefficients. The energy of activation of any reaction is given by the difference between the potential energy of the intermediate activated

complex and the zero-point energies of the reactants. If it be assumed that the potential energies of the activated complexes (OHH) and (ODD) are identical, the difference between the energies of activation of reactions II*a* and II will be given by the difference in zero-point energies of H_2 and D_2 respectively, namely 1800 cal. (Urey and Teal 1935). However, in view of the fact that many activated complexes themselves appear to possess zero-point energy, this figure is probably too high, and may be reduced to as little as 400 cal. if it be assumed that the difference in potential energies of (OHH) and (ODD) is equivalent to the difference in zero-point energies of OH and OD. Some evidence may be provided by the work of Wynne-Jones (1936) on the ionic products of H_2O and D_2O, in which it was calculated that the difference in free energy of the two reactions

$$D + OD = D_2O,$$

$$H + OH = H_2O,$$
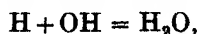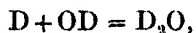
was 970 cal. Although these small differences in energy of activation play a part in fixing the absolute value of k_2/k_2' they will not produce in it any appreciable variation with temperature in the region of 800° abs. used in these experiments.

Assuming that the relative masses of H_2, O and D_2 are 2, 16 and 4 respectively, the value of k_2/k_2' derived from equation XIV is given by

$$\frac{k_2}{k_2'} = \sqrt{\left(\frac{\frac{1}{16}+\frac{1}{2}}{\frac{1}{16}+\frac{1}{4}}\right)} e^{\Delta E/RT} = 1 \cdot 34 \, e^{\Delta E/RT},$$

where ΔE = difference in energies of activation of reactions II*a* and II respectively. The foregoing analysis of all the constants involved in equation XVI indicates that the ratio of the upper pressure limits of ignition in mixtures sensitized by the same percentage of hydrogen and deuterium respectively is given by

$$\frac{P}{P'} = \sqrt{\left(\frac{k_2}{k_2'}\right)} = 1 \cdot 158 \, e^{\Delta E/2RT}.$$

The calculated values of P/P' at 530° C. for $\Delta E = 0$, 400, 970 and 1800 cal. are 1·16, 1·31, 1·57 and 2·04 respectively compared with the value 1·42 to which the observed ratio tends for small percentages of hydrogen and deuterium. A further calculation shows that for $\Delta E = 970$ cal. the variation in P/P' from the mean value over the temperature range studied could not be more than 2 %, which is less than the experimental errors involved in determining the ignition limits.

It may be concluded therefore that the relative effects of hydrogen and deuterium in this reaction may be explained by the slower rate of the elementary process IIa compared with II, due to a smaller collision number and a difference of about 800 cal. in the energies of activation. This satisfactory agreement between theory and experiment justifies the many assumptions involved and provides strong support to the kinetic mechanism adopted.

The effects of inert gases. In mixtures of carbon monoxide, oxygen and inert gas X, containing small quantities of hydrogen, it has been shown that the upper pressure limit of ignition is given by

$$2k_1 k_2 \frac{[H_2]}{[CO]} = \{Z_{O_2}[O_2] + Z_{CO}[CO] + Z_X[X]\}\{Z'_{O_2}[O_2] + Z'_{CO}[CO] + Z'_X[X]\},$$
(XVII)

where the two terms on the right-hand side replace the quantities $k_5 M$ and $k_6 M$ respectively in equation XI. The collision constants are given by equations of the form

$$\left. \begin{aligned} Z_X &= 2\sigma^2 \bigg/ \sqrt{\left\{2\pi R T\left(\frac{1}{m}+\frac{1}{m_x}\right)\right\}}, \\ Z_X &= 2\sigma^2 \bigg/ \sqrt{\left\{2\pi R T'\left(\frac{1}{m'}+\frac{1}{m_x}\right)\right\}}, \end{aligned} \right\}$$
(XVIII)

where m and m' are the masses of HO_2 and CO_2 respectively and m_x is the mass of the third molecule X. σ^2 and σ'^2 are defined as the effective cross-sectional areas of the processes

$$H + O_2 + M = HO_2 + M,$$
(V)

$$O + CO + M = CO_2 + M.$$
(VI)
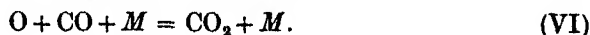
The ratio of each of these quantities to the square of the actual diameter of the corresponding intermediate complex will be a measure of the efficiency of the third particle in completing a reaction of the type V or VI.

For a given inert gas the values of σ and σ', and therefore Z_X and Z'_X, will be of the same order of magnitude, and as a first approximation it may be assumed that their ratio is the same for each of the inert gases used, i.e.

$$\frac{Z_{He}}{Z'_{He}} = \frac{Z_A}{Z'_A} = \frac{Z_{N_2}}{Z'_{N_2}} = \frac{Z_{CO_2}}{Z'_{CO_2}}.$$

Applying this approximation to equation XVII, it will be found that in mixtures containing constant partial pressures of carbon monoxide, hydrogen and oxygen, the partial pressures of different inert gases required to suppress ignition at a given temperature will be given by

$$Z_{He}[He] = Z_{N_2}[N_2] = Z_{CO_2}[CO_2] = Z_A[A].$$
(XIX)

The ratios [A]/[He], [A]/[N₂] and [A]/[CO₂] given in Table V are seen to be independent of temperature, and their mean values may be interpreted by equation XIX as the experimental values of Z_{He}/Z_A, Z_{N_2}/Z_A and Z_{CO_2}/Z_A. By means of the formula given in equation XVIII it is then possible to calculate the experimental values of

$$\frac{\sigma^2_{HeHO_2}}{\sigma^2_{AHO_2}}, \quad \frac{\sigma^2_{N_2HO_2}}{\sigma^2_{AHO_2}} \quad \text{and} \quad \frac{\sigma^2_{CO_2HO_2}}{\sigma^2_{AHO_2}},$$

which are recorded in Table VI.

In Table VI are also given the corresponding theoretical values of these quantities deduced from the values of the molecular diameters calculated from measurements of the coefficients of viscosity, diffusion and thermal conductivity of gases (Jeans 1925). The ratio of the experimental to the theoretical value of $\sigma^2_{HeHO_2}/\sigma^2_{AHO_2}$, etc., will be a measure of the relative efficiency E_{He}/E_A, etc., of helium compared with argon in a triple collision. On this basis it may be calculated from Table VI that the relative efficiencies of helium, nitrogen and carbon dioxide are respectively 0·90, 1·22 and 1·98, taking the efficiency of argon as unity.

TABLE VI

	$\sigma^2_{HeHO_2}/\sigma^2_{AHO_2}$	$\sigma^2_{N_2HO_2}/\sigma^2_{AHO_2}$	$\sigma^2_{CO_2HO_2}/\sigma^2_{AHO_2}$
Experimental	0·58	1·27	2·49
Gas-kinetic	0·64	1·04	1·26

In view of the assumptions made in the calculation, these values of the relative efficiencies must be regarded as approximate, and probably represent a mean for the two reactions

$$H + O_2 + M = HO_2 + M, \tag{V}$$

$$O + CO + M = CO_2 + M. \tag{VI}$$
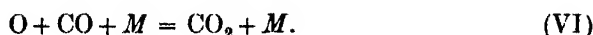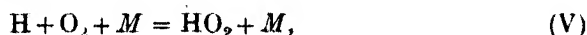
It is seen that the larger the number of degrees of freedom of the third molecule, the higher is its efficiency at a given triple collision. A similar result is provided by the specific quenching coefficients of added CO_2, N_2, O_2 and H_2 in the fluorescence of NO_2, which were found by Baxter (1930) to be 0·87, 0·29, 0·24 and 0·15 times that of NO_2 itself. However the quenching of fluorescence often involves specific transfers of electronic energy, which forbid a close comparison with ternary collision processes such as V and VI. A more analogous reaction is

$$O + O_2 + M = O_3 + M,$$
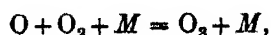
in which the efficiencies of helium and argon are about one-tenth, and that of nitrogen one-half the efficiency of carbon dioxide as third bodies (Beretta and Schumacher 1932).

It may be concluded that the effects of inert gases on the ignition limits confirm the view that the chain-ending processes in this reaction involve ternary collisions in the gas phase.

Conclusion

The results described above provide a link between two closely related reactions—the combustion of hydrogen and that of moist carbon dioxide—and provide further evidence on the nature of the branching chain mechanism involved in the explosion of hydrogen and oxygen. It appears that in the latter system, reaction chains branch at two distinct links, one of which has a high energy of activation and does not involve the breaking of an H—H bond, while the other is an efficient reaction between a chain carrier and a hydrogen molecule. In mixtures of hydrogen and oxygen the first reaction alone is prevented by ternary collisions, while in mixtures containing a high percentage of carbon monoxide, a second three-body process is introduced in competition with the second link. Extensive multiplication of chain centres can only occur when both elementary branching chain reactions are completed, and the absence of the second link involving molecular hydrogen in mixtures of moist carbon monoxide and oxygen provides an explanation of the fact that while water may supply those radicals necessary for chain propagation, its presence has no effect on the ignition limits.

Summary

It has been found that mixtures of carbon monoxide and oxygen containing only traces of hydrogen resemble oxy-hydrogen mixtures in that both ignite over the same range of temperatures, and both possess upper pressure limits of ignition not markedly affected by change of vessel diameter, which vary in the presence of inert gases in a manner suggesting that the processes

responsible for multiplication of chain carriers may be prevented by collisions of the second kind with other molecules. In mixtures of $2CO + O_2$ of constant $CO : H_2$ ratio the relation between $1/T$ and $\log P$ (P being the pressure limit of ignition at $T°$ abs.) is linear when the concentration of hydrogen is less than about 2 %, with a slope corresponding to an apparent energy of activation of 13,300 cal., approximately one-half the corresponding figure given for mixtures of $2H_2 + O_2$, while for mixtures of $2CO + O_2$ containing higher percentages of hydrogen the curves show a variable slope. These facts suggest that carbon monoxide introduces additional chain-ending processes into the mechanism of the hydrogen-oxygen reaction. A similar value for the apparent energy of activation is obtained in mixtures of $2CO + O_2$ containing 0·5 % of deuterium, while the ratio of the values of the pressure limits of ignition of mixtures sensitized by the same percentage of hydrogen and deuterium respectively becomes constant at 1·42 when the concentration of sensitizer is below about 2 %.

The catalytic effect of hydrogen on the combustion of carbon monoxide, and the difference in kinetic characteristics between this reaction and that between pure hydrogen and oxygen can be completely described by introduction of the two additional elementary reactions $O + CO + M = CO_2 + M$ and $OH + CO = CO_2 + H$ into the mechanism for the ignition of mixtures of $2H_2 + O_2$ proposed by Kassel and Storch (1935) and modified by von Elbe and Lewis (1937).

REFERENCES

Baxter, W. P. 1930 *J. Amer. Chem. Soc.* **52**, 3920.
Beretta, U. and Schumacher, H. J. 1932 *Z. phys. Chem.* B, **17**, 417.
Bodenstein, M. and Schenke, P. W. 1933 *Z. phys. Chem.* B, **20**, 420.
Bonhoeffer, K. F. and Haber, F. 1928 *Z. phys. Chem.* A, **137**, 281.
Cook, G. A. and Bates, J. R. 1935 *J. Amer. Chem. Soc.* **57**, 1775.
Farkas, L. and Sachsse, H. 1934 *Z. phys. Chem.* B, **27**, 111.
Foord, S. G. and Norrish, R. G. W. 1935 *Proc. Roy. Soc.* A, **152**, 196.
Frost, A. A. and Alyea, H. N. 1933 *J. Amer. Chem. Soc.* **55**, 3227.
Frost, A. A. and Alyea, H. N. 1934 *J. Amer. Chem. Soc.* **56**, 1251.
Grant, G. H. and Hinshelwood, C. N. 1933 *Proc. Roy. Soc.* A, **141**, 29.
Groth, W. 1937 *Z. phys. Chem.* B, **37**, 307.
Haber, F., Farkas, L. and Harteck, P. 1930 *Naturwissenschaften*, **18**, 266.
Harteck, P. and Geib, K. H. 1932 *Ber. dtsch. chem. Ges.* **66**, 1815.
Harteck, P. and Kopsch, U. 1931 *Z. phys. Chem.* B, **12**, 327.
Hinshelwood, C. N., Williamson, A. T. and Wolfenden, J. H. 1934 *Proc. Roy. Soc.* A, **147**, 48.
Jackson, W. F. 1934 *J. Amer. Chem. Soc.* **56**, 2631.
Jeans, J. H. 1925 "The Dynamical Theory of Gases", p. 327.
Kassel, L. S. and Storch, H. H. 1935 *J. Amer. Chem. Soc.* **57**, 672.
Kistiakowsky, G. B. 1930 *J. Amer. Chem. Soc.* **52**, 1868.

Norrish, R. G. W. and Foord, S. G. 1936 *Proc. Roy. Soc.* A, **157**, 503.

Sagulin, A., Kowalsky, A., Kopp, D. and Semenoff, N. 1930 *Z. phys. Chem.* B, **6**, 307.

Semenoff, N. 1928 *Z. Phys.* **48**, 571.

Semenoff, N. 1932 *Phys. Z. Sowjet.* **1**, 725.

Spence, R. 1932 *J. Chem. Soc.* 686.

Thompson, H. W. and Hinshelwood, C. N. 1929 *Proc. Roy. Soc.* A, **122**, 610.

Urey, H. C. and Teal, G. K. 1935 *Rev. Mod. Phys.* **7**, 34.

van Heiningen, J. 1936 *Rec. Trav. chim. Pays-Bas*, **55**, 65.

von Elbe, G. and Lewis, B. 1937 *J. Amer. Chem. Soc.* **59**, 656.

Wynne-Jones, W. F. K. 1936 *Trans. Faraday Soc.* **32**, 1397.

Photochemical reactions in monolayers
II. The photochemistry of proteins

By J. S. Mitchell* and E. K. Rideal, F.R.S.

Department of Colloid Science, The University, Cambridge

The examination of monolayers has been found to afford a quantitative method of investigation of the photochemical behaviour of many organic compounds of high molecular weight and appears to be especially suitable for macromolecular substances of physiological interest such as the proteins (Rideal 1932; Mitchell 1936a, 1937a; Rideal and Mitchell† 1937). The photochemical reactions occurring in the compounds spread in monolayers, at an air-water interface, on irradiation with monochromatic ultra-violet light, are observed by measurement of the changes in phase boundary potential and surface pressure; the light intensity is measured by chemical actinometers. The experimental methods were developed with particular reference to proteins and related simpler compounds, and, as a preliminary investigation, the photochemical properties of the keto-imino linkage have been examined.

The present work on the photochemistry of monolayers of typical proteins was undertaken from the point of view of radiation therapy, with the object

---

of providing elementary data for interpretation of the biological actions of radiation. The investigation is quantitative and is accordingly limited to proteins for which the amino acid analyses are sufficiently complete, namely, wheat gliadin, zein, insulin and ovalbumin. The application of the analytical data to the interpretation of the results of the photochemical experiments demands a detailed knowledge of the physical processes of light absorption in monolayers and of the photochemical significance of the absorption spectra of proteins in bulk solution. Only very general assumptions with regard to the molecular configuration of the monolayers are necessary. The results of photochemical experiments on proteins in bulk solution are required in the discussion of the chemical interpretation of the physical measurements on the monolayers.

GENERAL THEORY

The absorption spectrum of the monolayer must be determined quantitatively in order to evaluate the absolute quantum efficiency of the photochemical process. Direct precision measurements are not yet available, but theoretical considerations (Mitchell 1936*b*) show that it is possible to deduce the "molecular extinction coefficient in the film" to a first approximation from absorption measurements in polar solution, Hughes and Allsopp (1936) have shown directly in one case, namely, magnesium naphthalocyanine which gives visible green monolayers, that the molecular extinction coefficient in the film is of the same order as in solution; further, the observed velocity of simple photochemical reactions (I) shows that in monolayers the absorption bands are not usually displaced by more than 100 A from the position in solution. The theoretical considerations, confirmed by the experimental results with stearic anilide monolayers (I), emphasize the importance of the Hardy-Langmuir principle of molecular orientation in photochemical reactions in monolayers. It has been shown that molecular extinction coefficient in the monolayer, ϵ_λ, at the wave-length λ, is related to the molecular orientation by the relation

$$\epsilon_\lambda = \tfrac{3}{2}\overline{\sin^2\theta}\,f(\lambda),\tag{1}$$

where θ is the angle between the axis of the effective molecular electric dipole and the direction of the incident light, assumed to be normal to the film, and $\overline{\sin^2\theta}$ is the mean value of $\sin^2\theta$ for those values of θ allowed by the usually small thermal agitation and orientational oscillation at any given molecular area. $f(\lambda)$ is an extremely complicated function of λ, which cannot

be calculated theoretically in terms of the molecular extinction coefficient ϵ'_λ measured in polar solvents, but to a first approximation one must assume that $f(\lambda) = \epsilon'_\lambda$, as appears justified *a posteriori* by the experimental results for stearic anilide (I). With this assumption the number of quanta, $\Delta J/h\nu$, absorbed by the monolayer per sq. cm. per sec. from a normally incident beam of intensity J and frequency ν is given by

$$\frac{\Delta J}{h\nu} = \frac{2\cdot303}{6\cdot06 \times 10^{20}} \epsilon' n \frac{J}{h\nu} \tfrac{3}{2} \overline{\sin^2\theta}, \tag{2}$$

where n is the number of absorbing molecules per sq. cm.

For the analysis of the photochemical reactions in protein monolayers, observation of the phase boundary potential at constant surface area is the method of choice. The elastic hysteresis renders exact measurement of the reaction velocities at constant surface pressure almost impossible, and, moreover, from the observed change of phase boundary potential, $\delta\Delta V$, on irradiation at constant area, can be deduced the proportion of the total number of amino acid residues undergoing photochemical transformation. As discussed below, the proteins in the monolayers must be regarded as macromolecular polycondensation products in which only a small fraction, F, usually of the order of 10 %, of the total number of the repeating units possesses the chromophoric groups and can take part in primary photochemical changes. The inert residues are not of importance, and it is found that, as in the simple case previously discussed (I), the photoreactions at constant total surface area follow a unimolecular law, thus:

$$\frac{\partial \Delta V t}{\partial t} = K(\Delta V_f - \Delta V_t), \tag{3}$$

where ΔV_t and ΔV_f are respectively the phase boundary potentials characteristic of the film at equilibrium after irradiation for time t and at the end of the transformation. The constant K is, of course, proportional to the light intensity, and from its measured value can be deduced the true quantum efficiency, ϕ, for the total photochemical changes per chromophor by means of the equation

$$\phi = \frac{K}{\dfrac{2\cdot303}{6\cdot06 \times 10^{20}} \epsilon^* \dfrac{J}{h\nu} \tfrac{3}{2} \overline{\sin^2\theta}}, \tag{4}$$

where ϵ^* is the (mean) molecular extinction coefficient per chromophor, as measured in solution.

PHOTOCHEMICAL SIGNIFICANCE OF THE ABSORPTION
SPECTRA OF PROTEINS

The measurements of the ultra-violet absorption spectra of the gliadin, insulin and ovalbumin, in bulk solution have been described and figured elsewhere (Mitchell 1938). The results are required for the interpretation of the photochemical experiment on monolayers and will be given as needed, but here it is necessary to discuss in general terms the quantitative significance of the absorption spectra of proteins in relation to their amino acid composition.

The early investigations, in particular those of Hartley (1887), Blyth (1899) and Dhéré (1909), suggested that the characteristic absorption spectra of proteins were due to the constituent aromatic amino acids, especially tyrosine. Later, it was found possible to account semi-quantitatively for the absorption curves in certain cases, e.g. the serum proteins (Stenström and Reinhard 1925), insulin (Kuhn, Eyer and Freudenberg 1931), on the assumption that the proteins in solution behave, in relation to light absorption, as mixtures of the constituent amino acids.* Recent work (cf. Holiday 1936) has shown that for typical proteins in alkaline aqueous solution (pH 13), at wave-lengths greater than 2800 A, where tyrosine and tryptophane are the only effective chromophores, additivity is sufficiently exact for estimation of these two amino acids, with an error of the order of $\pm 4 \%$.

The validity, and limitations, of the "mixture hypothesis"† are in agreement with the well-known empirical facts that in complex organic molecules, two chromophores behave independently to a first approximation when separated by $—(CH_2)_2—$ and accurately when separated by three or more CH_2 groups (cf. Arnold and Kistiakowsky 1932; Ramart-Lucas 1934). The examination of insulin shows that at pH 12 at the wave-length of the absorption maximum 2920 A, the "molecular extinction coefficient" can be calculated, within the limits of experimental error, on the assumption of exact additivity; further, of the total light absorption 97·8 % is due to the

* The error in the absolute values of the calculated absorption coefficients was of the order of 25 % over the wave-length range 3100–2350 A.

† See Mitchell (1938) for further discussion and experimental details. It is of importance that there is no significant difference over the wave-length range 2350–3150 A and at pH 2–12 between the absorption spectra of glycyl-tyrosine and tyrosine (cf. Abderhalden and Haas 1927); however, the difference in the absolute values of the molecular extinction coefficients of glycyl-tyrosine and stearyl-tyrosine ethyl-ester in solution in ethyl alcohol suggests the possibility of modification of the tyrosine chromophor under certain conditions in large molecules.

tyrosine present, 1·8 % to the cystine and 0·3 % to the arginine. At pH 2 and 7·2, the assumption of linear additivity is a poor approximation and may underestimate the contribution of the tyrosine residues. Simple calculations using the analytical data available for wheat gliadin (*Tabulae Biologicae* 1926; Chibnall 1933) and zein (Kestner 1925; Waldschmidt-Leitz 1931; Pauli and Valko 1933) show that for these two proteins, over the wave-length range 2350–3150 A, at least 85 % of the total light absorption is due to the tyrosine, phenyl-alanine and tryptophane present; the only other amino acids making any appreciable contribution to the light absorption are cystine and arginine.

In general, while the significance of photochemical changes in the disulphide linkages and possibly also arginine (Lieben and Urban 1931) cannot be neglected, it is evident that, since in the wave-length region 2350–3150 A, 85–100 % of the total light absorption by typical proteins occurs in the residues derived from tyrosine, phenyl-alanine and tryptophane, the changes in relation to these three "aromatic" groups must be expected to play by far the most important and fundamental part in the photochemical behaviour of the proteins. From the above discussion it appears that these considerations, with insignificant quantitative modifications, are equally valid for proteins in monolayers. Further, the conclusions are probably consistent, not only with the Fischer-Hofmeister peptide theory of protein structure but also with the more recent suggestions associated with the names of Abderhalden (1923), Bergmann (1924), Ssadikow (1926) and Wrinch (1937).*

EXPERIMENTAL

The technique of investigation of photochemical reactions in monolayers has been described in detail in I, and the apparatus and methods employed here were essentially the same. For the greater part of this work, the hydrogen discharge tube was used as the light source, under the conditions described, in conjunction with the large quartz monochromatic illuminator. A rectangular area of film 6 × 5 cm. was uniformly irradiated with light of intensity of the order of 10^{13} quanta/sq. cm./sec. for the wave-length bands 2350–2400 A and 2980–303 A, and 10^{14} quanta/sq. cm./sec. for the band 2500–2550 A. The measurements of the light intensity were made by means

---

* Aliphatic diketopiperazines do not absorb at wave-lengths greater than 2500 A (Abderhalden and Rossner 1929) and the formation of diketopiperazine rings produces no significant modification of the tyrosine chromophor, in the case of 3-6-di-*p*-hydroxybenzyl-2-5-diketopiperazine (Abderhalden and Haas 1927).

of the uranyloxalate actinometer of Forbes and Heidt (1934), modified as described in I.

The photochemical reactions were examined by observation of the changes in phase-boundary potential on irradiation of the protein monolayers at constant total surface area and under true equilibrium conditions. On account of the complexity of the chemical processes and to render possible the application of equation (3), the method of fractional irradiation has been introduced, i.e. the monolayer is illuminated for repeated short periods of, usually, 5 min. duration, with intervals of darkness of the order of 10–40 min. to allow the attainment of equilibrium conditions. In this way, not only can the completion of the photochemical changes be observed but also the dark reactions following irradiation (and hence to some extent the behaviour of the unstable intermediate photochemical products) can be studied.

The protein monolayers

The preparation and mechanical properties of the protein monolayers used in the photochemical experiments have been described previously (Mitchell 1937 b), so that here only the relevant features will be discussed. The monolayers* were spread from aqueous or alcoholic solutions of the proteins, the method of preparation was characterized by:

(1) The employment of very dilute (0·01 %) spreading solutions of the proteins.

(2) The introduction of prolonged time intervals (1–36 hr.) to allow the attainment of apparent equilibrium, which was always confirmed by phase boundary potential measurements.

The volume of the protein solution dropped on to the surface of the substrate was measured by means of the "agla" micrometer syringe. The optical homogeneity of the monolayers was demonstrated by means of the dark ground ultra-microscopic technique introduced by Zocher and Stiebel (1930). It was found, in the case of gliadin, that monolayers with almost identical mechanical properties are obtained by the present method and by that of Hughes and Rideal (1932).

The solvent used for the gliadin and zein was aqueous ethyl alcohol of concentrations varying from 60 to 80% by volume; the insulin was dissolved in N/100 sulphuric acid. Except in the case of ovalbumin where the substrate was a standard phosphate buffer of pH 7·0, the results described refer to

* Except in the case of ovalbumin where the monolayers were spread from the crystalline protein by the method of Hughes and Rideal (1932) (cf. Hughes 1933).

monolayers spread on N/100 sulphuric acid. All the experiments were performed at room temperatures (16·5–21·5° C.).

The wheat gliadin was investigated in detail to explore the possibilities of the experimental methods; it was selected because monolayers with reproducible properties could easily be prepared, very pure specimens were available, and its amino-acid composition was known more fully than in the case of most proteins. Then more rapid examinations were made of monolayers of zein, insulin and ovalbumin. The relevant analytical data are given in the appendix.

Very pure specimens of the proteins have been used. The wheat gliadin was kindly given by Dr E. A. Fisher and the zein by Dr R. Gortner. The apparent water content of these prolamines was determined by drying in air to constant weight at 110° C. (Hughes and Rideal 1932); the value for the gliadin was found to be 9·9 and for the zein 5·4 %. The specimen of crystalline insulin was kindly given by Dr H. C. Hagedorn and had a physiological activity of 23·7 units/mg.; the apparent water content determined by drying in air to constant weight at 105° C. was 3·4 %. The specimen of crystalline ovalbumin was prepared and kindly given by Dr G. S. Adair; its apparent water content (see Sörensen 1917; Adair and Adair 1936) determined by drying in air to constant weight at 105° C., as described by Svedberg and Nichols (1926), was 13·4 %.

The specimen of stearic acid used in routine work for checking the zero-potential measurements was a Kahlbaum specimen, twice recrystallized from ethyl alcohol, corrected m.p. 69·1° C.

The compressibility curves of the monolayers of gliadin, zein and insulin are shown in fig. 1 where the surface pressure, F dynes/cm., is plotted against the surface density of dried protein, γ, mg./sq. m. Each curve is the mean of 5–8 almost coincident curves, and consists of three regions:

(1) A region where the surface pressure is not measurable (i.e. is less than 0·05 dyne/cm.), possibly corresponding to the region of surface vapour pressure.

(2) A "low-pressure" region of high compressibility and negligible elasticity and rigidity, extending from the limiting area to a surface pressure of the order of 1–2 dynes/cm.

(3) A "high-pressure" region of low compressibility extending to the collapse point.

The most characteristic mechanical criteria are the *extrapolated* limiting densities of the low and high pressure regions; these are independent of instrumental factors, identical values having been obtained with three dynamometers of widely different sensitivities. In the case of gliadin, the

limiting density of the low pressure region coincides with the transition between the electrically homogeneous and inhomogeneous regions.

The interpretation of the observed properties of the monolayers in terms of the properties of the repeating units, which may be *represented* as
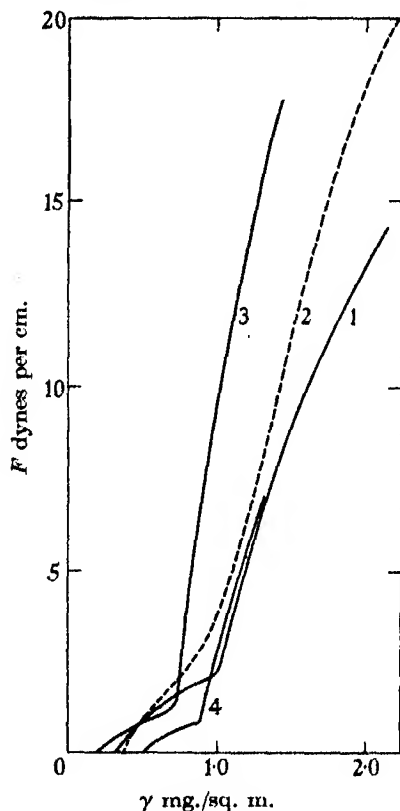
Fig. 1. Compressibility curves of protein monolayers spread on N/100 sulphuric acid (16·5–22·0° C.). 1. Gliadin spread from solution. 2. Gliadin spread from the solid (Hughes and Rideal 1932). 3. Zein. 4. Insulin.

CO-NH-CHR residues, is independent of theories of detailed structure and involves only the analytical results. The mechanical properties of the monolayers are summarized in Table I, where also are given the values for the mean properties per residue calculated on the hypothesis of the polypeptide structure (see Mitchell 1937b). While a flexible polypeptide chain structure*

* Experimental evidence that polypeptide chains can form monolayers is provided by the results of examination of films of polyesters—neutral and acidic ethylene succinates—by Moss (1934) and of the tripeptide of α-amino-caprylic acid by Gorter, Meyer and Philippi (1934).

TABLE I. MECHANICAL PROPERTIES OF PROTEIN MONOLAYERS

Protein	Gliadin	Zein	Insulin
Limiting density of low-pressure region (mg./sq. m.)	0·35	0·21	0·50
Limiting density of high-pressure region (mg./sq. m.)	0·85	0·67	0·81
Collapse density (mg./sq. m.)	2·10	1·40	1·30
Mean molecular weight per CO-NH-CHR residue	121·00	106·00	137·00
Calculated mean length of side chain in A	3·51	3·48	4·24
Percentage of polar side chains	60·00	39·00	60·00
Mean area per residue at limiting area of low-pressure region in sq. A: Obs.	56·50	85·20	45·20
Calc.	42·50	42·50	47·50
Mean area per residue at limiting area of high-pressure region in sq. A, obs.	23·30	26·10	27·80
Mean cross section of head per CO-NH-CHR in sq. A, calc.	23·80	23·00	24·20
Mean area per residue at collapse in sq. A, obs.	9·50	12·50	17·40
Approximate calculation	15·20	9·60	15·80

(cf. Hughes and Rideal 1932) appears consistent with the mechanical properties of the monolayers in question, it is evident that the occurrence, in parts of the film, of ring structures, e.g. cyclols (Wrinch 1937) or diketo-piperazines (Mitchell 1937 *b*), cannot be excluded. However, the only assumption of detailed molecular structure required for the present work is that near the limiting area of the low pressure region, the aromatic nuclei of the side chains derived from tyrosine, phenylalanine and tryptophane lie approximately parallel to the plane of the surface. This assumption is naturally fulfilled in the polypeptide chain model of film structure, but its validity is obviously much more general.

The phase boundary potential measurements, ΔV, refer to monolayers at equilibrium after standing at constant area for periods varying from 1–36 hr., until stationary values of ΔV are attained, with variations not greater than ± 1 mV over intervals of the order of 30 min. In the case of the gliadin monolayers spread on N/100 sulphuric acid at 17·5–22° C., a large number of measurements have been made at different surface densities, so that it has been possible to obtain the equilibrium ΔV-γ curve. The results are shown in fig. 2, where each experimental point was obtained from a separate monolayer. The values given by Hughes and Rideal (1932) for monolayers of

gliadin spread, from the solid,* on N/100 hydrochloric acid at 15–20° C. are included in fig. 2. For the monolayers of gliadin measured under equilibrium
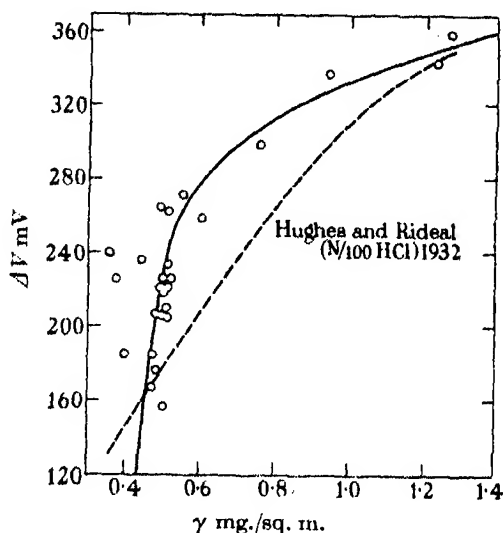
FIG. 2. —O—O— Equilibrium ΔV-γ curve for monolayers of gliadin spread on N/100 H_2SO_4 (17·5–22·0° C.). - - - - Measurements of Hughes and Rideal (1932).
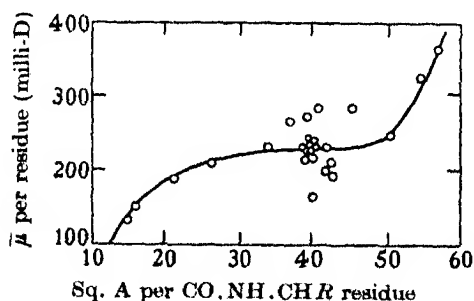
FIG. 3. Variation with mean area per CO.NH.CHR residue of the mean vertical component, $\bar{\mu}$ of the apparent dipole moment per residue, for monolayers of gliadin spread on N/100 H_2SO_4 (17·5–22·0° C.) and examined under equilibrium conditions.

conditions, fig. 3 shows the variation with mean molecular area per CO–NH–CHR residue of the mean value of the vertical component, $\bar{\mu}$, of the apparent electric dipole moment per residue, calculated with the aid of Helmholtz's equation on the assumption that the mean molecular weight per residue is

---

* As in the case of the F-γ curves, it is possible that the final equilibrium values were not reached in the transition region between the low- and high-pressure regions.

121.* The maximal error in the absolute determination of $\bar{\mu}$ for each individual value of γ is of the order of $\pm 25 \%$ in the low pressure region, and of $\pm 15 \%$ in the high pressure region. However, the absolute values are not of immediate interest but it is important to note that the curve shows the approximate constancy of $\bar{\mu}$ in the region where the mean area per residue is 35–45 A, i.e. $\gamma = 0.44$–0.58 mg./sq. m., in agreement with previous general considerations of film structure (cf. Hughes and Rideal 1932; Mitchell 1937b). The electrical properties of the monolayers of the other proteins will be discussed below.

PHOTOCHEMICAL EXPERIMENTS

As previously described (Rideal 1932; Mitchell 1936a, 1937a), the characteristic changes produced on ultra-violet irradiation of protein monolayers are:

(1) Liquefaction of the film, if it is initially in the gel state.

(2) At constant total surface area, a rapid rise of surface pressure, and an increase of phase boundary potential, which may be as great as 120 mV as in the case of zein, but is usually considerably smaller.

A typical example of the changes in phase boundary potential on irradiation of protein monolayers is shown in fig. 4; this summarizes the experimental data for the fractional irradiation of a monolayer of gliadin, spread on N/100 sulphuric acid at 18° C., at constant area ($\gamma = 0.55$ mg./sq. m. corrected) with light of the wave-length band 2350–2400 A (Exp. 23, Table II). Almost without exception, for the first few periods of illumination, ΔV has fallen by perhaps 10–30 mV when observed immediately after the cessation of irradiation and then rises slowly, while the film is unilluminated, to a value considerably above that measured before irradiation. At the end of the reaction, there is no change on further irradiation. In fig. 5a the changes in phase boundary potential on irradiation of gliadin monolayers are summarized for three experiments, only the equilibrium ΔV values after each period of irradiation being given; in fig. 5b it is shown that these examples of the photochemical reactions accurately obey the unimolecular law (eqn. (3)). It is to be noted that there is no induction period; further, it is of great interest that with radiation of the wave-length band 2500–2550 A, the photoreaction is not cyanide sensitive so that the measured reaction velocity constant K must be assumed to correspond to the unsensitized photochemical process (see below).

* The analytical results summarized in *Tabulae Biologicae* (1926) correspond to a value of the mean molecular weight per residue of 120 and the more recent data compiled by Chibnall (1933) give 122.
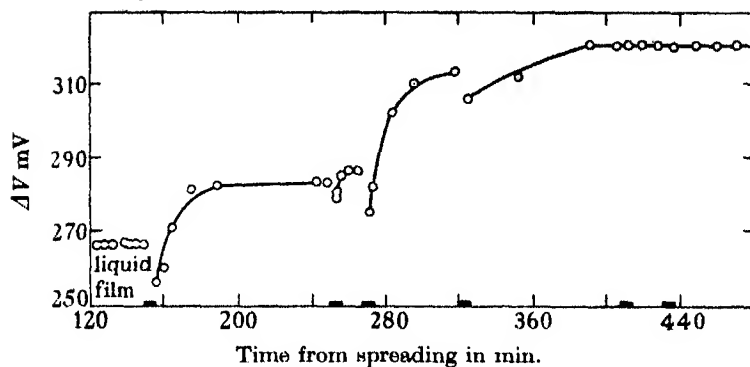
Fig. 4. A typical example of the changes in phase boundary potential on fractional irradiation of a monolayer of gliadin (Exp. 23, Table II). ■ Illumination.
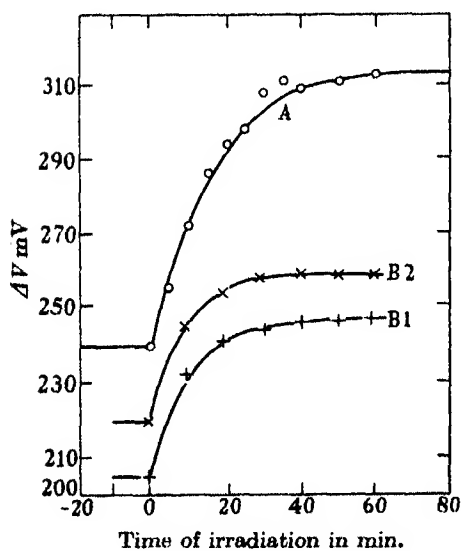
Fig. 5a
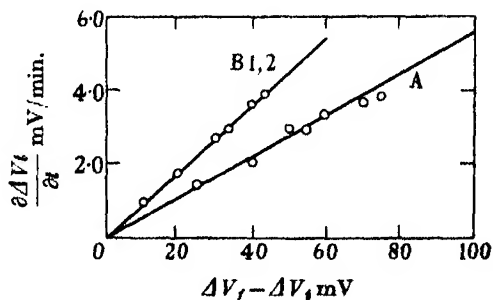
Fig. 5b

Fig. 5a. Further examples of the changes in phase boundary potential on irradiation of gliadin monolayers.

A. Exp. 1, Table II, $\lambda = 2350$–2400 A.

B 1. Exp. 18, Table II, $\lambda = 2500$–2550 A.

B 2. Exp. 13, Table II, $\lambda = 2500$–2550 A. After addition to the substrate of 5·0 c.c. M/100 KCN.

Fig. 5b. Kinetics of photoreactions shown in fig. 5a.

A. Exp. 1, Table II, $K = 5·5 \times 10^{-2}$ min.$^{-1}$.

B. Exps. 13 and 18, Table II. Curves coincident. For each $K = 9·2 \times 10^{-2}$ min.$^{-1}$.

TABLE II. IRRADIATION OF GLIADIN MONOLAYERS

Exp. no.	Temp. °C.	γ mg./sq. m. (corr.)	ΔV_{mV} initial	n residues per sq. cm.	$\bar{\mu}$ per residue milli-Debyes	sq. A per residue	Wave-length band	$\delta \Delta V_{mV}$ on irradiation	$\frac{\delta \Delta V}{4\pi n}$ milli-Debyes
1	19·5	0·35	240	$1·75 \times 10^{14}$	365	57·1	a	72	109
2	20·0	0·37	227	1·85	324	54·1	a	48	69
3	20·5	0·40	185	1·98	248	50·5	c	69	92
4	20·0	0·44	237	2·21	285	45·2	c	29	35
5	18·0	0·47	185	2·34	212	42·7	a	79	90
6	15·5	0·47	169	2·34	192	42·7	—	—	—
7	20·0	0·48	179	2·39	199	41·8	—	—	—
8	18·0	0·48	208	2·39	322	41·8	c	49	54
9	20·0	0·48	179	2·39	199	41·8	—	—	—
10	20·0	0·49	265	2·45	287	40·8	—	—	—
11	18·0	0·50	158	2·49	169	40·2	a	39	41
12	18·0	0·50	225	2·49	240	40·2	c	35	37
13	19·5	0·50	220	2·49	234	40·2	b	40	43
14	19·5	0·50	224	2·49	238	40·2	c	29	31
15	18·0	0·50	206	2·49	218	40·2	—	—	—
16	20·0	0·51	210	2·54	224	39·3	b	40	42
17	20·0	0·51	225	2·54	240	39·3	b	42	44
18	18·5	0·51	205	2·54	217	39·3	c	37	39
19	18·0	0·51	221	2·54	231	39·3	d	40	42
20	22·0	0·51	226	2·54	236	39·3	—	—	—
21	20·5	0·51	233	2·54	243	39·3	d	40	42
22	20·0	0·52	263	2·56	273	39·1	d	37	38
23	18·0	0·55	266	2·73	258	36·6	a	54	52
24	18·0	0·60	259	2·97	232	33·7	a	9	8
25	17·5	0·76	299	3·78	210	26·5	a	21	15
26	19·0	0·94	339	4·68	192	21·4	a	0	0
27	19·0	1·27	360	6·33	152	15·8	a	−30	−12
28	19·0	1·33	342	6·62	137	15·1	a	−37	−15

Substrate: N/100 sulphuric acid.
Wave-length bands: a, 2350–2400 A, b, 2500–2550 A, c, 2980–3030 A, d, 3125–3175 A. Sensitized.

The total increase in phase boundary potential $\delta\Delta V$ observed on irradiation appears to be of especial significance. The general conclusion from the results obtained is that $\delta\Delta V$ differs for the different proteins in a characteristic manner and, as will be discussed below, can be correlated quantitatively with the amino-acid analyses. $\delta\Delta V$ increases slowly with increasing acidity
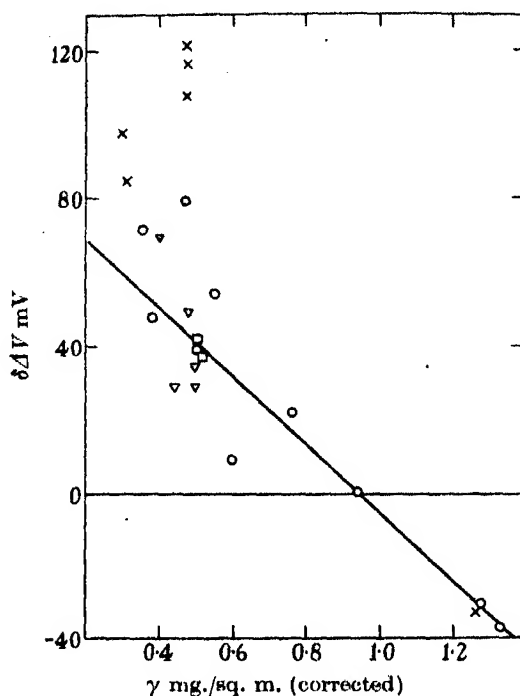
FIG. 6. Summary of changes in phase boundary potential on irradiation of mono-layers of gliadin and zein. Substrate N/100 H₂SO₄. 17·5–22·0° C. (see Tables II and III). Protein Exp. Wave-length band (A).

Gliadin	O	a, 2350–2400
	□	b, 2500–2550
	▽	c, 2980–3030 } Sensitized
	△	d, 3125–3175
Zein	×	a, 2350–2400

of the substrate and decreases approximately linearly with increasing initial surface density of the protein in the monolayer; at high initial surface densities, negative values of $\delta\Delta V$ have been observed with gliadin and zein. It is of interest that at any given surface density, $\delta\Delta V$ appears independent of the wave-length of the incident light, no significant differences being observed for the wave-length bands examined.

The results of the photochemical experiments with *gliadin* monolayers spread on N/100 sulphuric acid are summarized in Table II. Four wave-length bands have been employed for the irradiation, namely, 2350–2400 A, 2500–2550, 2980–3030, and 3125–3175 A; with the last two bands, the results recorded correspond to reactions which are cyanide sensitive. In the last column of Table II are given the values of $\delta\Delta V/4\pi n$, which are required later and represent the apparent mean change, on irradiation, of the vertical
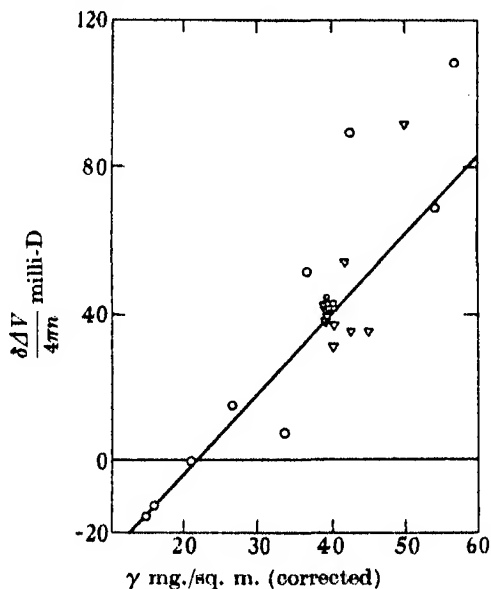
Fig. 7. Summary of the changes on irradiation of the mean vertical component of the apparent dipole moment per residue for monolayers of gliadin. (Experiments labelled as in fig. 6. See Table II.)

component of the electric dipole moment per residue. The variation of $\delta\Delta V/4\pi n$ with the mean area per residue, for gliadin, is summarized in fig. 7. The results of irradiation of monolayers of *zein*, spread on N/100 sulphuric acid, with light of the wave-length band 2350–2400 A are given in Table III, and the observed variation of $\delta\Delta V$ with the initial surface density of the protein for both gliadin and zein is shown in fig. 6.

In the case of *insulin*, the results are modified by the partial solution of the film on irradiation. This was evident in the preliminary experiments and was confirmed by the measurements of the phase boundary potential, e.g. on irradiation with light of the wave-length band 2350–2400 A of a monolayer of insulin spread on N/100 sulphuric acid at 19° C. with $\gamma = 0.65$ mg./sq. m. (corrected) and $\Delta V = 285$ mV initially, $\delta\Delta V$ was 15 mV.

The photochemical liberation into the substrate of molecular fragments containing aromatic groups has been demonstrated in the case of monolayers of insulin* by means of the colour reaction with diazotized p-amino-benzoic acid. The substrate beneath an insulin monolayer ($\gamma = 1\cdot45$ mg./sq. m.) illuminated for 45 min. with the total radiation from a quartz mercury vapour lamp gave a faint but quite definite colour reaction approximately equal to that of 1×10^{-6} M tyrosine solution. The substrate beneath a control film ($\gamma = 1\cdot52$ mg./sq. m.) illuminated through a glass filter with radiation of wave-lengths greater than 3300 A gave no colour reaction. The total amount of aromatic compounds liberated appeared to be significantly higher† than that anticipated from the tyrosine content, probably because the histidine residues were carried into solution and perhaps also on account of the photo-oxidative changes in the tyrosine groups.

TABLE III. IRRADIATION OF ZEIN MONOLAYERS

Exp. no.	Temp. ° C.	γ mg./sq. m. (corr.)	ΔV_{mv} initial	$\delta \Delta V_{mv}$ on irradiation
1	18·0	0·30	123	98
2	19·0	0·31	106	85
3	20·0	0·48	179	117
4	19·0	0·48	173	122
5	22·0	0·48	225	107
6	19·5	1·26	336	−32

Substrate: N/100 sulphuric acid. Wave-length band: 2350–2400 A.

TABLE IV. IRRADIATION OF OVALBUMIN MONOLAYERS

Exp. no.	Temp. ° C.	pH	ΔV_{mv} initial	γ mg./sq. m. (corrected)	n residues per. sq. cm.	$\delta \Delta V_{mv}$ on irradiation
1	19	2·0	216	0·52	$2\cdot60 \times 10^{14}$	45
2	21	7·0	158	0·55	2·77	23
3	23	7·0	164	0·55	2·77	26

Monochromatic radiation: wave-length 2537 A.

The relevant experimental data for the irradiation of monolayers of ovalbumin are given in Table IV. The monolayers were prepared by spreading from the solid and examined under equilibrium conditions, the surface density being deduced from the phase boundary potential measurements (cf. Hughes 1933; Philippi 1936). Continuous irradiation with monochromatic light of wave-length 2537 A was employed. The photoreactions obey

* Spread on N/100 sulphuric acid.
† The value was consistently of the order of 10 times that calculated for unchanged tyrosine.

the unimolecular law, e.g. in Exp. 1, where the incident intensity was $1 \cdot 4 \times 10^{13}$ quanta/sq. cm./sec., $K = 9 \cdot 7 \times 10^{-2}$ min.$^{-1}$.

The photochemical liquefaction of protein monolayers in the gel state is completely inhibited by the presence in the substrate of $0 \cdot 1 \%$ hydroquinone, so that it must be concluded (cf. Gee and Rideal 1935) that the photochemical changes in the proteins involve oxidative processes as an essential step. No detectable changes are produced in unilluminated films by exposure to ozone, or by addition of H_2O_2 to the substrate.*

The determination of the long wave-length threshold for the photochemical changes in protein monolayers presents considerable experimental difficulties, both on account of the very low velocity of the photoreactions at wave-lengths considerably greater than the absorption maximum, and also because of the presence of photosensitizers. Unexpectedly fast photochemical reactions have been encountered with radiation of wave-lengths 2980–3030 and 3125–3175 A in the case of the gliadin, and with wave-lengths greater than 3350 A in the experiments of Schulman on ovalbumin monolayers (Rideal 1932). In the present work, the anomalous reaction velocities were invariably reduced to the normal order of magnitude by addition to the substrate of excess KCN, e.g. for irradiation with the wave-length band 2980–3030 A, addition of $5 \cdot 0$ c.c. M/1000 KCN to the substrate in Exp. 15, Table II reduced K from the value $4 \cdot 0 \times 10^{-2}$ min.$^{-1}$ (cf. Exp. 14) to approximately $2 \cdot 0 \times 10^{-4}$ min.$^{-1}$ which is normal for these wave-lengths. It has been suggested (Mitchell, Rideal and Schulman 1937, and I) that these and similar anomalous results are due to photosensitization by traces of metallic ions. For the unsensitized photodecomposition of protein monolayers, changes have never been detected with the wave-length band 3125–3175 A or at longer wave-lengths. This observation provides further evidence that, in the monolayers, the absorption spectrum is not displaced towards longer wave-lengths by more than 100 A from the position in solution.

In accordance with the chemical interpretation of the results discussed below, a series of experiments have been made to determine the order of the absolute quantum efficiency of the total photochemical changes per aromatic residue in monolayers of gliadin spread on N/100 sulphuric acid. The most reliable results are summarized in Table V. The value of the absolute quantum efficiency ϕ is deduced from the measured reaction velocity constant K by means of eqn. (4) in which, at the area of observation, corresponding to 40 sq. A per residue, $\overline{\sin^2 \theta} = 1$ to a first approximation. The mean molecular extinction coefficient per chromophoric residue is deduced, with the aid of

---

* In the absence of ferrous ions.

the analytical data (see Appendix), from the measurements of the ultra-violet absorption spectrum of gliadin in solution in 70–80% by volume ethyl alcohol (Mitchell 1938) and refers to the side chains derived from tyrosine, phenyl-alanine and tryptophane only; the small corrections for cystine, methionine and arginine are negligible. The values of K refer to the un-sensitized photoreactions, and it must be concluded that, for the wave-length regions examined, the value of ϕ is of the order of one-half.

<div align="center">TABLE V</div>

Exp. no.	Wave-length band A	Intensity q./cm.²/sec.	T ° C.	γ mg./sq. m. (corr.)	K min.⁻¹	Mean $\bar{\epsilon}$ per chromophor	ϕ
1	2350–2400	$2 \cdot 90 \times 10^{13}$	18	0·50	$1 \cdot 80 \times 10^{-2}$	4010	0·45 ($\pm$ 0·09)
2	2500–2550	$8 \cdot 10 \times 10^{13}$	20	0·50	$1 \cdot 23 \times 10^{-2}$	798	0·55 ($\pm$ 0·11)
3	2500–2550	$9 \cdot 50 \times 10^{13}$	21	0·50	$1 \cdot 25 \times 10^{-2}$	798	0·48 ($\pm$ 0·10)
4	2980–3030	$0 \cdot 45 \times 10^{13}$	21	0·50	$\leqslant 2 \times 10^{-4}$	214	$\leqslant 0 \cdot 6$

<div align="center">DISCUSSION</div>

The observed liquefaction of protein monolayers on ultra-violet irradiation, with accompanying increase of surface pressure at constant total surface area, indicates the occurrence of photochemical fragmentation of the molecules of protein in the monolayer. In view of the fundamental importance of oxidative changes, this process is almost certainly analogous to the "photo-oxidative fragmentation" of proteins in bulk solution (Neuberg 1908; Becker and Szendrö 1931; Spiegel-Adolf 1934; cf. Mitchell 1938) and also of keratin (Becke 1912, 1919; Sauer 1916; Bergen 1925, 1926).

The quantitative examination of the absorption spectra has shown that the only residues of importance in the absorption of radiation of wave-lengths 3150–2350 A by typical proteins are those derived from the three aromatic amino acids—tyrosine, phenyl-alanine and tryptophane—and also to a much less extent, cystine and arginine. In the photochemical experiments on monolayers, cystine cannot play any part on account of its oxidation (cf. Andrews 1932, 1933) during the prolonged interval when the film is standing to attain apparent equilibrium as determined by the phase boundary potential measurements. Further, in the proteins examined light absorption by arginine has been shown to be negligible, and also arginine may not undergo photodecomposition in the wave-length region concerned (Lieben and Urban 1931). Thus on general grounds it is evident that the primary photochemical processes in the monolayers are limited, at least to a first approximation,* to the "aromatic" residues.

* Error may possibly be introduced by neglect of methionine.

On the basis of the classical work of Neuberg (1908), the examination of keratin referred to above and the observed photochemical behaviour of ovalbumin, insulin and glycyl-tyrosine, it has been suggested (Mitchell 1938) that the photo-oxidative fragmentation of proteins in solution with light of wave-lengths 3150–2350 A is due, at least in part, to a process of indirect oxidative photolysis of peptide linkages adjacent to the tyrosine chromophores. The experiments on glycyl-tyrosine can provide direct evidence for splitting of one only of the two peptide linkages adjacent to each tyrosine chromophor and suggest that the mechanism of the fragmentation is a series of photo-oxidative and intramolecular changes, followed by photochemical hydrolysis of the N—CO linkage in a manner analogous to that described by Baudisch and Hoschek (1916) and Rideal and Mitchell (1937). However, the results suggest the inherent probability of photohydrolytic cleavage of both the peptide linkages adjacent to each tyrosine side chain as a result of the photo-oxidative transformations; this conclusion is supported both by the observed increase of amino-nitrogen on irradiation of proteins (Fort and Lloyd 1914; Fort 1916; Eckstein and Lieben 1933) and by the ultra-filtrability of the pigment produced on ultra-violet irradiation of ovalbumin (Becker and Szendrö 1931). It appears reasonable to assume that phenyl-alanine may take part in a series of changes similar to those of tyrosine (cf. Bachér 1929) but, apart from photo-oxidative destruction (Lieben 1927), the role of the tryptophane residues of proteins is unknown. It is possible that light absorption in the tryptophane side chains leads to splitting of the adjacent peptide linkages; the occurrence of this process will be assumed but definite experimental evidence as to the validity of the assumption could not be obtained on account of the small numbers of the tryptophane residues and the magnitude of the experimental and analytical errors.

These conceptions of the photochemical behaviour of proteins in bulk solution appear directly applicable to the quantitative interpretation of the results of ultra-violet irradiation of the protein monolayers. Without any assumptions as to the detailed molecular structure, the proteins in the boundary state are to be regarded as polycondensation products in which a fraction, F, of the total number of repeating units is characterized by chromophoric side chains derived from tyrosine, phenyl-alanine or tryptophane. If both peptide linkages* adjacent to each chromophoric side chain undergo a process of photolysis, the end result of which is equivalent to hydrolysis, and the liberated chromophoric residue is removed by solution,

---

* Or the corresponding groups capable of undergoing intramolecular rearrangement to form peptide linkages, as in a cyclol fabric.

it can be shown that the total change of phase boundary potential, $\delta\Delta V$, observed on irradiation at a surface density corresponding to n residues per sq. cm. is given by:

$$\frac{\delta\Delta V}{4\pi n} = F\{\mu_{\text{COOH}} + \mu_{\text{NH}_2} - \mu_{\text{arom}} - 2\mu_{\text{CO.NH}}\}, \tag{5}$$

where μ_{COOH}, μ_{NH_2}, μ_{arom} and $\mu_{\text{CO.NH}}$ respectively refer to the *vertical* component of the apparent dipole moment per COOH, NH$_2$ CHR (aromatic) residue and peptide group.

It is well-known that the group represented by . CO . NH . CH . makes only a very small contribution to the mean vertical moment per residue for protein monolayers in the low pressure region (Hughes and Rideal 1932; Schulman and Rideal 1933). Further, in the case of stearic anilide monolayers (I) the NH . CO . C$_{17}$H$_{35}$ group appears to make a negligible contribution to the vertical component of the total apparent moment.* Thus, to a first approximation,† $\mu_{\text{CO.NH}}$ may be assumed to be zero in the low pressure region. The examination of mixed films (Schulman 1937, also private communications) has shown that, for equimolecular mixtures of acids and amines, linear addition of the vertical moments does not hold. The most exact experimental values available for $\mu_{\text{COOH}} + \mu_{\text{NH}_2}$ are, for pH 2·0, 746 milli-Debyes at 40 sq. A per two molecules, and for pH 7·0, 500 milli-Debyes at 36 sq. A per two molecules; data are not available at appreciably smaller areas.

To evaluate μ_{arom}, it must be assumed as discussed above, that near the limiting area of the low pressure region, the aromatic rings of the tyrosine, phenyl-alanine and tryptophane side chains lie parallel to the plane of the surface. Thus the only first order contribution (cf. Stuart and Volkmann 1933) to μ_{arom} is from tyrosine. The phase boundary potentials of tyrosine derivatives have not yet been measured but comparison of the vacuum values of the electric moments of phenol and aliphatic alcohols (Gurney and Jackson 1934) suggests that the required value for tyrosine must approximate to that measured for aliphatic alcohols in monolayers; hence it can be assumed that for the tyrosine side chains, the vertical component moment in the low pressure region near the limiting area is, at pH 2·0 and 7·0, approximately 210 milli-Debyes (Schulman and Hughes 1932; Adam, Danielli and Harding 1934). Fortunately, it is not necessary to know this

---

* The direction of the apparent molecular dipole moment is probably parallel to the plane of the benzene ring, in stearic anilide in monolayers (I).

† This may not be true in the immediate vicinity of the limiting area of the low pressure region where $\bar{\mu}$ per residue shows a rapid increase with increasing surface areas.

value with great accuracy, since the effective μ_{arom} is the mean value for the aromatic side chains and is usually small with respect to the value of $\mu_{COOH} + \mu_{NH_2}$. With the aid of the analytical data (see Appendix), it is found that μ_{arom} has the approximate value 80 milli-Debyes for gliadin, 90 milli-Debyes for zein and ovalbumin and 210 milli-Debyes for insulin.

On compression of the monolayers, μ_{arom} increases rapidly, so that, according to eqn. (5), $\delta\Delta V/4\pi n$ must decrease with increasing initial surface density of protein in the monolayer, and may have negative values at high initial densities. It is of great interest that the experimental observations summarized in figs. 6 and 7 receive a simple general explanation in this way in terms of the Hardy-Langmuir principle of molecular orientation in monolayers. On account of the structural complexity, more detailed quantitative interpretation is not possible but it is to be noted that both with gliadin and zein, $\delta\Delta V$ passes through zero value at surface densities slightly greater than the limiting values for the high pressure region.

To deduce the values of F from the experimental data, the surface density selected for analysis must satisfy the following conditions:

(1) No "phase change" occurs during the reaction.

(2) The mean vertical component of the apparent dipole moment per $CO.NH.CHR$ residue has an approximately stationary value, for small variations of the surface density, i.e. re-orientation of the inert residues is excluded.

(3) Solution of the film is negligible, only the chromophoric residues liberated photochemically leaving the surface.

The examination of the gliadin monolayers shows that the initial surface density must approximately correspond to the value 40 sq. A for the mean area per residue; then, for the substrate at pH 2, eqn. (5) takes the simplified form

$$\frac{\delta\Delta V}{4\pi n} = F(746 \times 10^{-21} - \mu_{arom}). \tag{5a}$$

Gliadin. The mean values of $\delta\Delta V/4\pi n$ deduced from nine experiments [Table II, Nos. 11–14, 17–20, and 22] is 39·7 milli-Debyes. Hence $F = 6\cdot0$ ($\pm 0\cdot4$) %, the value in brackets being the estimated *mean* error. The theoretical value, assuming fragmentation of both peptide linkages adjacent to the residues derived from tyrosine, phenyl-alanine and tryptophane, lies between 5·7 and 4·5 %; the upper limit is determined from the available analytical data and the lower limit by the assumption that the total number of residues per Svedberg unit is 288 (cf. appendix and Bergmann and Niemann 1937).

Zein. The mean value of $\delta\Delta V/4\pi n$ deduced from Exps. 3, 4, 5, Table III is 114 milli-Debyes; hence $F = 17\cdot3$ $(\pm 2\cdot0)$ %. The theoretical value lies between $13\cdot2$ and $11\cdot5$ %.

Ovalbumin. Exp. 1 (Table IV) gives $F = 7\cdot0$ $(\pm 1\cdot3)$ % and Exps. 2 and 3 give $F = 5\cdot7$ $(\pm 0\cdot8)$ %. The theoretical value is $8\cdot3 - 7\cdot3$ %.

Insulin. The total increase of phase boundary potential on irradiation is greatly reduced by the partial solution of the film so that eqn. (5) is no longer applicable; the value of F deduced from the data given above is $2\cdot6$ % while the theoretical value is $11\cdot6 - 8\cdot3$ %.‡

These results are summarized in Table VI. In the comparison of theory and experiment, it is essential to note that the maximal error in the experimental determination of the F values, is, under the most unfavourable conditions, of the order of $\pm 37\cdot5$ % and that the theoretical values given, although deduced from recent analytical data, may possibly be too low on account of incomplete estimation (cf. Carpenter 1931; Holiday 1936). Accordingly, it must be concluded from Table VI that the experimental values of F,

TABLE VI. THEORETICAL INTERPRETATION OF THE RESULTS OF ULTRA-VIOLET IRRADIATION OF PROTEIN MONOLAYERS

Protein	Wave-length of incident radiation A	pH of substrate	Percentage of chromophoric residues F	
			Experimental	Theoretical
Gliadin	2350–2400 2500–2550 *2980–3030 *3125–3175	2·0	6·0 ($\pm 0\cdot4$)†	5·7– 4·5
Zein	2350–2400	2·0	17·3 ($\pm 2\cdot0$)	13·2–11·5
Ovalbumin	2537	2·0	7·0 ($\pm 1\cdot3$)	8·3– 7·3
		7·0	5·7 ($\pm 0\cdot8$)	

* Sensitized reactions.

† The estimated *mean* error is given in the brackets.

calculated from the phase boundary potential measurements on the assumptions specified, are not inconsistent with the theoretical values at present available for the gliadin, zein and ovalbumin. Although the observed agreement cannot be regarded as proof of the occurrence of a particular mechanism of photolysis, it is of great interest that the suggested hypothesis, which is based on considerations of the absorption spectra and

‡ These observations suggest the possibility that monolayers of insulin may possess a structure somewhat different from that of the other proteins examined, perhaps being characterized by less frequent cross linkages.

on photochemical experiments in bulk solution, is found to provide a quantitative interpretation of the photochemical behaviour of monolayers of certain typical proteins.

<center>APPENDIX</center>

<center>*Relevant analytical data*</center>

Wheat gliadin. The data quoted in *Tabulae Biologicae* (1926) account for 90·7 % by weight of the initial material, while those collected by Chibnall (1933) account for 98·4 %. The latter values show that 1 Svedberg unit (34,500) contains 5·8 molecules of tyrosine (Looney 1926), 4·9 of phenylalanine (Osborne and Guest 1911) and 1·8 of tryptophane (Jones, Gersdorff and Moeller 1924). The total number of residues per Svedberg unit is not less than 227, and probably of the order of 280 (cf. Bergmann and Niemann 1937).

Zein. The data collected by Kestner (1925), Waldschmidt-Leitz (1931) and Pauli and Valko (1933) account for 101·3 % by weight of the initial material, and show that 1 Svedberg unit contains not less than 252 residues of which 14·5 are derived from tyrosine and 18·2 from phenyl-alanine.

Insulin. The results of Du Vigneaud, Jensen and Wintersteiner (1928), Jensen and Wintersteiner (1932), Gerlough and Bates (1932), Jensen and Evans (1935) and Harington and Neuberger (1936) account for at least 88 % by weight of the initial material and show that the micelle of weight 35,100 (Sjögren and Svedberg 1931) contains 24 tyrosine residues, no tryptophane and a small, as yet undetermined, amount of phenyl-alanine.

Ovalbumin. The compilation given in *Biochemisches Handlexikon* (1933) shows that 1 Svedberg unit (34,500) contains 8 molecules of tyrosine and 2 of tryptophane; probably there are also 11 molecules of phenyl-alanine (*Tabulae Biologicae* 1926).

The work of Bergmann and Niemann (1937) suggests that the molecule of ovalbumin contains exactly 288 residues; on the basis of the cyclol theory, Wrinch (1937) suggests the same number for insulin.

<center>SUMMARY</center>

This paper is an account of a quantitative investigation of the photochemistry of proteins in monolayers. Wheat gliadin, zein, insulin and ovalbumin have been examined. The photoreactions were studied by observation of the changes in phase boundary potential of the protein monolayers on irradiation, at constant surface area and under equilibrium conditions, with monochromatic ultra-violet light of wave-lengths 2350–3175 A.

The general theory of photochemical reactions in protein monolayers is summarized. The proteins in the monolayers are to be regarded as macromolecular polycondensation products in which the primary photochemical processes are limited, to a first approximation, to the "aromatic" chromophores.

The experimental technique, including the method of fractional irradiation, and the preparation and properties of the monolayers are described.

The characteristic changes on ultra-violet irradiation of protein monolayers are:

(1) Liquefaction, if the film is gelatinous.

(2) At constant area, an increase of phase boundary potential, and also of surface pressure.

Oxidative processes play a fundamental part. Photo-sensitization, probably by traces of metals, is described.

It is suggested that, in these photoreactions, both "peptide linkages" adjacent to each side chain derived from tyrosine, phenyl-alanine and possibly also tryptophane, may undergo a process of oxidative photolysis, the end result of which is equivalent to hydrolysis, and the transformed chromophoric residues liberated pass into solution. This hypothesis is in quantitative agreement with the total changes in phase boundary potential observed on irradiation of the monolayers of gliadin, zein and ovalbumin (the insulin films undergo partial solution). The importance of the Hardy-Langmuir principle is demonstrated.

The absolute quantum efficiency of the total changes per aromatic residue in monolayers of gliadin on N/100 sulphuric acid is of the order of $\frac{1}{2}$ for unsensitized photodecomposition at wave-lengths between 2350 and 3030 A.

References

Abderhalden 1923 *Hoppe-Seyl. Z.* **128**, 119.

Abderhalden and Haas 1927 *Hoppe-Seyl. Z.* **166**, 78.

Abderhalden and Rossner 1929 *Hoppe-Seyl. Z.* **178**, 156.

Adair and Adair 1936 *Proc. Roy. Soc.* B, **120**, 422.

Adam, Danielli and Harding 1934 *Proc. Roy. Soc.* A, **147**, 491.

Andrews 1932 *J. Biol. Chem.* **97**, 657.

— 1933 *J. Biol. Chem.* **102**, 263.

Arnold and Kistiakowsky 1932 *J. Amer. Chem. Soc.* **54**, 1713.

Arnow 1936 *Physiol. Rev.* **16**, 671.

Bachér 1929 *Handb. biol. ArbMeth.* Abt. i, Chemische Methoden, 2, 11, i, pp. 1475, 1635. 1599. Berlin: Urban and Schwarzenburg.

Baudisch and Hoschek 1916 *Ber. dtsch. chem. Ges.* **49**, 2579. Quoted by Bachér, p. 1717.

Becke 1912 *Lehnes Färbenztg*, **24**, 45.
— 1919 *Lehnes Färbenztg*, **30**, 101.
Becker and Szendrö 1931 *Pflüg. Arch. ges. Physiol.* **228**, 755.
Bergen 1925 *Melliands Textilberichte*, **6**, 745.
— 1926 *Dtsch. Wollengew.* **58**, 705.
Bergmann 1924 *Hoppe-Seyl. Z.* **140**, 128.
Bergmann and Niemann 1937 *J. Biol. Chem.* **118**, 301.
Biochemisches Handlexikon, 1933 **14**, 113. Berlin: Springer.
Blyth 1899 *J. Chem. Soc.* **75**, 1162.
Carpenter 1931 *J. Amer. Chem. Soc.* **53**, 1812.
Chibnall 1933 "Amino acid constituents of proteins." Private communication.
Dhéré 1909 "Recherches spectrographiques sur l'absorption des rayons ultra-violets par les albuminoïdes, les protéides et leurs dérivées." Fribourg: Fragnière.
Du Vigneaud, Jensen and Wintersteiner 1928 *J. Pharmacol.* **32**, 367.
Eckstein and Lieben 1933 *Biochem. Z.* **263**, 366.
Forbes and Heidt 1934 *J. Amer. Chem. Soc.* **56**, 2363.
Fort 1916 *J. Soc. Dy. Col., Bradford*, **32**, 184.
Fort and Lloyd 1914 *J. Soc. Dy. Col., Bradford*, **30**, 73.
Gee and Rideal 1935 *Proc. Roy. Soc.* A, **153**, 116.
Gerlough and Bates 1932 *J. Pharmacol.* **45**, 19.
Gorter, Meyer and Philippi 1934 *Proc. Acad. Wete. Amst.* **37**, 355.
Gurney and Jackson 1934 "Dipole Moments." Faraday Society Discussion, Appendix, pp. xxxix, xl, xlii. London.
Harington and Neuberger 1936 *Biochem. J.* **30**, 809.
Hartley 1887 *J. Chem. Soc.* **51**, 59.
Holiday 1936 *Biochem. J.* **30**, 1795.
Hughes 1933 *Trans. Faraday Soc.* **29**, 211.
— 1936 *Proc. Roy. Soc.* A, **155**, 710.
Hughes and Allsopp 1936 *Nature, Lond.*, **137**, 502.
Hughes and Rideal 1932 *Proc. Roy. Soc.* A, **137**, 62.
Jensen and Evans 1935 *J. Biol. Chem.* **108**, 1.
Jensen and Wintersteiner 1932 *J. Biol. Chem.* **98**, 281.
Jones, Gersdorff and Moeller 1924 *J. Biol. Chem.* **62**, 183.
Kestner 1925 "Chemie der Eiweisskörper." Braunschweig.
Kuhn, Eyer and Freudenberg 1931 *Hoppe-Seyl. Z.* **202**, 97.
Lieben 1927 *Biochem. Z.* **187**, 307.
Lieben and Urban 1931 *Biochem. Z.* **239**, 250.
Looney 1926 *J. Biol. Chem.* **69**, 519.
Mitchell 1936*a* *Proc. Roy. Soc.* A, Discussion on Surface Phenomena-Films, **155**, 696.
— 1936*b* *J. Chem. Phys.* **4**, 725.
— 1937*a* *Communications to the Second International Cancer Congress, Brussels*, p. 420.
— 1937*b* *Trans. Faraday Soc.* **33**, 1129. See also Discussion, p. 1145.
— 1938 *Strahlentherapie* (in the press).
Mitchell, Rideal and Schulman 1937 *Nature, Lond.*, **139**, 625.
Moss 1934 *J. Amer. Chem. Soc.* **56**, 41.
Neuberg 1908 *Biochem. Z.* **13**, 305.
Osborne and Guest 1911 *J. Biol. Chem.* **9**, 425.
Pauli and Valko 1933 "Kolloidchemie der Eiweisskörper." Leipzig: Steinkopff.

Philippi 1936 "On the Nature of proteins." Thesis, Leiden. N. V. Noord-Hollandsche Uitgeversmaatschappij. Amsterdam.

Ramart-Lucas 1934 "Traité de Chimie Organique (Grignard). II. Structure des Molécules et Spectres d'Absorption", p. 71. Paris: Masson.

Rideal 1932 *Kolloidzschr.* **61**, 218.

Rideal and Mitchell 1937 *Proc. Roy. Soc.* A, **159**, 206.

Sauer 1916 *Z. angew. Chem.* **29**, 424.

Schulman 1937 *Trans. Faraday Soc.* **33**, 116.

Schulman and Hughes 1932 *Proc. Roy. Soc.* A, **138**, 430.

Schulman and Rideal 1933 *Biochem. J.* **27**, 1581.

Sjögren and Svedberg 1931 *J. Amer. Chem. Soc.* **53**, 2657.

Sörensen 1917 *C.R. Lab. Carlsberg*, **12**.

Spiegel-Adolf 1934 *Biochem. J.* **28**, 372.

Ssadikow 1926 *Biochem. Z.* **179**, 326.

Stenström and Reinhard 1925 *J. Biol. Chem.* **66**, 819.

Stuart and Volkmann 1933 *Z. Phys.* **80**, 107.

Svedberg and Nichols 1926 *J. Amer. Chem. Soc.* **48**, 3081.

Tabulae Biologicae 1926 *J. Berlin*, **3**, 263.

Waldschmidt-Leitz 1931 "Neuere Untersuchungen über den Aufbau der Eiweisskörper." Leipzig.

Wrinch 1937 *Proc. Roy. Soc.* A, **161**, 505.

Zocher and Stiebel 1930 *Z. phys. Chem.* A, **147**, 401.

The comparison of series of measures on different hypotheses concerning the standard errors

By HAROLD JEFFREYS, F.R.S.

1. The test for the significance of the difference of two means, when the standard errors of one observation are unequal, has been the subject of much recent discussion (Fisher 1935; Bartlett 1936; Welch 1937; Daniels 1938), but the appropriate treatment remains in doubt. A significance test for the difference of two means, on my principles, has already been given (Jeffreys 1937a), but is not altogether satisfactory, for two reasons. The result was, for large numbers of observations,

$$K = \frac{P(q \mid \theta h)}{P(\sim q \mid \theta h)} = \left(\frac{2}{\pi} \frac{\sigma^2 + \tau^2}{\sigma^2/m + \tau^2/n}\right)^{\frac{1}{2}} \exp\left(-\frac{1}{2} \frac{(\bar{x} - \bar{y})^2}{\sigma^2/m + \tau^2/n}\right), \tag{1}$$

where $\bar{x}$ and $\bar{y}$ are the means in the two series, m and n the numbers of observations, σ and τ the (estimated) standard errors of one observation. The most serious practical defect of this formula is that the numbers of observa-

tions are supposed large enough for the uncertainty of the standard errors to be neglected. This was due to a premature approximation and could be corrected easily; the resulting change would be similar to the difference between the normal law and "Student's" formula, as has already been shown in other cases. There is, however, another anomaly, less serious in practice, but of theoretical importance. We notice that if $\tau = 0$, when the observations in the second series are exact, the first factor reduces to $(2m/\pi)^{\frac{1}{2}}$, which is the usual form for the test of one new parameter, and is satisfactory. But if $\sigma = \tau$, and n is very large, so that the uncertainty of the true value in the second series is again negligible, we should again expect the outside factor to reduce to $(2m/\pi)^{\frac{1}{2}}$, since we are again comparing the mean of the first series with an accurate value. Actually it reduces to $(4m/\pi)^{\frac{1}{2}}$. This is not of much practical importance, since if formula (1) gives $K = 1$, the correct formula would give $K = 1/\sqrt{2}$, and the result would still be indecisive, though slightly in favour of $\sim q$.

The analysis of the case $\sim q$ (genuine difference present) involves the estimation of two means and two standard errors. The weighted mean of the two means would be taken as the estimate of a parameter on q from the two series together. The problem is therefore one of assessing the significance of one new parameter when there is an additional parameter whose significance is not in question, and has analogies with several cases already considered. In the problem of function fitting the main effect of the allowance for each such parameter is to increase the index of the factor $\{1 + \chi^2/(n-m)\}^{-\frac{1}{2}(n-3)}$ by $\frac{1}{2}$. There was little change in the actual analysis, mainly because the new functions fitted were supposed chosen so as to be orthogonal with the old ones at the actual weights, so that allowance for the new ones does not affect the estimates of the coefficients of the old ones. The analogy suggests, however, that if this condition is necessary to a correct treatment the weighted mean of the true values and the difference of the true values should be introduced separately as two independent unknowns, the weights being chosen so that the former will have the same value on both hypotheses q and $\sim q$. A similar device has already been adopted (Jeffreys 1937*b*) in treating the comparison of two samples, of numbers (x, y) (x', y'), where $x + y$ and $x' + y'$ are initially fixed. On the hypothesis q that the chances of a number having the property ϕ in the two cases are really identical they are equal to p, to be found from the two samples together. On $\sim q$, the chances are respectively p and p', but the quantity b defined by

$$(x + y + x' + y')\,b = (x + y)\,p + (x' + y')\,p'$$

has the same value on both hypotheses, and would receive the same estimate on both. Its significance is not in question; but whatever its value may be, it will not by itself give us any information about whether $p = p'$. If we introduce b as an unknown explicitly we therefore ensure that information relevant only to its value will not be confused with information relevant to whether $p = p'$. In my first analyses (1935, 1936) this was not done. But if b is introduced in this way it imposes a restriction on the possible values of p and p'; values of p' that might be possible *a priori* would imply negative p when b is given. Allowance for this complication has removed a serious inconsistency between the results obtained for three sampling problems, where the conditions of sampling are slightly different, but if the numbers tested for proportionality are the same we should not expect any notable difference in the criterion for significance. The possible range of p' now depends on b, and this introduces a new factor into the prior probability, which just removes the previous inconsistencies.

If we should, by analogy, introduce a suitably weighted mean of the true values as a fundamental unknown in the comparison of series of measures, it may lead to a further restriction on the possible range of the difference, which will now have to be assessed subject to whatever value may be found for this mean, and this may alter the result. The change will not be so great as in cases already examined, since the result already found is of the right order of magnitude, but it is possible that the K found for large numbers of observations is too high and would sometimes lead to the rejection of a difference that a more accurate analysis would interpret as significant. On such an analysis the systematic difference would not be able to account for the whole expectation of the difference between two representative observations.

On hypothesis q, then, we shall introduce an unknown x, which will be the true value for both sets, and two standard errors s and t; we express the previous ignorance and independence of these by taking

$$P(q, dx\,ds\,dt \mid h) \propto dx\,ds\,dt/st. \qquad (2)$$

If $\bar{x}_1$ and $\bar{x}_2$ are the means and σ and τ the standard deviations of the two series of observations, denoted collectively by θ, we have

$$P(\theta \mid qh\,dx\,ds\,dt) \propto s^{-m}t^{-n}\exp\left[-\frac{m}{2s^2}(\bar{x}_1 - x)^2 - \frac{m\sigma^2}{2s^2} - \frac{n}{2t^2}(\bar{x}_2 - x)^2 - \frac{n\tau^2}{2t^2}\right]. \qquad (3)$$

The maximum posterior probability density and maximum likelihood for x are then given by

$$\left(\frac{m}{s^2} + \frac{n}{t^2}\right)x = \frac{m\bar{x}_1}{s^2} + \frac{n\bar{x}_2}{t^2}. \qquad (4)$$

On $\sim q$, we must regard $\bar{x}_1$ and $\bar{x}_2$ as estimates of two separate unknowns x_1 and x_2, of which x is a weighted mean. Attention is needed to the meaning of s and t. On q, since x is the true value, s^2 and t^2 are the expectations of the square of a departure from x. On $\sim q$ they must retain these meanings, but the departures of x_1 and x_2 from x will make contributions to s^2 and t^2, so that the actual standard errors will be smaller. Then x will be defined by

$$\left(\frac{m}{s^2}+\frac{n}{t^2}\right)x = \frac{mx_1}{s^2}+\frac{nx_2}{t^2}, \tag{5}$$

and if we put $x_2 - x_1 = z$ we have

$$x_1 = x - \frac{n/t^2}{m/s^2+n/t^2}z; \quad x_2 = x + \frac{m/s^2}{m/s^2+n/t^2}z, \tag{6}$$

while the standard errors s' and t' are given by

$$s'^2 = s^2 - (x_1 - x)^2; \quad t'^2 = t^2 - (x_2 - x)^2. \tag{7}$$

The limits for z will be fixed by the fact that $|x_1 - x|$ cannot exceed s, nor can $|x_2 - x|$ exceed t. Thus if $|z| \leqslant c$,

$$\frac{n/t^2}{m/s^2+n/t^2}c = s \quad \text{or} \quad \frac{m/s^2}{m/s^2+n/t^2}c = t, \tag{8}$$

whichever gives the smaller value of c. The immediate question is therefore which of s/m and t/n is the greater. If the former, we must take the first value of c; if the latter, the second. This distinction therefore introduces an asymmetry into the treatment. The prior probability distribution is given by

$$P(\sim q,\, dx\,ds\,dt\,dz \mid h) \propto dx\,ds\,dt\,dz/2stc, \tag{9}$$

and

$$
\begin{aligned}
&P(\theta \mid \sim q,\, dx\,ds\,dt\,dz\, h) \\
&\quad \propto s'^{-m}t'^{-n}\exp\left[-\frac{m}{2s'^2}(\bar{x}_1-x_1)^2-\frac{m\sigma^2}{2s'^2}-\frac{n}{2t'^2}(\bar{x}_2-x_2)^2-\frac{n\tau^2}{2t'^2}\right]. \tag{10}
\end{aligned}
$$

Hence combining (2) with (3), and (9) with (10), we have

$$
\begin{aligned}
&P(q\,dx\,ds\,dt \mid \theta h) \\
&\quad \propto s^{-m}t^{-n}\exp\left[-\frac{m}{2s^2}(\bar{x}_1-x)^2-\frac{m\sigma^2}{2s^2}-\frac{n}{2t^2}(\bar{x}_2-x)^2-\frac{n\tau^2}{2t^2}\right]\frac{dx\,ds\,dt}{st}, \tag{11}
\end{aligned}
$$

$$
\begin{aligned}
&P(\sim q\,dx\,ds\,dt\,dz \mid \theta h) \\
&\quad \propto s'^{-m}t'^{-n}\exp\left[-\frac{m}{2s'^2}(\bar{x}_1-x_1)^2-\frac{m\sigma^2}{2s'^2}-\frac{n}{2t'^2}(\bar{x}_2-x_2)^2-\frac{n\tau^2}{2t'^2}\right]\frac{dx\,ds\,dt\,dz}{2stc}. \tag{12}
\end{aligned}
$$

Now $\dfrac{m}{s^2}(\bar{x}_1 - x)^2 + \dfrac{n}{t^2}(\bar{x}_2 - x)^2 = \left(\dfrac{m}{s^2} + \dfrac{n}{t^2}\right)\left(x - \dfrac{m\bar{x}_1/s^2 + n\bar{x}_2/t^2}{m/s^2 + n/t^2}\right)^2 + \dfrac{(\bar{x}_1 - \bar{x}_2)^2}{s^2/m + t^2/n},$

$$\tag{13}$$

and the integration of (11) with regard to x gives

$$P(q\,ds\,dt \mid \theta h)$$
$$\propto s^{-m} t^{-n} \exp\left[-\frac{m\sigma^2}{2s^2} - \frac{n\tau^2}{2t^2} - \frac{(\bar{x}_1 - \bar{x}_2)^2}{2(s^2/m + t^2/n)}\right]\left\{\frac{2\pi}{(m/s^2 + n/t^2)}\right\}^{\frac{1}{2}}\frac{ds\,dt}{st}, \quad (14)$$

and that of (12) gives

$$P(\sim q\,ds\,dt\,dz \mid \theta h)$$
$$\propto s'^{-m} t'^{-n} \exp\left[-\frac{m\sigma^2}{2s'^2} - \frac{n\tau^2}{2t'^2} - \frac{(z + \bar{x}_1 - \bar{x}_2)^2}{2(s'^2/m + t'^2/n)}\right]\left(\frac{2\pi}{m/s'^2 + n/t'^2}\right)^{\frac{1}{2}}\frac{ds\,dt\,dz}{2stc}.$$

$$\tag{15}$$

If the number of observations is enough for the standard error of z to be much less than c, we can replace the limits for z in (15) by $\pm\infty$; integrating we find

$$P(\sim q\,ds\,dt \mid \theta h)$$
$$\propto s'^{-m} t'^{-n} \exp\left[-\frac{m\sigma^2}{2s'^2} - \frac{n\tau^2}{2t'^2}\right]\left(\frac{2\pi}{(m/s'^2 + n/t'^2)}\right)^{\frac{1}{2}} \{2\pi(s'^2/m + t'^2/n)\}^{\frac{1}{2}}\frac{ds\,dt}{2stc}$$
$$\propto s'^{-m} t'^{-n} \exp\left[-\frac{m\sigma^2}{2s'^2} - \frac{n\tau^2}{2t'^2}\right]\frac{2\pi s't'}{\sqrt{(mn)}}\frac{ds\,dt}{2stc}. \tag{16}$$

We can integrate (14) once by the substitution $t = su$, which gives

$$P(q \mid \theta h) \propto \{\tfrac{1}{2}(m + n - 3)\}!$$
$$\times 2^{\frac{1}{2}(m+n-3)} \int_0^\infty u^{-n}\left\{m\sigma^2 + \frac{n\tau^2}{u^2} + \frac{mn(\bar{x}_1 - \bar{x}_2)^2}{mu^2 + n}\right\}^{-\frac{1}{2}(m+n-1)}\left(\frac{2\pi}{mu^2 + n}\right)^{\frac{1}{2}} du. \quad (17)$$

In the important cases we can temporarily replace s and t in (16) by s' and t'; for if these were not good approximations the systematic difference would be comparable with at least one of the standard errors of one observation and significance would be obvious. Also we take $t/n < s/m$. Substituting for c we find

$$P(\sim q \mid \theta h) \propto \int\int s'^{-m} t'^{-n} \exp\left(-\frac{m\sigma^2}{2s'^2} - \frac{n\tau^2}{2t'^2}\right)\pi\Big/\sqrt{\left(\frac{n}{m}\right)}\frac{s'\,ds'\,dt'}{mt'^2 + ns'^2}, \quad (18)$$

or, putting $t' = s'u$,

$$\propto \pi\Big/\sqrt{\left(\frac{n}{m}\right)}\{\tfrac{1}{2}(m + n - 3)\}!$$
$$\times 2^{\frac{1}{2}(m+n-3)} \int_0^\infty u^{-n}\left(m\sigma^2 + \frac{n\tau^2}{u^2}\right)^{-\frac{1}{2}(m+n-1)}\frac{du}{n + mu^2}. \quad (19)$$

The factors in the integrand of (19) that have m or n in their indices give rise to a Beta-function. The same would apply to (17) if it were not for the $mu^2 + n$ in one of the denominators. The same term introduces complications into evaluation by the method of steepest descents. Now this is the only term that involves the difference of the means, and if we approximated directly it would lead to the $\exp(-\frac{1}{2}\chi^2)$ factor that arises when the numbers of observations are so large that we can neglect the uncertainties of the standard errors. The reason for dissatisfaction with this approximation is that with moderate numbers of observations the estimated standard error may be appreciably too high or too low, and the critical value of a difference is usually two to three times its estimated standard error. In this range the chance of a random difference is small anyhow if the true standard error is equal to or less than the estimate, but if the estimate is the lower, the chance of a random error in this range may be substantially greater. This complication is present both in problems of estimation and significance tests. In the latter, the observed difference may lead to the inference that the estimate of one of the standard errors is too low, rather than to an assertion of significance. A closer approximation than the simple exponential one is therefore needed in cases where the standard error is to be found from the actual scatter of the observations.

In the present case the estimated standard error of the difference $\bar{x}_1 - \bar{x}_2$ is $(\sigma^2/m + \tau^2/n)^{\frac{1}{2}}$ and the estimate of u is about τ/σ; thus $mu^2 + n$ depends on the (true) standard error of the difference, and the requisite improvement of the approximation depends on allowance for the variation of $mu^2 + n$ near the maximum of the integrand. Unfortunately this term, in its exact form, prevents any compact expression for the maximum of the integrand from being obtained; but if we try to fit a form $Cu^{-2} + D$, such that it and its first derivative are equal to $(mu^2 + n)^{-1}$ and its first derivative when $u = \tau/\sigma$, we shall allow for the variation with a possible error of order $(\bar{x}_1 - \bar{x}_2)^4$, and therefore one of order $(\bar{x}_1 - \bar{x}_2)^6$ in the integrand. The result is

$$C = \frac{m\tau^4}{(m\tau^2 + n\sigma^2)^2}; \quad D = \frac{n\sigma^4}{(m\tau^2 + n\sigma^2)^2}. \tag{20}$$

With this substitution (17) also can be reduced to a Beta-function except for a slowly varying factor, for which an approximate value can be substituted. Dropping some irrelevant factors, we have

$$P(q \mid \theta h) \propto \int_0^\infty u^{m-1}[\{m\sigma^2 + Dmn(\bar{x}_1 - \bar{x}_2)^2\}u^2 \\ + \{n\tau^2 + Cmn(\bar{x}_1 - \bar{x}_2)^2\}]^{-\frac{1}{2}(m+n-1)}\frac{du}{(mu^2 + n)^{\frac{1}{2}}}, \tag{21}$$

$$P(\sim q \mid \theta h) \propto \sqrt{\frac{\pi n}{2m}}\int_0^\infty u^{m-1}\{m\sigma^2 u^2 + n\tau^2\}^{-\frac{1}{2}(m+n-1)}\frac{du}{mu^2 + n}. \tag{22}$$

Now if we put
$$\frac{u^2}{Au^2+B} = \frac{v}{A},$$
(23)

we find
$$\int_0^\infty \frac{u^{m-1}}{(Au^2+B)^{\frac{1}{2}(m+n-1)}}\,du = \frac{\{\frac{1}{2}(m-2)\}!\,\{\frac{1}{2}(n-3)\}!}{\{\frac{1}{2}(m+n-3)\}!}\,\frac{1}{2A^{\frac{1}{2}m}\,B^{\frac{1}{2}(n-1)}},$$
(24)

and the maximum of the integrand is near
$$u^2 = \frac{mB}{nA}.$$
(25)

Approximating on this basis and simplifying we have
$$
\begin{aligned}
K &= P(q\,|\,\theta h)/P(\sim q\,|\,\theta h) \\
&= \left(\frac{2m}{\pi}\,\frac{m\tau^2+n\sigma^2}{n\sigma^2}\right)^{\frac{1}{2}} \left(1 + \frac{(m^3\tau^4+n^3\sigma^4)\,(\bar{x}_1-\bar{x}_2)^2}{(m\tau^2+n\sigma^2)^3}\right)^{-\frac{1}{2}} \\
&\quad \times \left\{1 + \frac{n^2\sigma^2(\bar{x}_1-\bar{x}_2)^2}{(m\tau^2+n\sigma^2)^2}\right\}^{-\frac{1}{2}(m-1)} \left\{1 + \frac{m^2\tau^2(\bar{x}_1-\bar{x}_2)^2}{(m\tau^2+n\sigma^2)^2}\right\}^{-\frac{1}{2}(n-1)}.
\end{aligned}
$$
(26)

A correction is needed for the replacement of s and t in (16) by s' and t', and therefore ultimately by σ and τ. The factor needed in K is the estimated value of
$$
\begin{aligned}
\frac{stc}{s't'c'}\,\frac{\partial(s',t')}{\partial(s,t)} &= \frac{s^2t^2c}{s'^2t'^2c'} \\
&= \left\{1 + \frac{(m^3\tau^4+n^3\sigma^4)\,(\bar{x}_1-\bar{x}_2)^2}{(m\tau^2+n\sigma^2)^3}\right\} \left(1 + \frac{n^2\sigma^2(\bar{x}_1-\bar{x}_2)^2}{(m\tau^2+n\sigma^2)^2}\right)^{\frac{1}{2}} \left(1 + \frac{m^2\tau^2(\bar{x}_1-\bar{x}_2)^2}{(m\tau^2+n\sigma^2)^2}\right),
\end{aligned}
$$
(27)

so that the indices in (26) should be changed respectively to $+\frac{1}{2}$, $-\frac{1}{2}(m-2)$, $-\frac{1}{2}(n-3)$. On inspection this formula shows some novel and satisfactory features. The asymmetry with respect to m and n comes from the restriction that $t/n < s/m$; if $\tau/n > \sigma/m$ we must interchange σ with τ and m with n. But the factor $(\sigma^2+\tau^2)^{\frac{1}{2}}$ in (1) has disappeared. If $\tau = 0$, the outside factor still reduces to $(2m/\pi)^{\frac{1}{2}}$, as it should. If $\tau = \sigma$, but n much greater than m, the factor is multiplied only by $(1+m/n)^{\frac{1}{2}}$ instead of by $\sqrt{2}$, as it was before. The anomaly present in the previous solution has therefore disappeared. If however $\tau/n < \sigma/m$, it does not follow that $\tau^2/n < \sigma^2/m$, and if τ is greater than σ but is associated with a larger number of observations the standard of significance may be substantially increased. But in this case the outside factor cannot exceed $\{2(m+n)/\pi\}^{\frac{1}{2}}$, and n is greater than m. If the first series was absolutely accurate the factor would be $(2n/\pi)^{\frac{1}{2}}$, so that this form is reasonable.

The interest of the other factors is that the difference whose significance is in question does not rise wholly through its ratio to its standard error, as in previous tests; the ratio of the two contributions to the standard error is also relevant. If m and n are large, so that exponential approximations are permissible, these factors do reduce to $\exp\left\{-\dfrac{(\bar{x}_1-\bar{x}_2)^2}{2(\sigma^2/m+\tau^2/n)}\right\}$, as we should expect; but for moderate values of m and n there is no analogous simplification. Now this is essentially reasonable when we recall that the departure from the exponential form represents the uncertainty of the estimated standard errors. If one set of observations gives a very small standard error of its mean, we are effectively comparing the mean of the other with an accurately determined value, and the test should reduce to the test for the significance of the difference between the mean of a moderate number of observations and zero. But if $\tau^2/n \ll \sigma^2/m$ these factors do reduce to $\{1+(\bar{x}_1-\bar{x}_2)^2/\sigma^2\}^{-\frac{1}{2}(m-3)}$, which is the result already found for the latter case (Jeffreys 1938a, p. 177, equ. (28)).

The formula is rather complicated, but one factor in (26) and (27) enters only with index $\frac{1}{2}$, and is of minor importance. If we replace $m^3\tau^4+n^3\sigma^4$ in it by $n^2\sigma^2(m\tau^2+n\sigma^2)$ we shall commit an inappreciable error; and then the first two factors involving $\bar{x}_1-\bar{x}_2$ coalesce to give

$$K = \left(\frac{2m}{\pi}\frac{m\tau^2+n\sigma^2}{n\sigma^2}\right)^{\frac{1}{2}}\left(1+\frac{n^2\sigma^2(\bar{x}_1-\bar{x}_2)^2}{(m\tau^2+n\sigma^2)^2}\right)^{-\frac{1}{2}(m-3)}\left(1+\frac{m^2\tau^2(\bar{x}_1-\bar{x}_2)^2}{(m\tau^2+n\sigma^2)}\right)^{-\frac{1}{2}(n-3)}.$$
$$(28)$$

This reduces to the correct form when $\tau=0$. When $\tau^2/n \gg \sigma^2/m$, with τ/n still $< \sigma/m$, we are comparing the second series with an accurate value. The first factor then approaches $\{2(n+m)/\pi\}^{\frac{1}{2}}$, (with $n \gg m$), the second to 1, the third to $\{1+(\bar{x}_1-\bar{x}_2)^2/\tau^2\}^{-\frac{1}{2}(n-3)}$, as it should. It appears therefore that (28) is sufficiently nearly correct in all cases where $\tau/n < \sigma/m$. When this inequality is reversed we must interchange m with n and σ with τ in the first factor. The approximations used, however, are not reliable unless both m and n are at least 5.

2. *Comparison when the standard errors are equal.* It often happens that the two series of observations are made under such similar conditions that it is legitimate to take as part of our data that the standard errors are equal. This is the opposite extreme from the last problem. Here, if there are many observations in one set and only a few in the other, the scatter of the first set is relevant to the accuracy of the mean of the second; in the usual language, there is only one standard error, determined from $m+n-2$ degrees of freedom, whereas in the last problem there are two, determined respectively

from $m-1$ and $n-1$. This problem can be treated as a case of the test for one new parameter, when there is another parameter, the mean of the whole set of observations, whose significance is not in doubt.

As before, we introduce a parameter x, which is the true value on q, while on $\sim q$ it is defined by

$$(m+n)\, x = mx_1 + nx_2. \tag{1}$$

We take also a function f, whose mean value over the observations is 0 and whose mean square is 1, and with the same value for each observation of either set. Then

$$f = (n/m)^{\frac{1}{2}}; \quad f = -(m/n)^{\frac{1}{2}} \tag{2}$$

for the respective sets; and we can write

$$x_1 = x + (n/m)^{\frac{1}{2}} a; \quad x_2 = x - (m/n)^{\frac{1}{2}} a, \tag{3}$$

where a is the new parameter to be found. The test for it is got from a previous one (Jeffreys 1938 a, p. 177, equ. (28)) by replacing the m of that formula, the number of new degrees of freedom, by 1, and n, the number of observations, by $m+n$; while since one unknown irrelevant to the test has to be eliminated the index of the last factor must be increased by $\frac{1}{2}$. Then we have

$$K = \left\{\frac{2(m+n)}{\pi}\right\}^{\frac{1}{2}} \left(1 + \frac{\alpha^2}{\sigma'^2}\right)^{-\frac{1}{2}(n+m-4)}, \tag{4}$$

where α is the estimate of a and σ'^2 is the mean square residual after allowing for α. Then

$$\bar{x}_1 - \bar{x}_2 = \{(n/m)^{\frac{1}{2}} + (m/n)^{\frac{1}{2}}\}\alpha = (m+n)\,\alpha/(mn)^{\frac{1}{2}}, \tag{5}$$

$$(m+n)\,\sigma'^2 = m\sigma^2 + n\tau^2, \tag{6}$$

σ and τ being the standard deviations in the respective series. Then

$$K = \left\{\frac{2(m+n)}{\pi}\right\}^{\frac{1}{2}} \left\{1 + \frac{mn(\bar{x}_1 - \bar{x}_2)^2}{(m+n)\,(m\sigma^2 + n\tau^2)}\right\}^{-\frac{1}{2}(m+n-4)}, \tag{7}$$

which is the form required. If we introduce the usual estimate σ_m of the standard error of $\bar{x}_1 - \bar{x}_2$,

$$\sigma_m^2 = (m+n)\,\sigma'^2/mn, \tag{8}$$

$$K = \left\{\frac{2(m+n)}{\pi}\right\}^{\frac{1}{2}} \left\{1 + \frac{(\bar{x}_1 - \bar{x}_2)^2}{(m+n)\,\sigma_m^2}\right\}^{-\frac{1}{2}(m+n-4)}, \tag{9}$$

the second factor in which reduces to $\exp(-\frac{1}{2}\chi^2)$ when $m+n$ is large. The result is quite different in form from that of the last section, the difference coming from the fact that σ and τ here are estimates of the same quantity, whereas in the last they were estimates of two entirely separate quantities.

K will be larger for small values of $\bar{x}_1 - \bar{x}_2$, in relation to its standard error, and smaller for large values.

3. *The test for the significance of one parameter, when the standard error is initially unknown.* In this problem, the simplest of this type, if there is only one observation and no irrelevant parameter is to be found, there is no way of saying whether the departure of this observation from zero is random or systematic, and the test should be wholly indecisive; that is, K should be exactly 1. In this case we have, without approximation,

$$P(q, ds \mid \theta h) \propto s^{-1} \exp\left(-\frac{\bar{x}^2}{2s^2}\right)\frac{ds}{s}, \tag{1}$$

$$P(\sim q, ds\,dx \mid \theta h) \propto (s^2 - x^2)^{-\frac{1}{2}} \exp\left\{-\frac{(x - \bar{x})^2}{2(s^2 - x^2)}\right\}\frac{ds\,dx}{2s^2}, \tag{2}$$

where, in (2), s is restricted to be greater than $|x|$. $\bar{x}$ is here of course identical with the single observation, and $\sigma = 0$. Integration of (1) gives

$$P(q \mid \theta h) \propto (\tfrac{1}{2}\pi)^{\frac{1}{2}}/\bar{x}. \tag{3}$$

To integrate (2), put $x = s \sin\phi$. Then

$$P(\sim q \mid \theta h) \propto \int_0^\infty \int_{-\frac{1}{2}\pi}^{\frac{1}{2}\pi} \exp\left\{-\frac{(s\sin\phi - \bar{x})^2}{2s^2\cos^2\phi}\right\}\frac{ds\,d\phi}{2s^2}$$

$$\propto \frac{1}{2}\int_0^\infty \int_{-\frac{1}{2}\pi}^{\frac{1}{2}\pi} \exp\left\{-\frac{(\sin\phi - k\bar{x})^2}{2\cos^2\phi}\right\} dk\,d\phi$$

$$\propto \frac{1}{2\pi}(\tfrac{1}{2}\pi)^{\frac{1}{2}}\int_{-\frac{1}{2}\pi}^{\frac{1}{2}\pi} \cos\phi\left\{1 + \operatorname{erf}\left(\frac{1}{\sqrt{2}}\tan\phi\right)\right\} d\phi$$

$$\propto (\tfrac{1}{2}\pi)^{\frac{1}{2}}/\bar{x} = P(q \mid \theta h). \tag{4}$$

Hence if there is only one observation K is exactly 1, and the test is indecisive, as we should expect.

Attention to such special cases is often desirable as a check on the general procedure, at any rate when only one parameter is under discussion. We have had similar cases already, notably that of the testing of an even chance (Jeffreys 1938 b, p. 487), where the first specimen gave exactly $K = 1$; and if a sample of $2x$ is equally divided, then the addition of a further specimen does not alter the value of K, which was again to be expected since the last specimen must be of one type or the other, whether the chance is even or not. A little care is needed, however, since the result does not hold if the chance tested is not even. The exact formula is

$$K = \frac{(x + y + 1)!}{x!\,y!}\,p^x(1 - p)^y.$$

If we are testing a $3 : 1$ ratio, $p = \frac{3}{4}$, and if we get $x = 1$, $y = 0$, then $K = \frac{2}{3}$; but if $x = 0$, $y = 1$, $K = \frac{1}{2}$. In this case there is an asymmetry in the trial hypothesis q; if q is true we should expect the first result and not the second from the first trial, so that the results would naturally be expected to be different.

It might appear that if m new parameters arose at once and just m observations were available we should again get $K = 1$. I have tried to prove this, but did not succeed, and on further thought believe it to be untrue, even when the new functions are strictly orthogonal at the weights. On hypothesis q the whole variation is random, and the m coefficients are a sample of values derived from the normal law. But we could take the $m - 1$ smallest, and these would lead to a definite probability distribution for the largest. On $\sim q$, the $m - 1$ may contain systematic parts, and the normal distribution will in general be less extended than on q. If then the largest coefficient found lies beyond the range where this probability is appreciable it will afford evidence that the m coefficients are not a normal sample, and therefore evidence for $\sim q$. Thus we may be able to assert the significance of at least one of the parameters even when the observations are too few to estimate a standard error according to the usual rules, because the smaller coefficients suggest a value for it.* If the new functions are strongly non-orthogonal the problem is formally easier. Thus if the functions are a cosine and sine, there may be two observations in opposite phases of the argument, say 0 and π. Then we have two observations capable of estimating a cosine term, and two are enough to give a judgement of significance (the constant term being supposed already known), though naturally not a very strong one.

If may be mentioned that the transformation $x = s \sin \phi$ will reduce $1/K$ to a single integral even if there are many observations, and could be used to obtain more accurate values for K than the present ones, which rest on an approximation by steepest descents, and cannot be used when n is less than about 5.

4. The value of K to adopt for practical use must involve other considerations than those of pure knowledge. Omitting cases of selection, where the treatment can easily be adapted, we may say that $\sim q$ is supported by the data whenever K is less than 1, and q when $K > 1$. But if $K = 1$, $\sim q$ has the same probability as the statement that an unbiased coin will throw a head at the next trial or that an estimate is right within its probable error, neither of which need be taken very seriously. If we are to assert either q or $\sim q$ with much confidence K must be much more or much less than 1. If we must

---

* The point is somewhat analogous to the occasional use in agricultural experiments of high-order interactions to provide an estimate of error.

draw an absolute line somewhere, $K = 1$ is likely, as far as we know now, to produce a minimum number of mistakes; but we are at liberty to surround $K = 1$ by two other values and say that within this range the data are not sufficiently decisive, and even this device would be purely one of convenience and sacrifice some information given by the actual values of K. Now these conditions of convenience are biased. At the least the introduction of a new parameter involves additional computation, the labour of which is not negligible. In economic applications, if action is to be taken on a discovery, it may involve a temporary loss during the transition, and it will be a matter for the economic advisers to say whether the ultimate advantage will compensate for this. It cannot be expected that these ethical values will be the same in all cases, but it is clear that they will tend to encourage future action on q even when the evidence is slightly against it. Some idea of the amount of this bias may be obtained from observations of behaviour. A physicist would hardly introduce a new parameter if it was only twice its standard error as estimated from the observations, even if it was predicted by a reliable theory independent of these observations, simply because the reduction of the residuals by allowing for it would not compensate for the extra trouble. Now the 5 % point of the normal law is at 1·96 times the standard error, and this point also is extensively used as the lower limit of significance in many current tests. It seems fair to say, therefore, that our limit, for practical use, should never be drawn below the 5 % point. A constant value of K does not correspond to one of P, though with ordinary numbers of observations it usually lies between $P = 0.05$ and $P = 0.01$. But at small numbers of observations $K = 1$ lies below the 5 % point, and this consideration should suggest a suitable value of K to take. The normal and χ^2 distributions are not suitable as standards of comparison, because they say nothing about the number of observations, and the latter is useless at small numbers, but the t distribution is suitable. With Fisher's definition of t (1936, p. 126), in the notation of the present paper,

$$t^2 = (n-1)\,\bar{x}^2/\sigma^2,$$

but the n of his table is my $n - 1$. My formula

$$K = \left(\frac{2n}{\pi}\right)^{\frac{1}{2}} \left(1 + \frac{\bar{x}^2}{\sigma^2}\right)^{-\frac{1}{2}(n-3)}$$

can therefore be written

$$K = \left(\frac{2n}{\pi}\right)^{\frac{1}{2}} \left(1 + \frac{t^2}{n-1}\right)^{-\frac{1}{2}(n-3)},$$

each of Fisher's values of n being increased by 1. His 5 % values of t then give the following values of K:

n (Fisher's $n+1$)	K	n (Fisher's $n+1$)	K
5	0·610	9	0·519
6	0·552	10	0·522
7	0·529	20	0·612
8	0·520	30	0·719

For the first few entries my formula may be appreciably inaccurate, but for $n = 8$ and more it should be fairly good. It appears therefore that the 5 % point of the t distribution never corresponds to a value of K less than about 0·5, or to 2 to 1 odds on the need for the new parameter. If we are entitled to interpret this as indicating at what value of K we may consider a new parameter as worth introducing, the value should be about 0·5; but there will then be just about as much confidence in the need for it as in a statement that an estimate of a parameter, whose relevance is not in doubt, is right within its standard error.

The inequality is reversed at large numbers of observations; thus for $K = 1$ and large n we have the approximation

$$t^2 \fallingdotseq \log_e 2n/\pi,$$

whereas the 5 % point of the t distribution tends to $t = 1·96$. The properties of the logarithm make the rise very slow; when $n = 100,000$, t is still only 3·32. But if the 5 % rule was used habitually there would be cases, with large numbers of observations, when a new parameter is asserted on evidence that is actually against it. Users of the rule usually advocate it with considerable caution, which would agree with the indications of the present theory up to about 30 observations, but at large numbers it is definitely too lax. It would mean drawing the line at such a limit as to give a fixed percentage of what Neyman and E. S. Pearson call errors of the first kind, with respect to the number of cases where q is true; but as the limit is at our disposal we are entitled to take it further out and reduce this percentage still further if there is no special reason to expect values of the new parameter in the range affected. To reject the null hypothesis in any cases at all where it is true is not a desirable action for its own sake. It is an evil that becomes necessary if we are to have any criterion for detecting cases where q is untrue, and we are justified in taking such steps as will reduce its importance to a minimum.

It may be worth while to call attention again to the reason for the increase of t and its analogues in other tests when the number of observations is very

large. If we start with the minimum of information about the new para-
meter, which is quite likely to be zero but might account for most of the
outstanding variation until we have actually analysed the data, then as we
increase the number of observations the standard error of the estimate
steadily falls. If the parameter is not zero, however, it is independent of the
number of observations, and will ultimately become several times the
standard error of its estimate and asserted to be genuine. If the estimate
persists within the order of magnitude of its standard error, our confidence
that this is because the parameter is really zero will naturally increase, on the
ground that with a large number of observations it is increasingly unlikely
that we should have failed to find it if it was there. This of course is a well-
known phenomenon in physics, where an estimated difference, always in
doubt, strengthens that doubt by diminishing every time the number of
observations is increased or the experimental technique improved; and it is
represented in the present theory by the increase of the outside factor in K.
When the number of observations is small, this factor is not much more than
1, and it is impossible to obtain strong support for q however well the ob-
servations may agree with it; and in sampling problems in similar conditions
it is also impossible to obtain strong support for $\sim q$. It may be recalled that
in the problem of sampling to test an even chance it took an $80 : 80$ sample to
give 10 to 1 support for q and a $7 : 0$ one to give 10 to 1 support for $\sim q$. It is
in such cases that we say that there is not enough evidence to make a de-
cision, and any definite rule will make a considerable number of mistakes of
one kind or the other. Mathematically, the ratio of the estimate to its stan-
dard error must increase with the number of observations because it has to
counteract this factor to reduce K to any fixed value. In general terms, it
must increase because the number of cases where q is still acceptable remains
the same, but those where it is untrue and its falsehood still undetected
become fewer. (I am not here considering cases where selection of an extreme
value, or previous knowledge indicating a restriction on the possible values
of a new parameter, needs to be taken into account; they only complicate
the matter without altering the general principle.) What the increase of the
critical value does beyond, say, the 5 % point, is to reduce the probability
of an error of the first kind, while possibly slightly increasing that of one of
the second, and when it has reached the 1 % point it may well be considered
that there is little to gain in any case. If a difference beyond the 1 % point
gives $K > 1$, it will often be worth while to test whether some unconsidered
dependence between the observations such as that discussed already
(Jeffreys 1938a, pp. 187–90) has led to an underestimate of uncertainty.
Such correlations are far commoner than differences in this range are likely

to be in their absence, and such a result may be regarded as an indication of the need for investigation. The use of a fixed P limit at large numbers of observations involves a definite danger that discrepancies due to correlations may be interpreted as systematic.

My own inclination, which is definitely a matter of personal impression of the economic factors involved, is that it would be worth while to consider separately the cases $K = 1, 1/3, 1/10$, and $1/30$. If $K > 1$, the evidence is in favour of q. If $1 > K > 1/3$, it is in favour of $\sim q$, but not sufficiently to repay special attention; $1/3 > K > 1/10$, $\sim q$ is worth adopting with reserve; $1/10 > K > 1/30$, less reserve is needed; and if $K < 1/30$, $\sim q$ may be definitely asserted.

5. It is often convenient for numerical purposes to round off or group data before analysis, and there has been some discussion on the method of allowance for the resulting increase of the standard error. Should the standard error of a mean, for instance, be taken from the grouped data, or should it be first corrected for grouping? Fisher (1936, p. 79) pronounces definitely in favour of the first alternative, but the second has occasionally been adopted. There are also cases, such as the discussion of gravity, where the data include a random error of observation, and this slightly inflates the variation of the residuals; but possible systematic effects are confined to the part not so explained, which is much larger. In a previous analysis (1936, p. 440) I obtained an intermediate result for this case. The uncorrected standard error appeared in the factor depending on the new parameters, but the outside factor was somewhat reduced. This test does not need much discussion, because it was a generalization of one already known to be seriously wrong when more than one degree of freedom arises, but the analysis contains a mathematical complication, which would arise even in a problem of estimation. The integrals used to obtain the result would in fact always diverge at the lower limit for the standard error. In the case where the standard error might be 0, convergence at the lower limit is saved by the exponential factor; but when the standard error includes a known observational part the exponential factor cannot tend to zero, and the integrals diverge. The analysis in the case of gravity would say that we can never dispose of the possibility that the whole variation is due to the known observational error; whereas in fact it is already disposed of by the comparison of observations in different places with the differences between observations repeated at the same place. If a known random error is introduced by grouping, its range is finite and this possibility is excluded by the distribution of the observations before grouping; even if some device introduces a normally distributed error, the possibility that there is no other variation is

similarly excluded. In fact the analysis used sacrificed an important piece of information; but since I did not notice the divergence and confined my attention to the contributions from the neighbourhood of the maximum likelihood solution, this information was restored, without my noticing that it had ever disappeared.

It appears from general considerations that Fisher's recommendation is nearly right. If we take the approximate form, for one parameter,

$$K = \frac{m}{\sqrt{(2\pi)}\,\sigma_\alpha} \exp\left(-\frac{\alpha^2}{2\sigma^2_\alpha}\right),$$

and consider the argument leading up to it, it is clear that σ_α is the standard error of the estimate as actually obtained, and therefore includes the additional errors. m, the permitted range of a, no longer reaches the whole $2s$, where s^2 is the expectation of the outstanding variation, since the known part s'^2 is not due to a systematic variation. The only change needed from the case where the range of variation is initially completely unknown is that K should be multiplied by the estimate of $(1-s'^2/s^2)^{\frac{1}{2}}$. Further, since the permitted range in the corrected test for several degrees of freedom arises only to the first power, the same correction is needed. But it would be unimportant unless s' was very near s. In the case of grouping or a superposed normal error, this would mean that the additional error accounted for most of the variation; and the appropriate comment would be that we should consider the data as they stood originally. If it should happen in some analogue of the gravity problem, an accurate determination of s' would be so important that it would be desirable to treat it also as originally unknown and assemble all the data relevant to it, and not reject the possibility that the current ones may lead to a revision of it. But then we are back to the case where the whole variation is treated as initially unknown, and the ordinary test will apply.

6. As many of the tests that I have given in previous papers have had to be revised to take account of the condition that the parameters accepted as significant on the null hypothesis must have exact analogues in the statement of the contrary one, or for other reasons, it is desirable to give here a list of the tests and of the places where they are corrected:

1935, pp. 203–5. Comparison of two samples (there called contingency). Approximately correct if $x+y <$ any of $x+x'$, $y+y'$, $x'+y'$; improved discussion in 1937 b.

  pp. 206–7. Measurement when the standard errors are known. pp. 211–13. Measurement when the standard errors are previously unknown. Revised in

the present paper; but relevant only when the permitted range is already indicated as much less than the total variation, and this is treated in 1938*a*, p. 178.

pp. 213–17. Test for a difference between a correlation coefficient and zero. Correct.

pp. 217–21. Periodicity. Superseded by 1938*a*, pp. 173–9.

1936, pp. 427–32. General contingency and multiple sampling. Superseded by 1937*b* and the discussion of selection in 1938*a*.

pp. 432–7. Representation of a set of measures by assigned functions. Superseded by 1938*a*, pp. 173–9.

p. 440. Ditto, where part of the variation is known to be random. Superseded by § 5 of the present paper.

p. 440. Example on test of bias in dice. Correct.

p. 441. Test of randomness in the occurrence of earthquakes in widely separated regions. Approximately correct.

p. 445. Test of the anomalous movement of the plane of the orbit of Venus. Revised in 1938*a*, with a better test and more recent data. But the possibility that the apparent anomaly is due to non-independence of the errors remains untested.

1937*a*. Comparison of series of measures. Revised in the present paper. In the example at the end the allowance for selection would be better treated as suggested in 1938*a*, p. 164, but the main conclusions are correct.

1938*b*. Frequency of aftershocks of earthquakes. This was written before some papers that were published earlier. If I was doing the problem now I should determine the general law of decline, with allowance for a possible departure of the index from − 1, by the minimum χ^2 approximation (Jeffreys 1938*c*); I should also use a rather less drastic grouping in testing some of the periodicities suggested (Jeffreys 1937*c*, p. 313) and adapt the test of 1938*a*. But as the number of observations is such that my $K = 1$ comes beyond the 5 % point, and none of the results reached the latter, I do not think revision necessary.

SUMMARY

A test previously given for the significance of the difference of two means, when the standard errors are unequal, is revised to take account of the uncertainties of the standard errors and of a theoretical complication that

has given trouble in other tests. The case where the standard errors can be assumed equal is derived from an existing formula. Some incidental points are discussed and a list is given of tests that have been revised in later work.

REFERENCES

Bartlett, M. S. 1936 *Proc. Camb. Phil. Soc.* **32**, 560–6.
Daniels, H. E. 1938 *Proc. Camb. Phil. Soc.* (in the Press).
Fisher, R. A. 1935 *Ann. Eugen., Lond.*, **6**, 391–8.
— 1936 "Statistical Methods for Research Workers." Edinburgh: Oliver and Boyd.
Jeffreys, H. 1935 *Proc. Camb. Phil. Soc.* **31**, 203–22.
— 1936 *Proc. Camb. Phil. Soc.* **32**, 416–45.
— 1937 a *Proc. Camb. Phil. Soc.* **33**, 35–40.
— 1937 b *Proc. Roy. Soc.* A, **162**, 479–95.
— 1937 c *Proc. Roy. Soc.* A, **164**, 307–15.
— 1938 a *Proc. Roy. Soc.* A, **165**, 161–98.
— 1938 b *Beitr. Geophys.* **53**, 111–39.
— 1938 c *Proc. Camb. Phil. Soc.* **34**, 156–7.
Welch, B. L. 1937 *Biometrika*, **29**, 350–62.

On the absorption of light by crystals

By N. F. MOTT, F.R.S., *H. H. Wills Physical Laboratory, University of Bristol*

1. THEORY OF THE ABSORPTION OF LIGHT

The purpose of this paper is to discuss the absorption of light by non-metallic solids, and in particular the mechanism by which the energy of the light absorbed is converted into heat.

If one considers from the theoretical point of view the absorption spectrum of an insulating crystal, one finds that it consists of a series of sharp lines leading up to a series limit, to the short wave-length side of which true continuous absorption sets in (Peierls 1932; Mott 1938). In practice the lattice vibrations will broaden the lines to a greater or less extent. When a quantum of radiation is absorbed in the region of true continuous absorption, a free electron in the conduction band and a "positive hole" are formed with enough energy to move away from one another and to take part in a photo-current within the crystal. When, however, a quantum is absorbed in one of the absorption *lines*, the positive hole and electron formed do not have

enough energy to separate, but move in one another's field in a quantized state. An electron in a crystal moving in the field of a positive hole has been termed by Frenkel (1936) an "exciton".

When an exciton is formed by the absorption of a quantum of radiation, there are three things which can happen to it. These are:

(a) The electron and positive hole may separate, the necessary energy W being provided by the thermal agitation of the surrounding atoms. If (a) happens with appreciable probability, the crystal will show photo-conductivity for the wave-length concerned. We shall denote by Pdt the probability per time dt that the electron and hole separate, and shall assume that P varies with the temperature according to the law

$$P = \nu e^{-W/kT},$$

where ν is of the order of the atomic frequency, 10^{13} sec.$^{-1}$.

(b) The electron and positive hole may recombine, with the emission of radiation; we denote the probability that this occurs per time dt by Adt; A will be of the same order as for an atom, namely, about 10^8 sec.$^{-1}$, and will be approximately independent of temperature. If process (b) happens with appreciable probability, the crystal will show luminescence. The frequency of the re-emitted radiation will in general be less than that of the absorbed radiation, because, as pointed out by Frenkel (1936) and others, the atoms move into new positions of equilibrium after the absorption act, and some energy is dissipated as heat. This is discussed below.

(c) The electron and positive hole may recombine, giving up their energy in the form of heat. This process has been investigated from the theoretical point of view in a number of papers (Peierls 1932; Frenkel 1936). No estimate has, however, been made of the probability of this process and of its variation with temperature. We shall therefore give a discussion of this for halide crystals, following a scheme for the excited levels due to Seitz (1938).

When a halide crystal absorbs a quantum of radiation, the electron is removed from a halogen ion into an "orbit" in which it revolves round the "hole" so formed.*

Suppose now that either before or after the absorption act we displace the ion or atom of the halogen a distance d in any direction and plot in fig. 1 the energies of the normal and excited states of the crystal as a function of d. Clearly it will require more energy to displace the large halogen negative

* Various authors (de Boer 1935; Hilsch and Pohl 1931; von Hippel 1936) have assumed that the electron is removed onto a neighbouring metal ion; while this may be approximately correct for the alkali halides, it does not seem to be a good approximation for the silver salts, as we shall see below.

ion than the smaller halogen atom. The energy for the normal state will thus rise more steeply than for the excited state, as shown. It is possible that the curves cross, as in the diagram.

If now the electron returns directly from A to B, it must get rid of several electron volts energy and thus excite perhaps 100 quanta at once. This process has been discussed theoretically by Peierls (1932) who shows that it can occur, but only if there is very strong coupling between the electron and the lattice vibrations. We shall, then, tentatively assume that the electron will only jump from the excited to the normal state if thermal agitation
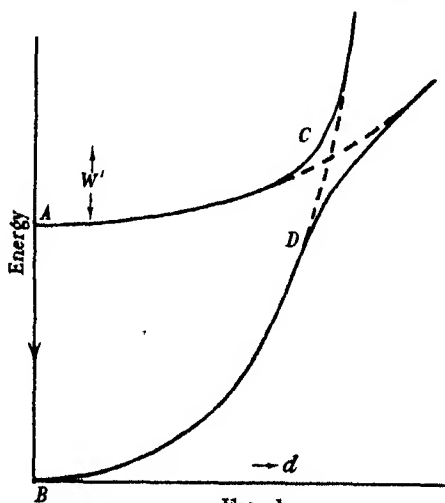
Fig. 1

brings the central atom to the point C, from which it can return to the normal electronic state at D by giving up only a few quanta of radiation. With this assumption, if $B\,dt$ is the probability per time dt that the electron returns to its ground state with the emission of heat, we should expect that

$$B = \nu' e^{-W'/kT},$$

where W' is the energy necessary to bring an electron from A to C, and ν' will be of the same order (but perhaps rather less than) the atomic frequency.

We may now write down the number η_e of free electrons and the number η_q of re-emitted quanta obtained per quantum absorbed. These are

$$\eta_e = P/(P+A+B)$$
$$= \left[1 + \frac{A}{\nu} e^{W/kT} + \frac{\nu'}{\nu} e^{(W-W')/kT} \right]^{-1},$$

and $\qquad \eta_q = A/(P+A+B).$

Consider first η_e, remembering that $\nu/A \sim 10^5$.

In fig. 2 η_e is plotted as a function of temperature for different values of the ratio W'/W (the value of ν'/ν is consistently taken to be $\frac{1}{2}$, so that for high temperatures η_e approaches the value $\frac{2}{3}$). If $W' > W$ there will be a sharp
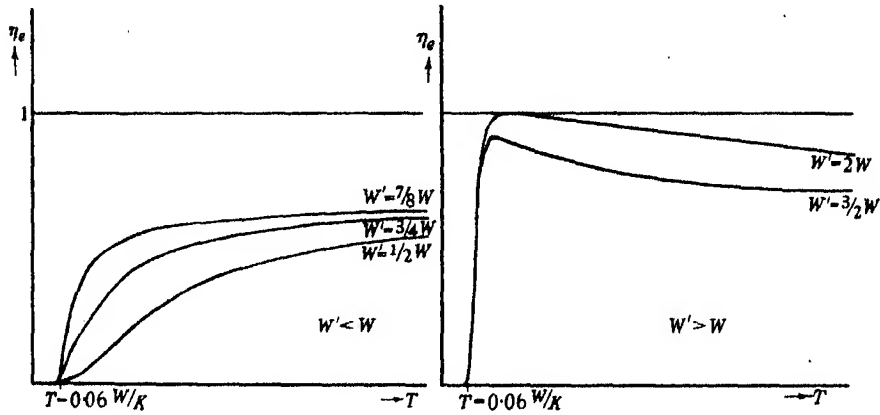
Fig. 2. Free electrons produced per absorbed quantum.
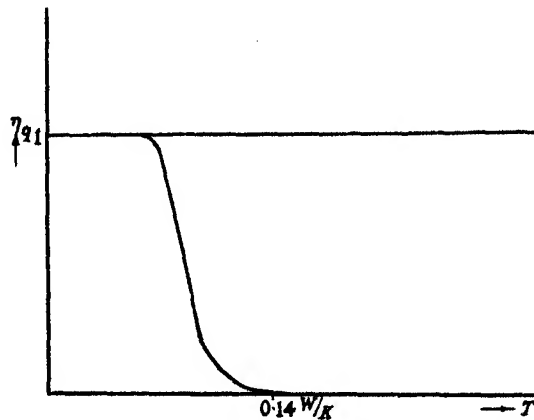
Fig. 3. Number of quanta re-emitted per quantum absorbed.

drop as the temperature is lowered; η_e reaches about 1 % of its original value for a temperature T_e, given by

$$\frac{A}{\nu} \exp\left(\frac{W}{kT_e}\right) \sim 100,$$

and thus by

$$T_e = W/k \log_e\left(\frac{\nu}{A} \times 100\right) \sim 0.06 \frac{W}{k}. \tag{1}$$

If $W > W'$, η_e will fall somewhat less sharply (the drop being caused here mainly by the term $(\nu'/\nu)\,e^{(W-W')/kT}$).

We now consider the number η_q of quanta reradiated per quantum absorbed

$$\eta_q = \left[1 + \frac{\nu}{A} e^{-W/kT} + \frac{\nu'}{A} e^{-W'/kT} \right]^{-1}.$$

η_q will have fallen to about 1 % of its low temperature value at one of the temperatures T_q or T_q' given by

$$\frac{\nu}{A} e^{-W/kT_q} \sim 100 \quad \text{and} \quad \frac{\nu'}{A} e^{-W'/kT'_q} \sim 100$$

and hence by $T_q \sim 0 \cdot 14\, W/k, \quad T_q' \sim 0 \cdot 14\, W'/k,$ (2)

whichever is the lower. The form of η_q is shown in fig. 3.

2. Comparison with experiment

(a) *Alkali-halides with F centres.* As shown by the work of Pohl and his co-workers on photoconductivity (Pohl 1937), the current per absorbed quantum in coloured alkali-halides drops sharply by a factor of the order of 1000 as the temperature is lowered below a critical temperature, $-150°$ C. in sodium chloride. Gurney and Mott (1938) have interpreted this on lines similar to those of this paper, but have taken A and B independent of T, so that

$$\eta_e = \left[1 + \frac{A+B}{\nu} e^{W/kT} \right]^{-1}.$$

They found fair agreement with experiment with

$$W = 0 \cdot 075\,\text{e-volt} \quad \text{and} \quad (A+B)/\nu = 0 \cdot 0033.$$

With the larger number of variables available in the present theory it will certainly be possible to obtain a fit, but one can no longer deduce a value for W, i.e. the work required to remove an electron from an excited F centre.

(b) *Pure alkali-halides.* No photoconductivity is observed, probably because the work W necessary to separate an "exciton" into an electron and positive hole is too large. Theoretical estimates of W are made below.

(c) *Silver halides.* The work of Lehfeldt (1935) has shown that even at liquid-air temperatures η_e is greater than $0 \cdot 5$. No measurements of the primary photoelectric current have been made at lower temperatures, but the *secondary* current shows, according to Lehfeldt, a very sharp drop at about $50°$ K. for AgCl and $25°$ K. for AgBr. The drop in the secondary current is believed to be due to a drop in the primary current.

We believe these sharp drops must correspond to the temperature T_c discussed above, and that the curves are of the type for which $W' > W$ shown in fig. 2. This conclusion is strengthened by the fact that these salts show luminescence at low temperatures.* We conclude that the energy W necessary to separate a positive hole and electron is (for AgBr)

$$W = 25° k/0.06$$

$$\sim 0.035 \text{ e-volt.}$$

This very low activation energy will be discussed in the next section.

The experimental result, that in silver halides the drop in the photo-electric current occurs at such low temperatures, has interesting consequences for the theory of the photographic latent image in halide emulsions. The primary action of the light is believed to be the production of free electrons; if this happens at low temperatures, they become trapped at surface levels, whence they are released when the emulsion is warmed up for development, the actual latent image formation then taking place. Berg and Mendelssohn (1937) find that emulsions still have considerable sensitivity at liquid hydrogen temperature; we should expect a very marked drop in the sensitivity as the temperature is lowered to that of liquid helium.

3. THE ACTIVATION ENERGY W

As we have already stated, for the alkali-halide crystals various authors have assumed that in the first excited state the electron is removed from a halogen atom on to a neighbouring metal atom. Such an assumption gives

$$W = e^2/\kappa r,$$

W being pictured as the work necessary to remove an electron from a metal atom adjacent to a neutral halogen atom, to a metal atom at infinity. κ is here the dielectric constant. This model gives energies of the order 0.5 e-volt for the *silver* halides, which is much too big, and we do not believe that it is necessarily correct.

An electron and positive hole in a crystal attract one another with a force

$$e^2/\kappa r^2,$$

when they are at a large distance r from one another. If then they are in a stationary state of principal quantum number n and high azimuthal

---

* I am grateful to Dr R. Hilsch for a private communication about this.

quantum number, the energy required to separate them must be given by the hydrogen-like formula

$$W = \frac{m_0 e^4}{2\hbar^2 \kappa^2 n^2},$$

where $m_0 = m_1 m_2/(m_1 + m_2)$ and m_1, m_2 are the "effective" masses of electron and positive hole. We shall assume m_0 equal to the mass m of a free electron, so that

$$W = 13 \cdot 5/n^2 \kappa^2 \text{ e-volts.} \tag{3}$$

For the first excited state we shall assume an effective quantum number n^* which we determine from experiment, as follows: The absorption spectra of the alkali-halides consist of a number of peaks, and it is possible to estimate with some certainty the interval W_0 between the first excited state and the series limit, and to compare the values with (3). We must, however, take for κ the value κ_0 for fields of frequencies large compared with the residual rays (so that $\sqrt{\kappa_0}$ is the refractive index), because by the Franck-Condon principle the absorption process takes place too quickly for the ions to move into new positions. The values obtained are as follows:

	NaCl	KCl	KBr
First absorption line (e-volts)	7·8	7·6	6·6
Series limit† (e-volts)	9·64	9·42	8·3
Difference, W_0(obs.) (e-volts)	1·8	1·8	1·7
κ_0	2·33	2·17	2·35
n^* (deduced from (3))	1·2	1·3	1·2

† Cf. Mott (1938).

We shall thus take $n^* = 1 \cdot 2$ as a mean value for the alkali halides, and shall assume this value to be valid for silver halides also, for which it has been possible to separate the various peaks in the absorption spectrum.

In working out the energy necessary to separate an electron and positive hole *thermally*, we must take κ to be the dielectric constant for static fields, since after the absorption act the ions surrounding the positive hole will move into new positions, cutting down its field from $e/\kappa_0 r^2$ to $e/\kappa r^2$. The calculated values of W are thus:

	NaCl	KCl	KBr	AgBr
Dielectric constant κ	5·3	4·3	4·4	12
W (e-volts)	0·34	0·58	0·49	0·06$_5$

Owing to the larger dielectric constant of AgBr we see that W has a much lower value for this salt than for the alkali halides; a slightly larger choice of n^* would bring it down to the value 0·035 e-volt which we deduced above.

In order that, for the alkali halides, no photoconductivity should be observed up to a temperature T, it is necessary by (1) that W should be greater than $\kappa T/0.06$. Taking T to be $300°$ K., this gives a value in the neighbourhood of 0.4 e-volt. We should thus expect, on the pure alkali halides illuminated on the long wave-length tail of the absorption band, that photoconductivity would be observed near or above room temperature. Experiments above room temperature do not seem to have been made.

SUMMARY

The mechanism of the absorption of light by solids is discussed from the theoretical point of view. The energy of a quantum of radiation can be converted into heat, re-emitted as fluorescent radiation, or used up in producing a photoelectric current within the solid; estimates are made of the dependence on temperature of the relative probabilities of these processes, which are compared with experiment.

REFERENCES

Berg and Mendelssohn 1937 *Proc. Phys. Soc.* **49** (extra part).
de Boer 1935 "Electron Emission and Absorption Phenomena." Cambridge.
Frenkel 1936 *Phys. Z. Sowjet.* **9**, 158.
Gurney and Mott 1938 *Trans. Faraday Soc.* **34**, 506.
Hilsch and Pohl 1931 *Z. Phys.* **68**, 721.
Lehfeldt 1935 *Nachr. Ges. Wiss. Göttingen*, No. 1, 170.
Mott 1938 *Trans. Faraday Soc.* **34**, 500.
Peierls 1932 *Ann. Phys., Lpz.*, **13**, 905.
Pohl 1937 *Proc. Phys. Soc.* **49** (extra part), 3.
Seitz 1938 *J. Chem. Phys.* **6**, 151.
von Hippel 1936 *Z. Phys.* **101**, 680.

The sorption of polar and non-polar gases by zeolites

By Richard M. Barrer

(Communicated by Eric K. Rideal, F.R.S.—Received 2 May 1938)

Details of zeolite structures have been obtained by X-ray methods, complete (W. H. Taylor and co-workers 1933–4) in the cases of natrolite, scolecite, mesolite, edingtonite and thomsonite, and partially complete in the cases of chabasite (Wyart 1931, 1933), analcite (Kastner 1931; Taylor 1930) and heulandite (Parsons 1932; Wyart 1933). Three types of zeolite framework have been recognized:

A. Three dimensional networks (chabasite, analcite).

B. Fibre structures (natrolite, scolecite, thomsonite, mesolite, edingtonite).

C. Plate-like structures (heulandite, and possibly mesolite).

These frameworks are anionic Si-O-Al networks, containing interstitial and exchangeable cations, and also neutral molecules of water, which are replaceable in some instances by molecules of ammonia, iodine, mercury or gases.

This paper describes an attempt to relate the sorptive properties towards permanent gases (Part I) and towards ammonia (Part II) to the structures and properties revealed by the X-ray method. While it is usual in sorption studies to focus attention upon the gases being sorbed, in these researches the influence of lattice structure upon the sorption processes has been especially considered. Samples of zeolites were chosen from each of the three classes listed above, and the sorption on them of the permanent gases helium, hydrogen, argon, and nitrogen and of the polar gas ammonia was measured. The former gases possess no dipoles; therefore in their sorption only van der Waals forces were encountered. This purely physical sorption revealed that van der Waals interactions could be multiplied* by the peculiar environment of the sorbed atom within the lattice. Such effects having been elucidated, the more complex interactions of the polar gas ammonia may be studied. Here powerful ion-dipole interactions occur, and

* De Boer and Custers (1934) calculated that van der Waals sorption heats in long cylindrical channels may as an optimum have six times the value of the sorption heat on a plane surface.

[392]

a variety of new and specific properties (Part II) appears. Heats of sorption of polar gases on zeolites have been reported of sufficient magnitude to suggest chemical reaction. The sequel will show however, that these heats could feasibly be comprised of ion-dipole and van der Waals interactions multiplied by the environment.

For certain zeolites of known detailed structure it is possible to calculate the potential of sorbed gases within the lattice, using the Kirkwood (1932) approximation to the dispersion forces, which has been found to give the best semi-empirical representations of sorption forces (e.g. Barrer 1937); the attempt to do this was carried out in this paper.

PART I. SORPTION OF PERMANENT GASES BY ZEOLITES

EXPERIMENTAL

The apparatus (Barrer and Rideal 1935) and methods of temperature measurement (Barrer 1937) have been described elsewhere. The zeolites used and their outgassing were as follows:

Chabasite ($Ca_2Al_4Si_8O_{24}.12H_2O$). Dehydration was carried out *in vacuo* at progressively increasing temperatures for several days. The temperature was finally raised to 480° C. for 1 day.

Analcite ($Na_{16}Al_{16}Si_{24}O_{96}.24H_2O$). Dehydration *in vacuo* at 330° C. for 3 days.

Natrolite ($Na_{16}Al_{16}Si_{24}O_{80}.16H_2O$). Dehydration as for analcite.

Scolecite ($Ca_8Al_{16}Si_{24}O_{80}.24H_2O$). Dehydration *in vacuo* at 260° C. for 2 days. After a number of experiments the scolecite was further dehydrated at 330° C. and experiments were repeated. The more severe treatment removed more water.

*Heulandite** ($(Na, K)_x Ca_y Al_{x+2y} Si_{36-(x+2y)} O_{72}.24H_2O$, where

$$6 < x + 2y < 10. \quad 4 < x + y < 6.$$

Dehydration *in vacuo* for 2 days at 130° C. After a number of experiments further evacuation at 330° C. removed more water, although the dehydration at 130° C. developed a large sorptive capacity for water.

It is seen that complete removal of water requires very prolonged outgassing at 330–350° C. Dehydration was only partial for heulandite and scolecite, for example, below these temperatures. The formulae given (Hey 1937) are those for the structure repeat as indicated by the X-ray method.

---

* The chemical composition of all zeolites is somewhat variable, but that for heulandite is very variable (Hey 1937).

The zeolites are prone to isomorphous replacements of the types $2Na^+ \rightarrow Ca^{++}$ and $(NaSi)^{5+} \rightarrow (CaAl)^{5+}$; so that variations in the structure repeat formulae may occur.

The permanent gases were often recovered after an experiment by condensing at 89° K. in a side limb containing dehydrated chabasite.

<div align="center">THE ISOTHERMS</div>

<div align="center">Zeolites with rigid frameworks</div>

X-ray measurements show that analcite and chabasite are rigid three-dimensional networks which do not collapse when interstitial water is removed* (Taylor 1934).

The sorption isotherms of hydrogen, nitrogen and argon on chabasite are given in figs. 1 a, b, and c. By extrapolating the isotherms plotted as $\log x/p$ against $\log x$ until the curves become vertical, the saturation values at liquid air temperatures may be observed. At 89° K. these values were:

$H_2 \sim 280$ c.c. at N.T.P. per g. of original chabasite.

Argon ~ 250 c.c. at N.T.P. per g. of original chabasite.

$N_2 \sim 164$ c.c. at N.T.P. per g. of original chabasite.

This weight of chabasite would contain 266 c.c. of water vapour. Thus at 89° K. and at saturation of sorption one may write for the unit cell

$$Ca_2Al_4Si_8O_{24} + 12(H_2 \text{ or } A), \quad \text{and} \quad Ca_2Al_4Si_8O_{24} + 7 \cdot 5 N_2.$$
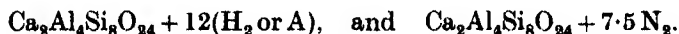
Penetration of the lattice can be as complete for these gases as for water and ammonia. The peculiar diminution in the saturation value for nitrogen has been observed before (Rabinowitsch and Wood 1936), but the saturation value is more than one-half that for hydrogen, water, and argon, so that nitrogen occupies less than two† of the chains of cells which may be supposed to compose the sorption channels. There is no reason why N_2, H_2 and A, without dipoles, should be strongly anchored in any cell; simply nitrogen with the greatest diameter, is least sorbed—less of it fills the sorption volume.

When expressed as the $\log x/p$-$\log x$ curves of fig. 1 a (for hydrogen) the isothermals on chabasite show a point of inflexion occurring at an x-value of ca. 90 c.c./3·98 g. This may indicate that all the available spaces in the chabasite skeleton are not similar, and that the resultant isotherm is

---

* A certain amount of shrinkage in analcite is however suggested by density measurements (Friedel 1896).

† Cf. Hey (1935), who allocates two cells to each nitrogen molecule.
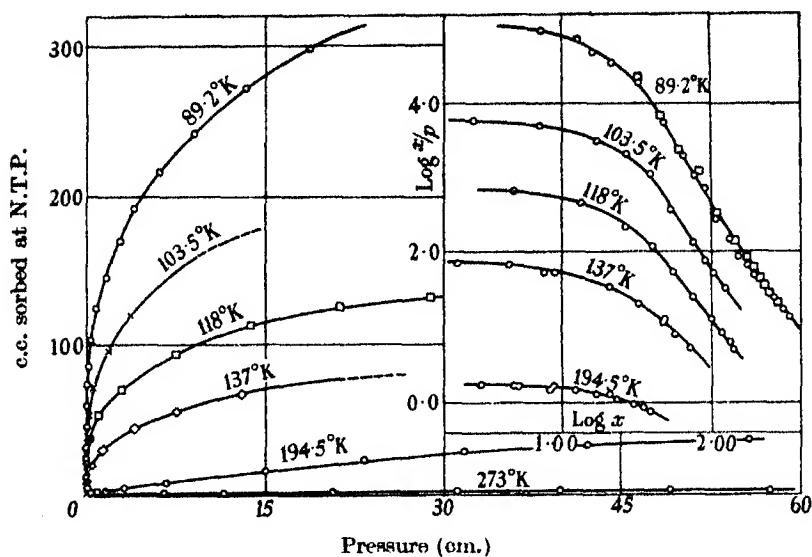
FIG. 1 a. H₂ on chabazite.
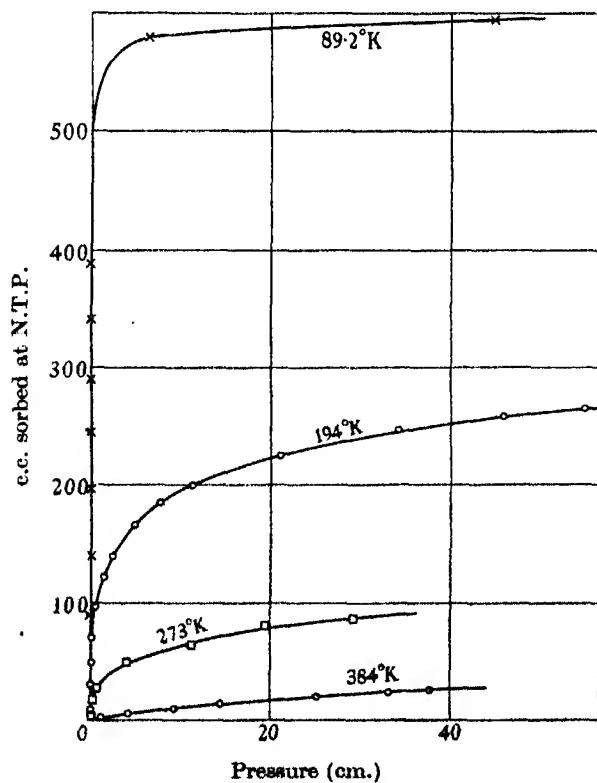
FIG. 1 b. N₂ on chabazite.

composed of two superposed isotherms. One should therefore write the sorption complex as

$$Ca_2Al_4Si_8O_{24} + (12-x)\,H_2, A + x\,H_2, A,$$
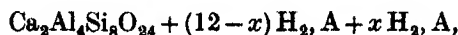
where x denotes the number of spaces of the second type per structure repeat. The point of inflexion may be a result of, or superposed upon, the trend in the sorption heats as a function of gas charge discussed later.
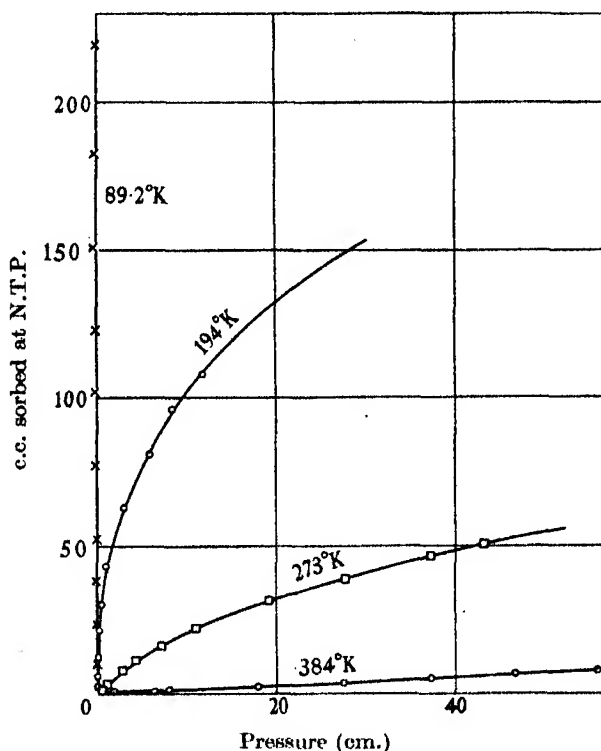
FIG. 1 c. Argon on chabazite.

The isothermals for hydrogen, nitrogen, argon and helium upon analcite outgassed at 330° C. are given in figs. 2 a and b. Those for helium obey Henry's law down to 65° K. None of the isothermals when plotted as $\log x/p$ against $\log x$ give points of inflexion, and although it will be shown later that the sorption heats decrease somewhat as the charge increases, this decrease is not great, and one can say that the available spaces in analcite are nearly all of one kind. When one tests the Langmuir isotherm by plotting p/x against p, both for analcite and chabasite instead of straight lines, one gets curves with
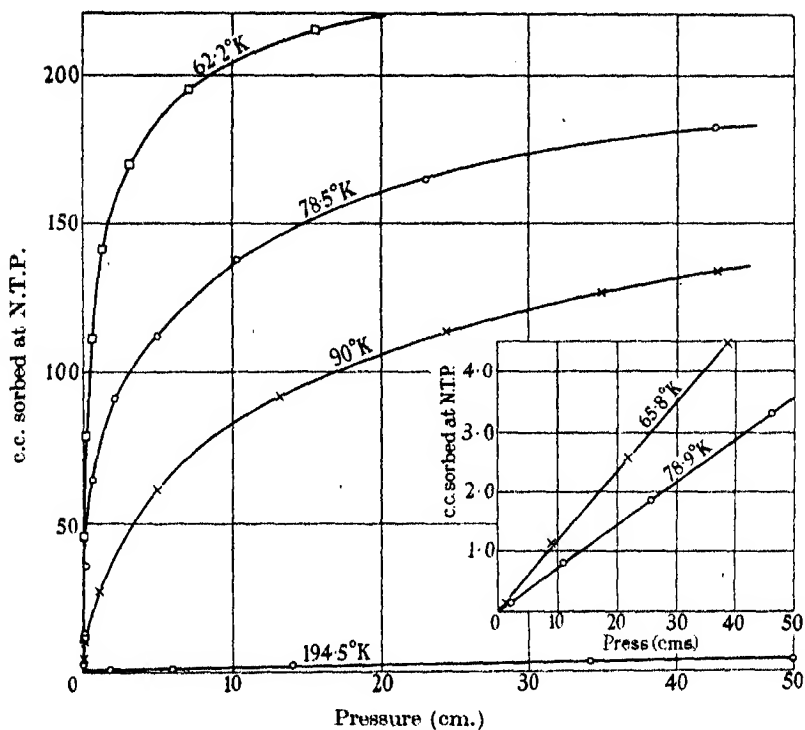
FIG. 2 a. H_2 on analcite (inset He on analcite).
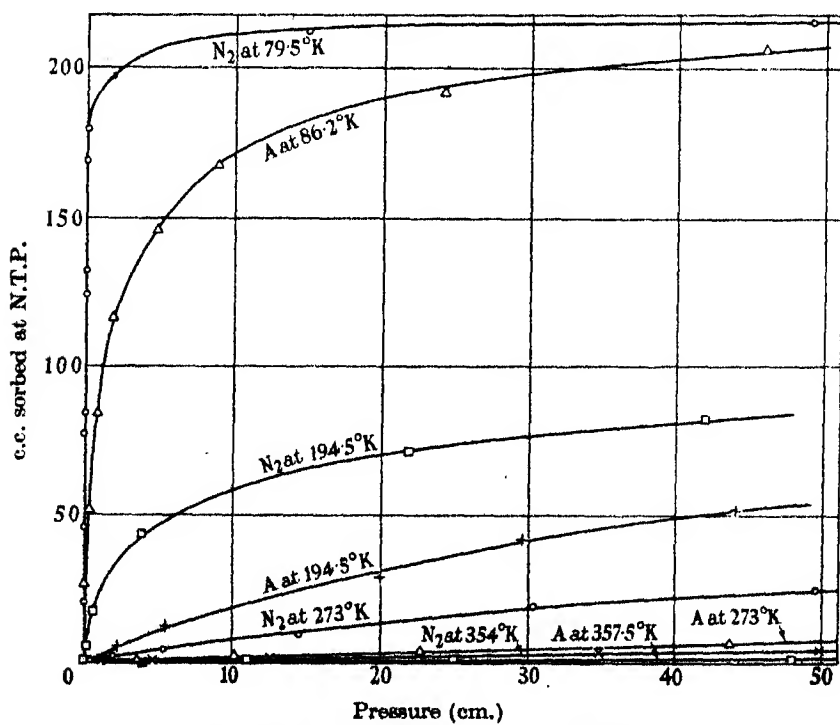
FIG. 2 b. Nitrogen and argon on analcite.

the maximum curvature near the origin, and an approach to linearity for larger amounts sorbed. This behaviour was the same as that observed in sorption by Acheson graphite (Barrer 1937) and as for the systems there described is to be associated with the trend in the sorption heat with the gas charge.

The amounts sorbed by analcite (*ca.* 230 c.c./7·86 g.) fall far short of the theoretical value of 1260 c.c. at N.T.P. corresponding to the formula $Na_{16}Al_{16}Si_{24}O_{80}.24H_2O$. Further outgassing at 330° C. failed to give a sorption saturation for ammonia approaching the theoretical (Part II). Thus a partial collapse followed prolonged outgassing at 330° C. The variation in the apparent saturation of sorption is given in Table I, which should be compared with Table I, Part II:

TABLE I. THE APPARENT SATURATION OF SORPTION AT
DIFFERENT TEMPERATURES

Zeolite	Gas	Temp. ° K.	Apparent saturation (c.c. at N.T.P./g.)
Chabasite	N_2	89·2	164·0
		194·5	75·2
	N_2*	83·0	170·0
		193·0	90·0
Analcite	N_2	79·5	30·3
		194·5	15·1
	H_2	62·2	33·0
		78·5	27·7
		90·0	23·7

* Data of Rabinowitsch and Wood (1936). A similar ratio was found for Ca, Sr, Ba, Na, K, and Cd chabasites with slight variations in the absolute values.

The apparent saturation values fall off nearly linearly with temperature, so that one might say that the co-volume of each sorbed molecule in the lattices increases linearly with temperature. This could be a property of a gaseous system contained within a constant sorption volume. It argues against finite chemical associations of the sorbed molecules with the lattice, since the composition should not then alter with temperature. Similar variations in the sorption saturation were observed in Part II for ammonia-zeolite systems wherein no new phase was formed by sorption.

Zeolites with fibrous structures

Natrolite, scolecite, mesolite, thomsonite and edingtonite all consist of similar chains of Si-O-Al tetrahedra cross-linked in different ways (Taylor

1934). The interstitial cations can of course be different, as may the quantities of interstitial water. Natrolite and scolecite with the cations Na^+ and Ca^{++} and different amounts of interstitial water can be regarded as typical of the series.

The thermal treatments given were less severe than that given to chabasite, which had showed no signs of collapse. The isothermals for argon and hydrogen on natrolite and scolecite show that sorption was confined to the external surfaces only. Under no circumstances could these zeolites be induced to sorb any but small amounts of gas (several c.c. on 8 g.). Natrolite sorbed more than scolecite and more vigorously.

Thus the evidence indicates that the modification of the water-bearing channels on dehydration was enough to exclude the permanent gases. X-radiograms of the scolecite samples used when compared with hydrous crystalline scolecite showed a blurring out of some lines, but that the actual dimensions of the unit cell had not altered much.* The same result had been earlier observed for natrolite (Hey 1932). Thus either the original channels were too small to admit argon, or a reorganization occurred about the channels which filled in the water-bearing channel without appreciably altering the lattice dimensions. The problem was attacked from a theoretical viewpoint by calculating the absorption potential in a natrolite lattice, the large positive heats of sorption there calculated indicating ample space in the original channels. The removal of ammonia from a natrolite-ammonia was then carried out by evacuation at 125° C., in the hope that at this temperature the evacuated crystal would be robust enough to retain its pore structure. An argon isotherm at 80·5° K. showed however that apart from capillary condensation at higher gas pressures the sorptive capacity was not altered. The data given in Part II indicate that penetration of most fibrous zeolites by ammonia or water involves formation of new phases; whenever this occurs, permanent gases unless they too yield new phases must be excluded, since, as pointed out in Part II, phase formation occurs with reorganization within the unit cell, the capacity to cause which is limited to gases showing a powerful affinity for the lattices (ammonia and water). In the case of scolecite-ammonia however, even ammonia failed to enter the dehydrated lattice, and behaved like the permanent gases (Part II). Like the other permanent gases helium was also unable to penetrate the dehydrated lattices of natrolite and scolecite, in spite of its small diameter (2·5 A).

---

* I am indebted to Drs Hey and Bannister for examination of the scolecite by the X-ray method.

Zeolites with laminar structure

Heulandite and probably stilbite are members of this class. The anionic laminae are thought to be bound together by cations, and between them also is the interlaminal water, some of which is removed very easily (Taylor 1934). Dehydration is accompanied by a great shrinkage in a direction normal to the planes of the laminae (Wyart 1930). In an attempt to avoid too great a shrinkage, dehydration of heulandite was at first carried out at 130° C. for 2 days; but argon and nitrogen sorption showed that for heulandite the interlaminar spaces are not available to permanent gases and that the sorptive capacity was about 1 c.c. at N.T.P. per 7·35 g.

More vigorous heating, for 2 days at 330° C., removed more water. The sorptive capacity after this treatment was unaltered.

To summarize, the sorptive capacity of dehydrated zeolites for non-polar gases depends upon the structure of the lattice. Three-dimensional networks are powerful adsorbents, sometimes taking up a quantity of permanent gas equivalent to the water of hydration. The fibrous and platy zeolites, on the other hand, do not after outgassing admit permanent gases into the lattice. Thus the sorptive properties could be used to determine whether an unknown zeolite was three-dimensional, or fibrous or platy, that is, to measure the stability of the crystal.

The heats of sorption

From the isotherms at various temperatures the Clapeyron-Clausius equation in the form

$$\log\left(\frac{p_{T_1}}{p_{T_2}}\right)_x = \frac{\Delta H}{R}\left[\frac{1}{T_2} - \frac{1}{T_1}\right],$$

(where ΔH is the heat of sorption including the heat of compression, RT cal./mol.) the sorption heats of the permanent gases were calculated.[*] Fig. 3 and Table II give the results of these calculations for chabasite, analcite, and for scolecite and natrolite respectively. In general, the heats diminish as the amount sorbed increases, but in all cases the heat approaches asymptotically a final value, and the best curve through the experimental points is a smooth one. In chabasite the sorption heats assume the high initial values for nitrogen, argon and hydrogen of 8800 cal., 6000 cal., and 4000 cal./mol. respectively. This serves to show how a suitable environment can increase van der Waals interactions, and suggests that the heats of 30,000—20,000 cal. (Part II) obtained with water and ammonia upon some

---

[*] Since the apparent saturation value varies with temperature, one may not use the Clapeyron equation at too large a value of the amount sorbed.

zeolites are logically explained as ion-dipole interactions added to van der Waals interactions, both multiplied by the environment, rather than as specific chemical interactions.

Tables were constructed for chabasite giving ΔH as a function of the amount sorbed and of temperature, which show that ΔH does not depend
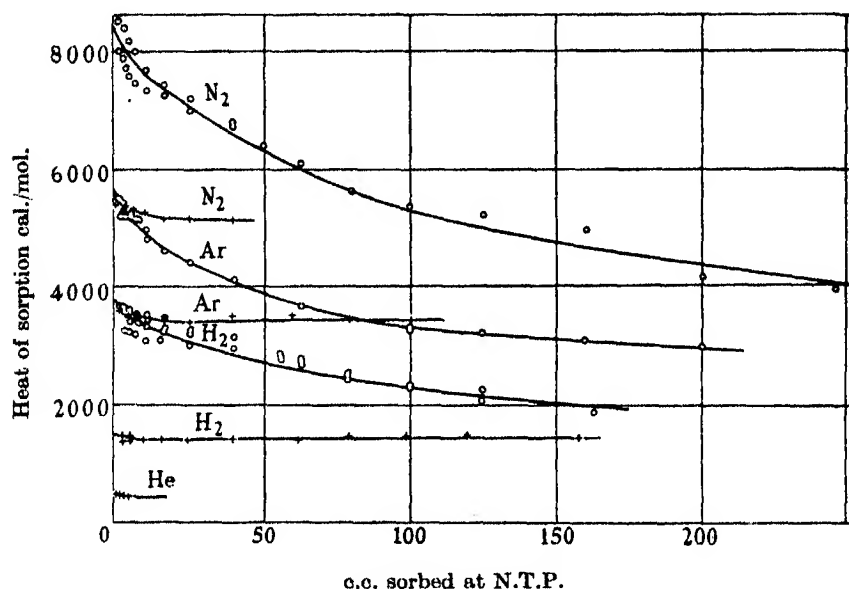
FIG. 3. Heats of sorption of N_2, H_2, He, Ar (without heats of compression). ○ Chabazite (3·98 g.).   + Analcite (7·86 g.).

TABLE II. HEATS OF SORPTION ON NATROLITE AND SCOLECITE

Amount sorbed (c.c./N.T.P. per 4·75 g. natrolite and per 6·25 g. scolecite)	Heats (cal./mol. including heat of compression)		
	Ar-natrolite	Ar-scolecite	H_2-scolecite
0·010	—	1900	1200
0·025	—	1840	1090
0·040	4400	1760	1040
0·100	—	—	900
0·150	4200	—	780
0·250	4100	—	—
0·400	—	—	590
0·600	3800	—	560
1·000	3800	—	540

upon the temperature. Thus for hydrogen, with 1 c.c. sorbed on 1 g. of the original chabasite one has:

Temperature range °K.	237–194	194–137·5	137·5–118·0	118·0–103·9
ΔH (cal./mol.)	3970	3580	3830	3710

With analcite similar tables showed that ΔH was not dependent upon temperature, for hydrogen, nitrogen and argon. The same result was found for these gases sorbed by Acheson graphite (Barrer 1937). van Itterbeek and van Dingenen (1937) in contrast considered their results to show a variation in ΔH with temperature. However, the variations appear to be random, rather than to show definite trends.

The following points emerge from a consideration of sorption heats on these various sorbents (zeolites and graphite):

(1) The initial and final sorption heats are summarized in the following table. (Table III.)

The most constant heats are those in the analcite lattice. Acheson graphite showed the most rapid diminution in heat with amount sorbed, and most rapid approach to the final value (Barrer 1937).

TABLE III

Adsorbent	Gas	Cal./mol. initial heat	Cal./mol. apparent limiting heat
Chabasite	N_2	8800	4400
	A	6000	2900
	H_2	4000	1700
Analcite	N_2	5500	5000
	A	3700	3300
	H_2	1500	1400
	He	500	——
Graphite	N_2	4600	2500
	A	4100	2400
	H_2	2000	1100
Natrolite	A	4600	3400
Scolecite	A	2000	——
	H_2	1250	500

(2) The relative magnitudes of the heats for argon and nitrogen vary in a regular way: the heat of sublimation of argon (2030 cal./g. atom) is greater than that of nitrogen (1860 cal./g. mol.); the sorption heat on the graphite surface is a little less for argon than for nitrogen; and the heat of sorption inside a chabasite lattice is much greater for nitrogen than for argon. The

reasons for this are revealed on calculating the potential in a zeolite lattice (as is done in the next section). The diameters of nitrogen and argon are 4·08 and 3·83 A. respectively; and the size of the hole needed to produce a large heat for nitrogen differs from that needed for argon. That is, the effects are due to molecular diameters rather than to polarizabilities, within chabasite.

The shape of the curves in fig. 3 agrees with that of similar curves plotted from the data of Lamb and Ohl (1935). One observes their very great initial value of ΔH for C_2H_4 of 15,600 cal./mol.

Calculated potentials in the natrolite lattice

Although natrolite, owing to reorganization of ions surrounding channels on dehydration, fails to absorb much gas, the detailed structure of its unit cell is known. Thus if permanent gases were supposed to replace water molecules in the lattice the potential of the permanent gases could be worked out employing an appropriate force law, and using Kirkwood's approximation to the dispersion forces. The absolute potentials for various degrees of shrinkage may be calculated and compared with heats commonly found in zeolites, and the sorption heats of different gases compared at various stages of collapse.

In the calculations the force law

$$E = A\left(\frac{1}{r^6} - \frac{1}{2}r_0^6\frac{1}{r^{12}}\right) \tag{1}$$

was used. The value taken for r_0, the equilibrium distance between a sorbed molecule and a lattice ion, was $\frac{1}{2}(d_1 + d_2)$, where d_1 and d_2 are the diameters of molecule and ion respectively. A was given by Kirkwood's expression

$$A = 6mc^2\chi_1\chi_2\bigg/\left(\frac{\chi_1}{\alpha_1} + \frac{\chi_2}{\alpha_2}\right). \tag{2}$$

Here c = the velocity of light, and m = the mass of the electron, α_1, χ_1 = the polarizability and magnetic susceptibility of the molecule, and α_2, χ_2 = the polarizability and magnetic susceptibility of the ion.

The total potential for all ions of a given kind in the lattice is then

$$E_i = \Sigma E = a\Sigma\left[\frac{1}{r^6} - \frac{1}{2}r_0^6\frac{1}{r^{12}}\right], \tag{3}$$

while the total potential for all kinds of ion is

$$E_{\text{total}} = \Sigma E_i.$$

In making the calculations the co-ordinates of every lattice ion were referred to a sorbed molecule which had replaced a water molecule as origin. The values of α, χ and d are collected in the following table (Table IV), and were obtained from papers by Pauling (1927) and Muller (1936).

TABLE IV

Atom or ion	Diameter $\times 10^8$ (cm.)	$-\alpha \times 10^{24}$	$-\chi \times 10^{30}$
He	2·54	0·2050	3·13
Ne	3·10	0·3930	11·80
Ar	3·83	1·6230	30·80
CH$_4$	4·18	2·4900	27·30
O^{--}	2·62	3·9000	20·80
Na$^+$	1·96	0·1800	6·95
Al^{+++}	1·14	0·0540	4·12
Si^{++++}	0·78	0·0331	3·46
Ca^{++}	2·12	0·4400	21·95

In Table V are given the constants a and r_0 determined from equation (2) and Table IV.

TABLE V

Gas	Ion	$a \times 10^{44}$ cal./mol.-ion pair	$r_0 \times 10^8$ (cm.)
He	Na$^+$	2·850	2·25
	O^{--}	22·250	2·58
	Al^{+++}	0·990	1·94
	Si^{++++}	0·717	1·66
	He	2·260	2·54
Ne	Na$^+$	8·540	2·53
	O^{--}	48·800	2·86
	Al^{+++}	3·220	2·12
	Si^{++++}	2·120	1·94
	Ne	16·330	3·10
Ar	Na$^+$	26·200	2·90
	O^{--}	185·500	3·22
	Al^{+++}	11·400	2·49
	Si^{++++}	7·040	2·30
	Ca^{++}	9·180	2·99
	Ar	176·000	3·83
CH$_4$	Na$^+$	27·000	3·02
	O^{--}	237·000	3·40
	Al^{+++}	9·080	2·66
	Si^{++++}	5·860	2·48
	CH$_4$	239·200	4·18

In making calculations upon the potentials in natrolite lattices, ions whose centres fell within a radius of 6·9 A of the central water molecule were considered. Within this surface were contained fifty-eight ion centres. Contributions to the potential of ions falling outside this sphere amount to not more than a few per cent. It is not possible without detailed X-ray analysis to indicate the new positions of the ions after lattice change

% contraction in water-bearing channel of a dehydrated natrolite
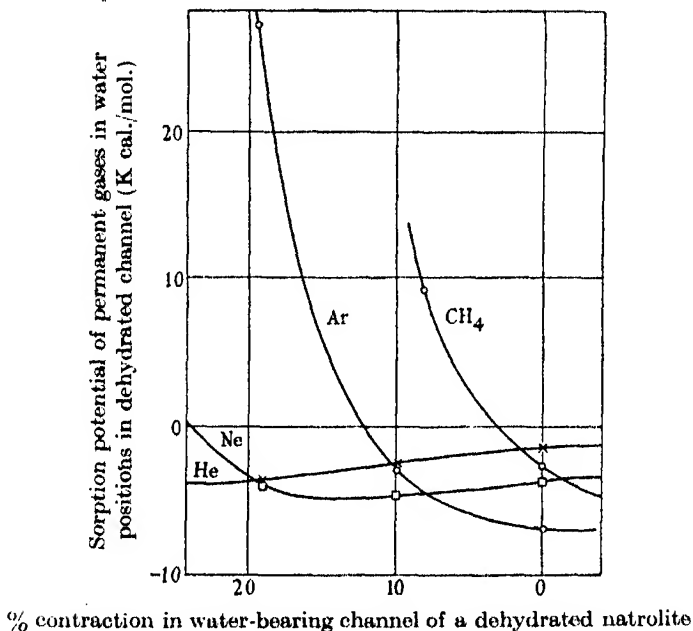
FIG. 4

following dehydration. As an approximation it was assumed that the c co-ordinates (parallel to the chains of Si-O-Al tetrahedra) did not alter appreciably but that up to 6·9 A from the centre of the original water molecule, the a and b co-ordinates altered by a fixed amount. The degree of collapse into the channels does not indicate that the cell constants will alter in the same ratios. There need be no simple connexion between the extent of channel collapse and of change in cell constants. Hey and Bannister's measurements on meta natrolite, the dehydrated form of natrolite, indicated little change in the a and b co-ordinates. Heulandite, however, shows a profound change in one co-ordinate on dehydration.

The results of calculation appear in fig. 4. They suggest that violent changes have occurred in the channels, since otherwise large positive heats would be found, whereas instead all the inert gases were excluded from these

26·2

lattices. The magnitude of the calculated heats in uncollapsed channels is of the same order as those experimentally observed in chabasite and analcite, where the channels have not collapsed.

SUMMARY

The sorption properties of argon, hydrogen, nitrogen and helium by five zeolites of known or approximately known crystal structure and chemical composition indicated well-defined sorption characteristics. Zeolites consisting of three-dimensional networks acted as powerful adsorbents (chabasite and analcite), chabasite taking up as much permanent gas (argon and hydrogen) as water of crystallization. Nitrogen was sorbed to a little more than half this extent by chabasite; and all three gases to about 25 % of the theoretical (based on the water content) with analcite. The fibrous zeolites natrolite and scolecite gave only slight surface sorption, as did the platy zeolite heulandite.

The sorption heats within chabasite and analcite, and on the surfaces of the other zeolites, diminished asymptotically from an initial high value towards a lower value. The initial sorption heats, and apparent limiting heats were compared with each other and with sorption heats on graphite. The initial sorption heat of 8800 cal./g. mol. for nitrogen in chabasite is the largest recorded van der Waals interaction energy for this molecule. Chabasite was energetically a stronger sorbent than analcite.

The saturation values obtained by extrapolation of isothermals diminish linearly with increasing temperature.

While X-ray diagrams show that the unit cell dimensions do not vary much on dehydration, a calculation of the potential of permanent gases within natrolite showed that if no reorganization of ions around the water-bearing channels occurred, these gases should be strongly sorbed. Decreases in effective diameter of these channels of 20 % or more were necessary before permanent gases would be excluded.

PART II. SORPTION OF AMMONIA BY ZEOLITES

The sorption of ammonia was measured for the five zeolites—chabasite, analcite, natrolite, scolecite, and heulandite. Sorption data exist for ammonia analcite and chabasite systems (Tiselius 1935; Rabinowitsch 1932); while on chabasite Evans (1931) has made a study of the sorption heats. Little could be found concerning sorption equilibria for ammonia upon the fibrous and the platy zeolites.

THE ISOTHERMALS

The sorptive properties of the fibrous and platy zeolites were dependent upon the thermal treatment given the crystals. The sorptive properties of chabasite and analcite, however, were not impaired by relatively severe thermal treatments which were carried out respectively at temperatures of up to 500 and 350° C.

Plotted in the usual way (x/m against p, where x/m denotes the amount sorbed per unit mass and p is the equilibrium pressure) the isothermals, as illustrated in figs. 5 a–d, show no peculiarities for chabasite or analcite; but there is evidence of an unusual behaviour in heulandite, while natrolite exhibits a threshold pressure and only above this pressure was the ammonia sorbed copiously. When, however, the ·isothermals are plotted as curves $\log (x/p)$ against $\log x$, their behaviour indicates a steady gradation. In the $\log (x/p)$ against $\log x$ curves, a section horizontal to the isothermal indicates that Henry's law is obeyed; a vertical section, that sorption saturation has been reached; and a section of slope $+1$ denotes an invariant system. These $\log (x/p)$ against $\log x$ isothermals are given in figs. 5 a–d. The chabasite isothermals show a normal steady trend towards saturation; and the analcite isothermals show in every case a point of inflexion, but no well-defined peculiarity. Thus the two zeolites in the form of three-dimensional networks sorb ammonia copiously without ammoniate formation. The platy zeolite heulandite, when carefully outgassed at low temperatures, showed a much more pronounced step in the isothermal, but could not be said to have formed any ammoniate. Natrolite, however, gave the remarkable set of curves of fig. 5 d, indicating for a considerable ammonia uptake that the system natrolite-ammonia was nearly invariant, which means in terms of the phase rule that a new phase, an ammoniate, has appeared, the system becoming comparable to the system $CaO + CO_2 \rightleftharpoons CaCO_3$ at constant temperature. The sorption kinetics provided further information to the same effect. Scolecite, on the other hand, failed to sorb ammonia save on its external surface. Thus the zeolites studied show a great diversity of behaviour.

Since the zeolites often prove sensitive to thermal treatment a brief account of the conditions under which the isothermals of figs. 5 a–d were obtained may be given. The chabasite remained a good sorbent of ammonia after periods of ignition from 400 to 500° C., provided that the thermal treatment was not too prolonged. Analcite could be maintained for 12 hr. periods at 350° C. without marked diminution in its sorptive property. Natrolite underwent alterations on heating to 330° C. Scolecite changed so
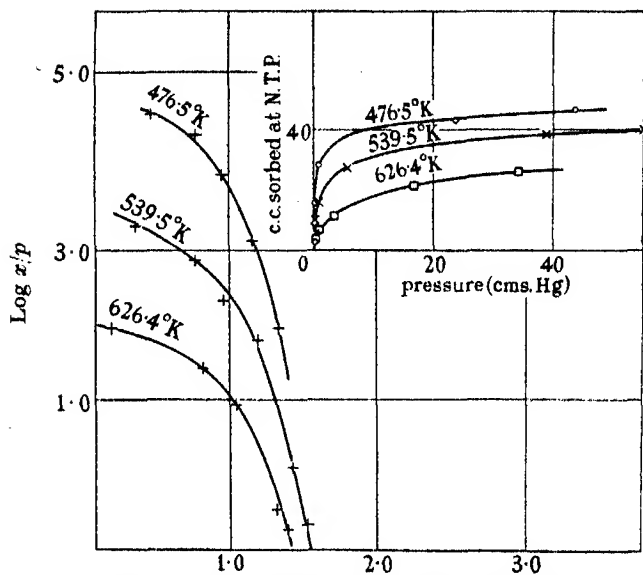
FIG. 5 *a*, NH₃ on chabasite (inset NH₃ on chabasite).
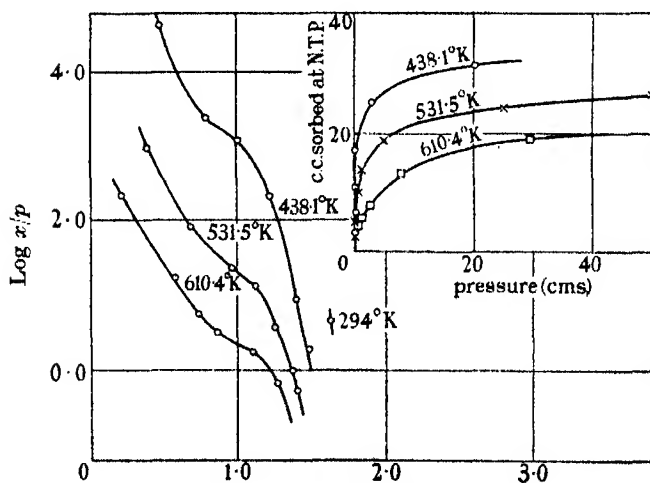
FIG. 5 *b*. NH₃ on analcite.
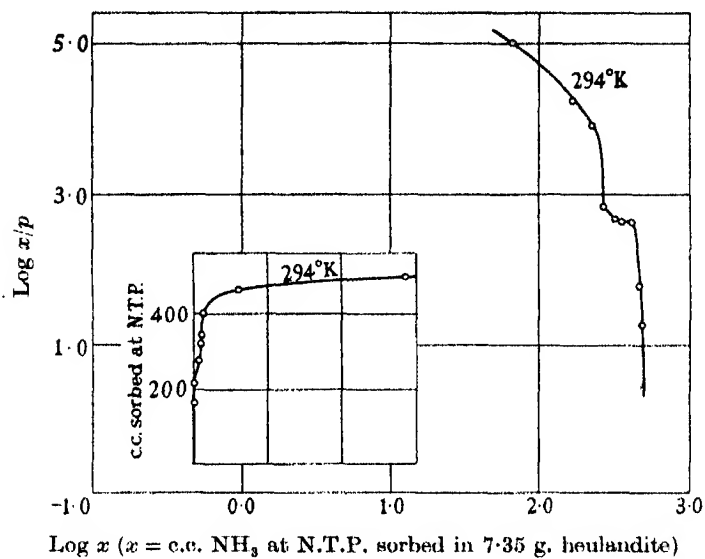
Fig. 5c. NH$_3$ on heulandite.
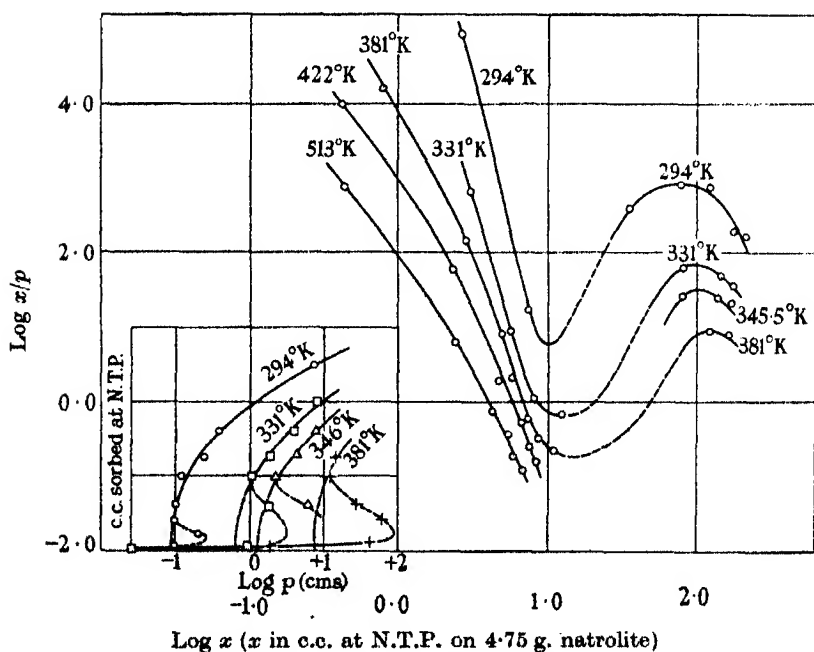
Fig. 5d. NH$_3$ on natrolite (inset x-log p isothermals).

completely at 330° C. that ammonia subsequently failed to enter the lattice. On heulandite outgassed at 130° C. ammonia sorption was copious and relatively rapid; after ignition at 330° C. sorption was extremely slow even at 126° C., so that equilibria could not be observed.

The saturation maxima in sorption for NH_3-chabasite and NH_3-analcite systems at 21° C. were respectively 170 c.c. at N.T.P./g. and 45 c.c. at N.T.P./ g. The apparent sorption maxima diminished with rising temperature. This phenomenon has been observed on charcoal (McBain and Britton 1930), graphite (Barrer 1937) and zeolites (Part I this paper; Rabinowitsch and Wood 1936); and seems to be of general occurrence in sorption (Langmuir and Sweetser 1918; Wilkins 1938). For this reason the Clapeyron equation has not been applied in regions of sorption approaching saturation. The sorption maxima at 21° C. for ammonia fall short of the theoretical values of 264 c.c. at N.T.P./g. and of 160 c.c. at N.T.P./g. for chabasite and analcite respectively. Similar data for heulandite and natrolite are given in Table I. For the latter substance a long extrapolation is necessary. Since for natrolite an ammoniate is formed the saturation value for ammonia sorption should not depend upon temperature.

TABLE I. APPARENT SATURATION VALUES OF AMMONIA
IN ZEOLITES

Zeolite	Gas	Temp. ° K.	Apparent saturation and calculated theoretical maximum (c.c. at N.T.P./g.)
Chabasite	NH_3	—	264·0 (theoretical)
		294·0	~170·0
		490·5	~126·0
		552·8	~100·0
		637·5	~ 80·0
Analcite	NH_3	—	160·0 (theoretical)
		294·0	~ 45·0
		457·4	~ 36·0
		514·0	~ 32·0
		623·0	~ 28·5
Natrolite	NH_3	—	118·0 (theoretical)
		294·0	~110·0
Heulandite	NH_3	—	~185·0 (theoretical)
		294·0	~ 65·0 (some strongly held water still present)

The figures in Table I may be compared with the data in Part I (p. 398) for the saturation values of the permanent gases in chabasite at 89° K., where argon and hydrogen gave theoretical sorption, and nitrogen some 70 % of

the theoretical. Analcite with these gases still-falls, at 89° K., far short of the theoretical maximum. These effects may have their origin in overheating during the original outgassing, with resultant impaired sorptive capacity. In decreasing order of stability and increasing order of internal rearrangement, as judged by the sorptive properties towards ammonia and permanent gases, the zeolites used may be arranged in the order:

Chabasite,
Analcite,
Natrolite,
Heulandite,
Scolecite.
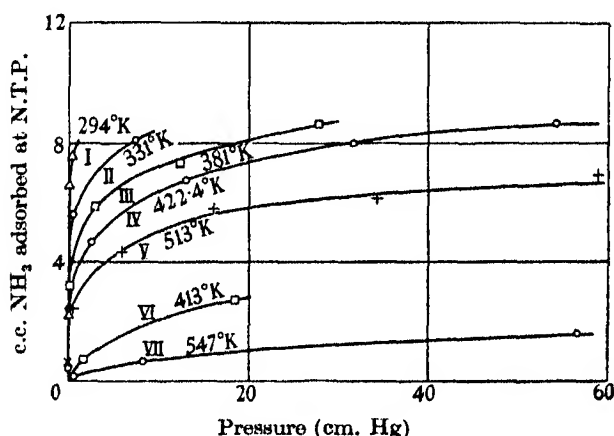
Fig. 6. Isotherms I—V: NH_3 adsorbed on natrolite (4·75 g.).
Isotherms VI and VII: NH_3 adsorbed on scolecite (7·85 g.).

A further point of interest from Table I is that the apparent saturation value for ammonia does not diminish exponentially with temperature, as recently reported by Wilkins (1938) for the permanent gases on platinum foil. The present result agrees with McBain and Britton's (1930) findings for permanent gases on charcoal and Rabinowitsch and Wood's (1936) finding for permanent gases on chabasite. From the data of Table I, and of Table I of Part I, the influence of temperature upon apparent saturation values appears nearly linear.

Surface sorption of ammonia on natrolite and scolecite

On these two lattices it was possible to study separately the sorption of ammonia upon the external surface of the adsorbents; for natrolite because

of the threshold pressures for ammoniate formation, and for scolecite because lattice penetration did not occur at all. In each case the amounts of ammonia thus taken up were comparable with the amounts of argon sorbed (Part I). Fig. 6 gives these isothermals for natrolite and scolecite.

Heats of sorption of ammonia by zeolites

Heats of sorption were calculated both for the surface sorption of ammonia by natrolite and for the absorption of ammonia inside the lattices of natrolite, chabasite and analcite. These sorption heats for natrolite-ammonia are given in the Tables II–IV. The sorption heats fall off very rapidly for surface sorption of ammonia, and much less rapidly for lattice penetration. Heats for adsorption depend upon the temperature; for ammoniate formation within the lattice they depend only slightly on the temperature. The data for NH_3-scolecite were not numerous enough to obtain heats for surface sorption accurately, but the heats are similar in magnitude to those on natrolite.

The sorption heats for chabasite-ammonia are given in Table III. As the extraordinary affinity of ammonia for the dehydrated lattice indicated, these heats are very large indeed. Since however there may be powerful ion-dipole interactions with ammonia inside the lattice, and since the van der Waals

TABLE II. SORPTION HEATS OF AMMONIA BY NATROLITE

Surface sorption (c.c. NH_3 at N.T.P./g. of original hydrous natrolite)	ΔH (cal./mol. NH_3) between temperature ranges		
	294–381° K.	381–422° K.	422–513° K.
0·084	—	—	12400
0·126	—	—	11600
0·210	—	16000	11400
0·333	—	13700	10700
0·527	15050	13000	10600
0·840	13000	11550	9200
1·260	10150	—	8000
1·680	8040	—	—

Lattice absorption (c.c. NH_3 at N.T.P./g. of original hydrous natrolite)	Mol. NH_3 per unit cell	ΔH (cal./mol. NH_3) between temperature ranges		
		294–331° K.	331–346° K.	346–381° K.
21·0	2·86	11830	11760	11620
25·3	3·45	11500	10950	11000
29·5	4·10	11500	11300	10400
33·7	4·60	11450	11300	—
37·9	5·16	11150	—	—
42·1	5·74	10500	—	—

TABLE III. SORPTION HEATS OF AMMONIA IN CHABASITE

c.c. at N.T.P. of ammonia/g. of chabasite	ΔH (k.cal./mol.) between	
	626·4–539·5° K.	539·5–476·5° K.
3·2	28·6	—
5·0	27·2	30·1
8·0	25·7	29·4
12·6	24·3	28·9
20·0	23·1	27·2
25·0	22·7	25·5
32·0	—	23·5
40·0	—	21·8
50·0	—	21·0

TABLE IV. HEATS OF SORPTION OF AMMONIA IN ANALCITE

c.c. at N.T.P. of ammonia/g. of analcite	ΔH (k.cal./mol.) between	
	611·4–542·5° K.	554·5–500·5° K.
Series A		
1·8	23·5	—
2·3	23·1	—
3·6	22·8	—
5·7	19·5	20·7
9·0	15·3	18·8
11·3	·14·3	17·7
14·5	13·9	16·8
16·3	13·8	16·3
Series B	442·5–500·5° K.	
5·7	20·8	—
9·0	20·8	—
11·3	20·0	—
14·5	14·6	—
16·3	18·4	—
Series C	610·4–531·5° K.	531·5–438·1° K.
1·4	22·7	—
2·3	22·1	22·5
3·6	20·9	21·5
5·7	19·9	21·1
9·0	19·1	20·9
11·3	18·2	20·5
14·5	15·5	19·3
16·3	14·2	17·3

sorption heats can themselves rise to the remarkably high values of 8800 for nitrogen (Part I) and 15,000 for ethylene (Lamb and Ohl 1935), within the chabasite lattice, one has little difficulty in understanding their magnitude, without recourse to a quantum mechanical type of chemical bonding. Reference to figs. 5 *a* and *b* shows that sorption follows a Langmuir type of isotherm, without a new phase appearing. The heats of sorption not only appear to increase appreciably as the temperature diminishes—a characteristic of dipole interactions—but also decrease steadily as the amount of ammonia sorbed increases.

The corresponding sorption heats obtained for the analcite-ammonia system from three separate series of measurements, A, B, and C are summarized in Table IV. These sorption heats are also large, but like the sorption heats of the permanent gases (Part I) inside the analcite lattice, they are smaller than are the sorption heats inside the chabasite lattice. Both heats are, however, much greater than the heat of ammoniate formation for natrolite-ammonia.

The sorption heats of ammonia-analcite also tend to increase with decreasing temperature (cf. NH_3-chabasite); but the temperature coefficient increases with the amount of ammonia sorbed. If the ammonia initially sorbed is very vigorously held in non-rotating states, and if rotation increases as the sorption approaches saturation, one might explain the behaviour by saying that the temperature-sensitive region is a transition region of states of sorbed ammonia not rotating at low temperatures, but rotating at high temperatures. The onset of rotation, in ion-dipole interaction, means a diminished energy of interaction.

The sorption kinetics

The sorption of ammonia by chabasite and analcite required for the lowest pressures about two hours per point, and was more rapid as the charge of ammonia increased. The sorption by heulandite required several days; but after degassing at high temperatures equilibrium was not established after several weeks. Natrolite also required a very long time (several weeks) for equilibrium to be established, while as described earlier scolecite excluded ammonia altogether. The distances of closest approach of pairs of molecules in the crystal lattices of the various gases used are:

$$NH_3 \qquad 3{\cdot}60\,A$$
$$He \qquad 2{\cdot}50$$
$$H_2 \qquad 3{\cdot}85$$
$$Ar \qquad 3{\cdot}83$$
$$N_2 \qquad 4{\cdot}08$$

In chabasite and analcite ammonia sorption though very rapid did not reach equilibrium so rapidly as did the sorption of permanent gases, indicating that molecular size does not control the diffusion rates into the crystal skeleton. The sorption velocities may be considered to be in the inverse order of the heats of sorption, i.e. the speed of heat dissipation governs the rate of approach to equilibrium. Also the polar gas ammonia would encounter intense periodic ion-dipole interactions which would tend to anchor it at special points and impede its diffusion rate.
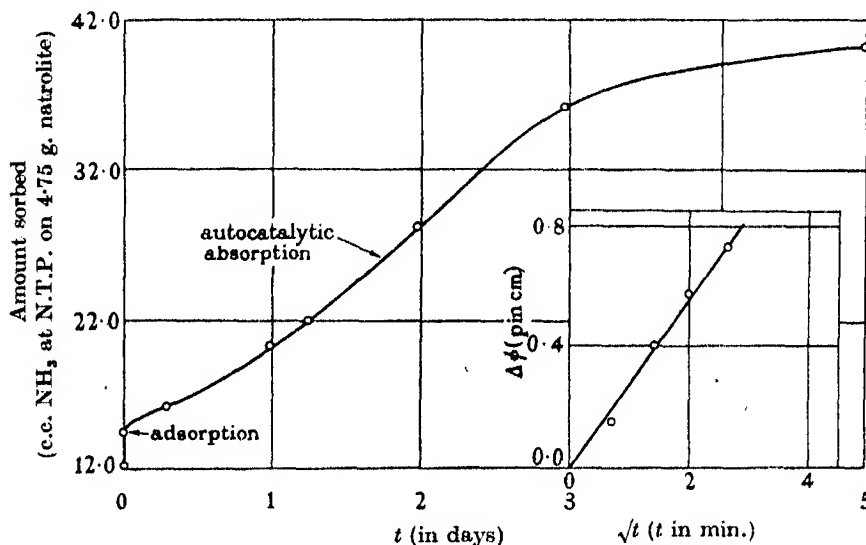
Fig. 7. Sorption velocities. NH_3 on natrolite, showing tendency to autocatalytic sorption rate curves. (NH_3 sorbed before commencing expt = 12·11 c.c. at N.T.P.) (Inset shows NH_3 on heulandite, sorption rate following the parabolic diffusion law.)

Many sorption rate curves were obtained for ammonia-heulandite. Some of these curves in their initial stages obeyed the $\sqrt{t}$ diffusion law:

$$(\text{c.c. sorbed at N.T.P.})^2 = K \times \text{time}.$$

This law, however, very quickly failed. Fig. 7 gives the curve of Δp (proportional to the amount sorbed) against $\sqrt{t}$, both for the early stage of diffusion and for longer periods, and illustrates the behaviour described. The curves are for heulandite degassed at 330° C., whose sorption rate for ammonia was powerfully depressed (loc. cit.) by this rigorous treatment. Because of the great anisotropy of the original heulandite, and its subsequent diffusion anisotropy (Tiselius 1934), no detailed analysis of the curves was made.

The sorption process in natrolite did not commence until a threshold pressure, increasing with increasing temperature, was reached, and thereafter there was the tendency, recorded in fig. 6 to an autocatalytic type of curve. Around this threshold pressure, furthermore, each successive charge of ammonia was sorbed more rapidly than the preceding one. When the quantity of ammonia sorbed was nearing its saturation value, the autocatalytic nature of the sorption was no longer apparent. It is clear that this system resembles in its early stages the hydration and dehydration of crystals and crystal hydrates (Topley 1932), or the decomposition of substances like lead azide (e.g. Garner and Marke 1936). It is an interface process, initiated at certain centres and propagated by the spreading of the centres. The facts are explained by assuming initial ammoniate formation to commence at the ends of the needles of the dehydrated natrolite, being autocatalytic until the end of the needle is covered, after which the phase boundary diffuses uniformly down the length of the needle. Thus, because of the geometry of the needle-like crystal the autocatalytic nature of sorption became submerged in a general linear diffusion of interfaces down the length of a crystal. One must distinguish between the sorption of a gas in a zeolite by diffusion down a concentration gradient in the lattice, and sorption by the diffusion of the interface ammoniate-dehydrated zeolite.

A comparison with earlier data

One may compare some of the systems studied here with the same systems studied by other workers. Chabasite-ammonia was examined by Evans (1931) who gave a calorimetric value of ΔH, the sorption heat, of 17 k.cal. at a 25 c.c./g. ammonia content, a value lower than the value found here; and not at all in keeping with the remarkably vigorous sorption observed. It is indeed but little greater than Lamb and Ohl's initial ΔH of ~15 k.cal. for ethylene. It may, however, be that at sufficiently high ammonia content a value of this order would be approached by the present data, since (Tables II, III and IV) ΔH falls off steadily with charge. The thoroughness with which the dehydration process is carried out and the chemical composition of the zeolite also have a marked effect upon ΔH (cf. Lamb and Ohl 1935; Lamb and Woodhouse 1936).

The sorption heats obtained by Tiselius (1935) for analcite-ammonia are in satisfactory agreement with the values for the larger ammonia content which have been observed in this paper. The high initial heats, however, were not observed by Tiselius, whose sorption isotherms at similar temperatures (302–385° C.) are not so rectangular as those which we have obtained. Tiselius outgassed his zeolite for several hours at 550–600° C. This severe

treatment may have caused considerable reorganization in the lattice, according to the properties recorded here, so that the two dehydrated analcite-ammonia systems may not be entirely comparable. The rates of establishment of equilibrium were also different, Tiselius finding that below 275° C. sorption equilibrium could not be approached, and that an apparent activation energy of 1½·5 k.cal. was required. In this connexion may be recalled the great slowness of sorption of ammonia by heulandite (p. 410), after too drastic a heat treatment as compared with its relatively rapid sorption after evacuation at only 130° C. For the analcite samples studied here sorption equilibrium was rapid and certain for analcite as for chabasite, and for ammonia as for permanent gases.

One may summarize the position as follows:

(1) The heat-charge curves had initial high values approaching asymptotically a lower value. These findings agree with Lamb and Ohl's (1935) data for various zeolites, both for polar and non-polar gases, and for the data in Part I on permanent gases. Other workers (Evans 1931; Tiselius, 1935) did not observe the initial high value. This may be due to incomplete outgassing or to differences in chemical composition.

(2) Very great differences exist between the present data on sorption velocities of ammonia in analcite, and the data of Tiselius. It is suggested that the difference has its origin in the different thermal treatments accorded the analcite, by analogy with similar effects found in this work for heulandite-ammonia.

DISCUSSION

No reason has yet been adduced as to why one zeolite system yields an ammoniate while a second system yields a simple sorption isotherm. This is a problem general throughout chemistry, which is here brought home by the fact that in a single family of substances, the zeolites, one has the limiting cases of ammoniate and simple sorption (and also various intermediate states, e.g. ammonia-heulandite). It is clear that there can be a range of systems exhibiting peculiar properties as sorption systems, but not comprising definite phases in the Phase Rule sense. In the following table the data of Milligan and Weiser (1937) on zeolite-water systems, and of the author on zeolite-ammonia systems, are compared and correlated with the stability data obtained from X-ray diagrams (Milligan and Weiser 1937) and from ammonia sorption subsequent upon thermal treatment. It should be noted that it is not sufficient to measure the unit cell dimensions by X-rays—these may not change appreciably as was the case for dehydration of scolecite (Part I, p. 399)—but yet the contents of the unit cell may undergo

reorganization around the original water-bearing channels upon whose stability the sorbent properties depend.

Reference to Table V will show that hydrates or ammoniates, or states intermediate between sorption and hydrate or ammoniate always appear whenever dehydration of the original zeolite causes a reorganization of the

TABLE V. ZEOLITE HYDRATES, AMMONIATES AND SORPTION SYSTEMS
AND ZEOLITE STABILITY TO THERMAL TREATMENT

Zeolite	Water	Ammonia	Stability to thermal treatment
Three-dimensional networks			
Chabasite	Sorption	Sorption	High, up to 500° C.
Analcite	Sorption	Sorption	High, up to 350° C.
Fibrous zeolites			
Natrolite	Hydrates	Ammoniate	Slight change in X-ray diagram by 160–180° C. Marked changes by 330° C.
Scolecite	Hydrates	No uptake after outgassing at 330° C.	Profound changes by 330° C. Lattice breakdown by 400° C.
Mesolite	Intermediate		Changes slight up to 230° C. Lattice breakdown by 400° C.
Thomsonite	Sorption	—	Changes slight only
Platy zeolites			
Heulandite	Intermediate	Intermediate	Slight changes by 130° C. Profound changes by 330° C.
Stilbite	Non-reversible water uptake (paths on desorption and sorption isobars different)	—	Marked changes by 120° C. Lattice breakdown by 400° C.

unit cell content. Thus lattice changes and hydrate formation tend to be coupled. It is then suggested that in general, when sorption of a gas occurs within a solid a new phase appears when reorganization of the lattice is necessary to accommodate the gas. The occurrence of a third phase demands an interface reaction; the third phase is a result of lattice rearrangement necessary for gas uptake. The formation or otherwise of a new phase has no connexion with the magnitude of the heat of uptake. The greatest heats occur for the simple sorption systems chabasite-ammonia, and analcite-ammonia. Nor is it due to operation of quantum mechanical forces. The forces encountered in chabasite-ammonia are undoubtedly those encountered in natrolite-ammoniate, i.e. van der Waals and ion-dipole interactions. On the basis of forces involved chabasite-ammonia has as much right to be

called a chemical compound as natrolite-ammoniate. On the basis of the phase rule only the natrolite-ammoniate should be thus classified. On the other hand, the intermediate cases, e.g. heulandite-ammonia, cannot be classified by the phase rule.

SUMMARY

The sorption equilibria of ammonia on five zeolites have been studied. The zeolites give sometimes ammoniates and sometimes simple sorption systems, as well as intermediate systems. When dehydration causes changes in the lattice, ammoniates tend to form; more rigid anionic frameworks of Si-O-Al give sorption systems (chabasite, analcite). The magnitude of the sorption heat bears no relation to the formation of ammoniates.

The sorption kinetics of ammonia by zeolites reveal two types of gas uptake: by diffusion of ammonia down concentration gradients within the solid; and by diffusion of the phase-boundaries in an ammoniate-dehydrated zeolite. Sorption was rapid for chabasite and analcite (with rigid frameworks) and slow for fibrous and platy zeolites. The thermal treatment in dehydrating the zeolite had a marked influence on the sorption rates in heulandite.

The heats of sorption of ammonia in analcite and chabasite, and on the external surface of natrolite, diminished as the charge of gas increased. The initial values were 30, 23·5, and 12·4 k.cal. respectively; but the sorption heats decreased somewhat as the temperature was raised. The heat of ammoniate formation in natrolite was 11·7 k.cal., independent of the amount of ammonia taken up, within limits, and only slightly dependent upon the temperature.

The amounts of ammonia sorbed at saturation approached the theoretical maximum for chabasite and natrolite but were only one-third of this maximum for analcite and heulandite. The saturation maxima decreased linearly with increasing temperature.

REFERENCES

Barrer, R. M. 1937 *Proc. Roy. Soc.* A, **161**, 476–93.
Barrer, R. M. and Rideal, E. K. 1935 *Proc. Roy. Soc.* A, **149**, 253–69.
De Boer, J. H. and Custers, J. F. 1934 *Z. Phys. Chem.* **25** B, 225–37.
Evans, M. G. 1931 *Proc. Roy. Soc.* A, **134**, 97–102.

Friedel, G. 1896 *Bull. Soc. Franc. Min.* **19**, 363.

Garner, W. E. and Marke, D. S. 1936 *J. Chem. Soc.* pp. 657–64.

Hey, M. 1932 *Min. Mag.* **23**, 243–89.

— 1935 *Min. Mag.* **24**, 99–130.

— 1937 *Ceramic Soc.* pp. 84–96.

van Itterbeek, A. and van Dingenen, W. 1937 *Physica*, **4**, 389.

Kastner, F. 1931 *Z. Kristallogr.* **77**, 353–80.

Kirkwood, J. 1932 *Phys. Z.* **33**, 57–60.

Lamb, A. B. and Ohl, E. N. 1935 *J. Amer. Chem. Soc.* **57**, 2154–61.

Lamb, A. B. and Woodhouse, J. C. 1936 *J. Amer. Chem. Soc.* **58**, 2637–46.

Langmuir, I. and Sweetser, S. P. 1918 *J. Amer. Chem. Soc.* **40**, 1376–1403.

McBain, J. W. and Britton, G. T. 1930 *J. Amer. Chem. Soc.* **52**, 2198–2222.

Milligan, W. and Weiser, H. 1937 *J. Phys. Chem.* **41**, 1029–40.

Muller, A. 1936 *Proc. Roy. Soc.* A, **154**, 624–39.

Parsons, A. L. 1932 *Univ. Toronto Studies*, **14**, 54.

Pauling, L. 1927 *Proc. Roy. Soc.* A, **114**, 181–211.

Rabinowitsch, E. 1932 *Z. Phys. Chem.* B, **16**, 50–71.

Rabinowitsch, E. and Wood, W. C. 1936 *Trans. Faraday Soc.* **32**, 947–56.

Taylor, W. H. 1930 *Z. Kristallogr.* **74**, 1–19.

— 1934 *Proc. Roy. Soc.* A, **145**, 80–103.

Taylor, W. H., Meek, C. A. and Jackson, W. W. 1933 *Z. Kristallogr.* **84**, 373–98.

Tiselius, A. 1934 *Z. phys. Chem.* A, **169**, 425–58.

— 1935 *Z. phys. Chem.* A, **174**, 401–23.

Topley, B. 1932 *Proc. Roy. Soc.* A, **136**, 413–28.

Wilkins, F. J. 1938 *Proc. Roy. Soc.* A, **164**, 510–31.

Wyart, J. 1930 *C.R. Acad. Sci., Paris*, **191**, 1343–6.

— 1931 *C.R. Acad. Sci., Paris*, **192**, 1244–6.

— 1933 *Bull. Soc. Franc. Min.* **56**, 81.

An X-ray investigation of slowly cooled copper-nickel-aluminium alloys

By A. J. Bradley, D.Sc., *Warren Research Fellow*
and H. Lipson, M.Sc.

National Physical Laboratory

In a recent letter to *Nature* (Bradley, Goldschmidt, Lipson and Taylor 1937) it was shown that even a complicated ternary equilibrium diagram might be rapidly and efficiently investigated by means of X-rays. A diagram for the copper-nickel-aluminium system worked out by the authors of the present paper was given as an example. Since then we have completed the investigation, solving some problems which had been left in abeyance. The whole of the ternary system has now been completely explored for slowly cooled alloys.

The copper-nickel-aluminium system has previously been investigated by a number of workers. Austin and Murphy (1923) determined the liquidus and part of the solidus, exploring the whole system at high temperatures, but without locating the phase fields. Bingham and Haughton (1923) made a more concentrated attack on the aluminium corner of the diagram. In a careful thermal investigation they found many complicated transformations. Gridnew and Kurdjumow (1936) have investigated the effect of adding nickel to the copper-rich copper-aluminium alloys. Recently Alexander and Hanson (1937) measured the hardness and electrical conductivity of alloys lying on the boundary of the face-centred cubic phase in the neighbourhood of pure copper. From these results they determined the change of solid solubility with temperature.

The copper-nickel-aluminium alloys include only one phase which is not found in the binary systems Cu-Ni, Cu-Al and Ni-Al. This is the τ phase, first discovered by Bingham and Haughton (1923). It is one of a group of phases which are related to a body-centred cubic lattice. Such deformed body-centred cubic lattices are found in both the copper-aluminium system (Preston 1931; Bradley, Goldschmidt and Lipson 1938) and in the nickel-aluminium system (Bradley and Taylor 1937*a, b*). Altogether there are eight such structures in this ternary system.

In addition there are three face-centred cubic phases, one with a super-lattice (Ni₃Al), the others without; two special types of structure (CuAl₂ and

27-2

NiAl$_3$) are less closely related to the rest of the system. We have investigated the phase boundaries of each of these phases, and fixed the positions of the two- and three-phase areas.

EXPERIMENTAL

Alloys were made from pure electrolytic copper, Hilger nickel No. 7636 (99·97 %), and aluminium from the British Aluminium Company and Aluminium Française (99·992 %). All the alloys were practically pure, and the compositions were in some cases checked by chemical analysis. This was only important in the β phase, where the melting-point is very high and the heat of reaction is so great that the metal tends to spit. Here differences up to 1·3 % were observed between the weighed and analysed compositions. Elsewhere, it was unnecessary to make any accurate determinations of composition, since we were only working to about 0·5–1 % in fixing the phase boundaries.

The melts were made in a high-frequency induction furnace, under a small pressure of hydrogen which was subsequently pumped off. The alloys were lump annealed for 3 days and powder annealed at the temperatures given in the respective tables. In powder annealing the alloys were allowed to cool from the given temperature to room temperature at the rate of 10° C. per hour.

Powder photographs were taken in a camera of 9 cm. diameter except where some special difficulty necessitated the use of a 19 cm. camera. Copper $K\alpha$ radiation was used throughout the first series of photographs. Some special cases required additional photographs with cobalt or nickel radiations.

GENERAL ACCOUNT OF TERNARY DIAGRAM

Fig. 1 shows the whole of the ternary system, an enlargement of the more complicated region between γ and τ being given in fig. 2. There are eleven single-phase areas, twenty two-phase areas and ten three-phase areas. The γ area is further subdivided into three regions (γ, γ_1 and γ_2) which have different superlattices.

The construction of these diagrams entailed fixing the boundaries of the single-phase areas, and finding the points of contact of the three-phase triangles. The alloys used for this purpose are indicated on the diagrams by circles. As far as possible compositions were chosen to be just outside the single-phase fields.

The method used consisted chiefly in the recognition of small amounts of the second or third constituent. The proportions of these constituents were estimated from the intensities of the lines on the powder photograph. Very consistent results were obtained. There was some tendency to give excessive amounts of the soft α phase (due to the greater readiness with which filings are removed), but this had no serious influence on the results.
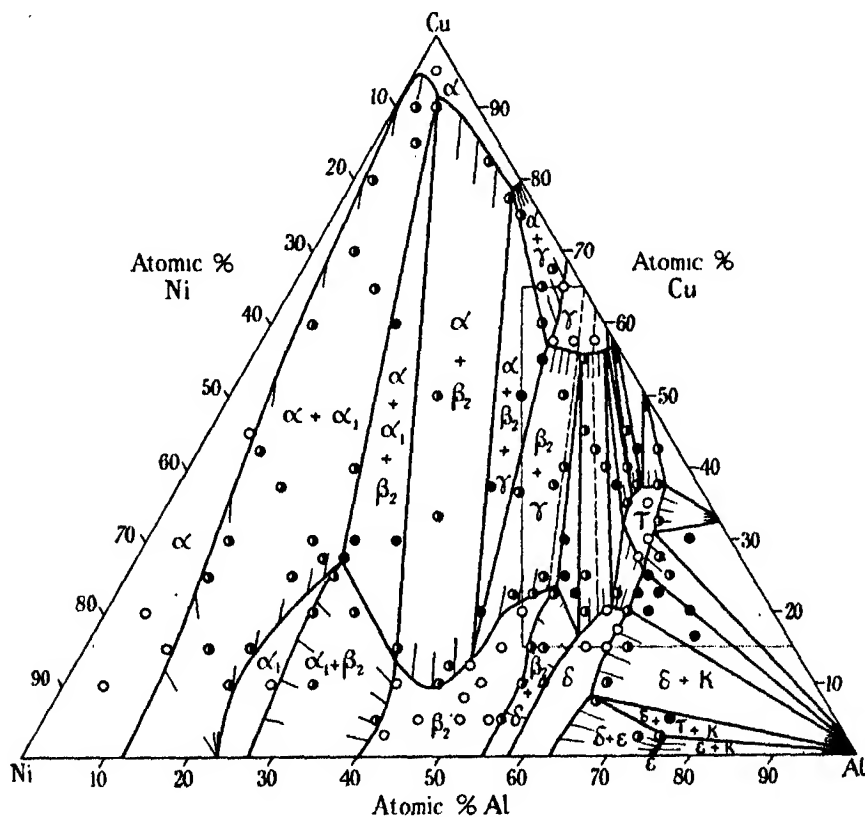
Fig. 1

Sufficient accuracy could be obtained to fix the approximate position of each alloy with respect to the nearest phase boundary. The method is particularly suitable for fixing the corners of the three-phase triangles, which give the key to the whole diagram. Where an alloy fell in a two-phase region it was necessary to find the directions of the tie-lines, from measurements of lattice spacings.

In the diagrams the directions of the tie-lines are shown as short lines emerging from each single-phase field. A particularly interesting point is

27·3

the change in direction of the tie-lines in the $\alpha + \alpha_1$ region. Starting parallel to the binary nickel-aluminium edge they rapidly swing round to a direction almost at right angles. This then remains the general direction of the tie-lines throughout the greater part of the system.
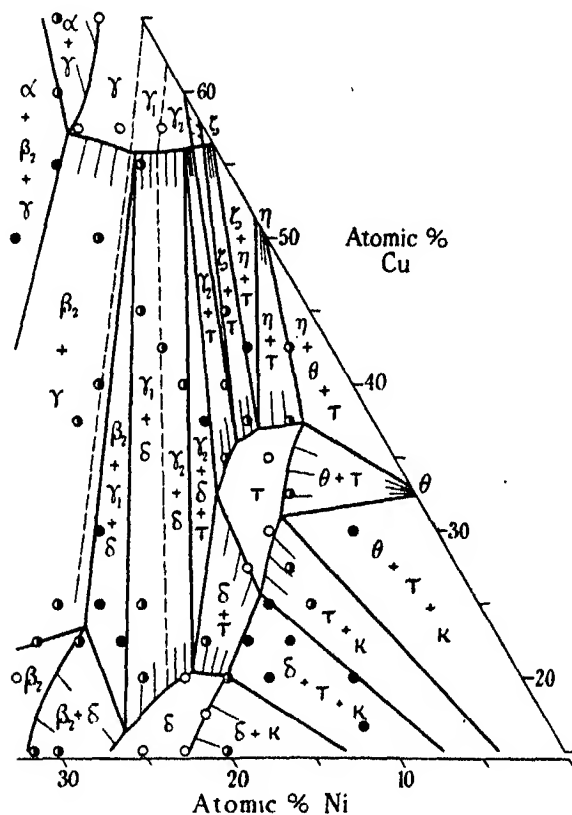
FIG. 2

The single-phase areas

The single-phase fields listed in Table I have been named in sequence starting from the aluminium-poor end and proceeding to the aluminium-rich end, using symbols which could later be employed in the quaternary Fe-Cu-Ni-Al system, on which we are working. The nomenclature is further chosen to fit in with the general usage in the Cu-Al system (Stockdale 1922; Hisatsune 1934; Hansen 1936), except in the γ region, where a special type of nomenclature is required to cope with the exceptional circumstances.

TABLE I. LIST OF SINGLE-PHASE FIELDS IN THE Cu-Ni-Al
SYSTEM AFTER SLOW COOLING

	Ideal formula	Structure
(a) Phases occurring in the binary copper-aluminium system		
α	$Cu-Cu_4Al$	Face-centred cubic
γ	Cu_9Al_4	Complex cubic
γ_1	$Cu_{32}Al_{19}$	Deformed γ
γ_2	Cu_3Al_2	Deformed γ
ζ_2	Cu_4Al_3	*Monoclinic (derived from δ type)
η_2	CuAl	*Orthorhombic (derived from δ type)
θ	$CuAl_2$	Tetragonal
κ	Al	Face-centred cubic
(b) Phases based on the binary nickel-aluminium system		
α	Ni-Cu	Face-centred cubic
α_1	Ni_3Al-Ni_2CuAl	Face-centred cubic superlattice
β_2	NiAl	Body-centred cubic superlattice
δ	$Ni_2Al_3-NiCuAl_3$	Trigonal
ϵ	$NiAl_3$	Orthorhombic
κ	Al	Face-centred cubic
(c) Phase not found in the binary systems		
τ	Cu_3NiAl_6	Deformed body-centred cube

* These are probably distinct from the high temperature forms ζ_1 and η_1 investigated by Preston (1931).

The α and α_1 phases are face-centred cubic, but whereas in the former phase the atoms are probably distributed at random, in the latter they form a superlattice. This is of the type X_3Al, X being nickel with one part in three replaceable by copper. The phase limits are therefore Ni_3Al and approximately $CuNi_2Al$. The aluminium composition is less variable.

The β_2 phase is body-centred cubic with a clear distinction between cube centres and cube corners. As far as possible nickel atoms occupy one position and aluminium the other. Copper may to some extent replace nickel. The ideal formula is NiAl. With less aluminium, nickel or copper atoms replace this element, but beyond 50 atomic % aluminium, there is no replacement of nickel by aluminium. The atomic proportions are then adjusted by leaving empty places in the lattice in lieu of the missing nickel atoms.

In addition to β_2, γ, γ_1, γ_2, δ, ζ, η and τ are all derived from a body-centred cubic lattice. Certain atomic sites are left vacant, the remaining atoms being subject to displacements in accordance with symmetry laws. The structure of ϵ alloys ($NiAl_3$) is also related to this type. A detailed account of the structure relationships will be given elsewhere.

The two- and three-phase areas

Table II gives a list of the two- and three-phase areas surrounding each single-phase area in the order in which they appear in the diagram. At least one representative alloy has been examined in each of the two- and

TABLE II. CLASSIFIED LIST OF TWO- AND THREE-PHASE
FIELDS IN ORDER OF APPEARANCE

The numbers indicate the tables giving details of alloys belonging to a given phase field. For example, data concerning alloys belonging to the $\alpha + \alpha_1$ phase field are given in Table IV.

4	$\alpha + \alpha_1$	4	$\alpha_1 + \alpha$	5	$\beta_2 + \alpha_1$
6	$\alpha + \alpha_1 + \beta_2$	6	$\alpha_1 + \alpha + \beta_2$	6	$\beta_2 + \alpha_1 + \alpha$
5	$\alpha + \beta_2$	5	$\alpha_1 + \beta_2$	5	$\beta_2 + \alpha$
7	$\alpha + \beta_2 + \gamma$			7	$\beta_2 + \alpha + \gamma$
7	$\alpha + \gamma$			7	$\beta_2 + \gamma$
					$\beta_2 + \gamma_1$
7	$\gamma + \alpha$		$\zeta + \gamma_2$	8	$\beta_2 + \gamma_1 + \delta$
7	$\gamma + \alpha + \beta_2$		$\zeta + \gamma_2 + \tau$	8	$\beta_2 + \delta$
7	$\begin{cases} \gamma + \beta_2 \\ \gamma_1 + \beta_2 \end{cases}$	9	$\zeta + \tau$		
		9	$\zeta + \tau + \eta$		$\theta + \eta$
8	$\gamma_1 + \beta_2 + \delta$		$\zeta + \eta$		$\theta + \eta + \tau$
8	$\begin{cases} \gamma_1 + \delta \\ \gamma_2 + \delta \end{cases}$			9	$\theta + \tau$
			$\eta + \zeta$	10	$\theta + \tau + \kappa$
9	$\gamma_2 + \delta + \tau$	9	$\eta + \zeta + \tau$		$\theta + \kappa$
9	$\gamma_2 + \tau$	9	$\eta + \tau$		
	$\gamma_2 + \tau + \zeta$		$\eta + \tau + \theta$	10	$\tau + \kappa$
	$\gamma_2 + \zeta$		$\eta + \theta$	10	$\tau + \kappa + \delta$
				9	$\tau + \delta$
	$\kappa + \theta$	8	$\delta + \epsilon$	9	$\tau + \delta + \gamma_2$
10	$\kappa + \theta + \tau$	10	$\delta + \epsilon + \kappa$	9	$\tau + \gamma_2$
10	$\kappa + \tau$	10	$\delta + \kappa$		$\tau + \gamma_2 + \zeta$
10	$\kappa + \tau + \delta$	10	$\delta + \kappa + \tau$	9	$\tau + \zeta$
10	$\kappa + \delta$	9	$\delta + \tau$	9	$\tau + \zeta + \eta$
10	$\kappa + \delta + \epsilon$	9	$\delta + \tau + \gamma_2$	9	$\tau + \eta$
	$\kappa + \epsilon$	8	$\delta + \gamma_2$		$\tau + \eta + \theta$
		8	$\delta + \gamma_1$	9	$\tau + \theta$
	$\epsilon + \kappa$	8	$\delta + \gamma_1 + \beta_2$	10	$\tau + \theta + \kappa$
10	$\epsilon + \kappa + \delta$	8	$\delta + \beta_2$		$(\tau + \kappa)$
8	$\epsilon + \delta$				

three-phase fields except for $\gamma_2 + \zeta + \tau$ and $\eta + \theta + \tau$. The binary alloys are not included in the present paper as they have been discussed elsewhere. Data referring to the $\gamma_2 + \zeta$ and $\zeta + \eta$ phase fields are given in a recent account of the intermediate phases of the copper-aluminium system (Bradley, Goldschmidt and Lipson 1938).

The α-phase (face-centred cubic) boundaries

This phase field includes the whole of the copper-nickel system, which forms a continuous series of solid solutions, together with the α phases of the copper-aluminium and nickel-aluminium systems. The structures are all face-centred cubic, without superlattices. The limits of solid solubility, as shown in fig. 1, divided the phase field into two branches; one part extends from pure copper to pure nickel, gradually widening as the nickel content increases: the other part extends along the copper-aluminium binary edge of the diagram. The first may be considered as a solid solution of aluminium in copper-nickel alloys, the second as a solid solution of nickel in copper-aluminium alloys.

TABLE III. SINGLE-PHASE ALLOYS—FACE-CENTRED AND BODY-CENTRED CUBIC

Atomic composition			Phase field	Lattice spacings	Radiation	Heat treatment*	
Cu	Ni	Al				Lump	Powder
95·0	2·5	2·5	α	3·6093	Cu	960°	830°
45·0	50·0	5·0	α	3·5638	Cu	900	700
20·0	75·0	5·0	α	3·5427	Cu	900	700
15·0	75·0	10·0	α	3·5442	Cu	900	700
10·0	85·0	5·0	α	3·5358	Cu	950	880
10·0	65·0	25·0	α_1	3·5699	Cu	900	740
10·0	50·0	40·0	β_2	2·8671	Cu, Co	900	800
10·0	40·0	50·0	β_2	2·8943	Cu	900	830
15·0	35·0	50·0	β_2	2·9102	Cu	900	830
12·5	40·0	47·5	β_2	2·8908	Cu	950	920
8·0	43·0	49·0	β_2	2·8878	Cu	900	740
5·0	50·0	45·0	β_2	2·8737	Cu, Co	900	850
5·0	45·0	50·0	β_2	2·8882	Cu, Co	800	700
5·0	41·5	53·5	β_2	2·8781	Cu, Co	950	880
3·0	55·0	42·0	β_2	2·8661	Cu, Co	900	830
20·0	30·0	50·0	β_2	2·9058	Cu	950	880

* For details see text.

The limits of solid solubility were fixed by comparing powder photographs of single-phase alloys with those of two-phase alloys, measuring up the lattice spacings and estimating the amounts of the second phase wherever present. In Table III are given the lattice spacings of the single-phase alloys. These are lowest near pure nickel, rising with the addition of either copper or aluminium. The maximum values of the lattice spacings are found near the copper-aluminium edge of the diagram.

Tables IV, V, VI and VII give a list of the two-phase and three-phase fields containing α. The most important of these is $\alpha + \alpha_1$, where two face-

centred cubic lattices are in equilibrium. Table IV gives a list of alloys in this phase field, from which the approximate positions of the phase boundaries were obtained. In many cases, e.g. 65, 25, 10,* the duplex character of the alloy is obvious from the first glance at the X-ray photograph. The high order reflections each give two separate α doublets, one corresponding to α, the other to α_1. In these cases, accurate measurement of the lattice spacing of each phase is possible, and by comparing the relative intensities of the corresponding lines estimates can be made of the amounts of the two phases. By this means a first approximation can be made to the positions of the phase boundaries.

The accurate position of the α boundary is more difficult to fix than might be thought from a preliminary glance at the powder photographs. The trouble arises from the similarity in the spacings of α and α_1. In the nickel-rich $\alpha + \alpha_1$ alloys, α_1 has the higher spacing; in the copper-rich alloys the α spacing is greater. Evidently an intermediate series of alloys exists, for which the α and α_1 constituents have exactly the same lattice spacings (3·566A). It is difficult to distinguish whether alloys in this neighbourhood consist of one or two phases. For example, in 60, 35, 5 the lattice spacing of the α_1 constituent is so near to that of the α constituent that it is impossible to give a separate measurement.

In such cases, the presence of small quantities of the α_1 phase is recognized by the superlattice lines. α has no superlattice, but α_1 has a superlattice of the Ni_3Al type. The extra lines of the structure can be seen faintly even when there is only a little α_1 present, especially if a camera with a large diameter is used. The alloys near the α boundary were all examined in a camera of 19 cm. diameter, in order to show up the presence of the superlattice lines. Cobalt radiation was used for this purpose as it increases the intensities of these lines.

The phase boundary shown in fig. 1 between α and $\alpha + \alpha_1$ was entirely constructed from the estimates of the intensities of the superlattice lines in duplex alloys. It is interesting to notice that a different result would have been obtained if we had used the intensities of the α doublets. For example, the alloys 90, 7·5, 2·5 and 80, 17·5, 2·5 give no sign of the 331 and 420 reflexions for the α_1 phase, although there should be quite an appreciable difference between the spacings of the two phases in these alloys. 85, 10, 5 which gives fairly strong superlattice lines suggesting that the alloy is far removed from the phase boundary, shows only faint reflexions from the main lattice planes of the α_1 phase.

---

* The numbers represent atomic percentages of copper, nickel and aluminium in that order.

TABLE IV. ALLOYS WITH TWO FACE-CENTRED CUBIC STRUCTURES

Atomic composition			Approximate proportion of phases		Lattice spacings	Remarks (see footnotes)	Heat treatment	
Cu	Ni	Al					Lump	Powder
90·0	7·5	2·5	α	15	3·6015	LS	900	800
			α_1	1				
85·0	10·0	5·0	α	8	3·6054	LS	900	750
			α_1	1		FF		
80·0	17·5	25·0	α	12	3·5909	LS	1000	950
			α_1	1				
70·0	25·0	5·0	α	8	3·5839	LS	850	750
			α_1	1				
65·0	25·0	10·0	α	2	3·6004	FF	900	700
			α_1	1	3·5804			
60·0	35·0	5·0	α	10	3·5768	LS	900	800
			α_1	1				
42·5	50·0	7·5	α	6	3·5658	S	950	900
			α_1	1		FF		
40·0	40·0	20·0	α	1	3·6105	FF	900	760
			α_1	5	3·5846			
37·5	50·0	12·5	α	2	3·5798	FF	1000	750
			α_1	3	3·5701			
30·0	50·0	20·0	α	1	3·5977	FF	900	760
			α_1	6	3·5752			
30·0	60·0	10·0	α	6	3·5585	FF	900	750
			α_1	1	3·5710			
27·5	50·0	22·5	α	1	—	FF	900	830
			α_1	12	3·5814	S		
25·0	65·0	10·0	α	8	3·5527	FF	950	900
			α_1	1				
25·0	55·0	20·0	α	1	—	LFF	850	830
			α_1	12	3·5721			
15·0	70·0	15·0	α	3	3·5499	FF	950	900
			α_1	1	3·5706			
15·0	65·0	20·0	α	1	—	LFF	900	750
			α_1	30	3·5672			
10·0	70·0	20·0	α	1	—	FF	850	820
			α_1	10	3·5651	S		

L = Powder photograph taken in longer camera.
S = Superlattice lines observed with cobalt radiation.
FF = Two face-centred cubic patterns observed.
All photographs were taken with copper radiation.

TABLE V. FACE-CENTRED + BODY-CENTRED CUBIC ALLOYS

Atomic composition			Approximate proportions of phases		Lattice spacings	Radiation	Heat treatment	
Cu	Ni	Al					Lump	Powder
82·5	2·5	15·0	α	100	3·6412	Cu, Ni	950	920
			β_2	1				
77·5	2·5	20·0	α	30	3·6527	Cu, Ni	1000	950
			β_2	1				
50·0	25·0	25·0	α	3	3·6195	Cu, Ni	850	750
			β_2	2	2·8728	Co		
33·3	33·3	33·3	α	1	3·6236	Cu, Ni	850	750
			β_2	2	2·8734	Co		
15·0	47·5	37·5	α	1	—	Cu	900	760
			β_2	25	2·8681	Co		
12·5	42·5	45·0	α	1	—	Cu	900	850
			β_2	25	2·8824	Co		
10·0	45·0	45·0	α	1	—	—	1000	900
			β_2	100				
25·0	50·0	25·0	α_1	100	3·5869	Cu	850	750
			β_2	1				
20·0	55·0	25·0	α_1	50	3·5846	Cu	950	880
			β_2	1				
20·0	50·0	30·0	α_1	3	3·5840	Cu	—	—
			β_2	1	2·8656			
10·0	60·0	30·0	α_1	4	3·5768	Cu	900	760
			β_2	1	2·8637	Co		
5·0	55·0	40·0	α_1	1	—	Cu	850	830
			β_2	40	2·8630	Co		

TABLE VI. ALLOYS WITH TWO FACE-CENTRED CUBES IN EQUILIBRIUM WITH A BODY-CENTRED CUBE

Atomic composition			Approximate proportion of phases		Lattice spacings	Radiation	Heat treatment	
Cu	Ni	Al					Lump	Powder
90·0	5·0	5·0	α	100	3·6105	Cu	1000	950
			α_1	?				
			β_2	1				
60·0	25·0	15·0	α	15	3·6116	Cu	950	900
			α_1	10	3·5869			
			β_2	1	—			
30·0	45·0	25·0	α	1	—	Cu	850	830
			α_1	20	3·5880			
			β_2	2	2·8669	Co		
27·5	47·5	25·0	α	1	—	—	850	800
			α_1	60	3·5886	Cu		
			β_2	3	2·8642	Co		
30·0	40·0	30·0	α	2	3·6110	Cu	900	760
			α_1	1	3·5856	Cu		
			β_2	5	2·8664	Co		

TABLE VII. SOME ALLOYS CONTAINING γ

Atomic composition			Approximate proportion of phases		Lattice spacings	Radiation	Heat treatment	
Cu	Ni	Al					Lump	Powder
65·0	2·5	32·5	γ		8·6720	Cu	950	900
57·5	7·5	35·0	γ		8·6797	Cu	900	850
57·5	5·0	37·5	γ		8·6940	Cu	950	920
57·5	2·5	40·0	γ		——	Cu	550	500
75·0	2·5	22·5	α	3	3·6533	Cu, Ni	900	740
			γ	1	8·6714			
67·5	2·5	30·0	α	1	3·6553	Cu, Ni	850	820
			γ	2	8·6780			
65·0	5·0	30·0	α	1	3·6538	Cu	850	820
			γ	2	8·6728			
50·0	10·0	40·0	β_2	1	2·9054	Cu	900	740
			γ	3	8·6937			
37·5	17·5	45·0	β_2	1	2·9076	Cu	900	800
			γ	1	8·6928			
34·6	23·1	42·3	β_2	1	2·8932	Co	1000	750
			γ	1	8·6765	Cu		
40·0	15·0	45·0	β_2	1	——	Cu	900	800
			γ	1				
60·0	7·5	32·5	α	1	3·6534	Ni	900	800
			β_2	?	——			
			γ	5	8·6706	Cu		
55·0	10·0	35·0	α	1	——	——	950	920
			β_2	3	(2·8907)	Cu		
			γ	20	8·6720			
50·0	15·0	35·0	α	2	3·6533	Cu	950	900
			β_2	3	(2·8902)	Ni		
			γ	6	8·6706	Co		
37·5	25·0	37·5	α	10	3·6543	Cu	1000	750
			β_2	10	2·8900	Co		
			γ	1	——			
20·0	35·0	45·0	α	1	——			
			β_2	40	2·8934	Cu	900	800
			γ	10	——			

These rather perplexing results may perhaps be explained in the following way. During cooling, some of the α_1 phase is precipitated from the α phase. Evidence for this fact can be found from the work of Alexander and Hanson (1937), who showed that the phase boundary of the α phase extends considerably further from the copper corner at high temperatures than at room temperature. The process of precipitation apparently occurs in two stages. First little "islands" of α_1 form within the α lattice. These have the lattice spacing of the original lattice, not that of the final state. Only when

the islands of α_1 have grown sufficiently to break away from α will they crystallize as a separate lattice. Slow cooling appears to "freeze in" the intermediate metastable state.

It is possible that the effect here described is a general phenomenon, to be observed whenever a precipitating phase imperfectly crystallizes from the parent lattice. If the precipitating phase has no superlattice it cannot then be detected by means of X-rays. This is probably the origin of the view that small quantities of a second phase may not be observed by X-ray methods. The second phase can, in fact, be observed as soon as it has crystallized apart from the parent lattice. For example, as little as one part in 600 of a body-centred cubic structure may be visible on an X-ray powder photograph taken in a 19 cm. camera.

A good example of the small amount of a body-centred cubic phase which can be observed on a powder photograph is shown by the alloy 90, 5, 5 which contains only 1 % of the body-centred cubic phase (see Table VI). This alloy is very near the α phase boundary, and marks the corner of the three-phase triangle $\alpha + \alpha_1 + \beta_2$, since the lattice spacing of the α phase is here lower than that in any of the $\alpha + \beta_2$ alloy, and almost the same as that of other three-phase alloys. The amount of α_1 is too little to be seen merely from the superlattice. From this point, the course of the boundary between α and $\alpha + \beta_2$ was followed from the photographs of 82·5, 2·5, 15 and 77·5, 2·5, 20. The data for the $\alpha + \beta_2$ phase field in Table V show that the amounts of β_2 are so small that these alloys must also be near the α phase boundary. The lattice spacings of the α constituents of 77·5, 2·5, 20 of the $\alpha + \beta_2 + \gamma$ alloys and of 75, 2·5, 22·5 increase in this order. The α corner of the three-phase triangle therefore lies between the two points representing these alloys.

The α_1 phase boundaries

Although we have examined only one ternary α_1 alloy which has proved to be single-phase, a number of other specimens has been found to contain almost pure α_1, mixed with small quantities of other phases. Five alloys contain small amounts of α mixed with α_1. This is proved by the doubling of the high order reflexions, which can easily be observed in the larger camera, although it is not always visible in the 9 cm. camera. These photographs establish the position of the α_1 boundary on the aluminium-poor side. On the aluminium-rich side, the data given in Table V show the exact position of the α_1 boundary and the point of contact of the three-phase triangle. 27·5, 47·5, 25 containing just a trace of the α and β_2 phases gives the exact position of the point of contact.

The β_2 phase boundaries

A large number of alloys has been found to contain only the body-centred cubic β_2 phase. These are listed in Table III. The lattice spacings change in the irregular manner which is characteristic of the NiAl type of structure (compare the results for the FeNiAl system). The maximum spacing was found for 15, 35, 50. There is a fall in spacing with the addition of either Cu, Ni or Al to this alloy.

The phase boundary is given by the two- and three-phase alloys in the regions indicated in Tables V and VI. Powder photographs of the $\beta_2 + \alpha$ and $\beta_2 + \alpha_1$ alloys (Table V) reveal the slightest trace of the α or α_1 constituent. In the 19 cm. camera 1 part in 400 is visible. The least amount observed in the present experiments was 1 part in 100 in the case of 10, 45, 45. The composition of the β_2 constituent of the $\alpha + \alpha_1 + \beta_2$ alloys is fixed by 15, 47·5, 37·5 and 30, 40, 30. The lattice spacing of the face-centred cubic constituent of the former proves that this belongs to the α phase and not α_1. The considerable amount of α_1 in the latter fixes the position of the boundary between the $\alpha + \beta_2$ and $\alpha_1 + \beta_2$ fields.

The composition of the β_2 constituent of the $\alpha + \beta_2 + \gamma$ field is given by the three-phase alloys in conjunction with 12·5, 40, 47·5 which contains only β_2. The boundary between the β_2 and $\beta_2 + \gamma$ fields was fixed by the presence of a small amount of γ in three alloys (Table VII). The γ pattern was recognized by the presence of line 66 which is one of its strongest lines and does not overlap any line of the β_2 pattern.

Four alloys lie just beyond the β_2 boundary in the $\beta_2 + \delta$ region (Table VIII). The small amount of δ is readily recognized, since the strong lines of the δ pattern, although close to the β lines, do not exactly superimpose them, except at low angles. 25, 22·5, 52·5 also contains γ_1 lines and enables this corner of the $\beta_2 + \gamma_1 + \delta$ triangle to be fixed.

The γ phase boundaries

Table VII shows that three single-phase ternary γ alloys were found, in addition to a single-phase γ_2 alloy. As in the binary copper-aluminium system, the lattice spacing of γ rises with increasing aluminium content. Only the α and β_2 phases are in equilibrium with γ; of these α is readily distinguished, but β_2 presents difficulties. These are greatest in the $\alpha + \beta_2 + \gamma$ region, where every line of the β_2 pattern exactly overlaps a line of the γ pattern. Small amounts of β_2 are, therefore, indistinguishable from γ. As the amount of β_2 increases it becomes possible to recognize changes in the relative intensities of the lines, those which are typical only of γ becoming relatively weaker than those lines which are common to γ and β_2.

Beyond the three-phase triangle in which α is in equilibrium with β_2 and γ_1, the lattice spacing of β_2 rises much more rapidly than that of γ. The β_2 lines gradually move away from those of γ and it becomes possible to distinguish them from one another at high angles. With cobalt radiation line 10(310) for β_2 now becomes quite separate from line 90(930) for γ. It is then easy to distinguish the two-phase alloy 50, 10, 40 from the single-phase alloy 57·5, 5, 37·5.

The alloy 60, 7·5, 32·5 is placed in the three-phase triangle, on account of the lattice spacings, which agree with those of the other three-phase alloys, although it is impossible to detect the presence of β_2 from the small change of intensity. 55, 10, 35, however, just shows an intensity change sufficient to prove the presence of β_2, fixing the composition of the γ constituent of the $\alpha + \beta_2 + \gamma$ alloys.

The differences between γ, γ_1 and γ_2 found for the binary copper-aluminium alloys are also observed in the ternary system. The essential point is a debasement of symmetry leading to a modification of the high order reflexions. This change occurs suddenly at a definite composition but is not accompanied by any great change in crystal structure. The majority of the atoms have the same positions in the structures of γ, γ_1 and γ_2, but whereas in γ extra aluminium atoms enter at random, in γ_1 and γ_2 they occupy definite sites. These sites are distributed in a manner which is inconsistent with cubic symmetry, so producing the observed effects. The differences between γ, γ_1 and γ_2 are scarcely sufficient to be regarded as real phase changes, so that there are no observable two-phase fields separating the γ, γ_1 and γ_2 regions on the phase diagram.

In the ternary system 57·5, 5, 37·5 is still γ; 55, 5, 40 is nearly pure γ_1, while 57·5, 2·5, 40 is γ_2. The positions of these three alloys show that the changes from γ to γ_1 and from γ_1 to γ_2 do not occur with a fixed aluminium composition. The addition of nickel enables more aluminium to be tolerated by the γ and γ_1 structures. This suggests that the transformation is essentially an electronic effect, nickel having less electrons, aluminium more electrons than copper.

The δ phase boundaries

The δ phase has a considerable extension in the ternary diagram, four single-phase alloys being found. One half of the nickel atoms in Ni_2Al_3 are replaceable by copper, the alloy $CuNiAl_3$ being just within the phase boundary. Characteristic lines of the δ pattern enable it to be distinguished from all neighbouring phases with which it comes into contact. For example, in the $\beta_2 + \delta$ alloys there is no difficulty in recognizing the 200

line of β_2 side by side with the corresponding δ line. In spite of the general resemblance between the β and δ patterns the lines never quite overlap except at low angles.

Similarly the γ_1 and τ patterns although extremely like δ, differ just sufficiently to enable the lines of one structure to be distinguished from those of another. Nevertheless, there is sufficient overlapping, especially in the low orders, to cause confusion unless every precaution is taken. Although the present work was satisfactorily carried out in a camera of 9 cm. diameter, it would certainly be advisable to use a much bigger camera to resolve the lines of the different patterns. Preferably one should use a monochromator in which the α_1 radiation only is allowed to reach the specimen. The corresponding lines of the pseudo body-centred structures are so close together that the presence of α_2 is a real handicap.

Special temperatures of lump annealing are required to make the copper-rich δ alloys homogeneous. At first the temperatures used for this purpose were too low and mixtures with neighbouring phases were obtained. This is due to coring. The first portions to solidify are richer in nickel than the rest of the material and the liquid crystallizes without reacting with

TABLE VIII. SOME δ ALLOYS

Atomic composition			Phase field	Approximate proportion of phases	Lattice spacings of β_2 phase	Radiation	Heat treatment	
Cu	Ni	Al					Lump	Powder
20·0	20·0	60·0	δ	—	—	Cu	810	750
17·5	20·0	62·5	δ	—	—	Cu	900	800
15·0	25·0	60·0	δ	—	—	Cu	810	750
15·0	22·5	62·5	δ	—	—	Cu	900	840
22·5	25·0	52·5	$\beta_2 + \delta$	50/1	2·9044	Cu	900	840
15·0	31·5	53·5	$\beta_2 + \delta$	10/1	2·8781	Cu, Co	850	820
15·0	30·0	55·0	$\beta_2 + \delta$	3/2	2·8993	Cu	900	800
10·0	35·0	55·0	$\beta_2 + \delta$	15/1	2·8900	Cu	900	800
10·0	32·5	57·5	$\beta_2 + \delta$	1/30	—	Cu	900	800
5·0	40·0	55·0	$\beta_2 + \delta$	30/1	2·8749	Cu, Co	850	830
55·0	5·0	40·0	$\gamma_1 + \delta$	40/1	—	Cu	900	840
45·0	10·0	45·0	$\gamma_1 + \delta$	3/1	—	Cu	810	750
20·0	22·5	57·5	$\gamma_1 + \delta$	1/10	—	Cu	900	850
25·0	20·0	55·0	$\gamma_1 + \delta$	1/4	—	Cu	810	750
42·5	10·0	47·5	$\gamma_2 + \delta$	3/2	—	Cu	720	660
40·0	10·0	50·0	$\gamma_2 + \delta$	1/1	—	Cu	720	660
30·0	20·0	50·0	$\beta_2 + \gamma_1 + \delta$	15/1/4	2·9103	Cu	830	700
25·0	22·5	52·5	$\beta_2 + \gamma_1 + \delta$	6/1/3	2·9084	Cu	950	920
22·5	22·5	55·0	$\beta_2 + \gamma_1 + \delta$	1/1/6	2·9095	Cu	950	920
7·5	27·5	65·0	$\delta + \epsilon$	15/1	—	Cu	550	500
2·5	25·0	72·5	$\delta + \epsilon$	1/3	—	Cu	750	640

the solid. To promote reaction, temperatures of at least 800° were required.

The δ phase is in equilibrium with β, γ_1, γ_2, τ, κ and ϵ (Tables VIII–X). Examples of two-phase alloys containing δ together with each of the above have been obtained, also examples of δ in four different three-phase areas. $\gamma_2 + \delta + \tau$ is an extremely narrow region about which it is difficult to get direct information; but one alloy has been found in this field.

TABLE IX. SOME τ ALLOYS

Atomic composition				Approximate proportion of phases	Heat treatment	
Cu	Ni	Al	Phase field		Lump	Powder
35·0	7·5	57·5	τ	—	650	550
30·0	10·0	60·0	τ	—	720	660
27·5	12·5	60·0	τ	—	750	640
40·0	7·5	52·5	$\gamma_2 + \tau$	1/2	650	550
35·0	10·0	55·0	$\gamma_2 + \tau$	1/25	720	660
22·5	17·5	60·0	$\delta + \tau$	2/1	900	750
37·5	10·0	52·5	$\gamma_2 + \delta + \tau$	6/1/10	720	660
37·5	7·5	55·0	$\zeta + \tau$	1/30	650	550
32·5	7·5	60·0	$\theta + \tau$	1/20	650	550
37·5	5·0	57·5	$\eta + \tau$	1/?/100	650	550
42·5	2·5	55·0	$\eta + \tau$	2/3	580	—
45·0	5·0	50·0	$\zeta + \tau$	2/3	650	550
42·5	5·0	52·5	$\zeta + \eta + \tau$	—	580	—

TABLE X. ALLOYS CONTAINING κ

Atomic composition				Approximate proportion of phases	Heat treatment	
Cu	Ni	Al	Phase field		Lump	Powder
30·0	5·0	65·0	$\theta + \tau + \kappa$	4/6/1	580	550
27·5	10·0	62·5	$\tau + \kappa$	30/1	650	550
25·0	10·0	65·0	$\tau + \kappa$	15/1	650	550
25·0	12·5	62·5	$\delta + \tau + \kappa$	1/50/1	710	680
22·5	15·0	62·5	$\delta + \tau + \kappa$	30/30/1	710	680
20·0	15·0	65·0	$\delta + \tau + \kappa$	8/4/1	710	680
16·7	11·1	72·2	$\delta + \tau + \kappa$	6/2/3	710	680
20·0	10·0	70·0	$\delta + \tau + \kappa$	3/10/3	710	680
22·5	12·5	65·0	$\delta + \tau + \kappa$	3/15/2	710	680
20·0	17·5	62·5	$\delta + \kappa$	100/1	900	750
10·0	25·0	65·0	$\delta + \kappa$	15/1	510	500
15·0	20·0	65·0	$\delta + \kappa$	15/1	710	680
5·0	20·0	75·0	$\delta + \epsilon + \kappa$	5/1/3	490	470
2·5	22·5	75·0	$\delta + \epsilon + \kappa$	—	580	—

The τ phase boundaries

The τ phase, situated in the interior of the ternary diagram, has a considerable extension, but mutual replacement of copper and nickel does not occur to the same extent, as in α_1 and δ. Of the three single-phase alloys found during this investigation, the simplest formula is Cu_3NiAl_6. This alloy contains considerably less aluminium than any investigated by Bingham and Haughton, in their discovery of the τ phase. The most homogeneous alloy reported by them was Cu_2NiAl_5 which is just outside the τ phase field, on the aluminium-rich side.

Considerable difficulty was at first experienced in removing segregation in τ alloys rich in aluminium. Before obtaining satisfactory results it was necessary to try lump annealing at several different temperatures. If the temperature is too high the alloy partially melts; if too low the reaction is too slow.

The difficulty of finding a suitable temperature for the heat treatment of the τ alloys arises from the following facts. The liquidus surface, as shown by Austin and Murphy has a steep gradient in the neighbourhood. The first phase to solidify is probably δ. τ is situated in a region where the liquidus temperature is much lower, but not so low as for θ and κ. The separation of δ crystals displaces the composition of the liquid phase towards the copper-aluminium edge of the diagram. It appears that τ next precipitates, leaving the eutectic of $\kappa + \theta$ (or possibly the ternary eutectic of $\tau + \kappa + \theta$) as the last composition to solidify. Finally the solid contains four phases δ, τ, κ and θ. It is necessary to heat-treat the alloy at a temperature where these four phases will react to give an equilibrium product. 650–700° C. covers the ideal temperature range.

ε and κ phases

The ε phase includes the composition $NiAl_3$. There is some solubility of copper as is proven by the 2·5, 25, 72·5 and 2·5, 22·5, 75 which contain only $\epsilon + \delta$. If there were no solid solubility these alloys would also contain κ.

The κ phase is of small extent. For details reference should be made to the work of Bingham and Haughton. Here we have only attempted to fix the phase sequence, showing that there are no fewer than seven phase fields bordering on the aluminium solid solution (see Table II). The system is therefore even more complicated than had previously been supposed.

We are indebted to Professor W. L. Bragg, F.R.S. for his great interest in the work which was commenced in the Physical Laboratories of the

University of Manchester and completed at the National Physical Laboratory under Dr C. H. Desch, F.R.S. One of us (H. Lipson) has been in receipt of a grant from the Department of Scientific and Industrial Research. The work is being continued with help from the Permanent Magnet Association and the Electrical Research Association.

SUMMARY

From an X-ray examination of slowly cooled CuNiAl alloys, a phase diagram has been constructed. The boundaries of the single-phase, two-phase and three-phase fields have been fixed from powder photographs. A novel feature of the work is the use made of the relative intensities of the X-ray reflexions to estimate the proportions of the constituents in two- and three-phase alloys.

The single-phase fields are derived from the copper-aluminium and nickel-aluminium systems, with the exception of τ (Cu_3NiAl_6), which has a new type of structure, derived from a deformed body-centred cube.

REFERENCES

Alexander, W. O. and Hanson, D. 1937 *J. Inst. Met.* **61**, 83.

Austin, C. R. and Murphy, A. J. 1923 *J. Inst. Met.* **29**, 327.

Bingham, K. E. and Haughton, J. L. 1923 *J. Inst. Met.* **29**, 71.

Bradley, A. J., Goldschmidt, H. J. and Lipson, H. 1938 In the Press.

Bradley, A. J., Goldschmidt, H. J., Lipson, H. and Taylor, A. 1937 *Nature, Lond.*, **140**, 543.

Bradley, A. J. and Taylor, A. 1937a *Proc. Roy. Soc.* A, **159**, 56.

— 1937b *Phil. Mag.* **23**, 1049.

— 1938 *Proc. Roy. Soc.* A, **166**, 353.

Gridnew, V. and Kurdjumow, G. 1936 *Metallwirtschaft*, **15**, 229.

Hansen 1936 "Der Aufbau der Zweistofflegierungen." Springer.

Hisatsune, C. 1934 *Mem. Coll. Sci. Engng Kyoto*, **8**, 74.

Preston, G. D. 1931 *Phil. Mag.* **12**, 980.

Stockdale, D. 1922 *J. Inst. Met.* **28**, 273.

The mechanism of chain breaking in the thermal decomposition of ethane

By J. E. HOBBS AND C. N. HINSHELWOOD, F.R.S.

The decomposition of ethane in the neighbourhood of 600° occurs largely by a chain mechanism in which free radicals are formed. In the course of experiments on the inhibition of the reaction by nitric oxide, Staveley (1937) found that the mean chain length diminished with increasing ethane pressure. From this he reached the conclusion that the chains were broken predominantly by a ternary collision process involving two radicles and an ethane molecule.

The important question whether chains are ended by binary or by ternary collisions can be approached in another way, the exploration of which is described in the following pages.

The reaction rate falls rapidly with increasing concentration of nitric oxide. The nitric oxide is in competition with the normal chain-ending agencies: therefore the form of the curve showing the rate as a function of its concentration, with ethane constant, can provide confirmation of the usual assumption that the chain-breaking process depends upon the square of the radicle concentration. Furthermore, the dependence on the ethane pressure of the constants in the equation for this curve may tell us what part the ethane molecules play in the recombination of the radicals.

The curve has therefore been determined for four different ethane pressures from 50 to 450 mm. The experimental method was the same as that described by Staveley.

The rates given in the tables are unimolecular velocity constants calculated from the directly observed initial reaction rates, and are expressed in sec.$^{-1}$ All measurements were made at 600°. The values of ρ_0 and ρ_∞ in each case are the mean of three concordant determinations.

The measured rates, ρ_0, in the absence of nitric oxide agreed with those given by Staveley: e.g. 24·3 at 100 mm. compared with 24·6, and 25·6 at 450 mm. compared with 21·0. (These are expressed as velocity constants in sec.$^{-1} \times 10^5$.) For the limiting rates, ρ_∞, at higher nitric oxide concentrations the present values are rather higher: e.g. 3·8 at 100 mm. compared with 1·4, and 6·2 at 450 mm. compared with 3·3. This probably means that a residual surface reaction is more in evidence now than in Staveley's

experiments, though it is evident from a difference between the inhibited reaction rates in two of Staveley's tables that a drift was occurring in the course of his experiments. However, neither baking out the reaction bulb with oxygen, nor decomposing acetone vapour in it—a device which sometimes poisons surface reactions—changed our values. The chain length, being fairly long, is sensitive to small changes in ρ_∞: consequently our values are somewhat lower than those given by Staveley, but we still find the characteristic decrease with increasing pressure, upon which he based the conclusion about the mechanism of chain-breaking. The only difference is that we find a variation with an inverse power of the ethane pressure of 0·35 while Staveley gave 0·5. As regards the variation of ρ_∞ with the ethane pressure, we find exactly the same result as Staveley. The occurrence of a small proportion of surface reaction may make some of the numerical values of chain lengths uncertain: it is therefore an advantage that the present method of approach largely eliminates the influence of any surface reaction which may be present.

The theory is as follows: let a be the concentration of the activated ethane molecules which yield radicals, n that of the normal ethane molecules, R that of the radicles or atoms which propagate the chain, and we have in the stationary state:

$$dR/dt = k_1 a - k_2 R^2 n^y - k_5 R[\text{NO}] = 0,$$

whence
$$R = \frac{-k_5[\text{NO}] + \{(k_5[\text{NO}])^2 + 4k_1 k_2 a n^y\}^{\frac{1}{2}}}{2k_2 n^y}.$$

The term $k_2 n^y$ allows for the operation of either binary or ternary recombination mechanisms. a is an unknown function of the ethane concentration, which we will represent approximately by n^x. In addition to the chain reaction there is a rearrangement process the rate of which is $k_3 f_2(n)$ and possibly a surface reaction of rate S. The total rate, ρ, is $k_3 f_2(n) + k_4 Rn + S$, it being assumed that the chain propagating reaction is proportional to the product of the ethane and of the radical concentrations.

$$\rho = S + k_3 f_2(n) + \frac{k_4 n}{2k_2 n^y}[-k_5[\text{NO}] + \{(k_5[\text{NO}])^2 + 4k_1 k_2 n^x n^y\}^{\frac{1}{2}}],$$

when $[\text{NO}] = 0$, rate $= \rho_0$,

$$\rho_0 = S + k_3 f_2(n) + \frac{k_4 n}{2k_2 n^y}\{4k_1 k_2 n^x n^y\}^{\frac{1}{2}}.$$

Let ρ_∞ be the limiting rate when $[\text{NO}]$ is large,

$$\rho_\infty = S + k_3 f_2(n),$$

whence
$$\frac{\rho - \rho_\infty}{\rho_0 - \rho_\infty} = \{(\gamma[NO])^2 + 1\}^{\frac{1}{2}} - \gamma[NO], \tag{1}$$

where
$$\gamma = c[C_2H_6]^{-(x+y)/2}. \tag{2}$$

When ethane is constant γ is also a constant, while for different ethane pressures γ varies according to (2).

Tables I–IV and fig. 1 show that equation (1) is satisfied at a given ethane pressure. In the figure the continuous lines are those calculated from the equation with the values of γ in Table V.

TABLE I. PRESSURE OF ETHANE = 57 MM.

[NO] mm.	ρ sec.$^{-1} \times 10^5$	$(\rho - \rho_\infty)/(\rho_0 - \rho_\infty)$
∞	2·18	0·00
4·08	2·42	0·013
3·44	2·83	0·034
2·76	2·91	0·038
2·00	3·42	0·065
0·916	4·93	0·144
0·381	8·48	0·330
0·206	11·5	0·489
0·0	21·3	1·000

TABLE II. PRESSURE OF ETHANE = 100 MM.

[NO] mm.	ρ sec.$^{-1} \times 10^5$	$(\rho - \rho_\infty)/(\rho_0 - \rho_\infty)$
∞	3·80	0·000
3·75	4·95	0·056
2·61	5·29	0·073
1·77	6·84	0·148
0·95	8·82	0·245
0·84	9·96	0·301
0·53	11·5	0·376
0·30	14·0	0·496
0·15	18·0	0·694
0·00	24·3	1·000

TABLE III. PRESSURE OF ETHANE = 300 MM.

[NO] mm.	ρ sec.$^{-1} \times 10^5$	$(\rho - \rho_\infty)/(\rho_0 - \rho_\infty)$
∞	4·80	0·000
3·54	7·79	0·126
2·07	9·6	0·203
1·62	10·5	0·241
0·97	13·3	0·359
0·46	17·5	0·536
0·35	22·5	0·747
0·00	28·5	1·000

TABLE IV. PRESSURE OF ETHANE = 454 MM.

[NO] mm.	ρ sec.$^{-1} \times 10^5$	$(\rho - \rho_\infty)/(\rho_0 - \rho_\infty)$
∞	6·20	0·000
3·53	10·4	0·223
2·09	12·8	0·339
0·96	16·9	0·552
0·50	19·7	0·696
0·00	25·6	1·000

TABLE V. VALUES OF γ USED IN THE EQUATION

$$(\rho - \rho_\infty)/(\rho_0 - \rho_\infty) = \{(\gamma[NO])^2 + 1\}^{\frac{1}{2}} - \gamma[NO]$$

[C$_2$H$_6$] mm.	γ
57	3·60
100	2·10
300	1·15
454	0·65

TABLE VI. VARIATION OF APPARENT CHAIN LENGTH
WITH ETHANE PRESSURE AT 600°

[C$_2$H$_6$] mm.	Mean chain length
57	9·8
100	6·5
300	5·9
454	4·1

Plotting $\log \gamma$ against $\log [C_2H_6]$, as in fig. 2, we find to what power of the ethane pressure γ is most nearly proportional. The value lies between the limits $-0·73$ and $-0·87$, the best approximation over the range of pressure used being $-0·83$. If the chains were broken by binary collisions, y would be zero and if by ternary y would be unity. To obtain y from the experimental results, we must first find x. x cannot be less than unity since the reaction is unimolecular: it probably lies, as is usual, between one and two. Thus y must be between 0·66 and zero, since it could not be negative. This would suggest a combination of binary and ternary collisions. Now it is only when x is near its lowest limit that the mean chain length decreases with increasing pressure as found experimentally. The apparent chain length being measured by ρ_0/ρ_∞ is

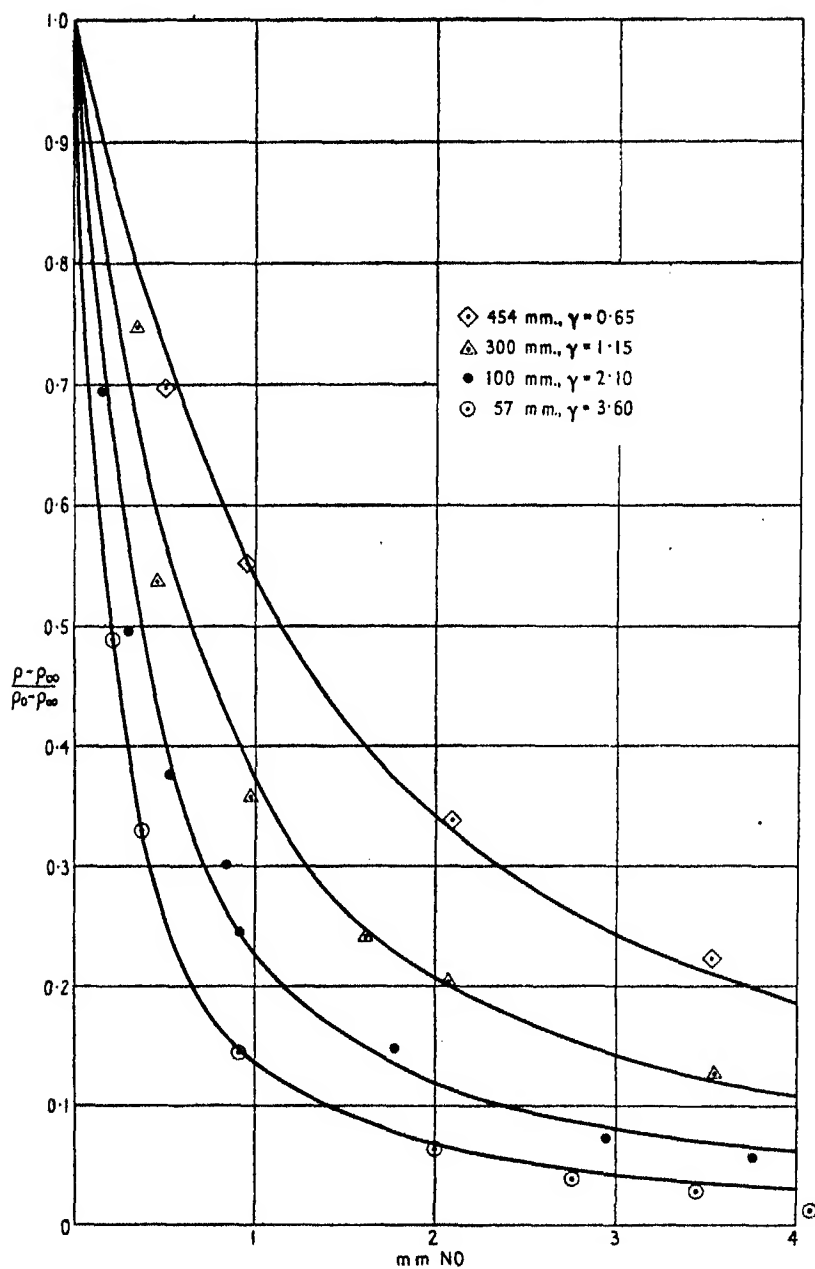$$\rho_0/\rho_\infty = 1 + K \sqrt{\frac{[C_2H_6]^{2+x}}{[C_2H_6]^y \{k_3 f_2(n) + S\}^2}}. \tag{3}$$

Fɪɢ. 1. Inhibition of thermal decomposition of ethane. (Continuous lines are those given by theoretical formula.)

$(S + f_2(n))$, the rate of the inhibited reaction, has been found empirically to be representable over the pressure range in question by an expression with $[C_2H_6]^{1\cdot5}$. Equation (3) then simplifies to

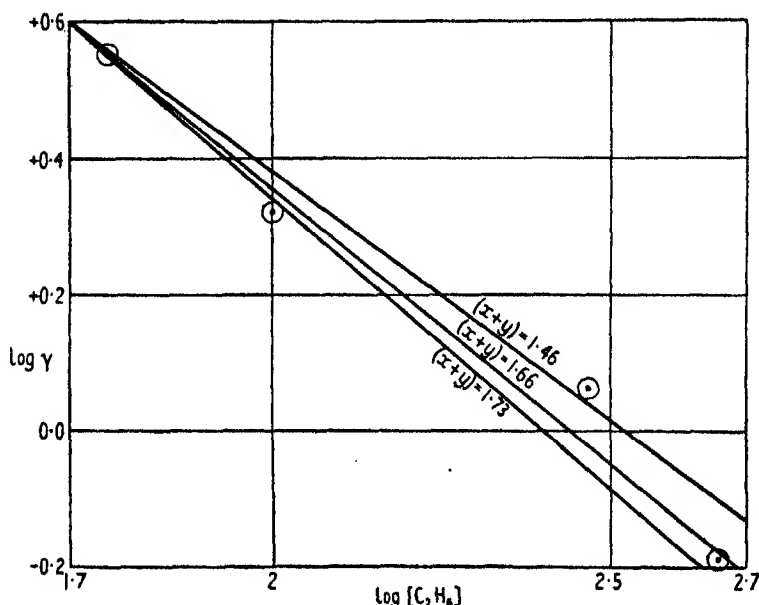$$(\rho_0/\rho_\infty - 1) = constant[C_2H_6]^{(x-y-1)/2}.$$

FIG. 2. Variation of γ with ethane pressure.

We consider first the case where x has its lowest value, unity. Since $x + y = 1\cdot66$, y will be $0\cdot66$, and $(\rho_0/\rho_\infty - 1)$ will vary as $[C_2H_6]^{-0\cdot33}$. The upper and lower limits of the exponent, corresponding to the experimental uncertainty of $x + y$, being $-0\cdot23$ and $-0\cdot36$ respectively. In the present series of measurements $(\rho_0/\rho_\infty - 1)$ varies as $[C_2H_6]^{-0\cdot35}$ with an uncertainty of about $0\cdot1$ in the exponent, for which Staveley gave the value $-0\cdot5$. Thus we see that there is nearly agreement between the observed and predicted variations of chain length. The agreement becomes less good if any other admissible value is assumed for x. Again, if the contribution, S, to the rate from the surface reaction is appreciable, this does not affect the value of γ, and therefore of $x + y$. The mean chain length $(\rho_0 - S)/(\rho_\infty - S)$, however, would decrease with increasing pressure faster than the apparent value, ρ_0/ρ_∞. This could only be accounted for by decreasing x below unity, which is inadmissible. For this reason the values assigned to x and y separately remain the most probable even if there is appreciable surface

reaction. Therefore we take x as unity and y as 0·66. The result $[C_2H_6]^{0·66}$ must be an approximation, justified empirically over the limited range studied, for some expression of composite form.

If there are two independent chain-ending mechanisms, one involving binary collisions and one ternary, then the exact expression should be $k_2 + k_2'[C_2H_6]$, which can be made to vary with ethane pressure in the required way by a suitable choice of the ratio k_2'/k_2. With a value of $1·32 \times 10^{-2}$ for the ratio, when $[C_2H_6]$ is expressed in mm., the linear expression varies in the same way as $[C_2H_6]^{0·66}$, with an average deviation of about 5 %. Thus on this assumption the ratio of ternary to binary collision processes is $1·32 \times 10^{-2}[C_2H_6]$, which is unity at a pressure of 76 mm., the binary processes predominating at lower pressures and the ternary at higher pressures. Since 76 mm. is near the lower limit of the pressure range, this conclusion is in agreement with that reached by Staveley in another way.

There is also the possibility of a single chain-ending process, the order of which depends upon the pressure. If the time between collisions is comparable with the mean life of the activated association product of the radicles, then it is easy to show that the rate of chain breaking will depend upon the ethane concentration according to an expression of the form $[C_2H_6]/(b + [C_2H_6])$, which can also be represented over the range in question by a fractional power of 0·66, if the constant b is assumed to be about 300: the average deviation being about 5 % as before.

In principle it should be possible to distinguish between the two hypotheses by seeing from the curve of $\log \gamma$ against $\log [C_2H_6]$ whether y itself tends towards unity or towards zero at high pressures, but unfortunately the experimental results do not allow this to be done. If there are two kinds of recombination process, then it would be natural to assume, as Staveley did, that the ternary collisions involve hydrogen atoms and the binary organic radicals. If, on the other hand, we have a single recombination process of varying order, then the predominating order below about 300 mm. is ternary with a tendency to become binary at higher pressures. The average life of the activated association product must be of the same order of magnitude as the time between two collisions which it suffers with ethane at 300 mm. and 600°, which is about 5×10^{-10} sec. This assumes that every collision with ethane would deactivate with perfect efficiency, which is open to considerable doubt in view of experiments on the addition of other gases such as nitrogen. 5×10^{-10} sec. is therefore a lower limit. Such a life is high for a pair of hydrogen atoms, but is within the possible range for the association product of a pair of organic radicals, or of an organic radical and a hydrogen atom (cf. Kimball 1937). It may well be that the

first alternative is the more probable for the ethane decomposition, since hydrogen atoms and organic radicals are almost certainly involved, but in simpler reactions, where only alkyl radicals appear, the application of the methods which we have discussed might lead to interesting results about the lives of activated molecules.

SUMMARY

In the decomposition of ethane there are chains which appear normally to be broken by the recombination of radicals, but, in presence of nitric oxide, by reaction between it and the radicals. The equation for the curve showing the rate of reaction as a function of nitric oxide concentration contains constants which depend differently upon the ethane concentration according to the mechanism assumed for the normal recombination of the radicles. Experimental investigation gives evidence that the predominant mechanism for chain ending in the absence of nitric oxide is a ternary collision between two radicals and an ethane molecule, but that binary collisions are also in some degree effective. This result is discussed.·

REFERENCES

Kimball 1937 *J. Chem. Phys.* **5**, 310.
Staveley, L. A. K. 1937 *Proc. Roy. Soc.* A, **162**, 557.

Reaction chains in the thermal decomposition of hydrocarbons. A comparison of methane, ethane, propane and hexane

By J. E. Hobbs and C. N. Hinshelwood, F.R.S.

The inhibition by nitric oxide of the thermal decomposition of ethane at 600° shows that the reaction proceeds partly by a chain mechanism, the apparent chain length, as measured by the ratio of the normal rate to that of the chain-free reaction, being of the order 5–15 over the range of pressure 50–500 mm., and falling with increasing pressure (Staveley 1937; Hobbs and Hinshelwood 1938).

In passing up a homologous series of compounds the chain length may rise or fall. With the series of ethers, for example, it decreases rapidly, whereas with the aldehydes it increases (Staveley and Hinshelwood 1937).

In order to ascertain the behaviour of the hydrocarbons in this respect the investigations with ethane have been extended to include propane and hexane. Some observations on the behaviour of methane have also been made.

PROPANE

The apparatus and general experimental methods were as described by Staveley. The propane was prepared by liquefaction and fractionation of commercial propane, stated to be chemically pure. Propane reacts at a convenient rate at 550°. The products are not simple, and the question arises, as always, how far the rate of pressure change may legitimately be used as a measure of the progress of the reaction. In principle this use would be questionable in the present case, but, for the range of conditions in which we apply it, it is justified empirically in the following way. Between 100 and 300 mm. the pressure-time curves could be brought into almost exact coincidence throughout their course if the pressures were made to correspond at any one point. This shows that the initial rates of pressure change can be used for comparative purposes over this range. The relation between pressure change and propane decomposed might easily vary with the amount of nitric oxide in the system: but the pressure changes after the

completion of the main reaction were the same within about 3 % whether the propane reacted alone or whether enough nitric oxide had been added to cut down the initial rate to one-fifth of the original. In these circumstances it is difficult to believe that the reduction of 80 % in the rate of pressure change is due to anything but a corresponding reduction in the true reaction rate.

In general the results are very similar to those found for ethane. The chain length is slightly greater than that found for ethane under comparable conditions, but the difference is not so great that it may not be due to small uncontrollable changes in these conditions.

The expression which gave the variation of rate with nitric oxide concentration for ethane (Hobbs and Hinshelwood, Staveley *loc. cit.*) is also applicable to propane as shown in the figure.

The chain length increases with decreasing pressure as found for ethane, being approximately proportional to $[C_3H_8]^{-0.5}$. The rate of the fully inhibited reaction over the pressure range investigated can be expressed empirically by a proportionality to $[C_3H_8]^{1.5}$ approximately.

TABLE I. VARIATION OF THE RATE OF PROPANE DECOMPOSITION IN PRESENCE OF NITRIC OXIDE. INITIAL PRESSURE OF PROPANE = 100 MM.

TEMPERATURE 550°

Pressure of nitric oxide mm.	Initial rate ρ	$(\rho - \rho_\infty)/(\rho_0 - \rho_\infty)$
0·000	25·5	1·000
0·278	16·4	0·590
0·475	13·5	0·460
0·878	8·9	0·252
2·02	6·1	0·125
2·81	5·2	0·085
3·75	4·8	0·066
7·20	3·8	—
14·5	3·3	—
24·4	3·35	—
34·4	3·49	—
51·5	4·29	—

The reaction is predominantly homogeneous. Experiments were made in a bulb packed with silica beads (surface/volume ratio twelve times greater than that for the unpacked bulb). At 500 mm. propane pressure the unimolecular velocity constant ($1/p \cdot dp/dt$) of the fully inhibited reaction was increased from $8\cdot9 \times 10^{-5}$ to $9\cdot5 \times 10^{-5}$ sec.$^{-1}$, and at 300 mm. from 6·6 to $7\cdot4 \times 10^{-5}$. The uninhibited reaction, on the other hand, was slower in the packed bulb, at 500 mm. being decreased from 29 to 25×10^{-5} sec.$^{-1}$ and

$[C_3H_8] = 100$ mm.

$$\frac{p-p_\infty}{p_0-p_\infty} = \left([\gamma.NO]^2 + 1\right)^{\frac{1}{2}} - [\gamma.NO]$$

with $\gamma = 2.00$
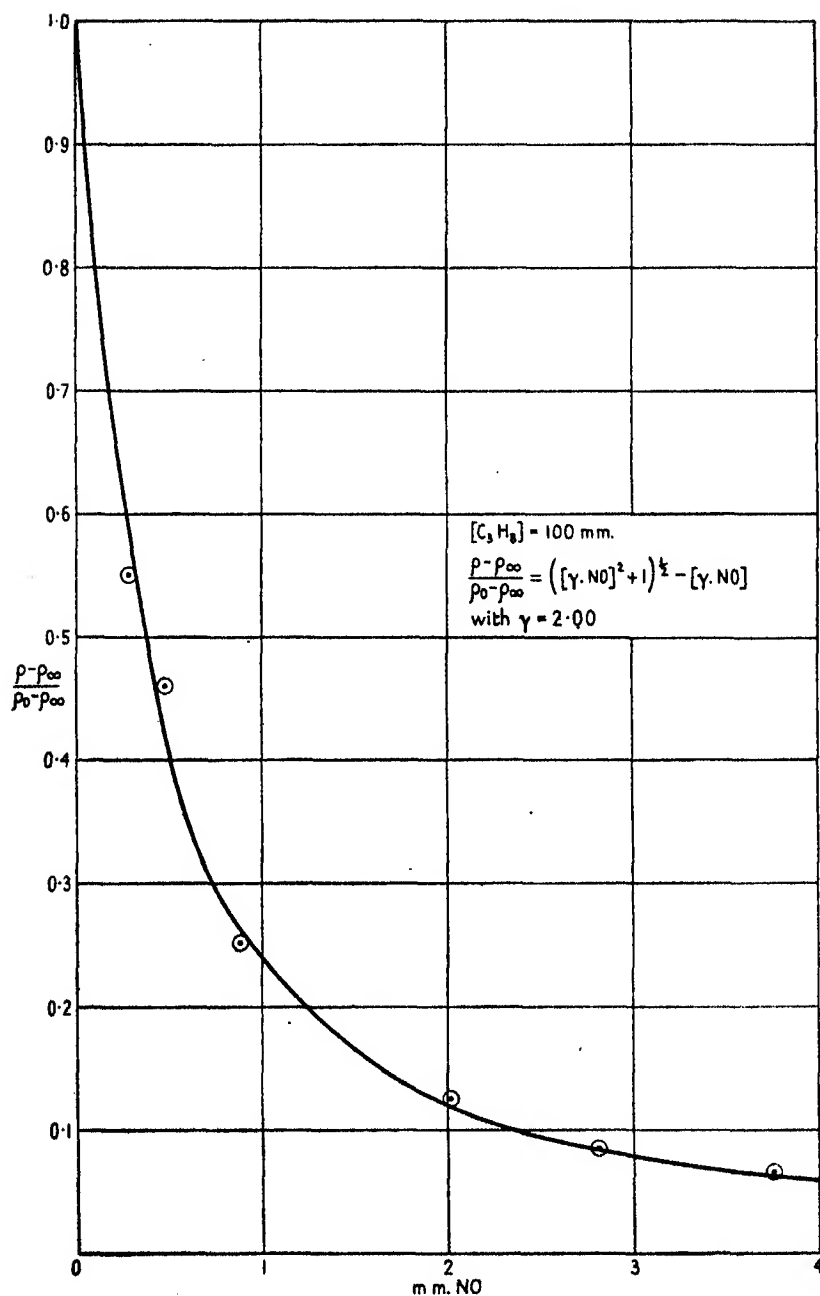
FIG. 1. Inhibition by nitric oxide of the thermal decomposition of propane.
(Continuous line is that given by theoretical equation.)

at 300 mm. from 27 to 21×10^{-5}, an effect attributable to the breaking of chains at the wall of the vessel.

TABLE II. VARIATION OF RATE OF FULLY INHIBITED
REACTION WITH PROPANE PRESSURE

Propane pressure mm.	$k \times 10^5$ (sec.$^{-1}$)
23	1·97
51	2·47
102	3·44
211	5·07
301	6·59
508	8·93

TABLE III. VARIATION OF APPARENT CHAIN LENGTH
(ρ_0/ρ_∞) WITH PROPANE PRESSURE. TEMPERATURE 550°

Propane pressure mm.	Chain length
23	10·1
50	9·9
103	7·5
211	4·9
306	4·1
501	3·3

HEXANE

The hexane was kept as liquid in a small bulb attached to the apparatus, all of which, including the Bourdon gauge, was warmed electrically to a temperature high enough to stop any condensation at the partial pressures used.

According to Dintzes and Frost (1933) the primary decomposition of hexane occurs in two principal ways, to give on the one hand methane and pentylene, and on the other ethane and butylene. The unsaturated compounds then break up further. Our experiments were carried out at 530° where any subsequent decomposition of the ethane is slow and that of the methane is negligible. To render possible certain general conclusions about chain length, we first established, as with propane, that the initial rate of pressure change measured on the Bourdon gauge can be regarded empirically as a measure of the relative reaction rate over the range of conditions used.

The results are similar in general to those found with propane: the inhibi-

tion by increasing amounts of nitric oxide is shown in fig. 2. The mean chain length is lower than that for propane, as shown in Table IV, the values falling as the pressure of hexane increases.

TABLE IV

Pressure of hexane mm.	Mean chain length
60	2·3
100	1·9
200	1·8
350	1·4

TABLE V. VALUES OF $k \times 10^5$ (SEC.$^{-1}$). TEMPERATURE 530°

	Uninhibited reaction		Inhibited reaction	
	Hexane 100 mm.	Hexane 60 mm.	Hexane 100 mm.	Hexane 60 mm.
Packed vessel	20	17	19·7	16·5
Unpacked vessel	35	31	18·2	13·6
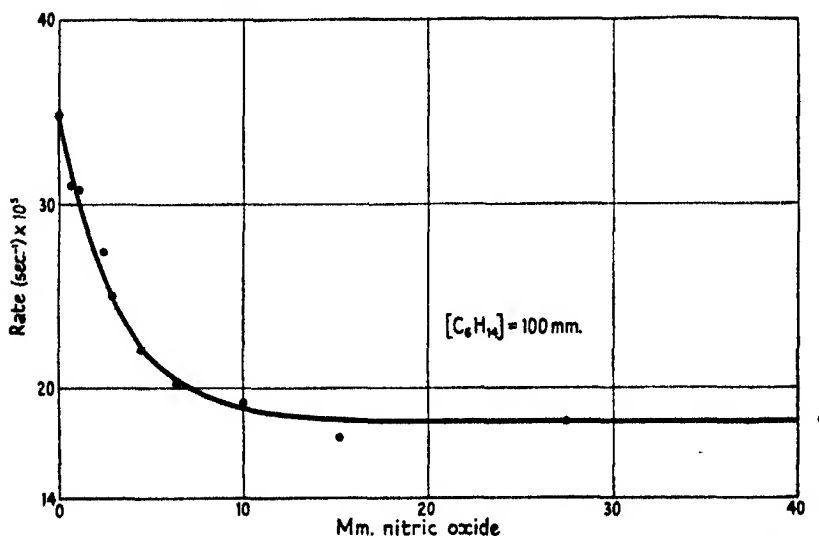
FIG. 2. Inhibition by nitric oxide of the thermal decomposition of hexane.

The variation is expressed approximately by Chain length $= c[C_6H_{14}]^{-0.8}$. The rate of the fully inhibited reaction varies as $[C_6H_{14}]^{1.5}$ approximately. The absolute rates found for the uninhibited reaction are in agreement with those found by other observers.

The results obtained by the use of a packed reaction vessel are of interest. The inhibited reaction is very little changed, showing that the reaction is homogeneous. The uninhibited reaction, on the other hand, is quite appreciably slowed down, showing that here the walls have a considerable influence in breaking the chains.

METHANE

The decomposition temperature of methane is much higher, and we expected that no definite results would be obtainable, since nitric oxide would react rapidly with methane itself, or at least with the hydrogen produced in the reaction. It proved possible, however, to obtain quite definite evidence of the occurrence of chains.

The methane was prepared from a natural gas containing over 90 % methane. This was freed from oxygen by pyrogallol, from hydrogen and carbon monoxide by passage over copper oxide heated to 350°, and then condensed at the temperature of liquid nitrogen. The condensate was fractionated until it showed the vapour pressure of methane, when a fraction was collected for use. Different preparations showed the same reaction velocity.

At 780° the decomposition was very slow, and the rate could only be reduced by about 15 % on addition of nitric oxide. This shows that the results at higher temperatures where inhibition is found can hardly be attributed to contamination with lower hydrocarbons.

Most of the experiments were made at 850°, where Kassel (1932) found a rate which is comparable with that of the ethane, propane and hexane reactions under the conditions of our previous measurements. Here the inhibition by nitric oxide is considerable.

Nitric oxide reacts with methane and, if the experiment is prolonged, the inhibition initially observed disappears and the rate rises to its normal value as shown in fig. 3. The disappearance, however, is not rapid enough to affect the initial rate measured on the Bourdon gauge. With increasing amounts of nitric oxide the initial rate falls to a minimum, but instead of remaining constant as with the other hydrocarbons (cf. figs. 1, 2) rises again rather steeply, owing to the increasing speed of the oxidation reaction between nitric oxide and methane, or possibly in some degree to a catalytic reaction. This is shown in fig. 4.

The rising part of the curve is nearly linear and may be extrapolated back, so that a correction may be applied to all the values on the falling part. In this way the value to which the rate would fall if there were no oxidation

or catalytic reaction can be found and the mean chain length calculated in the usual way. The value found is 4·7 at 100 mm. methane and 2·9 at 200 mm., varying thus approximately as $[CH_4]^{-0·7}$.
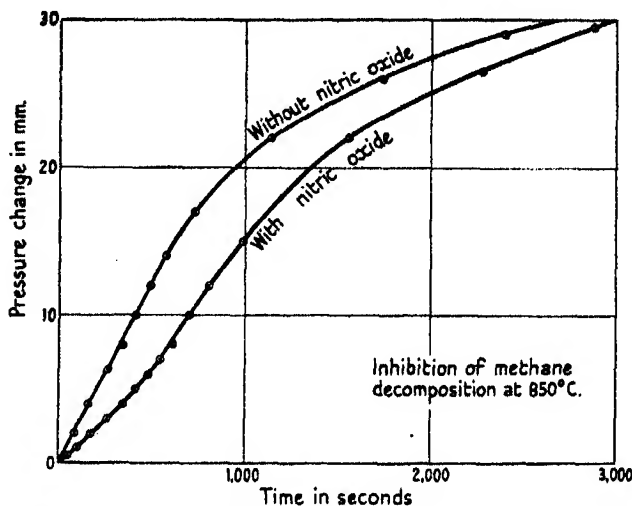

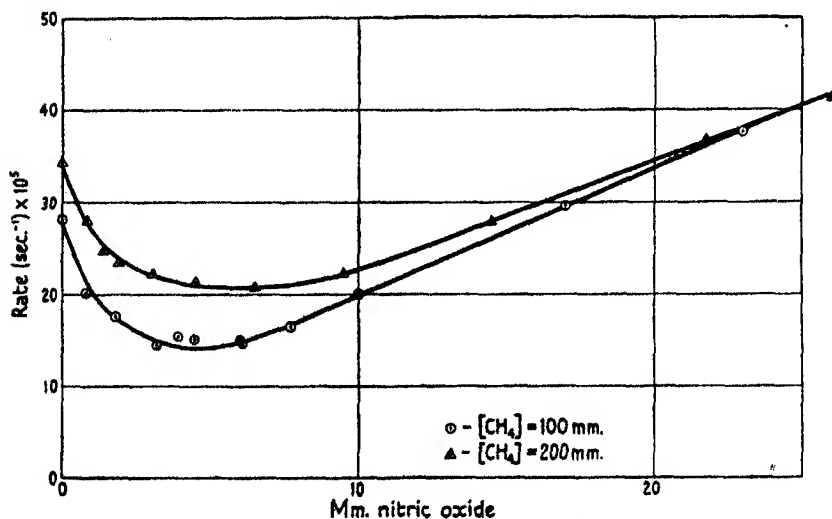FIG. 3. Inhibition by nitric oxide of the thermal decomposition of methane.

FIG. 4. Influence of nitric oxide on the rate of decomposition of methane at 850°.

The corrected curve can be expressed quite well by the usual formula (preceding paper, p. 441), but, in view of the indirect way in which it has to be obtained, no detailed deductions from the value of γ will be made.

TABLE VI. INITIAL PRESSURE OF METHANE = 100 MM. TEMPERATURE 850°

Pressure of nitric oxide mm.	0	0·77	1·77	3·2	3·9	4·6	6·1	7·7	10	17	23
$k \times 10^5$ sec.$^{-1}$		28·1	20·2	17·6	14·5	15·4	15·1	14·6	16·5	20·0	29·6	37·6

The formula of Kassel (*loc. cit.*) gives $k \times 10^5 = 26$ at 850°.

INITIAL PRESSURE OF METHANE = 200 MM. TEMPERATURE 850°

Pressure of nitric oxide mm.	0	0·85	1·40	1·9	3·1	4·5	6·5	9·5	14·5	22·0	26·0
$k \times 10^5$ sec.$^{-1}$		34·4	28·0	24·9	23·5	22·2	21·3	20·8	22·3	27·9	34·7	41·2

DISCUSSION

The mean chain length, as defined conventionally by ρ_0/ρ_∞, exhibits no marked trend on passing up the series from methane to hexane. It tends always to decrease as the pressure rises, usually depending upon a power of the pressure in the neighbourhood of -0.5. Detailed consideration of the case of ethane shows that this can be explained by assuming both binary and ternary collisions to play a part in the recombination of the radicles. Taking the results as a whole, they show that the reactions of the different hydrocarbons are built upon a rather constant plan.

Comparing the actual values of the mean chain lengths recorded in this and in the previous paper minor variations are, however, evident, the values for ethane and propane being greater than those for methane and hexane. The explanation is that the chain lengths depend upon three independently varying activation energies, those namely of radical formation, of the competing rearrangement process and of the chain propagation process (Staveley and Hinshelwood 1937). In the case of hexane, for example, the low mean chain length can plausibly be attributed to the fact that the competing rearrangement process has a low activation energy relatively to the radicle formation. A given value of the mean chain length may represent either a few long chains or many short ones. Which occur depends again upon the relative values of different activation energies. An approximate method (Staveley and Hinshelwood 1936) can be used for calculating the activation energy of the propagation process. Applied to the various results given above it yields for methane circa 10,000, for ethane 10,000, for propane 9000 and for hexane 6000. The lower value for hexane is essentially an expression of the fact that more nitric oxide is required to produce a given degree of inhibition with hexane than with the others. It leads us to expect that the relatively few chains starting should have

a considerably greater absolute length. This may explain why hexane is more sensitive than the others to the retarding influence of the vessel walls.

An incidental point of interest is that with ethane, propane and hexane the rates of the inhibited reaction vary over a certain range of about 400–50 mm. approximately as the 1·5th power of the pressure. This is probably due to the fact that in all three cases the curve has been determined in a region where the usual transition from first order to second order is occurring. On this view the three halves power would have no great significance. On the other hand, the three halves power law is itself followed by certain chain reactions, and one is led to wonder whether the residual inhibited reaction could itself depend upon a special kind of chain with carriers immune from the attack of nitric oxide. In view of the variety of reactions which nitric oxide effectively inhibits, one is reluctant to entertain such an hypothesis without other evidence, of which at present there is none.

SUMMARY

A comparison has been made of the inhibition by nitric oxide of the thermal decomposition of methane, ethane, propane and hexane. The mean chain length, as defined by the ratio of the rates of the uninhibited and fully inhibited reactions, shows no marked variation as the series is ascended, has values from 2 to 15 according to conditions, and, for a given hydrocarbon, decreases as the initial pressure increases. The curves showing the decrease in rate as a function of nitric oxide concentration can be expressed in terms of a simple theory of chain breaking. The mean chain length depends upon the relative values of three activation energies, namely those of radicle formation, of decomposition by internal rearrangement, and of chain propagation. Approximate evaluation of the last shows that it tends to decrease with the higher hydrocarbons.

REFERENCES

Dintzes, A. I. and Frost, A. V. 1933 *J. Gen. Chem. Russ.* 3, 747.
Hobbs, J. E. and Hinshelwood, C. N. 1938 *Proc. Roy. Soc.* A, 167, 439.
Kassel, L. S. 1932 *J. Amer. Chem. Soc.* 54, 3949.
Staveley, L. A. K. 1937 *Proc. Roy. Soc.* A, 162, 557.
Staveley, L. A. K. and Hinshelwood, C. N. 1936 *Proc. Roy. Soc.* A, 154, 335.
—— —— 1937 *J. Chem. Soc.* p. 1568.

A study of the chain reaction in the thermal decomposition of diethyl ether

By J. E. HOBBS

Trinity College, Oxford

In a recent paper (Hobbs and Hinshelwood 1938), information about the chain mechanisms involved in the thermal decomposition of ethane was obtained by studying the variation with the ethane concentration of the shape of the curve which represents the reduction in reaction rate as a function of minute quantities of added nitric oxide. This paper describes the results of a similar investigation carried out with diethyl ether, the behaviour of which shows an interesting contrast with that of ethane.

* *Notes by the Communicator:*

(1) This work is the natural continuation of the work of Staveley and Hinshelwood (1936, 1937) and of Hobbs and Hinshelwood (1938) on the chain processes involved in the decomposition of ether and of ethane respectively. The clear contrast which now emerges between the mechanism of chain breaking in the ether reaction and that in the reactions of the hydrocarbons necessitates the revision of one of the incidental calculations made by Staveley and Hinshelwood, who, from the amount of nitric oxide required to reduce the rate to a given fraction of its initial value deduced the probability of reaction and hence an energy of activation for the encounter between the chain propagating particle and the ether. This calculation, legitimate for e.g. ethane, should for ether be replaced by that given in the present paper, which leads not to a probability of reaction between radical and ether, but to the probability of spontaneous decomposition of one of the radicals.

(2) Confusion has arisen in some quarters about the relation between the inhibiting action of minute quantities of nitric oxide and the oxidation reactions which can occur with large quantities. It has been suggested (*a*) that the oxidation reactions mask or distort the pressure changes due to the normal decomposition and (*b*) that the oxidation reactions make it impossible to say whether the rate reaches a true limit with increasing nitric oxide concentration (cf. *Ann. Rep. Chem. Soc.* 1937, p. 47). With regard to (*a*) it may be pointed out that a few tenths of a millimetre of nitric oxide can very markedly reduce the rate of decomposition of 400 mm. ethyl ether over its whole course. It is impossible that one substance should stoicheiometrically affect 1000 times its own amount of another in the way implied by this criticism. With regard to (*b*) it should be pointed out again that with ether, for example, the rate falls rapidly to a limit over the range 0–1·0 mm. after which it remains steady for at least ten times this range, and later rises again slowly. The long steady region is quite unlike a mere minimum—as reference to published diagrams will show.

Finally, it may be observed that chemical reactions at higher pressures of nitric oxide with ethers, hydrocarbons and other substances are in no way inconsistent with the chain theories which themselves postulate the breaking of chains by reactions

The thermal decomposition of diethyl ether in the neighbourhood of 500° C. occurs partly by a chain mechanism in which free radicals are formed, and partly by intramolecular rearrangement (Staveley and Hinshelwood 1936, 1937). The end-products of the decomposition are methane, ethane, and carbon monoxide, with small amounts of hydrogen and unsaturated substances. Acetaldehyde is an intermediate product formed either in the rearrangement process, or, as in the mechanism put forward below, during the chain reaction (Fletcher and Rollefson 1936). The acetaldehyde, however, decomposes rapidly under the experimental conditions and the initial rate is sensibly that of the decomposition of the ether into the final products.

The decomposition of the ether is inhibited by nitric oxide, the rate falling rapidly to a steady limit with increasing concentration of the inhibitor. The mean chain length, as defined by the ratio of the uninhibited and fully inhibited reactions, is independent of the ether pressure: this also applies to the other members of the ether series. The mean chain lengths for the hydrocarbons, however, decrease as the pressure of the hydrocarbon increases: the average variation being as the -0.5 power of the hydrocarbon concentration. The reason for this difference between the two series is made clear in the present investigation.

The "inhibition curve" for diethyl ether has been determined at 504° C. for four different ether pressures from 50 to 400 mm. The experimental method was the same as that described by Staveley (1937).

The rates given in the Tables are initial reaction rates expressed in mm./sec. The values of ρ_0 and ρ_∞ in each case are the mean of at least three concordant determinations. The unimolecular velocity constant of the uninhibited reaction at 400 mm. and 504° C., calculated from the time for 50 % increase in pressure, is 28.3×10^{-5} sec.$^{-1}$. This is in fair agreement with the value 34.6×10^{-5} sec.$^{-1}$ extrapolated from the results of Hinshelwood (1927) for the limiting rate at high pressures and the same temperature.

The values of $(\rho - \rho_\infty)/(\rho_0 - \rho_\infty)$ have been calculated for each ether pressure and are plotted against the nitric oxide concentration in fig. 1. The

of nitric oxide with certain radicals. The whole point lies in the magnitude of the effect which minute amounts of nitric oxide can exert: this is the essential factor which distinguishes a chain reaction from any other type.

The clear-cut quantitative result of the present paper, revealing a distinction in detailed mechanism between ether and ethane, in entire accord with independent evidence, provides additional proof that the chain breaking theory of the action of nitric oxide is adequate, and that the experimental methods employed are quantitatively as well as qualitatively sound.

<div align="right">C. N. H.</div>

TABLE I. PRESSURE OF ETHER = 51 MM.

NO (mm.)	ρ mm./sec. $\times 10^3$	$(\rho - \rho_\infty)/(\rho_0 - \rho_\infty)$
0·00	10·55	1·000
0·15	5·10	0·357
0·30	4·49	0·285
0·46	3·19	0·131
0·78	3·14	0·125
∞	2·08	0·000

TABLE II. PRESSURE OF ETHER = 103 MM.

NO (mm.)	ρ mm./sec. $\times 10^3$	$(\rho - \rho_\infty)/(\rho_0 - \rho_\infty)$
0·000	29·9	1·000
0·115	16·8	0·458
0·127	17·4	0·484
0·276	12·9	0·298
0·415	10·1	0·182
0·550	8·35	0·109
0·795	7·42	0·071
0·935	7·52	0·075
1·020	6·55	0·035
∞	5·70	0·000

TABLE III. PRESSURE OF ETHER = 200 MM.

NO (mm.)	ρ mm./sec. $\times 10^3$	$(\rho - \rho_\infty)/(\rho_0 - \rho_\infty)$
0·000	68·0	1·000
0·040	41·4	0·488
0·121	37·6	0·415
0·202	29·8	0·265
0·409	23·6	0·146
0·582	20·6	0·088
0·765	17·4	0·027
1·120	19·6	0·069
∞	16·0	0·000

TABLE IV. PRESSURE OF ETHER = 400 MM.

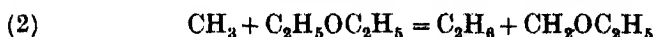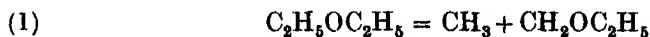| NO (mm.)	ρ mm./sec. $\times 10^2$	$(\rho - \rho_\infty)/(\rho_0 - \rho_\infty)$
0·000	20·40	1·000
0·069	14·16	0·613
0·150	12·96	0·538
0·265	8·96	0·289
0·352	7·00	0·167
0·450	6·48	0·134
0·553	6·52	0·137
0·703	6·00	0·104
0·933	4·84	0·032
∞	4·32	0·000
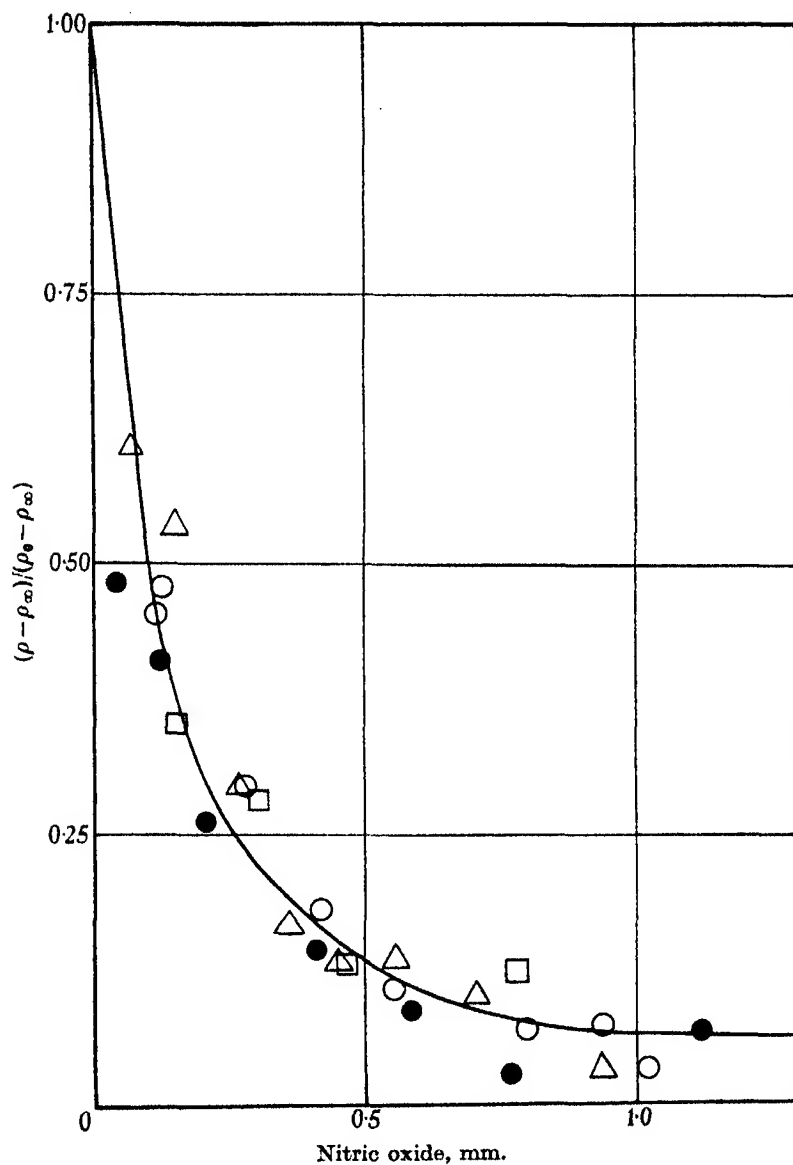
FIG. 1. Showing that the course of the "inhibition curve" is independent of the pressure of diethyl ether. □ 51 mm. of ether; ○ 103 mm. of ether; ● 200 mm. of ether; △ 400 mm. of ether.

important result is that the points for all the different ether concentrations lie on one single curve.

This result is strikingly different from that obtained with ethane where a series of separate curves are found, the amount of nitric oxide required for a given degree of inhibition increasing steadily with the ethane pressure. With ethane the course of the curve is determined by the relative probability with which a radical is either removed by a molecule of nitric oxide or can attack an ethane molecule for the continuation of the chain. The amount of nitric oxide required to bring about the same degree of inhibition (i.e. to give the same value of $(\rho - \rho_\infty)/(\rho_0 - \rho_\infty)$) thus increases as the concentration of the ethane increases. Here, however, we find that, whatever the pressure of the ether, the amount of nitric oxide required to produce a given degree of inhibition is always the same. The removal of the radical by the nitric oxide thus appears to be in competition with some reaction, the rate of which is quite independent of the concentration of the ether. Since experiments with a tube-packed reaction bulb show that the radicals are not to any serious extent removed on the surface of the bulb, the only possible reaction of this type is a unimolecular dissociation of the radical itself.

A chain mechanism is required that will take this into account, and we find that the only one likely contains just that same process for the normal mechanism of chain breaking as was postulated by Rice and Herzfeld (1934) to explain the first order nature of the total decomposition.

The mechanism proposed is as follows:

(1) $$C_2H_5OC_2H_5 = CH_3 + CH_2OC_2H_5$$

(2) $$CH_3 + C_2H_5OC_2H_5 = C_2H_6 + CH_2OC_2H_5$$

(3) $$CH_2OC_2H_5 = CH_3 + CH_3CHO$$

(4) $$CH_3 + CH_2OC_2H_5 = Product.$$
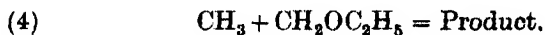
Reaction (4) is the normal chain process. In the presence of nitric oxide chain breaking occurs also by the reaction:

(5) $$NO + CH_2OC_2H_5 = Product.$$
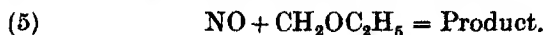
For the remainder of this discussion, in order to make it more general, the large radical, $CH_2OC_2H_5$, which is removed by the nitric oxide, will be called S, the small radical, CH_3, which reacts with the ether, will be called R, and the ether will be called A.

The contrasted behaviour of ethane and ether is due to the fact that in the reaction of the former the nitric oxide removes the radical corresponding

to R, while in that of the latter it must be assumed to remove the radical S, which does not itself propagate chains until it has suffered a decomposition.

It is interesting to note that the combination of this heavy radical S with the small radical R for chain breaking was found necessary by Rice and Herzfeld to explain the variation with the pressure of the rate of the uninhibited reaction. If this is the predominant method of chain breaking in the uninhibited reaction, then the radical R must react with the ether rapidly compared with the rate of decomposition of S, and the concentration of S in the system will be large compared with that of R. The nitric oxide, which attacks the chain at its most vulnerable point, will thus tend to remove S to a greater extent than it will remove R, and reaction (5) is more important than the corresponding process:

(6) $$NO + R = \text{Product.}$$

Apparently, however, in the ethane decomposition the radical corresponding to R attains an appreciable concentration in the system and chains are broken predominantly by the combination of two such radicals, or by the removal of one of them by nitric oxide when the latter is present.

The further development of the theory is as follows, in the stationary state:

$$d[R]/dt = k_1[A] + k_3[S] - k_2[R][A] - k_4[R][S] = 0,$$

$$d[S]/dt = k_1[A] + k_2[R][A] - k_3[S] - k_4[R][S] - k_5[S][NO] = 0.$$

Here we have assumed that the rates of dissociation of the diethyl ether, A, and of the large radical, S, are directly proportional to the first power of their concentrations; this is essential if the rate of the chain reaction as a whole is to be unimolecular with respect to the ether concentration.

From the above equations we have:

$$[R] = \frac{-k_2 k_5[NO] + [(k_2 k_5[NO])^2 + 8k_2 k_4(k_1 k_5[NO] + 2k_1 k_3)]^{\frac{1}{2}}}{4k_2 k_4}.$$

In addition to the chain reaction there is a rearrangement process and possibly a surface reaction, the joint rate of which may be written $k'f(A)$. The total rate is then

$$\rho = k'f(A) + k_2[R][A],$$

it being assumed that the chain propagating reaction is proportional to the ether and radical concentrations.

$$\rho = k'f(A) + \frac{k_2[A]}{4k_2 k_4} \{[(k_2 k_5[NO])^2 + 8k_2 k_4(k_1 k_5[NO] + 2k_1 k_3)]^{\frac{1}{2}} - k_2 k_5[NO]\}.$$

When NO = 0, rate = ρ_0

$$\rho_0 = k'f(A) + \frac{k_2[A]}{4k_2k_4}(16k_1k_2k_3k_4)^{\frac{1}{2}}.$$

The rate of the uninhibited chain reaction, $[A](k_1k_2k_3/k_4)^{\frac{1}{2}}$ is thus proportional to the first power of the ether pressure.

ρ_∞ is the limiting rate when [NO] is large, then

$$\rho_\infty = k'f(A),$$

and

$$(\rho - \rho_\infty)/(\rho_0 - \rho_\infty) = \frac{[(k_2k_5[NO])^2 + 8k_2k_4(k_1k_5[NO] + 2k_1k_3)]^{\frac{1}{2}} - k_2k_5[NO]}{4(k_1k_2k_3k_4)^{\frac{1}{2}}}$$

$$= [(\alpha[NO])^2 + \beta[NO] + 1]^{\frac{1}{2}} - \alpha[NO], \qquad (a)$$

where

$$\alpha = k_2k_5/4(k_1k_2k_3k_4)^{\frac{1}{2}}$$

and

$$\beta = k_5/2k_3$$

$(\rho - \rho_\infty)/(\rho_0 - \rho_\infty)$ is thus independent of the concentration of the ether.

In equation (a) the term $\beta[NO]$ is found from comparison with the experimental results to be very small and so can be neglected in this case. The continuous line in fig. 1 is calculated from the equation

$$(\rho - \rho_\infty)/(\rho_0 - \rho_\infty) = [(\alpha[NO])^2 + 1]^{\frac{1}{2}} - \alpha[NO].$$

using $\alpha = 7\cdot4$.

This mechanism for the chain reaction also explains the variation with the ether concentration of the mean chain length. The latter is given by

$$\rho_0/\rho_\infty = \frac{k'f(A) + [A](k_1k_2k_3/k_4)^{\frac{1}{2}}}{k'f(A)}.$$

Staveley and Hinshelwood (1936) found that the rate of the uninhibited reaction, $k'f(A)$, was of the first order with respect to the ether concentration, so that the above expression shows that the mean chain length is independent of the ether concentration.

The difference between the ether and ethane reactions is now quite clear. In the latter case the course of the inhibition curve depends on the probability with which a nitric oxide molecule removes the chain-propagating radical before this reacts with a molecule of ethane. As we should expect, this is dependent upon the ethane concentration. On the other hand, in the former case the course of the curve depends upon the probability with which a radical, S, is removed by nitric oxide before it dissociates. Since this depends only upon the mean life of S and the concentration of nitric oxide it is understandable why the curve is independent of the ether pressure.

The amount of nitric oxide required for half inhibition must be such that there is an equal chance for the radical S to decompose and to meet a nitric oxide molecule. The mean life of S is thus comparable with the time between its collisions with nitric oxide molecules at the pressure corresponding to this point. The amount of nitric oxide required for half inhibition is 0.1 mm. If we identify S with the complex $CH_2OC_2H_5$, then its average life is of the same order as the time between two collisions that it suffers with nitric oxide at 0.1 mm. and $504°$ C. which is 1.2×10^{-6} sec. This value is within the possible range for a large complex of this type.

The author is grateful to Professor Hinshelwood for much valuable advice in connexion with this work.

Summary

The course of the curves showing the rate of decomposition of diethyl ether as a function of minute additions of nitric oxide is independent of the concentration of diethyl ether. The removal of a radical must thus be in competition with some reaction the rate of which is entirely independent of the ether concentration. This must be a unimolecular dissociation of the radical itself. This is in contrast to the inhibition of the decomposition of ethane where the nitric oxide removes a radical which otherwise would have reacted with an ethane molecule. A chain mechanism explaining these results is the same as that put forward by Rice and Herzfeld (1934) to explain the first order nature of the reaction. This mechanism gives an expression for the shape of the "inhibition curve" and accounts for the variation of the mean chain length with the ether pressure. From the amount of nitric oxide required for a given degree of inhibition the average life of the radical can be calculated to be of the order of 1.2×10^{-6} sec.

References

Fletcher and Rollefson 1936 *J. Amer. Chem. Soc.* **58**, 2129.
Hinshelwood 1927 *Proc. Roy. Soc.* A, **114**, 84.
Hobbs and Hinshelwood 1938 *Proc. Roy. Soc.* A, **167**, 439.
Rice and Herzfeld 1934 *J. Amer. Chem. Soc.* **56**, 284.
Staveley 1937 *Proc. Roy. Soc.* A, **162**, 557.
Staveley and Hinshelwood 1936 *Proc. Roy. Soc.* A, **154**, 335.
—— — 1937 *Proc. Roy. Soc.* A, **159**, 192.

The posterior probability distributions of the ordinary and intraclass correlation coefficients

By Harold Jeffreys, F.R.S.

1. The accurate form of the probability distribution of an estimated correlation coefficient in a sample, the true correlation being taken as a datum, has been given by Fisher in two well-known papers (1915, 1921). Pearson and others (1917) have studied the adaptation of the formula, which is rather complicated, for numerical work, but a transformation suggested by Fisher in his earlier paper and applied in his later one offers great advantages. The present paper deals with the inverse problem: given the estimate from a sample, what is the probability distribution of the true value, the latter being supposed initially unknown?

Much of the mathematics of correlation depends on the hypothesis of the normal correlation surface. As this is a generalization of the normal law of error for one variable, it is subject to similar criticisms. It can be derived from the hypothesis that the two variables considered are subject to a number of independent component disturbances, m of which affect both in the same sense and n in opposite senses (Jeffreys 1935, pp. 213–17). If they are all equal in amount, then even if m and n are fairly small they lead to a good approximation to the normal correlation surface with correlation $(m-n)/(m+n)$. We could regard $m/(m+n)$ as a frequency to be estimated from a sample, and such frequencies are taken, in the absence of special knowledge, as having their prior probabilities uniformly distributed. The idea of the normal correlation surface therefore suggests that we should take the prior probability of the correlation coefficient as uniformly distributed between -1 and $+1$.

The intraclass correlation coefficient, also studied by Fisher, arises when we have a number of classes of k members each. If there is a component variation common to all members of a class, with variance τ^2, and superposed on it is a random variation with variance σ'^2, the ratio of the two can be estimated from the ratio of the variation of the class means to that of the whole sample. In the case $k=2$, the expectation of the squared difference between members of the same pair is $2\sigma'^2$, between members of different pairs $2(\sigma'^2+\tau^2) = 2\sigma^2$. By analogy with the simple correlation coefficient

we may introduce a correlation ρ, and if x and y are members of the same pair

$$E(x-y)^2 = E(x^2) + E(y^2) - 2E(xy)$$

$$= 2(1-\rho)\,\sigma^2,$$

and also $\qquad\qquad\qquad = 2\sigma'^2,$

whence $\qquad\qquad\qquad \rho = \tau^2/\sigma^2.$

The last relation provides a definition of ρ even when there are many members in each class. For if there are k observations in each group, σ and τ will retain their meanings, and it would still be a valid procedure to pick two members at random out of each group, and for these the same argument will hold; thus we can agree always to define ρ as meaning τ^2/σ^2, which has a meaning independent of the number of groups and of the number of observations per group. The intraclass correlation coefficient cannot be negative.

Brunt (1931, p. 171), following Kapteyn, analyses the meaning of the correlation coefficient in general by regarding m as the number of component disturbances common to x and y, while n are independent. The correlation ρ would then be equal to $m/(m+n)$, and could be interpreted as a ratio to be estimated by sampling, with its prior probability uniformly distributed between 0 and 1. This appears to be a valid analysis of the intraclass correlation. Thus in the correlation of height between brothers it may be supposed that there is an inherited part common to both, on which random differences due to segregation are superposed. Negative values are excluded; but if the common components all produced opposite effects on x and y we could deal similarly with negative correlations. If it was known that all common components either produced effects with the same sign, or all with opposite signs, but it was unknown which, we should again have the prior probability uniform between -1 and $+1$, and the result would become equivalent to mine for simple correlation. The correlation between brothers, however, is a typical one, and Brunt's analysis as it stands is sufficient. We should therefore expect a close parallel between the ordinary and intraclass coefficients.

The rule suggested is intended as a pure statement of initial ignorance of the value of the correlation, in either case, suggested by the idea of the conditions for the normal correlation surface to be a valid approximation. It is emphatically not asserted that all correlations in the world are uniformly distributed in frequency; this would suppose our work finished, and our problem is to show how it can begin. Some of the writings even of Pearson

(1917, pp. 353–60) show this confusion. He appears to suppose that the uniform distribution of prior probability cannot be used unless previous correlations have been found uniformly distributed; but without some way of saying how we can proceed from a sample to an estimate of a true value, without previous knowledge of the latter, there would be no way of ever estimating even one correlation. Deductive logic is inadequate for the purpose, and additional rules are necessary. The problem is to state these in such a way that they will involve the minimum number of independent postulates, be sufficiently general to cover the actual needs of learning from experience, and be consistent; but to identify a statement of ignorance with one of complete knowledge is to miss the point completely. Most modern statisticians, quite correctly, reject the idea of the statement of complete knowledge, but unfortunately appear to consider it a requisite of the principle of inverse probability, which it is not. Bayes, in his memoir of 1763, repeatedly says that the uniform distribution of the prior probability of a chance is intended only for the case where we have no previous information whatever about what the chance is. Laplace says (1820, Introduction, p. 142): "The theory of probability is at bottom only good sense reduced to calculation; it exhibits with accuracy what reasonable minds feel by a kind of instinct, without often being able to describe it to themselves." I can find nothing in the works of the pioneers of the principle of inverse probability to suggest that they identified the prior probability with a known frequency, and believe that if such an idea had occurred to them they would have repudiated it as definitely as I do. The function of a prior probability used to express ignorance is simply to express formally the transition from an inference about different possible data, given the same hypothesis, to one about different hypotheses given the same data, and this transition must be made somehow on any theory. It is usually apparently made unconsciously or else made to rest on a prediction of frequency in the long run by Bernoulli's theorem, the application of which is often open to grave suspicion since it rests on a dubious postulate of irrelevance. Apart from mere reduction of the standard error by multiplying observations, the whole of scientific progress reduces to the discovery of cases where Bernoulli's theorem has been found inapplicable. The principle of inverse probability is the only method that treats the transition formally and gives a clear statement of the information given by a unique and known sample about a definite set of hypotheses.

It is to be expected that the ignorance expressed by the uniform distribution of prior probability will be partially dispelled by actual determinations, and these may legitimately be used to reassess the prior probability to be

used at more advanced stages of knowledge; if, for instance, a concentration of values about a particular one is found in any subject. But a very strong concentration is needed if the correction is to have any important effect on the posterior probability when the number of immediately relevant observations is large enough to give much information by itself. The rule will enable us to find out what the particular sample says about the true value; other information can be used in addition if there is any, but we cannot provide for it in advance. Thus Pearson remarks on the tendency of correlations between brothers to collect about $+0.5$; that could be taken into account now, but it was not known and could not have been taken into account when such correlations were first investigated. In meteorology, on the other hand, significant correlations seem to be very evenly distributed over the whole possible range, and there is little need for revision. Even if there is a concentration, it does not provide completely against possible exceptions, and a significance test may be needed to decide whether a remarkably high or low correlation is consistent with the usual one, before we can treat information about the usual one as relevant to it.

There may, again, be a dominant component variation; in that case the whole idea of the normal correlation surface in inapplicable. This is what happens in a physical law, where nearly the whole variation of one parameter may be linearly related to that of the other, which may have a uniform distribution within the range of the experiment. But I think that the normal correlation surface is a valid approximation in the cases where methods of correlation are actually used. The fitting of a linear approximation by least squares would represent the opposite extreme.

2. *Interclass correlation.* Let us suppose that the variation is represented by a normal correlation surface about zero, the probability of a pair of observations, given the law, being

$$P(dx\,dy \mid \sigma_1\sigma_2\rho h) = \frac{1}{2\pi\sigma_1\sigma_2(1-\rho^2)^{\frac{1}{2}}} \exp\left[-\frac{1}{2(1-\rho^2)}\left(\frac{x^2}{\sigma_1^2} - \frac{2\rho xy}{\sigma_1\sigma_2} + \frac{y^2}{\sigma_2^2}\right) \right] dx\,dy.$$

(1)

Taking σ_1, σ_2, and ρ as initially unknown, we have

$$P(d\sigma_1 d\sigma_2 d\rho \mid h) \propto d\sigma_1 d\sigma_2 d\rho / \sigma_1\sigma_2.$$

(2)

If we have n observations, denoted collectively by θ, we write

$$\Sigma x^2 = ns_1^2, \quad \Sigma y^2 = ns_2^2, \quad \Sigma xy = nrs_1 s_2$$

(3)

and

$$P(\theta \mid \sigma_1\sigma_2\rho h) \propto \frac{1}{(\sigma_1\sigma_2)^n (1-\rho^2)^{\frac{1}{2}n}} \exp\left[-\frac{n}{2(1-\rho^2)}\left(\frac{s_1^2}{\sigma_1^2} - \frac{2r\rho s_1 s_2}{\sigma_1\sigma_2} + \frac{s_2^2}{\sigma_2^2}\right) \right].$$

(4)

Then, combining (2) and (4), we have

$P(d\sigma_1 d\sigma_2 d\rho \mid \theta h)$

$$\propto \frac{1}{(\sigma_1 \sigma_2)^{n+1}(1-\rho^2)^{\frac{1}{2}n}} \exp\left[-\frac{n}{2(1-\rho^2)}\left(\frac{s_1^2}{\sigma_1^2} - \frac{2r\rho s_1 s_2}{\sigma_1 \sigma_2} + \frac{s_2^2}{\sigma_2^2}\right)\right] d\sigma_1 d\sigma_2 d\rho. \quad (5)$$

To obtain the total probability that ρ is in a particular range $d\rho$ we must integrate with regard to σ_1 and σ_2. Making Fisher's substitutions

$$\frac{s_1 s_2}{\sigma_1 \sigma_2} = \alpha; \quad \frac{s_1 \sigma_2}{s_2 \sigma_1} = e^\beta, \quad (6)$$

and dropping factors independent of the unknowns, we have

$$P(d\rho \mid \theta h) \propto d\rho \int_0^\infty \int_{-\infty}^\infty \frac{\alpha^{n-1}}{(1-\rho^2)^{\frac{1}{2}n}} \exp\left[-\frac{n\alpha}{1-\rho^2}(\cosh\beta - \rho r)\right] d\alpha \, d\beta \quad (7)$$

$$\propto d\rho \int_0^\infty \frac{(1-\rho^2)^{\frac{1}{2}n}}{(\cosh\beta - \rho r)^n} d\beta. \quad (8)$$

A similar integral appears in Fisher's analysis, which, however, takes σ_1, σ_2 and ρ as given and integrates with regard to s_1 and s_2, thus obtaining the probability distribution of r given ρ.* His result is equivalent to

$$I_n = \int_0^\infty \frac{d\beta}{(\cosh\beta - \rho r)^n} = \frac{1}{(n-1)!} \frac{d^{n-1}}{d(\rho r)^{n-1}} \frac{\cos^{-1}(-\rho r)}{(1-\rho^2 r^2)^{\frac{1}{2}}}, \quad (9)$$

and Pearson and his collaborators (1917) give numerous transformations of it. I have tried to obtain an asymptotic expansion by putting

$$\cosh\beta - \rho r = (1-\rho r)e^u, \quad (10)$$

which should give a result in descending powers of n, but when more than three terms were wanted the algebra became prohibitive. But if we put, instead,

$$\cosh\beta - \rho r = \frac{1-\rho r}{1-u}, \quad (11)$$

the integral transforms to

$$I_n = \frac{1}{2^{\frac{1}{2}}(1-\rho r)^{n-\frac{1}{2}}} \int_0^1 \frac{(1-u)^{n-1} u^{-\frac{1}{2}} du}{\{1 - \frac{1}{2}(1+\rho r)u\}^{\frac{1}{2}}}, \quad (12)$$

---

* In previous papers I have used Greek letters for functions of the observations and italic ones for quantities to be estimated. The opposite usage is adopted by Fisher, and I follow him in this section to avoid confusion in comparison.

in which we can expand the denominator in powers of u, and the terms give Beta functions on integration. We find

$$I_n = \frac{(n-1)!\,(\tfrac{1}{2}\pi)^{\frac{1}{2}}}{(n-\tfrac{1}{2})!\,(1-\rho r)^{n-\frac{1}{2}}}\left[1 + \frac{1}{n+\tfrac{1}{2}}\frac{1+\rho r}{8} + \frac{1^2\cdot 3^2}{2!\,(n+\tfrac{1}{2})\,(n+\tfrac{3}{2})}\left(\frac{1+\rho r}{8}\right)^2 + \dots\right],$$

(13)

which converges for all ρr less than 1, and the terms diminish rapidly for large n. We denote the series by $S_n(\rho r)$.

Expanding $(n-1)!\,n^{\frac{1}{2}}/(n-\tfrac{1}{2})!$ and the series in descending powers of n as far as n^{-4}, we find agreement with the formula of the Co-operative Study (Pearson 1917, p. 348, eq. 49). Our result is therefore

$$P(d\rho \mid \theta h) \propto \frac{(1-\rho^2)^{\frac{1}{2}n}}{(1-\rho r)^{n-\frac{1}{2}}}\,S_n(\rho r)\,d\rho.$$

(14)

The series, in spite of the attention paid to it by Pearson and his collaborators, does not appear to be very important.* Even for the extreme case of $n = 2$ and $\rho r = 1$ the second term is only $0\cdot10$. If any allowance for it is needed it could be replaced by $\exp\left\{\dfrac{1+\rho r}{8n+4}\right\}$, which happens to represent the third term closely for $n = 2$. But we are interested in the variation of the function, since there is an irrelevant constant factor in any case, and the variation will be represented by $\exp\dfrac{r(\rho-r)}{8n+4}$. The displacement of the mode by allowance for this term will be of order n^{-2} and may safely be neglected. In (14) we can therefore replace S_n by 1. The mode of (14), to order n^{-1}, is given by

$$\rho = r - \frac{r}{2n}(1-r^2).$$

(15)

The bias shown by the second term is well known. The skewness of the distribution, however, is a more serious matter. Fisher deals with it in his problem by the substitution

$$r = \tanh z; \quad \rho = \tanh \zeta; \quad \zeta = z + x.$$

(16)

---

* I very much doubt whether it is ever worth while to carry the arithmetic beyond two places in the standard error. It seems to me that if a decision depends on whether the standard error is $1\cdot0$ or $1\cdot1$ it must be doubtful in any case. Rounding to one figure, however, is definitely undesirable; the difference between $\pm0\cdot15$ and $\pm0\cdot25$ may be very important.

Applying this to (14) and introducing a factor to make the expression unity for $x = 0$, we have

$$P(d\zeta \mid \theta h) \propto \frac{d\zeta}{\cosh^{-\frac{1}{2}} z \cosh^{\frac{1}{2}} \zeta \cosh^{n-\frac{1}{2}} x}, \qquad (17)$$

which approaches normality rapidly with increasing n because the factor raised to a high power is an even function of x. For large x, however, it approaches the median law, and if a Pearson law was fitted it would give one of Type IV, or Type VII if the asymmetry was neglected. But all the moments of finite order are finite, so that no law of these types could represent the large departures. The mode for ζ is given by

$$(n+2)\tanh x + \tfrac{5}{2}\tanh z + (n-\tfrac{1}{2})\tanh z \tanh^2 x = 0. \qquad (18)$$

Solving this as a quadratic in $\tanh x$ to order n^{-2} we find

$$\tanh x = -\frac{5}{2(n+2)}\tanh z - \frac{25(2n-1)}{8(n+2)^3}\tanh^3 z, \qquad (19)$$

whence, since x is small,

$$x = -\frac{5r}{2(n+2)} - \frac{25(3n-1)\,r^3}{12(n+2)^3}. \qquad (20)$$

It may be noticed that for $n = 3$ the maximum is at $x = -\tfrac{1}{2}z$ exactly, and for small r this agrees with the first term. There is no need to allow specially for the second, which will always be of order n^{-2}. Fisher, for the mode of z given ζ, gets (1915, p. 521)

$$\zeta - z = -\frac{r}{2n}, \qquad (21)$$

and the same expression, to this order, for the mean (1921, p. 13). (There is a misprint in the earlier paper, shown by reference to the previous line.) The corrections to z differ by a factor 5. In a sense this is not important, because a bias of order $1/n$ is small compared with the standard error, which is of order $n^{-\frac{1}{2}}$ in ordinary cases. Differences of this order are liable to occur in the comparison of direct and inverse methods (Jeffreys 1938a), and even within the range of the direct methods when there is a question of the best way of locating a skew distribution. Before discussing the matter further, however, it will be best to remove a difference between my problem and Fisher's. So far I have taken the distribution of (x, y) to be about zero; he takes it to be about a pair of unknowns m_1 and m_2, which in my problem would also have to be found from the data. If we write

$$x' = x - m_1; \quad y' = y - m_2, \qquad (22)$$

$$ns_1^2 = \Sigma(x-\bar{x})^2; \quad ns_2^2 = \Sigma(y-\bar{y})^2; \quad nrs_1s_2 = \Sigma(x-\bar{x})(y-\bar{y}), \qquad (23)$$

and take the prior probabilities of m_1 and m_2 as uniformly distributed, (1) stands, with the introduction of accents in the exponent, and (4) with the introduction of a factor

$$\exp\left[-\frac{n}{2(1-\rho^2)}\left\{\frac{(m_1-\bar{x})^2}{\sigma_1^2}-\frac{2\rho(m_1-\bar{x})(m_2-\bar{x})}{\sigma_1\sigma_2}+\frac{(m_2-\bar{x})^2}{\sigma_1^2}\right\}\right]. \qquad (24)$$

(5) then needs the inclusion of $dm_1\,dm_2$ on both sides, and of the last factor on the right. Integration with regard to m_1 and m_2 reproduces (5) with an extra factor $\sigma_1\sigma_2(1-\rho^2)^{\frac{1}{2}}$. Further work will therefore give only an irrelevant function of n as a factor and replace n in (8) by $n-1$. With this change the result will be

$$P(d\rho\mid\theta h)\propto\frac{(1-\rho^2)^{\frac{1}{2}(n-1)}}{(1-\rho r)^{n-\frac{1}{2}}}\,S_{n-1}(\rho r)\,d\rho, \qquad (25)$$

and in place of (20) we should have

$$\zeta-z=-\frac{5r}{2(n+1)}. \qquad (26)$$

Now Fisher's result can be written, apart from a constant factor,

$$P(dr\mid m_1,m_2,\sigma_1,\sigma_2,\rho,h)\propto\frac{(1-\rho^2)^{\frac{1}{2}(n-1)}(1-r^2)^{\frac{1}{2}(n-4)}}{(1-\rho r)^{n-\frac{1}{2}}}\,S_{n-1}(\rho r)\,dr, \qquad (27)$$

and as this is independent of m_1, m_2, σ_1, σ_2 these may be dropped and the left side replaced by $P(dr\mid\rho h)$. Also if we take the prior probability of ρ as uniformly distributed, then since for a given sample r and dr are fixed we are left with

$$P(d\rho\mid rh)\propto\frac{(1-\rho^2)^{\frac{1}{2}(n-1)}}{(1-\rho r)^{n-\frac{1}{2}}}\,S_{n-1}(\rho r)\,d\rho, \qquad (28)$$

which is identical with my result (25) except that r appears in the data instead of θ. The latter, being the complete data, enable r to be calculated; what the result shows is that the data contain no information relevant to ρ that is not contained in the summary value r. This proves, if proof is considered necessary, that r is a sufficient statistic for ρ.[*] The relation between

---

[*] In my treatment, the form of (5) shows that s_1, s_2 and r are jointly sufficient statistics for σ_1, σ_2 and ρ, since no other functions of the observations occur. The proof that s_1 and s_2 are irrelevant to ρ is contained in their disappearance from (8), while r remains and therefore is a sufficient statistic for ρ. Analogous results always follow from the principle of inverse probability when sufficient statistics exist. There is no need to think of a possible statistic and then investigate whether it is sufficient or efficient; the principle shows the proper statistics in the course of the work. They are, of course, identical with those given by the likelihood, which is the only part of the posterior probability that involves the observations.

Fisher's method and mine is exactly analogous to that between "Student's" and mine for the t distribution (Jeffreys 1937). The maximum likelihood solution obtained from (27) by differentiating with regard to p is identical with the point of maximum probability density obtained similarly from (25).

When we consider a transformation of variables, however, there is a difference. To take a more general case, suppose that the probability distribution for an observed sufficient statistic ξ, given a true value x, is

$$P(d\xi \mid xh) = f(\xi, x)\, d\xi, \tag{29}$$

and that the prior probability of x is uniformly distributed; it will follow that

$$P(dx \mid \xi h) \propto f(\xi, x)\, dx, \tag{30}$$

since ξ and $d\xi$ are the same for all values of x. Then the maximum likelihood and maximum posterior density for x are both given by

$$\frac{\partial}{\partial x} f(\xi, x) = 0. \tag{31}$$

But if we put $\xi = g(\eta)$, $x = g(y)$, (29) leads to

$$P(d\eta \mid yh) = f(\xi, x) \frac{d\xi}{d\eta}\, d\eta, \tag{32}$$

and (30) to

$$P(dy \mid \eta h) \propto f(\xi, x) \frac{dx}{dy}\, dy. \tag{33}$$

The maximum likelihood solution given by (32) is where

$$\frac{dx}{dy} \frac{\partial}{\partial x} f(\xi, x) = 0, \tag{34}$$

which is equivalent to (31); but the maximum posterior density for y, as given by (33), is where

$$\frac{dx}{dy} \frac{\partial}{\partial x} f(\xi, x) + \frac{d^2 x}{dy^2} = 0, \tag{35}$$

and the two will in general differ by a quantity of order $1/n$. The invariance of the maximum likelihood solution is not, however, much advantage. If the relation between x and y is linear, the extra term in (35) vanishes and there is no difference. If it is not linear, $f(\xi, x)$, regarded as a function of x or of y, is skew for at least one of them, and the maximum has no dominating importance in comparison with, say, the median. The advantage of the posterior probability is that (30) and (33) are the same differential element. If they are integrated between corresponding values of x and y they will

always give the same result, thus attaching an invariant value to the probability that x lies between two given values on fixed data. The median and the quartiles of the distribution, for instance, are unaltered by transformations.

The discrepancy between Fisher's result and mine is therefore only apparent and has arisen through the transformation applied to r and ρ. The maxima of (25) and (27) with regard to ρ are the same, but when we transform from ρ to ζ the maximum likelihood is not displaced but the maximum posterior density is, on account of the distortion. The transformation has introduced a factor $\mathrm{sech}^2\zeta$ into (17); if this was removed we should have a function whose maximum was at Fisher's value. But this factor comes from the interpretation of ρ in terms of an unknown ratio to be estimated by sampling, and the uniform distribution of the prior probability of such a ratio is quite satisfactory. A uniform one for ζ would be equivalent to $d\rho/(1-\rho^2)$ for ρ, implying a practical certainty that the correlation is ± 1, which may be approached in some physical laws but hardly in any case where methods of correlation would actually be used. There would usually be a dominating variation, and the normal correlation surface would cease to be a valid approximation.

I think that it is of theoretical interest to show how the different invariant properties of *maximum likelihood* and *inverse probability* are related, in an actual case where they are not quite identical, but in practice I should doubt whether the difference, where there is any, is ever important in problems of estimation. In this case, if the number of observations is large, the correction will be small compared with the standard error of ζ; if the number is small but the estimated correlation high, the corrected value will also be high; if the number is small and the correlation moderate the result will not be of much interest in any case. Fisher's comments are similar, but he suggests, rather tentatively, that the correction, being systematic, may become important when many series are combined. Now the question here is, how far are the series mutually relevant? If they are not, we cannot combine the evidence. If we go to the other extreme and regard them as cases where the correlation will be the same in all, we can write down the likelihood for the whole jointly, and it will be the product of those for the separate series. If we can take σ_1, σ_2, m_1 and m_2 also the same in all series, they can be eliminated as before. The data will give a summary value for r; and the displacement of the maximum likelihood solution for ζ from it will be $-r/2\Sigma n$, and that of the mode of the posterior probability $-5r/2\Sigma n$. Thus it would be wrong in either case to average the biases; it will become more and more accurate to take z without modification as the best value of ζ.

If σ_1 and σ_2 are not the same, e.g. if the correlation between the heights of brother and sister is to be estimated from British and Chinese data together, they must be eliminated separately. The joint likelihood for r will be the product of expressions like (27); and as the number of series combined increases the correction x will tend to Fisher's value. In expressions analogous to (17) the factor $\operatorname{sech}^{\frac{1}{2}} \zeta$ contributed by the likelihood will appear every time, but the $\operatorname{sech}^2 \zeta$ from the prior probability only appears once. In intermediate cases there may be doubts as to whether all the correlations are identical or not. It would then be legitimate to test them for consistency and to combine them if they are consistent and keep them separate if they are not. I have given a test (1935) that will say whether a correlation coefficient differs significantly from zero. Tests for whether it differs from a preassigned value other than zero, or for whether two estimates of a correlation are consistent, have not yet been constructed, but their construction would involve no new principle. If a number of related cases differ significantly, but yet appear to belong to a definite distribution, this could be used to assign a revised prior probability for other similar cases; but even then allowance for the bias would only make a change of order $1/n$ in the scale of this distribution, and the whole effect of reassessing the prior probability for a new case would also be of order $1/n$, so that the correction for bias in previous cases would only produce an effect of order $1/n^2$ in a new one. On the whole, therefore, I think that the correction is negligible in all cases of practical importance.

With reference to some examples given by Pearson to illustrate the effects of little or much previous knowledge, my comment would be that we must distinguish between an assessment based on the sample alone and one based on the whole of the previous knowledge. Both have definite meanings; but we need not say that the sample is all we know if we have other relevant information, and equally if we have other relevant information we must not say that we found it out from the sample. If we know so much already that the sample can tell us nothing new, we are still entitled to combine the evidence and apply the principle of inverse probability, though it becomes little more than a mathematical exercise. I should agree with Fisher (1921, p. 17) that in such a case it is quite wrong to speak of the conclusions as drawn from the sample; they would be drawn from the whole of the available experience, of which the sample, in such a case, would be a negligible part. To put the matter formally, if h represents the general principles of correlation theory, θ_0 the previous evidence, and θ the sample under discussion, we must not confuse $P(d\rho \,|\, \theta h)$ with $P(d\rho \,|\, \theta_0 \theta h)$, and with an adequate notation we cannot.

To obtain an estimate of uncertainty, we may use the expectation of x^2, since the distribution is nearly normal. Using the substitution

$$\cosh x = 1/(1-u), \tag{36}$$

neglecting the bias, and retaining two terms of the respective series,

$$\int_{-\infty}^{\infty} \frac{dx}{\cosh^{n-\frac{1}{2}} x} = \frac{(2\pi)^{\frac{1}{2}}(n-\frac{3}{2})!}{(n-1)!}\left(1+\frac{1}{8n}\right), \tag{37}$$

$$\int_{-\infty}^{\infty} \frac{x^2\,dx}{\cosh^{n-\frac{1}{2}} x} = \frac{(2\pi)^{\frac{1}{2}}(n-\frac{3}{2})!}{n!}\left(1+\frac{13}{8(n+1)}\right), \tag{38}$$

$$E(x^2) = \frac{1}{n}\left(1+\frac{3}{2n}\right) = \frac{1}{n-\frac{3}{2}}, \tag{39}$$

nearly. In the case where there are two means to be eliminated at the outset, this will be replaced by $1/(n-\frac{5}{2})$. Fisher gives $1/(n-3)$; the difference is slight and of the order n^{-2} and of the error due to neglecting the bias.

Thus where the distribution is centred on zero the solution for ζ can be taken to be

$$\zeta = z - \frac{5r}{2(n+2)} \pm \frac{1}{(n-\frac{3}{2})^{\frac{1}{2}}}, \tag{40}$$

and where it is centred on a pair of values to be found the solution is

$$\zeta = z - \frac{5r}{2(n+1)} \pm \frac{1}{(n-\frac{5}{2})^{\frac{1}{2}}}, \tag{41}$$

with negligible errors; the second term is usually negligible, and is better neglected if several series with the same standard errors are likely to be combined.

3. *The intraclass correlation coefficient.* The estimation of this parameter can be considered at the same time as the test that it is different from zero; if it passes the test the analysis will yield its posterior probability as a by-product. The conditions are very similar to those considered in my test for the significance of a departure from independence in a series of measures (1938 b), when the data are the means and variances in successive groups; there being a displacement $a_i - a$ derived from a normal law with standard error t and common to all members of a group. There will be parameters a and s that have meanings on both hypotheses, but a change is needed with respect to the additional parameter t that arises on $\sim q$. I took its prior probability uniformly distributed from 0 to s; but $\rho = t^2/s^2$, and the analogy

with sampling suggests that we should now take that of ρ uniformly distributed from 0 to 1. Thus if we put $t = su$, the previous rule was

$$P(du \mid \sim q, sh) = du, \tag{1}$$

and the present one would be written in either of the forms

$$P(d\rho \mid \sim q, sh) = d\rho; \quad P(du \mid \sim q, sh) = 2u\,du. \tag{2}$$

With this modification the analysis follows that of the previous test, a factor $2u$ being applied in each equation on $\sim q$. The result will therefore be

$$P(\sim q, du \mid \theta h) \propto \frac{2u\,du(1 - u^2)^{\frac{1}{2}(m-1)}\{1 + (k-1)u^2\}^{\frac{1}{2}m(k-1)}}{\{1 + (k - \gamma^2 k - 1)u^2\}^{\frac{1}{2}(mk-1)}} \tag{3}$$

$$\propto \frac{d\rho\,(1 - \rho)^{\frac{1}{2}(m-1)}\{1 + (k-1)\rho\}^{\frac{1}{2}m(k-1)}}{\{1 + (k - \gamma^2 k - 1)\rho\}^{\frac{1}{2}(mk-1)}}, \tag{4}$$

where m is the number of groups, k the number of observations in a group, and γ the ratio of the mean square deviations of the group means and the entire series.* Then $1/K$ is the integral of this from 0 to 1.

The first two checks given previously still apply. If $m = 1$, $\gamma^2 = 0$, and $K = 1$. If $k = 1$, $\gamma^2 = 1$, and again $K = 1$. The third check analogous to a previous one is for the case $m = 2$, $\gamma^2 = 0$; then

$$\frac{1}{K} = \int_0^1 \left\{ \frac{1 - \rho}{1 + (k-1)\rho} \right\}^{\frac{1}{2}} d\rho \tag{5}$$

which is integrated by the substitution

$$(k - 1)\rho = k\cos^2\theta - 1, \tag{6}$$

giving
$$\frac{1}{K} = \frac{k}{(k-1)^{\frac{1}{2}}} \left\{ \tan^{-1}\sqrt{(k-1)} - \frac{\sqrt{(k-1)}}{k} \right\}, \tag{7}$$

and K tends to $2k^{\frac{1}{2}}/\pi$ when k is large. The outside factor is therefore of the usual order of magnitude for the comparison of two means. Complete agreement is not to be expected, because in the comparison of means the prior probability of the difference is taken uniform over the possible range, while in this problem the means are estimates of two values from a normal distribution whose standard error can range from 0 to s, and this must give some concentration towards 0 and decrease K. The same criticism applies to the use of this check in the previous case. The agreement found was accidental, because the comparison case was the test of the difference between two means of k observations each with the same standard error,

* There is a misprint in the second index of the numerator in 1938b, equation (22).

and the outside factor in this should be $(4k/\pi)^{\frac{1}{2}}$, not $(2k/\pi)^{\frac{1}{2}}$ as I supposed. Agreement in order of magnitude is as much as should be expected.

In the general case the discussion follows previous lines. We put

$$w = \frac{k\rho}{1+(k-1)\rho}, \tag{8}$$

$$\frac{1}{K} = \int_0^1 \frac{k(1-w)^{\frac{1}{2}(m-1)}\,dw}{(1-\gamma^2 w)^{\frac{1}{2}(mk-1)}\{k-(k-1)\,w\}^2}. \tag{9}$$

When $\gamma^2 < 1/k$, K approaches $\frac{1}{2}k(m-m\gamma^2 k-5)$ provided this is positive. For $\gamma^2 = 1/k$, $K \doteqdot k(m/\pi)^{\frac{1}{2}}$; for $\gamma^2 \gg 1/k$,

$$K \doteqdot \frac{m^{\frac{1}{2}}}{2\sqrt{\pi}} \frac{k^{\frac{1}{2}mk-1}}{(k-1)^{\frac{1}{2}mk-\frac{1}{2}m-\frac{1}{2}}} \gamma^{m-3} (1-\gamma^2)^{\frac{1}{2}mk-\frac{1}{2}m-1}. \tag{10}$$

On putting

$$\gamma^2 = \frac{1}{k} + \frac{\beta}{k\sqrt{m}} \tag{11}$$

and simplifying, we get

$$K \doteqdot \frac{m^{\frac{1}{2}}}{2\sqrt{\pi}} \frac{k^{\frac{1}{2}}}{(k-1)^{\frac{1}{2}}} \exp\left\{-\frac{k\beta^2}{4(k-1)}\right\}, \tag{12}$$

which should be a good approximation in the range where the test is required.

In a pure problem of estimation we may return to (4), and consider what would happen if the variations just reached their expectations. $\sigma^2 - \tau^2$ would be the expectation of the variance of k observations from their mean, namely $s'^2(1-1/k)$. τ^2 consists of two parts. The t component would give $t^2(1-1/m)$. But each value will have a standard error $s'/k^{\frac{1}{2}}$ from the s' component, and this will give a contribution $(s'^2/k)(1-1/m)$ to the variance from the mean. Hence we should have

$$\frac{k(m-1)}{m} \frac{t^2 + s'^2/k}{s'^2(k-1)} = \frac{\tau^2}{\sigma^2 - \tau^2}, \tag{13}$$

and substituting the values of the ratios we should have

$$\frac{m-1}{m(k-1)} \frac{1+(k-1)\rho}{1-\rho} = \frac{\gamma^2}{1-\gamma^2}. \tag{14}$$

If r is the value of ρ defined by this equation, we have

$$(m-1+\gamma^2)(k-1)r = (mk-1)\gamma^2 - (m-1). \tag{15}$$

Put also

$$\frac{1+(k-1)\rho}{1-\rho} = e^{2\zeta}; \quad \frac{1+(k-1)r}{1-r} = \frac{m(k-1)\gamma^2}{(m-1)(1-\gamma^2)} = e^{2z}. \tag{16}$$

Then

$$P(d\zeta \mid \theta h) \propto \frac{2k\,e^{2\zeta}d\zeta}{(k-1+e^{2\zeta})^2} \frac{e^{m(k-1)\zeta}\{m(k-1)+(m-1)e^{2z}\}^{\frac{1}{2}(mk-1)}}{\{m(k-1)e^{2\zeta}+(m-1)e^{2z}\}^{\frac{1}{2}(mk-1)}}, \tag{17}$$

where the possible values of ζ range from 0 to ∞. The mode is easily seen to be near $\zeta = z$, provided z is positive. A second approximation gives

$$\zeta - z = \frac{mk-1}{m(m-1)(k-1)}\frac{k-1-e^{2z}}{k-1+e^{2z}} \pm \left\{\frac{mk-1}{2n(k-1)(m-1)}\right\}^{\frac{1}{2}}. \tag{18}$$

The resemblance of (17), as regards the factors raised to high powers, to Fisher's z distribution may be noticed. The other factors are due to various complications, notably the effect of the transformation and the fact that s' contributes to the observed value of τ^2; indeed the need for a significance test arises from the fact that it may account for the whole of it.* If (17) was integrated from 0 to ∞, it would yield again the function $1/K$.

4. The test (12) is substantially different in appearance from the previous one (1938b, equation (35)), which contained a factor $m^{\frac{1}{2}}k^{\frac{1}{2}}\beta^{\frac{1}{2}}$. It is intended to deal with different conditions from those contemplated before, but the resemblances of the previous problem to the present conditions may be more important than the differences. I have no doubt that the present test is right when we have to test a series of means that are not arranged in some definite order by the conditions of the problem, and these means are estimates of group parameters themselves derived from a normal law. If the last condition is not satisfied, if, for instance, the group parameters are derived from a rectangular law, the change needed would hardly be more than a factor of 2,† which is not worth introducing. The previous problem was intended to test a series of observations made in a known order for

---

* Mr W. O. Storer, in an unpublished paper, has applied the present methods to the following problem. Given one set of n_1 measures derived from the normal law, what is the probability that a future set of n_2 measures, presumed derived from a normal law with the same parameters, will give an observed standard deviation in the range ds? The result is exactly the z distribution. This case was chosen as an illustration of a problem where the complications just mentioned would be absent.

† I have worked out a rough solution for this case. It is very awkward in appearance, but $1-\gamma^2$ enters to a power $\frac{1}{2}(mk-m-2)$ as above, and the range between the extremes of $\bar{x}_i$ to a power of $m-3$. As the data enter so similarly the critical values are unlikely to be very different.

internal correlation; the fluctuation of the group means suggested an analogy with the problem of function-fitting, in which the prior probability of an amplitude is taken uniform within the range permitted, and the function itself will usually have a limited range. The method of analysis, however, made no use of the order of the group means, merely of their values, so that the analogy with function-fitting had already been abandoned. The actual variation suggested a set of interpolates obtained by fitting a polynomial to a set of random values, the comparative constancy of the ratio of the extreme range to the mean square deviation of the group means suggesting a rectangular distribution rather than a normal one (Jeffreys 1938c, p. 266). The analogy with function-fitting would require the function considered to be a highly selected one, not a simple one or one suggested by theory, such as we should usually consider in such a test, and at the least we should expect a corresponding increase in the outside factor to allow for selection. But in testing a function from km observations K would be of order $(km)^{\frac{1}{2}}$ if the expectation of the amplitude on the hypothesis of randomness was just realized; the correct one would be expected to be larger. (12) satisfies this condition; the previous test did not.

Applying the present test to Pearson's data, used previously, we get the following values of K:

	Bisection		Bright line
1	5×10^{-2}	1	$0 \cdot 21$
2	3×10^{-139}	2	9×10^{-7}
3	3×10^{-865}	3	9×10^{-20}

The numbers are changed a little, but the decisions and the comments need no change. (Most of the change in the very small values is due to the retention of $k/(k-1)$ in the last factor.) The test for the first bright line series, which gave the largest value of K before, namely $0 \cdot 096$, now gives $0 \cdot 21$; it appears that in spite of the different forms of K they both give nearly the same critical value of γ^2. It may be noticed that these series would have given 65 or 72 to 1 odds on independence if γ^2 had agreed with expectation on this hypothesis.

It may appear that the complication could be avoided if we abandoned the rule in function-fitting that the prior probability of an amplitude a is to be taken as uniform between $\pm s$, where s^2 is the expectation of the total variance, and replaced it by distributing that of a^2 uniformly; in other words if we replaced $P(da \mid \sim q, sh) = da/2s$ by $P(da \mid \sim q, sh) = |a| \, da/s^2$. But when we are seriously considering the possibility that a is 0 in a significance test it seems undesirable to say that if it is not 0 the probability

density at small values is infinitesimal. The effect of such a change would be to make the outside factor in K of order n instead of $n^{\frac{1}{2}}$, and the ratio of an estimate to its standard error at the critical value would vary more rapidly with the number of observations than my test gives. It seems better to retain the present rule, which is closer to the one used in problems of estimation; in any case a rule would be subject to modification if subsequent evidence suggested it, but it is at least not obvious that such modification is needed yet.

This kind of internal correlation could hardly be considered as either an accidental error or a systematic one in the usual sense. It is not accidental because the mean of a batch of 10 errors does give information about the mean of the next batch; it is not systematic because the correlation is not perfect and the errors may in fact have either sign. The usual distinction is far too sharp. The kind of effect that internal correlation may produce may be illustrated by two conditions in coin-tossing. Suppose in each case that the first throw is random, but that in Case 1 there is such a correlation that every throw must repeat the previous throw, and in Case 2 every throw must reverse the previous one. Then in Case 1 after 100 throws we have 100 similar results; on the usual analysis we should say that there was overwhelming evidence of bias. In Case 2 we should have 50 heads and 50 tails, and we should say that the evidence was against bias. Actually in each case all that we should be entitled to say is that there is no evidence for or against bias, since whether there was bias or not the first throw must give either a head or a tail, but if there is any it is likely to be in the sense of the first result. This is an extreme case, but serves to show how internal correlation may invalidate the usual methods. In Case 2, if we follow the apparent intentions of some discussions, the result of the whole series would be taken as evidence of the existence of a chance $\frac{1}{2}$; but inspection of the results of groups of throws arranged in tens would show no variation at all, which is not what a law of chance predicts. Alternatively, since the chances of a persistence and a repetition in consecutive throws are equal if there is a chance $\frac{1}{2}$, but not if there is a correlation, the numbers of persistences and repetitions could be used to test the existence of a correlation and would reveal it at once.

5. I think that the problem of function fitting, when there may be an internal correlation, must be analysed as follows. q is the statement that there is no internal correlation and that the function suggested is absent, but we may consider two alternatives, $\underset{p}{\sim} q$ saying that there is an internal correlation but no extra function, $\underset{a}{\sim} q$ saying that there is an extra function but otherwise no internal correlation. We cannot consider both complica-

tions together, since it is quite possible that one may be present without the other. But we can work out

$$K_\rho = \frac{P(q \mid \theta h)}{P(\underset{\rho}{\sim} q \mid \theta h)}; \quad K_a = \frac{P(q \mid \theta h)}{P(\underset{a}{\sim} q \mid \theta h)}.$$

For the first the present solution is available; for the second, the test for function-fitting. If both are more than 1, or if one is less than 1 and the other greater than 1, we need go no further. If both are less than 1, we have at once

$$P(\underset{\rho}{\sim} q \mid \theta h)/P(\underset{a}{\sim} q \mid \theta h) = K_a/K_\rho$$

so that we can consider the departure established that gives the smaller K. But now we are at liberty to consider the other afresh; if ρ is more strongly supported than a, that does not dispose of a. Hence if ρ is the more strongly supported we can consider a further alternative $\underset{\rho,a}{\sim} q$ and test it against $\underset{\rho}{\sim} q$. This will be done effectively by regarding the group means as data with an initially unknown variance (the rejection of q having implied that the variance of the data as a whole is not a datum relevant to the variance of the group means) and applying the test for function-fitting to them. Conversely if a is the more strongly supported we can allow for it and test the corrected group means for a correlation, which may lead to an increase in the estimated uncertainty of a if the correlation is established. This method has the advantage that it treats internal correlation and function-fitting as two separate parts of the problem. It distinguishes at the outset between a contribution to an observation that, if known, would determine the corresponding contributions for every observation available, and one that would give information about neighbouring observations but practically none about observations separated by, say, a tenth of the total range.

In the above Case 2, the test for the correlation of successive throws would reveal it strongly, while that for bias would deny it; hence we could assert correlation at once, and admitting it there would be no evidence relevant to bias. In Case 1, the first tests would both give K very small, the value for bias being about half that for correlation. Accepting either, the evidence would be indecisive in regard to the other.

If we form χ^2 for the group means in the intraclass correlation problem, it is

$$\chi^2 = S\bar{x}_l^2 \div \sigma^2/k = km\gamma^2,$$

the expectation on q being $m - 1$. Thus when such correlation is suspected of having increased the uncertainty of summary values χ^2 contains the same information about it as γ^2 does. To correct for it we may multiply all the

standard errors by $\chi/\sqrt{(m-1)}$, where m is the number of contributions to χ^2, provided $\chi^2 > m$. If $\chi^2 < m$ the evidence is against correlation and no correction is needed.

6. The general rules about the prior probability, which have been found adequate in all cases that have arisen so far, are as follows:

(1) For a quantity unrestricted initially in value except for sign, the ds/s rule; in particular for any case where it is equally natural to take either of two different powers of the same quantity as the unknown to be estimated.

(2) For the number of members of a given type in a population, a chance, a correlation, or the coefficient of a function introduced in fitting a series of measures, uniform distribution within the range permitted by the conditions of the problem. Where several functions arise simultaneously for consideration in a significance test, their coefficients may be regarded as the components of a vector, the prior probability distribution of its direction being taken as uniform and that of its resultant uniform within the permitted range.

(3) In significance tests, where there is a serious possibility that a new parameter may be zero or well within the standard error of an estimate of it, the prior probability that it is zero may be taken as $\frac{1}{2}$. When the question is whether some one out of a set of m possible parameters is genuine, allowance for selection may be made by considering the extreme departure, multiplying K by m if the acceptance of one would afford any inductive (not decisive) reason for accepting another, and by $1\cdot4\ m$ if it would afford no reason at all (1938 b).

The data for the correlation of measures might be regarded as an instance for the application of the m rule; if there is such a correlation in one series it would afford ground for suspecting it, but not for asserting it, in another. Thus the smallest value of K should strictly be multiplied by 6. The rule for other values can be stated rather more simply than has been done before (1938 b). If r and s are the numbers of values already accepted as normal and abnormal respectively, the extra factor needed will be $(r+1)/(s+1)$. We shall begin with the smallest value of K, and end at the pth smallest. But if this is to be the last we shall have $s = p-1$, $r = m-p$, so that the factor may be written $(m-p+1)/p$, as was noticed before. But this may actually always be used; there is no need to allow for the fact that fewer members than $m-p$ have yet been declared normal. It is correct for the first test and the last; at intermediate ones it is a little too high, but it cannot affect the place where we draw the line between the normal and abnormal values. In testing the above set of correlations in turn, we can

therefore take $m = 6$ and p in turn from 1 to 6, giving the factors 6, $\frac{5}{2}$, $\frac{4}{3}$, $\frac{3}{4}$, $\frac{2}{5}$, $\frac{1}{6}$. The largest value of K is 0·21, and when corrected in this way gives $P(q \mid \theta h)/P(\sim q \mid \theta h) = 0·035$. The odds are therefore about 28 to 1 that there is an internal correlation in every series. This method of treatment removes the complication that members originally taken as normal might be adjudged abnormal in the later stages of the test.

SUMMARY

The posterior probabilities of the ordinary and intraclass correlation coefficients are obtained from an analogy with sampling theory, suggested by the applicability of the normal correlation surface in both cases. The results cast some further light on the relation between direct and inverse methods in problems of estimation; for practical purposes the recommendations made would not differ appreciably. A significance test is obtained for the difference between an intraclass correlation coefficient and zero, and the application to internal correlation in series of measurements is discussed.

REFERENCES

Brunt, D. 1931 "The Combination of Observations." Camb. Univ. Press.
Fisher, R. A. 1915 *Biometrika*, **10**, 509–21.
— 1921 *Metron*, **1**, Part 4, 3–32.
Jeffreys, H. 1935 *Proc. Camb. Phil. Soc.* **31**, 203–22.
— 1937 *Proc. Roy. Soc.* A, **160**, 325–48.
— 1938a *Ann. Eugen. Lond.*, **8**, 146–51.
— 1938b *Proc. Roy. Soc.* A, **165**, 179–90.
— 1938c *Philos. Trans.* A, **237**, 231–71.
Laplace 1820 "Théorie Analytique des Probabilités."
Soper, H. E., Young, A. W., Cave, B. M., Lee, A. and Pearson, K. 1917 *Biometrika*, **11**, 328–413.

Influence of radiation on ionization equilibrium

By B. N. Srivastava, M.Sc.

Lecturer in Physics, University of Allahabad

The ionization formula for an assembly of atoms, ions and electrons in thermodynamical equilibrium was first given by M. N. Saha in a series of papers (1920a, 1920b, 1921) and later extended by Darwin and Fowler (1923) and Milne (1921b) to include the different excited states of the atom. Milne (1921a) and Russel (1922) calculated the equilibrium in the case when the electron concentration can be regarded as an independent variable. In all these cases, however, the system is supposed to be in thermodynamical equilibrium, i.e. the reaction space is supposed to be traversed by radiation having the same temperature as the assembly. Let us, however, consider the case when radiation traversing an assembly consisting of the neutral atom, the ion and the electron is not in temperature equilibrium with the components of the system. The problem was attacked by M. N. Saha and R. K. Sur (1926), but the correct solution was obtained by Woltjer (1925a, 1925b) and Milne (1924) for the case of a non-relativistic non-degenerate system and was applied by Pannekoek (1926) to the explanation of the ionization of the earth's atmosphere by sunlight. Eddington (1926) in this way calculated the ionization in gaseous nebulae for which a more elaborate theory has been given later by Ambarzumian (1935). The purpose of the present communication is to extend the analysis to such systems in which the electrons are degenerate but the atoms and the ions are non-degenerate. Such cases occur in the interior of white dwarfs and of the planets as shown by D. S. Kothari (1936).

For the sake of completeness we have derived in § 1 the generalized ionization formula when the constituents obey any statistics. In § 2 the ionization in presence of incident radiation of any composition is considered, the electrons being supposed to be either degenerate or non-degenerate.

1. System in thermodynamic equilibrium

For calculating the probability of the system we shall adopt the simplified method due to Bothe (1928), Majumdar (1931) and Milne (1930). Let A_s be

the number of cells of energy ϵ_s, and N_s the number of particles contained in those cells. The probability of such distribution for the system when the particles obey any statistics (Fermi-Dirac or Bose-Einstein, but not classical) can be written in the generalized form*

$$W = \prod_s \frac{(A_s!)^\beta}{\{(A_s - \beta N_s)!\}^\beta\, N_s!}, \tag{1}$$

where β should be put equal to $+1$ for systems obeying Fermi-Dirac statistics and $\beta = -1$ for systems obeying Bose-Einstein statistics. It is easy to see that for $\beta = +1$ we get

$$W = \prod_s \frac{A_s!}{N_s!(A_s - N_s)!} \quad \text{(F.D. statistics)},$$

and for $\beta = -1$ we get

$$W = \prod_s \frac{(A_s + N_s)!}{N_s!\, A_s!} \quad \text{(B.E. statistics)},$$

which is practically identical with the expression in Bose-Einstein statistics.

Suppose any such general system whose probability is expressed by (1) is in equilibrium. Then we must have

$$\delta(\ln W) = 0. \tag{2}$$

Now with the help of Stirling's theorem we obtain

$$\ln W = \sum_s [\beta A_s(\ln A_s - 1) - \beta(A_s - \beta N_s)\{\ln(A_s - \beta N_s) - 1\} - N_s(\ln N_s - 1)]$$

$$= \sum_s [\beta A_s \ln A_s - \beta(A_s - \beta N_s)\ln(A_s - \beta N_s) - N_s \ln N_s],$$

since $\beta^2 = 1$ for both statistics. Hence

$$\delta \ln W = \sum_s [\beta^2 \delta N_s \ln(A_s - \beta N_s) + \beta^2 \delta N_s - \delta N_s \ln N_s - \delta N_s]$$

$$= \sum_s \delta N_s \left[\ln \frac{A_s - \beta N_s}{N_s}\right]. \tag{3}$$

For equilibrium this should be equated to zero.

---

* The result in this form does not appear to be stated anywhere. Brillouin (1931, p. 168) has stated the result in the form

$$W = \prod_s \frac{\beta^{N_s}\, \Gamma(A_s/\beta + 1)}{N_s!\, \Gamma(A_s/\beta - N_s + 1)}.$$

The form given in the text is, however, found to be more convenient.

Let us now consider the single-stage ionization of an atom into an ion and an electron. We have

$$\text{Atom} + U \rightleftharpoons \text{ion} + \text{electron},\tag{4}$$

where U is the energy necessary to ionize the atom. The probability of the system is

$$W = W_a \cdot W_i \cdot W_e,\tag{5}$$

where W_a, W_i, W_e, denote the probabilities of the atom, ion and electron respectively.

Consider a unit reaction from right to left as expressed by equation (4). We have

$$\left.\begin{aligned}
\delta \sum_s N_{sa} - 1 &= 0,\\
\delta \sum_s N_{si} + 1 &= 0,\\
\delta \sum_s N_{se} + 1 &= 0.
\end{aligned}\right\}\tag{6}$$

The energy equation for the reaction (4) is

$$\delta \left\{ \sum_s \epsilon_{sa} N_{sa} + \sum_s \epsilon_{si} N_{si} + \sum_s \epsilon_{se} N_{se} \right\} - U = 0.\tag{7}$$

For the equilibrium of the system we must have

$$\delta(\ln W) = 0.$$

Hence from (5) we get as in (3) the result

$$\sum_{a,i,e} \sum_s \delta N_s \ln \frac{A_s - \beta N_s}{N_s} = 0.\tag{8}$$

Combining (6), (7) and (8) the condition of equilibrium becomes

$$\sum_s \left[\delta N_{sa} \left(\ln \frac{A_{sa} - \beta N_{sa}}{N_{sa}} + \gamma \epsilon_{sa} + \alpha_a \right) + \delta N_{si} \left(\ln \frac{A_{si} - \beta N_{si}}{N_{si}} + \gamma \epsilon_{si} + \alpha_i \right) \right.$$
$$\left. + \delta N_{se} \left(\ln \frac{A_{se} - \beta N_{se}}{N_{se}} + \gamma \epsilon_{se} + \alpha_e \right) - \alpha_a + \alpha_i + \alpha_e - \gamma U \right] = 0.\tag{9}$$

Hence we must have

$$\alpha_i + \alpha_e = \alpha_a + \gamma U\tag{10}$$

and

$$\ln \frac{A_{sa} - \beta N_{sa}}{N_{sa}} + \gamma \epsilon_{sa} + \alpha_a = 0.\tag{11}$$

From (11) we get

$$N_{sa} = \frac{A_{sa}}{e^{-\alpha_a - \gamma \epsilon_{sa}} + \beta}.\tag{12}$$

It can be shown that $\gamma = -1/kT$. Hence

$$N_{sa} = \frac{A_{sa}}{f_a\, e^{\epsilon_{sa}/kT} + \beta}, \tag{13}$$

where

$$f_a = e^{-\alpha_a},$$

or

$$\ln\left(1/f_a\right) = \alpha_a. \tag{14}$$

We can in a similar way deduce expressions for N_{si} and N_{se}.

Combining (10) and (14) we get

$$\ln\frac{f_i f_e}{f_a} = -\gamma U,$$

or

$$\frac{f_i f_e}{f_a} = e^{-\gamma U} = e^{U/kT}. \tag{15}$$

This is the generalized Saha equation for thermodynamical equilibrium when the constituents obey any statistics.

In order to find the value of f we utilize equation (13). The number A_s of cells having the energy between ϵ_s and $\epsilon_s + d\epsilon_s$ is given by the relation

$$A_s = \frac{Vg \cdot 2\pi(2m)^{\frac{3}{2}}\, \epsilon_s^{\frac{1}{2}}\, d\epsilon_s}{h^3}, \tag{16}$$

since the total phase volume at the disposal of the particles of energy between ϵ_s and $\epsilon_s + d\epsilon_s$ is equal to

$$\iiint dx\,dy\,dz \iiint dp_x\,dp_y\,dp_z = V \cdot 2\pi(2m)^{\frac{3}{2}}\, \epsilon_s^{\frac{1}{2}}\, d\epsilon_s,$$

and the volume of each cell is h^3. g denotes the quantum weight of the particle and hence the foregoing expression for phase volume has been multiplied by g in equation (16). Thus we obtain from (13)

$$N_s = \frac{Vg \cdot 2\pi(2m)^{\frac{3}{2}}\, \epsilon_s^{\frac{1}{2}}\, d\epsilon_s}{h^3(f e^{\epsilon_s/kT} + \beta)}.$$

Or the number of particles per c.c. in that energy interval is given by

$$n_s = \frac{2\pi g(2m)^{\frac{3}{2}}\, \epsilon_s^{\frac{1}{2}}\, d\epsilon_s}{h^3(f e^{\epsilon_s/kT} + \beta)}. \tag{17}$$

Hence the total number of particles per c.c. is given by

$$n = \sum_s n_s = \frac{2\pi g(2m)^{\frac{3}{2}}}{h^3} \int_0^\infty \frac{\epsilon_s^{\frac{1}{2}}\, d\epsilon_s}{f e^{\epsilon_s/kT} + \beta}. \tag{18}$$

For $f \gg 1$ (i.e. non-degenerate systems) (18) yields* as a first approximation the result

$$n = \frac{2\pi g(2m)^{\frac{3}{2}}}{h^3}(kT)^{\frac{3}{2}}\frac{\frac{1}{2}\sqrt{\pi}}{f},$$

or

$$f = \frac{g(2\pi mkT)^{\frac{3}{2}}}{nh^3} \text{ approx.} \tag{19}$$

For $f \ll 1$ (i.e. systems degenerate in the sense of Fermi-Dirac statistics) we obtain, following Sommerfeld's method, the approximate result

$$n = \frac{2\pi g(2m)^{\frac{3}{2}}}{h^3}(kT)^{\frac{3}{2}} \cdot \frac{2}{3}\left(\ln\frac{1}{f}\right)^{\frac{3}{2}},$$

or

$$\ln\frac{1}{f} = \left(\frac{3n}{4\pi g}\right)^{\frac{2}{3}}\frac{h^2}{2mkT} \text{ approx.} \tag{20}$$

When all the constituents are non-degenerate we can substitute the value of f from (19) in (15) and we get the usual Saha formula. When the electrons are degenerate but the atom and the ion are non-degenerate we get

$$\left(\frac{n_i}{n_a f_e}\right)_{\text{Eq.}} e^{U/kT} = \frac{g_i}{g_a}, \tag{21}$$

where f_e is given by (20).

2. Assembly and Radiation not in Thermodynamic Equilibrium

We shall now consider the system

$$\text{Atom} + \text{radiation} \rightleftharpoons \text{ion} + \text{electron} \tag{22}$$

and assume that it is traversed by radiation of any composition and intensity. Further, suppose that the electrons may be degenerate or non-degenerate while the atoms and the ions are non-degenerate.

We shall adopt the method based on the kinetic theory of gases first given by E. A. Milne (1924) for solving such problems.

Let n_a = number of neutral atoms per c.c. moving with velocity v_a,

n_i = number of positive ions per c.c. moving with velocity v_i,

n_e = number of free electrons per c.c. moving with velocity v_e.

* For the deduction see Saha and Srivastava (1935, p. 766).

Let this assembly be traversed by radiation coming in a small solid angle Ω and suppose that this radiation is a function of the direction. Thus if $I(\nu, \theta, \phi)$ denotes the specific intensity of radiation of frequency ν coming in the direction θ, ϕ, the total radiation of this frequency is

$$J(\nu) = \int I(\nu, \theta, \phi)\, d\omega, \tag{23}$$

where $d\omega$ denotes the elementary solid angle.

When a quantum of radiation falls on a neutral atom we have from the law of conservation of energy

$$h\nu + \tfrac{1}{2}m_a v_a^2 = h\nu_0 + \tfrac{1}{2}m_i v_i^2 + \tfrac{1}{2}m_e v_e^2, \tag{24}$$

where ν_0 is the frequency which is just able to ionize the atom and m_a, m_i, m_e denote the masses of the neutral atom, the ionized atom and the electron respectively. We are considering the non-relativistic case, but we shall assume that the electrons may be degenerate or non-degenerate. Now the atoms and the ions, being heavy, will be slow-moving in comparison with the free electrons. We can therefore, to a sufficient degree of approximation, neglect the velocity of the atom and of the ion. Equation (24) then yields

$$h\nu = h\nu_0 + \tfrac{1}{2}m_e v_e^2. \tag{25}$$

Consider a small element of volume dV of this assembly and suppose it is traversed by this radiation pencil. The number of acts of ionization in this volume element dV in unit time will be given by the expression

$$n_a \phi(v_a)\, dv_a\, dV \cdot J(\nu)\, d\nu \cdot \psi^*(\nu, v_a, v_i, v_e)\, [1 - \beta N_s/A_s]_e, \tag{26}$$

where $n_a \phi(v_a)\, dv_a\, dV$ is the number of atoms whose velocity lies within the range $v_a, v_a + dv_a$, $\psi^*(\nu, v_a, v_i, v_e)$ is the probability that a quantum of light on collision with an atom will ionize it according to equation (24), and $[1 - \beta N_s/A_s]_e$ is the probability that an electron can find a cell A_s with energy corresponding to v_e vacant. For the electron system $\beta = 1$ as it obeys Fermi-Dirac statistics.

To find N_s/A_s we must know the law of distribution of energy among the electrons. As the assembly is not in thermodynamic equilibrium and the incident radiation has any arbitrary composition, the distribution in the steady state will not correspond accurately to any temperature. We shall, however, assume that the distribution corresponds to the temperature T determined by the translational energy of the electrons so that it is given by (13), where T may be called the effective temperature of the assembly.

With this approximation (26) reduces to

$$n_a \phi(v_a) dv_a dV \cdot J(\nu) d\nu \cdot \psi^*(\nu, v_a, v_i, v_e) \left[\frac{f e^{\epsilon_s/kT}}{f e^{\epsilon_s/kT} + 1} \right]_e$$

$$= n_a \phi(v_a) dv_a dV \cdot J(\nu) d\nu \cdot \psi^*(\nu, v_a, v_i, v_e) \left[\frac{f e^{h(\nu - \nu_0)/kT}}{f e^{h(\nu - \nu_0)/kT} + 1} \right]_e \text{ from (25)}$$

$$= n_a J(\nu) d\nu dV \cdot \psi(\nu) \left[\frac{f e^{h(\nu - \nu_0)/kT}}{f e^{h(\nu - \nu_0)/kT} + 1} \right]_e, \qquad (27)$$

where
$$\psi(\nu) = \int_0^\infty \psi^*(\nu, v_a, v_i, v_e) \cdot \phi(v_a) dv_a$$

$$= \int_0^\infty \psi_1^*(\nu, v_a) \cdot \phi(v_a) dv_a.$$

We have neglected v_i, v_e in ψ_1^*, since $v_i \doteqdot v_a$ and v_e is a function of ν.

Let us now calculate the number of acts of recombination. This is proportional to the number of collisions between positive ions and electrons. Consider positive ions moving with velocities lying between v_i and $v_i + dv_i$ and electrons having velocities within the range v_e and $v_e + dv_e$. In unit volume the number of ions of this type is $n_i \phi(v_i) dv_i$ and the number of such electrons is $n_e \phi(v_e) dv_e$, where ϕ denotes the distribution function.

The number of collisions in unit volume per second between these ions on the one hand and the electrons on the other can be shown from kinetic theory methods to be given by

$$n_i n_e \phi(v_i) \phi(v_e) dv_i dv_e \cdot \sigma^2 V_r \cos\theta \cdot 2\pi \sin\theta d\theta,$$

where σ = collision radius of the ion, V_r = relative velocity of approach, and θ = angle between the directions of the two velocities.

In this particular case the ions move very slowly in comparison with the electrons, hence V_r is very nearly equal to v_e. We shall drop the suffix e and denote by v the velocity of the electron.

The total number of collisions in the volume element dV between ions of any velocity from 0 to ∞ and electrons having velocities lying in the range v and $v + dv$ for all angles of approach is given by

$$\int_{v_i = 0}^{v_i = \infty} \int_{\theta = 0}^{\theta = \pi/2} n_i n_e \phi(v_i) \phi(v) dv_i dv dV \cdot \sigma^2 v \cos\theta \cdot 2\pi \sin\theta d\theta$$

$$= \pi n_i n_e \phi(v) dv \sigma^2 v dV, \qquad (28)$$

since
$$\int_0^\infty n_i \phi(v_i) dv_i = n_i.$$

But every one of these collisions does not result in a capture. We write the probability of capture in the form

$$\lambda(v) + J(\nu)\,\mu(v),$$

the second factor being due to stimulated emission as postulated by Einstein. Hence the number of recombinations becomes

$$\pi n_i\,n_e\phi(v)\,dv\,dV\,.\,\sigma^2 v[\lambda(v) + J(\nu)\,\mu(v)]$$

$$= \pi n_i\,n_e\phi(v)\,dv\,dV\,.\,v[\,F(v) + J(\nu)\,G(v)], \quad (29)$$

where we have put

$$\sigma^2[\lambda(v) + J(\nu)\,\mu(v)] = F(v) + J(\nu)\,G(v).$$

In (29) we have to substitute the value of $\phi(v)$, the distribution law for the electrons as given by (17). Since

$$\epsilon_s = \tfrac{1}{2}mv^2 \quad \text{and} \quad d\epsilon_s = mv\,dv,$$

we get in place of (17) the relation

$$n_e\phi(v)\,dv = 4\pi g_e\left(\frac{m}{h}\right)^3 \frac{v^2\,dv}{f e^{\frac{1}{2}mv^2/kT} + 1}. \quad (30)$$

Thus (29) gives for the number of acts of recombination the expression

$$\pi n_i\,.\,4\pi g_e\left(\frac{m}{h}\right)^3 \frac{v^3\,dv}{f e^{\frac{1}{2}mv^2/kT} + 1}[F(v) + J(\nu)\,G(v)]\,dV. \quad (31)$$

In order to form a clear picture of the problem we shall take an example. Suppose the system is traversed by black-body radiation at temperature T_s coming in a narrow pencil of solid angle Ω, and assume that T_s is higher than the temperature of the assembly. In this case the quanta emitted by the assembly (due to recombination of ion and electron) will on the average have less energy than the quanta absorbed and therefore they will be of lower frequency. This is evident from the relation

$$\tfrac{1}{2}m_e v_e^2 + h\nu_0 = h\nu',$$

where ν' denotes the frequency of the quanta emitted as a result of recombination. Now $\tfrac{1}{2}m_e v_e^2$ on the average will correspond to the mean energy at the temperature of the assembly and will be less than the value when the assembly is at the same temperature as the radiation, in which case the quanta emitted on account of recombination have the frequency ν. Hence $\nu > \nu'$. It is evident therefore that there can be no detailed balancing for quanta of every frequency in the case we are considering. The principle of

detailed balancing will, however, hold when the radiation and the assembly have the same temperature.

In general, therefore, there is no detailed balancing as regards separate frequency regions, but the total number of acts of ionization always equals the total number of acts of recombination, since in the steady state the number of atoms or ions in the assembly must remain constant. The state of affairs can be well depicted by means of the curves shown in fig. 1, where the curve* R gives the number of acts of recombination and the curve I the
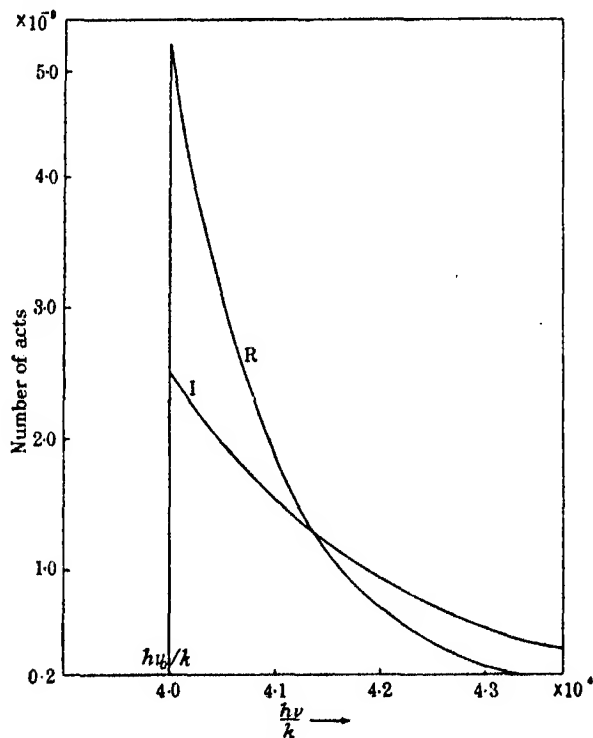
FIG. 1.

* Curve R is represented by the relation (see equation (37))

$$\frac{n_i}{g_i}\frac{g_a\,\{8\pi h\nu^3/c^2 + J(\nu)\}\,\psi(\nu)d\nu}{f\,e^{h(\nu-\nu_0)/kT} + 1} = \frac{n_a T_s}{T}\,e^{-\frac{h\nu_s}{k}\left(\frac{1}{T_s}-\frac{1}{T}\right)}\,e^{-\frac{h\nu}{kT}}.\frac{2h}{c^2}\,C\,d\nu\,.\,\Omega$$

obtained for the non-degenerate case by utilizing equations (40) and (35) and simplifying (40) in the manner employed in simplifying equation (41). Curve I is given by the relation

$$n_a\,J(\nu)\,d\nu\,.\,\psi(\nu)\,\frac{f\,e^{h(\nu-\nu_0)/kT}}{f\,e^{h(\nu-\nu_0)/kT} + 1} = n_a\frac{2h}{c^2}\,C\,e^{-h\nu/kT_s}d\nu\,.\,\Omega.$$

We have neglected the self-radiation of the gas coming from the different directions.

number of acts of ionization. The curves are drawn for the case when T_s is 2000° K., T the temperature of the assembly in the steady state is assumed to be 1000° K. and $h\nu_0/k = 4 \times 10^4$. $\psi(\nu)$ has been assumed to be zero for $\nu < \nu_0$ and equal to $C\nu^{-3}$ for $\nu > \nu_0$ (vide infra). Both curves indicate zero value for $\nu < \nu_0$, have a maximum for $\nu = \nu_0$, and then decay exponentially, the rate of decay in the ionization curve being much slower than in the recombination curve. The area enclosed between the curve and the x-axis is the same for both curves, since the total number of acts of ionization is equal to the total number of acts of recombination. When the temperatures of the radiation and the assembly are the same, the two curves will coincide.

Equating the total number of acts of both these types we get

$$n_a \int_{\nu_s}^{\infty} J(\nu)\, d\nu \,.\, \psi(\nu) \left[\frac{f e^{h(\nu-\nu_0)/kT}}{f e^{h(\nu-\nu_0)/kT} + 1} \right]$$

$$= n_i g_e \left(\frac{m}{h}\right)^3 .\, 4\pi^2 \int_0^{\infty} \frac{v^3 [F(v) + J(\nu)\, G(v)]\, dv}{f e^{\frac{1}{2} m v^2/kT} + 1}$$

$$= n_i g_e \left(\frac{m}{h}\right)^2 .\, 4\pi^2 \int_{\nu_s}^{\infty} \frac{v^2 [F(v) + J(\nu)\, G(v)]\, d\nu}{f e^{h(\nu-\nu_0)/kT} + 1}, \quad (32)$$

since

$$dv = \frac{h}{mv}\, d\nu.$$

Now consider for a moment the case of thermodynamical equilibrium with isotropic radiation at the same temperature as the assembly. In this case there is detailed balancing and hence for every frequency we should have

$$[n_a]_{\text{Eq.}} 4\pi B(\nu)\, d\nu \,.\, \psi(\nu) \left[\frac{f e^{h(\nu-\nu_0)/kT}}{f e^{h(\nu-\nu_0)/kT} + 1} \right]$$

$$= [n_i]_{\text{Eq.}} g_e \left(\frac{m}{h}\right)^2 4\pi^2 v^2 \frac{[F(v) + 4\pi B(\nu)\, G(v)]\, d\nu}{f e^{h(\nu-\nu_0)/kT} + 1}, \quad (33)$$

where $B(\nu)$ gives the specific intensity for the case of thermodynamical equilibrium and is given by Planck's law for the temperature T of the assembly.

Equation (33) yields

$$[n_a]_{\text{Eq.}} [f_e]_{\text{Eq.}} 4\pi B(\nu)\, \psi(\nu)\, e^{h(\nu-\nu_0)/kT}$$

$$= [n_i]_{\text{Eq.}} g_e \left(\frac{m}{h}\right)^2 4\pi^2 v^2 [F(v) + 4\pi B(\nu)\, G(v)]. \quad (34)$$

From (21) the ionization formula for thermodynamical equilibrium is

$$\left(\frac{n_i}{n_a f_e}\right)_{\text{Eq.}} e^{h\nu_0/kT} = \frac{g_i}{g_a}.$$ (35)

Substituting this value of the equilibrium concentrations in (34) we get

$$4\pi B(\nu).\psi(\nu) e^{h\nu/kT} = \frac{g_i g_e}{g_a}\left(\frac{m}{h}\right)^2 4\pi^2 v^2 [F(v) + 4\pi B(\nu)\,G(v)].$$

Or

$$4\pi B(\nu) = \frac{\dfrac{g_i g_e}{g_a}\left(\dfrac{m}{h}\right)^2 4\pi^2 v^2\, F(v)}{\psi(\nu)\, e^{h\nu/kT} - \dfrac{g_i g_e}{g_a}\left(\dfrac{m}{h}\right)^2 4\pi^2 v^2 G(v)}.$$

Now from Planck's law

$$B(\nu) = \frac{2h\nu^3/c^2}{e^{h\nu/kT} - 1}.$$

Hence on comparing we get

$$\left.\begin{aligned}
\frac{g_i g_e}{g_a}\left(\frac{m}{h}\right)^2 4\pi^2 v^2 G(v) &= \psi(\nu), \\
\frac{g_i g_e}{g_a}\left(\frac{m}{h}\right)^2 4\pi^2 v^2 F(v) &= \frac{8\pi h\nu^3}{c^2}\,\psi(\nu).
\end{aligned}\right\}$$ (36)

Or

$$\frac{F(v)}{G(v)} = \frac{8\pi h\nu^3}{c^2}.$$

Therefore

$$g_e\left(\frac{m}{h}\right)^2 4\pi^2 v^2\,[F(v) + J(\nu)\,G(v)] = \frac{g_a}{g_i}\left[\frac{8\pi h\nu^3}{c^2} + J(\nu)\right]\psi(\nu).$$

Substituting this in the general equation (32) for equilibrium we get

$$n_a \int_{\nu_\bullet}^{\infty} J(\nu)\,d\nu.\psi(\nu)\left[\frac{f e^{h(\nu-\nu_0)/kT}}{f e^{h(\nu-\nu_0)/kT} + 1}\right] = n_i \frac{g_a}{g_i}\int_{\nu_\bullet}^{\infty}\frac{\{8\pi h\nu^3/c^2 + J(\nu)\}\psi(\nu)\,d\nu}{f e^{h(\nu-\nu_0)/kT} + 1}.$$ (37)

Or

$$\frac{n_i}{n_a} = \frac{g_i}{g_a}\frac{\displaystyle\int_{\nu_\bullet}^{\infty} J(\nu)\,d\nu.\psi(\nu)\frac{f e^{h(\nu-\nu_0)/kT}}{f e^{h(\nu-\nu_0)/kT} + 1}}{\displaystyle\int_{\nu_\bullet}^{\infty}\frac{\{8\pi h\nu^3/c^2 + J(\nu)\}\,\psi(\nu)\,d\nu}{f e^{h(\nu-\nu_0)/kT} + 1}}.$$ (38)

With the help of (35) this yields

$$\frac{n_i}{n_a f} = \left(\frac{n_i}{n_a f}\right)_{\text{Eq.}}\frac{\displaystyle\int_{\nu_\bullet}^{\infty} J(\nu)\,d\nu.\psi(\nu)\frac{e^{h\nu/kT}}{f e^{h(\nu-\nu_0)/kT} + 1}}{\displaystyle\int_{\nu_\bullet}^{\infty}\frac{\{8\pi h\nu^3/c^2 + J(\nu)\}\,\psi(\nu)\,d\nu}{f e^{h(\nu-\nu_0)/kT} + 1}}.$$ (39)

This is the general formula giving the ionization when radiation of any kind is traversing the assembly, the electrons being supposed to obey Fermi-Dirac statistics. We shall now consider a few special cases.

Case 1. Electrons are non-degenerate, i.e. $f \gg 1$. Equation (39) then reduces to

$$\frac{n_i}{n_a f} = \left(\frac{n_i}{n_a f}\right)_{\text{Eq.}} \frac{\int_{\nu_0}^{\infty} \psi(\nu) J(\nu)\, d\nu}{\int_{\nu_0}^{\infty} \psi(\nu)\{8\pi h\nu^3/c^2 + J(\nu)\} e^{-h\nu/kT}\, d\nu}.$$

But f is given by (19), hence we get

$$\frac{n_i n_e}{n_a} = \left(\frac{n_i n_e}{n_a}\right)_{\text{Eq.}} \frac{\int_{\nu_0}^{\infty} \psi(\nu) J(\nu)\, d\nu}{\int_{\nu_0}^{\infty} \psi(\nu)\{8\pi h\nu^3/c^2 + J(\nu)\} e^{-h\nu/kT}\, d\nu}, \tag{40}$$

which is the Woltjer-Milne formula.

Case 2. Electrons are degenerate, i.e. $f \ll 1$.

In this case f is given by (20) and $g_e = 2$. Hence equation (39) yields

$$\frac{n_i}{n_a} e^{\frac{h^2}{2mkT}\left(\frac{3n_e}{8\pi}\right)^{\frac{2}{3}}} = \left[\frac{n_i}{n_a} e^{\frac{h^2}{2mkT}\left(\frac{3n_e}{8\pi}\right)^{\frac{2}{3}}}\right]_{\text{Eq.}} \frac{\int_{\nu_0}^{\infty} J(\nu)\, d\nu \cdot \psi(\nu) \dfrac{e^{h\nu/kT}}{f e^{h(\nu-\nu_0)/kT}+1}}{\int_{\nu_0}^{\infty} \dfrac{\{8\pi h\nu^3/c^2 + J(\nu)\}\psi(\nu)\, d\nu}{f e^{h(\nu-\nu_0)/kT}+1}}. \tag{41}$$

This equation cannot be integrated unless the function $\psi(\nu)$ is known. But $\psi(\nu)$ has been calculated only for the H-atom; in general, however, it is a good approximation to put $\psi(\nu) = C\nu^{-3}$. Further suppose that the incident radiation is coming in a small solid angle Ω from a black-body source at a higher temperature T_s and is uniform in that solid angle.* Then

$$J(\nu) = \frac{2h\nu^3}{c^2} \frac{\Omega}{e^{h\nu/kT_s}-1} = \frac{2h\nu^3}{c^2} e^{-h\nu/kT_s}\Omega,$$

since $e^{h\nu/kT_s} \gg 1$, as we are dealing with frequencies greater than ν_0. Also for the same reason $J(\nu) \ll 8\pi h\nu^3/c^2$.

---

* We are here neglecting the radiation coming from the other portions of the gas itself.

Hence the ratio of the integrands on the right-hand side of equation (41) becomes

$$\frac{\int_{\nu_s}^{\infty} \frac{2h\nu^3}{c^2} e^{-h\nu/kT_s} \Omega \cdot \frac{C}{\nu^3} \cdot \frac{e^{h\nu/kT} d\nu}{fe^{h(\nu-\nu_0)/kT}+1}}{\int_{\nu_s}^{\infty} \frac{8\pi h\nu^3}{c^2} \cdot \frac{C}{\nu^3} \cdot \frac{d\nu}{fe^{h(\nu-\nu_0)/kT}+1}} = \frac{\Omega}{4\pi} \frac{\int_{\nu_s}^{\infty} \frac{e^{\frac{h\nu}{k}\left(\frac{1}{T}-\frac{1}{T_s}\right)} d\nu}{fe^{h(\nu-\nu_0)/kT}+1}}{\int_{\nu_s}^{\infty} \frac{d\nu}{fe^{h(\nu-\nu_0)/kT}+1}}. \qquad (42)$$

$\Omega/4\pi$ is called the dilution factor W.

Let us put $\qquad\qquad u = h(\nu-\nu_0)/kT;$

then $\qquad\qquad du = h d\nu/kT.$

Expression (42) then becomes

$$W \frac{\int_0^{\infty} \frac{e^{\frac{h}{k}\left[\nu_s+\frac{kT}{h}u\right]\left[\frac{1}{T}-\frac{1}{T_s}\right]} du}{fe^u+1}}{\int_0^{\infty} \frac{du}{fe^u+1}}. \qquad (43)$$

The method of evaluating such integrals has been discussed at length by Sommerfeld (1928). He has shown that the integral

$$\int_0^{\infty} \frac{du}{fe^u+1} \cdot \frac{d\phi(u)}{du} = \phi(u_0) \qquad (44)$$

as a first approximation, where $u_0 = \ln(1/f)$ and $\phi(u)$ is such that it vanishes for $u = 0$. Using this result (43) yields

$$\frac{W e^{\frac{h\nu_s}{kT}\left(1-\frac{T}{T_s}\right)} \left[\int e^{\left(1-\frac{T}{T_s}\right)u} du + \text{const.}\right]_{u=u_0}}{[u+\text{const.}]_{u=u_0}} = \frac{W e^{\frac{h\nu_s}{kT}(1-x)}}{u_0} \left[\frac{e^{(1-x)u_0}-1}{1-x}\right],$$

since the constants have to be so determined that the function within the brackets [ ] is zero for $u = 0$. T/T_s has been put equal to x. Substituting $u_0 = \ln(1/f)$ the expression becomes

$$\frac{W e^{\frac{h\nu_s}{kT}(1-x)}}{\ln(1/f)} \cdot \frac{(1/f)^{1-x}-1}{1-x}.$$

Hence equation (41) for ionization becomes

$$\frac{n_i}{n_a f} = \left(\frac{n_i}{n_a f}\right)_{\text{Eq.}} \frac{W e^{\frac{h\nu_s}{kT}(1-x)}}{(1-x)\ln(1/f)}[(1/f)^{1-x}-1], \qquad (45)$$

where $x = T/T_s$ and f is given by (20).

It is easy to see that if $x = 1$, the multiplying factor in (45) reduces to W as it should be since we have assumed that no radiation comes from other directions.

For values of x not very near 1 equation (45) yields, since $f \ll 1$,

$$\frac{n_i}{n_a} = W\left(\frac{n_i}{n_a f}\right)_{\text{Eq.}} \frac{e^{\frac{h\nu_0}{kT}(1-x)}}{(1/f)^x (1-x) \ln(1/f)}$$

$$= W \frac{\frac{g_i}{g_a} e^{-\frac{h\nu_0}{kT}x}}{(1/f)^x (1-x) \ln(1/f)}. \tag{46}$$

For $1/f \to \infty$ the right-hand side tends to zero, indicating that the ionization will be negligible for a highly degenerate system. The degenerate electrons therefore appear to act like a screen tending to diminish the ionization of the atom even when it is acted on by incident radiation at a higher temperature.

As an illustration, suppose the gas is illuminated by a distant star of temperature T_s and radius r and the distance between the star and the gas is R. In this case $W = \Omega/4\pi = r^2/4R^2$ and the ionization is given by (46), where $x = T/T_s$.

So far we have assumed that the system is at the temperature T while it is exposed to radiation at the temperature T_s, but we have not enquired as to what this T will be. Evidently in the steady state T will depend upon T_s. In order to calculate the actual value of T we have to make some assumption regarding the electronic free path. If it is assumed that the expelled electrons remain free for a sufficient time so that most of them acquire a Fermi-Dirac velocity distribution as a result of collisions, and that the diffuse radiation from the gas corresponds to the temperature T, it can be shown* that

$$T = WT_s \frac{\ln(1 - e^{-h\nu_0/kT_s})}{\ln(1 - e^{-h\nu_0/kT})}. \tag{47}$$

From this we have approximately

$$\frac{T_s - T}{T} = \frac{kT_s}{h\nu_0} \ln(T/WT_s). \tag{48}$$

Thus knowing T_s, ν_0 and W we can calculate T. This may be used in equation (46) to give the ionization. Thus we get

$$\frac{n_i}{n_a} e^{\frac{h^2}{2mkT_s}\left(\frac{3n_e}{8\pi}\right)^{\frac{2}{3}}} \left(1 - \frac{T}{T_s}\right) \frac{h^2}{2mkT}\left(\frac{3n_e}{8\pi}\right)^{\frac{2}{3}} = W \frac{g_i}{g_a} e^{-h\nu_0/kT_s},$$

where T is given by (48).

* See Rosseland (*1936*, p. 322) for a deduction of this result.

In this paper we have considered the modification of the Woltjer-Milne formula when only one of the products of ionization, viz. the electron, behaves as a degenerate gas. In case the neutral atom or the ionized atom also behave as degenerate gases the formula will require further modification.

It is a pleasure to record my sincere thanks to Professor M. N. Saha, F.R.S., for his kind interest in this work and to Dr D. S. Kothari for a discussion of the problem.

SUMMARY

The generalized ionization formula in the case of thermodynamical equilibrium for an assembly consisting of atoms, ions, electrons and radiation is derived, the particles being supposed to obey any statistics.

The ionization produced in matter has been found for the case when the reaction space is traversed by radiation at a higher temperature. The electrons have been assumed to obey F.D. statistics, while the atom and the ion are taken to obey Boltzmann (classical) statistics. The general ionization formula for this case is derived and two limiting cases discussed. The Woltjer-Milne formula for ionization in any radiation field is readily obtained as a special case of the general formula. The ionization formula for the case when the electrons behave as a degenerate gas is also deduced from the general formula. On substituting the usual expression for the probability of ionization, viz. $\psi = C\nu^{-3}$, it is found that the ionization becomes much less when the electrons are highly degenerate.

REFERENCES

Ambarzumian 1935 *Mon. Not. R. Astr. Soc.* **95**, 469.
Bothe 1928 *Z. Phys.* **46**, 327.
Brillouin 1931 "Die Quanten-statistik."
Darwin and Fowler 1923 *Phil. Mag.* **45**, 1.
Eddington, A. S. 1926 *Proc. Roy. Soc.* A, **111**, 424.
Kothari, D. S. 1936 *Mon. Not. R. Astr. Soc.* **96**, 833.
Majumdar, R. C. 1931 *Astr. Nachr.* **242**, 145.
Milne, E. A. 1921 *a Observatory*, **44**, 261.
—— 1921 *b Observatory*, **44**, 269.
—— 1924 *Phil. Mag.* **47**, 209.
—— 1930 *Mon. Not. R. Astr. Soc.* **90**, 769.
Pannekoek, A. 1926 *Bull. Astr. Insts. Netherlds*, **3**, 207.
Rosseland 1936 "Theoretical Astrophysics."
Russel, H. N. 1922 *Astrophys. J.* **55**, 119.

Saha, M. N. 1920 a *Phil. Mag.* **40**, 472.
— 1920 b *Phil. Mag.* **40**, 809.
— 1921 *Proc. Roy. Soc.* A, **99**, 135.
Saha and Srivastava 1935 "A Treatise on Heat," 2nd ed.
Saha, M. N. and Sur, R. K. 1926 *Phil. Mag.* **1**, 1025.
Sommerfeld, A. 1928 *Z. Phys.* **47**, 1.
Woltjer 1925 a *Nature, Lond.*, March 14, April 11.
— 1925 b *Physica*, **5**, 406.

Investigation into the relation of shower frequency to general cosmic-ray intensity

By L. Jánossy*

(*Communicated by P. M. S. Blackett, F.R.S.*—
Received 12 *April* 1938. *Revised* 8 *June* 1938)

1. Introduction

Follett and Crawshaw (1936) have compared the transition curve of showers from lead at sea-level and under 30 m. of clay (60 m. water equivalent) and find that the number of showers decreases about in the same ratio as the vertical intensity. Other measurements of the showers below sea-level have been made by Clay and Clay (1935), Auger and Rosenberg (1935), Ehmert (1937 a, b), Wilson (1938) and by Pickering (1935, 1937).

The purpose of the work described in this paper was to investigate how the form of the shower transition curves at the two levels (i.e. sea-level and under 30 m. of clay) depends on the presence of large masses of light material (e.g. stone) over the lead absorber producing the showers. Drigo (1935) and Auger, Leprince-Ringuet and Ehrenfest (1936) had previously shown that at sea-level the presence of such light materials greatly reduces the number of showers and also alters the shape of the transition curve. Thus to get comparable results at the two levels it is necessary to use similar distributions of dense matter over the counting set. In the work of Follett and Crawshaw this was not the case.

The sea-level results were obtained under a light roof, but the underground measurements were necessarily made fairly close under the solid clay above

* John Harling Fellow in Physics, 1938.

the tunnel. It seemed therefore desirable to investigate whether the proportionality found between the shower frequency and the vertical intensity was really significant, or whether it was only due to the particular geometrical conditions.

2. THE EXPERIMENTAL METHOD AND THE RESULTS

The measurements were made with the pentagonal quintuple arrangement already described by Follett and Crawshaw (1936) and Hu (1937). The counters used had dimensions 30 × 2 cm. and the lead absorber to produce the showers was placed in a semicircle close around the five counters. With this arrangement the transition curve was determined under the following conditions:

TABLE I

Experiment	Location	Material over lead	Transition curve
1	Sea-level	⎧ Light roof	Fig. 2, curve 1
2	(under a light roof)	⎨ 30 cm. of stone of density 2·4	Fig. 2, curve 2
3		⎩ 100 cm. of stone	Fig. 2, curve 3
4	Holborn Tube	⎧ 3 m. below solid roof	Fig. 3, curve 1
5	Station	⎩ 100 cm. of stone	Fig. 3, curve 2

The relative vertical intensities observed with triple coincidences between three counters in the same vertical plane were:

TABLE II

Sea-level	16·6
Sea-level + 1 m. stone	13·4
Tube station	·1·0

The counter arrangement and the relative position of the lead and the stone are shown in fig. 1.
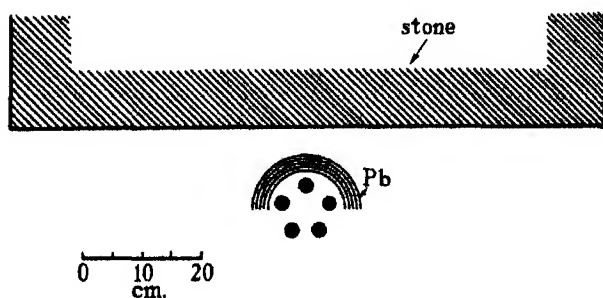
FIG. 1. The experimental arrangement.

Comparing the three sea-level curves of fig. 2, we see that the effect of placing dense material of low atomic number over the apparatus is to produce (*a*) an increase of the recorded shower frequency for small thicknesses of lead, (*b*) a reduction of the maximum frequency, (*c*) a shift of the maximum to lower thicknesses of lead.
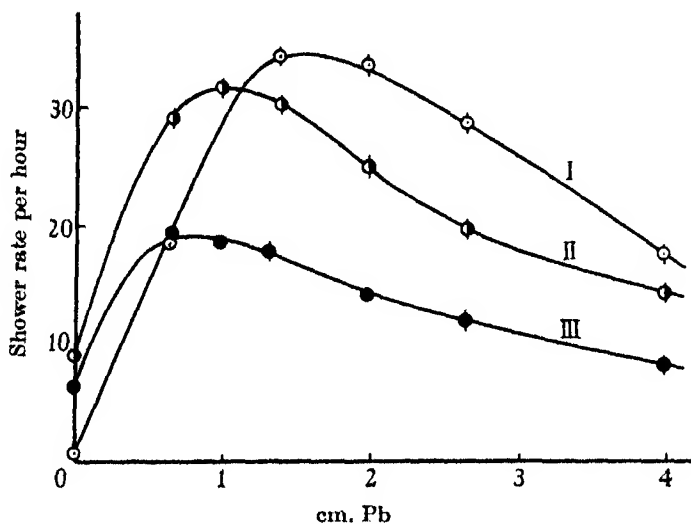
The shower transition curve. I. Under a light roof. II. Under 30 cm. stone. III. Under 100 cm. stone.

FIG. 2. The influence of light material above the lead on the shower transition curve at sea-level.
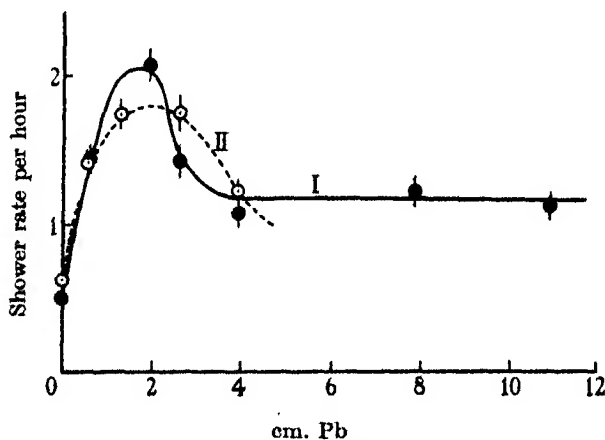
Transition curve. I. Under 30 m. of clay and 3 m. below the solid roof. II. Under 30 m. of clay and 1 m. stone close above the lead.

FIG. 3. Shower transition curves under 30 m. of clay.

Similar results have been reported by other workers. Drigo (1935) found that a layer of light material of mass 270 g./cm.² over the lead absorber reduced the intensity of the maximum to about a quarter of its value with no light material, and that the curve remained nearly constant for greater thicknesses of lead. The difference between Drigo's result and that in fig. 2 lies probably in the fact that Drigo's counter arrangement recorded two simultaneous rays, while our arrangement recorded only showers of three or more rays, and so excluded ordinary secondaries. Auger, Leprince-Ringuet and Ehrenfest (1936) observed a similar effect at a height of 3500 m. above sea-level by comparing the transition curve obtained under a heavy cement roof with that in free air.

3. DISCUSSION OF THE RESULTS

Fig. 4 shows the results of Exps. 2 and 5 (transition curve at sea-level and underground) plotted together. The ordinates of the underground curve have all been increased in the ratio (1 : 16·6) of the vertical intensities. Since the difference between the two curves is hardly outside the experimental error, it can be concluded that, for thicknesses of lead less than 4 cm., the transition curve 2 found under a light roof at sea-level is nearly the same shape as the curve obtained underground at a distance of 3 m. below the solid roof.
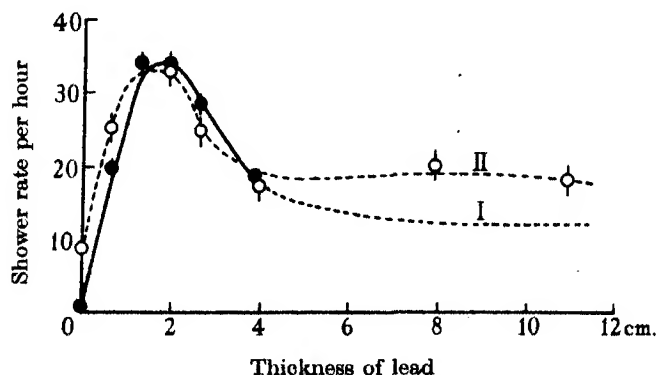
I. Sea level. II. Under 30 m. clay. Observed values multiplied by 16·6.

FIG. 4. Relative shower intensity at sea-level and underground with no dense material close above the lead.

Although, unfortunately, in our experiment the sea-level transition was not observed for thicknesses of lead greater than 4 cm., many other investigations have been made with much greater thicknesses. The data of

Schwegler (1935) have been used to give the probable continuation (shown dotted) of the sea-level transition curve I, fig. 4. The tail of the transition curve at sea-level is probably well below the corresponding part of the underground curve.

We therefore conclude from fig. 4 that the intensity of the showers for lead less than 4 cm. thick is proportional to the vertical intensity, but that showers from greater thicknesses of lead are relatively more frequent underground.
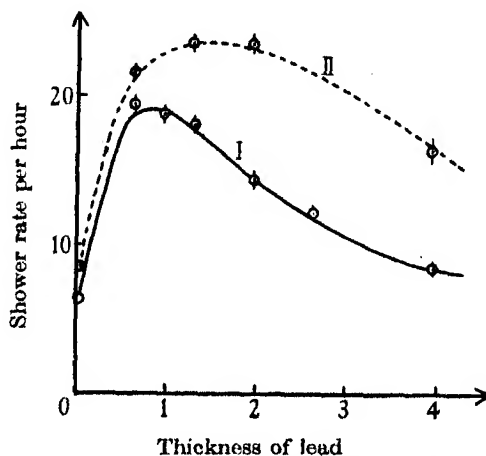
I. Sea level.   II. Under 30 m. of clay.   Observed values multiplied by 13·4.

FIG. 5. Relative shower intensities at sea-level and underground with 1 m. stone close above the lead.

A rather similar conclusion can be drawn from fig. 5, where the results of Exps. 3 and 5 at the two levels, both with 1 m. stone close above the lead, are plotted together; the ordinates of the former curve have been increased in the ratio (1 : 13·4) of the vertical intensities. Here the relative shower intensity at both levels is the same for thicknesses of lead up to 1 cm., but the relative number of showers from greater thicknesses of lead is considerably greater underground.

It may be mentioned that we now have an explanation of the apparent contradiction between the measurements of Clay and Clay (1935) and those of Ehmert (1937 a, b): Clay and Clay found that the shower intensity under 2–300 m. of water was proportional to the recorded general intensity, while Ehmert found that the shower frequency increased relatively with depth. But as Clay and Clay observed the shower intensity produced in 0·6 cm. Fe + 1·2 cm. Pb, they measured the showers producing the maximum of

the transition curve, whereas Ehmert used 5 cm. Pb for producing showers, and so observed the shower frequency in the tail.

The underground transition curves, fig. 3, show a maximum at about 2 cm. of lead. Follett and Crawshaw (1936) and Auger and Rosenberg (1935) did not find a maximum but observed a flat transition curve. The difference between their observations and ours is probably due to the different experimental arrangements. We placed the lead close around the counters, whereas Follett and Crawshaw used the lead at a distance of 2·5 cm. from the counters. So we measured showers of larger angular spread than Follett and Crawshaw. That the maximum in our transition curve is indeed due to the larger angular spread is supported by measurements of Hu (1937) and of Schmeisser and Bothe (1938) at sea-level, and Auger, Ehrenfest and Fréon (1936) at high altitudes, which show that the maximum is less pronounced for showers of small than for those of wide angular spread. The zero effect in our observations seems to be higher than that observed by Auger and Rosenberg (1935). Since our apparatus was placed in an iron hut (approximately 2 mm. wall thickness) our zero count may be due to showers emerging from the walls of the hut.

The presence of solid material of low atomic number above the apparatus may influence the number of showers and the shape of the transition curve in three main ways.

(a) Density transition effect

Even if the material (density ρ_2) above the apparatus were of the same atomic constitution as air (density ρ_1) so that only a change of density was involved, one still would expect a marked effect on the recorded number of showers, owing to the fact that showers have a finite angular spread. The particles from air which are recorded by the counters have their origin at a distance ρ_2/ρ_1 times farther away than those from stone, and so the showers from air are spread over a correspondingly larger area; thus the chance that an air shower will be recorded by the counting set is relatively small. It will be noticed that the number of showers recorded under no lead and no stone at sea-level is in fact very small.

Further, the change of density can have the effect of smoothing out the maximum of the transition curve (figs. 2 and 3). This can be seen by the following consideration: the number of secondary electrons reaching the lead absorber is the same for any density of the material above it, provided the total absorption is the same. But in the case of air above the lead the electrons mostly enter singly and *each* electron produces *one small* shower.

On the other hand, if stone is above the lead, simultaneous groups of electrons must enter the lead and will so produce *together one* large shower.

Hence for thicknesses of lead near the optimum value, we may expect in air a large number of relatively small showers due to single electrons, while under stone we may expect a smaller number of larger showers due to associated electrons. This is presumably the main origin of the large decrease of the number of recorded showers when stone is placed above the lead. A similar argument is given by Auger and Grivet-Meyer (1936).

It is clear that the degree of association of the rays will effect the recorded number of showers differently according as to whether the rays associated are of high or low energy. For in the case of high-energy rays, each single ray will produce (e.g. in the optimum thickness of absorber) so large a shower that the chance of its being recorded is nearly unity. Thus the association of several such rays can only have the effect that some showers will not be observed. On the other hand, in case of small showers there are some showers lost by association, but other showers which would not have been observed singly will now be observed when associated. So the decrease in number will be less for small than for large showers—it is even probable that the recorded number of sufficiently small showers increases by association.

It follows that an increased degree of association brought about by, say, the presence of dense material over the apparatus will bring the low-energy rays into relatively greater prominence than those of high energy. This may be the origin of the shift of the maximum of the transition curve to smaller thicknesses of lead, fig. 2.

The observations show that the process of association has no large effect on the first slope of the transition curve.

(b) *Atomic number transition effect*

This effect depends on the change of Z and would be expected even if the shower particles had no angular spread. Since the material used (stone) had a mean value of Z of about 15, its influence could be expected to be more like that of air, $\bar{Z} = 7\cdot2$, than that of a heavy element, e.g. lead ($Z = 82$), and so no large transition effect of this type is to be expected for the transition air to stone.

Bhabha (1938) has suggested that showers associated with the penetrating component consist of cascade showers produced by electrons set in motion by the close collision of heavy electrons. The number of such collisions is proportional to Z. The secondary electrons produced by these collisions give rise to cascade showers with a mean range proportional to $1/Z^2$. If there is equilibrium between the heavy particles and their secondaries, the frequency

of simultaneous groups of electrons (i.e. cascade showers) emerging from a material with the atomic number Z is roughly proportional to $Z \cdot 1/Z^2 = 1/Z$. Thus the number of showers decreases with Z, but their size increases. The numerical calculations of Bhabha show that the total number of electrons in lead should be about twice that in air or water.

(c) Filtration effect

A thick layer of light material will alter the composition of the incident beam. This effect is certainly appreciable at sea-level, where 1 m. stone corresponds to one-quarter of the thickness of the atmosphere. The absorption of the vertical rays due to 1 m. stone is about 20 % at sea-level, but at a depth of 60 m. water equivalent must be quite small. At sea-level fig. 2 shows that the maximum shower frequency is reduced to about one-half by 1 m. of stone; only a part of the reduction may be due to filtration.

This discussion leads us therefore to the general conclusion that the effect of dense light material (stone) over the apparatus is (a) to increase the degree of association of the rays falling on the lead and so to decrease the number of recorded showers emerging from the optimum thickness of lead, (b) to shift the maximum of the transition curve to a lower thickness, (c) to diminish somewhat the shower frequency along the whole transition curve by filtration.

4. Comparison with theory

The shape of the transition curve up to about 4 cm. of lead can be explained by the cascade theory of Bhabha and Heitler (1937) and of Carlson and Oppenheimer (1937). But without new assumptions this theory cannot explain (a) the presence of an appreciable number of electrons at sea-level and still less the number found underground, (b) the existence of the tail of the shower transition curve.

Both effects can be understood as being partly due to secondary electrons set in motion by the penetrating particles, which are themselves presumably heavy electrons. This view has been recently discussed by Bhabha (1938).

The transition curve under 30 m. of clay can thus be understood as the superposition of two effects. (1) Heavy electrons entering the lead produce secondary electrons in the lead which give rise to cascade showers. This process produces a flat transition curve without a maximum. (2) Electrons already produced by the heavy electrons in the earth above the apparatus enter the lead and produce cascade showers. These rays will produce a transition curve which has a maximum and then decreases to zero. The

superposition of (1) and (2) gives the observed curve. Whether the resulting curve is flat or shows a maximum, depends on the relative importance of the two mechanisms, and will thus vary considerably with the arrangement of the counters and the other conditions of the experiment.

It is possible that some part of the small showers contributing to the tail of the transition curves may be due to the heavy electrons, which constitute the penetrating component, giving rise to normal electrons, when their energy falls much below 2×10^8 e-volts (Blackett 1938). Such a transition of a heavy electron to a normal electron will be accompanied by the emission of radiation which will produce a small shower.

The initial slope of the transition curve at both levels is proportional to the vertical intensity. We therefore conclude that showers observed under thin layers of lead are mainly due to secondary electrons produced by the penetrating cosmic-ray particles, and that *even at sea-level* there is approximate *equilibrium* between the penetrating group and its secondaries.

That the shower frequency increases with height more rapidly than the vertical intensity, has been shown by Rossi and Beneditti (1934), Johnson (1935), Auger, Leprince-Ringuet, Ehrenfest (1936) and Braddick and Gilbert (1936). These high-altitude showers can be regarded as cascade showers produced by primary electrons on their way through the atmosphere. But few of these showers seem to be able to reach sea-level, for if they did one would find a greater relative intensity of showers at sea-level than underground, which is not the case.

This conclusion is in agreement with the theory of Bhabha and Heitler (1937) concerning the range of cascade showers, and the conclusion of Blackett (1938) that only about 1 % of the particles at sea-level with energy greater than 3×10^8 e-volts are electrons.

Summary

The frequency of cosmic-ray showers was observed at sea-level and under 30 m. of clay (60 m. of water equivalent). The shower frequencies at the two levels were compared with the corresponding vertical intensities.

Part of the experiments were carried out with layers of light material close above the lead in order to maintain similar geometrical conditions for the shower production at both levels. The marked observed effect of the stone on the transition curve can be understood as due mainly to the spatial association of the shower producing electrons emerging from the stone, rather than to filtration. The relative shower intensity, i.e. (shower frequency/vertical intensity), of the showers producing the first slope of the transition curve was found to be nearly the same at sea-level and underground; on the other hand, the shower frequency due to showers producing the tail of the transition curve increases relatively with depth. The conclusion was drawn that most of the showers at sea-level and underground are due to secondaries of some kind produced by the penetrating particles, and that consequently relatively few can be due to primary electrons.

REFERENCES

Auger, Leprince-Ringuet, Ehrenfest 1936 *J. Phys. Radium*, 1, 58.
Auger, Ehrenfest and Fréon 1936 *C.R. Acad. Sci., Paris*, 203, 1082.
Auger and Grivet-Meyor 1936 *C.R. Acad. Sci., Paris.*, 203, 246.
Auger and Rosenberg 1935 *C.R. Acad. Sci., Paris*, 201, 1116.
Bhabha 1938 *Proc. Roy. Soc.* A, 164, 151.
Bhabha and Heitler 1937 *Proc. Roy. Soc.* A, 159, 432.
Blackett 1938 *Proc. Roy. Soc.* A, 165, 11.
Braddick and Gilbert 1936 *Proc. Roy. Soc.* A, 156, 570.
Carlson and Oppenheimer 1937 *Phys. Rev.* 51, 220.
Clay 1937 *Proc. Acad. Sci. Amst.* 40, 564.
Clay and Clay 1935 *Physica*, 11, 1042.
Drigo 1935 *Ric. Sci.* 1, 11.
Ehmert 1937a *Z. Phys.* 106, 751.
— 1937b *Naturwissenschaften*, 25, 448.
Follett and Crawshaw 1936 *Proc. Roy. Soc.* A, 155, 546.
Hu Chien Shan 1937 *Proc. Roy. Soc.* A, 158, 581.
Johnson 1935 *Phys. Rev.* 47, 318.
Pickering 1935 *Phys. Rev.* 47, 423.
— 1937 *Phys. Rev.* 52, 1131.
Rossi and Beneditti 1934 *Ric. Sci.* 5, 379.
Schmeisser and Bothe 1938 *Ann. Phys., Lpz.*, 32, 161.
Schwegler 1935 *Z. Phys.* 96, 74.
Wilson 1938 *Phys. Rev.* 53, 337.

An interferometric wave-length comparison of the red cadmium radiation emitted by different sources

By W. Ewart Williams and D. V. Gogate

King's College, London

[Plate 13]

Introduction

The red line of cadmium with a wave-length value of 6438·4696A in "normal" air at 15° C. and 760 mm. pressure has long been used as the spectroscopic standard for accurate wave-length comparisons. From time to time, the type of discharge tube and the type and condition of the discharge tube have been defined with increasing stringency both by the International Astronomical Union and by the International Conference of Weights and Measures, but in some respects they are yet not completely specified. Thus, while a lower limit is set on the diameter of the capillary no mention is made of its length.

In many respects this discharge tube, which has to be maintained at 320° C. by means of an electric oven, is not a convenient source to employ. The high temperature gives rise to an enhanced Doppler width, and the comparatively high excitation voltage with its large electric field may cause a Stark broadening of the line. It can be easily shown that the errors due to optical defects in the Fabry-Pèrot plates have least effect when the light is passed through the plates as a parallel beam instead of being focused on the interferometer itself. A large magnification has to be used to enlarge the 2 mm. diameter disk source so that it fills the slit of the spectrograph. Since a high-aperture ratio lens cannot be used because of the limitations of the furnace and the capillary, the intensity of illumination at the slit is proportionately reduced.

Various alternative sources have been proposed at different times, the most successful probably being the hot-electrode cadmium lamp made by the A.E.G. in Germany and now manufactured in this country by the General Electric Company under the trade name of "Osira Cadmium Lamp". Sears and Barrell (1933) have shown that the wave-length of the red line emitted by one of these lamps with a current of 1 amp. was the same as that from a Michelson tube with a certainty of 1 part in 16 × 10⁶. Jackson (1936) carried out an extensive investigation, comparing this lamp

[509]

at different currents with a standard Michelson tube containing 1 mm. of air and employing etalons with plate separations of 2, 3, 6, 7½ and 10 cm. The vacuum form of Michelson tube specified by the International Astronomical Union and the International Conference of Weights and Measures could not be used for the 10 cm. etalon as the fringes were not sharp enough for accurate measurement. Jackson found that with a 2 amp. current the line is displaced by about 0·0002 A to the red, with a current of 1·7 amp. the red shift is just measurable and is about 0·0001 A, while with a current of 1·1 amp. no detectable difference occurred. He further compared the wave-length of the red line emitted by a Schüler hollow cathode discharge with the standard Michelson tube using etalons of 1·5 and 2·5 cm. gap and found them identical within ± 0·0001 A. Larger gaps could not be used as the work could not be carried out in the constant temperature room. No particulars are given regarding the current in the Schüler tube or the dimensions of the hollow cathode, and there is no indication whether a hot or water-cooled cathode was used.

One of us (W. E. W.) in conjunction with A. Middleton (1938) has recently determined the vacuum wave-lengths of a number of iron lines by means of the reflexion echelon grating, and the work has recently been extended to the ultra-violet region in conjunction with J. W. Drinkwater. For this purpose Schüler hollow-cathode discharge tubes were used, both for the red cadmium standard and for the iron lines. As is now well known, the Schüler lamp, suitably cooled if necessary, gives much narrower lines than any other form of discharge with the exception of a well-collimated atomic beam which would be too complicated for general use.

The original object of this investigation was to make a comparison between the three sources, the standard Michelson lamp, the Osira lamp and the Schüler tube. With the apparatus and facilities at our disposal, we found that the Michelson lamp could only be included in the comparison at the cost of a very considerable reduction in the standard of accuracy attainable on account of the comparatively low intensity of this source. In view of the work of Sears and Barrell and especially of Jackson the comparison was limited to the Osira lamp and the Schüler tube.

EXPERIMENTAL

The ideal method of comparing the wave-lengths of the same line from two different sources by means of the Fabry-Pérot interferometer would be to photograph the fringes simultaneously from both sources. In order to differentiate the fringe system of one source from that of the other,

the light from the one could be polarized in the horizontal plane and that from the other in the vertical plane. The two sets of fringes would overlap on the slit of the spectrograph but could be again separated on the photographic plate by including a weak double-image prism (of appropriate angle) in the parallel beam of the spectrograph. Equal density of the different sets of fringes could be obtained by suitably silvering the partially reflecting plate that reflects the light from one source into the path of the other; alternatively, a balance of intensity could be obtained even more easily by including a second nicol in the path of the stronger source and suitably rotating it. Any alteration, whether in the instrument or in the refractive index of air, would affect both sets of fringes equally, and the fringes being side by side would be in the best position to minimize any effects due to unequal shrinkage of the emulsion film on the photographic plate when it is dried after development and fixing. The double-image prism would have to be of good definition and cover an aperture equal to that of the spectrograph collimator objective. Before adopting this method, we decided to try a simpler arrangement, which, if it appeared to show any real wave-length difference, could be relinquished in favour of the above method in which any errors are automatically compensated.

The interferometer used for this work was a type of Fabry-Pèrot etalon designed by one of us (W. E. W.) in conjunction with Mr Twyman of Messrs Adam Hilger, Ltd., and manufactured by them (N. 71). It may be used with any plate separation between 2·5 and 100 mm. It has a bed of "invar" steel and differs from most other interferometers in the very high degree of accuracy to which the large diameter (6·5 cm.) plates have been optically worked and in the method of adjustment of parallelism of the plates, very fine-pitched tilting screws replacing the spring pressure devices previously used in such etalons. The parallelism of the plates is obtained by means of localized fringes from an independent mercury light source, and the plate separation is given by a vernier scale and microscope to within ± 0·005 mm.

The fringes are focused on the slit of a Hilger E 2 spectrograph (with glass train) by means of a 50 cm. achromatic objective mounted on the bed of the interferometer. In order to prevent any displacement of the fringe system on the spectrograph slit due to any small shift of one instrument with respect to the other, the two instruments are connected together with a rigid ball and socket coupling immediately beneath the slit; any small relative displacement of the instruments will then only produce a second order displacement of the fringes on the slit.

The normal plate carrier of the spectrograph is provided with a rack and

pinion movement so that successive exposures, one above the other, are obtained. With such an arrangement there is always the risk of unequal shrinkage of the film when the plate is fixed and dried. For this investigation a special plate-holder was made in which the plate could be moved in its own plane in a horizontal direction, so that successive exposures of the fringe pattern of a particular line will lie side by side. By controlling the lateral displacement accurately, one set of fringes would run on into the other and any vertical displacement of the fringes would become obvious. It is well known from experience with the coincidence type of range finder that the eye can set in, or detect a lack of, alignment to a far higher degree of precision than it can place a cross-wire at the centre.

To minimize the disturbing effects of heat from the light sources, the interferometer and the spectrograph were isolated by dividing the room, which was underground, with a double-walled low-conductivity partition. The light from either source was passed into the interferometer portion of the room through two small plate-glass windows, one on each side of the partition, which was also provided with a good-fitting heat-lagged door to give access to the instrument compartment.

The first point to be ascertained was the degree of accuracy with which the plate could be moved horizontally in its own plane through small known intervals. For this purpose the spectrograph slit was rotated to a horizontal position and its length adjusted to approximately 0·4 mm. by means of the V slit. Plate 13 shows with a magnification of 10 diameters the results of eighteen such exposures. Each horizontal line is a succession of three images (or exposures) of this narrow horizontal slit. At the end of every third exposure, the plate-holder was racked down so that sets of lines could be obtained and their separation (in different parts) measured by means of the travelling micrometer. The lines are straight and parallel to within the accuracy of measurement ($\pm 0\cdot001$ mm.).

The Fabry-Pèrot fringes for the Osira cadmium lamp, the Schüler tube and finally the Osira lamp again were then photographed in a similar manner, the plate being moved horizontally between each exposure. Before discussing these results, further details of the light sources chosen should be given. The Osira cadmium lamp was used with a current of 1·3 amp. This is a larger current than was used by Sears and Barrell or Jackson. With the particular lamp which we used, the intensity of the red cadmium line fluctuated considerably with currents of less than 1·3 amp., making it very difficult to arrange an exposure time to give a convenient density of image.

From previous experience with other lamps of this type we found that

the minimum current for an approximately constant brightness of the red line varies from lamp to lamp. Some lamps run steadily and give a constant and sufficient brightness of the red line with less than 1 amp., while others require 1·5 amp. for the same results. The discrepancy probably arises owing to the small differences in the hot-wire electrodes. In some lamps the bombardment is very local, causing a few turns of the electrode wire to become intensely hot with a small total current. In other lamps the whole of the heater coil appears uniformly bright, and these lamps require a larger total current. We therefore suggest that when these lamps are to be used as wave-length standards the current should not be numerically specified, but that they should be used with the smallest current that will give a constant brightness for the red line.

The Schüler tube source had an iron cathode 8 cm. long, 1·2 and 1·4 cm. internal and external diameters. A pure cadmium rod bored to within 2 mm. of the end with a 0·9 cm. diameter drill fitted closely into the iron cathode. Helium at a pressure of about 1 mm. was circulated through the tube, and the usual copper oxide furnace with liquid air-cooled chabazite traps was used to remove impurities. With this source the presence of even a small trace of mercury reduces the brightness of the cadmium spectrum very considerably, and it is advisable to reduce the heating of the diffusion pump even at the cost of lowering the efficiency of the circulation system, since the ordinary liquid air traps tend to allow some mercury vapour to pass. Both the anode and the cathode were water-cooled.

Normally this Schüler lamp would be used with a current of 100 mA. With a 10 cm. gap etalon the fringes are obviously narrower than with the Osira lamp. In order to make the comparison easier and more certain, the current in the Schüler lamp was increased to 200 mA. Even then, the hollow cathode source was the more homogeneous.

Most of the exposures were made with an etalon gap of 10 cm., although a number were made with gaps of 7·5 and 5 cm. The parallelism of the plates was adjusted at full aperture (6 cm.), and a diaphragm was placed close to the interferometer to limit the beam falling on the plates to a central disk of 1·5 cm. diameter. An exposure was first made with the Osira lamp, the photographic plate moved a small amount horizontally in its own plane, and a second exposure, now from the Schüler tube, obtained by removing the mirror used to reflect the first source into the line of the instruments. Finally, the photographic plate was moved again a similar amount and a second exposure of the Osira lamp obtained by replacing the mirror in its original position. The exposure times were chosen so that the three patterns should have approximately the same density.

RESULTS

No detectable wave-length difference was found between the two sources with a 5 cm. etalon gap. When 7·5 and especially when 10 cm. gaps were used, it was found impossible to obtain reliable photographs unless one observer remained in the instrument room (to move the photographic plate as required) while the other attended to the light sources. Since the etalon plates in this instrument are not screened, the mere act of opening the communicating door would set up draughts which cause fringe displacements. This may also, in part, be due to small pressure changes, since for this wave-length, with a 10 cm. etalon a pressure change of 0·05 mm. of Hg will cause a change of order of nearly 0·006. Temperature and pressure readings were taken before and after each complete exposure, and all plates taken when any detectable change occurred (0·1° C., 0·05 mm.) were rejected without further examination.

Since one observer had to remain in the instrument compartment, the temperature of the air would rise and the carbon dioxide content would increase, but the lowering of the refractive index of the air due to the increased temperature would be more than counterbalanced by the higher refractive index of the carbon dioxide replacing the oxygen of the air. The optical path difference of the interferometer was in consequence steadily increasing so that the original idea of testing the exact alignment of the first fringe of each of the three sets of fringes had to be abandoned. Fig. 2, Plate 13 shows a photograph (× 10) of the fringes with a 10 cm. gap. The thicker line of overlap occurs between the first Osira lamp exposure and that of the Schüler tube. The order of the difference between the successive exposures is less than 0·005, but is clearly visible to the eye in the central fringes.

The exact fractional part for each set was determined from measurements of the second to the fifth ring by means of the least squares method developed by Rolt and Barrell (1929). Table I gives the results of measurements on typical plates with an interferometer gap of 10 cm. corresponding to an order of interference of approximately 310,000. Fringe system (1) refers to the first Osram lamp exposure, (2) to that of the Schüler tube, and (3) to the second exposure of the first source. The corresponding fractional parts are given in the third column. In the fourth column are given the fractional parts for the same plate given by a remeasurement using another portion of the screw of the travelling micrometer. This is included to give an indication of the accuracy of measurement.

The change in the fractional part in the 21 min. required for the three

sets of exposures was normally about 0·01, and for these plates no detectable difference exists between the fractional part for the Schüler tube and the mean value for the two Osira lamp exposures. The results of plate 7 have been included, as it shows the greatest difference of all the plates that have been measured. If we assume that the path difference is increasing uniformly, the average value for the Schüler tube should have been $0·661_5$. A change of 0·0025 in f (which is not much greater than the error of measurement) implies a difference of wave-length of less than 1 part in 100×10^6, since the order of interference is over 300,000. The average value of the order difference from all the other plates is 0·0005, but since this is less than the possible error of setting no exact significance can be attached to it except to say that no detectable wave-length difference exists between these sources.

TABLE I

Plate no.	Fringe system	$f \times 10^3$	$f \times 10^3$	Average value
20	1	559	558	558_5
	2	563	561	562
	3	568	566	567_5
24	1	898	900	899
	2	902	905	903_5
	3	910	910	910
7	1	648	—	—
	2	664	—	—
	3	675	—	—

SUMMARY

A comparison is made between the wave-lengths of the red cadmium line ($\lambda = 6438$ A) emitted by a G.E.C. Osira cadmium lamp and a Schüler hollow-cathode discharge by photographing the Fabry-Pèrot fringes due to the two sources side by side in the same horizontal plane by means of

a specially designed plate-holder. Interferometer gaps up to 10 cm. were used, and the greatest difference recorded was less than 1 part in 100×10^6 or 0·00006 A.

References

Jackson, C. V. 1936 *Proc. Roy. Soc.* A, **155**, 407.
Rolt F. H. and Barrell, H. 1929 *Proc. Roy. Soc.* A, **122**, 131.
Sears, J. E. and Barrell, H. 1933 *Proc. Roy. Soc.* A, **139**, 202.
Williams, W. E. and Middleton, A. 1938 *Proc. Roy. Soc.* A. (In the press.)

Effusion phenomena in relativistic quantum statistics

By B. N. Srivastava, M.Sc.

Lecturer in Physics, Allahabad University

Considerable attention has been devoted in recent years to the investigation of properties of degenerate and non-degenerate matter. Quite recently the Joule-Thomson expansion of degenerate matter has been studied by Kothari (1938), while the present author (Srivastava 1938) investigated the same effect in non-degenerate matter and showed that the phenomenon of Joule-Thomson expansion may possibly serve as a means of experimentally testing the statistics obeyed by helium gas. In the present communication the effusion phenomena in degenerate and non-degenerate matter have been investigated, taking into account the effect of relativistic mechanics. In § 1 the effusion of non-degenerate matter has been discussed while degenerate matter has been considered in § 2.

1. Non-degenerate matter

Let us consider a gas contained in a vessel having a narrow orifice on one side and let the gas escape through this orifice into a vacuum outside. We shall assume that the pressure of the gas is so low that the mean free path is much greater than the dimensions of the orifice. Under these conditions we shall calculate the amount of matter effusing out through this hole.

The relativistic expression for the distribution law is*

$$N_\epsilon d\epsilon = \frac{a_s}{f e^{\epsilon/kT} + \beta},\tag{1}$$

where

$$a_s = \frac{4\pi g V}{c^3 h^3} (\epsilon^2 + 2mc^2\epsilon)^{\frac{1}{2}} (\epsilon + mc^2) d\epsilon.\tag{2}$$

Here ϵ denotes the kinetic energy, i.e.

$$\epsilon = mc^2 \left[\frac{1}{(1 - v^2/c^2)^{\frac{1}{2}}} - 1 \right],\tag{3}$$

m being the rest mass and v the velocity of the particle, $N_\epsilon d\epsilon$ the number of particles having their kinetic energy lying between ϵ and $\epsilon + d\epsilon$, g the quantum weight of the particles, and $\beta = +1$ for matter obeying Fermi-Dirac statistics and $\beta = -1$ for Bose-Einstein statistics.

The number of particles per c.c. of the gas having their velocity lying between v and $v + dv$ is given by

$$n_\epsilon d\epsilon = \frac{4\pi g}{c^3 h^3} \frac{(\epsilon^2 + 2mc^2\epsilon)^{\frac{1}{2}} (\epsilon + mc^2) d\epsilon}{f e^{\epsilon/kT} + \beta},\tag{4}$$

where ϵ and v are related by (3). The number of particles effusing out through unit area of the hole per second is given by

$$\int_0^\infty n_\epsilon d\epsilon \int_0^{\frac{1}{2}\pi} v \cos\theta \, \tfrac{1}{2} \sin\theta \, d\theta,$$

since $\frac{1}{2} \sin\theta \, d\theta$ is the solid angle between the directions θ and $\theta + d\theta$. Hence the number becomes

$$\int_0^\infty n_\epsilon d\epsilon \, \tfrac{1}{4} v = \tfrac{1}{4} n\bar{c},$$

where $\bar{c}$ is the mean velocity. Substituting the value of $n_\epsilon d\epsilon$ from (4) we have

$$\tfrac{1}{4} n\bar{c} = \int_0^\infty \frac{\pi g}{c^3 h^3} \frac{(\epsilon^2 + 2mc^2\epsilon)^{\frac{1}{2}} (\epsilon + mc^2) d\epsilon \, v}{f e^{\epsilon/kT} + \beta}.\tag{5}$$

Now from (3) we have

$$v = c \left\{ 1 - \frac{1}{\left(\frac{\epsilon}{mc^2} + 1 \right)^2} \right\}^{\frac{1}{2}}.$$

* See Majumdar (1932, p. 247).

Substituting for v and putting $\epsilon/kT = u$ we have

$$\tfrac{1}{4}n\bar{c} = \int_0^\infty \frac{\pi g}{c^3 h^3} \frac{(u^2 k^2 T^2 + 2ukT\,mc^2)\,ckT\,du}{fe^u + \beta}$$

$$= \frac{\pi g m}{h^3} k^2 T^2 \int_0^\infty \frac{\left(u^2\dfrac{kT}{mc^2} + 2u\right) du}{fe^u + \beta}. \tag{6}$$

We shall first consider the non-degenerate case $(f \gg 1)$.

Assuming the matter to obey Fermi-Dirac statistics $(\beta = +1)$ the term under the integral sign can be expanded in an infinite series for $f > 1$. Thus

$$\int_0^\infty \frac{\left[\dfrac{u^2 kT}{mc^2} + 2u\right] du}{fe^u + 1} = \int_0^\infty \left(\frac{u^2 kT}{mc^2} + 2u\right)\frac{1}{f}e^{-u}\left[1 + \frac{1}{f}e^{-u}\right]^{-1} du$$

$$= \int_0^\infty \left[\frac{u^2 kT}{mc^2} + 2u\right]\left[\frac{1}{f}e^{-u} - \frac{1}{f^2}e^{-2u} + \frac{1}{f^3}e^{-3u} - \ldots\right] du.$$

Similarly for the case of Bose-Einstein statistics $(\beta = -1)$ we get

$$\int_0^\infty \left[\frac{u^2 kT}{mc^2} + 2u\right]\left[\frac{1}{f}e^{-u} + \frac{1}{f^2}e^{-2u} + \frac{1}{f^3}e^{-3u} + \ldots\right] du.$$

Thus in the general case we can write the expression in the form

$$\int_0^\infty \left[\frac{u^2 kT}{mc^2} + 2u\right]\left[\frac{1}{f}e^{-u} - \frac{\beta}{f^2}e^{-2u} + \frac{1}{f^3}e^{-3u} - \ldots\right] du.$$

But

$$\int_0^\infty u^2 \frac{1}{f^k} e^{-ku}\,du = \frac{2}{k^3}\frac{1}{f^k},$$

and

$$\int_0^\infty u \frac{1}{f^k} e^{-ku}\,du = \frac{1}{k^2}\frac{1}{f^k}.$$

Hence the number of particles effusing out becomes

$$\frac{k^2 T^2}{h^3}\pi g m\left[\frac{kT}{mc^2}\left\{\frac{2}{f} - \frac{\beta}{f^2}\cdot\frac{2}{2^3} + \frac{1}{f^3}\cdot\frac{2}{3^3} - \ldots\right\} + 2\left\{\frac{1}{f} - \frac{\beta}{f^2}\cdot\frac{1}{2^2} + \frac{1}{f^3}\cdot\frac{1}{3^2} - \ldots\right\}\right]$$

$$= \frac{k^2 T^2}{h^3}\pi g m\frac{2}{f}\left[1 + \frac{kT}{mc^2} - \frac{\beta}{f}\left(\frac{1}{4} + \frac{kT}{8mc^2}\right) + \ldots\right], \tag{7}$$

neglecting small quantities of higher order.

This is the general expression, taking full account of the effect of relativistic mechanics. We shall consider two limiting cases of this expression. These

will be referred to as relativistic (when $\epsilon \gg mc^2$) and non-relativistic (when $\epsilon \ll mc^2$).

For the non-relativistic case it can be shown that*

$$\frac{1}{f} = \frac{1}{f_0}\left[1 - \frac{15}{8y} + \frac{\beta}{2^{\frac{3}{2}}} \cdot \frac{1}{f_0} \cdots \right], \tag{8}$$

where
$$f_0 = \frac{g(2\pi m k T)^{\frac{3}{2}}}{n h^3}, \quad y = \frac{mc^2}{kT}.$$

Hence the number effusing out in this case becomes

$$\tfrac{1}{4} n \sqrt{\frac{8kT}{m\pi}} \left\{ 1 - \frac{7}{8y} + \frac{\beta}{4f_0}(\sqrt{2}-1)\cdots \right\}. \tag{9}$$

For the completely non-relativistic case ($y \to \infty$) this expression reduces to

$$\tfrac{1}{4} n \sqrt{\frac{8kT}{m\pi}} \left\{ 1 + \frac{\beta}{4f_0}(\sqrt{2}-1)\cdots \right\}. \tag{10}$$

This expression can be obtained more simply by starting with the non-relativistic expression for the distribution law, viz.

$$n_\epsilon d\epsilon = \frac{2\pi g}{h^3} \frac{(2m)^{\frac{3}{2}} \epsilon^{\frac{1}{2}} d\epsilon}{f e^{\epsilon/kT} + \beta}$$

and proceeding as above. For completely non-degenerate systems ($f \gg 1$) this expression reduces to the simple formula for a classical perfect gas. For matter obeying Bose-Einstein statistics the effusion is less while for Fermi-Dirac statistics it is greater than that for a classical perfect gas. The departure is however small, being only about 1 % for $f = 10$.

For the relativistic case ($y \ll 1$) it can be shown that

$$\frac{1}{f^R} = \frac{n}{8\pi g}\left(\frac{ch}{kT}\right)^3\left[1 - y + \frac{\beta}{8} \frac{1}{f_0^R} \cdots \right], \tag{11}$$

where
$$\frac{1}{f_0^R} = \frac{n}{8\pi g}\left(\frac{ch}{kT}\right)^3.$$

Hence the number effusing out becomes

$$\tfrac{1}{4} nc(1 - \text{terms in } y^2). \tag{12}$$

For the completely relativistic ($y \to 0$) and completely non-degenerate system this reduces to $\tfrac{1}{4}nc$. This is obvious, since for the completely relativistic case the average velocity will be very nearly equal to c.

* For a complete list of such formulae see Kothari and Singh (1938, pp. 145–7).

It may prove of interest to find out the mass effusing out per unit time, since in the relativistic case the mass of all particles coming out is not the same. Proceeding as before the mass of gas effusing out per unit area per second is obtained by multiplying (5) by $m/\sqrt{(1-v^2/c^2)}$. We obtain

$$\int_0^\infty \frac{\pi g}{c^3 h^3} \cdot \frac{(\epsilon^2 + 2mc^2\epsilon)^{\frac{1}{2}} (\epsilon + mc^2) d\epsilon \, v \, \dfrac{m}{(1-v^2/c^2)^{\frac{1}{2}}}}{f e^{\epsilon/kT} + \beta} .$$

Substituting for v this becomes

$$\int_0^\infty \frac{\pi g}{c^4 h^3} \frac{(\epsilon^2 + 2mc^2\epsilon)(\epsilon + mc^2) d\epsilon}{f e^{\epsilon/kT} + \beta} .$$

Putting $\epsilon/kT = u$ we get for the mass effusing out

$$\frac{\pi g}{c^4 h^3} (kT)^4 \int_0^\infty \frac{\left(u^2 + \dfrac{2mc^2}{kT} u\right)\left(u + \dfrac{mc^2}{kT}\right) du}{f e^u + \beta} \tag{13}$$

$$= \frac{\pi g}{c^4 h^3} (kT)^4 \int_0^\infty \frac{\left(u^3 + \dfrac{3mc^2}{kT} u^2 + \dfrac{2m^2 c^4}{k^2 T^2} u\right) du}{f e^u + \beta} .$$

Expanding into an infinite series as before we get

$$\frac{\pi g}{c^4 h^3} (kT)^4 \left[\left\{\frac{6}{f} - \frac{6\beta}{2^4 f^2} + \frac{6}{3^4 f^3} \cdots\right\} + \frac{3mc^2}{kT}\left\{\frac{2}{f} - \frac{2\beta}{2^3 f^2} + \frac{2}{3^3 f^3} \cdots\right\} \right.$$

$$\left. + \frac{2m^2 c^4}{k^2 T^2}\left\{\frac{1}{f} - \frac{\beta}{2^2 f^2} + \frac{1}{3^2 f^3} \cdots\right\}\right]$$

$$= \frac{\pi g}{c^4 h^3} (kT)^4 \frac{2}{f}\left[3 + 3y + y^2 - \frac{\beta}{f}\left(\frac{3}{16} + \frac{3y}{8} + \frac{y^2}{4}\right) + \frac{1}{f^2}\left(\frac{1}{27} + \frac{y}{9} + \frac{y^2}{9}\right) \cdots\right], \tag{14}$$

where $y = mc^2/kT$.

For the non-relativistic case $(y \gg 1)$ we get, on substituting the value of f, the expression

$$\tfrac{1}{4} nm \sqrt{\frac{8kT}{m\pi}}\left[1 + \frac{9}{8y} + \frac{\beta}{4f_0}(\sqrt{2}-1)\ldots\right], \tag{15}$$

approximately. For the completely non-relativistic case $(y \to \infty)$ this reduces to

$$\tfrac{1}{4} nm \sqrt{\frac{8kT}{m\pi}}\left[1 + \frac{\beta}{4f_0}(\sqrt{2}-1)\right], \tag{16}$$

as is evident from (10).

For the relativistic case $(y \ll 1)f^R$ is given by (11). Hence the expression (14) for the mass effusing out becomes

$$\frac{3}{4}\frac{nkT}{c}\left[1+\frac{1}{16}\frac{\beta}{f_0^R}-\text{terms in }y^2 \ldots\right],\tag{17}$$

approximately. For the completely relativistic $(y \to 0)$ and completely non-degenerate case this reduces to

$$\frac{3}{4}\frac{nkT}{c}.\tag{18}$$

2. DEGENERATE MATTER

We shall now calculate the effusion of degenerate matter. The number of particles effusing out per second is given by equation (6), which has now to be evaluated for the degenerate case. Let us first consider matter obeying Fermi-Dirac statistics and since it is degenerate we have $f \ll 1$. We shall follow Sommerfeld's method (Sommerfeld 1928). Thus the number is equal to

$$\frac{\pi gm}{h^3}k^2T^2\left[\frac{1}{3}\frac{kT}{mc^2}\int_0^\infty\frac{\frac{d}{du}(u^3)\,du}{fe^u+1}+\int_0^\infty\frac{\frac{d}{du}(u^2)\,du}{fe^u+1}\right]\tag{19}$$

$$=\frac{\pi gm}{h^3}k^2T^2\left[\frac{1}{3}\frac{kT}{mc^2}u_0^3+u_0^2\right],\tag{20}$$

to a first approximation, where

$$u_0 = \ln\frac{1}{f} = \frac{mc^2}{kT}[(1+x^2)^{\frac{1}{2}}-1],\tag{21}$$

and

$$x = \frac{h}{mc}\left(\frac{3n}{4\pi g}\right)^{\frac{1}{3}}.\tag{22}$$

On substituting for u_0 this reduces to

$$\frac{\pi gm^3c^4}{3h^3}[2+x^2-2(1+x^2)^{\frac{1}{2}}][2+(1+x^2)^{\frac{1}{2}}].\tag{23}$$

This is the general expression giving the number of particles effusing out correct to a first approximation in the case of a Fermi-Dirac degenerate gas. We shall consider two limiting cases.

For the completely non-relativistic case $(x \to 0)$ this reduces to

$$\frac{3}{16}\left(\frac{3}{4\pi g}\right)^{\frac{1}{3}}\frac{h}{m}n^{\frac{4}{3}}.\tag{24}$$

33·2

This expression can be obtained more readily by starting with the non-relativistic expression for the distribution law. We can express (24) in terms of the pressure p with the help of the relation

$$p = \frac{4}{15} \frac{\pi g h^2}{m} \left(\frac{3n}{4\pi g}\right)^{\frac{5}{3}}.$$

Thus we get for effusion the expression

$$\frac{1}{4}\left(\frac{15}{4}\right)^{\frac{2}{5}} \left(\frac{\pi g}{mh^3}\right)^{\frac{1}{5}} p^{\frac{3}{5}},$$

i.e. the number of particles effusing out varies as $p^{\frac{3}{5}}$ and is independent of the temperature T to a first approximation. This should be contrasted with expression (10) for the non-degenerate case according to which the effusion varies as $p/\sqrt{T}$.

For the completely relativistic case $(x \to \infty)$ equation (23) reduces to $\frac{1}{4}nc$. Thus the number of particles effusing out in the completely relativistic case is the same whether the gas is highly degenerate or highly non-degenerate.

Following Sommerfeld's method we can evaluate (19) to a second approximation. Thus we obtain for the number of particles effusing out the expression

$$\frac{\pi g m}{h^3} k^2 T^2 \left[\frac{kT}{mc^2}\left\{\frac{u_0^3}{3}\left(1+\frac{\pi^2}{u_0^2}\right)\right\} + u_0^2\left(1+\frac{\pi^2}{3u_0^2}\right)\right]$$

$$= \frac{\pi g m}{h^3} k^2 T^2 u_0^2 \left[\frac{kT}{3mc^2}\left(u_0+\frac{\pi^2}{u_0}\right) + 1 + \frac{\pi^2}{3u_0^2}\right], \qquad (25)$$

where u_0 is given by

$$u_0 = \ln\frac{1}{f} = \frac{mc^2}{kT}\left[\left\{1+x^2\left(1-\frac{\pi^2}{3x^4y^2}(1+2x^2)\right)\right\}^{\frac{1}{2}} - 1\right], \qquad (26)$$

correct to small quantities of the first order. We can deduce this expression for $\ln 1/f$ in relativistic mechanics in the following manner:

From the distribution law in this case expressed by equation (4) we readily obtain, after making the usual substitutions, that

$$n = \frac{1}{3}\frac{4\pi g}{c^3 h^3}(kT)^3 \int_0^\infty \frac{\frac{d}{du}\left(u^2+\frac{2mc^2}{kT}u\right)^{\frac{3}{2}} du}{fe^u+1}$$

$$= \frac{4\pi g}{3}\left(\frac{kT}{ch}\right)^3 \left[\left(u_0^2+\frac{2mc^2}{kT}u_0\right)^{\frac{3}{2}}\right.$$

$$\left. + \frac{\pi^2}{?}\left(u_0^2+\frac{2mc^2}{kT}u_0\right)^{-\frac{1}{2}}\left(2u_0^2+\frac{4mc^2}{kT}u_0+\frac{m^2c^4}{k^2T^2}\right) + \dots\right],$$

following Sommerfeld's method. This after reduction yields, correct to small quantities of the first order, the equation

$$u_0^2 + 2u_0 \frac{mc^2}{kT} = \left(\frac{3n}{4\pi g}\right)^{\frac{2}{3}} \left(\frac{ch}{kT}\right)^2 \left[1 - \frac{\pi^2}{3}\left\{\frac{2}{\left(\frac{3n}{4\pi g}\right)^{\frac{2}{3}}\left(\frac{ch}{kT}\right)^2} + \frac{1}{\left(\frac{3n}{4\pi g}\right)^{\frac{4}{3}}\left(\frac{ch}{kT}\right)^4} \frac{m^2c^4}{k^2T^2}\right\}\right],$$

which yields the value of u_0 given by (26).

As a particular case of (25) we can consider the completely non-relativistic case ($y \to \infty$, $x \to 0$). In this case (25) yields

$$\frac{\pi g m}{h^3} k^2 T^2 u_0^2 \left[1 + \frac{\pi^2}{3u_0^2}\right] = \frac{3}{16}\left(\frac{3}{4\pi g}\right)^{\frac{1}{3}} \frac{h}{m} n^{\frac{4}{3}} \left[1 + \left(\frac{4\pi m kT}{h^2}\right)^2 \left(\frac{\pi g}{6n}\right)^{\frac{4}{3}} + \dots\right], \quad (27)$$

since u_0 in this case is given by

$$u_0 = \left(\frac{3n}{4\pi g}\right)^{\frac{2}{3}} \frac{h^2}{2mkT}\left[1 - \frac{1}{3}\left(\frac{4\pi m kT}{h^2}\right)^2 \left(\frac{\pi g}{6n}\right)^{\frac{4}{3}} + \dots\right]. \tag{28}$$

Equation (27) can be obtained easily by starting with the non-relativistic expression for the distribution law. This equation indicates a very slight dependence of effusion upon the temperature, there being a slight increase for higher temperature.

For the completely relativistic case (25) also reduces to $\frac{1}{4}nc$ approximately.

We shall now calculate the mass of gas effusing out in the degenerate case. This is given by (13) which can be written in the form

$$\frac{\pi g}{c^4 h^3}(kT)^4 \frac{1}{4} \int_0^\infty \frac{\frac{d}{du}\left(u^2 + \frac{2mc^2}{kT}u\right)^2 du}{fe^u + 1} \tag{29}$$

$$= \frac{1}{4}\frac{\pi g}{c^4 h^3}(kT)^4 \left\{u_0^2 + \frac{2mc^2}{kT}u_0\right\}^2 \text{ approx.}$$

$$= \frac{1}{4}\frac{\pi g}{c^4 h^3}(kT)^4 \left[\frac{mc^2}{kT}\left\{(1+x^2)^{\frac{1}{2}} - 1\right\}\right]^2$$

$$\times \left[\frac{mc^2}{kT}\{(1+x^2)^{\frac{1}{2}} - 1\} + \frac{2mc^2}{kT}\right]^2 \text{ from (21)}$$

$$= \frac{1}{4}\frac{\pi g m^4 c^4 x^4}{h^3}$$

$$= \frac{3}{16}\left(\frac{3}{4\pi g}\right)^{\frac{1}{3}} h n^{\frac{4}{3}} \tag{30}$$

with the help of (22). This expression shows that, to a first approximation,

the mass effusing out is the same whether we consider the relativistic mechanics or the non-relativistic mechanics (see equation (24)), though the number in the two cases is different.

The expression (29) for mass can be evaluated accurately by Sommerfeld's method. We thus get for the mass the expression

$$\frac{1}{4}\frac{\pi g}{c^4 h^3}(kT)^4\left[\left\{u_0^2+\frac{2mc^2}{kT}u_0\right\}^2+\frac{2\pi^2}{3}\left\{3u_0^2+\frac{6mc^2}{kT}u_0+\frac{2m^2c^4}{k^2T^2}\right\}+\frac{7\pi^4}{15}\right], \quad (31)$$

where u_0 is given by (26).

For the completely relativistic case this reduces to

$$\frac{3}{16}\left(\frac{3}{4\pi g}\right)^{\frac{1}{2}}hn^{\frac{4}{3}}\left[1+\frac{2^{\frac{1}{3}}\pi^2}{3^{\frac{2}{3}}}\left(\frac{8\pi g}{n}\right)^{\frac{2}{3}}\left(\frac{kT}{ch}\right)^2\cdots\right], \quad (32)$$

since u_0 in this case is given by

$$u_0=\frac{ch}{kT}\left(\frac{3n}{4\pi g}\right)^{\frac{1}{3}}\left[1-\frac{\pi^2}{2^{\frac{1}{3}}3^{\frac{2}{3}}}\left(\frac{8\pi g}{n}\right)^{\frac{2}{3}}\left(\frac{kT}{ch}\right)^2\cdots\right].$$

So far in this section we have considered matter obeying Fermi-Dirac statistics. In case of Bose-Einstein statistics the distribution law is expressed by (4) with $\beta=-1$. Here the state of degeneracy corresponds to $f\rightarrow1$. f cannot be less than 1, for then the number of particles having very small energy would be negative, which is absurd. The total number n of particles can be obtained by integrating the right-hand side of (4) as explained in §1 for $f>1$. If we put $f=1$ as the extreme degenerate case in this expression for n we get a fixed value for n which is obviously absurd, since the number of particles can have any value depending upon the mass of gas taken. This difficulty arises as the integral is not valid for $f=1$, hence for such values of f we must replace it by a sum extending over the discrete levels. Very simple arguments, however, show that the effusion of a Bose-Einstein degenerate gas will be negligible. Thus from equation (4) it follows that for $f=1$ (Bose-Einstein degenerate gas) the number of particles having very small kinetic energy or velocity is large, while the number of particles having large velocities is extremely small. Thus since the majority of the particles have almost zero velocity and zero energy any dynamical phenomenon such as effusion, etc., in the gas will be insignificant.

We have to make a few more remarks regarding the results obtained above. In the different cases we have found the number of particles as well as the total mass of gas effusing out. On dividing the latter by the former we get the average mass of the particles in the effusion stream. Thus in the

completely relativistic and completely non-degenerate case the average mass is given by

$$\frac{3}{4}\frac{nkT}{c}\Big/\frac{1}{4}nc = \frac{3kT}{c^2}, \tag{33}$$

while in the completely relativistic and completely degenerate case this is equal to

$$\frac{3}{16}\left(\frac{3}{4\pi g}\right)^{\frac{1}{4}}hn^{\frac{1}{4}}\Big/\frac{1}{4}nc = \frac{3}{4}\left(\frac{3}{4\pi g}\right)^{\frac{1}{4}}\frac{h}{c}n^{\frac{1}{4}}, \tag{34}$$

which is independent of m. In general, however, it can be easily verified for the relativistic degenerate and non-degenerate cases that if we retain small quantities of higher order and compare the energy or mass per particle in the effusion stream with that in the original gas at rest, it is greater in the former case. This should be so, since the faster molecules are able to escape very quickly through the orifice and hence are more abundant in the effusion stream than in the initial gas. In the completely relativistic case the two become equal as is obvious (see equations (17), (32) and (33), (34)).

Summary

In this paper the effusion phenomena in non-degenerate and degenerate matter have been investigated from relativistic mechanics. Matter obeying either Fermi-Dirac statistics or Bose-Einstein statistics has been considered. In § 1 non-degenerate matter has been considered, and the number of particles as well as the mass of matter effusing out has been calculated. The non-relativistic expressions are obtained as a limiting case. For $f = 10$ the departure from the value for a classical perfect gas amounts only to about 1%. In § 2 the effusion has been calculated for a degenerate gas, degenerate in the sense of Fermi-Dirac statistics, both to a first approximation and to a second approximation. The non-relativistic formulae are obtained as a limiting case. In this case it is found that to a first approximation the effusion varies as $p^{\frac{1}{4}}$ and is independent of T, but on working to a second approximation a slight dependence on temperature is observed. The average mass of particles in the effusion stream is calculated.

REFERENCES

Kothari, D. S. 1938 *Proc. Nat. Inst. Sci. India*, **4**, 69.
Kothari, D. S. and Singh, B. N. 1938 *Z. Astrophys.* **15**, 145.
Majumdar, R. C. 1932 *Astr. Nachr.* **247**, 217–52.
Sommerfeld, A. 1928 *Z. Phys.* **47**, 1.
Srivastava, B. N. 1938 *Proc. Nat. Inst. Sci. India*, **4** 75.

The diffraction of X-rays by age-hardening aluminium copper alloys

By G. D. PRESTON, M.A., *National Physical Laboratory*

(*Communicated by W. L. Bragg, F.R.S.*—*Received* 10 *May* 1938)

[Plates 14–18]

1. INTRODUCTION

The object of this paper is to draw attention to certain peculiarities in the X-ray diffraction spectra obtained from single crystals of an alloy of aluminium with 4 % by weight of copper. The experiments described below were carried out during an investigation into the property of age-hardening exhibited by these alloys, in the hope that some light would be thrown on the processes preceding precipitation of the compound $CuAl_2$, which are generally regarded as being the cause of the hardening in alloys of the Duralumin class, of which the simple 4 % copper alloy is the prototype.

The material used in the investigation was prepared from aluminium of high purity and after casting the ingots were forged and then drawn into wires of 1 mm. diameter. Pieces of the wire after annealing at 500° C. contained crystals of sufficient size (2–5 mm. in length) for X-ray examination by the oscillating crystal and Laue methods.

Oscillating crystal photographs of the alloy taken as soon after quenching as possible do not present any striking difference from those of pure aluminium, except in showing a small change of parameter which is measurable only in the high order reflexions. After ageing at 150° C. for 26 days or 200° C. for 10 hr. the intense diffraction spots of the solid solution on the oscillation diagrams are accompanied by two or three rather weak but fairly sharp satellites. These appear before the alloy is in its state of

maximum hardness and persist after that maximum has been passed. At the same time, observation of high order reflexions (511) and (333) shows that some material of spacing 4·04 A is making its appearance in the matrix of alloy in which the spacing is 4·033 A. The reflexions of the 4·04 A spacing are weak and diffuse. In the oscillation photographs of the alloy aged at room temperature for 6 or 8 months the diffraction spots due to the solid solution are accompanied by lines which pass through the positions occupied by the satellites observed in the spectra of the alloy aged at higher temperatures. The following sections, (2) and (3), are devoted to a more detailed description of these lines, the results of the oscillating crystal method being given in (2) and of the Laue method in (3). All the photographs have been taken with a hot cathode tube fitted with a copper target operated on an alternating supply of 40 kV (R.M.S.); tube currents of 10–15 mA (mean) with exposures of 1 or $1\frac{1}{2}$ hr. have been used for both the oscillation and Laue photographs. The latter have therefore been obtained in conditions in which the incident beam contained a much larger proportion of soft radiation than is usually the case.

2. Oscillating crystal method

A series of photographs has been taken of specimens aged for 6 months at room temperature and after different periods at 150 and 200° C. The orientation of the crystals selected for examination was determined by Laue photographs, and the specimens were adjusted so that a [110] or [100] direction was parallel to the axis of oscillation. The general nature of the results obtained by this method of investigation can be illustrated by a description of photographs of the alloy aged at room temperature for 6 months and at 150° C. for 26 days.

In the alloy aged at room temperature the reflexions due to the face-centred cubic structure are accompanied by a pair of lines diverging from each spot in the direction of increasing θ. These lines, in the alloy aged at 150° C., are resolved into two or three fairly sharp spots. Actually each reflexion is accompanied by three lines, one of which is masked in the central layer line by the "white" radiation, but can be seen in the first layer line. Similar results are obtained when the axis of oscillation is a (100) direction, but the V-shaped marks are not identical in shape with those observed when the axis is (011). Some idea of the nature of the observed effect may be obtained from fig. 1, where a number of diffraction spots with their accompanying lines are shown diagrammatically. The Laue photographs, fig. 2 a and b, Plate 14, also show the effect. The V-shaped lines on the left-hand

side of (a) accompany a (111) reflexion of the alloy aged at room temperature. In fig. 7 b, obtained from the alloy aged at 150° C., the lines are resolved into rather ill-defined spots.
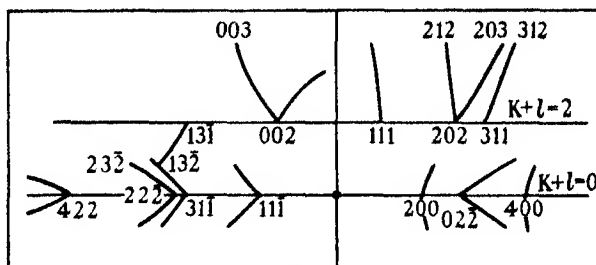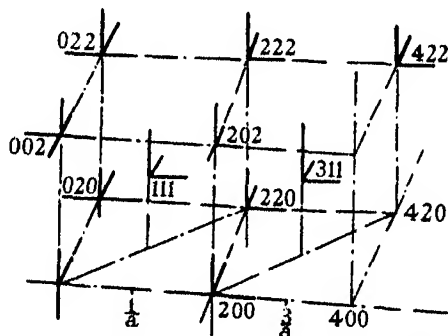

FIG. 1

FIG. 3. Reciprocal lattice showing short lines which give rise to V-shaped streaks in oscillation photographs.

Measurement of the films showed that the lines associated for instance with a (111) spot each proceeded towards the position where (211), (121) or (112) would occur, if it appeared in the X-ray spectrum. In terms of reciprocal space this means that the point (111) is accompanied by three mutually perpendicular lines parallel to the cube axes of the reciprocal lattice as illustrated in fig. 3. If we assume that each reciprocal lattice point is accompanied by three lines we can calculate the effect which should be observed. Taking the axis of oscillation to be (011) a point (x, y, z) referred to the reciprocal cube edges as axes will produce a reflected spot on a circular cylindrical film of radius R at a point (X, Y) on the film, when unwrapped, where

$$\cos \frac{X}{R} = \frac{\sqrt{2}}{\sqrt{(2 - (y+z)^2 l^2)}} \left\{ 1 - \frac{l^2}{2} (x^2 + y^2 + z^2) \right\}$$

and

$$\frac{Y}{R} = \frac{(y+z) l}{\sqrt{(2 - (y+z)^2 l^2)}},$$

where $l = \lambda/a$, the wave-length divided by the side of the cubic lattice. These formulae were used in preparing fig. 1: for the plane $(\bar{1}1\bar{1})$, for instance, we put $-x = y = 1$ and allow z to assume values between -1 and -2 which gives the line running out towards $(\bar{1}1\bar{2})$. The other two lines are obtained by putting $x = z = -1$, and $y = z = 1$ and allowing y and x to vary from 1 to 2 and -1 to -2 respectively. The line $(x1\bar{1})$ lies in the equatorial layer line $(y = 0)$ and cannot be observed, owing to the presence of "white" radiation. The X-ray photographs were superimposed on a diagram similar to fig. 1 and fitted in all cases. Similar results were obtained with [100] as oscillation axis.

3. The Laue method

The differences between Laue photographs of aluminium and of the age-hardened alloy are illustrated in figs. 2, 4 and 5, Plates 14–17. In fig. 4*a* the crystal aged at room temperature is orientated with a [110] direction parallel to the incident beam. The Laue diffraction spots are accompanied by quite intense streaks running round the principal zones and starting quite near the central spot. These streaks are not completely absent from photographs of the alloy taken immediately after quenching; they are, however, at first much fainter and broader. Fig. 4*b* shows a crystal aged at 150° C. for 25 days in the same orientation; the streaks are now resolved into short arcs. All these effects are absent from the Laue photographs of aluminium. Fig. 5*a* and *b* show crystals aged at room temperature and 150° C. for 25 days orientated with a (100) direction parallel to the X-ray beam with, in fig. 5*c*, a photograph of an aluminium crystal in the same orientation: fig. 5*d* is a crystal of slowly cooled alloy showing the spots due to $CuAl_2$, grouped near the centre of the pattern. Comparison of fig. 5*b* and *d* shows that $CuAl_2$ is not present in the alloy aged 26 days at 150° C. The results obtained by the oscillating crystal method were checked in the following way. The crystal aged at room temperature was mounted with a [011] direction parallel to the spectrometer axis, and rotated until a [111] direction was parallel to the X-ray beam. The position of the section by the (011) plane of the sphere of reflexion (for the $K\alpha$ radiation of Cu) is shown in fig. 6*a*. It passes very near to the point $(1\bar{1}1)$, from which three lines radiate, one PB parallel to (100) in the plane of the diagram and two others inclined at $\pm 45°$ to that plane, the projections of which are shown at PA. These two lines are almost tangential to the sphere of reflexion, so that, allowing for the finite divergence of the incident X-ray beam, the reflected rays from the whole of the pair of lines might be expected to appear on the Laue photograph. That

this is so may be seen in fig. 2. The V-shaped lines diverging from the point where the Bragg (111) reflexion of copper $K\alpha$ would occur are clearly visible. The (111) Laue spot is nearer the centre. When the orientation is changed by rotation about a vertical axis through a small angle so that the Laue spot passes out beyond the position of reflexion of (111) copper $K\alpha$ the V-lines no longer appear, the lines in reciprocal space being now within the sphere of reflexion, as shown in fig. 6 a by the dotted circle.
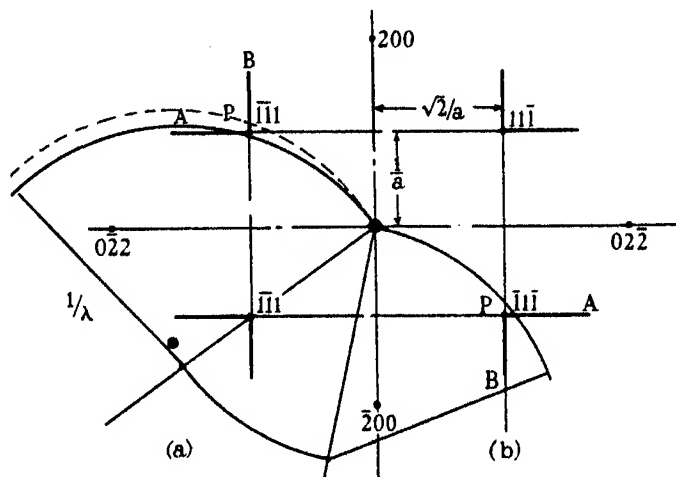
FIG. 6. Plan of (011) plane of reciprocal space.

Observations were also made on the plane $(\bar{1}1\bar{1})$ by taking Laue photographs at 2° intervals near the orientation shown in fig. 6 b. In this case the sphere of reflexion cuts the two lines, of which PA is the projection, at a steep angle so that the lines produce spots on the Laue diagram. If our assumption as to the position of the lines is correct, one of the spots will travel round the zone from $(\bar{1}1\bar{1})$ to $(\bar{1}2\bar{1})$ as the crystal rotates. In fig. 7 a–c, Plate 18, a few of the photographs are reproduced, and it is seen that this is the case. The results of a series of such photographs are shown in the stereographic projection (fig. 8). The Laue spots in successive photographs are displaced 2° along small circles such as AB (fig. 8). The spot arising from the line PA of fig. 6 b travels downwards along CD towards the equatorial plane and intersects the horizontal axis of the diagram at an angular distance 71° from the centre of projection. This is the complement of the Bragg angle of reflexion for the $K\alpha$ copper radiation, as it should be. The spots due to the $K\beta$ radiation are also recorded, $C'D'$, but are too faint to appear on the reproductions. The reflexions from all the photographs can be brought on to one

great circle by displacing the points through the appropriate angle. The Laue spots of one plane all coalesce into a single point, as shown along the circle QR: the angle of displacement has been chosen so as to bring the $(\bar{1}1\bar{1})$ Laue spot to 55° from the centre of projection which is now $(\bar{1}00)$. The spots arising from the lines PA of fig. 6 b all lie on the great circle running through $(\bar{1}1\bar{1})$ and $(\bar{1}2\bar{1})$ but move along the circle as the position of the crystal is altered, in just the way they should if the assumptions as to their origin in reciprocal space are correct.
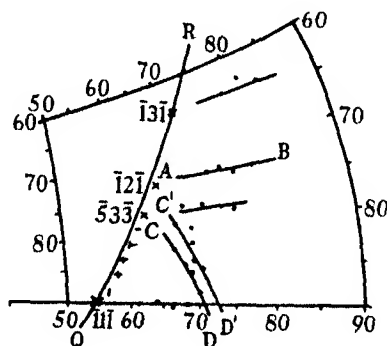
Fig. 8

It will be noticed in the photographs that the spots arising from the lines in reciprocal space are not so sharp as the Laue spots, although they are fairly clear. This suggests that the lines should really be thought of as rods having a finite volume, so that the reflected rays arise from a small area of the sphere of reflexion.

4. Origin of the lines

In order to see how lines of the type observed can be produced it will be simplest to give a description of the interference pattern produced by a two-dimensional lattice. This is equivalent to a pair of line gratings arranged with their rulings at right angles, so that the effect is to form a rectangular array of apertures. Such an array is shown in fig. 9 a. If the grating is illuminated with a beam of monochromatic radiation it will form a system of spectra of the type shown in fig. 9 b. We can call the two gratings which make the network of fig. 9 a A and B, and if A has its rulings vertical it would, in the absence of B, produce the horizontal row of spots $O, A_1, A_2, \ldots$ of fig. 9 b. The grating B alone, having its rulings horizontal, would produce the vertical line of spectra $O, B_1, B_2, \ldots$. The combination of the two gratings produces a

rectangular array of diffraction spots; the spectra A_1, A_2, etc., being diffracted by B to (11) and (21) as shown in the figure. In addition to these principal spectra there will be secondary maxima dividing the areas between the principal spectra into a rectangular network; the intensity and number of
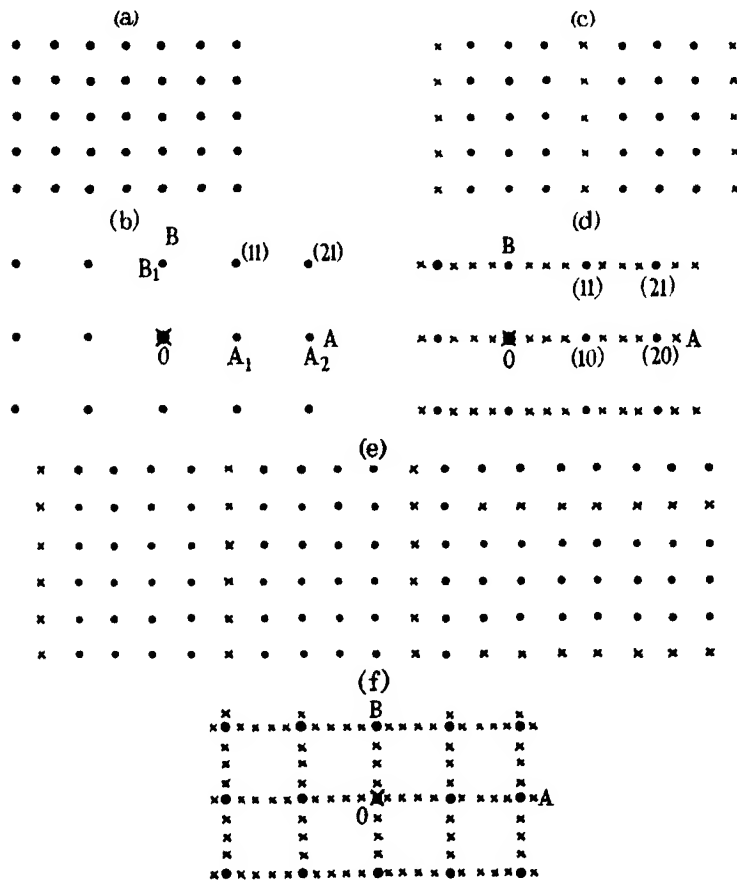
FIG. 9

these secondary maxima will depend on the number of apertures in the grating, and we may suppose that this number is so large that they can be neglected for the moment.

Now let us suppose that one of the gratings, say A, suffers from a periodic defect so that every nth aperture allows more light to pass than the intervening ones. This is illustrated in fig. 9 c, where the two columns marked with crosses represent the defective rulings. In terms of a plane of atoms or diffracting particles this corresponds to the weighting of these columns by

atoms of greater scattering power. This arrangement will produce the spectra shown in fig. 9 d. The normal diffractions are unchanged in position, but along the line OA, and lines parallel to it, the principal spectra are separated by spectra corresponding to a grating with the periodicity of the defective ruling. In the figure this periodicity has been taken to be four times that of the grating A, so that three new maxima are introduced between succeeding pairs of spectra as shown by the crosses in fig. 9 d. If the periodicity of the defect in the grating A varies in different parts of the grating the little supernumerary spectra will all run together into a smear joining the principal spectra along OA and the lines parallel to it. This begins to resemble the sort of effect observed in the crystal; it was pointed out in the preceding section that a spectral point (hkl) was accompanied by three lines running out towards the points $(h+1, k, l)$, $(h, k+1, l)$ and $(h, k, l+1)$. Here, in the two-dimensional model, we have produced lines running through a series of spectra $(0k)$, $(1k)$, $(2k)$, etc. This is one of the sets of lines we require, the other is of the type $(h0)$, $(h1)$, $(h2)$, etc. A point of some importance with regard to the structure of the crystal now arises. If in fig. 9 c we suppose the grating B to have a periodic defect as well as A, this will produce extra spectra along the line OB and parallel lines through *all* the spectra along OA. The area enclosed by, say, (11), (21), (20) and (10) will be filled with a network of points. Although this is not what is observed, it appears that the diffraction spectra within this area may, in certain circumstances, be much less intense than those along the lines OA and OB. It seems likely, however, that the observed pattern is due to an arrangement of the type shown in fig. 9 c. Here on the left the grating A has a periodic defect indicated by the columns of crosses, but grating B is perfect; on the right grating A is perfect and the horizontal row of crosses indicates a periodic imperfection in grating B. The resulting spectrum is shown in fig. 9 f; the principal spectra are joined by rows and columns of crosses, the horizontal rows being due to the imperfection of grating A, the vertical columns to those of B. This arrangement produces spectra in the places where they are observed in the alloy, namely, along lines where one index only of the normal spectra is allowed to vary. The production of the small streaks associated with the normal spectra in the alloy aged at room temperature must be ascribed to variations in the periodicity of the imperfection.

The above results may now be translated into terms of atoms in the alloy. The defect which was supposed to consist of the presence of a larger aperture in the grating represents, in the crystal, a (100) plane in which copper atoms, of approximately twice the scattering power of aluminium atoms, have become segregated. This plane gives rise to an intensity streak (or, if the

planes in which segregation occurs are regularly spaced, to a group of diffraction spots) running through a series of spectra (hkl), $(h \pm 1, k, l)$, $(h \pm 2, k, l)$, etc. In some other part of the crystal the copper will have selected a (010) and will produce a streak along (hkl), $(h, k \pm 1, l)$, $(h, k \pm 2, l)$, etc. The third streak running through (hkl), $(h, k, l \pm 1)$, $(h, k, l \pm 2)$ is due to enrichment of (001) by copper in yet a third region of the crystal. These are the three lines running through each point of the reciprocal lattice illustrated in fig. 3. Fig. 1 shows the parts of them which are actually observed.
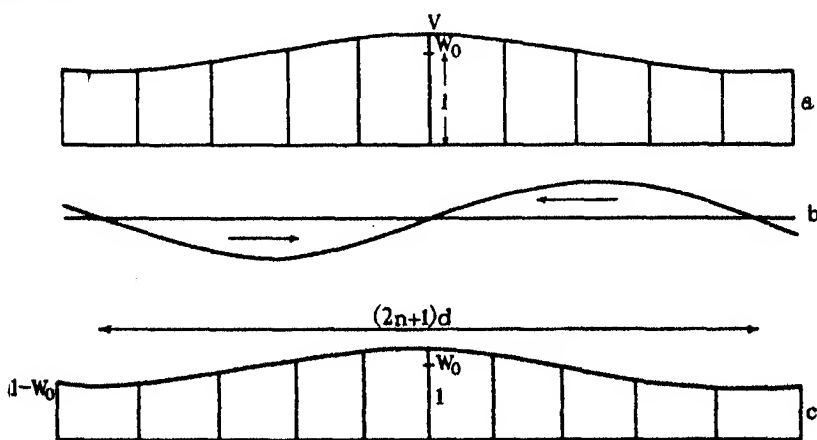
FIG. 10

The simple model of a pair of crossed gratings considered above gives a satisfactory account of the position of the lines and satellites observed on the photographs. One very characteristic feature still remains to be considered; this is the fact that in the photographs the lines (or spots) always occur at larger angles of diffraction than the spot from which they diverge, as is illustrated in fig. 2 a and b. We have to account for the distribution of intensity along a line such as $(11z)$, and in particular for the lack of symmetry of the intensity about the normal reflexions (111), $(11\bar{1})$, $(11\bar{3})$, etc.

5. INTENSITY DISTRIBUTION

An intensity distribution unsymmetrical about the normal reflexions will be produced if those elements of the grating which in the last section were supposed to have a high reflecting power are associated with a slightly smaller or larger spacing. In the case of the copper-aluminium alloy we would expect planes enriched in copper to be a little closer together than
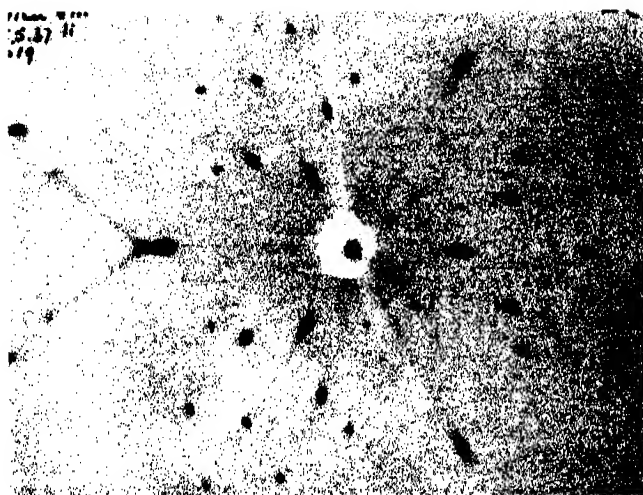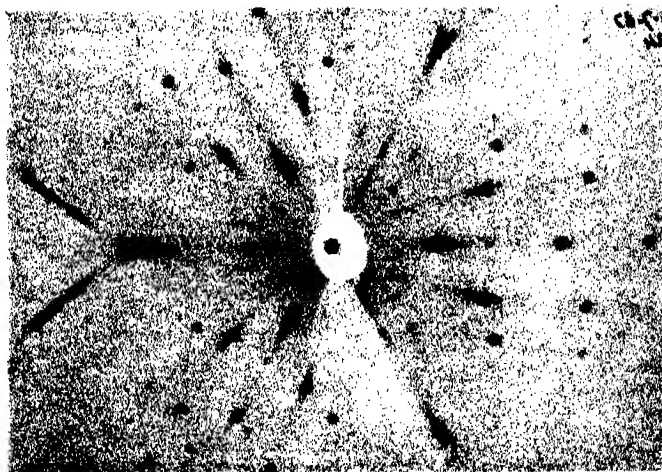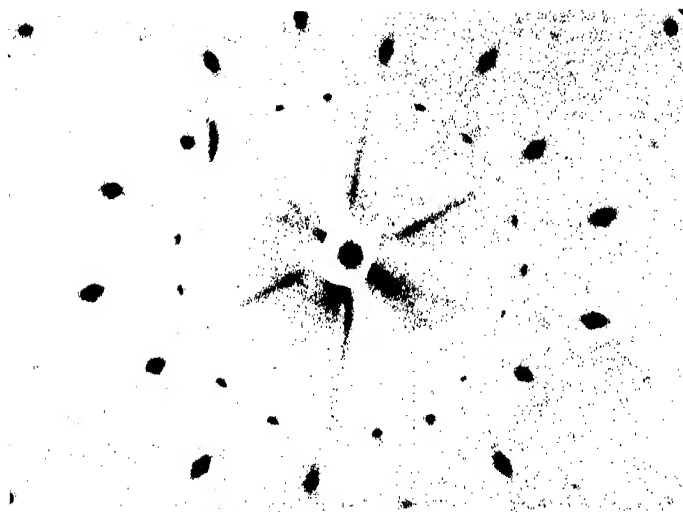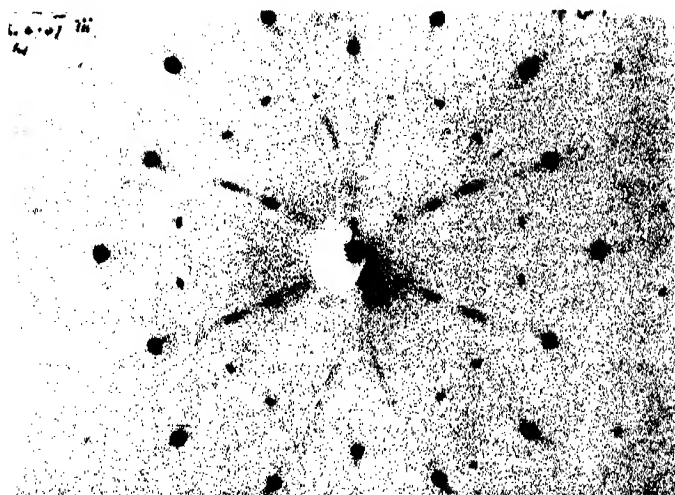
FIG. 2a

FIG. 2b

Preston

Proc. Roy. Soc., A, vol. 167, *Plate* 15

FIG. 4*a*

FIG. 4*b*

Preston

Proc. Roy. Soc., A, vol. 167, *Plate* 16
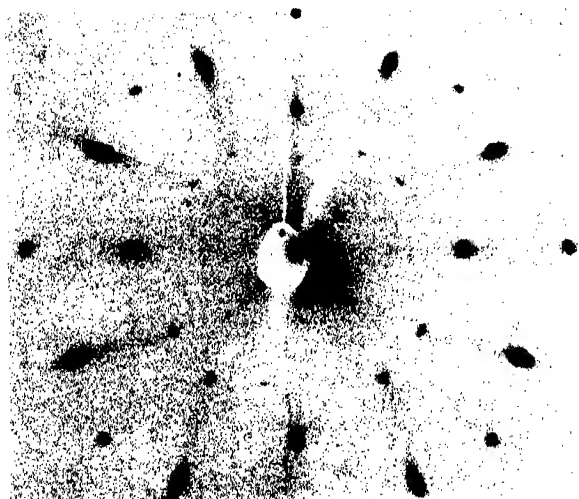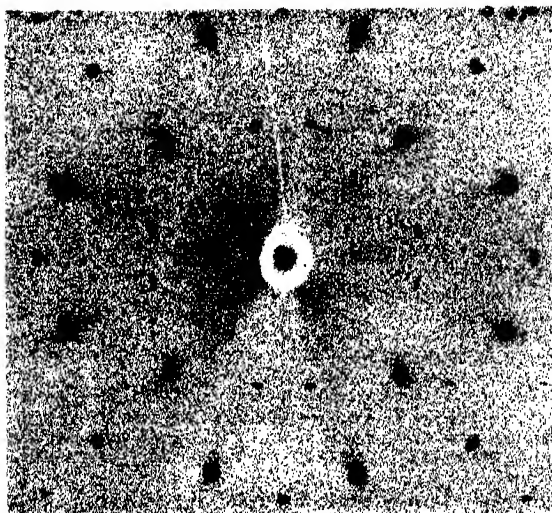

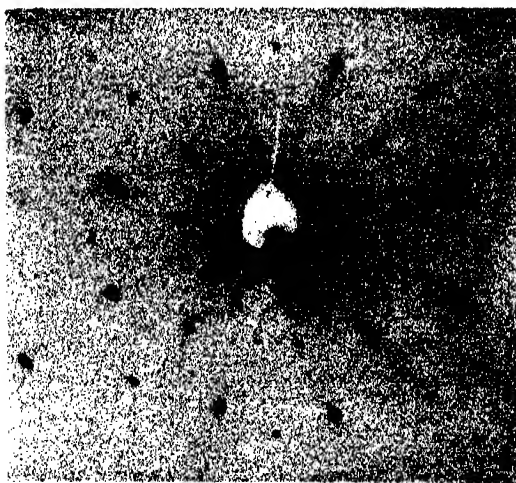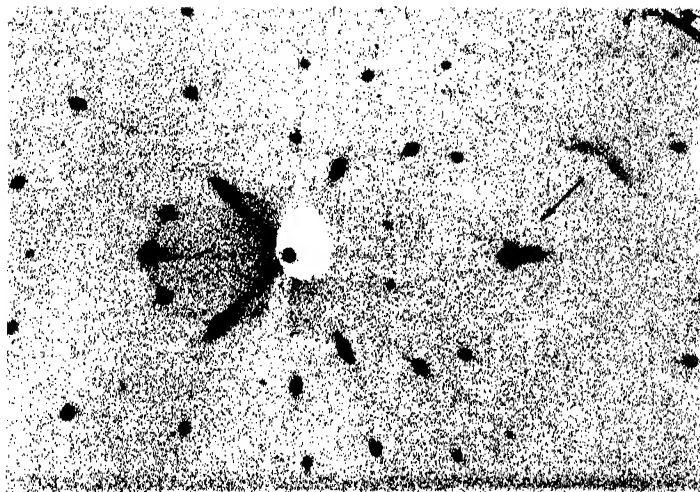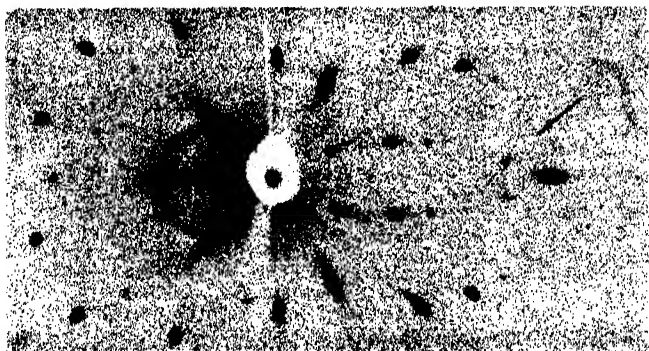Fig. 5a
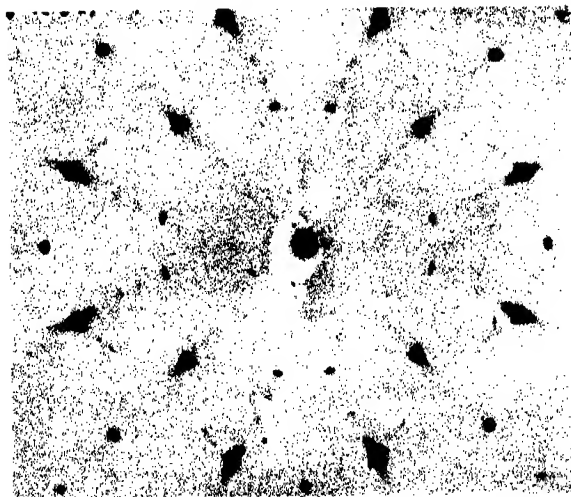
Fig. 5b

Fig. 5c

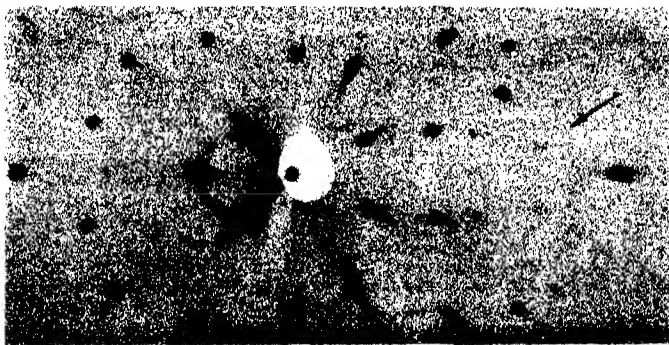Fig. 5d

Fig. 7a

Fig. 7b

Fig. 7c

those where the copper concentration is uniform, because copper in solid solution causes the aluminium to contract slightly. We can see in the following way that the association of high reflecting power with diminished spacing will produce a result of the observed type.

We consider a set of planes, spacing d, and reflecting power unity, and suppose that they are weighted so that the reflecting power varies by a small amount on each side of some plane chosen as origin. Let the reflecting power of the pth plane on either side of the origin be

$$f = 1 + w_0 \cos \frac{2\pi p}{2n+1},$$

so that f has a period $(2n+1)$ times the spacing. The effect is shown in fig. 10 a, where the planes are represented by a row of vertical equidistant lines whose tops are cut off by a cosine wave of amplitude w_0. The height of each line in the diagram is an indication of its reflecting power.

We now displace the planes in such a way that the heavier ones, grouped about the origin, are a little closer together than the lighter ones grouped about points at distances $\pm (2n+1)/2$ from the origin. In fig. 10 a the distance of the pth plane from the origin is pd; in the distorted structure we put the pth plane at a distance d_p from the origin, where

$$d_p = d\left(p + k \sin \frac{2\pi p}{2n+1}\right).$$

The quantity k is small, and if it is negative it will produce a diminution of the spacing near the origin and at points distant $\pm (2n+1)d$, $\pm 2(2n+1)d$, etc., from the origin. The curve $k \sin \dfrac{2\pi p}{2n+1}$ is shown in fig. 10 b, where the arrows in the loops indicate the directions of the displacements for a negative value of k. The final distribution of the reflecting planes is shown in fig. 10 c, the values of $w_0 = 0\cdot25$ and $k = 0\cdot2$ having been chosen sufficiently large to make their effect appreciable on the diagram.

The amplitude of the wave reflected by the system of planes illustrated in the figure is made up of the following contributions:

(1) the central plane $(p = 0)$: $(1 + w_0)$;

(2) a pair of planes on each side of the above $(p = 1)$:

$$2\left(1 + w_0 \cos \frac{2\pi}{2n+1}\right)\left(\cos\left(c + kc \sin \frac{2\pi}{2n+1}\right)\right);$$

(3) the next pair of planes ($p = 2$):

$$2\left(1 + w_0 \cos \frac{4\pi}{2n+1}\right) \cos \left(2c + kc \sin \frac{4\pi}{2n+1}\right);$$

and so on. For the pth pair the contribution is

$$A_p = 2\left(1 + w_0 \cos \frac{2\pi p}{2n+1}\right) \cos \left(pc + kc \sin \frac{2\pi p}{2n+1}\right).$$

In these expressions $c = \dfrac{2\pi d}{\lambda} \sin \theta$, so that $c = 2\pi, 4\pi, 6\pi$, etc., corresponds to the 1st, 2nd, 3rd, etc., order of reflexion from the planes with normal distribution, d; θ and λ have their usual meaning, the Bragg glancing angle and wave-length of the radiation. We now assume that kc is so small that $\cos kc = 1$ and $\sin kc = kc$, so that

$$A_p = 2\left(1 + w_0 \cos \frac{2\pi p}{2n+1}\right)\left(\cos pc - kc \sin \frac{2\pi p}{2n+1} \sin pc\right).$$

We can also assume that w_0 is so small that the term involving $w_0 kc$ is negligible and then

$$A_p = 2 \cos pc + (w_0 + kc) \cos p\left(c + \frac{2\pi}{2n+1}\right) + (w_0 - kc) \cos p\left(c - \frac{2\pi}{2n+1}\right).$$

The whole amplitude, arising from the $(2n + 1)$ planes in the interval $(2n + 1)d$ indicated in fig. 10c is

$$A = 1 + w_0 + \sum^{n} A_p,$$

$$A = \frac{\sin \dfrac{2n+1}{2} c}{\sin \dfrac{c}{2}} + \frac{w_0 + kc}{2} \frac{\sin \dfrac{2n+1}{2}\left(c + \dfrac{2\pi}{2n+1}\right)}{\sin \dfrac{1}{2}\left(c + \dfrac{2\pi}{2n+1}\right)} + \frac{w_0 - kc}{2} \frac{\sin \dfrac{2n+1}{2}\left(c - \dfrac{2\pi}{2n+1}\right)}{\sin \dfrac{1}{2}\left(c + \dfrac{2\pi}{2n+1}\right)}$$

$$= F + \frac{w + kc}{2} F_1 + \frac{w - kc}{2} F_2.$$

Now when we build up a grating each element of which is the unit illustrated in fig. 10c, these units will be separated by distances $(2n + 1)d$, so that the only values of c which are significant are those for which c is an integral multiple of $2\pi/(2n + 1)$. Let us put $c = 2\pi m/(2n + 1)$ and consider the terms F, F_1 and F_2 when this substitution is made. We see that F vanishes unless m is an integral multiple of $(2n + 1)$; F_1 vanishes unless $m + 1$ is an integral multiple of $2n + 1$, and F_2 vanishes unless $m - 1$ is an integral multiple of

$2n + 1$. The normal reflexions occur when $c = 2\pi$, 4π, etc., i.e. when $m = 2n + 1, 2(2n + 1)$, etc., and each of these is accompanied by two satellites, one on either side, when $c = 2\pi\left(1 \pm \dfrac{1}{2n + 1}\right)$, $2\pi\left(2 \pm \dfrac{1}{2n + 1}\right)$, etc. These are the only spectra which arise. The presence of a pair of satellites associated with each normal reflexion is a consequence of our original assumption involving a simple harmonic distortion. A less simple type of distortion would give satellites of higher order. Considering now the amplitude of the satellites associated with the first-order spectrum we have one at

$$c = 2\pi\left(1 - \frac{1}{2n + 1}\right)$$

with amplitude $\dfrac{1}{2}\left(w + 2\pi k\left(1 - \dfrac{1}{2n + 1}\right)\right)$; the amplitude of the other satellite at $c = 2\pi\left(1 + \dfrac{1}{2n + 1}\right)$ is $\dfrac{1}{2}\left(w - 2\pi k\left(1 + \dfrac{1}{2n + 1}\right)\right)$. If k is negative the former is smaller than the latter, so that the satellite occurring on the side of the normal reflexion remote from the zero-order spectrum will be more intense than that nearer the zero order. Table I shows the result numerically: it has been calculated with $n = 4$, $w_0 = 0.2$ and $k = -0.02$. The small intensity maxima, at $c = 320$ and $680°$, due to the term F_1 diminish as c increases: those at $c = 40, 400$ and $760°$, due to F_2, increase with c and are considerably greater than those due to F_1. Both F_1 and F_2 are small compared with the normal reflexion F. The model illustrates the observed intensity dissymmetry quite well, but owing to the restriction involved in the assumption that kc must be small the calculation cannot be extended to higher orders. This limitation is not of importance, as it is only intended to show that the association of high reflecting power with diminished spacing will produce an intensity distribution of the type observed.

TABLE I

Order	m	c	Source	Amplitude	Intensity
0	0	0°	F	9·00	81·00
	1	40	F_2	0·96	0·93
1	8	320	F_1	0·40	0·16
	9	360	F	9·00	81·00
	10	400	F_2	1·53	2·30
2	17	680	F_1	−0·17	0·03
	18	720	F	9·00	81·00
	19	760	F_2	2·11	4·50

6. CONCLUSION

The results described in the preceding sections must be regarded as preliminary. A fuller interpretation must depend on measurement of the intensity of the diffraction effects, when it should be possible to determine the size of the regions rich in copper and the number of copper atoms involved in each of them. It seems justifiable at the moment to conclude that the process of age-hardening in this alloy is associated with the segregation of copper atoms on the (100) planes of the crystal as suggested by Desch (1934). The observed effects resemble those described by Laves and Nieuwenkamp (1935) who attribute them to the presence of a two-dimensional super-lattice in the material (Ni_3As_2) which they were investigating, and are almost certainly connected with the formation of the "intermediate" phase discovered by Wasserman and Weerts (1935). The formation of this phase takes place at a stage of the process which follows those described in the present paper. When the alloy is aged at 200° C. for about 10 hr. one of the satellites, the outer one of fig. 2 b, disappears, the intermediate phase being then present in the alloy. It is difficult to say whether in this state the crystal is to be regarded as two phases or one, but in the earlier stages of the process it seems proper to regard the copper as being still "in solution", still occupying sites on the aluminium lattice. In the regions in which copper is segregating it is still not present in sufficient quantity to assert its individuality by precipitating $CuAl_2$. The state of the alloy seems to resemble the Fe-Ni-Al alloys described by Bradley and Taylor (1938), and it is possible that the high coercivity of these alloys and the age-hardening of duralumin may be manifestations of the same type of structural peculiarity.

REFERENCES

Bradley, A. J. and Taylor, A. 1938 "Magnetism", Lecture VI, p. 91. Institute of Physics.
Desch, C. H. 1934 "The Chemistry of Solids."
Laves and Nieuwenkamp 1935 *Z. Kristallogr.* 90, 279.
Wassermann, G. and Weerts, J. 1935 *Metallwirtschaft*, 14, 605.

Rotatory dispersion in the amine series.
IV. The optical activity of diamines

By W. C. G. Baldwin, M.A., Ph.D.

Laboratory of Physical Chemistry, Cambridge

Induced dissymmetry in amines

In Parts I and II of this series (Lowry and Baldwin 1937; Baldwin 1937), attempts were made to account for the effects on rotatory power which are observed when a simple optically active amine is ionized through neutralization by a mineral acid. It was found that the simple amino bases could be classified roughly into two groups, viz. (*a*) those whose specific rotation undergoes a large change of magnitude or even of sign on neutralization, and (*b*) a few which do not show this "acid effect". It was also shown that, when the "acid effect" occurs, (i) the amino group is usually in close proximity to an asymmetric carbon grouping; (ii) this configuration leads to circular dichroism of the absorption bands of the lone pair of electrons on the nitrogen atom, and thus to a large induced rotation due to the amino group; (iii) this induced rotation is eliminated on neutralization of the base, the rotatory power is reduced, and may even change in sign; whilst at the same time the dispersion constant in a Drude equation for the rotatory dispersion is displaced towards the Schumann region, owing to the elimination of absorption bands at longer wave-lengths. Confirmation of these results is found in the investigations of Raman spectra by Freymann and Freymann (1936), who showed that the frequencies characteristic of the basic NH radical disappear when the nitrogen atom becomes quadrivalent. In the work now described, it is shown that ionization by mere neutralization is not the only mechanism by which the "acid effect" can be produced. If it be correct to attribute the phenomenon in, say, *d*-secondary butylamine to the lone pair of electrons, the same type of effect should be observed when these electrons become bound in *any* way; and Table I shows that, in fact, conversion to a quaternary bromide leads to a result similar to that produced by simple ionization. The "acid effect" may therefore be associated directly with the existence of induced dissymmetry in the amino group.
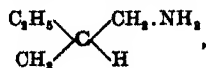
[539]

<div align="center">

TABLE I

</div>

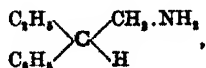|	$[M]^{20}_{5461}$
d-Secondary butylamine	$+6\cdot30°$ (homogeneous)
d-Hydrochloride	$-1\cdot26°$ (23 % solution)
Diethyl-d-secondary butylamine	$+131\cdot9°$ (homogeneous)
d-Hydrochloride	$+8\cdot21°$ (6 % solution)
d-Triethylbutylammonium bromide	$-29\cdot8°$ ($\frac{1}{4}$ % solution)

The reversal of sign in the case of d-triethylbutylammonium bromide is of particular interest, since it invalidates the general rule for the determination of configuration put forward by Boys in 1934. Nevertheless, his model finds great success when its application is restricted to the $-CH\begin{smallmatrix}\diagup NH_2 \\ \diagdown CH_3\end{smallmatrix}$ residue, and only one anomaly can be found when it is applied to the compounds of the amine series as described in Part II. These effects are, however, by no means general, as was shown by a full investigation of 1:1′-diamino-*cyclo*butane-*spirocyclo*butane (Lowry and Baldwin 1937). In this simple case ionization actually led to an *increase* in molecular rotatory power, and the assumption was made that a configuration such as is offered by a classical asymmetrical carbon grouping is usually necessary for development of induced dissymmetry in the amino group, and that molecular dissymmetry alone does not necessarily lead to the same activation of the lone pair of electrons on the amino nitrogen.

<div align="center">

BASES SHOWING ANOMALOUS BEHAVIOUR

</div>

Although the majority of optically active bases show induced dissymmetry in their nitrogenous groups, there is a large residue which gives rise to no "acid effect". In some of these cases the induced dissymmetry is only apparently absent, the change of magnitude on neutralization being concealed by other effects. Although amylamine

$$C_2H_5\diagdown \hspace{-6pt}\diagup CH_2.NH_2$$
$$CH_3\diagup \hspace{-6pt}\diagdown H$$

$\beta\beta'$-phenyl-ethyl-ethylamine

$$C_2H_5\diagdown \hspace{-6pt}\diagup CH_2.NH_2$$
$$C_6H_5\diagup \hspace{-6pt}\diagdown H$$

and $\beta\gamma$-diphenylpropylamine

$$C_6H_5.CH_2\diagdown \hspace{-6pt}\diagup CH_2.NH_2$$
$$C_6H_5\diagup \hspace{-6pt}\diagdown H$$
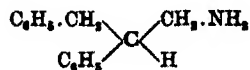
are all normal in their behaviour, a similar substance, β-phenylpropylamine, containing the same residue $>CH.CH_2.NH_2$, shows only a small reduction in specific rotation when it is neutralized. A few isolated exceptions of this type must naturally be expected in a generalization, but the uniformly anomalous behaviour observed with ring compounds seems to be of fundamental importance. The contrast between the two types of behaviour is brought out in Table II, which summarizes the results of the present investigations. The *spiro*-base of Janson and Pope (1936) was hitherto the only example which

TABLE II. NORMAL AND ABNORMAL OPTICALLY ACTIVE AMINES

Base	$[M]_D$	λ_1 A	λ_{11} A	Remarks and reference
l-Secondary butylamine	− 5·45	2300	1792	Part II. Normal in be-
Do. hydrochloride	+ 1·05	(2262)	—*	haviour
d-Diethyl-secondary butylamine	+ 110·8	2000	—*	Part II. Normal in be-
Do. hydrochloride	+ 7·02	1500	—*	haviour
l-Propylene-diamine	− 22·01	1900	1673	A normal amine
Do. hydrochloride	− 6·6	1850	1600	
Do. dihydrochloride	+ 5·94	1870	—*	Tables VIII, IX and X
d-*Spiro*heptane-diamine	+ 8·32	1360	—*	Part I. An abnormal
Do. hydrochloride	+ 9·6	1900†	—	amine
Do. dihydrochloride	+ 14·62	1934	—*	
l-Tetrahydroquinaldine	− 88·4	1410†	—	Calculated from data of
Do. hydrochloride	− 122	1750†	—	Pope and Read (1910). Apparently abnormal
l-Menthylamine	− 67	—	—	Calculated from Kenyon
Do. hydrochloride	− 70	1395†	—	and Pickard (1915), Read (1930). Probably abnormal
Ethylene-diamine sulphate crystals	$\alpha = \pm 15·4$ per mm.	1404	—*	Table V
l-1:2-*Cyclo*hexane-diamine	− 41·1	1870	0‡	Calculated from data by Jaeger and Bijkerk (1937). Classed as border-line case
Do. hydrochloride	− 48·2	1613	0‡	Table VI
Do. dihydrochloride	− 28·3	1431	—*	Table VII
l-1:2-*Cyclo*pentane-diamine	− 54·7	1793	0‡	Calculated from data by Jaeger and Blumendal (1928). Border-line case
Do. dihydrochloride	− 38·1	—	—	
Do. sulphate	− 22·8	—	—	

* Single-term equation.
† Approximate values.
‡ Two-term, three-constant Drude equation.

had been submitted to a full analysis of rotatory dispersion, and it was felt that, before definitely accepting the theory, which is outlined above, more evidence was necessary. Through the kindness of Professor F. M. Jaeger of Groningen, a specimen of *l*-1:2-diaminocyclohexane was available, and measurements have been made for this substance in both ionic states in combination with hydrochloric acid. For comparison, *l*-propylene-diamine has been investigated completely in the same way, whilst data for the rotatory dispersion of ethylene-diamine sulphate *crystals* are also put forward.

ABSORPTION SPECTRA OF DIFFERENT IONIC FORMS OF A POLYAMINE

The absorption spectra of ethylene-diamine in the three conditions of ionization were described in Part III, and in the present paper the effect of progressive neutralization of the simple tetramine

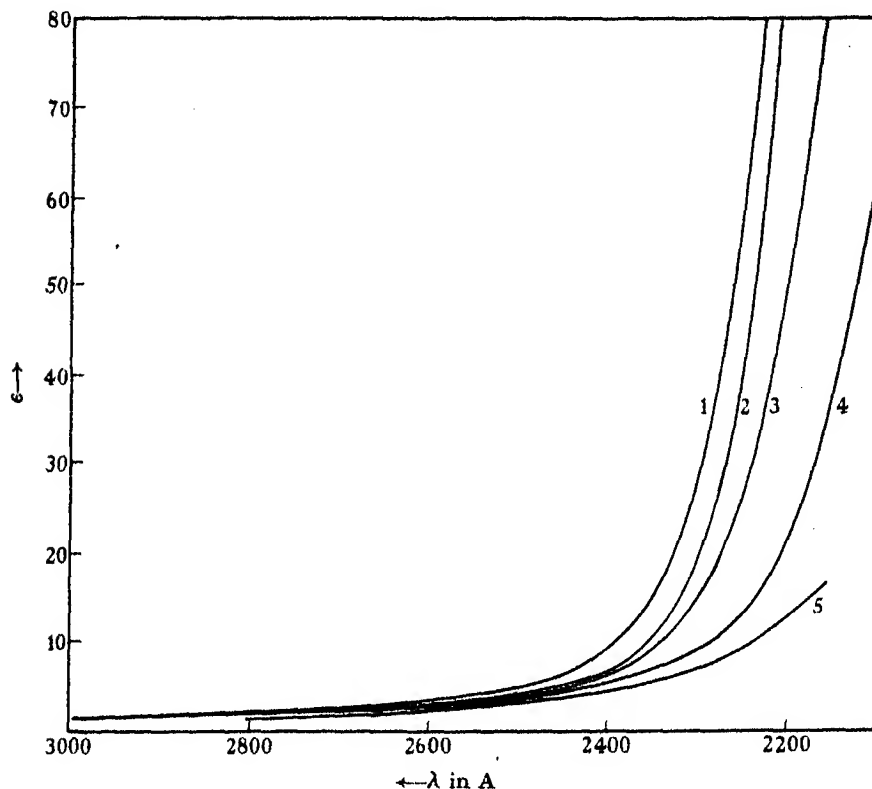$$NH_2.C_2H_4.NH.C_2H_4.NH.C_2H_4.NH_2$$

is shown in fig. 1. The progressive addition of equivalents of hydrochloric acid results in a regular decrease in the amount of absorption. Such behaviour is quite in harmony with that of ethylene-diamine under similar conditions, and merely represents an extension of the same effect. Each molecular equivalent of acid corresponds to the elimination of the absorption due to one lone pair, and at the final stage the absorption is similar to that given by a saturated straight-chain hydrocarbon, although somewhat greater in magnitude.

THE OPTICAL ACTIVITY OF CRYSTALLINE ETHYLENE-DIAMINE SULPHATE

This substance (von Lang 1872) crystallizes well as tetragonal bipyramids with good basal cleavage, and fairly high rotatory power. It was of importance to ascertain the nature of the rotatory dispersion of this salt for purposes of comparison with other diamines, and it was only by a fortunate accident, i.e. optical activity in the crystalline state, that such measurements could be made for a substance possessing molecular symmetry.

After cleavage of the crystals, measurements of rotatory power of both *d* and *l* samples were taken for visual light by means of radiation from metallic discharge lamps and arcs, the light being separated before reflexion from the microscope objective mirror by means of a good prismatic monochromator. The extinction positions were somewhat variable, and never perfect, and in most cases evidence of the intergrowth of mirror-image forms

was seen. Three crystals were, however, obtained which were almost optically pure, and a fourth showing very good extinctions was also measured. The final results are the averages of large numbers of readings for the first three crystals, and those for the fourth were included in the

Curve 1. $NH_2.C_2H_4.NH.C_2H_4.NH.C_2H_4.NH_2$ Base
  2. Base + 1 HCl ($\frac{1}{4}$ neutralized)
  3. Base + 2 HCl ($\frac{1}{2}$ neutralized)
  4. Base + 3 HCl ($\frac{3}{4}$ neutralized)
  5. Base + 4 HCl (All neutralized)

FIG. 1. Absorption spectrum of $H_2N.C_2H_4.NH.C_2H_4.NH.C_2H_4.NH_2$. Curve 1, in water; curve 2, in presence of 1 mol. HCl; curve 3, in presence of 2 mol. HCl; curve 4, in presence of 3 mol. HCl; curve 5, in presence of 4 mol. HCl.
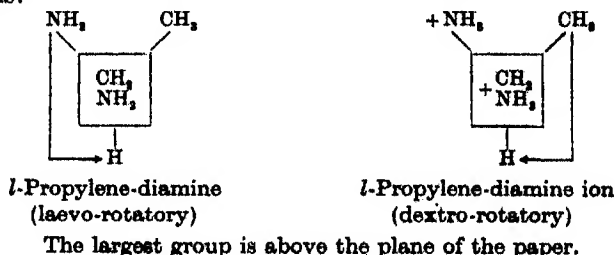
averages after allowing for contamination by the opposite isomer. The mean value α_D per mm., $\pm 15.4°$, compares well with that given by von Lang (1872). In spite of this agreement it is not claimed that this value is maximal, owing to the possibility of intergrowth, but the latter factor can have little

or no effect on the rotatory dispersion. The Drude equation expressing the dispersion is of one term, leading to an active wave-length at about 1404 A, a value which is in agreement with that expected. Little fundamental difference is introduced by the observations on symmetrical material in the dissymmetrical crystalline state, instead of those for asymmetrical molecules in solution. It seems certain that the same laws govern the dispersion for both crystalline and dissolved states, but a shift of the active wave-length from 1404 A for the sulphate crystals to 1870 A for the salt of l-propylene-diamine in solution is notable. On the other hand, the value of λ_0 for the *cyclo*hexane-diamine ion is almost identical with that for the ethylene-diamine salt.

THE APPLICATION OF BOYS'S MOLECULAR MODEL
TO PROPYLENE-DIAMINE AND ITS SALTS

It was mentioned in Part II that, according to the Boys model as applied to the $-CH.(NH_2)(CH_3)$ residue, the specific rotation of l-propylene-diamine should show a reversal of sign on neutralization of the base. According to the data in the literature (Tschugaeff and Sokolov 1907) the dihydrochloride of the laevo-base gave $[\alpha]_D = -4.04°$ and $[M]_D = -59.35°$, whereas the laevo-base itself had $[\alpha]_D = -29.7°$. The figure for the molecular rotatory power, $-59.35°$, is clearly a typographical error for $-5.94°$, but it has been found in a repetition of these measurements, that the laevo-dihydrochloride is in fact dextro-rotatory. The value found in the present work is identical in magnitude with that of Tschugaeff and Sokolov, but the predicted reversal of sign does in fact occur. This constitutes very strong evidence in favour of the molecular model under consideration, and indeed this work was begun with a view to clearing up the difficulty in finding a reason for the non-occurrence of the reversal of sign on ionization of the molecule. Carefully checked figures for this laevo-base and its salts are given in Tables VIII, IX and X, from which it is seen that the model explains the behaviour of the series with success as good as that found for the secondary butyl series, and enables the absolute configuration to be defined thus:

l-Propylene-diamine
(laevo-rotatory)

l-Propylene-diamine ion
(dextro-rotatory)

The largest group is above the plane of the paper.

The rotatory dispersion of *l*-propylene-diamine and its salts

The *l*-base at a concentration of 90·6 % by weight in water gave $[\alpha]_D = -29·75°$, $d_4^{23} = 0·883$, and $[M]_D^{22} = -22·1°$, whereas Tschugaeff and Sokolov (1907) recorded several slightly differing values for the carefully dried base, the most probable mean of which is $[\alpha]_D = -29·74°$ ($\pm 0·04°$ approximately), $d_4^{25} = 0·8586 \pm 0·0002$. The presence of 9·4 % water therefore does not affect the specific rotation, and for this reason the base was not subjected to the troublesome process of drying over sodium.

The rotatory dispersion between 6708 and 3100 A can be accurately expressed by a two-term, four-constant Drude equation which leads to calculated active wave-lengths at 1900 and 1673 A. The expression given in Table VIII shows that the dispersion should be classed as quasi-anomalous, because the calculated anomalies fall outside the range of observations, as follows: reversal of sign at 1994 A, maximum at 2150 A. Although the dispersion was rather low, it was necessary to introduce four constants in order to obtain a reasonable analysis, but in view of the flexibility of such an equation the values cannot be regarded as accurate. They merely show the approximate regions of the spectrum in which the active frequencies lie, and also the fact that the large negative component associated with the lone pair absorption bands is, in this case, of higher frequency than the "residual rotation" connected with the electrons of the CN and NH linkages. This is in contrast to the behaviour with butylamine, although both are regarded as "normal" amines.

The dispersions of the *l*-dihydrochloride and of the *l*-monohydrochloride are best expressed by equations of one and two terms respectively, with active wave-lengths at 1870 A in the first case, and at 1850 and 1600 A in the second. The value of about 1870 A common to all three forms, including the doubly charged ion, may be associated with the saturated electronic arrangements present in all three. Liberation of first one, and finally two basic groups with their associated lone pairs of electrons results in a progressive increase in the induced dissymmetry centred at about 1650 A.

Analysis of molecular rotations in the propylene-diamine series

Assuming the validity of Boys's model, some interesting deductions can be made from the results given in Tables VIII, IX and X. It is supposed that the first neutralization occurs predominantly at the lone pair in the end

position, since such a change causes no alteration in the Boys orientation of the model. The following scheme can then be constructed:

l-Base (negative rotation)	*l*-Monohydrochloride (negative rotation)	*l*-Dihydrochloride (positive rotation)

If now an almost unchanging dextro-rotatory core due to the saturated linkages be associated with all three forms, its effect will be superimposed on any induced dissymmetry due to the lone pairs of electrons, and the various contributions to the rotation can then be defined as follows:

TABLE III. APPROXIMATE ANALYSIS OF MOLECULAR ROTATIONS
IN THE PROPYLENE-DIAMINE SERIES

	Base	Mono-salt	Di-salt	
	-15.49	0.00	0.00	Lone pair (a)
	-12.46	-12.46	0.00	Lone pair (b)
	5.94	5.94	5.94	Fixed asymmetry
Total	-22.01	-6.52	5.94	

These figures can then be correlated with the values of the numerators K_1 and K_{11} in the Drude equations, and the approximate agreement in magnitude and sign between the ratios K_{11}/K_1 and $\dfrac{\text{lone pair contributions}}{\text{fixed contributions}}$, as set out in Table IV, confirms the general correctness of the analysis.

TABLE IV

	From Drude equations		K_{11}/K_1	Lone pair contributions A	Fixed contributions B	Ratio A/B
	K_1	K_{11}				
Base	3.2	-10.3	-3.2	-28	6	-4.7
Mono-salt	6.2	-8.5	-1.4	-12.5	6	-2.1
Di-salt	1.9	0	0	0	6	0

TABLE V. ROTATORY DISPERSION OF CRYSTALLINE ETHYLENEDIAMINE
SULPHATE .

Rotation per mm. (calc.) $= \pm 5 \cdot 14/(\lambda^2 - 0 \cdot 0197)$. $\lambda_0 = 1404$ A

| | Rotation/mm. | | |
λ	Obs.	Calc.	Obs. − calc.
6708	$\pm 12 \cdot 1°$	$\pm 11 \cdot 9°$	0·2
6104	$\pm 14 \cdot 6$	$\pm 14 \cdot 6$	$\pm 0 \cdot 0$
5893	$\pm 15 \cdot 4$	$\pm 15 \cdot 7$	− 0·3
5780	$\pm 17 \cdot 4$	$\pm 16 \cdot 3$	1·1
5461	$\pm 18 \cdot 3$	$\pm 18 \cdot 4$	− 0·1
5219	$\pm 20 \cdot 3$	$\pm 20 \cdot 3$	$\pm 0 \cdot 0$
4811	$\pm 24 \cdot 1$	$\pm 24 \cdot 3$	− 0·2
4722	$\pm 25 \cdot 2$	$\pm 25 \cdot 2$	$\pm 0 \cdot 0$
4678	$\pm 25 \cdot 8$	$\pm 25 \cdot 8$	$\pm 0 \cdot 0$
4358	$\pm 30 \cdot 5$	$\pm 30 \cdot 2$	0·3

TABLE VI. ROTATORY DISPERSION OF *l*-1 : 2-DIAMINO-*CYCLOHEXANE*
MONOHYDROCHLORIDE

$c = 19 \cdot 62$ g. per 100 c.c. in water. $L = 0 \cdot 4953$ dm., $t = 22°$ C.

$[M] = - 3 \cdot 155/(\lambda^2 - 0 \cdot 026) - 13 \cdot 64/\lambda^2$. $\lambda_0 = 1613$ A

λ	$[M]_{obs.}$	$[M]_{calc.}$	$[M]_{obs.} - [M]_{calc.}$
6708	− 37·2	− 37·8	0·6
6362	− 43·0	− 42·1	− 0·9
6104	− 46·5	− 45·8	− 0·7
5893	− 48·2	− 49·1	0·9
5782	− 50·2	− 51·0	0·8
5780	− 50·5	− 51·0	0·5
5700	− 52·6	− 52·6	$\pm 0 \cdot 0$
5461	− 56·5	− 57·3	0·8
5219	− 63·1	− 62·9	− 0·2
5106	− 65·7	− 65·7	$\pm 0 \cdot 0$
4811	− 74·0	− 74·4	0·4
4722	− 76·4	− 77·2	0·8
4602	− 81·5	− 81·4	− 0·1
4358	− 90·5	− 91·0	0·5
4294	− 92·8	− 93·9	1·1
4143	−101·2	−101·2	$\pm 0 \cdot 0$
4005	−106·5	−108·5	2·0
3912	−114·2	−113·9	− 0·3
3784	−122·0	−122·1	0·1
3696	−129·8	−128·5	− 1·3
3486	−145·1	−145·4	0·3
3329	−160·8	−160·3	− 0·5
3176	−177·1	−177·3	0·2
3024	−195·8	−197·6	1·8

TABLE VII. ROTATORY DISPERSION OF *l*-1 : 2-DIAMINO-*CYCLO*HEXANE
DIHYDROCHLORIDE

$t = 24°$ C. $c = 48·75$ g. per 100 c.c. in water. $L = 0·4953$ dm.
$[M] = -9·30/(\lambda^2 - 0·0205)$. $\lambda_0 = 1431$ A

λ	$[M]_{obs.}$	$[M]_{calc.}$	$[M]_{obs.} - [M]_{calc.}$
6708	− 22·1	− 21·7	− 0·4
6362	− 23·9	− 24·2	0·3
6104	− 26·3	− 25·7	− 0·6
5893	− 28·3	− 28·4	0·1
5782	− 30·4	− 29·6	− 0·8
5780	− 30·2	− 29·7	− 0·5
5700	− 30·3	− 30·6	0·3
5461	− 33·5	− 33·5	± 0·0
5219	− 37·0	− 36·9	− 0·1
4811	− 44·0	− 44·1	0·1
4722	− 46·1	− 45·9	− 0·2
4391	− 53·3	− 54·0	0·7
4358	− 55·1	− 54·9	− 0·2
4353	− 55·0	− 55·0	± 0·0
4200	− 59·5	− 59·7	0·2
4131	− 61·8	− 61·9	0·1
4045	− 64·9	− 64·9	± 0·0
3981	− 68·0	− 67·4	− 0·6
3892	− 71·9	− 71·0	− 0·9
3692	− 79·6	− 80·2	0·6
3547	− 88·9	− 89·3	0·4
3419	− 96·6	− 96·5	− 0·1
3338	−102·9	−102·4	− 0·5
3230	−110·6	−111·0	0·4
3146	−118·3	−118·4	0·1
3071	−126·1	−126·1	± 0·0
2992	−133·8	−134·7	0·9
2913	−144·4	−144·1	− 0·3
2824	−157·1	−157·0	− 0·1
2753	−168·7	−168·1	− 0·6
2689	−180·3	−179·5	− 0·8
2640	−189·0	−189·0	± 0·0
2570	−203·5	−204·3	0·8
2515	−219·0	−217·7	− 1·3

TABLE VIII. ROTATORY DISPERSION OF *l*-PROPYLENEDIAMINE IN
WATER AT 22° C.

$c = 80.0$ g. per 100 c.c. (90·6 % by weight).

$[M] = 3.159/(\lambda^2 - 0.0361) - 10.305/(\lambda^2 - 0.0280)$. $\lambda_{\mathrm{I}} = 1900$ A. $\lambda_{\mathrm{II}} = 1673$ A

λ	$[M]_{\mathrm{obs.}}$	$[\alpha]_{\mathrm{obs.}}$	$[M]_{\mathrm{calc.}}$	$[M]_{\mathrm{obs.}} - [M]_{\mathrm{calc.}}$
6708	−16·85	−22·78	−16·76	−0·09
6362	−18·54	−25·06	−18·79	0·25
6104	−20·47	−27·68	−20·52	0·05
5893	−22·01	−29·75	−22·13	0·12
5782	−23·07	−31·19	−23·01	−0·06
5780	−22·93	−30·96	−23·04	0·11
5700	−23·77	−32·12	−23·77	± 0·00
5461	−26·00	−35·13	−26·08	0·08
5219	−28·80	−38·94	−28·76	−0·04
5153	−29·65	−40·05	−29·64	−0·01
5086	−30·40	−41·06	−30·42	0·02
4825	−34·10	−46·05	−34·24	0·14
4811	−34·15	−46·13	−34·48	0·33
4800	−34·80	−47·01	−34·70	−0·10
4722	−35·82	−48·40	−35·94	0·12
4705	−36·15	−48·83	−36·21	0·06
4640	−37·40	−50·60	−37·37	−0·03
4597	−38·00	−51·36	−38·18	0·18
4520	−39·51	−53·40	−39·73	0·22
4495	−40·20	−54·37	−40·20	± 0·00
4358	−43·18	−58·38	−43·08	−0·10
4354	−43·20	−58·42	−43·21	0·01
4235	−46·05	−62·20	−46·05	± 0·00
4148	−48·30	−65·25	−48·30	± 0·00
3971	−53·90	−72·82	−53·50	−0·40
3807	−59·45	−80·38	−59·17	−0·28
3668	−64·62	−87·40	−64·66	0·04
3548	−70·40	−95·15	−70·20	−0·20
3428	−76·38	−103·1	−76·20	−0·18
3346	−81·90	−110·7	−81·20	−0·70
3245	−87·50	−118·2	−87·78	0·28
3136	−95·85	−129·5	−95·85	± 0·00
3055	−100·6	−135·9	−102·8	2·2
2990	−106·1	−143·5	−108·7	2·6

TABLE IX. ROTATORY DISPERSION OF l-PROPYLENEDIAMINE MONO-HYDROCHLORIDE AT 20° C.

$c = 57.90$ g. per 100 c.c. $L = 0.4953$ dm.

$[M] = 6.23/(\lambda^2 - 0.0342) - 8.53/(\lambda^2 - 0.0256)$. $\lambda_1 \equiv 1850$ A. $\lambda_2 \equiv 1600$ A.

Reversal of sign (calc.) at 2400 A.

λ	$[\alpha]_{obs.}$	$[M]$	$[M]_{calc.}$	$[M]_{obs.} - [M]_{calc.}$
6708	− 4.99	− 5.51	− 5.12	−0.39
6362	− 5.15	− 5.68	− 5.69	0.01
6104	− 5.83	− 6.45	− 6.17	−0.28
5893	− 5.90	− 6.52	− 6.63	0.11
5782	− 6.21	− 6.86	− 6.87	0.01
5780	− 6.35	− 7.01	− 6.88	−0.13
5700	− 6.49	− 7.17	− 7.07	−0.10
5461	− 7.01	− 7.76	− 7.69	−0.07
5219	− 7.57	− 8.37	− 8.40	0.03
5086	− 7.99	− 8.84	− 8.83	−0.01
4934	− 8.37	− 9.26	− 9.38	0.12
4811	− 8.86	− 9.80	− 9.84	0.04
4800	− 9.00	− 9.95	− 9.90	−0.05
4730	− 9.07	−10.03	−10.18	0.15
4722	− 9.14	−10.10	−10.21	0.11
4678	− 9.49	−10.49	−10.39	−0.10
4576	− 9.77	−10.80	−10.85	0.05
4358	−10.85	−11.99	−11.90	−0.09
4325	−10.47	−11.58	−12.08	0.50
4300	−11.16	−12.33	−12.17	−0.16
4107	−11.86	−13.10	−13.30	0.20
3997	−12.55	−13.87	−13.95	0.08
3738	−13.95	−15.41	−15.69	0.28
3682	−14.65	−16.20	−16.10	−0.10
3576	−15.35	−16.97	−16.88	−0.09
3483	−16.04	−17.73	−17.59	−0.14
3328	−16.74	−18.50	−18.76	0.26
3248	−17.79	−19.66	−19.42	−0.24
3080	−18.84	−20.82	−20.50	−0.32

TABLE X. ROTATORY DISPERSION OF LAEVO-PROPYLENEDIAMINE
DIHYDROCHLORIDE AT 20° C

$c = 20 \cdot 19$ g. per 100 c.c. in water. $t = 20°$ C. $L = 6$ dm. or $0 \cdot 4953$ dm.
$$[M] = + 1 \cdot 861/(\lambda^2 - \lambda_0^2), \ \lambda_0^2 = 0 \cdot 03487, \ \lambda_0 \equiv 1870 \text{ A.}$$

λ	$[\alpha]_{\text{obs.}}$	$[M]_{\text{obs.}}$	$[M]_{\text{calc.}} - [M]_{\text{obs.}}$
6708	$+3 \cdot 06$	$+4 \cdot 50$	$-0 \cdot 01$
6104	$3 \cdot 75$	$5 \cdot 51$	$\pm 0 \cdot 00$
5893	$4 \cdot 04$	$5 \cdot 94$	$0 \cdot 02$
5780	$4 \cdot 29$	$6 \cdot 30$	$-0 \cdot 08$
5700	$4 \cdot 37$	$6 \cdot 43$	$-0 \cdot 01$
5461	$4 \cdot 81$	$7 \cdot 06$	$0 \cdot 01$
5219	$5 \cdot 28$	$7 \cdot 76$	$0 \cdot 08$
5106	$5 \cdot 64$	$8 \cdot 30$	$-0 \cdot 05$
4811	$6 \cdot 50$	$9 \cdot 56$	$-0 \cdot 08$
4727	$6 \cdot 68$	$9 \cdot 82$	$0 \cdot 05$
4722	$6 \cdot 68$	$9 \cdot 82$	$0 \cdot 07$
4554	$7 \cdot 35$	$10 \cdot 80$	$\pm 0 \cdot 00$
4478	$7 \cdot 63$	$11 \cdot 21$	$0 \cdot 03$
4358	$8 \cdot 08$	$11 \cdot 88$	$0 \cdot 12$
4356	$8 \cdot 08$	$11 \cdot 88$	$0 \cdot 15$
4307	$8 \cdot 45$	$12 \cdot 42$	$-0 \cdot 05$
4128	$9 \cdot 28$	$13 \cdot 64$	$0 \cdot 10$
3995	$10 \cdot 09$	$14 \cdot 82$	$0 \cdot 10$
3869	$10 \cdot 94$	$16 \cdot 10$	$0 \cdot 12$
3821	$11 \cdot 5$	$16 \cdot 9$	$-0 \cdot 15$
3743	$11 \cdot 75$	$17 \cdot 29$	$0 \cdot 41$
3714	$12 \cdot 5$	$18 \cdot 4$	$-0 \cdot 3$
3656	$12 \cdot 60$	$18 \cdot 52$	$0 \cdot 34$
3626	$13 \cdot 5$	$19 \cdot 85$	$-0 \cdot 55$
3545	$14 \cdot 5$	$21 \cdot 3$	$-0 \cdot 8$
3400	$15 \cdot 5$	$22 \cdot 8$	$0 \cdot 3$
3384	$16 \cdot 5$	$24 \cdot 3$	$-0 \cdot 9$
3314	$17 \cdot 5$	$25 \cdot 7$	$-0 \cdot 9$
3244	$18 \cdot 5$	$27 \cdot 2$	$-0 \cdot 7$
3146	$19 \cdot 5$	$28 \cdot 7$	$0 \cdot 3$
2975	$24 \cdot 5$	$36 \cdot 0$	$-1 \cdot 3$
2885	$26 \cdot 5$	$39 \cdot 0$	$-0 \cdot 4$
2817	$28 \cdot 5$	$41 \cdot 9$	$\pm 0 \cdot 0$
2750	$30 \cdot 5$	$44 \cdot 9$	$0 \cdot 7$
2694	$32 \cdot 5$	$47 \cdot 8$	$1 \cdot 6$
2679	$34 \cdot 5$	$50 \cdot 7$	$-0 \cdot 2$
2603	$37 \cdot 5$	$55 \cdot 1$	$1 \cdot 5$
2566	$40 \cdot 5$	$59 \cdot 6$	$0 \cdot 4$

SIMPLE CYCLIC DIAMINES

Experimental values for the rotatory dispersions of *l-trans*-1:2-diamino-*cyclo*pentane, and -*cyclo*hexane have been recorded by Jaeger and co-workers (1928, 1937). Their data have now been analysed, and the results extended, in the case of the *cyclo*hexane derivative, to include the two ionic forms. The rotatory dispersion of the *cyclo*pentane compound can best be expressed by the equation:

$$[\alpha] = -9\cdot545/(\lambda^2 - 0\cdot03207) - 8\cdot44/(\lambda^2), \quad \lambda_0 = 1790 \text{ A.}$$

For the *cyclo*hexane-diamine the equation adopted is

$$[\alpha] = -2\cdot924/(\lambda^2 - 0\cdot0350) - 9\cdot28/(\lambda^2), \quad \lambda_0 = 1870 \text{ A.}$$

It must be emphasized that in both cases the values quoted for λ_0 are upper limits, but it is possible to derive similar equations of equal merit, leading to smaller dispersion constants. From the behaviour on neutralization, and from the evidence of the above equations, it is not possible to take a clear decision as to the nature of these two bases. It seems probable that they are both of an intermediate type, i.e. that the dissymmetry dependent on the ring structure has only a small effect on the lone pair of electrons, but that it is nevertheless present.

EXPERIMENTAL

Triethylbutylammonium Bromide. Pure *d*-diethylbutylamine and ethyl bromide were heated together in a sealed tube for 2 days. Combination between the two substances was not rapid, but a small quantity of crystalline quaternary salt was eventually formed. The substance had an extraordinary avidity for water, and this fact made complete purification difficult. Recrystallization was effected by suspending the salt in boiling ethyl acetate, and by adding alcohol dropwise until solution occurred. On cooling, the substance crystallized, and was dried over phosphorus pentoxide. A titration with silver nitrate showed the product to be essentially pure, but complete purity of the salt is not claimed owing to the experimental difficulty. In any case, possible impurities, being dextro-rotatory or inactive, would only lower the negative rotation, and for this reason, the argument set out above would not be vitiated.

l-Propylene-diamine. Thirty grams of specially purified *dl*-hydrate were combined with two molecular proportions of *d*-tartaric acid (Baumann 1895). The resulting salt was crystallized twenty times as two crops from

water, the second being crystallized from the mother liquor of the first, after 20 % evaporation. The *l*-propylene-diamine di-acid tartrate was distilled with aqueous alkali, and the distillate dehydrated by the usual methods. The final oil was analysed by titration for $C_3H_{10}N_2$—found 90·6 %, or 800 g. of propylene-diamine per litre. This material had a specific rotation identical with the best values in the literature, given by Tschugaeff and Sokolov (1907).

1-Trans-1:2-*Diamino*-cyclohexane. The pure material was supplied through the kindness of Professor F. M. Jaeger, and after conversion into the dihydrochloride, crystallized from alcohol.

Summary

Variations in Drude equations for the rotatory dispersions, and changes in specific rotation, which occur on neutralization, are utilized for the detection of induced dissymmetry in the amino-radical of optically active bases. When the lone pair of electrons of the nitrogen atom becomes bound in any way, the partial rotation associated with it disappears. An attempt is made to explain the behaviour of a few exceptional bases whose rotatory powers contain no contribution which can be attributed directly to the lone pair of electrons. Such bases do not give the large alteration in specific rotation which is usually produced by ionization.

The rotatory dispersion of crystalline ethylene-diamine sulphate is compared with that of *l*-propylene-diamine, *l*-diamino-cyclohexane, and of their salts in solution. Measurements and analyses are given for these two optically active bases, as well as for their mono- and di-hydrochlorides. The results are interpreted in terms of Boys's molecular model, and the absolute configuration of *l*-propylenediamine is defined. In spite of statements in the literature to the contrary, the sign of the specific rotation of this base is actually reversed on ionization, and this experimental fact constitutes strong evidence in favour of the proposed model.

It is shown that the major contribution to the optical activity of *l*-propylenediamine may be attributed to the absorption bands associated with the two lone pairs of electrons in the molecule. Assuming the presence of an unchanging dextro-rotatory nucleus common to all three ionic forms,

an attempt to estimate the other contributions to the rotatory power and dispersion is made.

The absorption bands between 2300 and 2000 A which are without exception common to all amines previously investigated are in the cases of *l*-propylenediamine and *l-cyclo*hexane not optically active. The induced dissymmetry is centred at wave-lengths between 1900 and 1400 A, and is associated with two groups of absorption bands in this region, one due to the lone pairs of electrons, and the other to the more saturated CN and NH linkages.

REFERENCES

Baldwin, W. C. G. 1937 *Proc. Roy. Soc.* A, **162**, 215.

Baumann, G. 1895 *Ber. dtsch. chem. Ges.* **28**, 1176.

Boys, S. F. 1934 *Proc. Roy. Soc.* A, **144**, 655.

Freymann, M. and Freymann, R. 1936 *J. Phys. Radium,* **7**, 506.

Jaeger, F. M. and Bijkerk, L. 1937 *Proc. Akad. Wet. Amst.* **40**, 12.

Jaeger, F. M. and Blumendal, H. B. 1928 *Z. anorg. Chem.* **175**, 161.

Janson, S. E. and Pope, Sir W. J. 1936 *Proc. Roy. Soc.* A, **154**, 53.

Kenyon, J. and Pickard, R. H. 1915 *J. Chem. Soc.* **107**, 35.

Levene, P. A., Mikeska, L. A. and Passoth, K. 1930 *J. Biol. Chem.* **88**, 27.

Lowry, T. M. and Baldwin, W. C. G. 1937 *Proc. Roy. Soc.* A, **162**, 204.

Lowry, T. M. and Walker, E. E. 1924 *Nature, Lond.,* **113**, 565.

Pope, Sir W. J. and Read, J. 1910 *J. Chem. Soc.* **97**, 2199.

Read, J. 1930 *Trans. Faraday Soc.* **26**, 441.

Tschugaeff, L. A. and Sokolov, W. 1907 *Ber. dtsch. chem. Ges.* **40**, 3461.

— — 1909 *Ber. dtsch. chem. Ges.* **42**, 55.

von Lang, V. 1872 *S.B. Akad. Wiss. Wien,* **11**, **65**, 30.

The molecular structures of carbon and silicon tetrafluorides

By C. R. Bailey, J. B. Hale and J. W. Thompson

The Sir William Ramsay and Ralph Forster Laboratories,
University College, London

The tetrahedral structure of the halides of Group IV is well established. The relation of the molecular constants to the force field governing the motion of the atoms is less certain; in particular, some difficulty has been found in reconciling the interatomic distances obtained by electron diffraction with those deduced by other means. We have obtained certain of these molecular constants from an examination of the infra-red absorption spectra of gaseous carbon and silicon tetrafluorides.

PREPARATIVE

Carbon tetrafluoride was formed by the direct action of fluorine on carbon. The halogen was generated by the electrolysis of fused potassium bifluoride in a copper vessel, the anode being a graphite rod; the gas was passed through a hard glass tube packed with sodium fluoride and then through charcoal. A stream of dry nitrogen had been passed through the absorbents and the molten electrolyte for some hours. The resulting gas was condensed in a liquid air trap, and separated; after evaporation through silver nitrate solution to remove oxygen and silicon fluorides, and through soda-lime to remove hydrogen fluoride and CO_2, it was again condensed and fractionally distilled, as far as was possible with the small yields obtained, over a small temperature range at about $-130°$ C.

Silicon tetrafluoride was prepared by heating a mixture of silica and calcium fluoride with 100 % sulphuric acid. The gas evolved was passed through a reflux condenser and a carbon dioxide-alcohol trap to remove SO_3 and hydrogen fluoride; it was condensed as a solid in liquid air and allowed to sublime at about $-90°$ C.

EXPERIMENTAL

The large Hilger D 42 spectrometer was fitted with quartz, fluorite, rock salt, and sylvine prisms for use in the appropriate spectral regions. The

equivalent slit widths in cm.$^{-1}$ are given in the tables of bands. Temperature corrections were applied where necessary.

RESULTS

The general appearance of the spectra is indicated in fig. 1: the experimental data are summarized in Tables I and II, and the contours of certain of the individual bands are displayed in figs. 2 and 3.

TABLES I AND II. THE INFRA-RED ABSORPTION SPECTRA OF CARBON TETRAFLUORIDE (I) AND SILICON TETRAFLUORIDE (II)

Band	Centre		Relative intensity at 5 cm. pressure	Slit width	Prism
	(μ)	(cm.$^{-1}$)			
			I		
A	3·935	2541	40	14	Fluorite
B	4·588	2179	30	10	,,
C	5·254	1904	28	8	,,
D	5·897	1696	19	7	,,
E	6·515	1535	44	6	,,
F	7·353	1360	40	4	,,
G	7·908	1265	100	3	,,
H	8·99	1112	79	9	Rock salt
K	11·04	906	52	5	,,
L	15·87	630	65	4	Sylvine
			II		
A	4·287	2332	19	12	Fluorite
B	4·875	2051	29	9	,,
C	5·488	1822	37	7	,,
D	6·910	1447	1	5	,,
E	7·770	1287	47	13	Rock salt
F	8·32	1202	97	11	,,
G	9·78	1022	100	7	,,
H	10·96	912	3	5	,,
K	11·93	838	46	4	,,
L	12·91	775	12	3	,,
M	15·50	645	1	4	Sylvine

The individual bands

Carbon tetrafluoride, fig. 2.

Band C, 1904 cm.$^{-1}$. There are faint inflexions on each side of the main peak separated by some 40 cm.$^{-1}$.

Band D, 1696 cm.$^{-1}$. This is a complicated region of absorption with two main maxima at 1711 and 1696, and subsidiary maxima on the long-wave
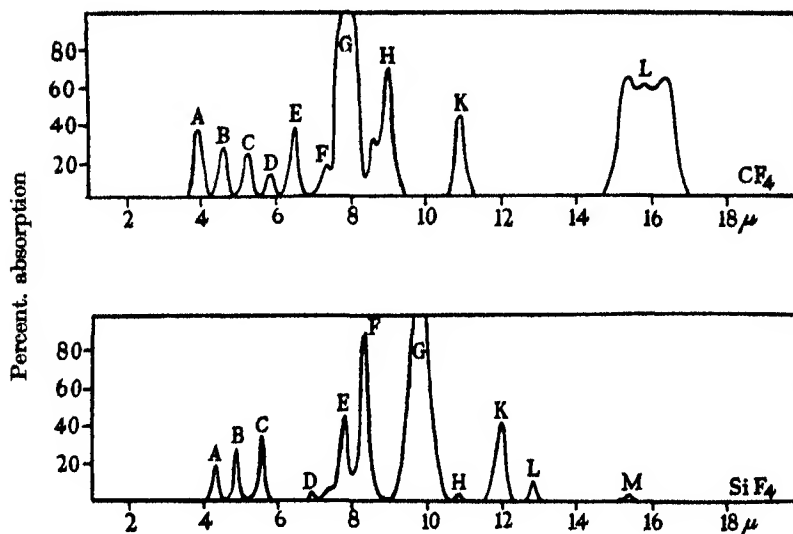
FIG. 1. The infra-red spectra of CF$_4$ (*a*) and SiF$_4$ (*b*)
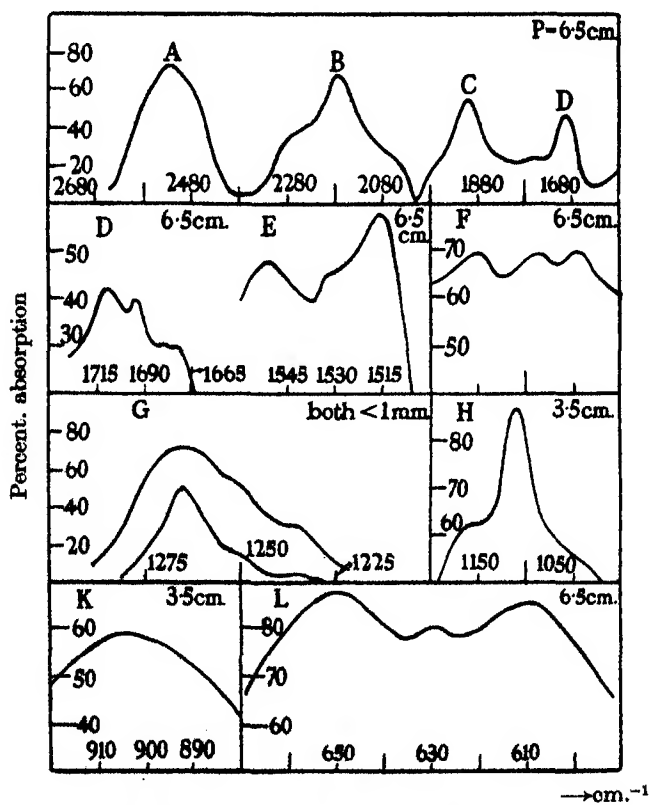
FIG. 2. Individual bands of CF$_4$.

side at 1681 and 1672 cm.$^{-1}$. 1681, 1696 and 1711 have been taken as P, Q, and R branches of a single band, since they are evenly spaced at intervals of 15 cm.$^{-1}$.

Band E, 1535 cm.$^{-1}$. We have given this frequency as the centre of the absorption region, but the band is asymmetrical, and the short-wave maximum is the less intense. The most likely impurity in the conditions of experiment is C_2F_6; and we are inclined to attribute the spread of some of the bands to the presence of this or a similar substance in small amounts. The most pronounced peak at 1516 is therefore taken as the band centre for the purposes of assignment.

Band F, 1360 cm.$^{-1}$. The intensity of this band together with its shape varied throughout the different samples examined, and we consider it as most likely due to traces of impurity.

Band G, 1265 cm.$^{-1}$. This band is so intense that it is difficult to reduce the absorption below 75 %, and the best resolution is not obtained. It can be seen to be composite, and we place the two centres at 1265 and 1247.

Band H, 1112 cm.$^{-1}$. There are also signs of a weak band at 1152.

Band K, 906 cm.$^{-1}$. In spite of a theoretical resolving power of 5 cm.$^{-1}$ in this region, no signs of structure were found. It may thus be due to some other substance than CF_4.

Band L, 630 cm.$^{-1}$. P and R branches are found at 611 and 649 cm.$^{-1}$, with a small Q branch at 630.

Silicon tetrafluoride, fig. 3.

The regions of absorption were generally narrow but intense. No structure was revealed in any of the bands, and it is hardly necessary to comment in detail on their individual shapes. Band F at 1202 cm.$^{-1}$ seems to be nearly as strong as G at 5 cm. pressure, but at about 3 mm. their respective relative intensities are 19 and 95.

Assignments

The infra-red spectrum of CF_4 was partially explored by Eucken and Bertram (1936) in an attempt to locate the fundamentals for a determination of the specific heat; two bands were found at 653 and 1350 cm.$^{-1}$. Yost, Lassettre and Gross (1936) examined the Raman spectra of both substances: gaseous CF_4 gave one line at 904, and the liquid two additional lines at 635 and 437 cm.$^{-1}$, whereas SiF_4 gave one line in both states at 800 cm.$^{-1}$.

The tetrahedral molecule YX_4 has high symmetry, and the nine possible vibrations are reduced by the degeneracy resulting from the isotropic motion to four. The classes with their spectral characteristics are taken from Placzek's tables (1934) and given in Table III (a): Table III (b) has been

compiled to show the activities of the binary summation tones. *R* and *I* denote bands active in the Raman effect alone, or in the infra-red alone, while *RI* bands are active in both.
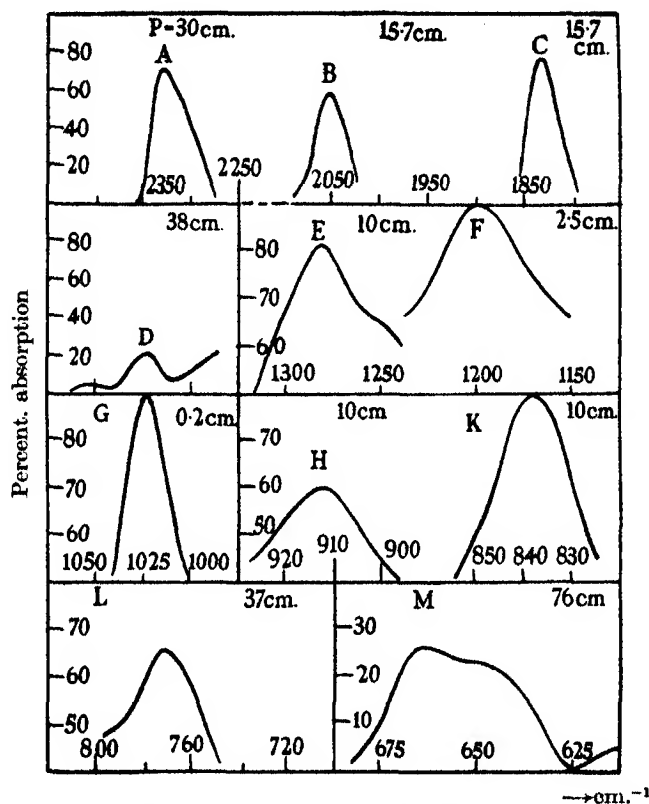
Fig. 3. Individual bands of SiF$_4$.

TABLE III*a*

Class	Mode	Degeneracy	Activity
A_1	ν_1	—	R
E	ν_2	2	$R(\rho = 6/7)$
F_2	ν_3; ν_4	3	$R(\rho = 6/7)$; I

TABLE III*b*

	ν_1	ν_2	ν_3	ν_4
ν_1 (R)	R	R	RI	RI
ν_2 (R)		R	RI	RI
ν_3 (RI)			RI	RI
ν_4 (RI)				RI

It will be seen that any band appearing in the infra-red spectrum must involve either or both ν_3 and ν_4.

The fundamental modes are shown in fig. 4; the representation of ν_4 is somewhat different from that usually given, but it is found that in the solution of the mechanical problem with symmetry co-ordinates the formulation here given is correct: furthermore, ν_4 now bears the same relation to ν_2 as ν_3 does to ν_1.

Both spectra have one very powerful band which may be taken as the high-frequency F_2 mode: hence ν_3 for CF_4 is *Band G* at 1265, and for SiF_4 is *Band H* at 1022 cm.$^{-1}$. The low-frequency F_2 mode ν_4 for CF_4 is probably *Band L* at 630 cm.$^{-1}$: the corresponding band for SiF_4 is thus outside our experimental region. All four fundamentals are active in the Raman effect, and both substances as gases show one strong line which is probably the
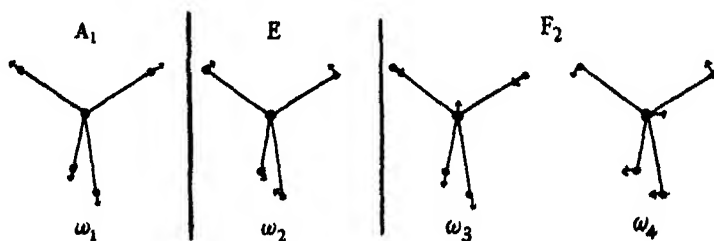
FIG. 4. The vibrational modes of the tetrahedral YX_4 molecule (only one component is shown for the degenerate cases).

symmetrical mode A_1; we therefore take ν_1 for CF_4 as 904, and for SiF_4 as 800 cm.$^{-1}$. Liquid CF_4 gives in addition two lines at 635 and 437 cm.$^{-1}$; we follow Yost, Lassettre and Gross (1936) in allotting the first to ν_4, and the second to the degenerate bending vibration, ν_2. The band at 906 in the infra-red spectrum cannot be interpreted as a combination tone: and if the suggested structure and assignments are correct, must be ascribed to the presence of an impurity. C_2F_6 and higher homologues are said to be formed when charcoal is used in the preparation, and avoided to some extent if lampblack is substituted. We found difficulty in getting the fluorine over and through the latter, and the pressure developed forced the gas back into the cell where explosions took place. The SiF_4 spectrum is free from awkward coincidences, but it is necessary to resort to comparison and calculation to estimate the approximate magnitude of ν_2 and ν_4. A comparison of the ratios of the known fundamentals for the chlorides and fluorides of carbon and silicon places ν_2 for the latter at c. 304 and ν_4 at c. 447 cm.$^{-1}$. Inspection of the observed bands suggests that a better fit is obtained with $\nu_2 = 260$ and

$\nu_4 = 420$ cm.$^{-1}$. Fortunately the absolute magnitude of these frequencies is not critical in a discussion of the force constants. The combination tones are assigned on the basis of these values as in Table IV.

TABLE IV. THE ASSIGNMENTS IN THE INFRA-RED AND
RAMAN SPECTRA OF CF_4 AND SiF_4

Mode	CF$_4$			SiF$_4$		
	IR	R	Calc.	IR	R	Calc.
ν_2	ia	437	—	ia	(260)	—
ν_4	630	635	—	(420)	—	—
ν_1	ia	904	—	ia	800	—
ν_3	1265	—	—	1022	—	—
$\nu_2 + \nu_4$	1112	—	1067	645	—	(680)
$\nu_3 - \nu_2$	—	—	828	775	—	(762)
$2\nu_4$	1250	—	1262	838	—	(840)
$2\nu_2 + \nu_4$	1516	—	1504	912	—	(940)
$\nu_1 + \nu_4$	1553	—	1534	1202	—	(1220)
$\nu_2 + \nu_3$	1696	—	1702	1287	—	(1282)
$\nu_3 + \nu_4$	1904	—	1895	1447	—	(1442)
$\nu_1 + \nu_3$	2179	—	2169	1822	—	1822
$2\nu_3$	2541	—	2530	2051	—	2044
$\nu_2 + 2\nu_3$	—	—	2967	2332	—	(2304)

Agreement on the whole is satisfactory: two complicating factors exist which make the selection of any values as the actual band centres a somewhat arbitrary proceeding for pentatomic molecules of tetrahedral symmetry. Not only does the interaction between vibration and rotation (Teller 1934) alter the line spacing within a band and hence its contour, but the type of motion involved in ν_3 and ν_4 produces a degeneracy which has far-reaching consequences. For both of these modes (or their combinations) all states in which the vibrational quantum number $n \neq 0$ are degenerate: the weight of the nth state is given by $g_n = \frac{1}{2}(n+1)(n+2)$ (Dennison and Ingram 1930). To a first approximation these levels are coincident, but when the anharmonicity is taken into account, this degeneracy is partly removed. Thus $2\nu_3$ or $2\nu_4$ consists of three separate near-lying levels of degeneracy 3, 2 and 1; while a high overtone such as $4\nu_3$ would be made up of no less than seven bands. An extension of the argument to the mode $\nu_3 + \nu_4$ shows that this is ninefold degenerate with two triple states, and in addition one double and one single state (Johnston and Dennison 1935). The irregular envelopes of certain of the bands may perhaps be explained in this way. It should also be observed that for CF_4, $2\nu_4(1264) = \nu_3(1265)$, and quasi-resonance between components of these two modes having the same symmetry is possible, although no direct evidence of this effect is obtained.

The force field

The complete potential energy expression for a pentatomic molecule requires nine force constants for its specification. The symmetry of the tetrahedral model reduces them to five, but in the absence of data from isotopic molecules or of measurements of the internal moment of momentum, only four relations (the fundamental frequencies) are observable, and hence certain physical assumptions are necessary to restrict the number of force constants. The equations of motion corresponding to the complete expression were set up and solved by Miss Rosenthal (1934*a*); a formal simplicity is obtained due to an elegant choice of variables, but the solution of a number of simultaneous equations is required to relate the constants which appear to those of the original expression. In later papers (1934*b*; 1936) Rosenthal restricts the generality of the complete expression, and certain relationships obtained by her are used below. We have found that the best approximate representation of the force fields within CF_4 and SiF_4 is given by the potential energy expression devised by Urey and Bradley (1931) for the YX_4 molecule: this includes forces along the bonds, perpendicular to them, and along the lines joining like atoms, and is fully expounded by Urey and Bradley in their readily accessible paper. We will therefore content ourselves with defining the force constants for the valence, central, and Urey and Bradley systems, and with summarizing the results of applying the systems to the molecules in question.

The valence force system. $K_1 = \partial^2 V/\partial r^2$; k_2 is defined by the potential energy term $\frac{1}{2}\sum_1^4 k_2 r_0^2 \Delta\theta_i^2$, with r_0 as the equilibrium value of the bond length r. V is the potential energy, and θ an angular displacement perpendicular to the bond direction. For a valence system to hold, Rosenthal (1934*b*) has shown that

$$\nu_1 \nu_2/\nu_3 \nu_4 = (3\mu/2)^{\frac{1}{2}},   (1)$$

and
$$\nu_3^2 + \nu_4^2 = (1/3)\,[\nu_1^2(2 + 1/\mu) + (2/3)\,\nu_2^2(1 + 2/\mu)],   (2)$$

where $\mu = M/(4m + M)$, with M as the mass of the central atom Y, and m that of the external atoms, X. Table V shows the measure of agreement.

The data for silicane are the frequencies given by Stitt and Yost (1936). It will be seen that agreement is generally better the larger the central atom and the smaller the external atoms, so that within the experimental error the valence force may be said to be satisfactory for the hydrides.

The central force system. K_1; $K_2 = (\partial^2 V/\partial q^2)$; and $K' = -(\sqrt{8}/q_0\sqrt{3})\,.\,\partial V/\partial q$, where q is the side of the tetrahedron. The solution was first given by Denni-

son (1925); as only three force constants are to be determined from four frequencies, it is possible to adjust them to give best agreement. The method is described in Dennison's paper, and has been applied by Trumpy (1930), and by Schaefer and Kern (1932). It is hardly necessary to give details of the calculations and accompanying curves: the results are to be found in Table VI.

TABLE V

	Equation (1)			Equation (2)		
	L.H.S.	R.H.S.	% diff.	L.H.S. (both × 10^{-4})	R.H.S.	% diff.
CH_4	1·127	1·061	6	1078	1132	− 5
CF_4	0·499	0·452	10	197	321	− 39
CCl_4	0·409	0·344	19	69	130	− 47
SiH_4	1·077	1·146	− 7	559	575	− 3
SiF_4	0·559	0·636	− 12	122	139	− 12
$SiCl_4$	0·470	0·500	− 6	42	54	− 22

TABLE VI. THE FORCE CONSTANTS OF THE MOLECULES CF_4 AND SiF_4

(Frequencies in cm.$^{-1}$; force constants in dynes × 10^{-5}/cm.)

Obs. CF_4	Valence		Central		U.B.	
	Calc.	% diff.	Calc.	% diff.	Calc.	% diff.
904	904	0	904	0	904	0
437	437	0	423	− 3·1	437	0
1265	1783	42	1265	0	1266	0·1
630	600	− 5	641	1·7	634	0·3
	K_1 9·10		K_1 3·08		K_1 3·99	
	k_2 2·13		K_2 1·51		k_2 0·67	
	—		K' − 2·00		g_3 0·73	
SiF_4						
800	800	0	800	0	800	0
(260)	280	—	260	—	300	—
1022	1168	14	967	− 5·3	1022	0
420	382	− 9	424	1·0	420	0
	K_1 7·13		K_1 4·95		K_1 5·60	
	k_2 0·87		K_2 0·55		k_2 0·57	
			K' − 0·84		g_3 0·25	

The Urey and Bradley force system. K_1; k_2; and $g_3 = 4nk_3/q_0^{n+2}$, where $k_3 = -(q^{n+1}/n)(\partial V/\partial q) = (q^{n+1}/n\sqrt{6})(\partial V/\partial r)$ by the geometry of the model. It will be seen that K' and g_3 provide terms measuring the potential energy due to strain within the molecule arising from the repulsion of the like atoms, and here assumed proportional to an inverse power ($n = 6$) of the distance: the marked success of this system in describing the structure of

CF_4 and SiF_4 justifies the assumption. The frequency expressions will be found in the original paper.

Interatomic distances

A collection of pertinent data has been made in Table VII. The following remarks apply: K, in dynes $\times 10^5$/cm., is taken from Urey and Bradley's paper for CCl_4 and $SiCl_4$, from Sutherland (1938) for the methyl halides, from the vibrational frequencies for the diatomic cases, and for CF_4 and SiF_4 from the present work; the molecule CCl has recently been identified by Asundi and Karim (1937); the electron diffraction value for the fluorine molecule is due to Brockway, cited in a paper by Garner and Yost (1937); the abbreviations signify electron diffraction (ED); interatomic distance (r), determined by the Badger rule (B), determined from the rotation-vibration spectrum (S); and the Pauling-Huggins radius sum (PH) as recently corrected by Pauling and Brockway (1937).

TABLE VII

| Link | Molecule | K | Interatomic distance, r | | | |
			ED	B	S	PH
C—F	CH_3F	5·8	1·42	1·34	1·38	1·41
C—F	CF_4	4·0	1·36	—	—	1·41
C—Cl	CH_3Cl	3·6	1·77	1·69	1·66	1·76
C—Cl	CCl_4	1·7	1·76	—	—	1·76
C—Cl	CCl	3·7	—	1·68	—	1·76
Si—F	SiF_4	5·6	1·54	1·59	—	1·81
Si—F	SiF	4·9	—	1·62	—	1·81
Si—Cl	$SiCl_4$	2·6	2·02	2·02	—	2·16
Si—Cl	SiCl	2·6	—	2·01	—	2·16
F—F	F_2	—	1·46	—	—	1·28
Cl—Cl	Cl_2	3·3	1·98	—	1·98	1·98

The relative values of the force constants for the first four molecules may be taken to confirm the existence of strain in the tetrahalides. The difficulty of reconciling the interatomic distances as determined by electron diffraction in the cases of methyl chloride and carbon tetrachloride was pointed out by Badger (1935), and has been the subject of a recent enquiry by Sutherland (1938). On the whole the spectral evidence indicates a stretched link in CCl_4: if Sutherland's separation of 1·66 A is accepted, the normal Cl radius should be 0·89 A instead of the Pauling value of 0·99. In this respect it is interesting to compare the Cl radius in the following compounds (the normal radius for the other element concerned being used in each case): CH_3Cl (S) 0·89, CCl (B) 0·91, $COCl_2$ (ED) 0·91, PCl_3 (ED) 0·92, $PSCl_3$ (ED) 0·91, $GeCl_4$ (ED) 0·89, $SnCl_4$ (ED) 0·90, HCl (S; H = 0·37) 0·90 A.

It is much more difficult to say anything with certainty about the fluorine radius. The electron diffraction values for this length vary throughout compounds in which no double bond formation is presumed; we have the following for r: F_2 0·73, F_2O 0·70, CH_3F 0·65, BF_3 0·63 (if we use the boron radius of 0·67 first estimated by Bailey, Hale and Thompson (1937), or if, as Bauer (1938) insists, we use $B = 0·86$, then $F = 0·44$), AsF_3 0·52, and PF_3 0·46. It is tempting to say that the discrepancies are due to the high electronegative nature of fluorine, but it is not always easy to predict the consequences. There are nevertheless two competing phenomena which are of interest to us in this connexion: high ionic states such as may occur in CF_4 (see below) tend to increase the size of the fluorine atom at the expense of the carbon, and so may bring into prominence the repulsion between the external atoms; on the other hand the same ionic states render possible

contributions from such structures as $:\ddot{F}:\ :C^+$ and $\begin{matrix} :\ddot{F}: \\ :\ddot{F}: \ :C^+ \\ :\ddot{F}: \end{matrix}$ and $:\ddot{F}\bar{\cdot}$, providing some

double bond character. As the shortening on the *PH* radii in CF_4 is according to electron diffraction some 15 %, and the maximum contribution for complete double bond formation is 10 %, the explanation is not complete. What is reasonably certain is that the force constants show the existence of strain in CF_4 and CCl_4 as compared with the methyl halides, and that in this respect the findings are opposed to those of electron diffraction.

The Badger relationship applies to unstrained bonds: Urey and Bradley showed that by connecting for strain the force constant for CCl_4 could be improved, and estimated that the observed C—Cl distance in this compound should be about 0·2 A greater than in the unstrained link, a calculation confirmed as to order by Badger (1935) and by Sutherland (1938). In $SiCl_4$ and SiCl the force constants are in close agreement. It therefore seems that the interatomic distance calculated by the Badger rule cannot be far from the truth, and that a double bond involving the unoccupied d orbitals of the Si atom results in an interatomic distance of 2·02 A, slightly less than that calculated for Si $=$ 1·17, Cl $=$ 0·89, i.e. 2·06. Both SiF and SiF_4 seem to have double bonds, but the electron diffraction value for the SiF link is so low that it would be of great interest if it were confirmed.

Mulliken (1935) gives an empirical equation by which the internal polarity of a YX_n molecule may be determined: it is

$$- Q_X/e = (P_X - P_Y)/3 - (P_X - P_Y)^3/48.$$

The P's are the electronegativity values of the corresponding elements as they appear in the scale devised by Pauling (1932), while Q is the actual net charge. Mulliken finds that it is only in CBr_4 and CI_4 that a real approach is made to electron pair bond formation; he shows CH_4 to be represented very approximately by $C^{-0.72}(H^{+0.18})_4$, CCl_4 by $C^{+0.52}(Cl^{-0.13})_4$, and CF_4 by $C^{+1.68}(F^{-0.42})_4$. In addition, we calculate SiH_4 as $Si^{-0.2}(H^{+0.05})_4$, SiF_4 as $Si^{+2.0}(F^{-0.50})_4$, and $SiCl_4$ as $Si^{+1.0}(Cl^{-0.25})_4$. For silicane electron pair bonds are also a good approximation: the obedience of silicane to a valence force system, and the considerable departure from additivity in the radii of SiF_4 and $SiCl_4$ with the consequent failure of the valence force system for those two compounds are in accord with the position of silicon as considerably more electropositive than carbon on Pauling's scale. Since the measure of electronegativity used is related to the deviation of the heats of linking from covalent additivity, we see that the small interatomic distance for SiF_4 runs parallel to the high force constant and large heat of formation. It would thus be a fundamental procedure to construct curves of atomic radii for elements on the basis of the relative electronegativity of their partners.

SUMMARY

The infra-red absorption spectra of gaseous CF_4 and SiF_4 have been examined between 1 and 18μ with a prism spectrometer. Data obtained for the Raman spectra by other workers have helped in the assignment of fundamental modes and combination tones. The Urey and Bradley force system provides a satisfactory picture of the two molecules, and the force constants for this and other systems have been calculated. The molecular structures are discussed with particular reference to the interatomic distances and extent of electron pair bond formation.

REFERENCES

Asundi, R. K. and Karim, S. M. 1937 *Proc. Ind. Acad. Sci.* 6, 328.
Badger, R. M. 1935 *J. Chem. Phys.* 3, 710.
Bailey, C. R., Hale, J. B. and Thompson, J. W. 1937 *Proc. Roy. Soc.* A, 161, 107.
Bauer, S. H. 1938 *J. Amer. Chem. Soc.* 60, 524.
Dennison, D. M. 1925 *Astrophys. J.* 62, 84.
Dennison, D. M. and Ingram, S. B. 1930 *Phys. Rev.* 36, 1451.
Eucken, A. and Bertram, A. 1936 *Z. phys. Chem.* B, 31, 361.
Garner, C. S. and Yost, D. M. 1937 *J. Amer. Chem. Soc.* 59, 2738.
Johnston, M. and Dennison, D. M. 1935 *Phys. Rev.* 48, 868.
Mulliken, R. 1935 *J. Chem. Phys.* 3, 586.
Pauling, L. 1932 *J. Amer. Chem. Soc.* 54, 3570.

Pauling, L., Brockway, L. O. 1937 *J. Amer. Chem. Soc.* **59**, 1223.
Placzek, G. 1934 *Handb. Radiol.* **6** (II), 205.
Rosenthal, J. E. 1934*a* *Phys. Rev.* **45**, 538.
— 1934*b* *Phys. Rev.* **46**, 730.
— 1936 *Phys. Rev.* **49**, 535.
Schaefer, C. and Kern, R. 1932 *Z. Phys.* **78**, 609.
Stitt, F. B. and Yost, D. M. 1936 *J. Chem. Phys.* **4**, 82.
Sutherland, G. B. B. M. 1938 *Trans. Faraday Soc.* **34**, 325.
Teller, E. 1934 *Hand. Jb. chem. Phys.* **9**, 125.
Trumpy, B. 1930 *Z. Phys.* **66**, 790.
Urey, H. C. and Bradley, C. A. 1931 *Phys. Rev.* **38**, 1969.
Voge, H. H. and Rosenthal, J. E. 1936 *J. Chem. Phys.* **4**, 137.
Yost, D. M., Lassettre, E. N. and Gross, S. T. 1936 *J. Chem. Phys.* **4**, 325.

The band spectrum of lead fluoride (PbF). II

By G. D. Rochester, Ph.D.

University of Manchester

[Plate 19]

Introduction

This investigation was undertaken to explain the apparently conflicting band-spectral evidence for the nature of the ground states of the diatomic germanium, tin and lead halides. Investigations of the band spectra of the germanium and tin monohalides by Jevons (1926, 1937), Jenkins and Rochester (1937) and others show that the ground states of these molecules are doublets of the electronic type $^2\Pi$, with $^2\Pi_{\frac{3}{2}} \sim {}^2\Pi_{\frac{1}{2}}$ separations of approximately 1000 cm.$^{-1}$ for the germanium compounds and 2400 cm.$^{-1}$ for the tin compounds. Ground states of the type $^2\Pi$ are predicted by theory if it is assumed that the molecules are formed from unexcited metal and halide atoms. The spectra of the lead monohalides, of which that of PbF is typical, apparently do not show doublet multiplicity, only one system (A_1) being found (Part I, Rochester, 1936). Morgan (1936) observed this system in absorption, and suggested that the apparent absence of a second component system (A_2) was due to the magnitude of the doublet separation in the ground state. He pointed out that if the doublet separation was as large

as 7000 cm.$^{-1}$ system A_2 would not occur in absorption but could occur in emission and would lie in the near infra-red region.

In the ultra-violet region of the spectrum the germanium and tin mono-halides have intense systems of the type $^2\Sigma \rightleftharpoons {}^2\Pi$ and it is to be expected that the spectrum of PbF will have similar spectra in the same region. The following paper gives an account of the results of a search for these spectra.

<center>EXPERIMENTAL.</center>

The absorption spectrum of PbF was photographed in the first order of a 30,000 lines per inch, Al-coated, concave grating, the property of the Department of Physics, the University of California, Berkeley. The plates were taken as part of a series of investigations of the ultra-violet absorption spectra of metal halides. As already described by Jenkins and Rochester (1937) the substances investigated were placed in carbon tubes in a carbon-tube furnace, the temperature of which could be varied continuously from room temperature to 2000° C. PbF vapour was produced by heating a few grams of lead fluoride (PbF$_2$) in the furnace to temperatures ranging from 600 to 1500° C. Details of the furnace, the source of continuum, photographic plates, and exposure times were as given in the former paper.

The study of the emission spectrum of PbF was carried out at King's College, Newcastle-upon-Tyne, with Hilger quartz spectrographs, a discharge tube and a high-frequency oscillator of the types described in Part I. Care was taken to obtain spectra as free as possible from SiF bands, a troublesome "impurity" caused by the chemical action of the hot lead fluoride on the silica walls of the discharge tube.

A preliminary survey from 2300 to 6000 A with the small quartz spectrograph showed that the emission spectrum was similar to the absorption spectrum except for a group of bands at 3700 A and a strong continuum stretching from 2800 to 3800 A. The band spectrum was photographed with a Hilger E1 spectrograph (dispersion 9 A/mm. at 3700 A), in 3 hr. on a "Monarch" plate.

Measurements of the band heads were made with a comparator and were reduced to wave-lengths using iron-arc wave-length standards and methods of reduction appropriate to the type of spectrograph. The heads photographed in absorption were very sharp, and since the dispersion of the grating was large (1·3 A/mm.), quite accurate measurements were made. Measurements of the same intense heads made on different grating plates seldom differed by more than ± 0·1 cm.$^{-1}$. The values given in the tables are usually the mean of several measurements from different plates. The wave

numbers of the heads photographed with the E 1 spectrograph are accurate only to $\pm 1 \cdot 0$ cm.$^{-1}$, however, because of the presence of a strong continuum which made exact setting difficult. Intensities were assigned visually on a 0–10 scale.

DESCRIPTION OF THE SPECTRA

Photographs of the spectra illustrating their main features are reproduced in Plate 19. Plate 19 (a) shows the absorption spectrum at a furnace temperature of 900° C. and Plate 19 (b) the emission spectrum. Both spectra were photographed with the small quartz spectrograph, the former on a Kodak "I.O.U.-V." plate and the latter on an Ilford "Monarch" plate. It is seen that the most notable features of the absorption spectrum are groups of bands, degraded to shorter wave-lengths, at 2200 and 2750, and an intense continuum extending from 2350 to 2650 A. No other bands occur below 4000 A. Raising the temperature of the furnace causes the groups of bands and the continuum to extend a little towards longer wave-lengths. Usually, at high temperatures, the absorption in the ultra-violet is so intense that no bands can be seen below 3300 A.

The emission spectrum is seen from Plate 19 (b) to consist mainly of an intense continuum extending from 2800 to 3800 A (upper limit uncertain), and groups of lines and bands. Most of the lines belong to the elements lead and silicon and the bands to SiF (Johnson and Jenkins 1927), but the groups of bands at 2800 and 3700 A are due to PbF. The continuum is also definitely not due to SiF and must therefore be ascribed to PbF.

Because of the rapid fall in the sensitivity of the photographic plate below 2400 A it is not possible to say whether the 2200 A group of bands occurs in emission.

Plate 19 (c) and (d) show in greater detail the appearance of the bands in the 2700 and 2200 A groups, in absorption, and Plate 19 (e) the appearance of the bands of the 3700 A group in emission. It is seen that most of the bands are double-headed and have long intense Q branches and short intense P branches. Well-resolved rotational structure is easily seen in several bands belonging to the 2700 A group.

VIBRATIONAL ANALYSES

All the absorption bands with the exception of three weak bands have been fitted into five systems (designated B_1, C, D, E, and F), and all the emission bands into one system (B_2). The systems B_1, C, D, E, and F have as

36-2

their lower electronic states the ground state (X_1) which is also the lower state of system A_1. The v'' numeration has therefore been made by comparing the observed values of $\Delta G(v'' + \frac{1}{2})$ with those of system A_1. The v' numeration has been made from a study of the intensity distributions. Vibrational constants of the electronic states have been derived in the usual way from graphs of $\Delta G(v + \frac{1}{2})$; $(v + 1)$.

System B_2 (3565–3795 A)

This system occurs only in emission and consists of six double-headed bands degraded to shorter wave-lengths. Tables Ia and Ib show in square array the wave numbers of the band heads and the intensity distribution. To within the accuracy of measurement the wave numbers of the Q heads are represented by the formula

$$\nu = 27377 + 612 \cdot 8(v' + \tfrac{1}{2}) - 3 \cdot 42(v' + \tfrac{1}{2})^2$$

$$- 531 \cdot 1(v'' + \tfrac{1}{2}) + 1 \cdot 50(v'' + \tfrac{1}{2})^2.$$

The vibrational constants of the upper state are taken from system B_1. O. – C. values are given in Table VII.

The absence of bands with $v' > 1$ is noteworthy and indicates that the upper electronic state of this system is crossed by a repulsive state at $v' = 2$.

TABLE Ia. SYSTEM B_2

v' \ v''		0		1		2		3
0	P	27,410	528	26,882	524	26,358		
		8		8		6		
	Q	418	528	890	526	364		
		603				605		
		604				607		
1	P	28,013				26,963	520	26,443
		9				8		7
	Q	022				971	521	450

TABLE Ib. SYSTEM B_2. INTENSITY DISTRIBUTION

v' \ v''	0	1	2	3
0	10	5	2	
1	3		3	2

System B_1 (2665–2925 A)

System B_1, which appears strongly at all temperatures from 700 to 1500° C., is the largest system occurring in absorption. It consists of fifteen double-

headed bands degraded to shorter wave-lengths. The average wave-number difference $\nu_Q - \nu_P$ is 7 cm.$^{-1}$ being approximately the same as for the bands of system B_2. The Deslandres' scheme is given in Table IIa and the intensity distribution in Table IIb. As is shown in Table VII the wave numbers of the Q heads are represented accurately by the formula

$$\nu = 35642\cdot8 + 612\cdot8(v' + \tfrac{1}{2}) - 3\cdot42(v' + \tfrac{1}{2})^2$$

$$- 507\cdot2(v'' + \tfrac{1}{2}) + 2\cdot30(v'' + \tfrac{1}{2})^2.$$

The intensity distribution is such as would be expected from the Franck-Condon principle for the observed $\omega_e' - \omega_e''$ difference. Several bands, notably the 0, 0; 0, 1; 0, 2 and the 1, 0 bands, have well-resolved Q branches extending a considerable distance from the head. Some 80 rotational lines of the 0, 0 band and 40 lines of the 1, 0 band have been measured and give average second differences of 0·040 and 0·036 cm.$^{-1}$ showing that $B' - B''$ is approximately 0·019 cm.$^{-1}$. No clearly resolved rotational structure is observed in bands having $v' > 1$.

The 0, 0; 0, 1 and 1, 0 bands of this system are observed in emission (*vide* Plate 19 (b)).

TABLE IIa. SYSTEM B_1

v' \ v''		0		1		2		3		4		5
	P	35,688·4	502·3	35,186·1	497·8	34,688·3		—				
		7·6		7·2								
0	Q	696·0	502·7	193·3		—		34,199·2				
		605·0										
		605·7						608·3				
	P	36,293·4						34,801·0	489·9	34,311·1		
		8·3						6·5		6·6		
1	Q	301·7						807·5	489·8	317·7		
		598·9								599·3		
		599·3								598·6		
	P	36,892·3	503·1	36,389·2	496·0	35,893·2				34,910·4	—	—
		8·7		7·7		6·8				5·9		
2	Q	901·0	504·1	396·9	496·9	900·0				916·3	483·4	34,432·9
		—		—								
		591·9		592·8								
3	Q	37,492·9	503·2	36,989·7				36,001·6				

TABLE IIb. SYSTEM B_1. INTENSITY DISTRIBUTION

v' \ v''	0	1	2	3	4	5
0	9	8	3	0		
1	10			3	1	
2	7	5	1		1	0
3	2	3		1		

System C (2570–2690 A)

This is a system of weak absorption bands lying between system B_1 and the continuum. The bands are grouped in sequences, as shown by the square arrays in Tables IIIa and IIIb. Most bands have only one head, presumably a Q head, but three of the strongest bands have P heads as well as Q heads, the $\nu_Q - \nu_P$ difference being approximately 10 cm.$^{-1}$. The numeration has been chosen to make the sequence having the strongest bands the 0 sequence. With this v' numeration the Q heads of all bands except the weakest are represented to within an error of ± 1 cm.$^{-1}$ by the formula

$$\nu = 38046 + 594 \cdot 0(v' + \tfrac{1}{2}) - 2 \cdot 50(v' + \tfrac{1}{2})^2$$

$$- 507 \cdot 0(v'' + \tfrac{1}{2}) + 2 \cdot 30(v'' + \tfrac{1}{2})^2.$$

At all temperatures the bands in this system are very diffuse, suggesting that the upper electronic state is strongly predissociated.

TABLE IIIa. SYSTEM C (Q HEADS)

v' \ v''	1		2		3		4		5
1	38,176	499	37,677	497	37,180				
	584		585		589				
2	38,760	498	38,262	493	37,769				
			574		579				
3			38,836	488	38,348	489	37,859		
							574		
4							38,433	485	37,948
									572
5									38,520

TABLE IIIb. SYSTEM C. INTENSITY DISTRIBUTION

v' \ v''	1	2	3	4	5
1	0	1	0		
2	0	2	2		
3		0	2	1	
4				1	0
5					0

System D (2245–2305 A)

System D consists of three bands with single sharp heads. It appears first at a temperature of 1000° C. and is intense at a temperature of 1400° C. ω_e' is approximately equal to 600 cm.$^{-1}$ and ω_e'' to 505 cm.$^{-1}$ (*vide* Table IV).

TABLE IV. SYSTEM D (INTENSITIES IN BRACKETS)

v' \ v''	0		1
0	43,863 (2)	503	43,360 (1)
	597		
1	44,460 (2)		

System E (2120–2250 A)

System E, the main system in the extreme ultra-violet region, appears at relatively low temperatures (i.e. at low vapour pressures), and consists of a group of intense bands degraded to shorter wave-lengths. A photograph of the system at a temperature of 1000° C. is reproduced in Plate 19 (*d*). The Deslandres' scheme and the intensity distribution are given in Table V, the intensity distribution being consistent with the fact that the system appears at low temperatures. Wave numbers are given to whole numbers only, because of the unfavourable wave number : wave-length ratio in this region. The v'' assignment has again been made by comparing the lower state first differences with those of system A_1 and the v' assignment from the intensity distribution. It is seen that bands in the v'' progression with $v' = 0$ have double heads, whilst all other bands in the system have single heads. Consideration of a possible explanation of this is deferred until later in the paper. Because of the uncertainty in the value of $x'_e \omega'_e$ a formula for the wave numbers of the band heads is not given. There is little doubt, however, that the vibrational constants of the lower state are the same as those of the lower state of system A_1 and that ω'_e is approximately equal to 565 cm.$^{-1}$.

TABLE V. SYSTEM E (INTENSITIES IN BRACKETS)

v' \ v''	0		1		2		3
	45,415	502	44,913	498	44,415		
	17		20		21		
0	432 (8)	499	933 (3)	497	436 (0)		
	—				—		
	561				563		
	—				—		
1	45,993 (10)				44,999 (1)		
	—						
	560						
	—						
2	46,553 (5)						45,055 (0)
	—						
	569						
	—						
3	47,122 (1)						

System F (2060–2130 A)

This system, lying between system *E* and the limit of the transmission of air, contains four bands with single sharp heads. It is observed only at relatively low temperatures and low vapour pressures. The lowest state is the ground state and therefore has the same vibrational constants as the lower state of system A_1. ω_e' is seen from Table VI to be approximately equal to 630 cm.$^{-1}$.

TABLE VI. SYSTEM *F* (INTENSITIES IN BRACKETS)

v' \ v''	0		1		2
0	47,927 (2)	505	47,422 (2)	499	46,923 (0)
	628				
1	48,555 (1)				

THE CONTINUA

Two broad continua are observed, one in absorption, having a maximum at 2440 A, and the other in emission with a maximum at 3050 A. The 2440 A continuum appears first at 700° C., at which temperature it extends from 2400 to 2500 A (estimated to half-absorption at either limit). With increasing temperature and therefore increasing lead fluoride vapour pressure, the continuum increases in width and intensity roughly in proportion to the increase in the intensity of the band systems with temperature. No useful purpose would be served by giving the observed width of the continuum at different temperatures because it is not possible to allow for the change in the vapour pressure with temperature. When the vapour pressure is high absorption in the ultra-violet region below 3200 A is complete. Up to the present no assumption regarding the origin of the continuum, i.e. whether it is due to the triatomic molecule PbF_2 or the diatomic molecule PbF, has been made. The fact of the variation of the intensity of the continuum with the intensities of the band systems favours its ascription to the molecule PbF. If this assumption is correct it follows that the continuum must be due to a transition from the stable lower state common to all the systems found in absorption, i.e. to A_1, B_1, C, D, E, and F, and an upper repulsive state.

The 3050 A continuum extends from approximately 2950–3250 A. As stated earlier in the paper it must be ascribed definitely to the molecule PbF and not to PbF_2. This continuum must be due to a transition from an upper stable state to a lower repulsive state.

Rochester

Proc. Roy. Soc. A., vol. 167, Plate 19
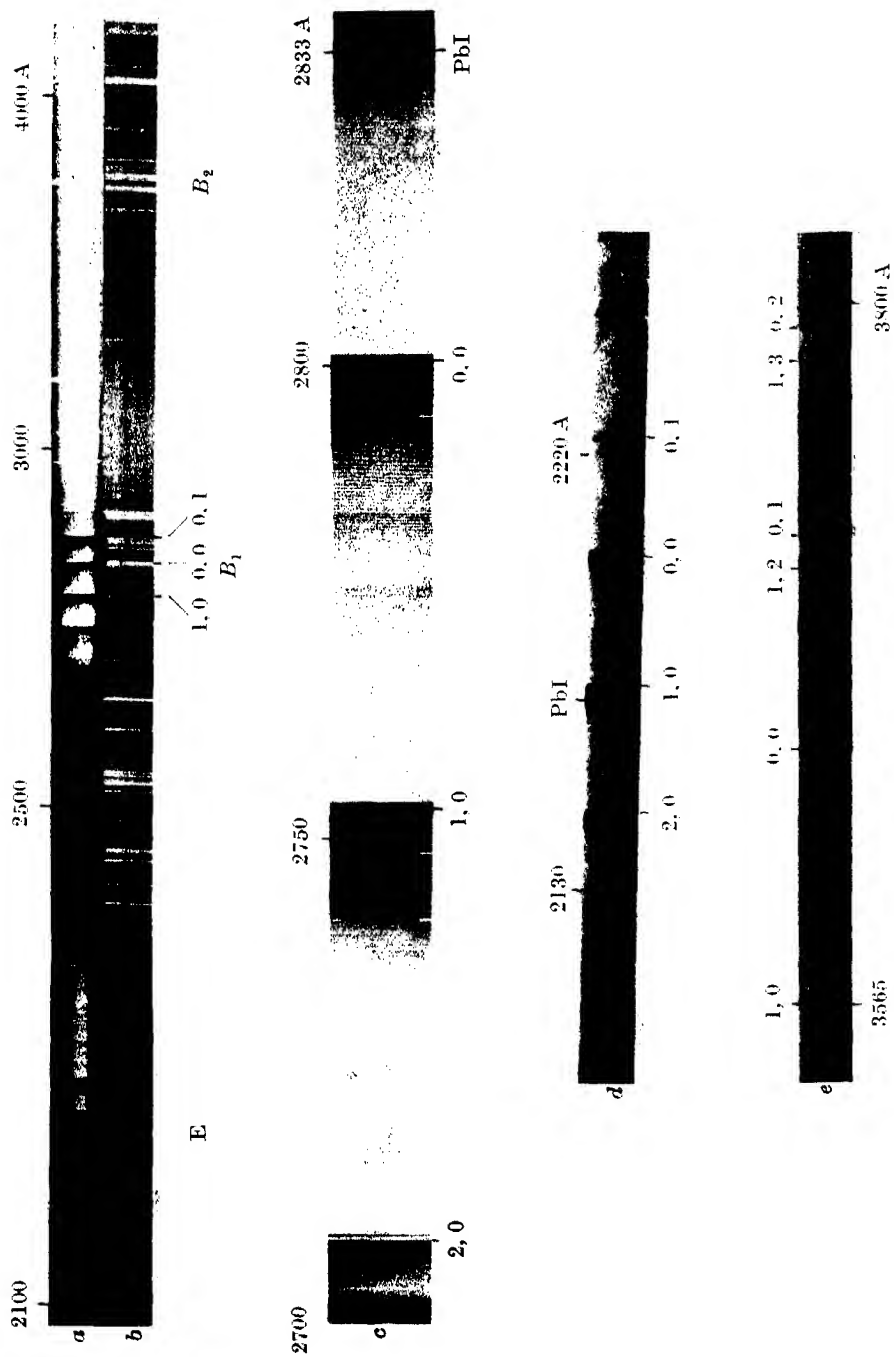
THE INTERPRETATION OF THE SPECTRUM

The close similarity of the electronic structures of PbF to those of the monohalides of germanium and tin suggests, as stated in the Introduction, that the ground state of PbF is a $^2\Pi$ state with an extremely large multiplet separation. The level X_1 common to all PbF absorption bands, is identified as the lower level of this multiplet state. To find the upper level of the ground state the emission spectrum must be examined for a wide doublet system the lower states of which have the same vibrational constants as the level X_1. System B is seen to be such a system for its component systems, B_1 and B_2, have the same upper state vibrational constants and almost the same lower state vibrational constants. Thus if state B is single (i.e. is a $^2\Sigma$ state), or has a narrow multiplet structure (i.e. is a $^2\Delta$ state), the difference

$$\nu_e(B_1) - \nu_e(B_2)$$
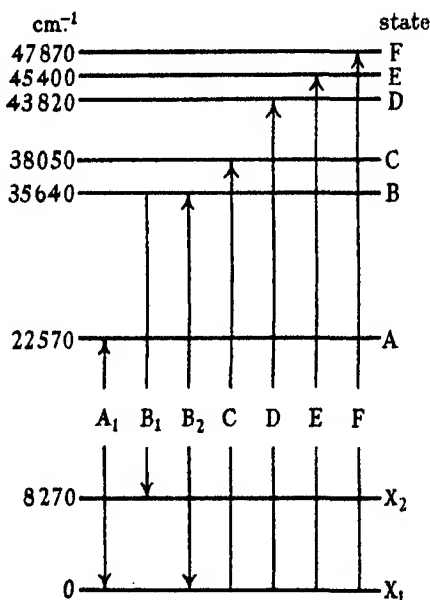
FIG. 1. Stable electronic states of PbF.

gives the width of the ground state. For two reasons it seems probable that system B is a $^2\Sigma - ^2\Pi$ system, first, because of the relative intensities of the P and Q branches, the Q branches being approximately twice as intense as the P branches, and secondly, because of its analogy to the strongest systems of the germanium and tin monohalides. It follows that the ground state has a width of 8270 cm.$^{-1}$—the largest yet recorded. System A_1 is then, as

TABLE VII. CLASSIFIED BANDS

System B_2

I	ν (cm.$^{-1}$)	O. – C. (cm.$^{-1}$)	Classification
	26,358		0, 2 P
2	364	– 1	0, 2 Q
	26,443		1, 3 P
2	450	2	1, 3 Q
	26,882		0, 1 P
5	890	0	0, 1 Q
	26,963		1, 2 P
3	971	1	1, 2 Q
	27,410		0, 0 P
10	418	1	0, 0 Q
	28,013		1, 0 P
3	022	– 1	1, 0 Q

System B_1

I	ν (cm.$^{-1}$)	O. – C. (cm.$^{-1}$)	Classification
0	34,199·2	– 2·2	0, 3 Q
	34,311·1		1, 4 P
1	317·7	– 0·8	1, 4 Q
0	34,432·9	– 0·5	2, 5 Q
3	34,688·3		0, 2 P
	34,801·0		1, 3 P
3	807·5	+ 0·2	1, 3 Q
	34,910·4		2, 4 P
1	34,916·3	– 1·3	2, 4 Q
	35,186·1		0, 1 P
8	193·3	+ 0·5	0, 1 Q
	35,688·4		0, 0 P
9	696·0	+ 0·6	0, 0 Q
	35,893·2		2, 2 P
2	900·0	+ 0·2	2, 2 Q
1	36,001·6	+ 2·9	3, 3 Q
	36,293·4		1, 0 P
10	301·7	+ 0·4	1, 0 Q
	36,389·2		2, 1 P
5	396·9	– 0·9	2, 1 Q
	36,892·3		2, 0 P
7	901·0	+ 0·6	2, 0 Q
3	36,989·7	– 0·4	3, 1 Q
2	37,492·9	+ 0·2	3, 0 Q

System C

I	ν (cm.$^{-1}$)	O. – C. (cm.$^{-1}$)	Classification
0	37,180	– 5	1, 3 Q
1	37,677	– 1	1, 2 Q
	37,759		2, 3 P
2	769	0	2, 3 Q
	37,849		3, 4 P
1	859	0	3, 4 Q
0	37,948	– 1	4, 5 Q

TABLE VII (*continued*)

0	38,176	0	1, 1 Q
2	38,262	0	2, 2 Q
	38,341		3, 3 P
2	348	0	3, 3 Q
1	38,433	0	4, 4 Q
0	38,520	2	5, 5 Q
0	38,760	0	2, 1 Q
0	38,836	−7	3, 2 Q

System D

1	43,360	0, 1
2	43,863	0, 0
2	44,460	1, 0

System E

	44,415	0, 2 P
0	436	0, 2 Q
	44,913	0, 1 P
3	933	0, 1 Q
1	44,999	1, 2 Q
0	45,055	2, 3 Q
	45,415	0, 0 P
8	432	0, 0 Q
10	45,993	1, 0 Q
5	46,553	2, 0 Q
1	47,122	3, 0 Q

System F

0	46,923	0, 2
2	47,422	0, 1
2	47,927	0, 0
1	48,555	1, 0

Morgan (1936) suggested, the high-frequency component of a $^2\Delta - {}^2\Pi$ system analogous to the $^2\Delta - {}^2\Pi$ system found in the spectrum of SnCl (Ferguson 1928). The width of the ground state being known it is possible to calculate approximately where system A_2 should lie, for

$$\nu_c(A_2) = \nu_c(A_1) - \Delta\nu_c(X)$$
$$= 22,600 - 8300 \text{ cm.}^{-1}$$
$$= 14,300 \text{ cm.}^{-1}.$$

System A_2 should therefore lie at about 7000 A and by analogy with system A_1 should consist of bands with line-like heads degraded to longer wavelengths.

TABLE VIII. UNCLASSIFIED BANDS

I	ν (cm.$^{-1}$)
1	47,707
1	47,780
1	48,802

Bands of system C have double heads which are presumably P and Q heads. Consequently state C must be either a $^2\Sigma$ or a $^2\Delta$ state. Bands of systems D and F have single heads showing that the states D and F must be of the electronic type $^2\Pi$.

Numerous examples of predissociation occur in the spectrum, and it is of interest to consider what information they give of the unstable states of PbF. It may be recalled that system B_2 has a sharp cut-off at the level $v' = 1$ and that this was interpreted as showing that a repulsive curve crosses state B at $v' = 2$. Since this state is also the upper state of system B_1 this system should show, in emission, the same cut-off as system B_2. No cut-off should be observed in absorption, but the bands with $v' > 1$ should have diffuse rotational structure. The only photograph available to test this point is the one reproduced in Plate 19 (b) which shows only three bands of system B_1, namely the 1, 0; 0, 0 and 0, 1 bands. Further work on the emission spectrum of system B_1 is therefore desirable. In agreement with expectation comparison of the rotational structure of absorption bands having $v' > 1$ e.g. the 2, 0 and 3, 0 bands, with those having $v' \leqslant 1$, e.g. the 1, 0; 0, 0; 0, 1 and 0, 2 bands, shows that bands in the second group only have clearly resolved rotational structure.

State C must be strongly predissociated because all the bands of system C are diffuse. The repulsive state responsible for the predissociation of state C may be the upper state of the 2440 A continuum.

Whether or not state E is predissociated depends upon the interpretation of the double-headed bands of system E. It will be recalled that all the bands of this system having $v' = 0$ have double heads whilst all bands having $v' > 0$ have single heads. The separation of the heads forming a double-headed band is approximately equal to 20 cm.$^{-1}$. The magnitude of this separation and the appearance of the heads suggests that the double heads are P and Q heads and that the other heads are Q heads.

If these assumptions are correct it is natural to assume that predissociation of state E is responsible for the absence of P heads from the bands having $v' > 0$. Predissociation phenomena of a similar kind are occasionally observed in emission spectra but not in absorption spectra. Thus in the Fulcher bands (a $3p\,^3\Pi$–$2s\,^3\Sigma$ transition), all bands for which $v' \leqslant 3$ have

normal P, Q and R branches while those bands for which $v' > 3$ have only Q branches. Dieke (1935), from a study of the analogous systems of the isotopic molecules HD and D_2, showed that the absence of the P and R branches from certain bands was caused by the predissociation of the "c" levels[*] of the $3p\,^3\Pi$ state into an overlying continuum belonging to the $3p\,^3\Sigma$ state. A similar explanation cannot be used in the present case, however, for all the bands in system E are *absorption* bands whose initial level is the stable unpredissociated ground state (X_1). Now if the double heads are P and Q heads state E must be either a $^2\Sigma$ or a $^2\Delta$ state and of these states only the latter can have "c" and "d" levels. The $^2\Sigma$ state will have only one set of levels, e.g. the "c" levels. Predissociation by another state will therefore affect all the levels and hence all the branches of a predissociated band. It is to be expected, then, that in absorption both the P and Q heads will become diffuse as a result of predissociation.

Similar considerations in the case of the $^2\Delta$ state show that predissociation will cause one set of branches, e.g. the P_1, Q_1 and R_1 branches, to become diffuse and leave unaffected the other set of branches, i.e. the P_2, Q_2 and R_2 branches. It seems, therefore, that the absence of the P heads cannot be explained by predissociation. The only other reasonable interpretation is that the P heads in the first v'' progression of system E are part of another system. It will be of considerable interest to examine system E in emission.

SUMMARY

An account is given of the emission and absorption band spectra of PbF. Six new systems and two continua are found. The vibrational constants of the stable electronic states of PbF are as follows in cm.$^{-1}$:

State	Probable type	ν_e	ω_e	$x_e\omega_e$	Observed in, emission (E), absorption (A)
X_1 X_2	$^2\Pi$	0 8266	507·2 531·1	2·30 1·50	E and A E
A	$^2\Delta$	22,567	397·8	1·77	E and A
B	$^2\Sigma$	35,643	612·8	3·42	E and A
C	$^2\Delta$	38,046	594·0	2·50	A
D	$^2\Pi$	43,820	600·0	—	A
E	—	45,400	565·0	—	A
F	$^2\Pi$	47,870	630·0	—	A
2440 A continuum maximum ~41,000					A
3050 A continuum maximum ~32,800					E

[*] I.e. one of the two sets of levels resulting from Λ-type doubling.

The width of the ground state, i.e. 8266 cm.$^{-1}$, is the largest yet recorded. Numerous examples of predissociation are found.

REFERENCES

Dieke, G. H. 1935 *Phys. Rev.* **48**, 610.
Ferguson, W. F. C. 1928 *Phys. Rev.* **32**, 607.
Jenkins, F. A. and Rochester, G. D. 1937 *Phys. Rev.* **52**, 1135.
Jevons, W. 1926 *Proc. Roy. Soc.* A, **110**, 365.
Jevons, W., Bashford, L. A. and Briscoe, H. V. A. 1937 *Proc. Phys. Soc.* **49**, 532.
Johnson, R. C. and Jenkins, H. G. 1927 *Proc. Roy. Soc.* A, **116**, 327.
Morgan, F. 1936 *Phys. Rev.* **49**, 47.
Rochester, G. D. 1936 *Proc. Roy. Soc.* A, **153**, 407.

DESCRIPTION OF PLATE 19

PbF band systems: (*a*) absorption; (*b*) emission; (*c*) system B$_1$, absorption; (*d*) system *E*, absorption; (*e*) system B$_1$, emission.

The electrical conductivity of the transition metals

BY A. H. WILSON

Trinity College, Cambridge

INTRODUCTION

1·1. The conductivity of a pure metal depends upon a large number of quantities, and it is difficult to decide the relative importance of the various constants since they often produce compensating effects. It is, however, generally agreed that the low conductivity of the divalent metals, and especially of bismuth, is due to the small effective number of conduction electrons. It has further been suggested by Mott (1935, 1936*a*, 1936*b*) that the low conductivity of the transition elements, which are even worse conductors than the divalent elements, is due to another cause, namely, to the abnormal smallness of the free path. The transition metals possess conduction electrons in an *s*-band and they also have unfilled *d*-bands.

Hence, in addition to the normal *s-s* transitions the electrons can also undergo *s-d* transitions, and this results in a shortening of the free path.

One of the difficulties in the way of a complete theory is the necessity of separating the normal *s-s* transitions from the *s-d* transitions, and so far it has not proved possible to do this. In the present paper it is shown that the resistances produced by the two different types of transition have different temperature variations, and therefore that it should be possible to estimate their relative importance by measurements over a sufficiently large range of temperature.

1·2. In order to obtain an insight into what happens we consider a simple model, for which quantitative calculations are carried out in §§2 and 3. Many of the results are, however, qualitatively true for more general models, but at present it is impossible to carry out the calculations completely except under the simplest assumptions. We take the energy zero at the bottom of the *s*-zone, and we assume that for this zone the energy is given by

$$E_s(\mathbf{k}) = \frac{h^2 |\mathbf{k}|^2}{8\pi^2 m_s},$$ (1)

where $\mathbf{k}$ is the wave vector of the state and m_s is the effective mass of an electron in the *s*-zone. The energy in the *d*-zone is assumed to be given by

$$E_d(\mathbf{k}) = A - \frac{h^2 |\mathbf{k}|^2}{8\pi^2 m_d} \quad (A > 0),$$ (2)

where m_d is the effective mass of an electron in the *d*-zone and is much greater than m_s. The quantity A and the number of electrons are such that there are some electrons in the *s*-zone and some vacant levels or holes in the *d*-zone. Let ζ be the Fermi energy of the conduction electrons. The value ζ_0 of ζ at $T = 0$ gives the energy of the highest occupied level, and for most purposes the variation of ζ with T is negligible. At $T = 0$ the electrons in the *s*-zone are contained in a sphere in $\mathbf{k}$-space of radius k_s, and the holes in the *d*-zone are contained in a sphere of radius k_d, where

$$\frac{h^2 k_s^2}{8\pi^2 m_s} = \zeta_0 = A - \frac{h^2 k_d^2}{8\pi^2 m_d}.$$ (3)

ζ_0 lies between 0 and A, and in general we should expect that $k_d > k_s$, but it is difficult to give any very accurate estimate of these quantities. The energy levels are shown schematically in fig. 1.

When an electron undergoes a transition from a state $\mathbf{k}$ to a state $\mathbf{k}'$ by

interacting with a lattice wave whose wave vector is $\mathbf{q}$, energy must be conserved, and hence

$$E(\mathbf{k}') - E(\mathbf{k}) \pm h\nu(\mathbf{q}) = 0, \tag{4}$$

where $h\nu(\mathbf{q})$ is the energy absorbed or emitted by the lattice wave. Since $h\nu(\mathbf{q})$ is very small, we can say that the energy of the electron must be practically unaltered by the collision. Further, on account of the exclusion principle, the final state must be an unoccupied one. Hence, if an electron is to undergo an s-d transition, its initial state must be one with $|\mathbf{k}|$ nearly equal to k_s, and its final state must have $|\mathbf{k}'|$ nearly equal to k_d. There is, however, one further condition which was omitted by Mott. Owing to the symmetry of the crystal lattice, the transition can only occur if (Wilson 1936, p. 199)

$$\mathbf{k} - \mathbf{k}' \pm \mathbf{q} = 0. \tag{5}$$
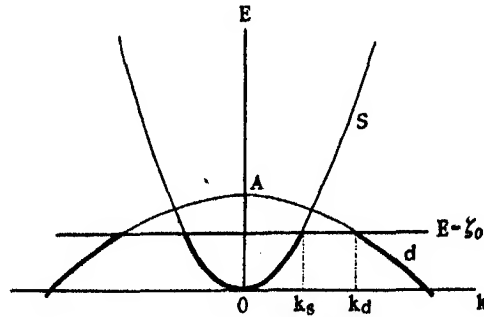
FIG. 1. The s and d levels in a transition element as functions of k. The thick lines represent levels occupied by electrons at the absolute zero.

This involves a considerable restriction on the possible transitions, since $k_s \neq k_d$, and hence a large value of $|\mathbf{q}|$ is required. We therefore deduce that lattice waves with small wave numbers are ineffective in producing s-d transitions. This is a general result and does not depend on the simplifications introduced by our model. A more complicated model would not change the result essentially, but it might change considerably the limiting wave number which produces transitions.

At high temperatures all the lattice vibrations are excited and the s-d transitions must be frequent. At low temperatures, however, only the low-frequency vibrations, with small values of $|\mathbf{q}|$, occur with appreciable intensity, and hence the s-d transitions must decrease exponentially with temperature. Thus, although the resistance may be dominated by the s-d transitions at high temperatures, the resistance at sufficiently low tempera-

tures should be entirely due to the normal *s-s* and *d-d* transitions. It should, therefore, be possible to separate the two effects.

The resistance of platinum does not show an abnormal decrease at low temperatures which can be ascribed to the falling off of the *s-d* transitions. The significance of this, and of the behaviour of the thermoelectric power, is discussed in §§ 2·3 and 3·2.

The quantitative theory is exceedingly complicated, even for the simplified model which is discussed here. Although approximations have finally to be made, the calculations have been given in detail so that the various assumptions can be clearly seen. This is particularly desirable, since the expressions obtained for the second-order quantities differ from those given by Mott.

The equations for the distribution function

2·1.   Let f denote the velocity distribution function of the electrons, and let $\mathscr{W}(\mathbf{k}, \mathbf{k}')$ be the probability that in unit time an electron makes a transition from the state $\mathbf{k}$ to the state $\mathbf{k}'$. Also let $[\partial f/\partial t]$ denote the net rate of increase in f due to the collisions. Then (Wilson 1936, p. 158)

$$\left[\frac{\partial f}{\partial t}\right] = \iiint [\mathscr{W}(\mathbf{k}', \mathbf{k}) f(\mathbf{k}')\{1 - f(\mathbf{k})\}$$
$$- \mathscr{W}(\mathbf{k}, \mathbf{k}') f(\mathbf{k})\{1 - f(\mathbf{k}')\}] \, dk_1' dk_2' dk_3'. \tag{6}$$

If we put $f = f_0 + f_1$, where f_0 is the Fermi function, and make various plausible assumptions, we can show that the net rate of change in f for the electrons in the *s*-band, due to transitions to and from the *d*-band, is

$$\left[\frac{\partial f_s}{\partial t}\right]_{sd} = \frac{\varpi_d C_{sd}^2 \Delta}{8\pi^3 M h} \iiint \frac{|\mathbf{q}|^2}{\nu(\mathbf{q})} \left[\{f_{1d}(\mathbf{k}+\mathbf{q})[N(\mathbf{q})+1-f_{0s}(\mathbf{k})] \right.$$
$$- f_{1s}(\mathbf{k})[N(\mathbf{q})+f_{0d}(\mathbf{k}+\mathbf{q})]\} \Omega\{E_s(\mathbf{k}) - E_d(\mathbf{k}+\mathbf{q}) + h\nu(\mathbf{q})\}$$
$$+ \{f_{1d}(\mathbf{k}+\mathbf{q})[N(\mathbf{q})+f_{0s}(\mathbf{k})] - f_{1s}(\mathbf{k})[N(\mathbf{q})+1-f_{0d}(\mathbf{k}+\mathbf{q})]\}$$
$$\left. \times \Omega\{E_s(\mathbf{k}) - E_d(\mathbf{k}+\mathbf{q}) - h\nu(\mathbf{q})\} \right] dq_1 dq_2 dq_3. \tag{7}$$

This only differs from the expression for one band (Wilson 1936, p. 204), because the initial and final states belong to different bands and must be distinguished by suffixes *s* or *d*. C_{sd} is an interaction energy which measures the effectiveness of the *s-d* transitions, Δ and M are the volume and mass of a unit cell of the crystal, $N(\mathbf{q})$ is the energy distribution function of the lattice, and Ω is a time factor whose effect is considered below. ϖ_d is the weight of the

d-states (apart from the weight factor 2 due to the spin); the weight of the s-states is taken as unity.

The reduction of the triple integral to a single integral proceeds in the usual manner. We take polar co-ordinates q, ϑ, ϖ in the $\mathbf{q}$ space, the polar axis being in the direction of $\mathbf{k}$. Then

$$E_s(\mathbf{k}) - E_d(\mathbf{k}+\mathbf{q}) \pm h\nu(\mathbf{q})$$

$$= \frac{h^2|\mathbf{k}|^2}{8\pi^2 m_s} - A + \frac{h^2}{8\pi^2 m_d}(|\mathbf{k}|^2 + 2\mathbf{k}.\mathbf{q} + |\mathbf{q}|^2) \pm h\nu(\mathbf{q})$$

$$= \left(\frac{1}{m_s} + \frac{1}{m_d}\right)\frac{h^2 k^2}{8\pi^2} + \frac{h^2}{8\pi^2 m_d}(2kq\cos\vartheta + q^2) - A \pm h\nu(\mathbf{q}). \qquad (8)$$

Now (Wilson 1936, p. 197)

$$\Omega(x) = \frac{\sin 2\pi xt/h}{2\pi x/h}.$$

Hence, putting

$$y = 2\pi t\{E_s(\mathbf{k}) - E_d(\mathbf{k}+\mathbf{q}) \pm h\nu(\mathbf{q})\}/h,$$

we have

$$\int_0^\pi \Omega\{E_s(\mathbf{k}) - E_d(\mathbf{k}+\mathbf{q}) \pm h\nu(\mathbf{q})\}\sin\vartheta\, d\vartheta = \frac{2\pi m_d}{hkq}\int_{\vartheta=\pi}^{\vartheta=0}\frac{\sin y}{y}\,dy. \qquad (9)$$

For large t, the integral on the right of (9) is π if the limits of integration are of opposite sign, and it is zero otherwise. It is not possible to express the limits simply, but if we neglect the small term $h\nu(\mathbf{q})$ we obtain much simpler expressions, which are adequate for our purpose. The condition for the top limit to be positive is that

$$q > \sqrt{\left(\frac{8\pi^2 m_s A}{h^2} - \frac{m_d}{m_s}k\right)} - k.$$

Since only the electrons near the top of the Fermi distribution contribute to the conductivity, we may put $k = k_s$. Then, by (3), the above condition becomes

$$q > k_d - k_s.$$

Similarly the bottom limit is negative provided that

$$q > k_s - k_d.$$

One or other of these conditions is always satisfied, and hence the condition for an s-d transition to be possible is

$$q > |k_d - k_s|. \qquad (10)$$

This condition is obvious from the arrangement of the energy surfaces. For, the smallest value of q is required when an electron jumps from a point

on the s-sphere in $\mathbf{k}$ space to the nearest point on the d-sphere. In this case $\mathbf{k}$ and $\mathbf{k}'$ have the same direction and hence $q = |k_d - k_s|$.

We may remark here that if the energy surfaces are not spheres it is possible for the s- and d-surfaces to cut. The minimum value of q is then 0. This applies, however, only to those electrons whose energy levels lie along the intersections. For the vast majority of the electrons a non-zero value of q is required to produce a transition, and the argument is not essentially altered by the presence of a negligible number of electrons which can be scattered from one band to the other by long lattice waves.

We now restrict ourselves to problems in which the current is along the x-axis, and we put

$$f_1 = -k_1 c(E) \frac{\partial f_0}{\partial E}. \tag{11}$$

We can replace any slowly varying functions of $\sin \vartheta$ by their values when $y = 0$, since practically the whole of the integral (9) comes from small values of y. The integration over ϖ can then be carried out. If θ and θ_1 are the angles between the x-axis and $\mathbf{k}$ and $\mathbf{q}$, we have

$$q_1 = q \cos \theta_1 = q(\cos \theta \cos \vartheta + \sin \theta \sin \vartheta \cos \varpi)$$

and

$$\int_0^{2\pi} q_1 d\varpi = 2\pi q \frac{k_1}{k} \cos \vartheta_0$$

$$= 2\pi k_1 \left[\frac{m_d}{2m_s E} (A \mp h\nu) - \frac{m_s + m_d}{2m_s} - \frac{h^2 q^2}{16\pi^2 m_s E} \right] \tag{12}$$

Finally, putting $x = h\nu/kT$ and $\eta = (E - \zeta)/kT$ (k here is Boltzmann's constant), we obtain

$$\left[\frac{\partial f_s}{\partial t} \right]_{sd} = -\frac{k_1}{E^{\frac{1}{2}}} \frac{\partial f_0}{\partial E} \varpi_d m_d P_{sd} \left(\frac{T}{\Theta} \right)^3 \int_{\Theta_E/T}^{\Theta/T} \frac{z^2 dz}{e^z - 1}$$

$$\times \left[\left\{ c_d(\eta + z) \left(E + \frac{m_d A}{2m_s} - \frac{m_s + m_d}{2m_s} E + \frac{m_d k T z}{2m_s} - D \frac{T^2}{\Theta^2} z^2 \right) - E c_s(\eta) \right\} \frac{e^\eta + 1}{e^\eta + e^{-z}} \right.$$

$$\left. + \left\{ c_d(\eta - z) \left(E + \frac{m_d A}{2m_s} - \frac{m_s + m_d}{2m_s} E - \frac{m_d k T z}{2m_s} - D \frac{T^2}{\Theta^2} z^2 \right) - E c_s(\eta) \right\} \frac{e^\eta + 1}{e^{\eta - z} + 1} \right]$$

$$= -\frac{k_1}{E^{\frac{1}{2}}} \frac{\partial f_0}{\partial E} \varpi_d m_d P_{sd} \left(\frac{T}{\Theta} \right)^3 \int_{-\Theta/T}^{-\Theta_E/T} + \int_{\Theta_E/T}^{\Theta/T} \frac{e^\eta + 1}{e^{\eta + z} + 1} \frac{z^2 dz}{|1 - e^{-z}|}$$

$$\times \left[c_d(\eta + z) \left\{ A \frac{m_d}{2m_s} - E \frac{m_d - m_s}{2m_s} + \frac{m_d k T z}{2m_s} - D \frac{T^2}{\Theta^2} z^2 \right\} - E c_s(\eta) \right], \tag{13}$$

where

$$D = \frac{(6\pi^2)^{\frac{2}{3}} h^2}{16\pi^2 m_s a^2}, \quad P_{sd} = \left(\frac{3}{4\pi} \right)^{\frac{1}{3}} \frac{3\pi^2 C_{sd}^2}{\sqrt{2m_s^{\frac{5}{2}} M a k \Theta}}.$$

37-2

Θ is, as usual, the Debye temperature, and $k\Theta_E = h\nu_E$, where ν_E is the frequency corresponding to the minimum value of q necessary to excite the s-d transitions. When $E = \zeta_0$ the value of q is $|k_d - k_s|$. It is to be noted that Θ_E is a function of E, and that (13) is to be taken as zero if $\Theta_E > \Theta$.

2·2. The formula we have just derived is so complicated that we must make some approximations before going any further. Since A, E and D are all of the same order of magnitude, the coefficient of c_d is probably considerably smaller than the coefficient of c_s, and we therefore neglect c_d. As a reasonable estimate we might take $A - E = \frac{1}{10}E$ and $E = D$. The approximation is then justified unless m_d/m_s is very large. Very large values of m_d/m_s of the order 10 to 20 have sometimes been proposed to account for the properties of the transition metals (e.g. Baber 1937). I cannot believe that such large values ever occur. Measurements of the specific heat or magnetic susceptibility give $\varpi_d m_d$ and not m_d. Now in an atom the d-states have a fivefold degeneracy. In a cubic crystal this degeneracy is partly removed (Bethe 1929), and the states split up into two sets, one of which is doubly and the other triply degenerate. It is not possible to say whether these states overlap or not. But, if we put $\varpi_d = 3$, then values of m_d/m_s of the order of 3 to 5 are sufficient to explain all the results. These values are small enough to justify our approximation.

It should be noted that the probability of scattering is proportional to $\varpi_d m_d$, but not to the density $\mathfrak{n}_d(E)$ of states in the d-band as stated by Mott. Thus the scattering probability is of the same order as that predicted by Mott but it has a different form, and this has important consequences in connexion with the second-order effects. The reason why he arrived at the wrong result is that he did not take account of the conditions (5) and assumed instead that every $\mathbf{k}'$ state is attainable from every $\mathbf{k}$ state.

The probability of scattering due to s-s transitions is (Wilson 1936, p. 207)

$$\left[\frac{\partial f_s}{\partial t}\right]_{ss} = -\frac{k_1}{E^{\frac{1}{2}}}\frac{\partial f_0}{\partial E}m_s P_{ss}\left(\frac{T}{\Theta}\right)^3$$
$$\times \int_{-\Theta/T}^{\Theta/T}\left[c_s(\eta+z)\left\{E + \tfrac{1}{2}kTz - D\frac{T^2}{\Theta^2}z^2\right\} - E c_s(\eta)\right]\frac{e^{\eta}+1}{e^{\eta+z}+1}\frac{z^2 dz}{|1-e^{-z}|}.$$

$$(14)$$

This has to be added to (13) in order to obtain the complete expression for $[\partial f_s/\partial t]$. The corresponding expressions for $[\partial f_d/\partial t]$ can be readily obtained, but we do not need them. The conductivity due to one band is (Wilson 1936, pp. 161 or 208),

$$\sigma = \frac{ne^2}{m}\tau(\zeta).$$

Hence, even if the time of relaxation is of the same order for both s- and d-bands, the conductivity due to the d-band can be neglected, since $m_d \gg m_s$ and since our theory is at best only an indifferent approximation. (Note that the weight ϖ_d does not come into the conductivity of the d-band if we assume, as is reasonable, that an electron in one of the d-bands can be scattered into any of the degenerate d-bands. There is then a factor $1/\varpi_d$ in the conductivity due to the ϖ_d possibilities of scattering, but there is also another factor ϖ_d due to there being ϖ_d bands to carry the current, and hence ϖ_d does not come into the expression for the conductivity except through the time of relaxation.) If we take into account the contributions of the d-electrons to the current, the conductivity is increased and the thermoelectric power is decreased.

2·3. After all the approximations have been made we have

$$\left[\frac{\partial f_s}{\partial t}\right] = -\frac{k_1}{E^{\frac{1}{2}}}\frac{\partial f_0}{\partial E}m_s P_{ss}\left(\frac{T}{\Theta}\right)^3$$

$$\times \int_{-\Theta/T}^{\Theta/T}\left[c_s(\eta+z)\left\{E+\tfrac{1}{2}kTz-D\frac{T^2}{\Theta^2}z^2\right\}-Ec_s(\eta)\right]\frac{e^\eta+1}{e^{\eta+z}+1}\frac{z^2\,dz}{|1-e^{-z}|}$$

$$+\frac{k_1}{E^{\frac{1}{2}}}\frac{\partial f_0}{\partial E}\varpi_d m_d P_{sd}\left(\frac{T}{\Theta}\right)^3\left\{\int_{-\Theta/T}^{-\Theta_E/T}+\int_{\Theta_E/T}^{\Theta/T}Ec_s(\eta)\frac{e^\eta+1}{e^{\eta+z}+1}\frac{z^2\,dz}{|1-e^{-z}|}\right\}. \quad (15)$$

To solve this equation for small values of Θ/T we adopt the usual method of expanding the integrands in terms of z and retaining only the leading terms. We obtain

$$\left[\frac{\partial f_s}{\partial t}\right] = k_1 c_s(\eta)\frac{\partial f_0}{\partial E}\frac{T}{\Theta}\frac{1}{E^{\frac{1}{2}}}\left\{\tfrac{1}{2}m_s P_{ss}D+\varpi_d m_d P_{sd}E\left(1-\frac{\Theta_E^2}{\Theta^2}\right)\right\}. \quad (16)$$

Since the time of relaxation τ_s, when it exists, is defined by

$$\left[\frac{\partial f_s}{\partial t}\right] = -\frac{f_s-f_{s0}}{\tau_s},$$

we have $$\frac{1}{\tau_s} = \frac{T}{\Theta}\frac{1}{E^{\frac{1}{2}}}\left\{\tfrac{1}{2}m_s P_{ss}D+\varpi_d m_d P_{sd}E\left(1-\frac{\Theta_E^2}{\Theta^2}\right)\right\}. \quad (17)$$

2·4. Although it is not possible to define a time of relaxation at low temperatures it is easy to obtain a solution for $c(\eta)$ when the only external influence is an electric field. This calculation follows exactly the same lines

as Bloch's calculation of the conductivity of monovalent metals (see, for example, Wilson 1936, p. 212); it gives

$$\frac{1}{\sigma} = \frac{2m_s}{n\epsilon^2\zeta^4}\left[m_s P_{s^*} D\left(\frac{T}{\Theta}\right)^5 \int_0^{\Theta/T} \frac{z^5 dz}{(e^z-1)(1-e^{-z})} \right.$$
$$\left. + \varpi_d m_d P_{sd} \zeta\left(\frac{T}{\Theta}\right)^3 \int_{\Theta_E/T}^{\Theta/T} \frac{z^3 dz}{(e^z-1)(1-e^{-z})}\right]. \quad (18)$$

This is the general expression for the specific resistance and can be used for all temperatures except very high ones. When τ_s exists it can be obtained from the relation $\sigma = n\epsilon^2\tau_s/m_s$.

2·5. The resistance of platinum does not show any abnormal decrease at low temperatures of the kind predicted. The resistance does indeed behave abnormally, but the variation is in the wrong direction. At very low temperatures the resistance is proportional to T^2, instead of to T^5 as for a normal metal. This variation with T^2 has been ascribed by Baber (1937) to the collisions between the s- and d-electrons.

The resistances of the other transition elements are not known accurately at low temperatures. If they behave like platinum we must conclude either that the s-d transitions are not important or that $k_s = k_d$ for all the metals. If this latter condition were found to be satisfied, it could only be so for some very general reason, connected presumably with the stability of the metallic state.

THE SECOND-ORDER EFFECTS

3·1. The effects, such as the thermoelectric power, which depend on the derivatives of τ, present considerable difficulties. Mott (1936b) has given a theory of the thermoelectric properties of the transition elements based on the assumption that the probability of s-d transitions is proportional to the density of d-states. We have seen in § 2·2 that this is not correct. The incorrectness of the assumption does not have much effect on σ, but it completely changes the theory of the second-order quantities. However, Mott and Jones (1936, p. 313) give some numerical values for $A - \zeta$ which seem to confirm Mott's theory. I believe that this confirmation is not as convincing as it seems.

Mott cites the large thermoelectric powers of the transition elements as evidence of the s-d transitions. The thermoelectric power of platinum at high temperatures is about $-1·8 \times 10^{-2} T\,\mu\text{V}/\text{degree}$ and that of palladium is about $-3·4 \times 10^{-2} T\,\mu\text{V}/\text{degree}$. These are very much smaller than the

thermoelectric powers of the alkalis and could be explained without much difficulty by the elementary theory based upon the assumption that the s-electrons are perfectly free. The thermoelectric power is $-\mathfrak{S}/\varepsilon$, where (Wilson 1936, p. 177)

$$\mathfrak{S} = \tfrac{1}{3}\pi^2 k^2 T \left(\frac{1}{E} + \frac{1}{l}\frac{\partial l}{\partial E} \right)_{E=\zeta}, \tag{19}$$

l being the free path. For perfectly free electrons l is proportional to E^2, and hence

$$\mathfrak{S} = \frac{\pi^2 k^2 T}{\zeta}. \tag{20}$$

If we take the number of s-electrons per atom to be $0\cdot6$ and assume that $m_s = m$, the mass of a free electron, we find for platinum that the thermoelectric power is $-2\cdot15\times10^{-2}T\,\mu\mathrm{V}/\text{degree}$. To explain the considerably higher thermoelectric power of palladium we should have to assume that m_s is larger than m, but this is quite a reasonable assumption and the value of m_s required is about $1\cdot5\,m$. On these grounds alone we are therefore not obliged to adopt Mott's hypothesis.
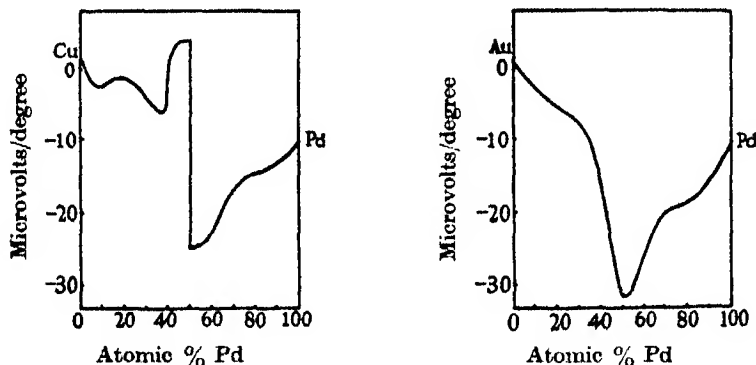
Fig. 2. Absolute thermoelectric powers of Pd alloys at $0°$ C.

Another piece of evidence which has been advanced is the dependence upon composition of the thermoelectric power of the palladium alloys. If copper, silver or gold is added to a transition metal, the holes in the d-band are filled up and at the same time $\mathfrak{S}$ becomes larger. When all the holes are full, further addition of the monovalent metal causes $\mathfrak{S}$ to decrease. The interpretation of this phenomenon is not, however, as unambiguous as might appear at first sight. In fig. 2 are shown the absolute thermoelectric powers of the two alloys PdCu and PdAu (Borelius 1935, pp. 404–5). The anomalies

in the PdCu curve at 75 and 50 % Cu are due to the formation of super-lattices. Since the formation of the superlattice CuPd is associated with a change in the crystal structure from face-centred to body-centred cubic, we consider only the superlattice Cu_3Pd. Even for this superlattice there is a slight change in structure, the ordered state being very slightly tetragonal. However, if our present ideas about superlattices are correct, there ought to be no essential difference in the electronic energy levels of the ordered and disordered Cu_3Pd lattices. On the other hand, the thermoelectric power of the ordered state is considerably smaller than that of the disordered state. This suggests that some of the change in the thermoelectric power of the alloys is due to the random distribution of the atoms. (Since condition (5) does not apply to electronic transitions caused by the random distribution of atoms, the s-d transitions might be more frequent in the disordered than in the ordered metal. It is difficult to say what effect this would have.) It is impossible to estimate what the thermoelectric power of an alloy would be if it were ordered at all compositions, and it may be that the effect would not be large. It is, however, obvious that the behaviour of these alloys indicates that the simple theory is inadequate, which assumes that the arrangement of the energy levels is independent of the composition and that all the effects can be ascribed to the change in the number of valency electrons.
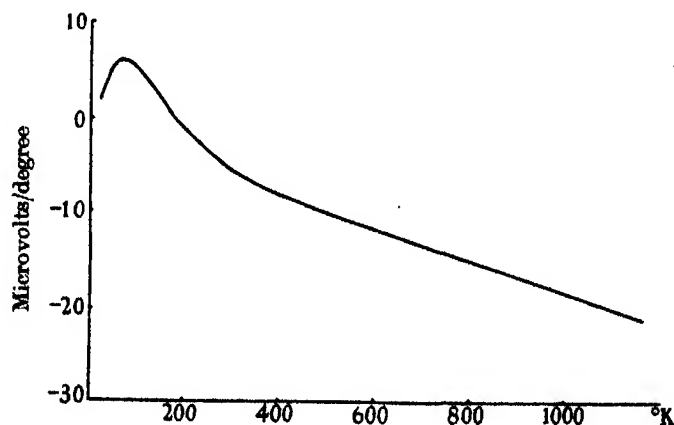
FIG. 3. Absolute thermoelectric power of Pt.

3·2. The thermoelectric power of platinum as a function of the temperature is shown in fig. 3 (Borelius 1935, p. 400). The thermoelectric power is negative at high temperatures and positive at low. The obvious interpretation is that the current is carried by electrons at high temperatures and by

positive holes at low temperatures, but it is extremely difficult to see how such a state of affairs could possibly happen. Another possible explanation is that $\partial l/\partial E$ is positive at high temperatures and negative at low temperatures. It is perhaps worth pointing out that such a behaviour is possible with the model we are considering.

If we take τ from equation (18) we have

$$\frac{\partial}{\partial E}\log l = \frac{\partial}{\partial E}\log(\tau E^{\frac{1}{2}})$$

$$= \frac{2}{E} - \frac{\partial}{\partial E}\log\left[m_s P_{ss}\left(\frac{T}{\Theta}\right)^5 \int_0^{\Theta/T}\frac{z^5\,dz}{(e^z-1)(1-e^{-z})}\right.$$

$$\left. + \varpi_d m_d P_{sd} E\left(\frac{T}{\Theta}\right)^3 \int_{\Theta_E/T}^{\Theta/T}\frac{z^3\,dz}{(e^z-1)(1-e^{-z})}\right]. \tag{21}$$

This expression cannot be used at very low temperatures since τ does not then exist. The correct expression can be obtained by a method which I have given recently (Wilson 1937), but the results are exceedingly complicated and (21) is sufficiently accurate for the present discussion. If the second term on the right of (21) is zero, that is, if the *s-d* transitions are unimportant, we regain (20). In order to obtain the desired behaviour of l, the second term must be small at high and large at low temperatures. The only factor which can possibly vary in such a manner is

$$\frac{\partial}{\partial E}\int_{\Theta_E/T}^{\Theta/T}\frac{z^3\,dz}{(e^z-1)(1-e^{-z})}. \tag{22}$$

The quantity $\partial\Theta_E/\partial E$ can be either positive or negative and is of the order[*] $\pm\Theta_E/E$. For, $\Theta_E = \text{constant}\,|k_d - k_s|$, and hence

$$\frac{\partial\Theta_E}{\partial E} = \frac{\partial\Theta_E}{\partial k_s}\bigg/\frac{\partial E}{\partial k_s}$$

$$= \pm\frac{\text{constant}}{2E}\left(k_s + \frac{m_d k_s^2}{m_s k_d}\right)$$

by (3). The plus sign is to be taken if $k_d < k_s$ and the minus sign if $k_d > k_s$. (This is obvious from fig. 1.) The expression (22) is therefore of the order

$$\mp\frac{1}{E}\frac{(\Theta_E/T)^4}{(e^{\Theta_E/T}-1)(1-e^{-\Theta_E/T})}, \tag{23}$$

---

[*] It is probably larger than this by a factor of the order m_d/m_s, but this does not affect the argument.

the numerical value of which is small for both large and small values of Θ_E/T but which is large for intermediate values of Θ_E/T. In order that $\partial l/\partial E$ may be negative for some range of temperature it is necessary that (22) should be positive, that is, that $k_d > k_s$.

Whether $\partial l/\partial E$ ever becomes negative is an extremely difficult question to answer, since the expression (23) occurs multiplied by a complicated factor, including powers of T. It seems probable, however, that this could be arranged by a proper choice of the constants. If the explanation put forward here is correct, then at low temperatures where (23) is small the thermoelectric power ought to become negative once more. This would be a decisive test of the theory, but unfortunately the measurements do not extend to sufficiently low temperatures. Changes in the sign of the thermoelectric power occur for some substances at liquid helium temperatures, but the thermoelectric power of platinum has not been measured in this region. Finally, although the present theory does give rise to the possibility of $\partial l/\partial E$ changing sign, yet the explanation advanced seems too artificial to be the correct one.

3·3.   The resistance of platinum at very high temperatures increases less rapidly than T. This is a second-order effect which depends on the second derivative of τ and therefore involves even greater refinements than does the theory of the thermoelectric power. We must now use a more accurate formula for σ than we have hitherto done. We have (Wilson 1936, p. 162)

$$\sigma = -\frac{\epsilon^2}{3\pi h^2}\iiint \tau \mid \operatorname{grad}_k E\mid \frac{\partial f_0}{\partial E} dk_1 dk_2 dk_3$$

$$= -\frac{16\sqrt{2}\pi^2 m^{\frac{1}{2}}\epsilon^2}{3h^3}\int \tau E^{\frac{3}{2}}\frac{\partial f_0}{\partial E}\, dE.$$

This can be evaluated by the approximate formula

$$-\int \phi(E)\frac{\partial f_0}{\partial E}dE = \phi(\zeta)+\frac{\pi^2}{6}k^2 T^2\left(\frac{\partial^2\phi}{\partial E^2}\right)_{E=\zeta}.$$

Now τ is given by (17). If we neglect the s-d transitions, we obtain (compare Wilson 1937, equation (14))

$$\sigma = \frac{\text{constant}}{T}\left[1+\left(\frac{\pi kT}{\zeta}\right)^2\right].$$

In order that this formula should fit the experimental results, the value of ζ must be small and therefore the effective mass of the s-electrons must be large, of the order $4m$. This is too large to be reasonable.

If we use the expression (17) for τ_s, which includes the effect of the s-d transitions, we obtain an even worse result if Θ_E is treated as constant. In fact, if we assume in addition that the s-d transitions are much more important than the s-s transitions, we find

$$\sigma = \frac{\text{constant}}{T}\left[1 + \frac{1}{3}\left(\frac{\pi k T}{\zeta}\right)^2\right].$$

In order to obtain a larger effect with the present model it is necessary to invoke the variation of Θ_E with E. It seems impossible, however, to obtain any numerical estimate of how much difference this would make, and the theory is very speculative.

SUMMARY

By using a model in which the energy surfaces are spheres, a complete theory is worked out of the s-d transitions in a metal containing incomplete d-bands. The results are of the same order of magnitude as those given by Mott's qualitative theory, but differ considerably in detail and in interpretation. It is shown that the s-d transitions should fall off exponentially as the temperature is lowered. A suggestion is put forward to explain the change in sign of the thermoelectric power of platinum at low temperatures.

REFERENCES

Baber, W. G. 1937 *Proc. Roy. Soc.* A, **158**, 383.
Bethe, H. 1929 *Ann. Phys., Lpz.* (5), **3**, 133.
Borelius, G. 1935 "Handbuch der Metallphysik." Leipzig.
Mott, N. F. 1935 *Proc. Phys. Soc.* **47**, 571.
— 1936*a Proc. Roy. Soc.* A, **153**, 699.
— 1936*b Proc. Roy. Soc.* A, **156**, 368.
Mott, N. F. and Jones, H. 1936 "The theory of the properties of metals and alloys." Oxford.
Wilson, A. H. 1936 "The theory of metals." Cambridge.
— 1937 *Proc. Camb. Phil. Soc.* **33**, 371.

INDEX TO VOLUME CLXVII (A)

END OF THE ONE HUNDRED AND SIXTY-SEVENTH VOLUME (SERIES A)

ABSTRACTS

OF PAPERS COMMUNICATED TO THE ROYAL SOCIETY OF LONDON

In accordance with a resolution of Council, summaries or abstracts of papers are to be published as soon as practicable. The publication of such abstracts in no way indicates that the papers have been accepted for publication in any fuller form. These abstracts will be issued for convenience with the "Proceedings of the Royal Society of London" but do not form a part of the "Proceedings".

Diffusion of electrolytic hydrogen through metals. By H. R. Heath and T. L. Ibbs. (*Communicated by M. L. Oliphant, F.R.S.—Received* 20 *May* 1938.)

Experiments were made to test whether hydrogen produced electrolytically on one side of a metal plate will diffuse through the plate. The Shakespear katharometer was used to detect and measure the diffused gas. The metals examined were aluminium, iron, nickel, cobalt, copper, zinc, silver, palladium, platinum and lead. Only in the case of iron and palladium was any diffusion observed.

Observations were also made with iron showing how the amount of diffused gas varied with the time, and how the rate of diffusion varied with the thickness of the plate.

The variation of the rate of diffusion with the electrolysing current density was observed for plates of iron and palladium. The results agree well with the conclusions of Borelius and Lindblom for large current densities; but show that a threshold value of current density, below which no diffusion occurs, does not really exist.

The diffused gas appears to be in the ordinary diatomic state. The absorption of electrolytic hydrogen by palladium was also studied.

The band spectrum of lead fluoride. II. By G. D. ROCHESTER. *(Communicated by W. E. Curtis, F.R.S.—Received 21 May 1938.)*

An account is given of the emission and absorption band spectra of PbF. Six new systems and two continua are found. The vibrational constants of the stable electronic states of PbF are as follows in cm.$^{-1}$:

State	Probable type	ν_e	ω_e	$x_e\omega_e$	Observed in emission (E), absorption (A)
X$_1$	$^2\Pi$	0	507·2	2·30	E, A
X$_2$		8266	531·1	1·50	E
A	$^2\Delta$	22567	397·8	1·77	E, A
B	$^2\Sigma$	35643	612·8	3·42	E, A
C	$^2\Delta$	38046	594·0	2·50	A
D	$^2\Pi$	43820	600·0	– –	A
E	——	45400	565·0	——	A
F	$^2\Pi$	47870	630·0	....	A
2440 A continuum		maximum	41000		A
3050 A continuum		maximum	32800		E

The width of the ground state, i.e. 8266 cm.$^{-1}$, is the largest yet recorded. Numerous examples of predissociation are found.

Studies on the ionosphere at Allahabad. By B. D. PANT and R. R. BAJPAI. *(Communicated by M. N. Saha, F.R.S.—Received 23 May 1938.)*

In this paper are described the results of study of the ionosphere at Allahabad from October 1936 to March 1938. Various types of reflexions, including complex echoes, are described and illustrated. A typical curve showing the diurnal variation of electron density is given. The results of measurements of the critical penetration frequencies for the O and X waves show that at times the X wave gets reflected from a layer where the electron concentration is given by the condition $p_0^2 = p^2 \dfrac{p^2 - p_h^2}{p^2 - p_L^2}$ instead of the usual condition $p_0^2 = p^2 - pp_h$.

A new Coriolis perturbation in the methane spectrum. I. Vibrational-rotational Hamiltonian and wave functions. By H. A. JAHN. *(Communicated by Sir William Bragg, O.M., P.R.S.—Received 25 May 1938.)*

The theoretically possible sub-levels into which the rotational levels of a threefold degenerate mode of vibration of methane can be split by a tetrahedrally symmetrical perturbation are given up to the tenth rotational quantum number together with the correct vibrational-rotational wave functions with which to carry out the perturbation calculation. Good approximations to the true modes of vibration of the methane molecule are found and used to evaluate certain Coriolis terms in the

Hamiltonian which couple the twofold and threefold degenerate modes of vibration. Table III which gives the tetrahedrally irreducible harmonic functions and extends calculations of Bethe (1929) from the fourth to the tenth quantum number will be useful in a number of connections.

Nature and causes of the adaptation of water-breathing creatures to air breathing. I. The bionomics structure and physiology of *Lepidocephalus*.

By B. K. DAS. *(Communicated by E. W. MacBride, F.R.S.—Received 25 May* 1938.)

This paper gives an account of the habits and structure of the fresh-water fish *Lepidocephalus*. The aim of the author is to show that the structure of the air-breathing organs depends entirely on the place in the body where the air bubbles are trapped. Thus in previous papers he had shown that the air-sac in *Anabas* is a part of the opercular cavity whereas in *Amphipnous euchia* and in Ophiocephalidae there exist a pair of pouches of the pharynx which contain air. In *Lepidocephalus*, with which the present paper deals, a part of the intestine is converted into an air-breathing organ. It is supplied with a rich blood plexus from which a large vessel is given off to the portal vein. The fish lies near the surface of the ponds and streams in which it lives and from time to time rises in order to swallow bubbles of air.

Thermal effects on bodies in an air stream.

By W. F. HILTON. *(Communicated by E. F. Relf, F.R.S.—Received 26 May* 1938.)

A theoretical expression derived from Pohlhausen's formula, giving the temperature due to laminar flow over a flat plate, has been tested experimentally in the one-foot diameter high-speed wind tunnel at the N.P.L. The temperatures were measured by using thermocouples, and good agreement between theory and experiment was obtained with the thermocouple near the leading edge of the flat plate, where the flow was probably laminar. A 26% discrepancy was found with the thermocouple near to the trailing edge, due probably to the flow being turbulent.

On all models tested the temperature difference was found to increase as the square of the wind speed, until a shock wave was formed, which gave an inflexion in the δT, V^2 curve. The present method can thus be used to detect the formation of a shock wave at a solid boundary, such as an aerofoil, or aeroplane body.

Besides tests on flat plates of four thicknesses, and a streamline bar at four incidences, measurements were made on a circular cylinder, and two other shapes. The circular cylinder was found to be a most unsatisfactory shape for the thermometry of moving fluids, unless placed along the wind. A flat plate with a thermocouple near the leading edge is suggested to be the best shape for a sensitive element.

Photochemical reactions in monolayers. II. The photochemistry of proteins. By J. S. MITCHELL and E. K. RIDEAL, F.R.S. (*Received 26 May* 1938.)

This paper is an account of a quantitative investigation of the photochemistry of proteins in monolayers. Wheat gliadin, zein, insulin and ovalbumin have been examined. The photo-reactions were studied by observation of the changes in phase boundary potential of the protein monolayers on irradiation, at constant surface area and under equilibrium conditions, with monochromatic ultra-violet light of wave-lengths 2350–3175 A.

The general theory of photochemical reactions in protein monolayers is summarized. The proteins in the monolayers are to be regarded as macromolecular polycondensation products in which the primary photochemical processes are limited, to a first approximation, to the "aromatic" chromophores.

The experimental technique, including the method of fractional irradiation, and the preparation and properties of the monolayers are described.

The characteristic changes on ultra-violet irradiation of protein monolayers are:

(1) Liquefaction, if the film is gelatinous.

(2) At constant area, an increase of phase boundary potential, and also of surface pressure.

Oxidative processes play a fundamental part. Photosensitization, probably by traces of metals, is described.

It is suggested that, in these photoreactions, both "peptide linkages" adjacent to each side chain derived from tyrosine, phenylalanine and possibly also tryptophane may undergo a process of oxidative photolysis, the end result of which is equivalent to hydrolysis, and the transformed chromophoric residues liberated pass into solution. This hypothesis is in quantitative agreement with the total changes in phase boundary potential observed on irradiation of the monolayers of gliadin, zein and ovalbumin (the insulin films undergo partial solution). The importance of the Hardy-Langmuir principle is demonstrated.

The absolute quantum efficiency of the total changes per aromatic residue in monolayers of gliadin on N/100 sulphuric acid is of the order of $\frac{1}{2}$ for unsensitised photodecomposition at wave-lengths between 2350 and 3030 A.

The subthreshold potentials in a crustacean nerve fibre. By A. L. HODGKIN. (*Communicated by E. D. Adrian, F.R.S.—Received 26 May* 1938.)

Experiments with isolated crustacean nerve fibres show that subthreshold shocks produce two quite distinct effects. When the stimulus is weak and cathodic, or anodic and of any strength, it produces a "polarization" potential which behaves as though it were due to the passive accumulation of charge at the nerve membrane. On the other hand, when the stimulus approaches threshold, it produces an additional wave of negativity which behaves like a subliminal response of the nerve fibre. These two processes have entirely different properties. Thus:

The size of the polarization potential is directly proportional to the strength of the shock, whereas the subliminal response increases at an accelerating rate as the shock approaches threshold.

The time relations of the processes are different. The polarization potential rises during the period in which the shock is applied and then declines in an approximately exponential way. On the other hand, the subliminal response starts with an initial inflexion and continues to grow for as much as $500\,\mu$sec. after the end of the shock.

The time relations of the polarization potential are independent of the strength of the shock; whereas the duration of the local response increases and its maximum occurs later as the shock approaches threshold.

When the local response has almost reached propagating size, it becomes unstable and varies from shock to shock. On the other hand, the polarization produced by successive shocks is always quite constant.

The local response can be greatly reduced or abolished by making the nerve refractory, whereas the polarizability is only slightly reduced by refractoriness.

The local response can be increased by making the nerve supernormal, whereas the polarization potential is slightly reduced or unaffected during the supernormal phase.

The spatial spread of the two processes is different. The polarization potential falls to one-third of its value in approximately 0·5 mm., whereas the local response usually declines to only two-thirds in that distance. Under certain conditions the local response may spread very much farther than the polarization.

The latency of the nerve fibre is determined by the time relations of the local response. The latency is short when the local wave has a rapid rise and fall, whereas it is long when the wave has slower time relations. It is suggested that the latency of the fibre is due to the time required for the local response to reach propagating size.

The potential at which the local response starts to propagate is increased during the relatively refractory period and decreased during the supernormal phase. In a normal nerve the response starts to propagate when its amplitude is equal to about one-fifth of the spike. During refractoriness this large safety margin may be reduced to the point at which a propagated action potential is only slightly larger than one which just fails to propagate. Under these conditions both sub- and superthreshold waves of activity at first spread along the nerve in the same way and do not finally separate until they have travelled a short distance from the cathode.

The comparison of series of measures when the standard errors are unequal. By H. JEFFREYS, F.R.S. (*Received* 27 *May* 1938.)

A test previously given for the significance of the difference of two means, when the standard errors are unequal, is revised to take account of the uncertainties of the standard errors and of a theoretical complication that has given trouble in other tests. The case where the standard errors can be assumed equal is derived from an existing formula. Some incidental points are discussed and a list is given of tests that have been revised in later work.

Statistical theory of superlattices with long-range interaction. By J. S. WANG. (*Communicated by R. H. Fowler, F.R.S.—Received* 30 *May* 1938.)

I. General Theory. Bethe's theory of order-disorder in superlattices is extended to cover the case of long-range interactions. The theory is applicable to any interaction energy of the form $V(r)$ subject to the condition $\int_0^\infty V(r)\, r^2 dr =$ finite, and to a general class of lattice structures which include the three lattices of the cubic system.

II. The simple cubic lattice and the body-centred cubic lattice. The general statistical theory of superlattices with long-range interaction given in the preceding paper is applied to the simple cubic lattice and the body-centred cubic lattice. It is shown that the assumption of an inverse power law for the interaction energy alters the calculated configurational energy in the direction required to make the agreement with experiment better than the assumption of interaction between nearest neighbours only, but the shift is not great enough to remove the discrepancy between theory and experiment completely.

The androgenic activity of ovarian grafts in castrated male rats. By R. DEANESLY. (*Communicated by Sir Henry Dale, F.R.S.—Received* 1 *June* 1938.)

Ovarian grafts were made into the ears of immature castrated male rats. All functional grafts showed oestrogenic activity, detectable by the fibrosis of the seminal vesicles. Most functional grafts, especially those established for three months or more, showed androgenic activity causing secretion and growth in the prostate and, occasionally, in the seminal vesicles. One rat, with a graft 135 days old, had a prostate of full adult size, though the seminal vesicles were not correspondingly large. The slighter response of the vesicular epithelium as compared with that of the prostate suggests that the androgenic substance produced by the grafts is not testosterone.

Androgenic activity does not depend on the temperature at which the rat is kept; it is associated with luteinization of the theca interna of the follicles, which occurs commonly in established grafts.

Gonadotrophic extracts which cause extensive luteinization of the granulosa do not appreciably affect the androgenic activity of the graft.

A new Coriolis perturbation in the methane spectrum. II. Energy levels. By H. A. JAHN. (*Communicated by Sir William Bragg, O.M., P.R.S.— Received* 3 *June* 1938.)

Using the vibrational-rotational wave functions derived in Part I, the perturbations of the rotational levels of the fundamental vibration ν_4 of the methane molecule, caused by the Coriolis term in the Hamiltonian which couples the rotational levels of

ν_4 with the rotational levels of ν_3, are calculated explicitly up to the tenth rotational quantum number. Table III, which gives the wave functions for the tetrahedral rotational sublevels of ν_3, will be useful in calculating the perturbations of the rotational levels of any fundamental or overtone subvibrational level of symmetry type E in a tetrahedrally symmetrical molecule.

Photographic sensitivity and the reciprocity law at low temperatures.
By W. F. Berg and K. Mendelssohn. (*Communicated by F. A. Lindemann, F.R.S.—Received* 3 *June* 1938.)

Experiments are described which were undertaken to test a theory on the formation of the latent image by Gurney and Mott which differs from earlier theories in stressing the importance of movements of silver ions. It is shown that photographic materials have an appreciable sensitivity down to 20° K. While the sensitivity drops by 93% by changing from room temperature to 90° K., very little change occurs between 90 and 20° K. The main difference between exposure at 90 and 20° K. is a drop in contrast and in maximum density. It is shown that no reciprocity failure takes place at these temperatures. It appears that at sufficiently low temperatures the latent image is formed in two distinct stages: an electronic process, in which the electrons are separated from the halide ions absorbing the light, and are trapped in the lattice, and an ionic process which takes place on warming up, and consists of a movement of silver ions and probably also of bromine atoms. These results confirm the importance of ionic movements for the latent image formation.

Relaxation methods applied to engineering problems. III. Problem involving two independent variables. By D. G. Christopherson and R. V. Southwell, F.R.S. (*Received* 8 *June* 1938.)

In this paper relaxation methods are applied with success to four problems involving Laplace's, Poisson's and similar equations in *two variables*, namely:

The torsion problem of Saint-Venant for triangular shafts (this, since the solution is known, serves to illustrate and in some degree to test the methods);

The same problem for a shaft pierced by axial holes (a multiply-connected cross-section);

The torsion problem modified by the imposition of a definite limit to the shear stress (Prandtl's problem);

The problem of magnetic induction in a field containing iron.

In all four problems the methods lead without difficulty to solutions of sufficient accuracy for practical purposes, and it seems reasonable to conclude that they will be applicable (suitably modified) to other problems which, like the last three above, would present great or insuperable difficulties if treated by orthodox methods.

The nuclear spin of iodine. III. Further measurements upon the fine structure in the first spark spectrum. By S. Tolansky. (*Communicated by P. M. S. Blackett, F.R.S.—Received* 8 *June* 1938.)

Earlier measurements by Tolansky upon the fine structures in the lines of the first spark spectrum of iodine are extended into the ultra-violet region with the aid of a quartz Lummer plate interferometer. Fine structures are now known for 58 lines, 39 of which have been allocated to terms which go either to the (^{4}S) or the (^{2}D) series limit.

An independent fine structure analysis is made for both the systems and is confirmed by the aid of intercombination lines in the ultra-violet. Fine structure interval factors are given for 13 (^{4}S) terms and 15 (^{2}D) terms. These exhibit anomalies which can be explained as arising from configuration interaction perturbation.

It is shown that the nuclear coupling of the $5p^3$ electrons in iodine is comparable with that of the 6s electron.

In three terms, deviations from the interval rule have been established. These are attributed to nuclear electrical quadrupole moment. The perturbation constants have been calculated, but these cannot as yet be employed to give a numerical estimate of the quadrupole moment, since the coupling constants have not yet been evaluated.

Experiments on the transmutation of fluorine by protons and deuterons. By W. E. Burcham, C. L. Smith and P. I. Dee. (*Communicated by E. V. Appleton, F.R.S.—Received* 8 *June* 1938.)

The transmutations of fluorine under bombardment with artificially accelerated protons and deuterons have been systematically investigated.

The energy of the group of α-particles which is emitted during bombardment of fluorine with protons has been accurately determined and leads to a value 19·0043 for the mass of ^{19}F, in good agreement with the mass spectroscopic value. From the value of the energy release in this process and from the absence of α-particle groups of smaller energy it is concluded that the α-particle emission from fluorine under proton bombardment arises from successive transitions of excited ^{20}Ne nuclei.

Five groups of α-particles were found to be emitted during bombardment of fluorine with deuterons, and the energies of these groups have been determined. From the energy values of these groups it is concluded that excitation levels at 0·83, 2·95, 3·77, and 4·49 × 10^6 e-volts above the ground state exist in ^{17}O nuclei.

The emission of a group of protons which is believed to be associated with the formation of ^{20}F has been observed. From the energy of these protons the value 20·0087 has been deduced for the mass of radioactive ^{20}F. An energy release of 9·2 × 10^6 e-volts is therefore to be expected in the radioactive decay process

$$^{20}\text{F} \rightarrow {}^{20}\text{Ne} + e^-$$

and the disagreement between this value and the observed end-point energy of the β-rays (5·2 × 10^6 e-volts) has been partially reconciled by the observation that a radioactive emission of γ-radiation accompanies the β-emission and decays with the same period.

ABSTRACTS

OF PAPERS COMMUNICATED TO THE ROYAL SOCIETY OF LONDON

In accordance with a resolution of Council, summaries or abstracts of papers are to be published as soon as practicable. The publication of such abstracts in no way indicates that the papers have been accepted for publication in any fuller form. These abstracts will be issued for convenience with the "Proceedings of the Royal Society of London" but do not form a part of the "Proceedings".

5 AUGUST 1938

A study of the chain reaction in the thermal decomposition of diethyl ether. By J. E. HOBBS. (*Communicated by C. N. Hinshelwood, F.R.S.—Received 8 June* 1938.)

The course of the curves showing the rate of decomposition of diethyl ether as a function of minute additions of nitric oxide is independent of the concentration of the diethyl ether. The removal of a radical by the nitric oxide must thus be in competition with some reaction the rate of which is entirely independent of the concentration of the ether. This must be a unimolecular dissociation of the radical itself. This is in contrast to the inhibition of the decomposition of ethane where nitric oxide removes a radical which would otherwise have reacted with a molecule of ethane. A chain mechanism explaining these results is the same as that put forward by Rice and Herzfeld to explain the first order nature of the reaction. The mechanism gives an expression for the shape of the inhibition curve and accounts for the variation of the mean chain length with the ether pressure. From the amount of nitric oxide required for a given degree of inhibition the average life of the radical can be calculated to be of the order of $1\cdot2 \times 10^{-5}$ sec.

An analysis of the mechanism of oestrogenic activity. By G. PINCUS and N. T. WERTHESSEN. (*Communicated by F. H. A. Marshall, F.R.S.—Received 8 June* 1938.)

To facilitate the study of a series of thirty synthetic oestrogenic substances a new method for the bio-assay of the materials in question was advised. Mice were used as the test animals. The substances were dissolved in oil and administered intraperitoneally. The value obtained by assay had an error of approximately 10%. A comparison between the time course of action for oestrone and the other oestrogens

was possible. It was found that the hydroxyl group contributes quantitatively to the oestrogenic activity. Structure, when approximating to that of natural hormones by adding the five-membered ring to the phenanthrene nucleus, also contributes to the activity. Activity is generally low—the maximum being 1·72% that of oestrone. Subcutaneous injection decreases the activity value many times. Oestrone and oestradiol in adequate doses show a definite difference in the time course of action from oestrone. The synthetic oestrogens do not. Simultaneous injection of several synthetic oestrogens with progesterone into rabbits ovariectomized after fertile copulation stimulated the progesterone effects. This was also found in the case of small doses of the native oestrogens. The synthetic agents are not progestins. Oestrone in higher doses inhibits both the progesterone induced proliferation of the uterus and also the growth of the eggs. Oestradiol and oestriol inhibit, when given in large doses, the proliferation of the uterus but do not affect the growth of eggs.

Problems on stability in hydrophobic colloidal solutions. I. By S. LEVINE. *(Communicated by E. K. Rideal, F.R.S.—Received* 13 *June* 1938.)

A method of obtaining the mutual electrical energy of two colloidal hydrophobic spherical particles has been developed by applying the Debye-Hückel theory of electrolytes. The final result is

$$\frac{Q_0^2}{Da}f\left(\frac{R}{a}, \kappa a\right) = \zeta^2 Da(1+\kappa a)^2 f\left(\frac{R}{a}, \kappa a\right),$$

where Q_0 is the charge on each particle, assumed to be constant, a its radius, ζ its potential, R the distance between the particles, D the dielectric constant of water and κ is the well-known Debye-Hückel constant, being proportional to the square root of the electrolytic concentration. Only the approximate Debye-Hückel equation has been considered.

The electrical forces are repulsive at small separations but become attractive at large, passing through a zero at some intermediate distance, where the energy is a minimum. The energy near contact decreases very rapidly with increase in electrolytic concentration even though the charge does not change. This suggests that the diminution of the mutual energy as electrolyte is added is chiefly due to the behaviour of the ionic atmospheres, the effect of the adsorption of ions tending to lower the charge being less important.

There are two distinct terms in the energy function. The first represents the repulsion that one particle experiences when it enters the field of a second particle, and is the more important term at small separation. The second term represents the attraction that is exerted upon the ionic atmospheres when overlapping occurs and is the dominating contribution at large distances.

The van der Waals attractive energy for a particular case is computed. The resultant total energy function exhibits a maximum at a little distance out from contact. The value of the energy at this maximum is the controlling factor in coagulation, its value diminishing with electrolytic concentration.

The theory suggests an explanation for the fact that with electrolytes which coagulate at low concentrations the critical potential is much lower than with electrolytes which precipitate at large concentrations.

The Schultz-Hardy rule is discussed. It is shown that the use of the approximate Debye-Hückel equation cannot explain this rule for the ions of higher valency and it is necessary to consider the complete equation.

The energy minimum is characteristic of all hydrophobic sols containing spherical particles, and, contrary to current belief, the energy is always negative at large distances. Whereas the van der Waals forces cannot be of a long range character, the electrical forces can yield a minimum in the energy at a distance of several particle radii and the minimum energy may be a small multiple of kT. In general, it is likely that, at least for hydrophobic sols, thixotropy and related phenomena are mainly due to the existence of this minimum in the electrical energy and not to the van der Waals energy.

The method of calculating the osmotic pressure from the expression for the interaction energy is indicated.

Problems of stability in hydrophobic colloidal solutions. II. By S. Levine. (*Communicated by E. K. Rideal, F.R.S.—Received* 13 *June* 1938.)

The mathematical method of deriving the mutual energy of two colloidal metallic particles is developed. Only a first and second approximation are obtained. In the appendix a statistical analysis of the free energy evaluated here is given. It is seen that the Debye-Hückel theory of electrolytes can be applied much more satisfactorily to colloidal solutions than to ordinary electrolytic solutions. This is true even if the electrolyte present in the sol is of an unsymmetrical type.

On the absorption of light by crystals. By N. F. Mott, F.R.S. (*Received* 14 *June* 1938.)

The mechanism of the absorption of light by solids is discussed from the theoretical point of view. The energy of a quantum of radiation can be converted into heat, re-emitted as fluorescent radiation, or used up in producing a photoelectric current within the solid; estimates are made of the dependence on temperature of the relative probabilities of these processes, which are compared with experiment.

The thermal properties and heats of adsorption of films on vitreous silica. By W. G. Palmer. (*Communicated by Sir William Pope, F.R.S.— Received* 14 *June* 1938.)

Isothermals have been obtained at temperatures between 70° and 25° for adsorption of the vapours of benzene, acetone and methyl alcohol on known surfaces of vitreous silica, by methods giving a check on the constancy of the surface condition. The values of the coefficients of thermal expansion, compressibility and the temperature variation of the lateral force have been calculated and discussed in relation to parallel properties of the bulk phase. The heats of adsorption have been calculated from the temperature variation of the adsorption potential. Their relations to the fraction of surface covered are in agreement with theoretical predictions for films with inter-action energy.

The electrical conductivity of the transition metals. By A. H. WILSON. (*Communicated by R. H. Fowler, F.R.S.—Received* 20 *June* 1938.)

By using a model in which the energy surfaces are spheres, a complete theory is worked out of the *s-d* transitions in a metal containing incomplete *d*-bands. The results are of the same order of magnitude as those given by Mott's qualitative theory, but differ considerably in detail and in interpretation. It is shown that the *s-d* transitions should fall off exponentially as the temperature is lowered. A suggestion is put forward to explain the change in sign of the thermoelectric power of platinum at low temperatures.

The posterior probability distribution of the ordinary and intraclass correlation coefficients. By H. JEFFREYS, F.R.S. (*Received* 21 *June* 1938.)

The posterior probability distributions of the ordinary and intraclass correlation coefficients are obtained from an analogy with sampling theory, suggested by the use of the normal correlation surface in both cases. The results cast some further light on the relation between direct and inverse methods in problems of estimation; for practical purposes the differences from the recommendations made by Fisher are inappreciable. A significance test is obtained for the difference between an intraclass correlation and zero, and the application to internal correlation in series of measures is discussed.

An electrical theory of nerve impulse propagation. By O. H. SCHMIDT. (*Communicated by A. V. Hill, Sec.R.S.—Received* 22 *June* 1938.)

A capacitative theory of the nerve impulse is offered which supposes the local excitatory process to consist largely in an increase of capacitance rather than exclusively in a resistance change. This theory is shown to satisfy all requirements in respect of structures, energy, and electrical properties.

An electrical model is developed and discussed which permits direct determination of the electrical constants involved in this or other electrical theories of excitation. The results obtained from the model are shown to resemble those from nerve.

A possible physico-chemical theory of nerve excitation is developed on the basis of the capacitance-shift hypothesis.

A new process of negative ion formation. IV. By F. L. ARNOT and C. BECKETT. (*Communicated by H. S. Allen, F.R.S.—Received* 22 *June* 1938.)

The three previous papers of this series described a new process of negative ion formation. This process is the formation of negative ions at metal surfaces by bombardment of the surface with positive ions, the negative ion being formed by the positive ion capturing two electrons from the surface. The present paper shows that a new modification of this process can also occur.

The experimental results show that a spectrum of negative ions is obtained when a surface is bombarded with positive ions of argon or nitrogen or mercury, and that practically identical negative ion curves over the range of mass numbers from 10 to 54 are obtained by each type of positive ion. The negative ions observed have mass numbers 12, 16, 24, 29, 32, 38, 44 and 51. It is concluded that these negative ions arise from atoms and molecules of gas and vapour adsorbed on the surface.

It thus appears that there are two processes leading to the formation of negative ions at surfaces. The initial stage in each process is the same; this is capture of an electron from the surface by the incident positive ion into an excited state of the atom, probably by a resonance process. This excited atom, on reverting to its normal state, may then capture a second electron from the surface, again probably by a resonance process, so forming a negative ion of the same element as the incident positive ion. The second process consists in the excited atom transferring by a collision of the second kind its excitation energy to an adsorbed atom on the surface, which then captures an electron from the surface, and so a negative ion of an element different to that of the incident positive ion is produced.

The previous results are reviewed in the light of this new work which shows that no negative ions of nitrogen are formed. Certain alterations in the interpretation of the CO_2 results must also be made. The previous work on the formation of negative ions of mercury, hydrogen and oxygen requires no amendment, except that the probabilities of formation of these ions may have to be raised.

It is shown that no O_2^- ions are formed at the surface of an oxidized tungsten filament, but that they readily appear when the filament is cleaned by flashing. It is suggested that this effect is due to the increased work function of the filament when oxidized. It is also found that a covering of oxygen on the filament suppresses the peaks of mass numbers 24 and 38.

New systems of normal co-ordinates for relativistic optics. By G. TEMPLE.

(Communicated by Sir Arthur Eddington, F.R.S.—Received 22 June 1938.)

This paper developes the theory of a new system of normal co-ordinates (y^μ) in an n-dimensional manifold with an indefinite metric of signature $+1 - (n-1)$. In this system of co-ordinates the expression for the metric has the form

$$ds^2 = h_{jk} dy^j dy^k + 2dy^{n-1} dy^n, \quad (j, k = 1, 2, ..., n-1).$$

Any arbitrary time-like curve C being taken as the base curve, the forward null cone at any point A on C is given by $y^{n-1} = \text{constant}$, C itself is given by the single equation $y^n = 0$, and any forward null geodesic G from A is given by $y^j = \text{constant}$ $(j = 1, 2, ..., n-1)$. y^n is the "projected length" defined in a general co-ordinate system (x^μ) by

$$y^n = \int K_\mu dx^\mu,$$

where the integral is taken along G from A, and K_μ is a unit vector transported along G by parallel displacement and forming the tangent to C at A.

Hadamard's theory of null geodesics as bicharacteristics leads to a generalization of this system of normal co-ordinates in which $y^{n-1} = \text{constant}$ is the equation of a system of wave fronts, $y^j = \text{constant}$ are the equations of the orthogonal null geodesics or rays, and y^n is a projected length measured along the rays.

The theory is applied to optical problems in general relativity. Fermat's principle of minimum time is established rigorously for any relativistic manifold. The discussion of astronomical determinations of distance is simplified by the use of the new system of normal co-ordinates, which gives explicit expressions for the various distance functions. These general results are illustrated by the case of a manifold representing an isotropic expanding universe. Incidentally the use of normal co-ordinates of Riemann's type in relativistic optics is justified by a new definition in terms of "projected distances".

A new Coriolis perturbation in the methane spectrum. III. Intensities and optical spectrum. By W. H. J. CHILDS and H. A. JAHN. (*Communicated by Sir William Bragg, P.R.S.—Received* 22 *June* 1938.)

Using the Coriolis perturbations evaluated in a previous paper, a theoretical envelope for the infra-red absorption band of the low-frequency fundamental ν_4 of the methane molecule is calculated and compared with the experimental envelope of Nielsen and Nielsen and also with that of a simple overtone band of methane in the photographic infra-red. Theoretical intensity factors for the methane molecule which take into account correctly the spin weights of the equivalent hydrogen nuclei are also given. It is emphasized that Coriolis perturbations will in general have an important effect on the spectra of all polyatomic molecules having a threefold or higher axis of symmetry.

Representative algebra and internuclear vibrations. By A. C. MENZIES and K. WEISSENBERG. (*Communicated by C. G. Darwin, F.R.S.—Received* 23 *June* 1938.)

In this paper is described a simplified treatment of representation algebra; designed to facilitate the application of representation theory to wave and quantum mechanics. The method is quite general. Here it is used for the production of tables dealing with the spectroscopy of nuclear oscillations (infra-red and Raman effect) in molecules and crystals. The paper is divided into two main parts. Part I contains a new invariant treatment of the algebra of unitary representation of a given symmetry group. We first characterize each matrix of such a representation by a set of integers which are the natural logarithms of the proper values of the matrix, multiplied by a factor $\omega/2\pi i$ (where ω is the order of the group operation). The whole representation, which is the aggregate of the matrices, is then characterized by the aggregate of the corresponding sets of integers, which we call "mode numbers" (abbreviated to m.n.). Representation algebra is thereby reduced to the arithmetic of simple integers, and rules are given which make possible a drastic reduction in the number of m.n. required. In application to wave mechanics the m.n. are simply related to quantum numbers of angular momentum type. Part II gives in the form of explicit tables the results obtained from the application of this treatment to the spectroscopic problem mentioned above. The nuclear oscillations are grouped into the various normal modes which

are distinguished from one another by the m.n. of their corresponding representations, so that the m.n. serve as a convenient nomenclature for the modes. In the tables are listed the fundamental modes and the fundamental oscillations and properties associated with each of them. By applying the algebra of Part I to the m.n. characterizing these fundamental modes, the properties of obertones and combinations are calculated.

The decomposition and ignition of peroxides. I. Diethylperoxide. By A. C. EGERTON, F.R.S., and E. J. HARRIS. (*Received* 24 *June* 1938.)

The decomposition of diethylperoxide in the range 130–190° C. occurs in a unimolecular manner and is very little affected by surface or by diluents. The rate is given by $\log_{10} K = -6890 \cdot 4/T + 14 \cdot 708$ with an apparent activation energy 31500 cal. However, as first shown by Neumann and Toutakin, above a certain critical pressure the reaction becomes explosive; this effect has been studied, and the critical pressure is found to depend on the diameter of the vessel and to a less extent on the presence of diluents; the results do not accord with the simpler forms of theory for thermal explosions, and further experiments are being made.

The ignition of the peroxide is related to its explosive decomposition, the slope of the $\{\log p/(I/T)\}$ curve being the same in a similar vessel; but the ignition takes place at a somewhat lower temperature than corresponds to the critical explosion pressures, owing to the increase in the exothermicity. Ignition of diethylperoxide can occur in propane oxygen mixtures without ignition of the propane; it is possible therefore that substances formed in slow oxidations of hydrocarbons may behave like diethylperoxide and give rise to cool flames or to cool flames succeeded by true ignition. Diethylperoxide greatly diminishes the induction period of the slow combustion of propane.

The dissociation of the ammonium ion and the basic strength of ammonia in water. By D. H. EVERETT and W. F. K. WYNNE-JONES. (*Communicated by Sir Harold Hartley, F.R.S.—Received* 24 *June* 1938.)

From measurements of the E.M.F. of cells comprising hydrogen electrodes in buffer solutions of ammonia and ammonium chloride the dissociation constants of the ammonium ion in water have been determined at different ionic strengths at 5, 15, 25, 35 and 45°. By combination with the data of Harned for the ionic product of water, these results give values for the ionization constants of ammonia. It is found that the dissociation of the ammonium ion varies with the temperature according to the equation:

$$-\log K = 2706/T + 0 \cdot 189,$$

corresponding to a heat of dissociation of 12,400 cal. The ionization of water and of ammonia, however, do not vary with the temperature in such a simple way and their heats of ionization decrease with rising temperature.

The difference in the behaviour of these substances is regarded as the consequence of the varying electrical type of the dissociation process. If ions are produced in a reaction, the orientation of solvent molecules by the ions causes an entropy decrease and also a decrease in the heat capacity, and therefore a changing heat of ionization. Where the dissociation process results in no change in the number of ions, or, more correctly, of charge centres, the heat of dissociation is practically constant.

On the corpora allata of dipterous insects. Part II. By E. T. Burtt. (*Communicated by A. D. Imms, F.R.S.—Received* 27 *June* 1938.)

Evidence is given concerning the function of Weismann's ring which, as was suggested by the author in 1937, represents in *Calliphora* the corpora allata of other insects. Methods are described for extirpating Weismann's ring in the larva of *Calliphora*. Pupation can be prevented either by removing Weismann's ring or by cutting the nerve connexions to this organ. Removal of the ring in larvae which are still feeding causes an arrest of development. Such larvae continue to feed for a period greatly exceeding the normal, and the growth of their imaginal buds is arrested. It is concluded that Weismann's ring secretes the pupating hormone discovered by Fraenkel, and in addition influences processes taking place prior to pupation. The work of Hadorn on Weismann's ring in *Drosophila* is briefly reviewed, and the somewhat discordant results obtained by workers who have removed the corpora allata in species of Orthoptera and Lepidoptera are discussed.

The low temperature properties of gaseous helium. By R. A. Buckingham and H. S. W. Massey. (*Communicated by J. E. Lennard-Jones, F.R.S.— Received* 27 *June* 1938.)

The viscosity and second virial coefficients of helium gas are calculated in the temperature range $0-26°$ K, using exact quantum formulation and the interatomic interaction given by Slater. It is found that there is very good agreement with the observed viscosity down to $15°$ K, but below this temperature the calculated values are too small. The correct form for the variation of the virial coefficient with temperature is obtained but the calculated behaviour is in error in predicting too low temperatures for the position of the maxima, etc. (The calculated Boyle point is $21°$ compared with the observed $23°$.)

It is shown that the discrepancies may be greatly reduced in both cases by small modification of the Slater field involving reduction of the van der Waals force at large distances and inclusion of dipole-quadripole interaction. No difference between the theoretical results obtained by assuming different statistics is sufficiently definite to be distinguished from small errors in the assumed interaction, in the temperature range from $1°$ K upward.

The separation of isotopes for the investigation of nuclear transmutations.
By E. LEIGHTON YATES. (*Communicated by E. V. Appleton, F.R.S.—Received 27 June* 1938.)

A mass spectrograph of simple design has been used to prepare deposits containing a few micrograms of the separated isotopes of lithium, boron and carbon. In the case of lithium, a filament type ion source was employed, while the boron and carbon ions were produced in a low voltage capillary arc running in boron trifluoride and in a mixture of heavy methane and helium respectively. On examination in artificial disintegration experiments, the samples were found to be of high purity.

Optical pyrometry. II. By F. A. CUNNOLD, A. C. EGERTON, F.R.S., and M. MILFORD. (*Received* 28 *June* 1938.)

The accuracy of the disappearing pyrometer as a means for determining high temperatures is emphasized; the sensitivity is such that temperature changes of about 1/5th of a degree can be detected. The simple means of determining the gold point described in *Proc. Roy. Soc.* A, **130**, 111, 1930, have been improved and an error due to the lack of equilibrium between the wire and the platinum tube eliminated by increasing the absorption coefficient of the wire. It is shown, as a development of the expression derived by Foote, that the effective wave-lengths used in the calibration of the pyrometer in terms of the current through the filament are those for which the temperature values are the brightness temperatures of the pyrometer filament.

The use of sectors in the calibration of the pyrometer is discussed, and greater accuracy can be obtained by means of a wide angle sector applied several times, rather than by using a single sector of narrow angle.

The best form in which to express the results of the calibration is discussed. The formula for one particular lamp used being:

$$T = a + bV^{-1} + cI,$$

where $a = +1224 \cdot 913$, $b = -288 \cdot 002$, $c = +417 \cdot 191$. The measurement of the effective wave-lengths of the special monochromatic colour filters used and of the transmission coefficients of the neutral absorbing glasses is described and the errors in the final extrapolation to very high temperatures determined.

The kinetics of electrode reactions. By J. N. AGAR and F. P. BOWDEN. (*Communicated by R. G. W. Norrish, F.R.S.—Received* 28 *June* 1938.)

Part I. The effect of local concentration changes on overpotential. We can distinguish three main causes of irreversibility in electrode reactions. These are:

(i) Concentration overpotential.
(ii) Activation overpotential.
(iii) Resistance overpotential.

A general theory of concentration overpotential is developed, and this shows how the overpotential will depend on the current density, concentration and temperature. An expression for the rate of growth of concentration overpotential after switching on the current is also given.

It is shown that the resistance of the diffusion layer may in some cases attain high values, and cause a resistive potential drop at least as great as the concentration overpotential. Finally the principal differences between concentration overpotential and activation overpotential are described.

Part II. Electrodeposition from a fused electrolyte. Measurements of the oxygen overpotential on nickel and platinum electrodes in fused sodium hydroxide have been made. The current densities used ranged from approximately 5×10^{-4} to 1 amp./sq. cm. At the highest current density the overpotential is of the order $0 \cdot 2$ V.

Although in some respects the observations might suggest that the overpotential is of the same kind as that observed in the deposition of OH′ ions in aqueous solutions, the evidence as a whole shows that this is not so. The overpotential in fused NaOH is due to the change in the concentration of *water* in the melt in the immediate vicinity of the electrode. A small trace of water is normally present in the fused hydroxide, and more water is produced by the anode reaction.

This view is supported by many different lines of evidence, including:

(*a*) the influence of stirring the electrolyte;

(*b*) the effect of adding small quantities of water;

(*c*) the rate of increase of the overpotential on switching on the current;

(*d*) the nature of the relation between overpotential and current density;

(*e*) the low value of the temperature coefficient;

(*f*) the fact that the overpotential is independent of the nature of the electrode.

The general behaviour is consistent with the theory of concentration overpotential developed in Part I.

On the polymerization of vinyl acetate. Part I. By A. C. Cuthbertson and E. K. Rideal, F.R.S. (*Received* 28 *June* 1938.)

Details are given for the preparation of pure vinyl acetate. Freshly distilled aldehyde-free vinyl acetate shows no appreciable reaction up to a temperature of $100°$ C over a period of 24 hr. It has been shown that the addition of acetaldehyde (prepared in air) to pure vinyl acetate catalyses the reaction at $100°$ C. Experimental data have been presented for the course of the polymerization of pure vinyl acetate catalysed by benzoyl peroxide at 60, 80 and $100°$ C and for the former in toluene solutions at $80°$ C. Chain lengths of the polymers at $60°$ C have been computed from viscosity data obtained from measurements made with an Ostwald viscometer which were shown to be in relative agreement with comparable measurements made with a Couette viscometer. At $80°$ C there is evidence that chain branching occurred particularly in the later stages of the reaction. During the reactions catalyst decomposition takes place as an independent side reaction. This effect is noticeable at 60 and $80°$ and is very marked at $100°$ C. The reactions are exothermic as a result of which there is a temperature rise during the course of the polymerizations. This rise is progressively more pronounced as the catalyst concentration is increased.

On the polymerization of vinyl acetate. Part II. By A. C. CUTHBERTSON and G. DEE. *(Communicated by E. K. Rideal, F.R.S.—Received 28 June 1938.)*

The interpretation of the experimental results described in Part I is discussed. The induction period in the polymerization is ascribed to the fact that the initiation process involves two concentive slow reactions, namely the formation and subsequent decomposition of a complex between the catalyst and monomer. A kinetic analysis is developed, on the basis of which it is concluded that the polymerization chains terminate by mutual deactivation. Correction has to be made for the decomposition of the catalyst which is found to be an important factor. The causes of the observed effect of toluene in reducing both rate and chain length are discussed, and two alternative explanations examined.

The experimental measurements of chain length are in some cases at least invalidated by the occurrence of branching, leading finally to the production of insoluble products. A kinetic treatment shows that branching is largely confined to the late stages of polymerization: this is in accord with experimental findings.

On the theory of coincidence experiments on cosmic rays. By N. ARLEY. *(Communicated by N. F. Mott, F.R.S.—Received 28 June 1938.)*

We have made further calculations on the cascade theory of showers put forward by Bhabha and Heitler and by Carlson and Oppenheimer. In § 1 the number of "slow" electrons in a shower is calculated, i.e. of electrons having an energy less than the critical energy of the shower producing material. In § 2 we discuss the fluctuations of the number of particles about the mean number. By means of a simplified model for the multiplication process it is made plausible that the Poisson formula holds for the fluctuation in small showers. In § 3 the energy spectrum of the soft component is discussed. With this energy spectrum the mean probabilities of finding one, two and so on particles emerging from a certain layer are calculated, giving the absorption curve and the Rossi transition curves. In §§ 4–6 we compare our results with experiments. *The quantitative agreement between theory and experiment for the absorption and the Rossi curves is satisfactory* both with regard to the shape of the curves and their dependence on the material. There is, however, a difficulty in understanding the Z^2 law found for the Rossi curve at small thicknesses. This is possibly explained by the simultaneous effects of a light quantum and an electron. The spread of showers from air is discussed in this connexion.

The rates of transformation in ethyl alcohol of ammonium and ethylammonium cyanates to the corresponding ureas. By CHRISTINA C. MILLER and J. R. NICHOLSON. *(Communicated by J. Kendall, F.R.S.—Received 29 June 1938.)*

The rates of transformation of ammonium cyanate to urea at 16, 24 and 32° C, and of ethylammonium cyanate to ethylurea at 0, 10 and 20° C have been found over

the concentration range 0·0002–0·04 M in ethyl alcohol containing 1·91 % of water, and compared with those for methylammonium cyanate at 0 and 10° C in the same solvent.

On the supposition that ammonium (or alkylammonium) and cyanate ions are the reactants, the applicability of the Brönsted-Gronwall, La Mer and Sandved theory to the results has been tested by assuming its validity and calculating the values of *a*, the mean distance of closest approach of the ions, required to give agreement. For all three cyanates *a* has been found to have a high positive temperature coefficient. A simplified form of Christiansen's equation for ionic reactions is not generally satisfied at infinite dilution, whether *r* the distance between colliding and reacting ions is taken to be constant or set equal to the temperature-variable *a* values.

The Arrhenius equation ($k = Ae^{-E_A/RT}$) is not fulfilled, except at the highest concentration. E_A and A vary in a parallel manner from one cyanate to another, and with change of concentration, temperature and solvent. An attempt has been made to explain the relative rates of transformation of the cyanates in water and ethyl alcohol at infinite dilution by supposing that the solvation of the reactants plays an important part.

The effect of androgenic substances on the growth of the teat and mammary gland in the immature male guinea-pig. By A. C. BOTTOMLEY and S. J. FOLLEY. (*Communicated by A. S. Parkes, F.R.S.—Received* 30 *June* 1938.)

In the young male guinea-pig between 150 and 430 g. body weight the teat grows isometrically with the body as a whole. This teat growth ceases after castration and is, therefore, maintained by the endocrine activity of the testes. The unsaturated androgens, Δ_5-*trans*-androstendiol, testosterone, Δ_5-*trans*-dehydroandrosterone and 17--methyltestosterone promote teat growth, Δ_5-*trans*-androstendiol being the most potent in this respect.

Data for the relative rates of teat growth under the stimulus of Δ_5-*trans*-androstendiol, Δ_5-*trans*-dehydroandrosterone, testosterone propionate and 17-methyltestosterone give good agreement with the law of simple allometric growth. The saturated androgens, *cis*-androsterone, *cis*-androstendiol, dihydrotestosterone and the unsaturated diketone Δ_4-androstendione, do not promote teat growth. Testosterone and its propionate were both more active in promoting teat growth when the volume of oil medium used for injection was decreased. Testosterone propionate was no more active than free testosterone.

The relative rate of teat growth caused by testosterone propionate was greater in intact guinea-pigs than in recently castrated ones. The activity of the androgens in promoting teat growth appears to be correlated with the presence of a double bond (Δ_4 or Δ_5) in the ring structure of the molecule, and the presence of at least one hydroxyl group in the 3 or 17 position also appears to be necessary for activity. The most active substance studied was an unsaturated 3–17 diol.

Histological examination showed the Δ_5-*trans*-androstendiol, testosterone propionate and 17-methyltestosterone stimulated the mammary ducts but caused very little alveolar development.

ABSTRACTS

OF PAPERS COMMUNICATED TO THE ROYAL SOCIETY OF LONDON

In accordance with a resolution of Council, summaries or abstracts of papers are to be published as soon as practicable. The publication of such abstracts in no way indicates that the papers have been accepted for publication in any fuller form. These abstracts will be issued for convenience with the "Proceedings of the Royal Society of London" but do not form a part of the "Proceedings".

---

6 SEPTEMBER 1938

The effects of thunderstorms and lightning discharges on the earth's electric field. By T. W. WORMELL. (*Communicated by C. T. R. Wilson, F.R.S.—Received* 29 *June* 1938.)

The results of an extended series of observations of the potential gradient during thunderstorms in the years 1926–36 are discussed. A capillary electrometer was used to record photographically the behaviour of the gradient, and continuous observations were possible even in the most intense fields and throughout heavy rainfall. The effects of lightning discharges could be detected up to about 40 km. distance. The time of response of the recording system to a sudden change in the field was about 0·05 sec. and the method thus yields an accurate record of the behaviour of the pre-discharge gradient, of the recovery of the field after a discharge and also a certain amount of detail during the change of field accompanying a discharge.

Records of a number of storms are reproduced and discussed in detail.

The values of the pre-discharge gradient beneath a thundercloud rarely exceeded 10,000 V/m. even just before a close lightning flash. Negative gradients were on the average more intense than positive ones at all distances from the storm. When discharges were occurring within 5 km., negative pre-discharge gradient was twice as frequent as positive; beyond 10 km., positive gradient predominated.

The magnitude of the field changes due to very close discharges was very variable. The biggest observed, of either sign, exceeded 50,000 V/m., but flashes within 1 km. occasionally caused changes of only a few thousand volts per metre.

The magnitude of the field changes at greater distances leads to an estimate of the electric moment of the discharges. The mean value deduced for this quantity (i.e. twice the product of the charge by its vertical displacement) was about 220 coulombs × kilometres. The values for positive and negative discharges were not greatly different.

The most distant discharges recorded showed an excess of negative field changes (i.e. of changes tending to reduce the value of a positive potential gradient). For discharges within 15 km. there was a considerable excess of positive field changes, the proportion increasing with decreasing distance until at about 5 km. distance positive changes were more than three times as frequent as negative ones. This well-known behaviour is commonly interpreted as due to the frequent occurrence of a discharge involving the main positive charge at the top and negative charge in the base of the thundercloud. For the very close discharges there was however, in the present series of storms, a marked increase in the proportion of negative field changes, positive and negative changes being about equally frequent for discharges within 3 km. The observations would seem to demand the not infrequent occurrence of a second type of cloud discharge which causes a negative field change at short distances, but a positive change beyond its small reversal distance, and must be very low down.

About one quarter of all the field changes recorded, even with this rather slow apparatus, showed components of both signs. For very close discharges the proportion was considerably higher. Such complex field changes were sometimes observed when only a single flash, either in the cloud or to earth, was visible in daylight. Many of the simple field changes showed appreciable duration on the records, in a few cases exceeding 0·5 sec. In some cases this was clearly due to the discharge being made up of several strokes but in others the change was recorded as a slow smooth variation of the field.

The form of the recovery of the field after a discharge is discussed in detail and it is concluded that the initial rate of regeneration of electric moment by the cloud is, on the average, about 0·15 of the moment destroyed by the flash per second.

A brief discussion is given of our present knowledge of some of the fundamental quantities connected with a thundercloud and of the theory of the mechanism of the production of the charges.

The use of a vertical pipe as an overflow for a large tank. By A. M. BINNIE. (*Communicated by R. V. Southwell, F.R.S.—Received* 30 *June* 1938.)

The performance of vertical pipes arranged as overflows in a tank was studied experimentally on a small scale with special apparatus, which ensured that the water reached the pipe inlet with no tangential component of velocity.

Under normal conditions the change of head with discharge was small at low heads. At this stage the flow was not rotational, but a considerable volume of air was drawn down the pipe in the form of bubbles. Above a sharply marked critical head, the pipe ran full and a large rise of head caused only a slight increase in the discharge. The effects on the critical head of lengthening the pipe and of sharpening its inlet end were comparatively small, but the insertion of a trumpet-shaped mouthpiece greatly improved the performance.

The types of flow described by Borda as free and full flow were possible with overflow pipes of uniform diameter, and they resulted in a serious reduction in the discharge.

The electromagnetic energy of a point charge. By M. H. L. PRYCE. (*Communicated by P. A. M. Dirac, F.R.S.—Received* 30 *June* 1938.)

A method of defining the energy of a point charge in a finite manner is developed. It is roughly equivalent to subtracting an infinite constant from the ordinary expression in an unambiguous and relativistically invariant way. The energy and momentum are quite simply given as the sum of a mechanical part and a (convergent) integral over all space. For a point charge in uniform motion the energy and momentum are the same as for a particle possessing inertia.

The equations of motion for a point charge are derived from the conservation of energy and momentum.

In § 5 the theory is presented symmetrically with regard to the advanced and retarded fields.

An absolute determination of the acceleration due to gravity at the National Physical Laboratory. By J. S. CLARK. (*Communicated by W. L. Bragg, F.R.S.—Received* 5 *July* 1938.)

An absolute determination of the value of *g* at the N.P.L. has been carried out, using a reversible pendulum swinging *in vacuo* on a fixed knife-edge, the plane-bearing surface being part of the pendulum itself.

The pendulum was designed to be as rigid as possible, and special attention was given to the calculation of the correction due to the elastic deformation of the pendulum when oscillating.

Investigations were also made to determine the corrections due to curvature of the knife-edges, elasticity of the support, amplitude of swing, and the residual pressure.

The mean result of eighteen determinations gave the value of *g* at the N.P.L. (lat. 51° 25' 14" N., long. 0° 20' 21" W., and height above M.S.L. 10 m.) as 981·181₅ cm./sec.²

Specific heat-temperature curves of some age-hardening alloys. By N. SWINDELLS and C. SYKES. (*Communicated by W. L. Bragg, F.R.S.—Received* 5 *July* 1938.)

The changes in atomic configuration taking place during hardening affect the apparent specific heat of age-hardening alloys. Specific heat-temperature curves and hardness measurements have been obtained on five typical age-hardening alloys.

The results show that in certain cases, e.g. the silver-copper and copper-beryllium alloys, maximum hardness is attained when the major portion of the chemical energy associated with the supersaturated solid solution has been evolved, i.e. precipitation has taken place. In other cases, duralumin and aluminium-copper alloys, maximum hardness is associated with segregation of the solute atoms in the parent lattice prior to precipitation.

The classical equation of state of gaseous helium, neon and argon. By R. A. BUCKINGHAM. (*Communicated by J. E. Lennard-Jones, F.R.S.—Received* 11 *July* 1938.)

The problem of deriving the form of the interaction of rare gas atoms from their observed second virial coefficients is attacked by the method introduced by Lennard-Jones, using the classical equation of state and for the interaction energy

$$E(r) = \lambda r^{-s} - \mu r^{-t}. \tag{1}$$

The method of calculation used by Lennard-Jones for helium, neon and argon, assuming λ and μ constant, has been modified and then extended to allow for a possible slow variation of λ with r. The bearing of the results upon the true interaction of helium atoms is discussed, mainly in relation to the accuracy of the Slater field. For neon and argon it is emphasized that an unambiguous determination of the interaction energy requires an accurate knowledge of the properties of the crystalline form of these elements. The description of the repulsive potential by analytic expressions, such as $be^{-r/\rho}$ and $b_1 r^7 e^{-r/\rho_1}$, is considered, and parameters deduced which give the best correlation of gas and crystal data, on the assumption that (1) and kindred forms are valid for the interaction of neighbouring atoms only in the crystals.

The formation of negative ions by positive-ion impact on surfaces. By R. PRESS and R. H. SLOANE. (*Communicated by E. V. Appleton, F.R.S.—Received* 12 *July* 1938.)

It has been found that when a hot-cathode discharge is passed through mercury vapour, light negative ions are produced from surfaces exposed to positive-ion bombardment. The negative ions include some with energies greater than could be imparted to them in the existing electric fields. Experiments are described which eliminate the possibility that the excess energies could be produced through electrical oscillations. The conditions under which the negative ions appear indicate that they are produced mainly through sputtering of occluded electronegative films under the action of mercury positive-ion bombardment, but results from experiments of this type cannot be interpreted unambiguously. The existence of this process has been shown directly by a double mass spectrograph in which beams of positive ions of known kind are allowed to impinge normally on a metal disk in high vacuum and are found to produce a spectrum of negative ions, with properties similar to those of the negative ions obtained in the previous experiments. The existence of Hg^- as a stable entity seems to be still in doubt.

The porous diaphragm method of measuring diffusion velocity, and the velocity of diffusion of potassium chloride in water. By G. S. HARTLEY and D. F. RUNNICLES. (*Communicated by F. G. Donnan, F.R.S.—Received* 12 *July* 1938.)

A continuous reading apparatus for measuring the rates of diffusion of pure electrolytes through porous diaphragms is described.

Results obtained for the diffusion of potassium chloride as a function of concentration are presented and the absolute values obtained by extrapolation.

The comparison of the results obtained with the best available data by absolute measurements shows that there is still room for more accurate work in the whole problem, but it is believed that the diffusion coefficients in the range from $N/100$ to $N/10$ are accurate to within 2 %.

The determination of the size of paraffin-chain salt micelles from diffusion measurements. By G. S. HARTLEY and D. F. RUNNICLES. (*Communicated by F. G. Donnan, F.R.S.—Received* 12 *July* 1938.)

The porous diaphragm method has been applied to the measurement of the diffusion of paraffin-chain micelles in aqueous solution with a swamping excess of simple electrolyte.

For cetyl pyridinium salts the method is satisfactory and a radius for the micelle of about 26 A is found. The radius is independent, within experimental error, of the concentration of paraffin-chain or swamping electrolyte, and very little dependent on temperature. These results are in excellent agreement with the "spherical liquid micelle" theory. There is small, but definite, influence of the nature of the gegenion on the size of the micelle.

For cetane sulphonates and cetyl sulphates the method fails to give reliable results, probably owing to the building up of a structure within the pores of the diaphragm.

When the solutions are saturated with amyl alcohol or benzene the method again fails to give reliable results. A mechanism is suggested for the anomalies observed.

The simultaneous sorption of carbon bisulphide and water vapour by activated charcoals. By A. J. ALLMAND, F.R.S. and J. L. LIZIUS. (*Received* 12 *July* 1938.)

Although accurate work has recently been published in the *Proceedings* on the adsorption of *gaseous* mixtures on solid sorbents, the authors do not think that similar work of any value has appeared dealing with the simultaneous adsorption of two *vapours*. They have attempted to carry out such measurements, using water and carbon bisulphide as the sorbates, and three activated charcoals of varying character as the sorbents. The technique employed, including pressure measurements by means of a Pirani gauge, was an extension of that already described in the *Proceedings* of the Society.

Experiments were carried out on the effect of varying charges of water vapour on the pressure exerted by a constant charge of carbon bisulphide sorbed on charcoal, on the sorption isothermals of water on charcoal containing such a charge of carbon bisulphide, and also on the sorption isothermals of carbon bisulphide on charcoal containing a constant charge of water. The results are expressed in the form of diagrams. They are of some complexity, due to the complications involved in the use of water vapour.

The discussion is a somewhat detailed one, necessarily so in the opinion of the authors, in view of the complex nature of the systems studied. It commences with a résumé of our present knowledge of the nature of the sorption of water and carbon bisulphide vapours by the charcoals of the particular types used—points to a parallelism between certain results in the present paper and the sorption isothermals of water on charcoal—makes detailed suggestions regarding the nature of the different stages of the latter (adsorption of single molecules passing gradually over to the formation of a continuous adsorbed film, with irreversible capillary condensation superposed)—explains the effect of an increasing water charge on the pressure of a constant carbon bisulphide charge in the light of these suggestions—shows how the isothermals of carbon bisulphide on charcoals containing sorbed water are consistent with the same views.

The mammary gland of the rhesus monkey under normal and experimental conditions. By S. J. Folley, A. N. Guthkelch and S. Zuckerman. (*Communicated by W. E. Le Gros Clark, F.R.S.—Received* 13 *July* 1938.)

Examination of the mean mammary gland area of twenty-six non-pregnant normal female rhesus monkeys shows that over the body-weight range 3400–6060 g. the gland grows according to the simple allometric law. The first menstrual cycles of the rhesus monkey after puberty are usually anovular. Until ovulation occurs, mammary glands grow by proliferation of their ducts, and alveoli do not appear to form until after luteinization has occurred.

Normally the mammary gland of the male rhesus monkey consists of a relatively uncomplicated duct system which does not extend far beyond the base of the nipple. One otherwise normal male showed a condition of gynaecomastia, with clumps of fully formed alveoli. Thirteen male monkeys were injected daily with varying quantities of oestrone for periods ranging from 6 to 484 days. Only one of these animals (one that was injected for fewer than 15 days) failed to show duct proliferation. Only one showed alveolar formation, no alveoli being present in the two animals which received the longest treatment (368 and 484 days respectively).

Only two of four female rhesus monkeys which were spayed before the beginning of the treatment with oestrone (37–365 days) showed alveolar formation. Testosterone propionate appears to stimulate stunted duct development and alveolar formation in male monkeys.

No carcinomatous changes were observed in the mammary glands of any of six monkeys which were injected daily with oestrone either continuously or for the major part of periods varying between 365 and 938 days.

The thermal decomposition of nitrous oxide. By C. N. Hinshelwood, F.R.S. and R. M. Lewis. (*Received* 15 *July* 1938.)

Further experimental data relating to the thermal decomposition of nitrous oxide at 747° and 652° are recorded.

The variation of reaction rate with pressure is expressed both in terms of the reciprocal half time of reaction and in terms of the initial rates. The two curves

obtained are similar enough to show that previous conclusions based upon the half-time curves are confirmed by the initial rate curve.

The mean value of the activation energy falls at lower pressures, and the absolute magnitude of this energy agrees with most previous determinations, but not with those upon which has been based a theory that the reaction is abnormally slow for certain quantum mechanical reasons.

The influence of the products of reaction and of additions of nitrogen, argon and carbon dioxide has been studied. There is a contrast between the action of argon and that of carbon dioxide in that the former has a relatively greater effect at lower than at higher partial pressures of nitrous oxide. This fact is consistent with a greater complexity of the reaction mechanism than corresponds to the assumption of a single "quasi-unimolecular" reaction. The nature of this complexity is discussed.

On the stability of flow between parallel planes. By D. MEKSYN. *(Communicated by L. Bairstow, F.R.S.—Received 20 July 1938.)*

The equations of motion of a viscous fluid for the case of flow between two parallel planes are considered, and it is shown that at sufficiently high Reynolds numbers and sufficiently small wave-lengths, neutral vibrations of small amplitude can coexist with a laminar flow. For moderately large values of R neutral vibrations can exist only for discrete values of R and λ, the wave-length of the vibrations.

The band spectrum of silicon monosulphide and its relation to the band spectra of similar molecules. By R. F. BARROW and W. JEVONS. *(Communicated by A. Fowler, F.R.S.—Received 21 July 1938.)*

The spectrum of SiS is investigated in emission by heavy-current discharges through a mixture of SiS vapour and argon. In the region $\lambda 2585$–3959 is a system of some 70–80 red-degraded bands with single heads:

$$\nu_{\text{head}} = 35028 \cdot 8 + (512 \cdot 0u' - 2 \cdot 38u'^2 - 0 \cdot 045u'^3) - (749 \cdot 5u'' - 2 \cdot 56u''^2)$$

(where $u = v + \frac{1}{2}$). That the lower state is the ground state of SiS is proved by the fact that some of the band heads (with $v'' = 0$ and 1) have been measured in absorption by SiS vapour. In the region $\lambda 3491$–6169 in the SiS discharge are about 70–80 red-degraded bands, which form a part of a second extensive system, probably of SiS, with neither state in common with the first. The vibrational frequencies for the upper and lower states are of the same orders for the two systems. The first system almost certainly involves singlet states (either $^1\Sigma \rightleftarrows x^1\Sigma$ or $^1\Pi \rightleftarrows x^1\Sigma$), while the second system, which resembles the $^3\Sigma \rightleftarrows {}^3\Sigma$ system of S_2 in appearance, may involve triplet states of SiS. The first system occurs also in heavy-current discharges through Al_2S_3 vapour and argon, and through BCl_3 vapour and H_2S, in silica tubes, apparently without the second system. The energies of dissociation of SiS in the ground state and excited state of the first system are about $6 \cdot 0 \pm 0 \cdot 3$ and $2 \cdot 1 \pm 0 \cdot 5$ eV respectively,

and the products of dissociation are probably unexcited atoms, $Si(^3P) + S(^3P)$ in each case. The numerical constants for the ground states and certain excited states of the diatomic oxides, sulphides and selenides of group $IV(B)$ atoms are surveyed, and from the empirical relations described the constants for the expected systems of SiSe and GeSe are estimated.

The behaviour of polar molecules in solid paraffin wax. By R. W. SILLARS. (*Communicated by E. V. Appleton, F.R.S.—Received 25 July* 1938.)

The experiments described constitute an extension of previous work by Jackson and were carried out on solid samples of paraffin wax containing small concentrations of various long-chain esters. The esters are of molecular type similar to the wax, but have a permanent electric moment in virtue of the ester group. Dipole effects similar to those found by Jackson are observed, and the variations of the characteristic time constants with temperature and with chain length of the esters are studied. Variation with temperature is approximately exponential, the exponent being about the same for each ester. It is found that the time constant is a non-linear function of the total chain length of the ester molecule, but is relatively independent of the position of the ester group in the chain. It is confirmed that the observed losses are due to dipole effects and not to some adventitious cause. It is concluded that the whole ester molecule contributes to the time constant, and therefore that it behaves as a rigid structure and does not simply become deformed in the immediate neighbourhood of the dipole group. This is in agreement with evidence from other sources. The results do not suggest any simple relation between chain length and time constant, and a satisfactory theory to relate them has yet to be found.

The specific heat of β-brass. By R. EISENSCHNITZ. (*Communicated by Sir William Bragg, F.R.S.—Received 26 July* 1938.)

A theoretical investigation is made of the specific heat of β-brass. The following assumptions are made in the course of the calculation: The interaction energies of the atoms vary with the square of change of volume; the energy minimum of the average of Cu-Cu and Zn-Zn energies lying at higher volume than the minimum of Cu-Zn.

The partition function at constant volume is calculated according to the theory of Bragg and Williams; the corresponding partition function at constant pressure is obtained by taking an average over the variable volume.

It is shown that the specific heat curve can be adjusted so as to give good agreement with experiment for temperatures below the maximum of specific heat.

The theory of Bragg and Williams is applied to a lattice containing a finite number of atoms. By introducing this number, agreement is obtained with the experimental slope of the C_v curve beyond the maximum. A theoretical estimate is made which justifies the introduction of this finite number.

A general theorem of statistical mechanics is derived, according to which all thermodynamical quantities in physically realizable systems are analytic functions of the temperature.

The effect of solvents on the continuous absorption spectrum of bromine. By R. G. AICKIN, N. S. BAYLISS and A. L. G. REES. (*Communicated by F. G. Donnan, F.R.S.—Received 26 July* 1938.)

The visible and ultra-violet absorption spectrum of bromine has been investigated in the following solvents: water (2N sulphuric acid), cyclohexane, chloroform, carbon tetrachloride, benzene, chlorobenzene, toluene.

The weak ultra-violet absorption of gaseous bromine is enormously enhanced in solution, particularly by the aromatic solvents. The smallest effect occurs in carbon tetrachloride, where considerable deviations from Beer's law were found. Absorption maxima in the ultra-violet were found at 2500 A in cyclohexane, at 2725 A in chloroform, and in the neighbourhood of 2950 A in the aromatic solvents.

In the region of the visible continuum, the non-aqueous solvents cause a marked increase in absorption intensity combined with a small or zero shift of the maximum towards the ultra-violet. Water causes a large displacement (1750 cm.$^{-1}$) of the maximum to higher frequencies; but only a very small increase in intensity. If the A component of the visible continuum is complex, the displacement of the maximum in non-aqueous solvents can be interpreted as due to a greater solvent effect on $^1\Pi_u \leftarrow {}^1\Sigma_g^+$ than on $^3\Pi_{0_u}^+ \leftarrow {}^1\Sigma_g^+$. The transition $^3\Pi_{1u} \leftarrow {}^1\Sigma_g^+$ is less affected still. Difficulty is found in interpreting the observations if the B continuum is complex and A simple.

Oscillatory motion of a fluid along a circular tube. By D. G. CHRISTOPHERSON, A. GEMANT, A. H. A. HOGG and R. V. SOUTHWELL, F.R.S. (*Received 26 July* 1938.)

This paper is concerned with oscillatory motion (either free or forced) of a viscous fluid along a circular tube: the restoring force comes in both instances from the "gravity head" which results from the passage of fluid. Part I is a theoretical discussion of the problem. Part II deals from a practical standpoint with complicating factors (e.g. turbulence, or meniscus and other end effects) which the theory does not take into account, and briefly discusses the possible application to viscometry. Part III gives the results of experiments made to test the predictions of Parts I and II.

The surface migration of barium. By M. BENJAMIN and R. O. JENKINS. (*Communicated by R. H. Fowler, F.R.S.—Received 27 July* 1938.)

It is found that under similar vacuum conditions barium does not migrate over tungsten, although thorium does. It is also shown that barium does not migrate over nickel.

The yield of mild steel, with particular reference to the effect of size of specimen. By J. L. M. MORRISON. *(Communicated by R. V. Southwell, F.R.S.—Received* 28 *July* 1938.)

The paper describes an investigation carried out to determine by means of tests under various conditions of uniform and non-uniform stress distribution the criterion of yield in specimens of mild steel.

Apparatus is described for heat-treating material after machining in such a manner as to avoid surface decarburization, and for determining the stresses at yield of specimens tested in tension, compression, flexure, torsion and combined tension and torsion. Experiments are described which indicate that the material used is uniform and isotropic; and the results of certain earlier investigations are compared with those found in the present paper.

No differences are found between the yield of mild steel in tension and compression.

The tests in combined tension and torsion give results in accordance with the theory of yield at a critical value of the shear strain energy stored per unit volume of the material. It is later shown that this result is due to the size of specimen tested.

Tests in tension on solid specimens of varying size and on thin tubes indicate that the character of the yielding of mild steel is a result of the polycrystalline nature of the material.

It is shown that in all cases of non-uniform stress distribution the yielding depends on the size of the specimen. The explanation advanced to account for this result is that in such cases yield is delayed until a shear stress not less than the shear stress at yield under uniform stress is applied to a thickness of material of the order of a few crystal diameters.

The band spectrum of antimony fluoride (SbF). By H. G. HOWELL and G. D. ROCHESTER. *(Communicated by W. E. Curtis, F.R.S.—Received* 28 *July* 1938.)

The spectrum of SbF has been produced in active nitrogen and also by means of a high-frequency discharge. It consists of three groups of bands lying in the regions 3600–5000, 2600–2700 and 2200–2430 A. Most of the bands in the first region had already been shown by Rochester to belong to two systems. The remaining bands in this group are here allocated to a third system. As the vibrational constants of these three systems are very nearly the same they are considered to be due to transitions between triplet electronic levels. Similarly, the ultra-violet bands form a triplet system, one component being in the region 2600–2700 A and the other two between 2200 and 2430 A. The final state is common to both triplet systems and is probably $^3\Pi$. The multiplet separations of the states is not known nor is the nature of the other electronic levels.

The vibrational constants of all the SbF systems are as follows:

Visible triplet system

ν_e	w_e'	$x_e w_e'$	w_e''	$x_e w_e''$
21887·5	411·3	1·71	616·9	2·89
23992·5	420·0	1·75	612·6	2·58
27912·0	412·0	2·35	612·5	2·55

Ultra-violet triplet system

ν_s	w_s'	$x_s w_s'$	w_s''	$x_s w_s''$
37937·6	696·9	1·09	616·6	3·19
43513·7	698·8	1·93	612·6	2·63
44750	700	—	612	——

The comparative behaviour of mammalian eggs *in vivo* and *in vitro*. II. The development of fertilized and artificially activated rabbit eggs. By G. PINCUS. (*Communicated by J. Hammond, F.R.S.—Received* 3 *August* 1938.)

This paper describes:

(i) the sequence of changes occurring between sperm attachment and the first cleavage division in rabbit ova normally fertilized *in vivo*;

(ii) the cytological changes occurring in unfertilized rabbit ova during their sojourn in the fallopian tubes;

(iii) the cytological behaviour of unfertilized ova subjected to five activating treatments (exposure to (*a*) hypertonic solution, (*b*) supranormal temperatures, (*c*) treatment with rabbit sperm, (*d*) treatment with rat sperm, and (*e*) culturing in a moist chamber) is categorized, and the various events ensuing upon activation are described and discussed;

(iv) the effects of varying the intensity and duration of the hypertonic solution and heat treatments;

(v) the results of treating rabbit ova with the spermatozoa of six species of mammal other than the rat and rabbit;

(vi) a series of transplantations of artificially activated rabbit ova.

These experiments are taken to demonstrate that: (1) both ovarian and tubal ova activated by these treatments *in vitro* will in varying degrees exhibit development comparable to that of normally fertilized eggs; (2) the initiation of activation is an all-or-none process though its continuation probably is not; (3) haploid, diploid or tetraploid parthenogenesis results from the treatments employed; (4) the intervention of atretic processes may arrest the development of activated eggs at any developmental stage; (5) foreign sperm may activate rabbit eggs to a limited degree, but, except in certain instances with rat sperm, the foreign sperm do not penetrate the zona pellucida of the rabbit eggs; (6) living young may arise from artificially activated eggs, but only in a limited number of cases.

The heat of shortening and the dynamic constants of muscle. By A. V. HILL, Sec. R.S. (*Received* 3 *August* 1938.)

Further improvements in thermopile and galvanometer systems are described which have made it possible to read the initial heat production directly from photographic records, in absolute units and (for most purposes) without analysis.

When a muscle shortens, in a tetanically maintained contraction, it liberates extra energy in two forms, (i) as "shortening heat", in amount proportional to the shorten-

ing, and (ii) as external mechanical work. The shortening heat is independent of the load, and therefore of the work done and the speed of shortening. The rate of energy liberation, i.e. of work + heat, is a linear function of the load, increasing as the load diminishes.

The "dynamic constants" of muscle, in a maintained contraction, are defined and measured. They are:

a, the shortening heat per cm. of shortening;

P_0, the isometric tension;

b, the increase of energy rate per g. wt. of load.

At any temperature these quantities are very constant: a/P_0 is independent of temperature, b has a temperature coefficient of about 2·05 per 10°C. A "characteristic equation" is deduced for the speed of shortening v under a load P, viz.

$$(P+a)(v+b) = \text{const.}$$

This equation is very accurately obeyed. By fitting it to observations of v and P, the same constants a and b are obtained as are given by heat measurements.

When a contracting muscle is made to lengthen gradually by applying a load rather greater than the isometric tension there appears to be a negative heat of lengthening, and the total energy given out by the muscle is less than in an isometric contraction. The energy relations in lengthening are the converse of those in shortening and seem to be governed by the same rules.

The nature of the shortening heat, and the mechanism by which the energy rate is governed by the load are discussed. It is suggested that the chemical processes by which energy is liberated involve certain active points in the molecular machinery, and that when these are occupied in attracting one another and producing a tension they are not available to take part in chemical reaction.

The work done by a muscle in raising a load, or in overcoming an elastic resistance, is transformed into heat in relaxation.

The "visco-elasticity" of contracting muscle is shown to be the property of a two-component system, the one component being undamped and elastic, the other being governed by the characteristic equation $(P+a)(v+b) = \text{const.}$, and its corresponding energy relations. The fact that an active muscle shortens more slowly under a greater force is due, not to "viscosity" but, as Fenn has claimed, to the manner in which the energy liberation is regulated. A large force causes a low energy rate, which results in a low speed.

From this can be deduced (i) the form of the isometric contraction, (ii) the form of the force-distance curves made, at constant velocity, by the Levin-Wyman apparatus, and (iii) that the greatest rate of doing external work should occur with a load equal to about 30 % of the isometric tension.

The specific heat of gases at high temperatures. By R. W. Fenning and A. C. Whiffin. (*Communicated by W. L. Bragg, F.R.S.—Received 3 August 1938.*)

(a) *Introductory (reasons for enquiry).* At the time this investigation was authorized there was some uncertainty as to the accuracy of the "accepted" values of the molecular heat, at high temperatures, of the gases which comprise the working fluid

of the internal combustion engine, and in view of the experience that had already been gained at the N.P.L. in connexion with gaseous explosions in closed vessels, it was recommended that a redetermination of this fundamental physical property should be attempted.

(b) *Range of investigation.* By carrying out explosions of mixtures of the type $(2+a)\,CO+O_2+bA$, and replacing the argon in turn by CO, N_2 and CO_2, values have been obtained of the mean molecular heat of these gases between 373°K and about 2370, 2650, 2930 and 3060°K. By balancing the heat losses in each group of explosions, the direct measurement of such heat losses was avoided although their magnitude could eventually be obtained from the heat capacity equations.

Determinations have also been made of the mean molecular heats at constant volume of H_2 and H_2O (gas), the measurements being made from 373°K to temperatures ranging from about 2100 to 2900°K. Although the highest temperature is considerably below that attained in the case of CO, N_2 and CO_2, it is believed to be a considerable advance on earlier work, the temperature extension being obtained by the substitution of nitrous oxide for oxygen in the explosive mixtures. The H_2 and H_2O determinations are dependent on heat loss measurements for which a special device was employed.

(c) *Conclusions.* The values obtained for the mean molecular heats at constant volume of CO, N_2, CO_2, H_2 and H_2O (gas) are represented by the following equations over the specified temperature ranges:

Between 373°K and temperatures ranging from 2350 to 3070°K :

$$C_{CO} = 4\cdot854 + 0\cdot0_37725T - 0\cdot0_7875T^2,$$
$$C_{N_2} = 4\cdot795 + 0\cdot0_37675T - 0\cdot0_7875T^2,$$
$$C_{CO_2} = 8\cdot631 + 0\cdot001522T - 0\cdot0_615T^2.$$

Between 373°K and temperatures ranging from 2050 to 2930°K :

$$C_{H_2} = 4\cdot089 + 0\cdot0_2953T - 0\cdot0_798T^2,$$
$$C_{H_2O} = 4\cdot874 + 0\cdot002284T - 0\cdot0_6256T^2.$$

where $T =$ upper temperature in degrees Centigrade absolute.

These values are compared with molecular heats deduced by other investigation from spectroscopic data and, for the ranges specified above, represented by

$$C_{CO} = 4\cdot955 + 0\cdot0_37018T - 0\cdot0_7812T^2,$$
$$C_{N_2} = 4\cdot833 + 0\cdot0_37224T - 0\cdot0_7822T^2,$$
$$C_{CO_2} = 8\cdot672 + 0\cdot001555T - 0\cdot0_618T^2,$$
$$C_{H_2} = 4\cdot369 + 0\cdot0_26474T - 0\cdot0_7486T^2,$$
$$C_{H_2O} = 5\cdot244 + 0\cdot001893T - 0\cdot0_6194T^2.$$

The difference between the two sets of values is comparatively small and if equal weight be given to each, the appropriate equations would be:

$$C_{CO} = 4\cdot904 + 0\cdot0_37371T - 0\cdot0_7844T^2,$$
$$C_{N_2} = 4\cdot814 + 0\cdot0_3745T - 0\cdot0_7849T^2,$$
$$C_{CO_2} = 8\cdot651 + 0\cdot001538T - 0\cdot0_6165T^2,$$
$$C_{H_2} = 4\cdot229 + 0\cdot0_38002T - 0\cdot0_7733T^2,$$
$$C_{H_2O} = 5\cdot059 + 0\cdot002089T - 0\cdot0_6225T^2.$$

A further study of the problem of nuclear isomerism: the application of the method of coincidence counting to the investigation of the γ-rays emitted by uranium Z and the radioactive silver Ag^{106}. By J. V. DUNWORTH and N. FEATHER. (*Communicated by E. V. Appleton, F.R.S.— Received 3 August* 1938.)

The application of the method of coincidence counting by electrical means to the study of the time correlation of nuclear processes—particularly that of successive quantum emission—is discussed in detail. It is shown that a knowledge of the energy dependence of the sensitivity of the counters is essential for any interpretation of the results of such experiments. For the γ-ray counters employed in the present investigation some information on this point has been obtained by the use of sources of thorium-active deposit of short and long exposure. In the course of this work the general validity of the ideas of Ellis and Mott (1933) and of the nuclear level schemes of Oppenheimer (1936) has been established. Also the paired quanta of the annihilation radiation of positrons have been utilized in the calibration.

A study of the γ-radiations from UZ and the long-lived modification of Ag^{106} by the coincidence method has shown, in the former case, the emission of two quanta in succession in a very large fraction of the disintegrations, and, in the latter, the emission of four or five quanta in succession in the most probable mode. This result is in general accord with the view that nuclear isomers are to be distinguished one from the other by a small difference in energy content and a large difference in angular momentum. The particle emission from the short- and long-lived modifications of Ag^{106} has also been studied. It appears probable that the negative electrons of the long-period activity are internal conversion electrons associated with nuclear transitions following K electron capture, rather than that they represent a distinct mode of disintegration of the long-lived radioelement, Ag^{106}.

Relaxation methods applied to engineering. IV. Problems relating to elastic stability and vibrations. By K. N. E. BRADFIELD, D. G. CHRISTOPHERSON and R. V. SOUTHWELL, F.R.S. (*Received 3 August* 1938.)

Preceding papers in this series have been concerned with unique solutions: this paper deals with problems such that a complete solution would define an infinite number of configurations, all satisfying the governing equations and the terminal conditions, but each associated with some particular value of a critical loading or frequency (the "characteristic number", or *eigenwert*). The strut and vibrating rod (of non-uniform section) have been chosen for detailed treatment as the simplest examples, respectively, of elastic stability and vibrations; but the principles as distinct from the details of our "relaxation" treatment are quite general, and they provide a new method of attack on problems which are at once difficult and important.

In both problems the relaxation method appears capable of determining, with more than sufficient accuracy for practical purposes (when dimensions etc. are not known exactly), not only characteristic numbers but also the mode associated with each. (The modes are not determined by the well-known theorem of Lord Rayleigh.)

The nature of sliding and the analysis of friction. By F. P. Bowden and L. Leben. (*Communicated by G. I. Taylor, F.R.S.—Received 8 August* 1938.)

A detailed analysis of the kinetic friction between moving metals shows that the frictional force does not remain constant during sliding. Sliding is not a continuous process: the motion proceeds in jerks, and large and violent fluctuations occur in the friction. In the case of dissimilar metals the top surface sticks to the bottom one and moves with it until, as a result of the gradually increasing pull, a sudden and very rapid slip occurs. The process is then repeated indefinitely. A simultaneous measurement of the surface temperature shows that this too is fluctuating and, at the instant of slip, there is a sudden temperature "flash".

The exact behaviour depends upon the relative physical properties of the metals, particularly on the melting point, and there is evidence that three distinct types of sliding may occur. The experiments suggest that friction is due to a welding together of the metals at the local points of contact. These metallic junctions are large compared with the dimensions of a molecule and when they are broken the metal is distorted to a considerable depth.

Even if the surfaces are lubricated with mineral oils or other lubricants an intermittent clutching and breaking away of the surfaces occurs and the behaviour may be essentially the same. Certain long chain fatty acids may prevent stick-slip and allow continuous sliding to take place.

The area of contact between stationary and between moving surfaces. By F. P. Bowden and D. Tabor. (*Communicated by G. I. Taylor, F.R.S.—Received 8 August* 1938.)

An estimate of the real area of contact between stationary and between moving metal surfaces has been made by electrical and by visual means. Experiments with stationary surfaces show that the area of intimate contact is very small. It varies with the pressure, but for flat steel surfaces it may be less than one ten thousandth of the apparent area. The real area of contact is not greatly affected by the size, shape and degree of roughness of the surface: it depends mainly on the pressure. The general behaviour is consistent with the view that the surfaces are held apart by small irregularities. This means that even with lightly loaded surfaces the local pressure may be sufficiently great to cause the steel to flow plastically. This conclusion is supported by the observed relation between the pressure and the electrical conductivity. The slope of such a curve indicates that, at the points of contact, plastic flow of the metal has occurred. Although the stresses may cause elastic deformation in the bulk of the metal, the experiments suggest that the irregularities on which the bodies are supported are crushed down until their cross-section is sufficient to enable them to support the applied load.

Measurements made with moving surfaces show that the area of contact is not constant but is fluctuating rapidly during sliding. A detailed analysis shows a remarkable correlation between these fluctuations and the frictional and temperature

changes described in an earlier paper. It is clear that an intermittent clutching and breaking away of the surfaces is taking place and the results support the view that metallic junctions between the metals are being rapidly formed and broken. The nature of these junctions depends on the relative physical properties of the two metals and there is again evidence that three main types may occur.

The conductivity measurements show that even if the metals are lubricated with mineral oils and other lubricants, metallic contact may still occur through the film of lubricant. When the surfaces slide, fluctuations in the area of contact are observed and the behaviour may be essentially the same as for unlubricated surfaces.

Visual pathways concerned in gonadal stimulation in ferrets. By W. E. Le Gros Clark, F.R.S., T. McKeown and S. Zuckerman. (*Received 10 August* 1938.)

At the beginning of the non-breeding season lesions were made at various levels in the visual pathways of the brains of female ferrets. The animals were then exposed, at the end of each day, to bright artificial illumination for 6 hr. and 30 min. in order to discover whether or not they would come into heat during the anoestrum. Normal control animals, and ferrets whose optic nerves had been divided were exposed to the same conditions, while normal control animals were also kept under ordinary laboratory conditions.

The ferrets whose optic nerves had been divided either did not come into heat at all, or came into heat much later than the control animals. All the other animals came into oestrus either within or soon after the control period set by the normal animals exposed to additional light. The experiments showed that the normal response to visual stimulation occurs in the absence of the superior colliculi, when all retinal impulses to any part of the mid-brain have been interrupted and when retinal impulses to the dorsal nucleus of the lateral geniculate body and the visual cortex have been completely interrupted. Unless a few isolated normal cells in the dorsal nucleus of the lateral geniculate body provide the basis for adequate cortical stimulation, it was also found that a normal response can occur in the combined absence of the visual cortex and the superior colliculi, while another experiment strongly suggested that it can occur even after the interruption of retinal impulses passing to the dorsal nucleus of the lateral geniculate body, visual cortex, superior colliculi and pretectal area. This being so, the conclusion is suggested that the visual response depends on impulses passing either to the ventral nucleus of the lateral geniculate body, or to the subthalamus by way of the accessory optic tracts.

These results are discussed in relation to views on the exteroceptive stimulation of the pituitary in general and to the question of pituitary innervation in particular.

ABSTRACTS

OF PAPERS COMMUNICATED TO THE ROYAL SOCIETY OF LONDON

23 SEPTEMBER 1938

Growth and development in the pig with special reference to carcass quality characters. By C. P. McMEEKAN. (*Communicated by J. Hammond, F.R.S.—Received* 8 *August* 1938.)

Carcass quality in the meat animal is defined, in terms providing a fundamental basis for its scientific study, as being dependent upon the proportions of the body and upon its relative composition in the terms of bone, muscle, fat and offals. On the hypothesis that these characters are determined by growth and developmental changes, and that such changes are themselves controlled by hereditary and environmental influences, a series of experiments was designed to provide the knowledge of the principles operative, essential to increasing man's effective control over the animal body.

The composition of the bodies of some seventy closely inbred pigs of the Large White breed has been studied by complete anatomical dissection in the laboratory.

Analysis of postnatal changes with age under normal conditions has established the general order in development of the body proportions, tissues, and anatomical units. The different parts and tissues exhibit marked differential growth, so that the existence of well-defined growth gradients in the pig has been demonstrated.

The influence of quantitative differences in the plane of nutrition, operative from birth for the first 16 weeks of life, is such that the differential response of the different parts and tissues is dependent upon their differential growth relationships.

Complex experiments over the productive life of the pig as a meat producing animal afford convincing evidence of the influence of the nutritional environment as a directive and controlling force in the development of the animal body. The shape of the growth curve is revealed as a dominant factor in this connexion. Major modifications in form and anatomical composition do not occur as isolated effects but as orderly changes spread over a number of correlated parts.

By establishing the quantitative relationships between "internal" and "external" body measurements, and the anatomical composition, a scientific basis has been given their use in the study of carcass quality in the pig.

A new theory of melting-points. By F. C. FRANK. (*Communicated by N. V. Sidgwick, F.R.S.—Received* 11 *August* 1938.)

The only satisfactory existing theory of melting is the purely phenomenological thermodynamic description. This reveals no connexion with existing molecular theories, such as Lindemann's, and stands to some extent in contradiction with these. The modern recognition of order in liquids and disorder in solids raises the problem of explaining why there is an abrupt jump in physical properties on melting at all, instead of a continuous change, only showing discontinuity in a derivative quantity, e.g. in specific heat. Peierls has already succeeded in showing that discontinuity in certain properties is necessary.

In this paper the Bragg and Williams theory of order-disorder transformation is applied to melting. The basic assumption for this application is that the increasing disorderliness of a crystal near, and in fiction above, its melting-point can be described by a continuous numerical measure. An essential deviation from the cases considered by Bragg and Williams is that the lattice loses its rigidity on approaching states of low order. This causes one to anticipate a change of form in the $V(S)$ curve of Bragg and Williams such that the transition is regularly one of first order, whereas their cases could readily be of either first or second order, in sensitive dependence on minor changes of circumstance.

According to this interpretation there are critical temperatures above and below the melting-point limiting the range of existence of the metastable (superheated and supercooled) states. The probability that transformation will commence becomes great as the critical temperature is approached. It is shown that the melting-point may be expected to lie much closer to the upper critical point than the lower one, which may in certain circumstances be near the absolute zero. This explains why it is impossible to keep a crystal in the superheated state, but sometimes necessary to supercool to very low temperatures to produce crystallization nuclei in a liquid.

Progressive lightning. VI. By H. COLLENS, D. J. MALAN and B. F. J. SCHONLAND, F.R.S. (*Received* 15 *August* 1938.)

An account is given of some apparently anomalous lightning discharges observed with the Boys camera, and it is shown that their behaviour is in accordance with the same principles as govern the more usual type of discharge.

Certain abnormal first leader processes occur in two stages, the first rapid and the second involving a velocity close to the limiting value for negative streamer propagation. The first stage is considered to arise from the presence of space-charge concentrations in the air below the cloud. Dart streamers may travel down from the cloud during the second slow stage and catch up with the leader tip.

Changes in the lower portions of the channels used by successive strokes of the same flash are shown to be associated with long time intervals between strokes, whereby the conductivity and guiding power of the previous track is destroyed. A case of change in the upper portion of the channel is ascribed to the existence of a second centre of charge within the cloud.

The β-ray spectrum of Ra E. By L. H. Martin and A. A. Townsend. (*Communicated by T. H. Laby, F.R.S.—Received* 15 *August* 1938.)

The β-ray spectrum of Ra E has been studied by means of a magnetic spectrometer, the magnetic field for which was provided by an annular electromagnet, and has a geometrical form especially suitable for β-ray analysis.

Special attention was paid to the effect on the distribution of back scattering in the source support, and absorption in the window of the counter. The former was found to disturb the shape of the distribution to a greater extent than is generally appreciated. With the source mounted on thin mica and after correcting for absorption in the window of the counter, the maximum of the distribution was placed at 1210 gauss cm., a value much further towards the low-energy end of the distribution than has usually been found. The average energy of the β-particles is in good agreement, however, with the calorimetric values.

Both the Fermi theory and the modification of Konopinski and Uhlenbeck completely fail to describe the experimental distribution. The high-energy limit was placed at 5395 gauss cm.

Optical thickness of the transition layer between transparent media. By H. D. Bruce. (*Communicated by J. W. McBain, F.R.S.—Received* 16 *August* 1938.)

In view of the use that is being made in recent years of the properties of reflected plane polarized light to determine the nature and thickness of the adsorbed or transition layer, the theories of Drude and Maclaurin are discussed and found to reduce to an identical form not permitting of mathematical separation of thickness and refractive index of the transition layer, not even by the use of a series of observations as simultaneous equations. It is shown that the minimum thickness of the adsorbed layer compatible with the equations is derived by assuming the refractive index of the adsorbed layer to be the geometrical mean of the indices of the two media.

The spectral variation of the photosensitivity of visual purple. By C. F. Goodeve, R. J. Lythgoe and E. E. Schneider. (*Communicated by C. A. L. Evans, F.R.S.—Received* 18 *August* 1938.)

The photochemical bleaching of visual purple was measured quantitatively at wave-lengths ranging from 440 to 560 mμ using the method of photometric curves described previously. The experimental arrangement included a new high-intensity Hilger monochromator.

The results obtained for the photosensitivity of visual purple show that the quantum efficiency of bleaching is essentially constant and of the order of unity over the whole wave-length range. These facts lend further support to the previous arguments on the mechanism of the bleaching process.

The spectral variation of the photosensitivity is compared with the scotopic luminosity curve and good agreement between them is found. The significance of this result for the theory of scotopic vision is discussed.

A quantitative investigation into the enterohepatic circulation of bile salts in the cat. By J. MELLANBY, F.R.S., and S. F. SUFFOLK. (*Received* 23 *August* 1938.)

In a fasting cat about 95 % of the total bile salt is contained in the gall-bladder bile. The hepatic bile, continuously secreted by the liver, contains only traces of bile salt. In the fed cat the volume and bile-salt content of the hepatic bile shows a large increase, whilst the gall bladder contains only a small quantity of relatively dilute bile. The removal of the small intestine causes an immediate fall in the cholic acid content of the hepatic bile to that found in the fasting cat.

Bile salt are absorbed more rapidly from the ileum than from the duodenum and jejunum. A small amount of absorption occurs in the large intestine, but the absorption of water takes place much more rapidly than that of bile salt. Consequently the original concentration of bile salt may be increased fivefold in the unabsorbed bile. Bile salts injected into the blood are rapidly excreted in the hepatic bile. They are non-threshold substances in respect of the biliary apparatus. Bile salts are not stored in any tissue outside the enterohepatic system. The intravenous injection of secretin increases by 50 % the volume of bile secreted by the liver. It has no effect on the total quantity of cholic acid contained in the bile. Its action is therefore that of a hydrogogue.

Stimulation (acetyl choline) or paralysis (atropine) of the parasympathetic nerves to the liver has no influence on the volume or cholic acid content of the bile. Stimulation of the sympathetic nerves to the liver (adrenalin) diminishes to a small degree the volume of the bile secreted but augments the total amount of cholic acid contained in it. The sympathetic nerves may stimulate the formation of cholic acid from some inactive precursor by the liver cells.

After removal of the bile from a fasting cat, two-thirds of the cholic acid is re-synthesized in 2 days if the animal feeds well. In the absence of eating no synthesis of cholic acid takes place.

A cat contains approximately 100 mg. of cholic acid per kg. body weight. A rat contains approximately 25 mg. cholic acid per kg. body weight. The rate of flow of bile per unit of body weight is about six times as great in the rat as in the cat.